Magmatic dyke systems of the South Shetland Islands volcanic arc (West Antarctica): reflections of the geodynamic history

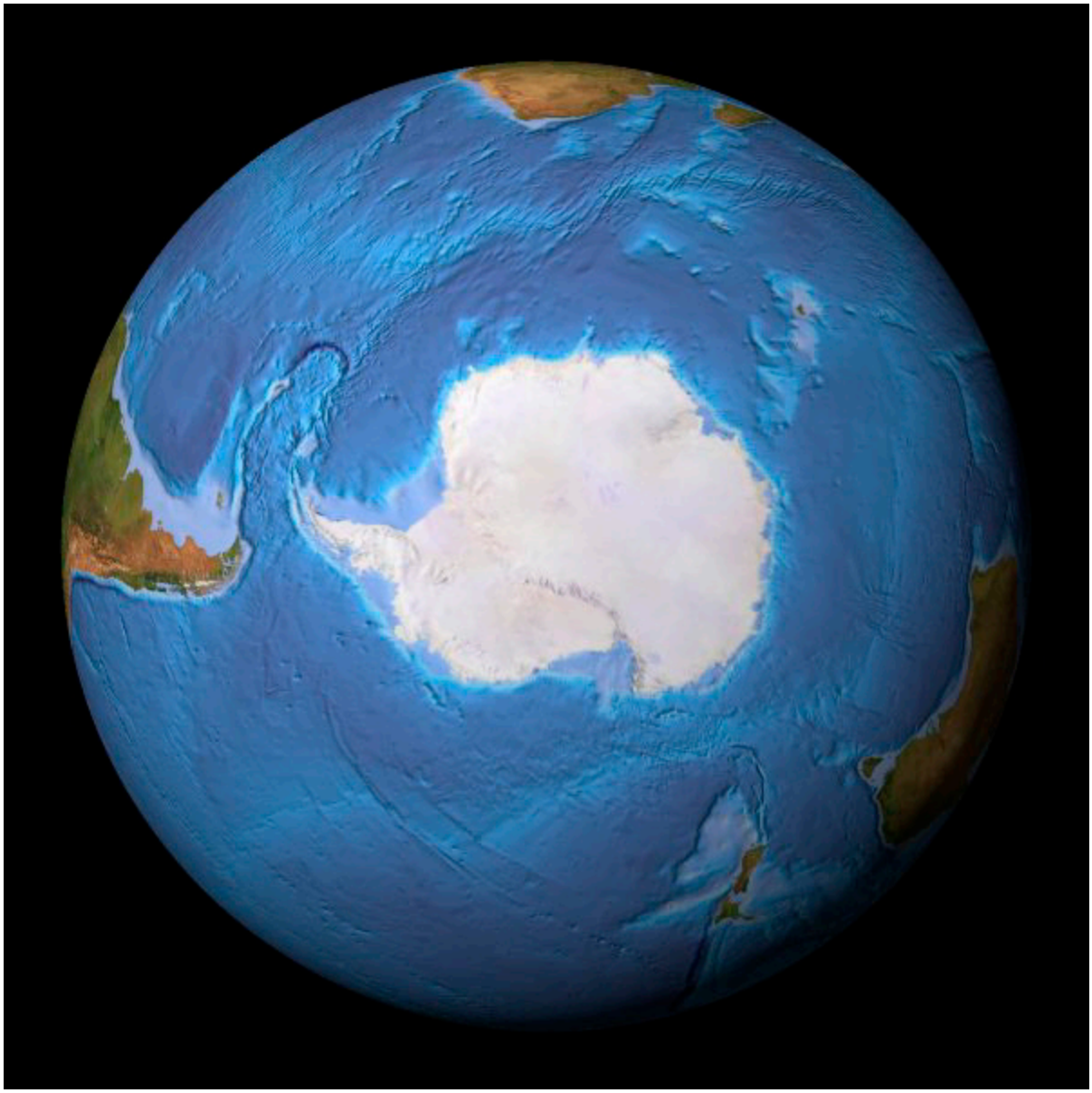

Als Dissertation eingereicht an der
Fakultät für Geowissenschaften
Ludwig-Maximilians-Universität München

von
Stefan Kraus

München, März 2005

Tag der mündlichen Prüfung: 2. Juni 2005
1. Berichterstatter: Prof. Dr. Dr. h.c. Hubert Miller
2. Berichterstatter: Prof. Dr. Ludwig Masch

Magmatische Gangsysteme auf den South Shetland Islands (West Antarktis): Reflexionen der geodynamischen Geschichte

Zusammenfassung

Der magmatische Bogen der Antarktischen Halbinsel entstand als Teil des andin-westantarktischen Kontinentalrandes ab der späten Trias bis zur Gegenwart. Die South Shetland Islands befinden sich an der Nordspitze der Antarktischen Halbinsel. Während der Kreide begann die Subduktion von protopazifischem Ozeanboden unter diesen Archipel und damit seine Entwicklung als eigenständiger magmatischer Bogen. Große Teile der South Shetland Islands bestehen aus Gesteinen, deren Entstehung auf die Aktivität dieses magmatischen Bogens zurückzuführen ist. Dazu gehören zahlreiche hypabyssale Intrusionen, welche die stratiforme vulkanische Sequenz durchschlagen.

Magmatische Gangschwärme gehören zu dieser letzteren Gruppe und sind auf den gesamten South Shetland Islands vertreten. Besonders häufig treten sie auf der Hurd Peninsula (Livingston Island) in Erscheinung. Über magmatische Gänge lassen sich hervorragend magmatische Ereignisse sowie tektonische Parameter identifizieren, da sie nicht nur die geochemischen und isotopischen Charakteristika der Magmenquelle widerspiegeln, sondern auch das tektonische Regime zur Zeit ihrer Platznahme. Außerdem können die relativen Altersbezüge der verschiedenen Intrusionsereignisse anhand sich schneidender Gänge bestimmt werden.

Während eigener früherer Arbeiten konnte ein enger Zusammenhang zwischen der Streichrichtung und der Chemie der Gänge nachgewiesen werden, welche die stratiforme vulkanische Sequenz auf der Potter Peninsula (King George Island, South Shetland Islands) durchschlagen. Auf diese Beobachtungen aufbauend und mit einer Erweiterung des Untersuchungsgebietes auf große Teile des Archipels, wurde ein Arbeitsansatz gewählt, der die Fragestellung von drei Seiten beleuchten sollte: kombiniert wurden tektonische, (isotopen-) geochemische und geochronologische Daten, um die in den Gangsystemen reflektierte geodynamische Entwicklung der South Shetland Islands zu rekonstruieren.
Hauptziele stellten zum einen die Identifizierung tektonischer Ereignisse dar, welche sich sowohl in der Orientierung der Gänge als auch in den Kluftsystemen widerspiegeln, zum anderen die Ermittlung der Magmenquellen einschließlich der möglicherweise auftretenden Veränderungen sowie eventuelle Verbindungen zwischen tektonischen und magmatischen Ereignissen.
Während der Südsommer 2000/2001 und 2001/2002 wurden an verschiedenen Stellen der South Shetland Islands Gangsysteme von bis zu 100.000 m² Größe kartiert, insbesondere auf King George und Livingston Island. Weitere Gänge wurden auf Nelson und Penguin Island untersucht. Es wurde eine

strukturgeologische Analyse des Nebengesteins und der Gänge durchgeführt, welche jeweils umfangreiche Kluftmessungen einschloss. Dabei wurde das Hauptaugenmerk auf sich kreuzende Gangsysteme gerichtet, welche die relativen Altersbeziehungen widerspiegeln. Insgesamt wurden etwa 250 Gänge beprobt.
Im Zuge der Laborarbeiten wurden Mikroskopie an Dünnschliffen aller 250 Proben, Mikrosondenanalysen (19 Proben), geochemische Analysen mittels ICP-MS (130 Proben) und Isotopenanalysen von Sr (12 Proben), Nd und Pb (jeweils 30 Proben) durchgeführt.
Um das daraus resultierende Gesamtbild in einen zeitlichen Rahmen setzen zu können, wurden Ar/Ar-Altersdatierungen an Plagioklas-Separaten von 19 Gängen vorgenommen. Zusätzlich wurden K-Ar-Datierungen von 7 Gängen gemacht (dabei handelte es sich um Gesamtgesteinsanalysen).

Der durchschnittliche Alterationsgrad der Gänge liegt in der Regel bei leicht bis mittel, in einigen Gebieten allerdings auch deutlich höher, und korreliert mit der geographischen Position. Die Gänge aus denjenigen Gebieten, die zur axialen, herausgehobenen Horststruktur von King George Island gehören, zeigen den höchsten Alterationsgrad. Bei der Hurd Peninsula (Livingston Island) könnte es sich um eine ähnlich herausgehobene Struktur handeln.

Die Gänge der South Shetland Islands gehören zur subalkalischen Serie und sind vorwiegend kalkalkalischer Affinität. Allerdings treten auch Tholeiite auf, die offensichtlich mit dem Anfangsstadium der vulkanischen Aktivität im jeweiligen Gebiet in Verbindung stehen. Das gilt für die Hurd Peninsula (Livingston Island), sowie für Weaver und Barton Peninsula und Admiralty Bay (alle King George Island).

Die geochronologischen Daten lassen darauf schließen, dass sich das Zeitintervall, in dem die Gänge in den Untersuchungsgebieten intrudiert sind, auf das Paleozän und Eozän beschränkt. Das schließt allerdings nicht aus, dass frühere Intrusionsereignisse in anderen Teilen des Archipels stattgefunden haben oder schlicht nicht aufgeschlossen sind.

Die wahrscheinlich ältesten Gänge treten auf der Hurd Peninsula auf und ergaben keine regulären Ar/Ar-Plateaus. Eine zeitliche Abschätzung, die auf den gemessenen Daten beruht, ergibt aber ein vermutliches Intrusionsalter im Bereich der Kreide/Paläogen-Grenze, wahrscheinlich im untersten Dan. Das wiederum zeigt, dass die Intrusion von Gängen auf der Hurd Peninsula (Livingston Island) offensichtlich früher begann (Dan) und länger andauerte (Priabon) als auf Nelson und King George Island. Hier konnten nur Gangalter von Thanet bis Lutet nachgewiesen werden. Das maximale Alter für das Einsetzen von Gangintrusionen auf der Hurd Peninsula wird durch Nannofossilien aus dem Campan gesetzt, welche in den metasedimentären Nebengesteinen nachgewiesen wurden.

Diese Daten schränken auch das Zeitintervall ein, in welchem die Hauptdeformation der Nebengesteine auf Hurd Peninsula (Livingston Island) stattfand. Dies umfasst die Faltung und die Ausbildung von primären und sekundären Schersystemen. Die Deformation ereignete sich offensichtlich innerhalb eines Zeitfensters von etwa 5-10 Ma zwischen dem späten Campan und dem frühesten Dan. Betrachtet man die geotektonische Herkunft dieser Gesteine, die einen Teil eines fossilen Akkretionskeils darstellen, ist ein solch verhältnismäßig kurzes Zeitintervall für die Deformation als möglich anzusehen. In den metasedimentären Nebengesteinen wurde Faltung um eine mit 24° streichende Achse nachgewiesen.

Ab dem Dan intrudierten die Gänge entlang der verschiedenen, den primären und sekundären dextralen und sinistralen Schersystemen zugehörigen Richtungen. Auf der Hurd Peninsula können sechs verschiedene Intrusionsereignisse unterschieden werden und auf King George Island bis zu sieben.
Gänge, die das gleiche relative Alter haben, weisen auch die gleiche Streichrichtung auf. Dies wiederum belegt, dass leichte Veränderungen der allgemeinen tektonischen Parameter zur Bevorzugung einer anderen Richtung führte, aber immer im Rahmen desselben übergeordneten Spannungsfeldes. Diese Beobachtung lässt sich in allen bearbeiteten Gebieten verfolgen.

Bei der Deformation der Gänge handelt es sich ausschließlich um Klüfte. Im Gegensatz zu ihren Nebengesteinen sind die Gänge nicht gefaltet. Ihre Intrusionsrichtungen drücken sich auch in den Klüften innerhalb der Gänge aus. In Folge dessen kann angenommen werden, dass das Spannungsfeld, welches die Deformation hervorgerufen hat, im Zeitraum der Gangintrusionen weitgehend stabil geblieben ist. Obwohl in den Arbeitsgebieten auf Nelson und King George Island keine Faltenachsen nachgewiesen werden konnten, sind die a- und b-Achsen sowie die Scherrichtungen, welche aus dem Streichen der Gänge und den Klüften in den Gängen und ihrem Nebengestein ermittelt wurden, den Richtungen sehr ähnlich, die auf der Hurd Peninsula festgestellt wurden. Das wiederum lässt auf ein einheitliches Spannungsfeld im gesamten Bereich der South Shetland Islands schließen, das zumindest vom Maastricht bis zum Priabon unverändert angehalten hat, also dem Zeitraum, in welchem die Intrusion der Gänge stattgefunden hat.

Die chemische und isotopische Zusammensetzung der Gänge, welche sich während der ersten magmatischen Phase auf der Hurd Peninsula gebildet haben, weist eine starke krustale Komponente auf. Diese äußert sich in Form von niedrigen εNd-Werten (0-1) und der Korrelation der Nd-Isotopendaten mit dem Differentiationsgrad des Magmas. Ich gehe davon aus, dass eine während des Anfangsstadiums der Intrusionsaktivität verhältnismäßig ungedehnte kontinentale Kruste, sowie Krustenverweilzeiten der Schmelzen in flach gelegenen Magmenkammern dafür verantwortlich sind. Die krustale Komponente nimmt mit der Zeit auf der Hurd Peninsula (Livingston Island) ab und ist in Gebieten, die weiter NE gelegen sind (Nelson und King George Island) generell schwach oder gar nicht ausgeprägt.
Im Gegensatz dazu lassen geochemische Daten (z.B. die LSEE-Fraktionierung, Th/Nb- und Ce/Th-Verhältnisse) vermuten, dass ein sedimentärer Eintrag in die Subduktionszone in der frühen Phase gering war.
Die jüngeren Gänge auf Hurd Peninsula hingegen, wie auch alle Gänge aus den Gegenden, die weiter NE liegen (Nelson und King George Island), weisen eine stärkere sedimentäre Komponente auf. Offensichtlich nahm der Sedimenteintrag in die Subduktionszone mit der Zeit zu.
Die Anreicherung der Mantelquelle durch Fluide aus der subduzierten Platte war offensichtlich im Bereich der Hurd Peninsula (Livingston Island) und der Barton Peninsula (King George Island) am stärksten. Dies wird durch die beträchtlich erhöhten Ba/Th-Verhältnisse belegt. Die Abwesenheit dieser Signatur in anderen Gegenden lässt auf einen heterogenen Mantelkeil schließen, was sich auch in der HFSE-Systematik widerspiegelt. Das Verhalten der HFSE lässt vermuten, dass große Teile der Mantelquelle vor der selektiven Anreicherung durch Fluide und Sedimente von der subduzierenden ozeanischen Kruste generell aus verarmtem Material bestanden. Dieser verarmte Mantelkeil lässt sich am deutlichsten in den Gängen der Admiralty Bay (King George Island) nachweisen, aber er zeigt sich auch in der

Zusammensetzung der viel jüngeren Gänge von Penguin Island. Residualer Granat scheint in der Mantelquelle nicht vorhanden zu sein, was durch die SEE-Muster und die fehlende negative Y-Anomalie belegt wird.

Auf King George Island begann der Magmatismus, der im Zusammenhang mit dem vulkanischen Bogen steht, schon während der Kreide, was durch publizierte Alter belegt ist, die aus Gesteinen der stratiformen vulkanischen Sequenz gewonnen worden sind. Diese sind vermutlich auch von hypabyssalen Intrusionen begleitet worden.
Die auf Nelson und King George Island untersuchten Gänge intrudierten jedoch erst ab der Grenze Paleozän/Eozän. Die Intensität der Gangintrusionen erreichte während des Lutets zwischen 47 und 45 Ma in sämtlichen untersuchten Gebieten (außer Penguin Island) ihren Höhepunkt. Diese Hauptphase ist durch das Fehlen von krustaler Kontamination (auch auf der Hurd Peninsula) charakterisiert, sowie durch einen stärkeren Beitrag der sedimentären Komponente zur Magmenbildung.
Die Zusammensetzung der Magmenquelle blieb dann bis zum Ende der Gangintrusionen (Priabon) stabil. Das Auftreten dieser jüngsten Gänge ist abermals auf die Hurd Peninsula (Livingston Island) beschränkt.

Hohe Mg-Zahlen, εNd-Werte und Nb/Y-Verhältnisse charakterisieren die radialen Gänge auf Penguin Island als primitive, undifferenzierte und leicht alkalische Gesteine. Sie zeigen eine tholeiitische Affinität. Derjenige Gang, der auf Penguin Island datiert worden ist, ergab ein unerwartet hohes Alter (Torton). Die Entstehung von Penguin Island wurde bisher mit dem „Backarc-Spreading" in Verbindung gebracht, welches die Öffnung der Bransfield Strait zwischen der Antarktischen Halbinsel und den South Shetland Islands zur Folge hatte. Man nimmt an, dass dieses „Backarc-Spreading" während des Pliozäns (etwa vor 4 Ma) begann. Nachdem sich das Alter des Ganges von Penguin Island allerdings als wesentlich höher (Torton) herausgestellt hat, erhebt sich die Frage, ob das „Backarc-Spreading" in der Bransfield Strait möglicher Weise schon zu einem beträchtlich früheren Zeitpunkt eingesetzt hat als bisher angenommen.

Magmatic dyke systems of the South Shetland Islands volcanic arc (West Antarctica): reflections of the geodynamic history

Abstract

The Antarctic Peninsula magmatic arc developed as part of the Andean-West Antarctic continental margin from late Triassic to recent times. The South Shetland Islands are located at the northern tip of the Antarctic Peninsula. Subduction of proto-Pacific ocean floor beneath this archipelago and its development as a separate magmatic arc commenced during the Cretaceous. Large parts of the South Shetland Islands consist of rocks related to the activity of the magmatic arc, including numerous hypabyssal intrusions piercing the stratiform volcanic sequence.

Magmatic dyke swarms belong to this latter group and are ubiquitous throughout the South Shetland Islands. They occur especially numerous on Hurd Peninsula (Livingston Island). Dykes offer considerable potential to identify magmatic events and tectonic parameters, because they do not only reflect the geochemical and isotopic characteristics of their magma source, but furthermore the tectonic regime at the time of their emplacement. Their crosscutting relations are especially suitable to establish relative time sequences of the identified intrusive events.

A tight correlation between strike and chemistry of the dykes cutting the stratiform volcanic sequence on Potter Peninsula (King George Island, South Shetland Islands) was recognized during own former work. Proceeding from these observations and extending the investigation to large parts of the archipelago, a threefold approach combining structural, (isotope-) geochemical and geochronological data was applied in order to reconstruct the geodynamic development of the South Shetland Islands as reflected by dyke systems. Major goals were the identification of tectonic events as reflected by the orientation of the dykes as well as by joint systems, the determination of the magma sources including possible changes, and relationships between tectonic and magmatic events.

During austral summers 2000/2001 and 2001/2002, dyke systems covering areas of up to 100,000 m^2 have been mapped at several locations of the South Shetland Islands, particularly on King George and Livingston Island. Further dykes were studied on Nelson and Penguin Island. A structural analysis of the host rocks and the dykes was undertaken, including extensive measurements of joint systems within both. Special attention was given to the determination of crosscutting relationships reflecting the relative ages. About 250 dykes were sampled.

Laboratory work included microscopy of thin sections from all 250 samples, microprobe analyses (19 samples), ICP-MS geochemical analyses (130 samples), Sr (12 samples), Nd and Pb (30 samples) isotopic analyses.

To fix the obtained pattern into a time frame, Ar-Ar age determinations were carried out on plagioclase separates of 19 dykes, further 7 dykes were K-Ar dated (whole rock).

The average degree of alteration of the dykes is mostly low to moderate, but in certain areas rather high and correlates with the geographic position. Those areas belonging to the axial, upthrown horst structure of King George Island show the highest average degree of alteration. A similar, upthrown situation is possible for Hurd Peninsula (Livingston Island).

The dykes from the South Shetland Islands comprise a subalkaline series of predominantly calc-alkaline affinity. Tholeiites occur also, apparently connected to the initial stages of intrusive activity in the respective areas. This is true for Hurd Peninsula (Livingston Island), Weaver and Barton Peninsula and Admiralty Bay (all King George Island).

The geochronological data suggest that the time interval, during which dyke intrusion occurred in the investigated areas, was restricted to the Paleocene and Eocene. This does not exclude possible earlier intrusive activity in other parts of the archipelago or beneath the actual outcrop level.

The supposedly oldest dykes crop out on Hurd Peninsula and did not yield formal Ar-Ar plateaus, but best estimates as deduced from the measured data indicate an intrusion age around the Cretaceous/Paleogene boundary, probably Danian. Thus, dyke intrusion obviously started earlier (Danian) and lasted longer (Priabonian) on Hurd Peninsula (Livingston Island) as compared to Nelson and King George Island (Thanetian - Lutetian). A maximum age for incipient dyke intrusion on Hurd Peninsula is set by Campanian nannofossil ages published for the metasedimentary host rocks.

These data also restrict the time interval during which the main deformation of the host rocks on Hurd Peninsula (Livingston Island) occurred, including folding and the creation of primary and secondary shear systems. It was limited to a time gap of approx. 5-10 Ma between Latest Campanian and Earliest Danian. Given the geotectonic position of these rocks forming part of an accretionary wedge, such a relatively short deformation time seems to be possible. Folding is evident in the metasedimentary host rocks around an axis striking 24°.

From Danian on, dykes intruded the different directions (first and second order dextral and sinistral shear systems) correlated with the folding axis. Six different intrusive events can be distinguished on Hurd Peninsula and up to seven on King George Island. Dykes of the same relative age also share the same strike direction, indicating that slight changes of the overall tectonic parameters led to different preferred directions, but within the same general stress field. This observation was made throughout all investigated areas.

The deformation of the dykes is restricted to jointing, but in contrast to their host rocks they are not folded. The directions used by the dykes are also expressed as joints within the dykes, indicating that the stress field that caused the deformation of the host rocks remained stable during the time of dyke intrusion. No folding axis could be determined for the areas investigated on Nelson and King George Island, but the a- and b-axes and the shear directions as deduced from the strike of the dykes and from jointing within the dykes and their host rocks are very similar to the directions observed on Hurd Peninsula. This suggests a uniform stress field throughout the South Shetland Islands at least from Maastrichtian to Priabonian, the time when dyke intrusion ceased.

The chemical and isotopic composition of the dykes generated during a first magmatic phase on Hurd Peninsula indicates a strong crustal component. This is reflected by low εNd values (0-1) and a correlation of Nd isotopic data with the degree of differentiation. A relatively unstretched continental crust during the initial stages of intrusive activity in that area and storage of the melts in shallow level magma chambers prior to intrusion is assumed to be responsible. This component decreases with time on Hurd Peninsula (Livingston Island) and is generally weak or nonexistent in the areas further to the NE (Nelson and King George Island).

In contrast, geochemical data (e.g. LREE fractionation, Th/Nb and Ce/Th systematics) indicate that sediment influx to the magma source was apparently low during this early phase. Later dykes from Hurd Peninsula as well as all dykes from the areas further to the NE (Nelson and King George Island) reflect a stronger sedimentary component.

Enrichment of the mantle source by fluids derived from the subducted slab was apparently strongest on Hurd Peninsula (Livingston Island) and on Barton Peninsula (King George Island), as reflected by the considerably elevated Ba/Th ratios. The absence of such a signature in the other areas indicates heterogeneities in the mantle wedge, which are also confirmed by other HFSE systematics. HFSE behavior suggests that large parts of this mantle source were generally of depleted nature prior to selective enrichment by fluids and sediment addition from the subducting slab.

This depleted mantle wedge is reflected especially by the dykes from Admiralty Bay (King George Island), but also by the composition of the dykes from the much younger Penguin Island. The mantle source is further characterized by the absence of residual

garnet, as indicated by the REE patterns and the missing negative Y anomaly.

On King George Island, magmatism related to the volcanic arc started already during Cretaceous times, as proved by published ages obtained for rocks from the stratiform volcanic sequence, possibly accompanied also by hypabyssal intrusions.

However, the dykes cropping out in the areas investigated on Nelson and King George Island indicate an onset of dyke intrusion around the Paleocene/Eocene boundary, culminating during the Lutetian at 47-45 Ma. This main phase is characterized by the absence of crustal contamination (also on Hurd Peninsula), and by stronger contribution of subducted sediments to arc magma genesis.

The characteristics of the magma source then remained stable, until dyke intrusion terminated during the Priabonian, those latest dykes once again being restricted to Hurd Peninsula (Livingston Island).

High Mg-numbers, εNd values and Nb/Y ratios characterize the radial dykes from Penguin Island as primitive, undifferentiated and moderately alkaline rocks. They are of tholeiitic affinity. The one dyke dated from Penguin Island yielded an unexpectedly high age (Tortonian). Penguin Island represents a volcano considered as being related to the backarc-spreading that opened the Bransfield Strait between the Antarctic Peninsula and the South Shetland Islands. This backarc-spreading is widely believed to have started during the Pliocene (approx. 4 Ma ago). The Tortonian age obtained for the dyke on Penguin Island therefore rises the question whether backarc-spreading in Bransfield Strait might have commenced considerably earlier than believed so far.

Contents

Preface

The idea for this project was born based on observations made during own former work on the South Shetland Islands.

The work was funded by the German Science Foundation (DFG-Project Mi 120/41-1) and financially further supported by a two-year scholarship according to the Bavarian law for support of young graduated scientists and artists (Graduiertenförderungsprogramm des Bayrischen Staates).

Logistical support including transport to the Antarctic Peninsula as well as accomodation in the German/Argentine Dallmann Laboratory (King George Island) was kindly provided by the Alfred-Wegener-Institute (AWI, Bremerhaven), as well as equipment necessary for field work in polar regions.

The realization, however, would have been impossible without the help, continuous support, critical comments and fruitful discussions led with my supervisor Prof. Dr. Dr. h.c. Hubert Miller. Herewith I want to thank him cordially for everything he did for me, including the considerable enhancement of my knowledge concerning structural geology. I will always remember with much pleasure the time we spent together at the Bulgarian Antarctic Base "St. Kliment Ohridski" on Livingston Island.

Further valuable comrades during field work were Dr. Rodolfo del Valle (Instituto Antártico Argentino, Buenos Aires), Prof. Dr. Christo Pimpirev and Prof. Dr. Dimo Dimov (both Bulgarian Antarctic Institute, Sofia). All the three of them deserve my heartily gratitude for their friendship, their support, for sharing their knowledge concerning the regional geology and last but not least for numerous pleasant evenings spent in a wind-lashed tent preparing "asado" or in the base singing Bulgarian folk songs.

Prof. Dr. Krzysztof Birkenmajer (Inst. of Geological Sciences, Polish Academy of Sciences, Kraków) shared a great deal in enhancing my knowledge concerning the regional geology of King George Island. I will not forget his cordial welcome at the Polish Antarctic Base "H. Arctowski" after having crossed the Warszawa Icefield during an eight hours lasting trip by ski.

Prof. Dr. Michael McWilliams (Stanford University, California) introduced me to Ar-Ar geochronology. I thank him herewith for the effort he put into the dating of my samples, for many fruitful discussions and especially for his hospitality during my stay at Stanford.

Dr. Zoltan Pecskay (Institute of Nuclear Research of the Hungarian Academy of Sciences in Debrecen) deserves much gratitude for dating some of my samples at no cost.

From the numerous people who supported me during my work at the Department of Earth and Environmental Sciences in Munich (Germany), I want to thank first of all my colleague Dr. Alexander Rocholl for countless fruitful discussions concerning geochemical topics, as well as for valuable help during measurements carried out at the mass spectrometer, and last but not least for critical and helpful comments on the geochemical part of this thesis.

Prof. Dr. Ernst Hegner and Dr. Frank Söllner deserve my gratefulness for introducing me to analytical methods concerning Sr, Nd and Pb isotopy and to mass spectrometry, as well as for helpful discussions regarding these topics.

My fellows Bettina Scheu, Ulrich Küppers, Dr. Ana Rieger, Dr. Andreas Veit and Dr. Martin Höckenreiner contributed a lot to numerous pleasant hours and helped a great deal to smooth the less pleasant ones.

Outside geoscience business, my family deserves my most heartily gratefulness for unlimited support throughout the years of this work. I want to thank especially my brother Florian for reading through the whole manuscript and applying linguistic corrections.

I want to thank especially and most cordially my girlfriend Wiebke Höfling for all her patience, unlimited support and understanding especially during the last year of this work. I know it was not always easy...

1. Introduction

1.1 Geography and history

The South Shetland Islands (Fig. 1-1) form an approx. 500 km long island chain located about 1000 km SE of Ushuaia (Tierra del Fuego, Patagonia) across Drake Passage and approx. 120 km NW of the Antarctic Peninsula across Bransfield Strait. They lie at 61-63° S and 54-63° W, thus located still N of the south polar circle.

Traditionally, they are regarded as the SW end of the Scotia Ridge, an U-shaped structure of archipelagos and drowned continental blocks linking the South Pacific with the South Atlantic and southern South America with the Antarctic Peninsula, respectively.

The South Shetland Islands comprise about a dozen medium to large sized islands, the biggest being King George Island (80x25 km) and Livingston Island (70x30 km), moreover hundreds of minor islands and shoals lying offshore.

The history of the archipelago is tightly connected to the activities of the whalers and seal hunters at the

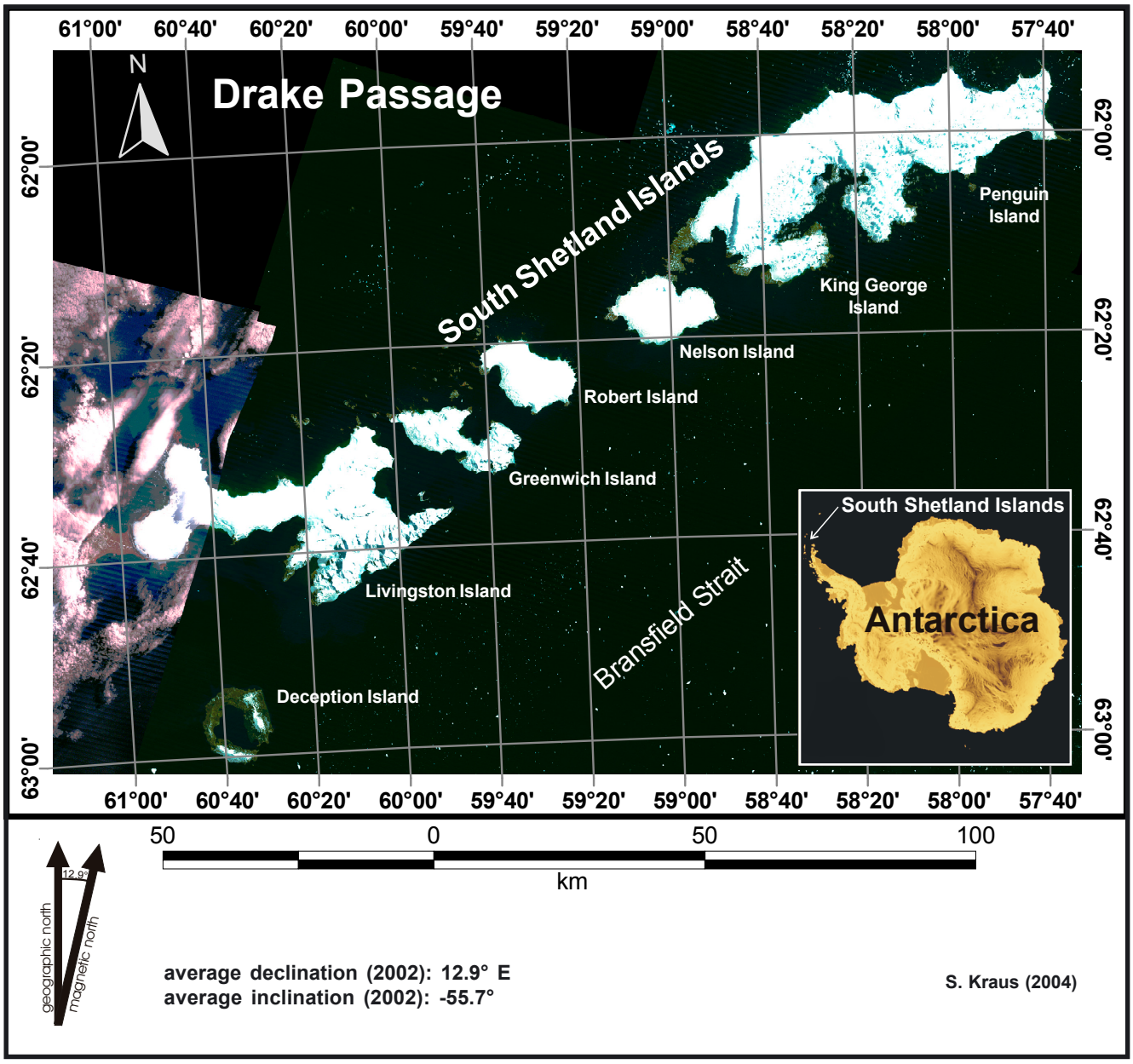

Fig. 1-1: Map of the South Shetland Islands (created and processed by S. Kraus, 2004). Satellite image courtesy of J. Sievers (Bundesamt für Kartographie und Geodäsie (BKG, formerly IFAG); Frankfurt am Main, Germany). Please refer also to Bennat et al. [1998]. The image is a subset taken from the "Geoscientific Information System Antarctica (GIA)": LandSAT TM mosaic Antarctic Peninsula (pixel resolution 30 m).

beginning of the 19th century. Most of the place names in the South Shetland Islands were introduced by them.
Whereas nearly all of the other islands south of the Atlantic convergence had already been discovered (and the economically interesting animals nearly been eradicated) at that time, the South Shetland Islands still remained untouched. In February 1819, the 82 ft. long English brigg 'Williams' sailed through Drake Passage heading south. The 28 year old captain William Smith was a whaler who had worked in the North Atlantic before. The 'Williams' was on its way from Buenos Aires around Cape Hoorn to Valparaiso and took, due to bad weather, a more southerly route than normal [GURNEY 1997].

On February 19th, 1819, shortly after daybreak, land was sighted, but Smith decided not to approach further due to another fierce storm. He came back the next day and, at 62°17' S / 60°12' W, sighted a promontory about 12 miles SW. The place is today known as 'Williams Point' and defines the NE tip of Livingston Island. He decided not to go onshore and instead sailed to Valparaiso, where he arrived on March 11th. He returned to the South Shetland Islands in October 1819 and went onshore at a place today called 'Venus Bay', where he took possession of the land in the name of King George III. After his return to Valparaiso, Smith gave a detailed report to the Royal Navy. Especially John Miers, a British engineer, was deeply impressed. He played a major role during the further discovery of the South Shetland Islands. The sedimentary 'Miers Bluff Formation' on Hurd Peninsula, Livingston Island, was named after him later. The Royal Navy decided to charter the 'Williams', Smith and his crew to undertake further investigations on the newly discovered land. In December 1819, under the command of E. Bransfield (the namer of the strait between the Antarctic Peninsula and the South Shetland Islands), the 'Williams' sailed towards south once more. Between January 16th and March 19th, 1820, Bransfield discovered and named not only most of the South Shetland Islands but also some parts of the coast of the Antarctic Peninsula [GURNEY 1997]. During the following decades, the South Shetland Islands experienced above all frequent visits of whalers and seal hunters, until these animals had almost disappeared.

For the rest of the 19th and the early 20th century, the South Shetland Islands served only as in-between bases for many of the great expeditions on their way further south or towards east into Weddell Sea.

From World War II on, as a consequence of the rivaling political claims of Argentina, Britain and Chile on the Antarctic Peninsula, numerous scientific bases have been set up on the South Shetland Islands and elsewhere on the Antarctic Peninsula. This generally led to increased scientific activity and also to a virtually continuous geological research program until the present day. Further nations which started scientific research on the Antarctic Peninsula and adjacent islands, putting up summer-only as well as all-year-bases, include all South American nations (except Bolivia, Colombia, Paraguay and Venezuela), furthermore China, Bulgaria, Germany, Poland, South Korea, Spain, Russia, Ukraine and the USA.

Today, especially the South Shetland Islands are also target of a yearly growing number of tourist vessels. On Fildes Peninsula (King George Island) even a hotel has been built, along with a post office and other facilities.

1.2 Geomorphology

Featuring a contrasting physiologic, geologic and glaciogenic terrain, the Antarctic Peninsula resembles much the southern cordillera of the Andes. It consists of a narrow (less than 250 km wide), elevated arcuate landmass (more than 1500 m high over much of its length) that stretches from the main continent approx. 1800 km to the north (Fig. 1-1, inset) towards South America and is the only part of Antarctica which extends into sub polar climates, subjecting its icecap to contrasting oceanographic and meteorological conditions with a strong east-west gradient.
Fragmentation and brittle response of the crust to a compressive and later extensional regime led to the opening of the Drake Passage during the Oligocene, associated with reorganization of spreading centers and complex plate tectonic movements in the Scotia Sea region [TARNEY et al. 1982]. This event was also responsible for the uplift and dissection of the Antarctic Peninsula (Paleogene to Neogene), which led to deep erosion and exposure of igneous plutons and related metamorphic/volcanic rocks of the Mesozoic arc. These units represent the backbone of the Antarctic Peninsula, now covered by a permanent icecap. The uplift probably had a major impact on the accumulation pattern of ice masses across the peninsula as well as on erosional and depositional patterns on the continental shelf [ELLIOT 1997]. In comparison, the younger South Shetland Islands volca-

nic arc is much less eroded and less significantly uplifted.
The increase of the average temperature due to climate changes resulted in a significant glacier retreat, which can be observed all over the Antarctic Peninsula since several decades. As a consequence, today many outcrops are accessible which have been buried underneath the icecaps until recently.

1.3 Previous geological investigations

As one of the first humans visiting the South Shetland Islands, the above mentioned John Miers was also the first one to draw geological deductions about the islands [Miers 1820]. The first proper determination of rocks from the South Shetland Islands, however, was undertaken by Anon [1821] and Traill [1822], who recognized correctly the volcanic character of the samples which had been brought back to England.
During the next decades, the interest of human activities was focused mainly on whaling and seal hunting. The only remarkable scientific discovery was the observation of Eights [1833], who found fossil wood incorporated in the volcanic rocks of an unspecified island. This was the first finding of fossils in the Antarctic, but unfortunately remained unnoticed for a long time because it was published in a paper on a new species of modern crustacean, thus being overlooked by geoscientists.
Among all the great and important expeditions during the rest of the 19th and early 20th century, which passed by the South Shetland Islands, only few carried out more than rudimentary geological work on this island group. In this context, Nordenskjöld's 1901-04 Swedish expedition should be mentioned. Besides his important geological work at Hope Bay and on James Ross Island, he also visited Nelson, Snow and Livingston Island. Regrettably, all samples collected by this expedition were lost, when their ship sank in the Weddell Sea later on.

It was not before 1921, that major geological information became available, when a prospector named Ferguson published the results of his geological observations he had made during the whaling season 1913-14. He had worked both in the Gerlache Strait and on the South Shetland Islands, focussing on King George Island in the latter area. Here, he distinguished a sequence of stratified sediments (?Middle Jurassic) with intercalated basaltic and andesitic lavas (Cenozoic), furthermore dioritic intrusions with attendant extensive quartz-pyrite mineralizations [Ferguson 1921]. Ferguson's emphasis on the sedimentary rocks in the Mesozoic sequence stood in contrast to another important, contemporary work which described the sediments as of minor importance and focussed more on the volcanic rocks [Tyrell 1921]. According to him, the volcanics comprised mainly andesitic and, more seldom, acidic types. Maybe the most important result of Tyrell's work was that he recognized Bridgeman, Penguin and also Deception Island as belonging to a younger volcanic phase, based on the field work carried out by N.A. Mackintosh and J.W.S. Marr during the 'Discovery II' expeditions in the years 1934 and 1937. He set up a stratigraphy divided into three phases: I. Andesitic to rhyolitic lavas and pyroclastic rocks with local sedimentary intercalations (Jurassic), II. Thick andesitic and pyroclastic sequence with dioritic intrusions (Cenozoic), III. Olivine basalts and andesitic rocks [Tyrell 1921, 1945].
Due to logistic difficulties, many of the geoscience-related papers published since then are restricted to investigations at relatively small, isolated outcrops, i.e. peninsulas comprising only a few square-km, which become ice- and snow-free during austral summer [e.g. Fourcade 1960]. During the sixties, mainly the British undertook overland and sea-ice travels, which led to the first comprehensive studies, above all of the major islands King George and Livingston [Barton 1965; Hawkes 1961; Hobbs 1968]. Hawkes [1961] and Barton [1965] were also the first who established a detailed stratigraphic standard for King George Island, comprising five and eight lithostratigraphic units, respectively.
It was also during that time, that more and more fossil remains were found, thus fixing the relative ages into a time frame (e.g. G. Hattersley-Smith in 1948, J.S. Bibby in 1957-58 and G.J. Hobbs in 1958-59). Mainly Chilean geologists showed that Mesozoic rocks are cropping out at numerous places in the western parts of the South Shetland Islands. A Middle Jurassic to Lower Cretaceous flora was identified in volcanic and tephra sequences on Snow and Livingston Island [e.g. Hernández & Azcárate 1971], moreover the same sequences contain Upper Jurassic to Lower Cretaceous marine molluscan faunas [e.g. González-Ferrán et al. 1970]. On King George Island, six Cenozoic plant fossil sites have been reported [e.g. Fourcade 1960], among them a Lower to Middle Miocene flora from Fildes Peninsula [Orlando 1963, 1964], which was correlated

with the Point Hennequin Group flora of Admiralty Bay.

Landbased and marine geophysical investigations have been undertaken as early as the sixties [Griffiths et al. 1964] and revealed that the archipelago seems to rest on a fragment of continental crust which has been separated from the Antarctic Peninsula during the opening of the Bransfield Strait as a backarc-basin-like extensional structure [e.g. Ashcroft 1972; Birkenmajer et al. 1990; Davey 1972].

In the meanwhile, also a lot of isotopic age determinations have become available, both on the arc-related volcanic rocks and their sedimentary intercalations [e.g. Birkenmajer 1997a and references therein; Jwa et al. 1992; Smellie et al. 1984] as on the metamorphic rocks of the Elephant Island Group [e.g. Trouw et al. 1990]. However, the reliability in many cases is difficult to estimate, as most age determinations are based on K-Ar or Rb-Sr isotopy, systems which react especially sensible to (hydrothermal) alteration processes. A more detailed summary of previous works is given by Birkenmajer [2003] and Smellie et al. [1984].

1.4 Geodynamic background

1.4.1 Relation to Gondwana

The Antarctic Peninsula has been part of the former Pacific margin of Gondwana at least since Carboniferous times [Tarney et al. 1982]. The western margin of Gondwana stretched from South America along the Antarctic Peninsula and Marie Byrd Land to New Zealand and existed until the Lower Cretaceous [Davey 1990; Elliot 1997; Thomson et al. 1983].

The original position of the Antarctic Peninsula with respect to South America has long been subject to acrimonious discussions. Several reconstructions have been proposed, and many former authors saw the Peninsula's position *east* of southern Argentina [e.g. Craddock 1975; Norton & Sclater 1979; Smith & Hallam 1970]. In the meanwhile, sufficient evidence is known for the pre-existence of continental crust in both areas - the Falkland Plateau and the Antarctic Peninsula - to make the overlap required by these reconstructions unacceptable [Barker et al. 1991]. Since the late seventies, this error has been corrected and geological evidence now suggests that the Antarctic Peninsula originally might have been located *west* of the southern tip of South America [Harrison et al. 1979; Miller 1981; Miller 1983; Suárez 1976]. However, most reconstructions require relative motion between the Antarctic Peninsula and East Antarctica, most probably during early phases of Gondwana breakup, prior to the initial opening of the South Atlantic at 137 Ma [Barker et al. 1991].

1.4.2 Plate tectonic history

Separate evolution of the Antarctic Peninsula commenced with Gondwana breakup during Early to Mid Jurassic times, reflected clearly by the magmatic history of the area. During the Late Jurassic, the Antarctic Peninsula formed probably a band of continental crust up to 400 km wide with a magmatic arc resting on it, breaking off the Pacific margin of Gondwana and thus initiating the opening of the Weddell Sea [Barker et al. 1991]. This event separated the Peninsula from East Antarctica, leaving it framed by oceanic crust on either side. Timing of the initial opening of the Weddell Sea, however, still remained speculative, as well as its relation to Patagonia. New data on the development of the ocean floor of the Weddell Sea [Ghidella et al. 2002; Jokat et al. 2003] show that its history can only be explained by a pre-Jurassic position of the Antarctic Peninsula block west of Patagonia. According to seismic data published by Guterch et al. [1991], the crustal thickness of the northern Antarctic Peninsula is 38-43 km, indicating a normal continental crustal thickness. Today, the approx. 900 km wide Drake Passage separates Patagonia and the Antarctic Peninsula by Cenozoic oceanic crust .

During Jurassic and Early Cretaceous times, the Pacific, Farallon and Phoenix plates probably formed a simple three-plate-system [Larson & Chase 1972]. Approx. 105 Ma ago, a segment of the very fast spreading Pacific-Phoenix-ridge collided with the subduction trench at the part of the Antarctic margin later forming New Zealand, resulting in the separation of New Zealand from West Antarctica along the new Pacific-Antarctic-ridge approx. 85 Ma ago [Bradshaw 1989]. Subsequently, this ridge propagated towards NE, resulting in a step-by-step replacement of the Pacific-Phoenix-ridge by paired segments of the Pacific-Antarctic- and the Antarctic-Phoenix-ridge [Cande et al. 1982]. As a consequence, large parts of the oceanic crust produced by the Pacific-Phoenix-ridge have been added to the Antarctic plate approx. 47 Ma (Eocene) ago (Fig. 1-2).

The remainder of the Phoenix plate, which is still existing today, is also called Aluk plate [Herron &

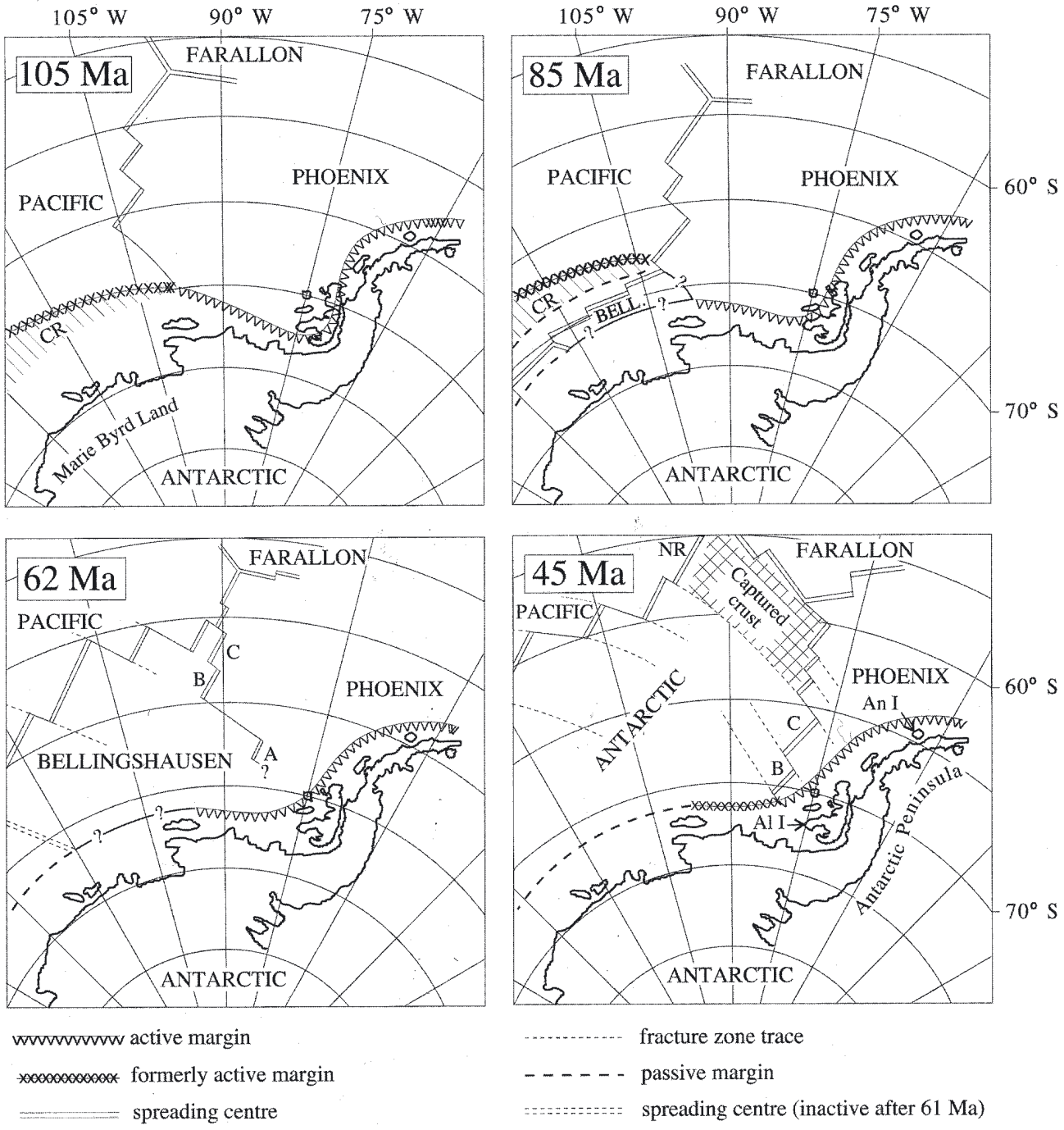

Fig. 1-2: Reconstructions of the South Pacific with respect to the Antarctic plate, assuming that since 105 Ma no relative motion occurred between the blocks forming West Antarctica, based on data of CANDE et al. [1982; 1995] and MAYES et al. [1990]. The 62 Ma reconstruction corresponds approximately to the time when the Bellingshausen plate probably was attached to the Antarctic plate [CANDE et al. 1995]. Al I: Alexander Island, An I: Anvers Island, BELL: Bellingshausen plate, A, B and C: ridge segments of the Antarctic-Phoenix ridge, CR: Chatham Rise, NR: new ridge segment produced by propagation of the Pacific-Antarctic ridge approx. 47 Ma ago. Fig. taken from MCCARRON & LARTER [1998], p. 256.

TUCHOLKE 1976] or Drake plate [BARKER 1982; BARKER et al. 1991]. It is represented by the microplate bordered by the spreading center in the western Drake Passage (the rest of the Antarctic-Phoenix-ridge), the Shackleton Fracture Zone in the N and the trench NW of the South Shetland Islands (Fig. 1-4). Since the formation of oceanic crust at the spreading centers bordering the Phoenix plate has been uninterrupted since the Mesozoic, the name 'Phoenix' will be used throughout this work. Based on paleomagnetic data published by DIVENERE et al. [1994] and LUYENDYK et al. [1996] it can be assumed, that most parts of West Antarctica, including the Antarctic Peninsula, formed a coherent, rigid plate since the middle Cretaceous [MCCARRON & LARTER 1998]. However, inconsistences between paleomagnetic poles of East Antarctica and Marie Byrd Land are interpreted as evidence for Late Cretaceous, clock-

wise rotations of - or between - Westantarctic microplates [LUYENDYK et al. 1996].

During the Cenozoic, large parts of the Antarctic-Phoenix-ridge collided with the subduction trench along the Antarctic Peninsula [BARKER et al. 1991; HERRON & TUCHOLKE 1976; LARTER & BARKER 1991]. The orientation of the fracture zones was the reason why the ridge segments collided with the subduction trench successively from SW (southern Alexander Island, middle Eocene) to NE (north of Anvers Island, Pliocene, Fig. 1-2) [LARTER & BARKER 1991; LARTER et al. 1997]. It was an unusual tectonic situation, with the oceanic crust west of the colliding ocean-crest segments and the overriding lithosphere on the east side of the trench both belonging to the Antarctic plate.

This made further subduction impossible, because even prior to collision no relative motion occurred between the two parts of the Antarctic plate. Instead, it was the activity of the spreading center, that pushed itself towards the trench. Thus, the collision of the ridge segments with the trench resulted in complete deactivation of both the spreading center and the subduction zone, elimination of the trench basement topography, and the margin became passive [LARTER & BARKER 1991]. Today, the trench NW of the South Shetland Islands is the only remaining part of the subduction zone which bordered the entire western margin of the Antarctic Peninsula before. The above mentioned small oceanic plate is the last remaining part of the Phoenix plate which has been largely subducted beneath the Antarctic Peninsula (Fig. 1-4).

MCCARRON & LARTER [1998] determined Late Cretaceous to Cenozoic plate movements for West Antarctica (Fig. 1-3). They calculated high convergence rates (110-121 mm/a increasing from N to S) of the Phoenix plate towards the Antarctic Peninsula for the Late Cretaceous (83.0 - 67.7 Ma). A calculated subduction direction of 93° at 60°S/60°W indicates a fairly oblique subduction in the area of the northern Antarctic Peninsula during that time. Such an oblique subduction is likely to cause a deformation pattern governed by contraction- and strike-slip-components in the overriding plate [TIKOFF & TEYSSIER 1994], possibly resulting in forearc-fragments splintering away [PLATT 1993]. Strike-slip faults are common in modern subduction zones at approx. 100-300 km distance from the trench within or near the volcanic arc, if the convergence angle exceeds 12° [JARRARD 1986]. Trench-parallel faults are the expected consequence. The NE-SW striking, dextral

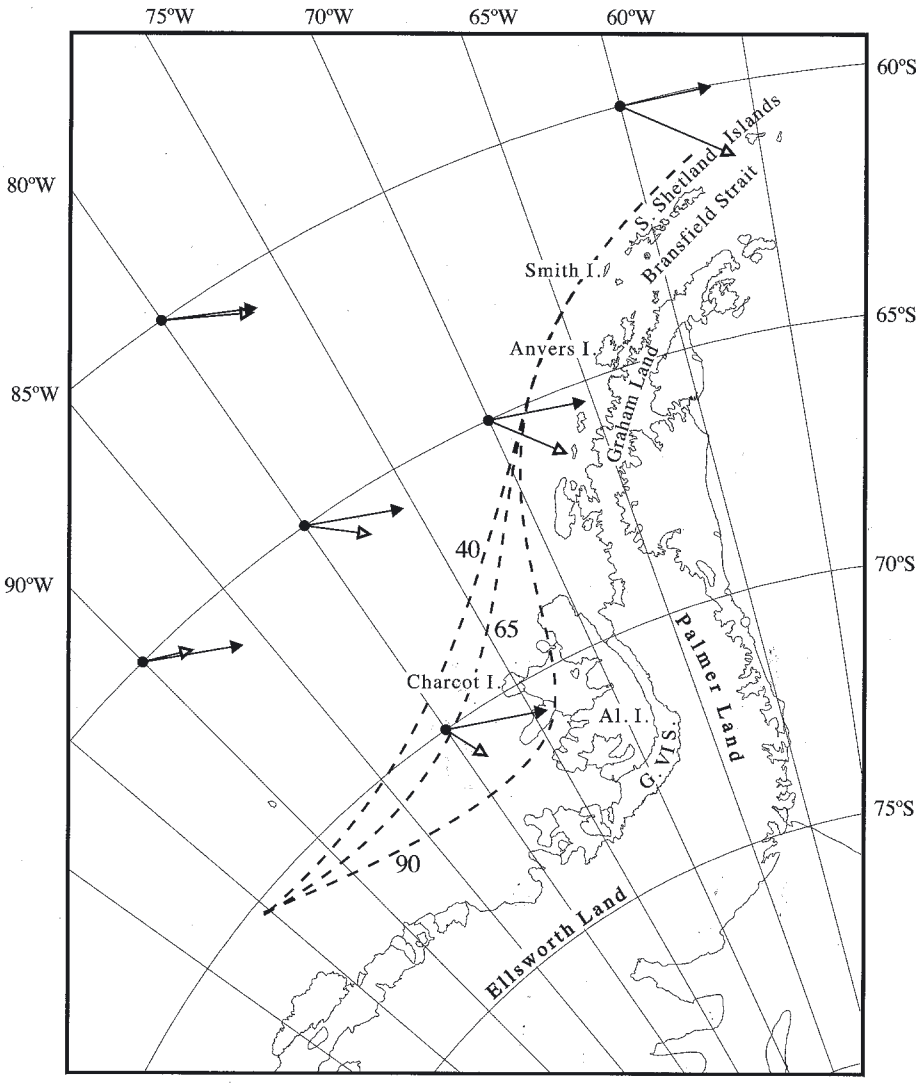

Fig. 1-3: Movement directions of the Phoenix plate relative to the Antarctic Peninsula, as deduced from calculations of plate rotations. Closed arrows indicate Late Cretaceous (83.0 - 67.7 Ma), open arrows Early Cenozoic (61.1 - 53.4 Ma) directions. The arrows' length is proportional to subduction velocity. Dashed lines indicate the position of the trench, adjacent numbers the corresponding age in Ma. AL I: Alexander Island; G VI S: George VI Sound. Fig. taken from McCARRON & LARTER [1998], p. 262.

and trench-parallel strike-slip faults, evident everywhere in the South Shetland Islands, may have this origin.

In the Early Cenozoic (61.1 - 53.4 Ma), the Phoenix - Marie Byrd Land rotational pole apparently shifted towards a position on the edge of Marie Byrd Land, resulting in a radical change of subduction parameters for the Antarctic Peninsula. Whereas in the Late Cretaceous convergence rates have been higher in the SW than in the NE, the shifting of the rotational pole resulted in reverse conditions in Early Cenozoic times. Convergence rates increased considerably to 145 mm/a in the NE (60°S/60°W) and slowed down to 56 mm/a in the SW (70°S/80°W).

The change in subduction direction of more than 30° clockwise (Fig. 1-3) was maybe even more important. As compared to the very oblique subduction during the Late Cretaceous, convergence was now nearly orthogonal at the northern tip of the Antarctic Peninsula [McCarron & Larter 1998]. Orientation of faults further to the NE indicates, that the subduction direction remained stable for the rest of the Cenozoic [Larter & Barker 1991].

Magnetic anomalies along a large magnetic profile NW of Alexander Island reveal an abrupt decrease of the spreading rate at the Antarctic-Phoenix-ridge 52.3 Ma ago. Assuming symmetric spreading, the rate decreased from 102 mm/a to 42 mm/a [McCarron & Larter 1998]. Such a dramatic change of the spreading rate and consequently also of subduction velocity probably caused a rollback of the underriding plate and subsequently an increase of extensional forces in the arc and forearc. The rise of the metamorphic rocks (blueschist facies) cropping out on Smith Island (South Shetland Islands) could be related to this process and probably happened long before any of the ridge segments of the Antarctic-Phoenix-ridge reached the nearby trench in the Pliocene [Grunow et al. 1992; Larter & Barker 1991]. However, reliable estimates on convergence rates and direction of subduction beneath the Antarctic Peninsula exist only for Late Cretaceous to recent times [Barker 1982; Larter & Barker 1991; McCarron & Larter 1998].

1.4.3 Plate tectonic parameters of the South Shetland Islands

According to seismic data published by Guterch et al. [1991], the crustal thickness of the northern Antarctic Peninsula is 38-43 km, but of the South Shetland block only about 30 km.

From Cretaceous times on, the location of the volcanic arc shifted towards NW, probably due to decreasing subduction velocity culminating at the 52.3 Ma event mentioned above. Interestingly, this event corresponds well with the onset of ridge crest-trench collisions of the Antarctic-Phoenix ridge with the trench off the Antarctic Peninsula.

Thus, the part of the volcanic arc settled upon the South Shetland Islands belongs to a much younger phase in geodynamic history. The spreading centre in the western Drake Passage (Fig. 1-4) became virtually inactive about 4 Ma ago [Barker 1976, 1982; Barker et al. 1991; Larter & Barker 1991] and the South Shetland trench was partly filled with sediments. Today, this last part of the formerly much larger subduction zone is the only area around the entire Antarctic continent where subduction probably still takes place, even though at very low velocities [Barker 1982]. Assuming that subduction is still continuing, the rate should resemble that of the opening of Bransfield Strait, which is estimated at approx. 10 mm/a [Dietrich et al. 2000]. Recent seismic data suggest active convergence along the South Shetland subduction zone, with earthquake locations indicating association of seismicity with slow subduction of young lithosphere, rifting, active volcanism and transcurrent plate boundaries [Robertson et al. 2002]. Based on the displacement of the South Shetland Islands to the NW, the amount of stretching and the width of new oceanic crust formed during rifting and spreading in the Bransfield Strait area, Henriet et al. [1992] estimate convergence rates of 2.5 to 7.5 mm/a for the last 2 Ma.

The oldest parts of oceanic crust of the Phoenix plate adjacent to the South Shetland trench lie in the NE close to the Shackleton Fracture Zone and are approx. 23 Ma old [Larter & Barker 1991]. The subducting lithosphere at 100 km depth is approx. 17 Ma old beneath Livingston Island, approx. 24 Ma beneath King George Island and approx. 30 Ma further to the NE [Barker 1982]. These age differences are due to the segmentation of the South Shetland archipelago along the NW-SE trending fracture zones separating also the three remaining, inactive parts of the Antarctic-Phoenix spreading ridge. Given that the southwesternmost segment of the ridge lies closest to the trench, it is also clear that the subducting oceanic lithosphere belonging to this segment provides the youngest oceanic crust at 100 km depth. The South Shetland subduction zone prob-

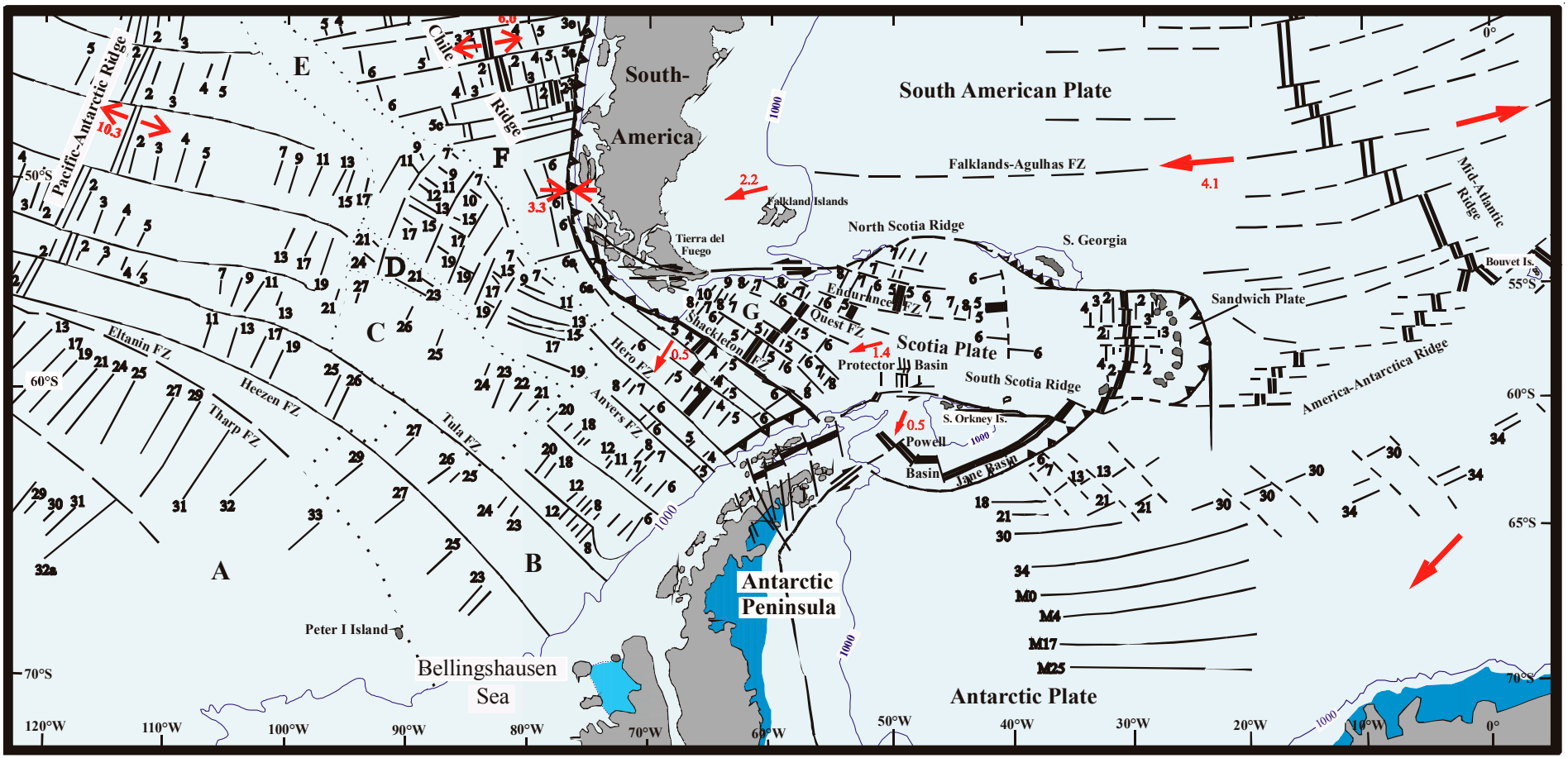

Sea floor divided into regions based on the spreading ridge at which oceanic crust was generated (from CANDE et al., 1982):

A = Pacific-Antarctic/Bellingshausen
B = Aluk-Antarctic/Bellingshausen
C = Pacific-Phoenix
D = Pacific-Farallon
E = Antarctic-Farallon
F = Antarctic-Nazca
G = Spreading on a now extinct ridge east of the Shackleton Fracture Zone

Compiled map of the Scotia Sea tectonics and seafloor magnetic anomalies:

The Antarctic Peninsula and southern oceans. Seafloor magnetic data and structural features from: ACOSTA & UCHUPI (1996), BARKER (1982), CANDE et al. (1982), DEL VALLE & RINALDI (1992), ELLIOT (1988), GALINDO-ZALDIVAR et al. (1996), GONZALEZ-FERRAN (1985), KLEPEIS et al. (1996), LABRECQUE et al. (1986), LIVERMORE et al. (1994), PELAYO & WIENS (1989), SLOAN et al. (1995).

Symbols used in the map:

- 5 /// Anomaly Number
- FZ Fracture Zone
- Spreading Ridge
- Subduction Zone
- Former plate boundary
- Edge of shelf ice
- 1000 m isobath

0 — 1000 km

Fig. 1-4: Tectonic map of the Southern Oceans. Slightly modified after VEIT [2002].

ably represents an extreme end-member of young and slow subduction zones on Earth.

The reason, why the Drake Passage spreading centre became inactive, is still subject of discussion. Maybe the rest of the Phoenix plate is now exposed to an E-W oriented compression due to reasons lying further to the east in the Scotia Sea [Barker et al. 1991; Forsyth 1975] and this was sufficient to deactivate the spreading centre. Ceasing subduction rates could have caused a slab-rollback of the subducting Phoenix plate and the opening of a slab window [Barker & Austin 1998], a subsequent oceanward migration of the trench and therefore extensional forces in the backarc area of the South Shetland Islands, probably leading to the opening of the Bransfield Strait [Barker & Dalziel 1983; Barker et al. 1991; Maldonado et al. 1994]. The geophysical data suggest that the archipelago rests upon a narrow fragment of continental crust split off the Antarctic Peninsula during that opening. According to Barker et al. [1991], opening started about 4 Ma ago, Birkenmajer [1992a] quotes evidence for incipient rifting to have started at the end of Oligocene, 26 to 22 Ma ago. The uniqueness of the Bransfield Rift is underlined by the fact that it may represent a transition between a rifting and a spreading regime [Barker & Austin 1994].

The South Shetland Islands' early geological history is quite similar to that of the rest of the Antarctic Peninsula's western margin. However, the archipelago exhibits the most complete record of subduction related volcanic rocks in the entire Antarctic Peninsula. Former studies reveal an episodic activity of the magmatic arc for that area, with rough maxima at 130-110, 90-70, 60-40, 30-20 Ma and rare later activity [Birkenmajer et al. 1986a; Pankhurst & Smellie 1983].

1.5 Stratigraphy of the Antarctic Peninsula

1.5.1 Basement

Only very scattered and incomplete information is available about the basement of the Antarctic Peninsula, but most authors refer to the Trinity Peninsula Group (TPG) and correlates, consisting of intermediate graded metasediments formed in an accretion wedge [Barker et al. 1991]. The TPG comprises siliciclastic turbidites varying in thickness between 1200 m (Antarctic Peninsula) and 3000 m (Livingston Island, South Shetland Islands). These sediments were probably derived from Gondwana and introduced into a marine marginal basin during Late Carboniferous to Jurassic times, maybe being the result of the progradation of turbiditic fans [Arche et al. 1992; Birkenmajer 1992b; Miller et al. 1987; Thomson 1992]. However, at least for the Miers Bluff Formation (Livingston Island, South Shetland Islands), which traditionally was assigned to the TPG, new fossil findings of Late Jurassic [Pimpirev et al. 2002] and Late Cretaceous age [Pimpirev et al. 2005; Stoykova et al. 2002] indicate a post-Triassic formation, raising severe doubts concerning its relation to the name-giving formation on Trinity Peninsula. No outcrop is known of the contact TPG - crystalline basement; it is unknown whether it is of sedimentary or tectonic character.

Older, crystalline basement is documented only from very scarce outcrops, boulders within Mesozoic conglomerates and mostly as xenoliths incorporated in magmatic rocks of the volcanic arc. Only in eastern Graham Land, gneisses and amphibolites crop out that may represent either part of the Gondwana craton or pre-breakup arc rocks [Barker et al. 1991]. Presence of continental basement beneath other parts of the eastern Antarctic Peninsula is indicated by the geochemistry of garnets extracted from andesitic volcanics [Moyes & Hamer 1983].

1.5.2 Arc-related magmatic rocks

Subduction related magmatism started in the Antarctic Peninsula area no later than during Early Jurassic times, with proto-Pacific oceanic crust subducting beneath the western margin of Gondwana. Plutonism and attendant volcanism continued also after breakup of Gondwana during much of the Mesozoic and Cenozoic.

The activity of the subduction zone and attendant volcanism led to the formation of a predominantly calc-alkaline magmatic arc. It consists mainly of mafic to felsic plutons ('Antarctic Peninsula Batholith'), which intruded between Middle Triassic and Neogene times and are associated with the Andean Orogeny [Pirrie 1991]. One of the oldest plutons crops out on the eastern coast of Graham Land and yielded a Triassic age (209 ± 3 Ma) [Barker et al. 1991]. Effusive activity produced basaltic and andesitic volcanic rocks with dacites and rhyolites occurring subordinately ('Antarctic Peninsula Volcanic Group'). These rocks formed between Middle Jurassic and Pliocene times [Smellie 1990].

The volcanic sequence unconformably overlies the uplifted older subduction-accretion complex.

Whereas Jurassic magmatism concentrated along the Peninsula's east coast, it was very broadly distributed during Early and mid-Cretaceous times. In the Late Cretaceous and Early Cenozoic, the activity was confined to the west coast and offshore islands [Barker et al. 1991]. Moreover, also along-arc magmatic trends are discernible. Especially the series of Cenozoic ridge crest - trench (RT-C) collisions mentioned above led to a northeastward migrating cessation of calc-alkaline, arc-related magmatism.

Volcanic activity in the South Shetland Islands - then still part of the Antarctic Peninsula - was widespread from Cretaceous (130 Ma) to Miocene (14 Ma) times and has been reactivated during the Late Pleistocene [Birkenmajer et al. 1991; Smellie et al. 1984]. It seems, that from Early Cretaceous times on the location of the magmatic arc shifted towards NW, moving also the focus of volcanic activity away from what is today the Antarctic Peninsula to the area that nowadays comprises the South Shetland Islands. Predominantly basaltic to andesitic, more seldom also rhyodacitic lavas, pyroclastics and all types of intrusions comprise a typical subduction-related suite with calc-alkaline affinity. The Late Cretaceous to Oligocene stratiform volcanic sequence (best investigated on King George Island) gives hints on different volcanic cycles of mainly effusive character. The products of this subaerial volcanism yield an overall thickness of approx. 3000 m [Birkenmajer 1994] and include pyroclastic intercalations with terrestrial plant fossils. This points towards a moderate warm to warm climate at the time of eruption; several horizons with glacial and glaciomarine sediments represent the Cenozoic glaciations [Birkenmajer 1989].

Starting in the Pliocene, an outbreak of alkali volcanism occurred along the Antarctic Peninsula, from western Alexander Island in the south through Jason Peninsula and Seal Nunataks to James Ross Island and Paulet Island in the north [Barker et al. 1991; Veit 2002]. Most of these locations lie at similar distances from the Pacific margin (300-400 km), nevertheless a simple and direct link with subduction is not very probable under the view of the long lasting and very variable subduction history along the arc.

With the onset of backarc-extension related rifting in the Bransfield Strait area (also Pliocene), a transitional component between calc-alkaline and E-MORB was added to the Peninsula's magmatic history, expressed in numerous seamounts along Bransfield Rift and some young volcanic islands like Bridgeman, Penguin and Deception Island. From some of these islands eruptions have been documented in historical time, e.g. the last series of eruptions on Deception Island at the end of the sixties, and Penguin Island is supposed to have erupted around 1905.

Though alkali volcanism, Bransfield Strait opening, and also the creation of George VI Sound may all be extension related and even similar in age, it is highly uncertain if they are triggered by the same reasons or are even structurally connected at depth [Barker et al. 1991].

1.5.3 Sedimentary rocks

Both the southern Andes' as well as the Antarctic Peninsula's eastern areas are characterized by a back-arc-basin stratigraphy of thick Jurassic to Cretaceous marine shales, siltstones, pyroclastic sediments (southern Antarctic Peninsula) and anoxic mudstones and airfall tuffs (northern Antarctic Peninsula) with the then active volcanic arc lying west [Barker et al. 1991; Domack et al. 2003]. Deposition of sediments within these basins (Larsen and/or James Ross Basin) continued throughout the Cenozoic. The western (Pacific) border of the Antarctic Peninsula features thick, partially tectonized forearc strata that comprise Mesozoic to Cenozoic volcanic and attendant sedimentary rocks. During deposition of this forearc strata, the final phases of ridge crest - trench collision along the Pacific margin of the peninsula took place and the subduction zone was closed successively from SW to NE from Paleogene times onward [Barker et al. 1991].

1.6 The role of dyke systems in magmatic arcs

Even though often disregarded, magmatic dykes are essential components of volcanic arcs, penetrating joints and fracture zones. Thus, they reflect the tectonic as well as the magmatic parameters at the time of their intrusion.

The timing of magmatic events is generally difficult to determine in deeply eroded magmatic arcs which comprise poorly preserved lava sequences and fine-grained, hydrothermally altered plutons. In such arcs, dyke systems yield a considerable potential to identify magmatic and tectonic events. Primarily, because crosscutting dykes reflect directly the relative age re-

lationships, giving the opportunity to identify different intrusive events and to establish a relative time sequence. Moreover, because their orientation is often tightly connected to the tectonic regime at the time of their intrusion, thus giving hints on how the tectonic parameters changed with time. There is no other element of volcanic arcs combining petrological, geochemical, isotopic and structural information like dykes do. Thus, magma genesis, tectonic regime at the time of emplacement, cooling conditions and postmagmatic hydrothermal as well as tectonic events are all reflected by dyke systems. Despite this great potential, dyke swarms in magmatic arcs traditionally have been referred to only as feeder systems for subaerial stratovolcanic centres, or as features comagmatic with arc-plutons, and therefore often been ignored.

Some recent works carried out on the Fiji Islands, Texas/Mexico, Sierra Nevada in California and also on the Antarctic Peninsula show clearly, that many dyke swarms are not related directly to subduction or subaerial volcanism. In fact, they can serve as indicators of crustal extension [Wharton et al. 1995], give evidence for ridge crest-trench (RT-C) collisions and slab-window formation [Scarrow et al. 1997a, 1997b] or also indicate post-subduction related intraplate magmatism [Henry et al. 1991]. The consequence is, that magmatic dykes may appear very similar in the field despite having completely different origins [Dilek et al. 1991; Scarrow et al. 1998].

RC-T collision events cause a magmatism of heavily extended chemical bandwidth [Rogers et al. 1985], e.g. high-Mg andesites and intraplate-like basalts rising through slab-windows opening temporarily in the subducting plate. These events are predominantly preserved by dykes intruding granitic plutons in active continental margins [Scarrow et al. 1997a]. Dykes intruding along faults give evidence, that melting of the different mantle sources available during a RC-T collision event is controlled by the geometry of the faults.

1.7 Questions and goals

As a by-product from own former work on Potter Peninsula (King George Island, South Shetland Islands) during austral summer 1998/1999, evidence was found for a tight correlation of strike and chemistry of the dykes cropping out there [Kraus et al. 2000]. Because of the high potential of dykes giving information not accessible through other arc-related features, the project presented here was initiated with the intention to gain further insight into the magmatic and tectonic development of the northern Antarctic Peninsula, especially in the area of the South Shetland Islands. The following questions have been of major importance:

(1) Is the correlation of strike and geochemical composition of the dykes only a local phenomenon on Potter Peninsula or does it apply also for other parts of the magmatic arc?
(2) Are there any relations between the age of the dykes and their chemism?
(3) Is there any indication for a relation between the characteristics of the dyke systems and changes in the tectonic position of the northwestern part of the Antarctic Peninsula (= South Shetland Islands) during its drift from the position west of Tierra del Fuego to its present geotectonic position?
(4) Is it possible to reconstruct different deformation phases of the arc expressed by the orientation of the dykes and the joint systems developed within them and their host rocks? Does this indicate changes in the geometry of the subduction zone or changing velocities/directions of the downgoing slab?
(5) Do the structural data (orientation of the dykes as well as joint systems developed within them) and the crosscutting relationships allow the identification of dyke swarms belonging to the same intrusive event? Do the geochemical data corroborate the structural results?
(6) Do the isotopic data allow the identification and maybe also changes of the magma source? If yes, is it possible to identify different sources? To what extent do the isotopic results copy the pattern obtained from the structural and geochemical data and what geodynamic conclusions can be drawn?
(7) Is it possible to reconstruct the geodynamic history of that part of the Antarctic Peninsula for the time interval covered by the dykes combining the structural data with the geochemical and isotopic evidence given by them?
(8) Do the dyke systems of the South Shetland Islands give any indication on RC-T collision events in that area, indicating which of the two models presented by Scarrow et al. [1997a] might be right?

To explain the last point more in detail:

According to Scarrow et al. [1997a], dyke systems investigated in the central part of the Antarctic Peninsula indicate RC-T collision events at three dif-

ferent times during the Mesozoic and Cenozoic. One of them (Upper Cretaceous) seems to have been associated both with dextral and sinistral shearing, allowing two different models for the subduction and attending RC-T collision events. One model assumes the collision events to have propagated from SW to NE, just like the model well established for the later collisions during Cenozoic times [Barker et al. 1991; Larter & Barker 1991; McCarron & Larter 1998]. The other model postulates the Upper Cretaceous RC-T collisions to have propagated from NE to SW, accompanied by sinistral shearing within the overriding plate. If this hypothesis proves to be true, the northern Antarctic Peninsula (and therefore also the area of the South Shetland Islands) should yield evidence for such a collision event. It was one of the goals of this project to find evidence whether this second model proposed by Scarrow et al. [1997a] might be correct or not.

1.8 Working conditions and cooperations

The results presented here are based on field work carried out by myself during austral summers 1998/1999, 2000/2001 and 2001/2002. The investigated area comprised all snow- and ice-free areas around Maxwell Bay and Admiralty Bay (both King George Island), as well as Hurd Peninsula on Livingston Island. Further work was carried out on Nelson and Penguin Island (Fig. 1-1).

Transport to and from the Antarctic Peninsula mostly took place on board of tourist vessels sailing from Ushuaia (Tierra del Fuego, Argentina) via the Falkland Islands to the Antarctic Peninsula. During recent years it became common practice for scientists to use these tourist ships to get to their destination, paying a small fee, giving oral presentations on board and guiding the tourists during onshore visits in exchange.

Furthermore, the Argentine icebreaker 'Almirante Irizar', the Spanish icebreaker 'Hespérides' and the British icebreaker 'Shackleton' were used for transport between the Antarctic Peninsula and Argentina / Falkland Islands, respectively. In one case the Argentine Navy provided transport to Seymour Island, location of the Argentine Air Force's Base 'Marambio', from where a Hercules C130 provided further transport to Buenos Aires, Argentina.

Field work has been accomplished under tight cooperation with the Instituto Antártico Argentino (Buenos Aires, Argentina) and the Bulgarian Antarctic Institute (Sofia, Bulgaria). Additionally, invaluable logistic support has been provided by the Alfred-Wegener-Institute (Bremerhaven, Germany), the British Antarctic Survey (Cambridge, England), the Argentine, Brazilian, Spanish and Uruguayan Navy, the Polish Antarctic Institute (Warsaw, Poland) and by the South Korean Antarctic Institute (Seoul, South Korea). Following scientific bases were used as platforms for field work: Teniente Jubany / Dallmann Laboratory (Argentina/Germany), King Sejong Station (South Korea), Artigas (Uruguay), Arctowski (Poland), all located on King George Island, moreover St. Kliment Ohridski (Bulgaria) on Livingston Island.

Due to the lack of roads or even paths in all areas but Fildes Peninsula (King George Island), access to the working areas has been achieved mainly by foot, very often also by Zodiac boat. Transport to and from other scientific bases was provided by Zodiac boats, helicopter and/or ship, in some cases the inland-icecaps have been crossed by ski. Penguin Island was visited and samples taken during a stop and onshore excursion of tourists of MS Hanseatic in 1999. The northern coast of Nelson Island has been investigated by means of a Zodiac boat during day trips from the Argentine Base Jubany. Field camps have been planned originally but proved unnecessary because most working areas are located within day-reach of a scientific base.

Due to their comparatively mild climate, especially the South Shetland Islands are home to an exceptionally rich wildlife with several large areas having been declared so-called SSSIs (Sites of Special Scientific Interest) by SCAR (Scientific Committee on Antarctic Research). To protect breeding animals (sea elephants, fur seals, giant petrels, seagulls, etc.) from disturbances, strict rules apply for those who wish to work inside such a SSSI, consequently certain outcrops could not be visited due to the close vicinity of penguin rookeries or other breeding animals.

On King George Island, especially on Potter and Barton Peninsula, large dyke systems crop out cutting offshore, extensive intertidal pyroclastic platforms which fall dry only during very low tide. Such extremely low tides occur at two subsequent days only once within three months, thus requiring rapid work, independent of time and weather.

2. Regional Geology and Tectonics

Several authors [Birkenmajer 1994; Birkenmajer et al. 1986b; Pankhurst & Smellie 1983] have argued, that the focus of magmatic activity on the South Shetland Islands apparently shifted from SW to NE.

Even though the magmatic history of the South Shetland Islands is rather complex and characterized by many different phases and episodes, the overall trend indicates northeastward decreasing ages of the volcanic and intrusive rocks. Therefore, the description of the field work areas will start in the SW (Livingston Island), continue towards the NE (Nelson and King George Island) and terminate with Penguin Island, the youngest rocks studied in this project (Fig. 1-1). The tectonic data were processed using the program SpheriStat (ver. 2.2).

2.1 Livingston Island (Hurd Peninsula)

Hurd Peninsula (62° 40' S / 60° 22' W) is located in southern Livingston Island, the second largest of the South Shetland Islands (Fig. 2-1). It is bordered by South Bay in the NW and False Bay in the SE and comprises about 27 km^2, stretching some 11 km from SW to NE and 4.5 km from NW to SE at its broadest part. The highest point lies at about 400 m a.s.l. It is located near the southern end of the Peninsula. Like many other parts of the South Shetland Islands, also the shape of Hurd Peninsula seems to be controlled strongly by block faulting. The interior of the Peninsula is covered by a large icecap (Hurd Glacier), complicating access and geological field work (Fig. 2-1). Besides Byers Peninsula, the coastal areas of Hurd Peninsula comprise the largest rock outcrops in Livingston Island, predominantly along the northwestern coastline. Major morphological features are plane erosion surfaces between 60 and 200 m a.s.l., moraine ridges, paleocliffs and raised beaches [López-Martínez et al. 1992].

Three main lithological sequences crop out on Hurd Peninsula: the sedimentary, turbiditic Miers Bluff Formation in the stratigraphically lowermost position, unconformably overlain by the Moores Peak Breccia and, uppermost, the volcanic rocks of the magmatic arc (Mount Bowles Formation). Dykes are widespread in all areas throughout the Peninsula. The dykes investigated within this project are located in the northwestern part of Hurd Peninsula (Fig. 2-1 & 2-5) and hosted without exception by the Miers Bluff Formation.

2.1.1 The host rocks: Miers Bluff Formation

General characteristics

The strongly deformed Miers Bluff Formation (MBF) forms the local basement and consists of very low-grade metamorphic turbiditic arkoses, arkosic-wackes, mudstones, conglomerates and breccias.

An outcrop was found consisting of a lens (approx. 80 x 10 cm) of strongly deformed limestone associated with limonitized breccia, sandwiched between a 13 m thick dyke (HP-6) and the wall rock (locality UTM 635579, 20E 3052248). Maybe the limestone has been dragged from below by the magma during dyke intrusion and is an indication for a different lithology at deeper levels. Neither limestone nor the associated limonitized breccia belong to the MBF's normal lithology.

The MBF crops out in large areas along the Peninsula's northwestern coast between the type locality Miers Bluff in the southwest and steep ice-cliffs NE of Hespérides Point in the northeast. Additional outcrops at the southeastern coast along False Bay are smaller and more difficult to access, as both scientific bases on Hurd Peninsula (the Spanish base 'Juan Carlos I' and the Bulgarian base 'St. Kliment Ohridski') are located at the northwestern coast (Fig. 2-1). Neither base nor top of the MBF are exposed, but an overall thickness of at least 3000 m has been assumed by several authors [e.g. Arche et al. 1992; Dalziel 1972; Smellie et al. 1984, 1995] and seems plausible. Upper mid-fan suprafan lobes to lower mid-fan settings with thin channel sequences characterize the depositional environment of these turbidites [Pimpirev et al. 2000; Smellie et al. 1995].

Age of the MBF

The age of the MBF is still a matter of debate, with proposals ranging from Late Carboniferous to Early Jurassic [Loske et al. 1988; Miller et al. 1987; Smellie 1991]. Recently, this discussion has been broadened considerably with the new findings of Late Cretaceous nannofossils [Pimpirev et al. 2005; Stoykova et al. 2002] and an Upper Jurassic ammonite [Pimpirev et al. 2002]. Besides these important new findings, fossil evidence is generally undiagnostic. Locally abundant trace fossils support a marine origin of the MBF [Doktor et al. 1994; Hobbs 1968]. Some poorly preserved plant remains were found by Hobbs [1968] and Dalziel [1969],

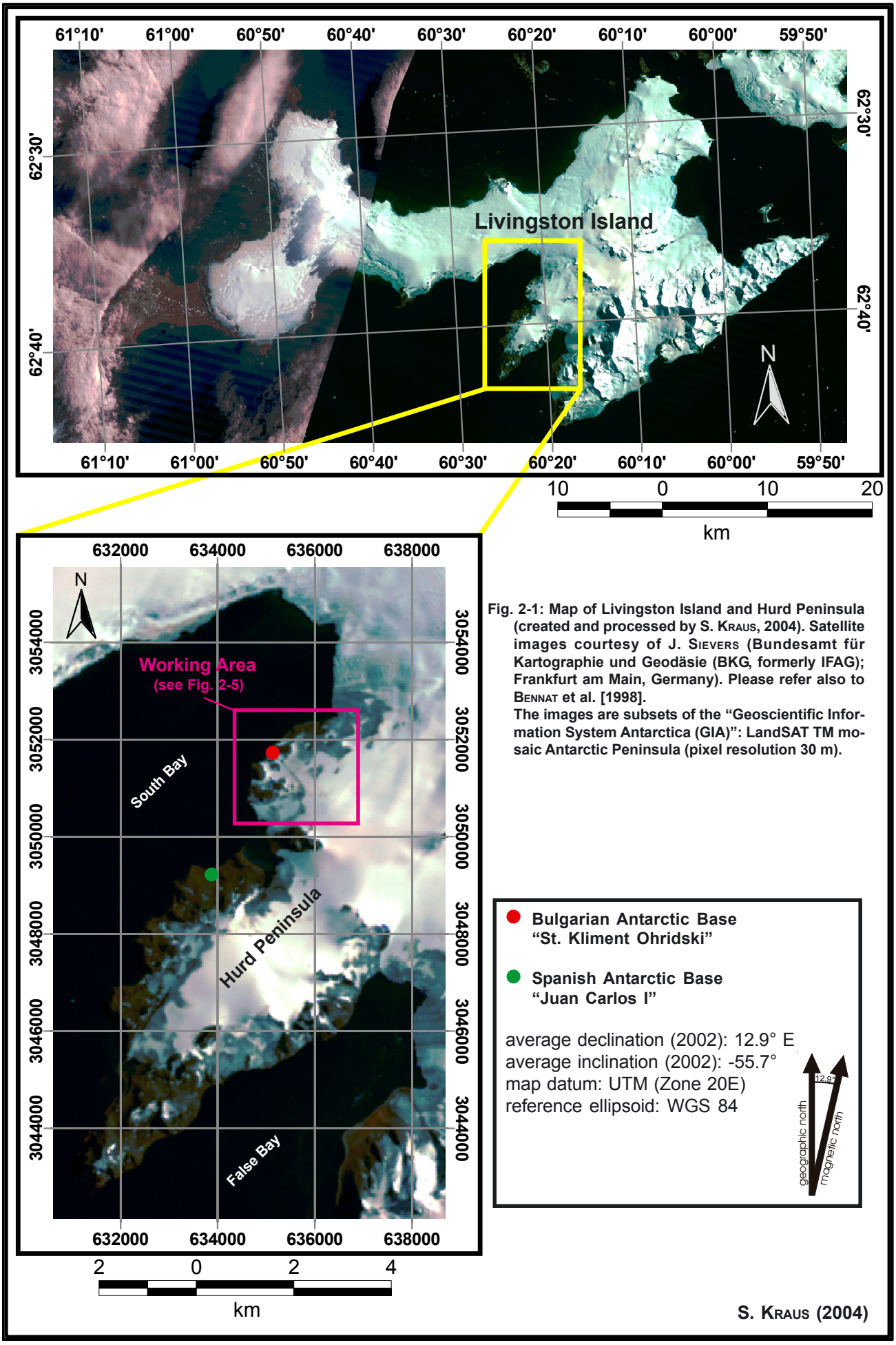

Fig. 2-1: Map of Livingston Island and Hurd Peninsula (created and processed by S. Kraus, 2004). Satellite images courtesy of J. Sievers (Bundesamt für Kartographie und Geodäsie (BKG, formerly IFAG); Frankfurt am Main, Germany). Please refer also to Bennat et al. [1998].
The images are subsets of the "Geoscientific Information System Antarctica (GIA)": LandSAT TM mosaic Antarctic Peninsula (pixel resolution 30 m).

reworked coal detritus and a single shell fragment favor an age younger than Carboniferous, maybe Mesozoic [Hobbs 1968]. Terrestrial palynomorphs reported by Xiguang et al. [2002] suggest a Late Triassic (probably Norian-Rhaetian) age.

Absolute age determinations also yielded uncertain data. Clay fractions gave Triassic ages, but it is questionable if these data represent true ages or rather periods of diagenesis or very low metamorphism [Dalziel 1972, 1982; Pankhurst 1983]. In any case, they should be younger than the real age of deposition. The volcanic rocks of the Mount Bowles Formation overlying unconformably the MBF are supposed to be of mid-Cretaceous age [Smellie et al. 1995, Willan 1996], standing in conflict with the aforementioned Upper Cretaceous fossil findings. Detrital zircons from sandstones of the TPG and the MBF yielded a Middle-Late Carboniferous age [Loske et al. 1988; Miller et al. 1987; Smellie 1991], giving hints on the provenance of the sediments and thus a maximum age. In case of the MBF, the maximum age seems to be even younger, as proved by a recently discovered Jurassic zircon population [Hervé et al. 2005]. These new data render the correlation with the TPG doubtful.

Regarding the paleogeography and provenance of the MBF, Arche et al. [1992] point out the freshness and similar size and roundness of the volcanic fragments and plagioclase clasts to the slate, sandstone and granitic fragments, inferring that the source area may have consisted of active volcanoes and low-metamorphic and granitic terranes. They conclude that the turbidites have probably been transported along the convergent Pacific Gondwana margin to the south, forming long-travelling systems along the trench. The finer grained beds of the MBF were deposited by NE-SW-oriented palaeocurrents, as indicated by abundant sole structures [Smellie et al. 1995].

Tectonic characteristics of the MBF

Constrained by the youngest fossil age (Campanian nannofossils, see above) and the assumed onset of dyke intrusion (earliest Danian, see chapter 5), the main deformation obviously took place during a time interval of 5-10 Ma, mainly during the Maastrichtian.

At most outcrops the sediments show inverted beds striking coast-parallel NE-SW and dipping to the NW (Fig. 2-5). They have been interpreted as forming the short and overturned limb of a fold several km in wavelength, featuring a subhorizontal axis (NNE-SSW) and an axial plane dipping 10°-45° to the NW or WNW [Arche et al. 1992; Smellie et al. 1995]. This large-scale fold is characterized by locally expressed tight later folding [Smellie et al. 1995], intrusion of Late Cretaceous gabbroic to quartzdioritic plutons and Eocene quartzdiorites [Kamenov 1997], several generations of Cretaceous quartz veins [Willan 1994], numerous dyke systems piercing it [Willan & Kelley 1999; Zheng et al. 2003] and by recent, active tensional and strike-slip faults.

The deformation history has been interpreted differently by several authors:

According to Smellie et al. [1995], three phases of open folding deformed the MBF. A first phase of possibly synsedimentary folds is locally expressed, faces east and yields NNW-SSE striking axial surfaces. A second generation (phase 2) is facing north and features subhorizontal E-W oriented axes. During main folding, a phase 3a produced the aforementioned large-scale open folds, which face SE and are characterized by steeply NW-dipping short limbs and NNE-SSW striking subhorizontal axes. Phase 3b folds have only local distribution and are N-S oriented. Smellie et al. [1995] conclude that folding was completed before the Cretaceous and postulate subsequent tilting to the ESE to overturn bedding and achieve the present bedding orientation.

In contrast, Tokarski et al. [1997] see only one early folding phase around a NNE trending axis and two later phases of strike-slip tectonics, the first featuring a maximum stress axis trending E-W and the second one N-S. Most studies, however, conformably interpret the folding to be open and state the general lack of cleavage. Joint systems are abundant in the MBF as in the dykes. They have been extensively measured within this project.

Two possible ways of defining the local geometry of the MBF folding can be applied. To obtain the general trend of strike and dip of the large-scale folding, the bedding must be measured avoiding the proximity of minor folds and the resulting data should plot as a cluster in the Schmidt Net rather than as girdle. Such data have been kindly provided by Prof. Dimo Dimov (p.c., Univ. Sofia, Bulgaria) and indicate a general orientation of the large-scale fold's overturned limb of 63/23 NW (Fig. 2-2A & 2-5). In contrast, in order to obtain a reliable b-axis, the bedding around the aforementioned minor folds was measured. Consequently, these data form a girdle plotted in the Schmidt Net. The measurements con-

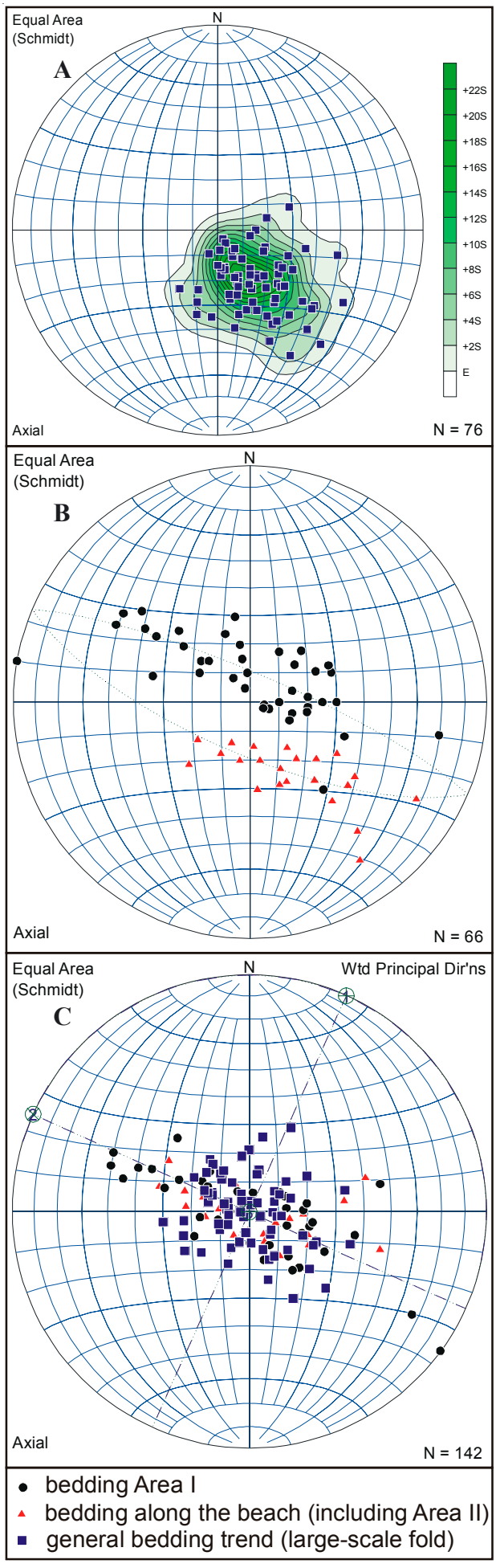

firm a folding axis oriented NNE-SSW (Fig. 2-2B & 2-2C). Also the overturned character of the MBF could be verified in the field (Fig. 2-3 & 2-5).

Rotating back the bedding includes rotation of the b-axis around the a-axis to a horizontal position, then reverting the inverse to normal bedding (rotation of approx. 160° around the b-axis) and finally shifting the c-axis to the centre of the Schmidt net (rotation around the b-axis).

Fig. 2-2C illustrates the result of rotating back the three datasets independently, i.e. applying the aforementioned method to each dataset separately and determining the individual back-rotational factor for each of them.

This factor, in case of the general bedding orientation, is a rotation of -164° (the rotation angle is negative for an anticlockwise rotation when the rotation axis is 'viewed' from the center of the unit sphere) around an axis trending (17.4/7.3).

For Area I (Fig. 2-5), it is a rotation of -178° around an axis oriented (203.1/5).

In case of the bedding along the beach, including Area II, this factor can be determined as a rotation of -160.4° around an axis trending (17.6/10).

Plotting then the three datasets into the same Schmidt Net (Fig. 2-2C) gives an orientation of 24/0 for the b-axis and 114/0 for the a-axis.

However, within the investigated area there is a remarkable difference between the bedding of the sediments measured in Area I and the data obtained along the beach, including Area II (Fig. 2-2B). If the different π-circles in Fig. 2-2B would be a consequence of cross folding, a homogeneous distribution of the two observed types of bedding could be expected within both areas, moreover the two π-circles should show a 'bridge' of datapoints between them, rather than being separated so clearly. This is not the case, in contrast, one π-circle in Fig. 2-2B is entirely defined by the bedding measured in Area I and the other nearly entirely by the data obtained along the beach including Area II.

Fig. 2-2: General bedding orientation of the large-scale fold (A) and bedding measured at minor folds, also showing the corresponding π-circles (B). The combined plot (C) shows the back-rotated bedding data indicating a NNE-SSW striking b-axis (24/0). Poles to planes. For contouring, the Gaussian method 'K=100' has been applied. This method gives an expected count, E, that is the same as the conventional 1% counting circle. The mean, or expected, value E is the count that should arise in each counting model if the data set was uniformly distributed. The weighting curve has a width at half-height of 8.1°. The contour levels are in multiples of s (standard deviation) above (or below) E.

A possible interpretation is, that the two areas are separated by a fault (Fig. 2-6) and that late block faulting with movement and/or tilting along the fault plane is responsible for the observed pattern.

This inferred fault is not visible in the field, but could well be masked by dyke HP-1A (Fig. 2-9). This dyke is the second youngest cropping out within the investigation area, one of the thickest (5.5 m) and moreover running where the fault could be located. Also, it is by far the longest observed dyke: it

Fig. 2-3: Flute casts on a NW-dipping bedding surface confirming the overturned character of the MBF. Hammer as scale.

can be traced over 2 km running along the northwestern coast of Hurd Peninsula.

It is difficult if not impossible to tell which of the two areas has been affected by tilting. Block faulting marks the last stage of deformation in the South Shetland Islands (as postulated by several authors) and might be responsible for the pattern observed in Fig. 2-2B. One logical possibility to determine the amount of movement during this last stage is to rotate the bedding data of the area that supposedly has been affected by tilting in such a way, that its a-, b- and c-axes are congruent with the axes of the other area. The amount of this rotation then should equal the movement during block faulting.

A good means to verify the correctness of this procedure is the behavior of the dykes piercing the MBF, especially dyke HP-1A, which can be traced over more than one km running through both, Area I and Area II (here its name is HP-7G, see Fig. 2-10). As block faulting probably took place during a late stage of deformation, it should have affected not only the MBF, but also the dykes cutting it, as these are supposed to be older than the block faulting. The present orientations of the two segments of HP-1A do not plot congruent in the Schmidt net (event V in Fig. 2-4A). This fact can either be due

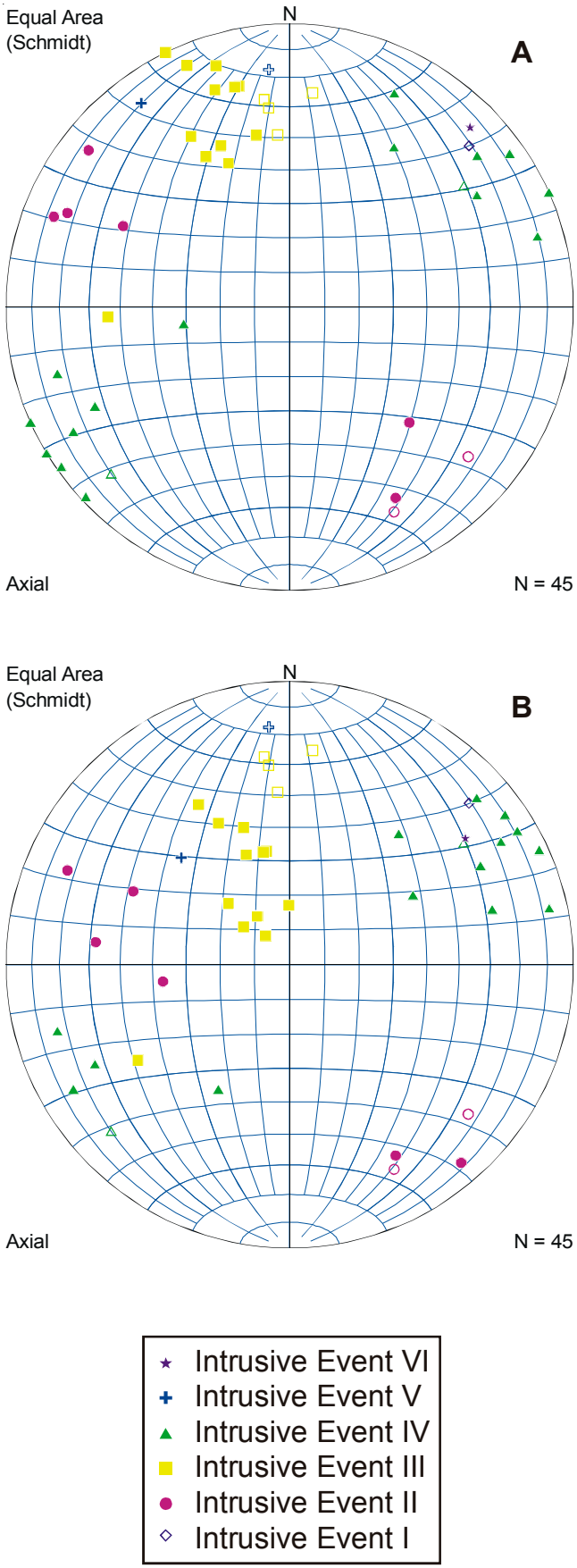

Fig. 2-4: Orientation of the dykes as observed in the field (A). Poles to planes. Applying the back-rotational factor determined for the bedding of Area I to the dykes cropping out in the same area leads to an even less homogeneous pattern (B). Filled symbols: dykes of Area I; open symbols: beach-dykes and Area II

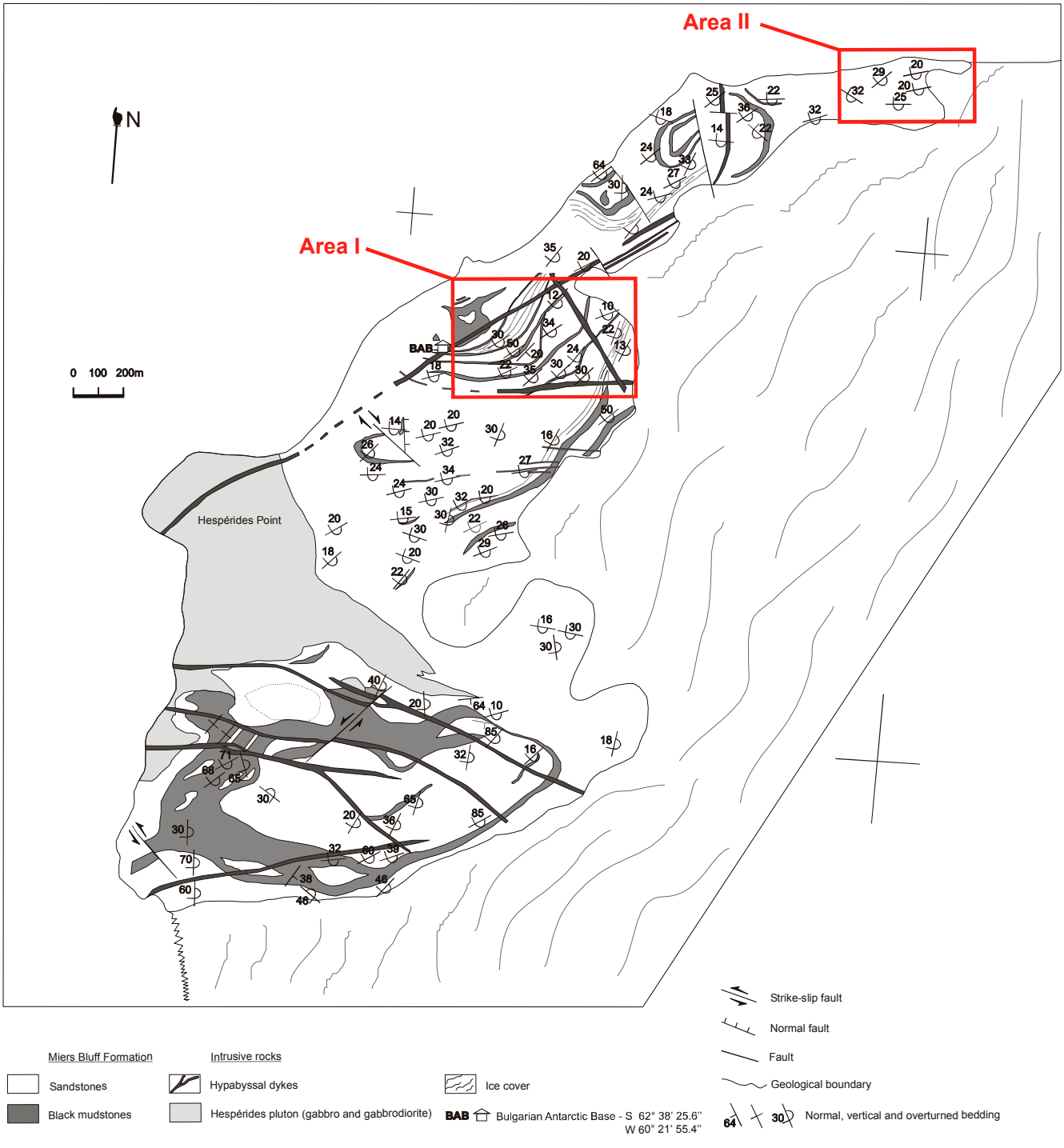

Fig. 2-5: Geological sketch map of the northwestern part of Hurd Peninsula, showing the location of Area I and II and the bedding orientation of the host rock (MBF). Slightly modified after D. Dimov (Univ. of Sofia, Bulgaria, kind p.c.).

to the dyke having changed its direction during emplacement, or to late block faulting rotating the two segments of the dyke relative to each other.

It is conspicuous, that all dyke groups of Area II are rotated 15-30° clockwise with respect to the corresponding dyke groups of Area I, though showing the same relative time sequence (Fig. 2-9 & 2-10). Applying the aforementioned rotational factor of the bedding data to the dykes should also lower the difference in orientation between the corresponding dyke groups of the two areas.

Determining the rotational factor for a possible block faulting induced movement of Area I yields a rotation of -35.7° around an axis oriented (71.2/2.9). Unfortunately, applying this factor to the dykes of Area I results in an even less homogeneous distribution of the dyke pattern (Fig. 2-4B). Checking for a possible rotation of Area II does not yield better results.

A possible interpretation is, that either *both* areas have been affected by tilting with *individual* rotational factors (which are very difficult, if not impos-

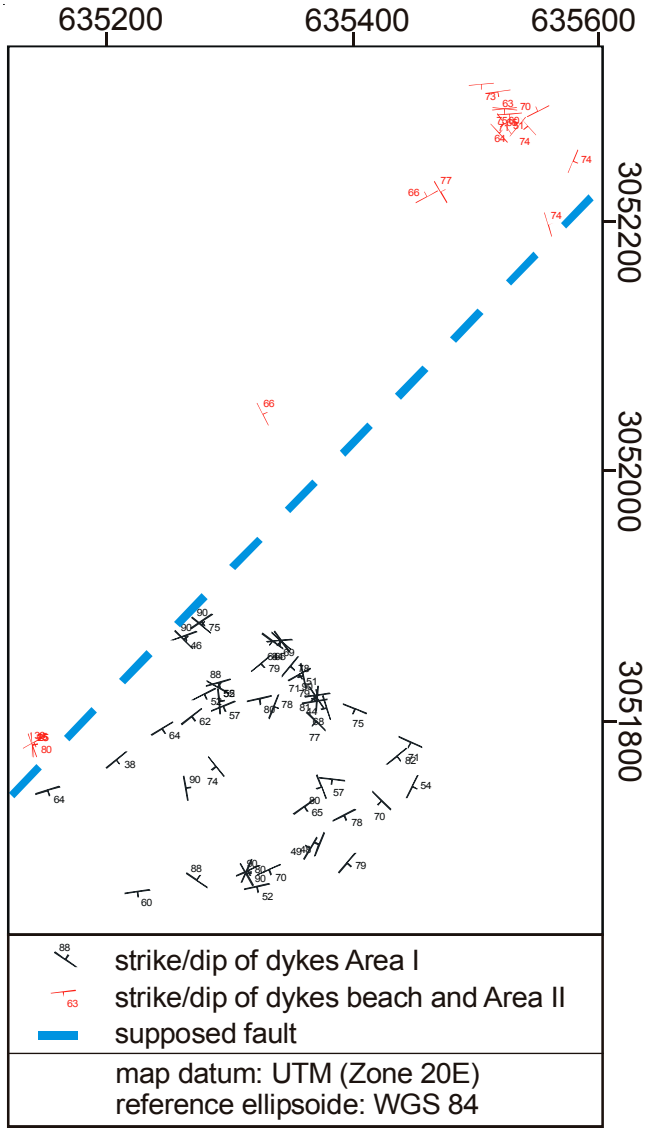

Fig. 2-6: Sketch map showing the geographical separation of the two areas and strike and dip of the investigated dykes. The inferred fault is just tentatively.

sible to reconstruct), or that further processes are responsible for the different bedding observed in the two areas. However, three points have to be emphasized:

(1) Whereas Area I lies entirely in the south of the investigated part of Hurd Peninsula, Area II lies - spatially clearly offset - towards the NW (Fig. 2-5 & 2-6). It is well known that late, postmagmatic block faulting has affected the South Shetland Islands and produced several deep-cutting, dextral strike-slip faults. One of these faults is supposed to run along South Bay [Hobbs 1968] (Fig. 2-1), and a minor, subparallel running fault could separate the two areas and be the reason for the observed different bedding.

(2) If comparing the bedding of the two areas (Fig. 2-2B) to the general bedding orientation of the large-scale fold (Fig. 2-2A), the data of Area II seem to correlate better with the general orientation than the data of Area I. This is also reflected by the very similar back-rotational factors displayed by the general bedding and Area II, as compared to the completely different factor of Area I. This leads to the speculation that Area I has been affected stronger by tilting than Area II.

(3) The most likely explanation for the differing structure and dyke directions in both host rock areas is the interpretation of the fault drawn in Fig. 2-6 as a major transcurrent fault that brought together two former distant parts of the MBF. The aforementioned new fossil findings prove differing sediment ages at both sides of the fault, a Late Cretaceous nannofossil age on one side [Stoykova et al. 2002] and a Late Jurassic ammonite age on the other [Pimpirev et al. 2002].

The most important conclusion to be drawn from the above discussed data is, that the absolute strike of the dykes is in no way diagnostic if compared between different areas. Much more reliable and indeed suitable to compare different areas is the angle between the different strike directions in combination with their relative time sequence.

Jointing is widespread in the MBF and extensive measurements lead to following results (Fig. 2-7): Clearly recognizable are ac-joints, averaging an orientation of 117/87 SW. Surprisingly, they are expressed almost exclusively within Area I, but far less in Area II (Fig. 2-7A, B). The reason is unclear.

First and second order shear systems are both reflected clearly by the joints observed in the field. Whereas first order shear systems (expressed as shear planes belonging to the zone σ_1-σ_3, with σ_2 as shared axis) are well known, the occurrence of a second order shear system is less frequently mentioned, though stated already 73 years ago [Schmidt 1932]. This second order shear system develops shear planes belonging to zone σ_1-σ_2 in case that the σ_2-value is closer to σ_3 than to σ_1 (practically this means elongation in direction of the strike of the orogeny). In case that the σ_2-value lies closer to σ_1 than to σ_3, the resulting shear planes would belong to zone σ_2-σ_3 (meaning shortening in direction of the strike of the orogeny). Theoretically, these shear planes should develop at angles of 45° to the respective σ-directions [Schmidt 1932]. However, the angle never exceeds 45°, but may become as low as 20°, due to internal friction.

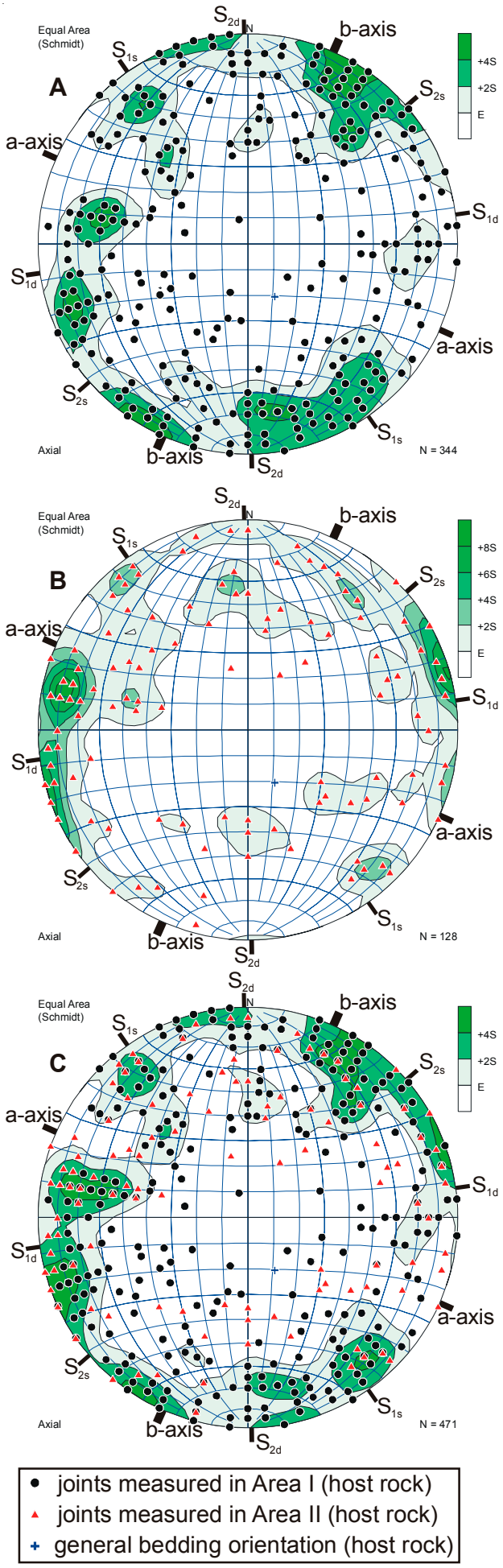

On Hurd Peninsula, dextral first order shear joints (S_{1d}) occur abundantly at angles of 25-30° to the a-axis of the main folding phase. Sinistral first order shear joints (S_{1s}) are less frequent. First order joints average 82/80 N (dextral) and 145/88 SW (sinistral) in orientation.

Second order shear joints (also dextral and sinistral; S_{2d}, S_{2s}) are abundant too and oriented at an angle of approx. 25° to the b-axis of the main folding phase. They could be interpreted as indications for cross-folding, though the observed pattern shown by the bedding rather indicates late block faulting (see above). Their orientation averages 179/84 E (dextral) and 49/87 NW (sinistral).

Most of the joints seem to be relatively young with respect to folding. Unambiguous rotations are rare and difficult to interpret in the frame of the given symmetry field. Folding axis parallel h0l-joints do also occur rarely and are pronounced weakly, maybe because they belong to the same overturned limb of the fold. The prominent, sinistral faults displacing some dykes of the second intrusive event (Fig. 2-9) belong to the first order shear system.

2.1.2 The dyke systems on Hurd Peninsula

The investigated area is situated in the northwestern part of Hurd Peninsula in the vicinity of the Bulgarian Antarctic Base 'St. Kliment Ohridski' (Fig. 2-1 & 2-5). The morphology is characterized by glacier-polished, smoothly shaped hills as well as steep and craggy cliffs and rock walls, mostly towards the sea. Compared to other parts of the South Shetland Islands, the outcrop situation of the dykes is especially good here, because the cover of moraine detritus tends to be thinner or even nonexistent. Moreover, the sedimentary MBF comprising the host rocks makes identification of dykes and their relative age

Abbr.	Explanation (with average strike)
b-axis	24° (folding axis)
a-axis	117° (ac-planes: 117/87 SW)
S_{1d}	dextral first order shear direction: 82°
S_{1s}	sinistral first order shear direction: 145°
S_{2d}	dextral second order shear direction: 179°
S_{2s}	sinistral second order shear direction: 49°

Fig. 2-7: Joints (host rock) in Area I (A), Area II (B) and a compilation of all joint data (C). The table summarizes the average tectonic features as deduced from the host rock joints. Contouring as explained in Fig. 2-2. Poles to planes.

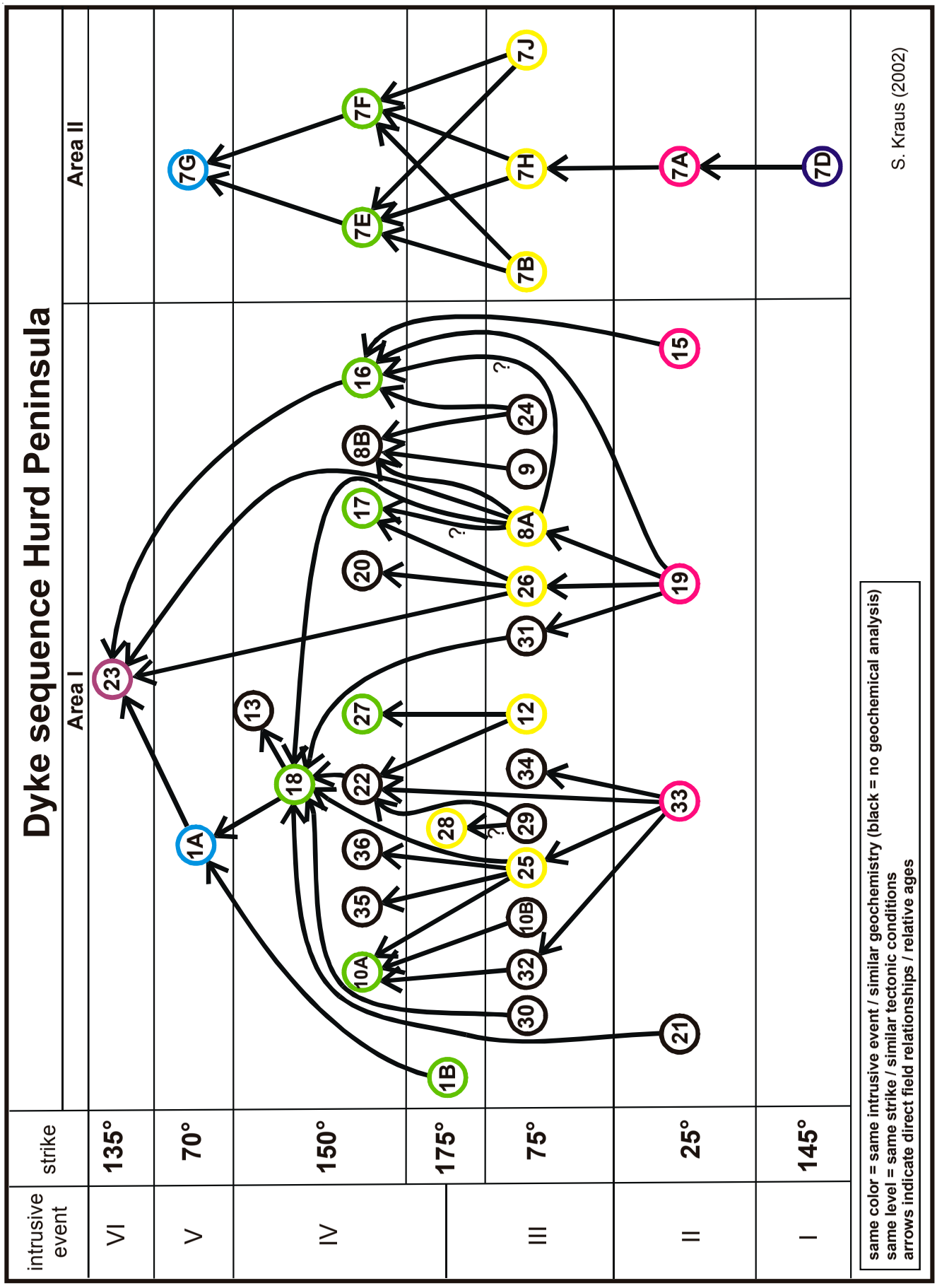

Fig. 2-8: Dyke sequence ('genealogical tree') of Hurd Peninsula, showing the relative age relationships observed directly in the field. Area I and II refer to the mapped systems illustrated on the following pages. Colors are corresponding.

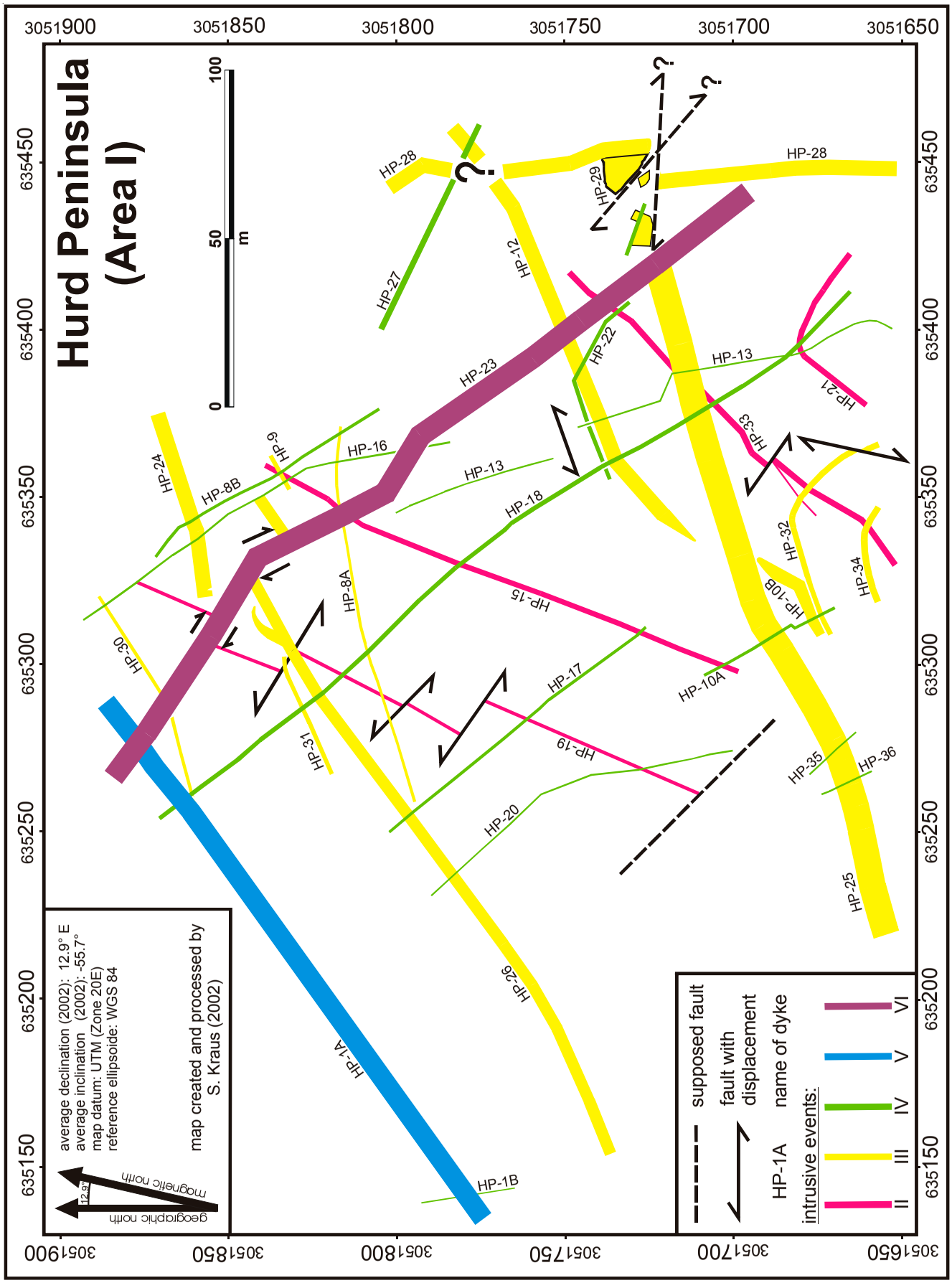

Fig. 2-9: Mapped dyke system 'Area I', counting 31 dykes which form 5 distinct groups representing the intrusive events II to VI. The mapped area comprises approx. 100,000 m². Note that groups II and III suffered a change of tectonic conditions during their respective emplacement time. Within group II, only the early dykes show sinistral displacement. Within group III, HP-28, probably the youngest dyke within this group, marks a change of the used joint direction towards the end of this intrusive phase. Note that the apparent bending of dykes HP-13, -21, -32 and -34 at the southern margin is only a topographical effect.

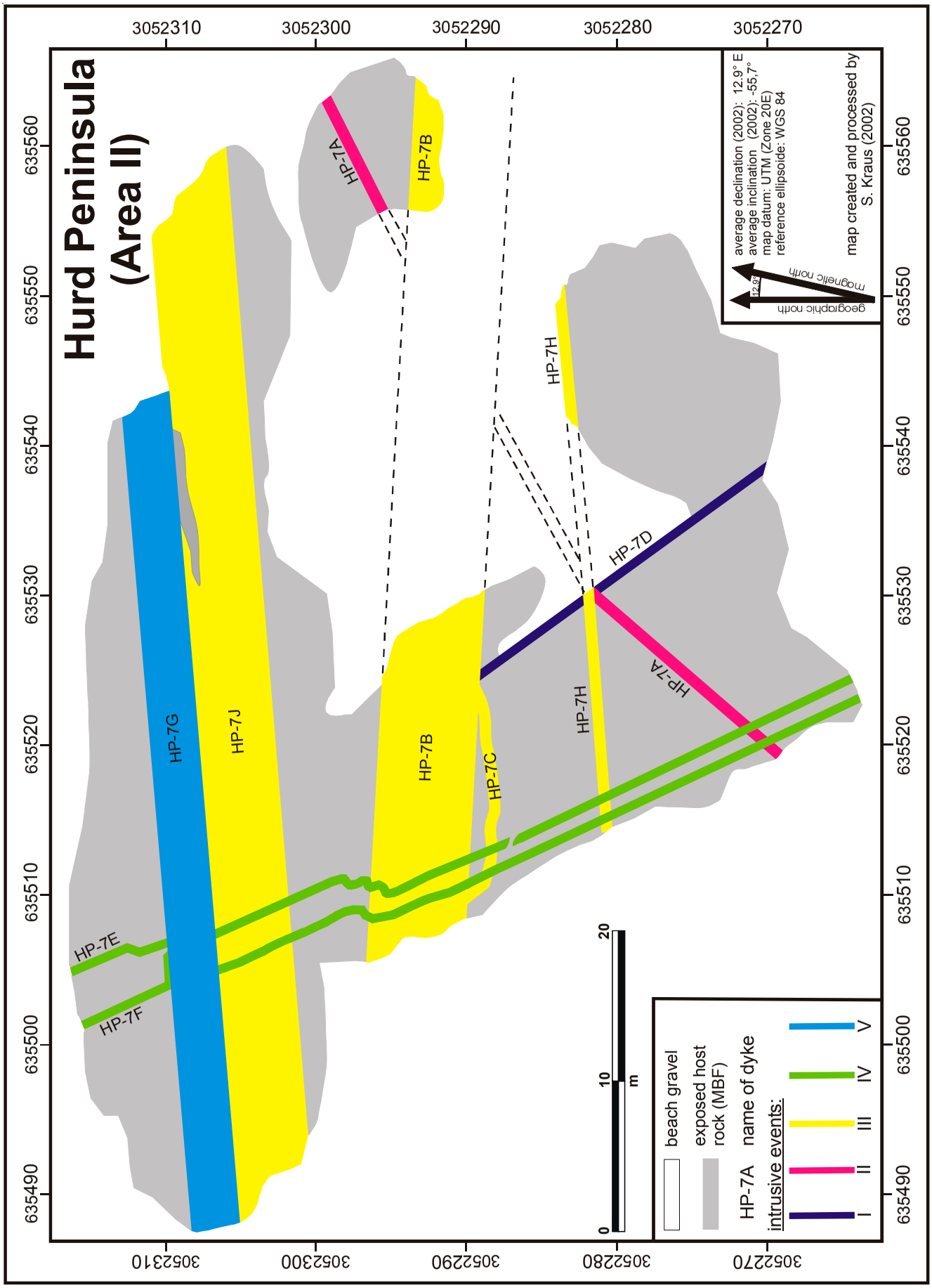

Fig. 2-10: Mapped dyke system 'Area II', counting 8 dykes which form 5 distinct groups representing the intrusive events I to V. The mapped area comprises approx. 4,000 m². Note the different strike of up to 30° clockwise of corresponding dykes as compared to Area I.

	Event I	Event II	Event III	Event IV	Event V	Event VI
Number of dykes	1	8	16	17	2	1
Prevailing strike	145°	25°	75°	150°	70°	135°
Average thickness	55 cm	262 cm	320 cm	90 cm	425 cm	600 cm
Lithology	Trachyandesite	Tephrite Andesite Dacite	Bas. Andesite Bas. Trachyandesite (Trachy-) Andesite Dacite Rhyolite	Basalt Trachybasalt Bas. Trachyandesite	Bas. Andesite Trachyandesite	Andesite
Mineralogy (magmatic)	**Pl**, opq, Ap	**Pl**, **Cpx**, opq, Ap	**Pl**, **Cpx**, **Zir**, opq, Ap	**Pl**, **Cpx**, **Opx**, opq, Ap	**Pl**, **Cpx**, opq, Ap	**Pl**, **Cpx**, opq, Ap
Mineralogy (sec. alteration)	Cc, Chl, Ser	Ab, Cc, Chl, Ep, Qz, Ser	Ab, Cc, Chl, Ep, Qz, Ser, Zeo	Ab, Cc, Chl, Ep, Qz, Ser, Zeo	Cc, Chl, Ep, Ser	Cc, Chl, Ep, Qz, Ser
average AI	3.50	3.56	3.34	3.38	2.5	2.5
average LOI	5.53	5.82	4.35	5.15	3.69	3.35

Table 2-1: Basic characteristics of the six intrusive events on Hurd Peninsula. Note the difference in frequency, thickness and lithology. Bold abbreviations indicate phenocrysts (for explanation see Appendix I). Especially noteworthy is the occurrence of a zircon-bearing dyke belonging to event III. AI = Alteration Index, LOI = Loss on Ignition.

relationships easy. This last point is of special importance, as nowhere on the South Shetland Islands so many relative age relationships can be observed directly in the field and complete dyke systems can be mapped like here, thus giving information not obtainable elsewhere. Furthermore, folding and joint systems of the host rock allow determination of the stress geometry of the intruding dykes.

The working area includes two distinct locations at about 500 m distance from each other (Fig. 2-5). A total number of 44 dykes have been investigated on Hurd Peninsula. 31 of them form the dyke system mapped in Area I (Fig. 2-9) and 8 the system in Area II (Fig. 2-10). Moreover, 5 dykes were studied located in between.

Generally, the dykes feature a compact, blocky appearance with chilled margins normally not thicker than 1-2 cm. Quite frequent is columnar jointing and cc-, ser- and qz-filled amygdales which are concentrated in the center of the dykes and elongated parallel to the dykes' strike.

AI	Explanation
1	absolutely fresh, no secondary minerals
2	slight signs of alteration; scarce secondary minerals in groundmass or along fractures/rims of phenocrysts
3	medium alteration; groundmass enriched in secondary minerals; many phenocrysts show partial alteration
4	heavy alteration; most phenocrysts at least partly altered
5	basically no primary minerals left; rock completely altered

Table 2-2: Classification of the AI (Alteration Index) used in Table 2-1, based on microscopic observations on thin sections.

Description of Area I

Area I (Fig. 2-9) comprises a smoothly shaped hill located approx. 50-70 m a.s.l. close to the Bulgarian base (Fig. 2-1 & 2-5). It is bordered by the glacier to the SE and the beach to the NW. The apparent abrupt change in the strike of HP-21, -32 and -34 to a southeasterly direction (Fig. 2-9) is due to the hills morphology and not to a real change in strike.

In Area I, the host rocks are pierced by 30 dykes and one small stock most probably representing the northeastern end (or start) of a long dyke (HP-25). Intrusive event I is not expressed within this area, the oldest group cropping out here is event II. With one exception, at all of the numerous dyke-crossings the relative age relationships could be observed directly in the field, giving invaluable support for setting up the time sequence. Normally, the dykes are xenolith-free and cut the MBF sharply (Fig. 2-

Fig. 2-11: A thin (60 cm), sharp-edged basaltic dyke (HP-3) showing columnar jointing pierces the Miers Bluff Formation close to Area I. View towards SE, Hammer as scale.

11), developing thin, well defined chilled margins (1-2 cm). Many of them can be followed in a straight line over a distance of dozens of meters, sometimes far more.

In some cases, however, a network of apophyses, dead ends and magmatic bodies has been developed. HP-10B marks such a locality in the south of Area I (Fig. 2-9) and carries host rock xenoliths mostly smaller than 5 cm, though at its northeastern tip a piece of MBF sandstone several meters in diameter has been incorporated by the magma. Obviously, the host rock has locally been affected by tectonic brecciation and the magma subsequently intruded the scattered rock taking different directions, sometimes forming wedge-shaped dead ends. Another similar outcrop is marked by the aforementioned small-sized (approx. 15x10 m), microgabbroic/doleritic intrusive body HP-29. It could well represent the spot from where dyke HP-25 (also a microgabbro) migrated towards WSW. Towards the end of magmatic activity on Hurd Peninsula, old directions apparently have been reactivated, reflected by the strike of the two youngest events (V & VI) which run subparallel to directions already used before (Fig. 2-8, 2-9).

From these, HP-23 is of special importance, because it is the youngest of all dykes cropping out in the investigation area. It is notable, that these two youngest dykes run parallel and orthogonal to Bransfield Strait, respectively, but a relation with Bransfield Strait opening is nevertheless unlikely, due to their Eocene age (see chapter 5).

Description of Area II

Area II is located directly at the shore (Fig. 2-5 & 2-12) and forms a small hill not higher than 5 m. A part of the outcrop is accessible only during low tide. 8 dykes are piercing the MBF here, belonging to the intrusive events I to V (Fig. 2-10). Event VI is not present in this area. Dyke HP-7D is of special importance, as it is the only representative of intrusive event I and thus not only the oldest dyke found within the investigation area on Hurd Peninsula, but moreover the oldest of all dykes investigated within this project on the South Shetland Islands.

The lithology comprises, like in Area I, mostly basalts and andesites, but some dykes are much more acid. Fig. 2-10 shows clearly, that some dykes have not intruded the host rock straight forward, but rather tend to change their direction, either with a single kink (HP-7A) or a kind of meandering (HP-7E and -7F). This behavior (Fig. 2-13) may indicate that the host rock was strongly fractured prior to intrusion and the magma then migrated along cracks and joints of different directions.

Area II hosts the oldest dyke investigated within this work, furthermore a "dyke-triple-crossing" (three dykes crossing in one point). After removing the beach gravel, we found the crossing of three dykes about 1 m beneath beach level (HP-7D, HP-7A, HP-7H). Every dyke-crossing visible in the field is a compelling evidence for relative age sequences. A crossing of three dykes is even more important, as it links three instead of only two intrusive events into a clear sequence, hence ruling out doubtable geochronological data obtained later in the laboratory. In this case, the oldest dyke HP-7D could be identified as such, subsequently crossed by HP-7A and later by HP-7H as the youngest of the three (Fig. 2-14 & 2-15).

Fig. 2-12: Area II, a small hill cropping out at the shore of Hurd Peninsula. It comprises around 4,000 m² and is cut by 8 dykes. On the left side the outcrop is partially drowned by high tide.

The genealogical tree

The dyke crossings observed in the field have been used to compose a 'genealogical tree' of the different dyke generations (Fig. 2-8). The arrows in Fig. 2-8 always reflect a crossing observed directly in the field and point towards the younger dyke, thus reflecting the relative age relationship. With only a few exceptions, all dykes showing the same strike are also of the same relative age, thus allowing to form groups representing 6 different intrusive events associated with different strike directions. With the exception of one subordinate tectonic phase (175°) represented by only two dykes, all other tectonic directions coincide strictly with a corresponding intrusive event. This means, that every slight change of the tectonic parameters also came along with a new intrusive event, showing geochemical and isotopic characteristics different from the preceding one (see chapter 4). However, the general tectonic stress regime seems to have changed only slightly, confirmed for example by the repetition of the approx. 145°- and the 70°/75°-directions. ICP-MS analyses of the dykes corroborate the genealogical tree, same color of the circles in Fig. 2-8 means similar geochemical characteristics. No ICP-MS analyses have been made of the black circled dykes, these have been assigned to their respective groups according to their orientation and the relative age relationship. The colors used in Fig. 2-8 correspond to those in Fig. 2-9 and 2-10. The 175° tectonic direction is the only one which is not expressed also by a new intrusive event, obviously it became active while event III was still in progress. Dyke HP-28, being the youngest of this group, marks the end of this event, before the chemistry changed and intrusive event IV began. With the 175° direction still being active, dyke HP-1B marks the beginning of this new intrusive phase, then tectonic parameters changed once more and led to a new strike direction (150°), though still fed by the same magma.

The two youngest intrusive events, despite using old directions, are not only geochemically distinctive from the preceding ones, but also defined clearly by the relative age relationships. However, it can be assumed that these dykes intruded old, reactivated faults or zones of instability. It is interesting, that they run parallel (event V) and perpendicular (event VI) to the Bransfield Strait, though, despite being the youngest dykes cropping out in the area, they are too old to be correlated with the opening of the

Fig. 2-13: Dyke HP-7E jumping from one crack to another by changing temporarily its direction. Note that this is not postmagmatic faulting but a synmagmatic process due to the brittle structure of the host rock.

Bransfield Strait. Table 2-1 compares the main characteristics of the intrusive events on Hurd Peninsula.

Obviously, magmatic activity has been low in the beginning, producing only few dykes during events I & II. This may reflect the initial stage of subduction zone volcanism in that area and therefore a still unstretched (continental) crust underneath. The geochemical and isotopic data corroborate this assumption, as the oldest dykes show the highest degree of crustal contamination (see chapter 4). During the subsequent events III & IV, activity was much higher and led to the formation of numerous dykes showing higher εNd values. Probably not only the quantity of ascending magma rose, but also shallow level storage times were shorter at this stage, thus leading to lower degrees of crustal contamination.

Events V & VI mark the end of magmatism on Hurd Peninsula and are expressed as scarce, single dykes.

Though the strike of the dykes changed from event to event, the overall change of the tectonic stress field has obviously been only minor. This is reflected by the possibility to assign all intrusive events to the different first and second order shear directions, some to the bc-direction or also to h0l-joints, but all geometrically related to the main folding phase. However, variations were sufficient to allow different preferred directions at different times. This leads to the speculation that the general geometry of the subduction zone, including subduction direction and velocity, remained relatively stable during the time of the dykes' emplacement.

Dipping of the dykes is quite variable. Generally, throughout the different intrusive events, the dykes are dipping moderately to steeply (45°-80°). Event I consists of only one, steeply SW dipping dyke (HP-7D). Event II features a 1:1 distribution of NW and SE dipping dykes, whereas event III consists only of S to SE dipping dykes. A NW direction is not expressed, maybe slight differences in the tectonic stress field have been sufficient to favor only one dipping direction instead of the expected two. Event IV once again shows a 1:1 distribution, this time of NE and SW dipping dykes. Event V dips uniformly towards SE and event VI towards SW (Fig. 2-16).

The changes in intensity (not direction) of the tectonic stress field are also expressed in the thickness of the dykes, which is varying considerably between only 30 cm and up to 13 m (averages shown in Table 2-1).

It is not surprising, that event I is expressed as a very thin dyke and that average thickness is rising with growing magma volumes, opening rising paths and maturity of the arc, though event IV with its numerous dykes shows an only slightly higher average thickness than event I.

The same scheme applies to the lithology. Whereas event I is a trachyandesitic dyke with shoshonitic characteristics, the subsequent events yielded mostly basalts, andesites, dacites and sometimes also rhyolites. There is only one exception: HP-19 (Fig. 2-9) belongs to event II but is a tephrite showing the same strong shoshonitic chemistry as event I. The eye-catching dissection of this dyke by the prominent sinistral faults (Fig. 2-9) indicates that it is the oldest dyke of event II and thus affected by similar strong crustal contamination as event I. As already mentioned earlier, these faults can probably be assigned to the first order shear system and very likely mark a shorttime event during emplacement of event II, dis-

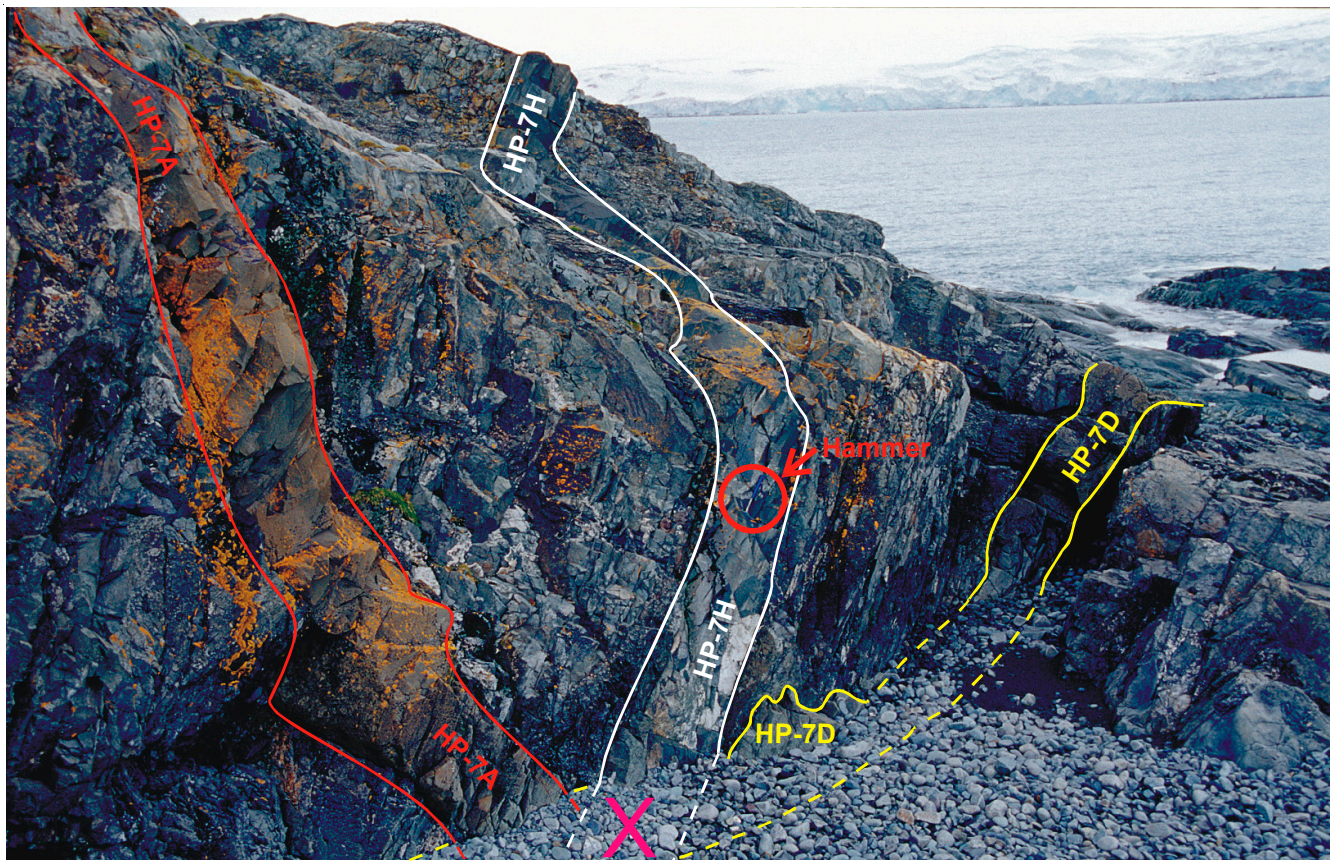

Fig. 2-14: Overview of the "dyke-triple-junction" in Area II. Dyke HP-7D runs parallel to the vertical rock wall, the crossing is located beneath the beach gravel marked by the X. Excavated crossing see below (Fig. 2-15). View towards W, Hammer as scale.

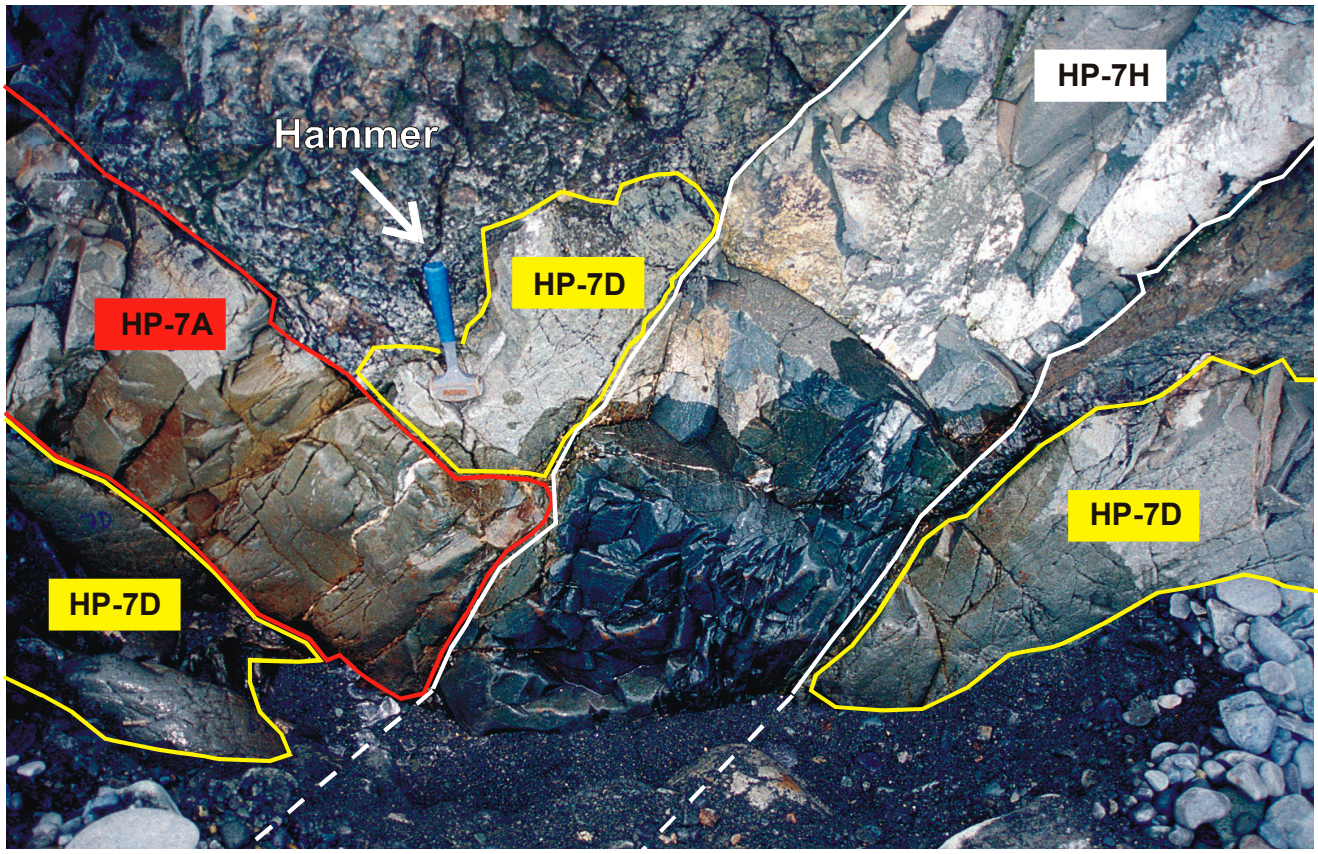

Fig. 2-15: The excavated dyke-crossing. The oldest dyke is HP-7D, with a fragment of it sandwiched between the two other dykes, followed by HP-7A and HP-7H (youngest). Hammer as scale.

placing the dykes already present but not affecting the younger dykes of this event.
The mineralogy is typical and not diagnostic for the different events. However, one dyke of event III must be mentioned specially because of the only occurrence of zircon. In a thin section of HP-12 (Fig. 2-9, 3-6) two euhedral zircon grains of approx. 80 µm length have been observed. For a detailed description see chapter 3.
(Hydrothermal) alteration is common in all dyke groups and reflected by typical minerals like albite, calcite, chlorite, epidote, quartz, sericite and sometimes zeolite. In order to obtain a measure for the degree of alteration, an alteration index (AI) has been introduced reflecting the degree of alteration observed under the microscope (Table 2-2) and applied to all investigated dykes. As expected, events I & II have the highest average AIs, and only events V & VI seem to be considerably fresher (Table 2-1). This pattern is confirmed by the LOIs obtained from ICP-MS analyses. The relatively high degree of alteration could be due to hydrothermal fluids circulating during a later phase in the fractured and jointed dykes. However, the type and distribution of the alteration minerals may also point towards autometasomatism shortly after crystallization of the magma. This would suggest that the dykes have been altered by fluids related to their own emplacement, and not during a later hydrothermal event.

Tectonic characteristics of the dykes

Most of the dykes can be assigned to the first order shear system (Table 2-3, Fig. 2-16). Event I (144/74 SW) intruded along the sinistral first order shear direction (S_{1s}).
The dykes of the second intrusive event can not be assigned unequivocally. 50% of them (average orientation 26/72 SE) may be assigned to bc-joints or (folding axis parallel) h0l-joints, the rest to the sinistral second order shear direction (S_{2s}; dykes averaging 52/64 NW).
Intrusive event III (74/63 SE) uniformly represents a dextral first order shear direction (S_{1d}), though scattering considerably (60-96/46-90 SE). Only the (probably) youngest dyke of this generation, HP-28 (177/54 E), may have intruded either along the dextral second order shear direction (S_{2d}) or along a h0l-joint. The same applies to the (probably) oldest dyke of event IV, HP-1B (171/31 E), which took a similar direction as HP-28 and can be interpreted accordingly. Afterwards, most of the dykes belonging to event IV intruded along the sinistral first order shear direction (S_{1s}; dykes averaging 149/89 SW). However, two dykes (HP-27 and HP-22) may be assigned to the ac-direction (119/65 SW).

intrusive event	used joint system	average orientation of the dykes
VI	**S_{1s}**	**135/79 SW**
V	**S_{1d}**	**69/75 SE**
IV	**S_{1s}** , S_{2d}, h0l, ac?	**149/89 SW**; 119/65 SW (ac)
III	**S_{1d}** , S_{2d}, h0l?	**74/63 SE**; 177/54 E (S_{2d})
II	**bc, h0l?**, S_{2s}	**26/72 SE**; 52/64 NW (S_{2s})
I	**S_{1s}**	**144/74 SW**

Table 2-3: Overview of the joint systems used by the intrusive events and their average orientation. Prevailing directions printed bold.

Two dykes representing event V intruded once more along the dextral first order shear direction (S_{1d}; dykes averaging 69/75 SE) and the youngest dyke within the investigation area, HP-23 (event VI), along the sinistral first order shear direction (S_{1s}; 135/79 SW).

The fabric of the dykes themselves displays joints of different origin, often healed with qz and/or cc. One group is represented by dyke-parallel and, above all, more or less dyke-orthogonal joints (columnar jointing). They are interpreted as cooling joints and not analyzed further. Their poles lie on great circles orthogonal and subparallel to the dykes themselves (dyke-parallel and -orthogonal joints, respectively). Joints of tectonic origin observed within the dykes can be indexed similarly as the joints cutting the host rock: the dextral first order shearing cutting the dykes averages 94/77 S, the sinistral first order shear direction 139/87 SW, the dextral second order shearing produced 0/85 E oriented joints and the sinistral second order shearing a 50/80 NW orientation.

Joints running through both, the host rock and the dyke, often change their orientation slightly when entering the dyke. This is reflected by the aforementioned slightly different average orientation of the joints within the dykes, as compared to the orientations observed in the host rock. It can be explained by the lithological differences between the sedimentary MBF and the magmatic material of the dykes, which apparently does not allow straight propagation of the joints when crossing lithological boundaries.

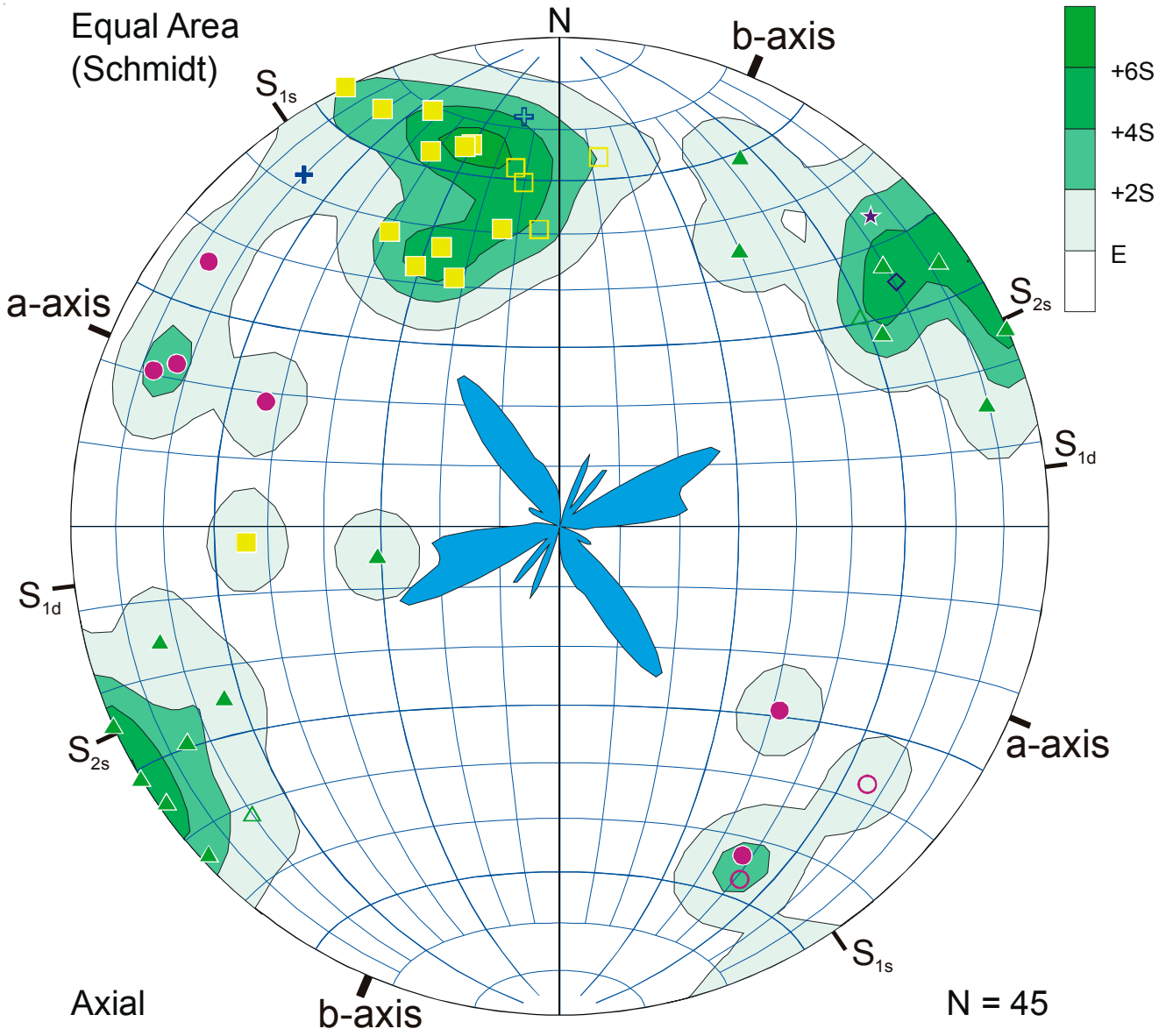

Abbr.	Explanation and orientation / strike
b-axis	203/10 (folding axis)
a-axis	113/2
S_{1d}	dextral first order shear direction: 83°
S_{1s}	sinistral first order shear direction: 146°
S_{2s}	sinistral second order shear direction: 65°

- Intrusive Event VI
- Intrusive Event V
- Intrusive Event IV
- Intrusive Event III
- Intrusive Event II
- Intrusive Event I

Filled symbols: dykes of Area I
Open symbols: beach-dykes and Area II

The existence of tectonic, non-cooling joints within the dykes, and the joints observed crossing the dyke rims show that the general stress field outlasted the dyke formation at similar geometrical conditions.

Fig. 2-16: Orientation of the dykes on Hurd Peninsula as observed in the field, and indication of the structural directions (strike of folding axis and joint systems as observed in the host rock). The rose diagram reflects the principal strike directions of the dykes. Contouring as explained in Fig. 2-2. Poles to planes. The supplementary table indicates the average strike of the different shear directions as deduced from the dykes. Note the existence of the second order shear system as discussed by Schmidt [1932].

2.2 Nelson Island

This member of the South Shetland Islands is located directly SW of King George Island (Fig. 2-18), stretching from 58° 50' to 59° 14.5' W, and from 62° 14' to 62° 21' S.
It is one of the least visited and therefore least known islands of the archipelago. It comprises approx. 160 km^2, but an estimated 95% of this area are covered by a permanent icecap, the Nelson Ice Dome. During austral summer 2000/2001 several day-trips have been undertaken by Zodiac boat from the Argentine base 'Jubany' (Potter Peninsula, King George Island, Fig. 2-18) to O'Cain Point (11.9 km), New World Point (11.3 km) and Duthoit Point (13.6 km).

2.2.1 Regional Geology

The lithology of the host rocks as of the dykes is fairly the same as on adjacent King George Island. The investigated dykes are basaltic, (basaltic) andesitic and dacitic in composition and are hosted by a calc-alkaline, mainly basaltic to andesitic stratiform succession of lavas and pyroclastic rocks. This succession is typically indurated, often closely jointed, and primary bedding is mostly difficult to recognize.

Epidote and/or pyrite mineralizations are locally abundant, as are jasper veins cutting the volcanic rocks (Fig. 2-17). The clastic (normally fine to coarse-grained lapilli) rocks feature a green, red-brown or purple color and occur subordinately to the lavas, usually forming beds not thicker than a few meters. At Harmony Point (SW Nelson Island), thin-bedded volcanic mudstones and fine volcanic sandstones have been observed, as well as a 1 cm thick bed of coal, conglomerates and fragments of carbonized wood [Smellie et al. 1984].

Further members of the succession are intrusive bodies of variable size and lithology, often microgabbros and gabbros. Such a gabbroic intrusive body has been recognized during field work at New World Point (Fig. 2-18), featuring a grain size of approx. 2-3 mm. A prominent feature of this intrusive body is its high grade of alteration and the way this alteration is distributed in the rock. Granular disintegration is common, but the crumbly parts often cut the fresher ones in a dyke-like manner with very sharp alteration-frontiers (mm-size). Locally the percentage of strongly alterated rock is higher than that of the remaining fresher part. Maybe this type of apparently dyke-like granular disintegration has been caused by fluids migrating along joints and propagating from there orthogonal to the joints into the rock, with a sharply defined alteration front. This gabbroic body shows many features similar to the much bigger and well-known intrusive body on Barton Peninsula (Noel Hill). Maybe their genesis is related and part of the same intrusive cycle.

Magmatic dykes have been found cropping out at O'Cain Point and New World Point, but none at Duthoit Point. Their thickness ranges from 2.5 m to 10 m, the lithology is characterized by a finegrained, light-grey fresh surface, sometimes with abundant pl- and px-phenocrysts of up to 5 mm in size. Maybe because of their higher resistance against erosion, the dykes do often form monadnocks and prominent morphologic reliefs.
Though O'Cain Point and New World Point belong to the same tectonic unit (Barton Horst) as Weaver and Barton Peninsula on King George Island, the average alteration index is slightly lower here (Fig. 2-21). For discussion of the tectonic units of King

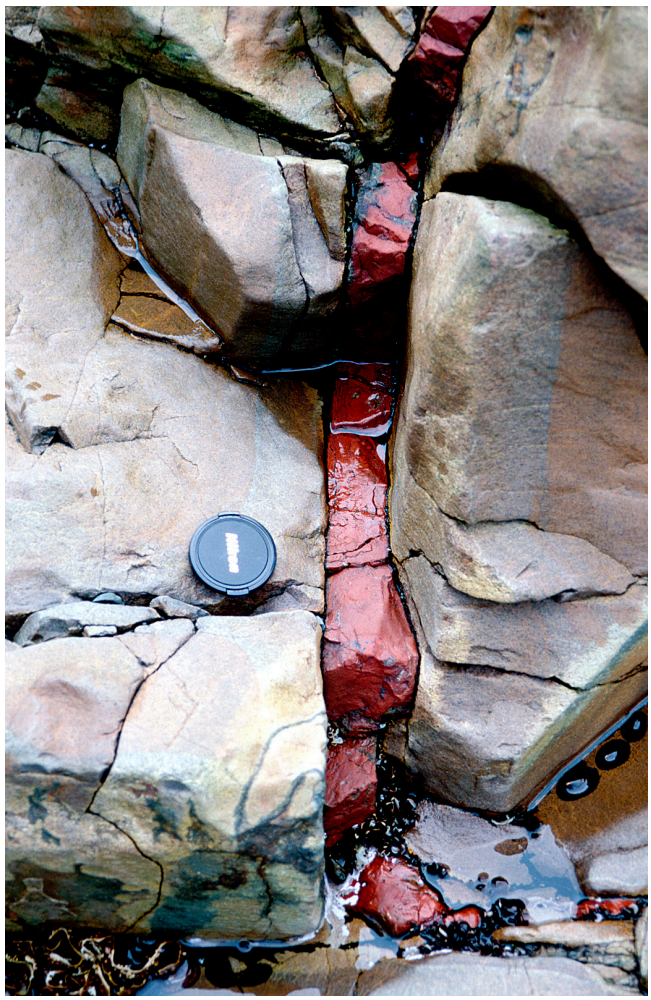

Fig. 2-17: Jasper vein cutting the volcanic host rock at New World Point, Nelson Island. Camera cap (6 cm diameter) as scale.

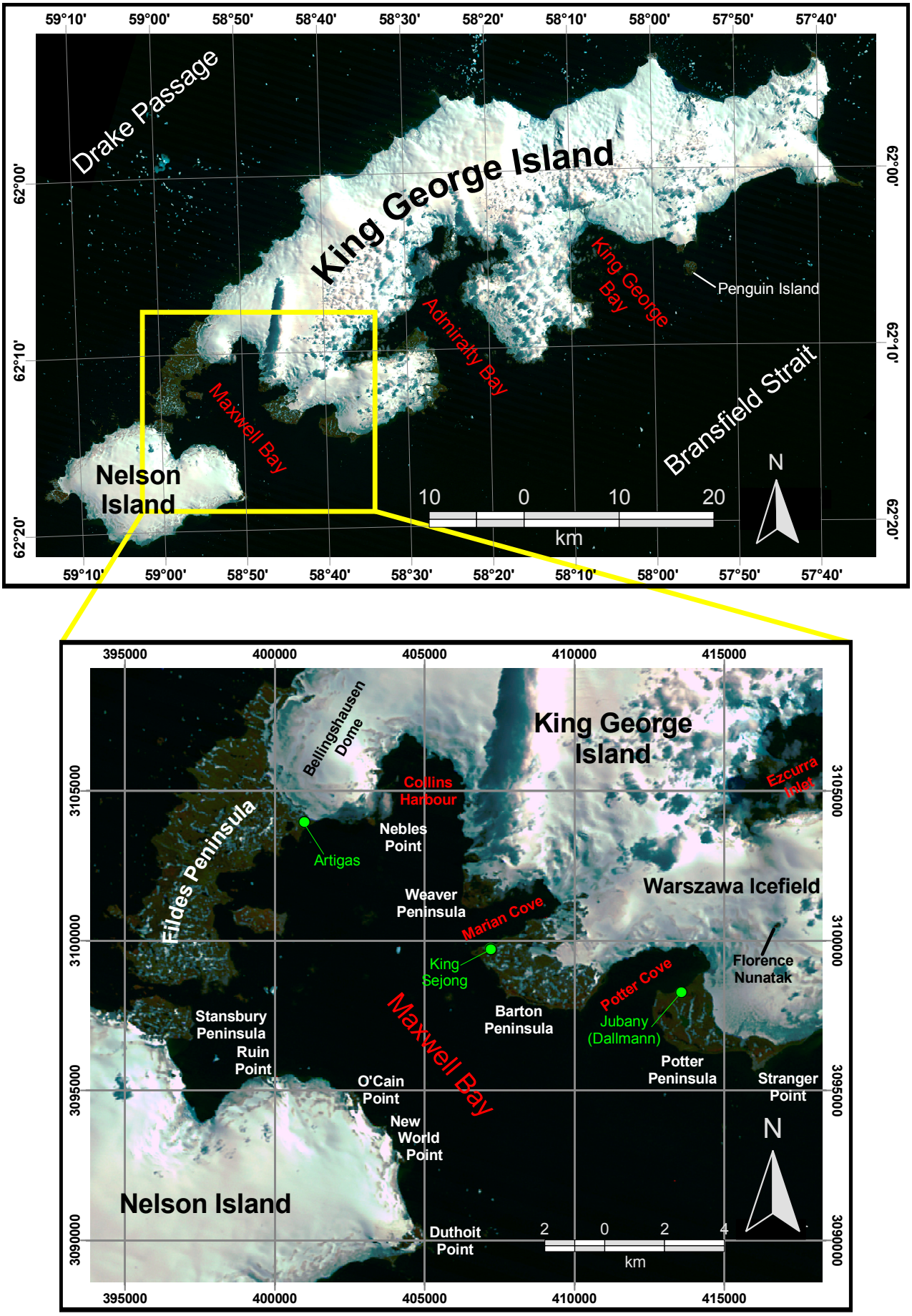

Fig. 2-18: King George and Nelson Island (upper map) and areas around Maxwell Bay visited for field work (lower map, UTM, WGS 84). Created and processed by S. Kraus (2004). Satellite image courtesy of J. Sievers (Bundesamt für Kartographie und Geodäsie (BKG, formerly IFAG); Frankfurt am Main, Germany). Please refer also to Bennat et al. [1998]. The images are subsets from the "Geoscientific Information System Antarctica (GIA)": LandSAT TM mosaic Antarctic Peninsula (pixel resolution 30 m).

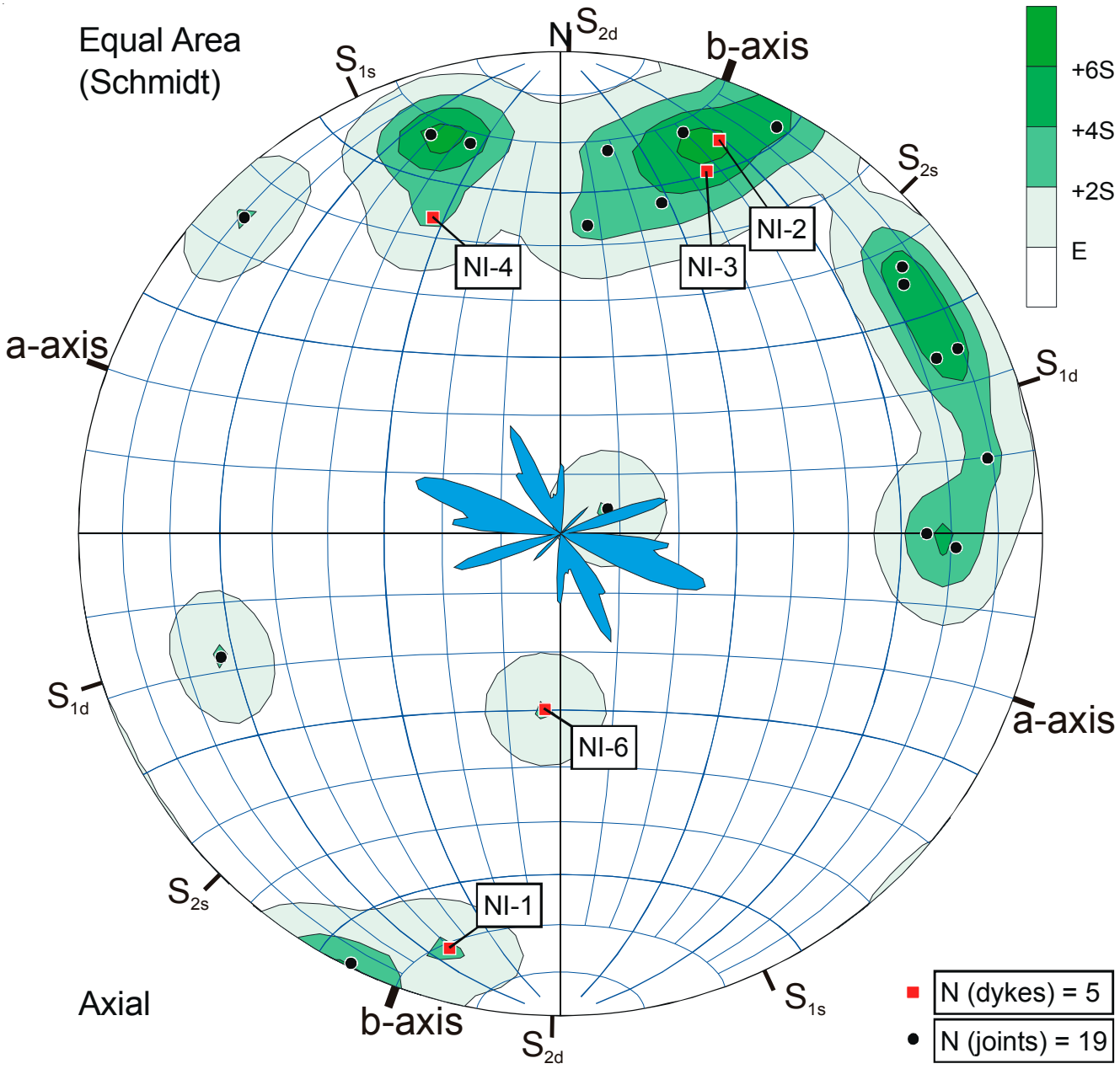

Abbr.	Explanation (with average strike)
b-axis	20°
a-axis	110°
ac	ac-joints: 110/80 S
S_{1d}	dextral first order shear direction: 72°
S_{1s}	sinistral first order shear direction: 155°
S_{2d}	dextral second order shear direction: 1°
S_{2s}	sinistral second order shear direction: 45°

Fig. 2-19: Schmidt net showing the orientation of joints (black circles) and dykes (red squares) on Nelson Island. Cooling joints within the dykes are not plotted. Density contours calculated as explained in Fig. 2-2. Principal strike directions reflected by the rose diagram in the center. The tectonic directions shown have been determined assuming a stress field oriented similar as on Hurd Peninsula. Poles to planes.

George Island and the respective characteristics please refer to chapter 2.3.

2.2.2 Tectonics

An eye-catching difference to the rocks investigated on Hurd Peninsula is the obviously stronger brittle deformation, giving some dykes on Nelson Island a virtually shattered appearance (Fig. 2-20).

In contrast to the conspicuous folding on Hurd Peninsula (Livingston Island), no direct signs of folding could be observed on Nelson Island. Therefore, no local folding axis could be determined, and, as a consequence, the shear directions defined by the joint

Fig. 2-20: Dyke NI-1 cropping out at O'Cain Point, Nelson Island. It forms an about 15 m high monadnock and is about 3 m thick. Note the shattered appearance, evidence for strong brittle deformation, possibly intensified by cryoclastic weathering.

systems have to be assigned with caution. Cooling joints within the dykes are present parallel and orthogonal to the dykes, but excluded from further analysis.

However, the joints as well as the orientation of the dykes indicate, that the same directions as observed on Hurd Peninsula are expressed on Nelson Island. Assuming, that the orientation of the b-axis of the overall stress regime on Nelson Island is at least similar as on Hurd Peninsula, the observed shear directions can tentatively be assigned as follows:

One prominent direction expressed by joints and also taken by some of the dykes (NI-1, NI-2, NI-3 and maybe NI-6, Fig. 2-19) averages 111/80 S and could correspond well to the ac-direction observed on Hurd Peninsula. Indeed, the difference is only 3° and it is very sharply defined with a scatter no more than ± 5°.

A first order shear system is weakly developed dextral (S_{1d}, averaging 72/71S) and much stronger sinistral (S_{1s}, averaging 151/90 NE), at angles of 39° and 40° to the a-axis, respectively. Dyke NI-4 can be assigned to S_{1d}.

The second order shear system is also present, clearly expressed dextral (S_{2d}, averaging 177/72 W) but only very weakly sinistral (S_{2s}, 45/82 SE) in both cases at an angle of 24° to the b-axis.

There is no final evidence that these directions are assigned correctly, but the fact that they differ only approx. 5° (except S_{1d}) from the ones observed on Hurd Peninsula, indicates that the tectonic regime might have been the same.

The only published work [Fontoura et al. 1988] mentioning the orientation of dykes on Nelson Island reports N-S (0-10°), E-W (80-90°) and NE-SW (approx. 45°) directions as prevailing strikes of 49 dykes cropping out on Stansbury Peninsula (Fig. 2-18). Their N-S direction could correspond to S_{2d}, the E-W direction to S_{1d} and their NE-SW direction to S_{2s}.

2.3 King George Island

King George Island (Fig. 2-18) is situated in the middle of the South Shetland Islands arc at (57° 35'-59° 01' W) and (61° 54' - 62° 16' S). It comprises about 1185 km^2, measures approx. 80 km in NE-SW direction and about 30 km across in NW-SE direction. During the austral summers 1998/1999, 2000/2001 and 2001/2002, extensive field work has been carried out predominantly around Maxwell Bay (Potter Peninsula, Barton Peninsula, Weaver Peninsula and Fildes Peninsula), moreover in Admiralty Bay between the shores of Bransfield Strait and Ezcurra Inlet, around Ezcurra Inlet including Dufayel Island and further N towards Mackellar Inlet.

General tectonic outlines

Like the whole archipelago, King George Island has been subjected to Cenozoic structural deformation related to the plate-tectonic history of the southeastern margin of the Pacific Ocean. This deformation resulted in a network of mainly strike-slip faults, expressed as several generations of tectonic directions which are best visible in the axial parts of the island (Fig. 2-21). Large- and small-scale folding related to the regional tectonic tension pattern like observed on Livingston Island (Hurd Peninsula), can be observed nowhere on King George Island. Only locally, intense folding is evident, but this deformation is most probably related to the movement of the above mentioned, deep cutting strike-slip faults and restricted to the areas adjacent to these faults. Therefore, no folding axes reflecting the regional stress field could be deduced from tectonic measurements carried out on King George Island. However, the following three major tectonic and structural elements can be distinguished:

(1) A first deformation phase produced NE-SW running, deep cutting longitudinal strike-slip faults parallel to the axis of the South Shetland Islands archipelago [Birkenmajer 1982a]. They influence to a great extent the shape of the islands and are reflected by the location and course of many fjord-like bays and coves like Ezcurra Inlet, Potter Cove or also Collins Harbour (all on King George Island, Fig. 2-18). Also South Bay and False Bay, framing Hurd Peninsula on Livingston Island (Fig. 2-1), owe their existence most likely to these strike-slip faults. Even the often linear arrangement of Cenozoic volcanic centres on King George Island may be related to them. Possibly these faults indicate a compressional (transpressional) tectonic regime during that time. This fault generation is assumed to have been active from Eocene to Miocene [Birkenmajer 1989]. On King George Island, two major faults belong to this first generation and have a deep impact on the island's geology:

(a) The *Ezcurra Fault* (named after the Ezcurra Inlet in Admiralty Bay, Fig. 2-21) has originally been interpreted as a normal fault [Barton 1965] and was later redefined as a dextral strike-slip fault [Birkenmajer 1980b]. It runs NE-SW and can be traced over more than 60 km all along King George Island and Nelson Island. It has been active at least until Neogene, probably Upper Miocene or around the Miocene-Pliocene boundary, proved by displaced plant-bearing strata of Early-Middle Miocene age [Birkenmajer 1982a]. Though it postdates the King George Island Supergroup (see below), it predates the Kraków Icefield Supergroup and has apparently been active during the time of the Admiralty Bay Group hypabyssal intrusions [Birkenmajer 1982a]. Along its course, the Ezcurra Fault is several times offset by transversal faults, sometimes up to more than 5 km (Fig. 2-21). Birkenmajer [1980b] calculated the apparent vertical throw of this fault to at least 2.5 km but states the amount of dextral horizontal movement to remain unknown.

(b) Another longitudinal fault running parallel to the aforementioned one is the *Collins Fault* (named after Collins Harbour in Maxwell Bay). It is possibly also a strike-slip fault, dissecting both Nelson and King George Island in a NE-SW direction like the Ezcurra Fault, but running 10-20 km NW of the latter. It has also been offset several times by transversal faults, sometimes as much as 15 km. Its age corresponds most likely to that of the Ezcurra Fault (also displacing Lower-Middle Miocene plant-bearing strata), but up to now a precise scale of its vertical and horizontal translation remains unknown. However, the vertical displacement of the northwestern tectonic unit, the downthrown Fildes Block, along the Collins Fault has been estimated at approx. 4 km [Birkenmajer 1982a].

(2) A subsequently produced set of NW-SE trending, predominantly strike-slip transversal faults (both dextral and sinistral) represents a second deformation phase during Late Cenozoic times and offsets

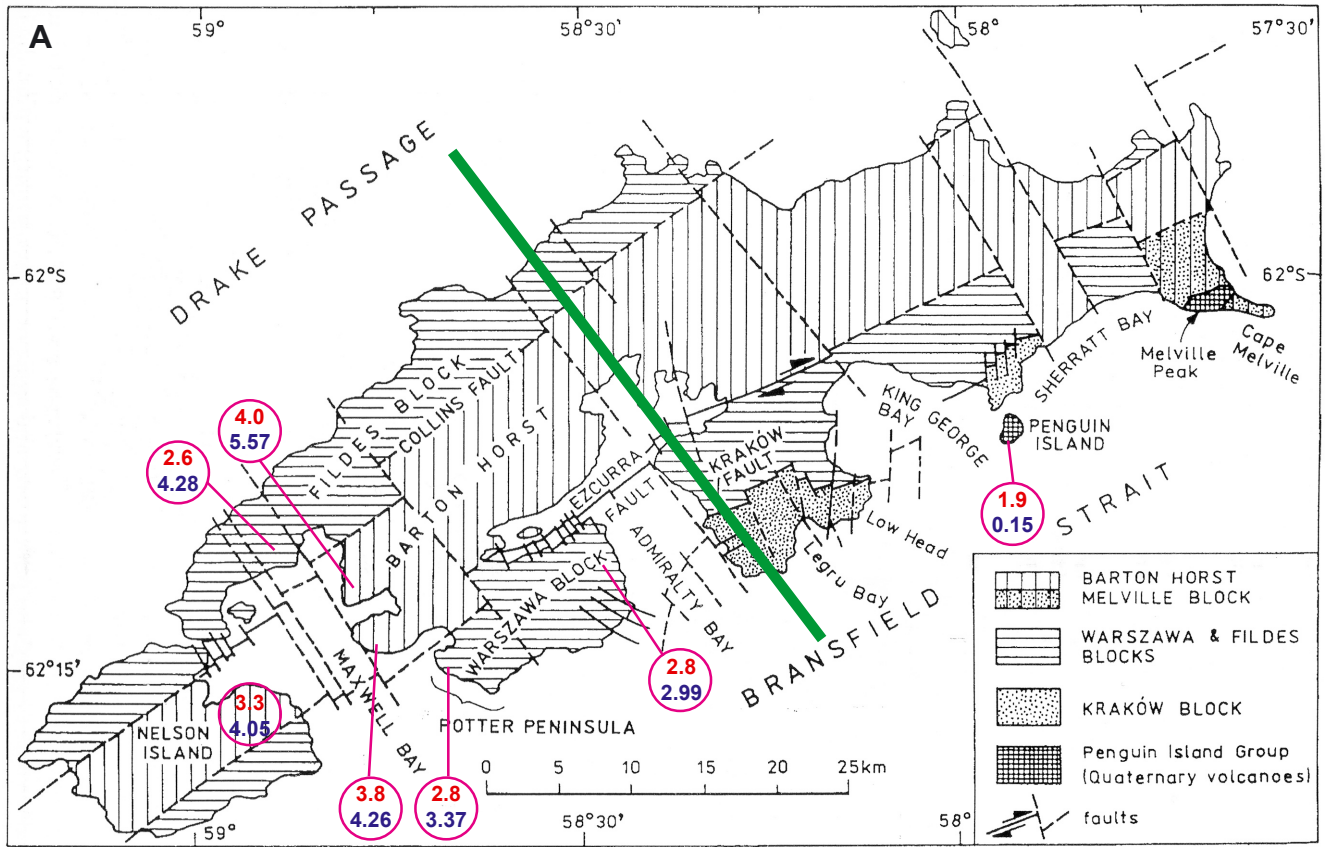

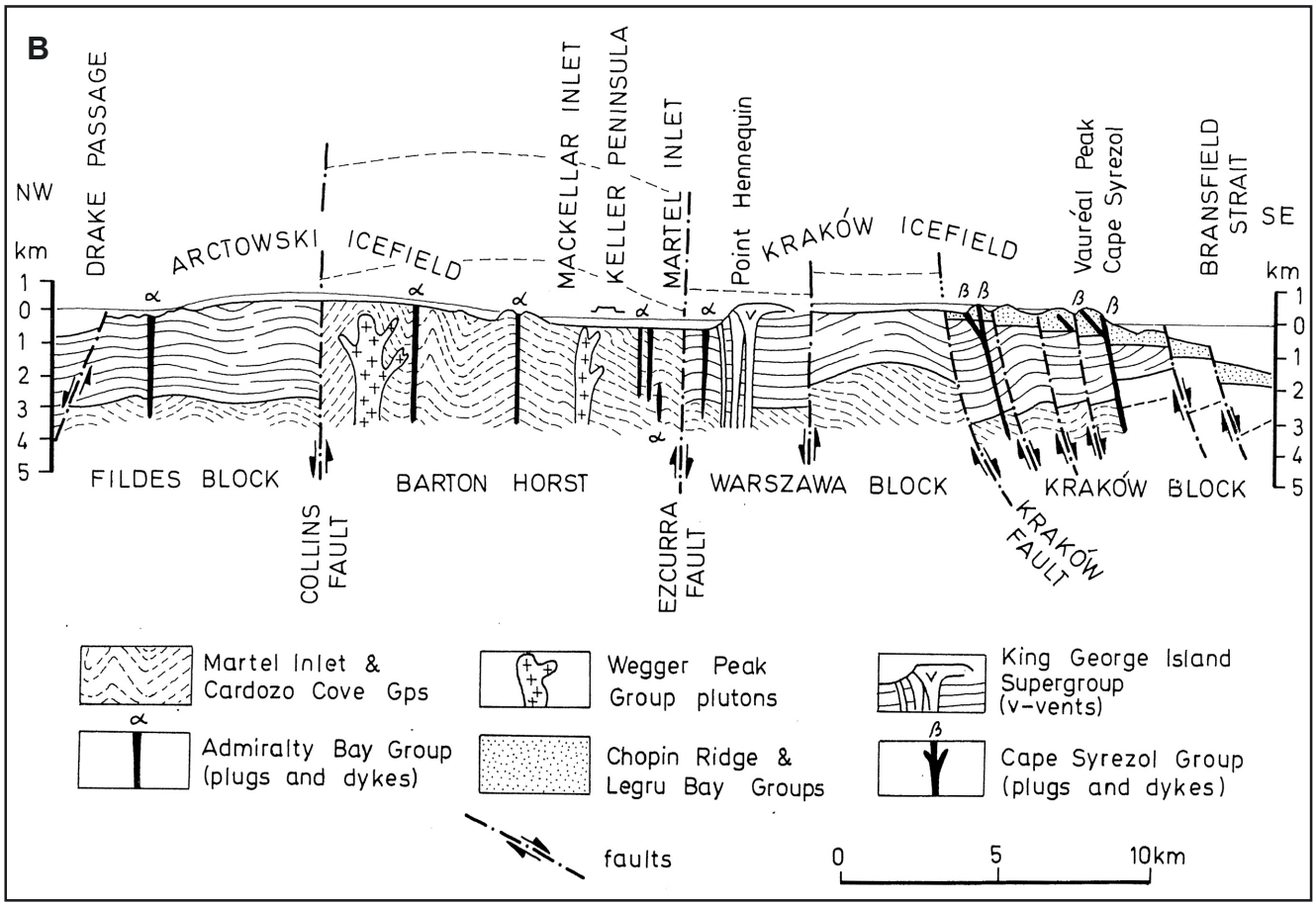

Fig. 2-21: (A) Structural elements, tectonic units and alteration of King George and Nelson Island (modified after Birkenmajer 1998b). The green line defines the location of the cross section. The red numbers indicate the average alteration index (AI, for explanation see Table 2-2), the blue numbers the average LOI of the dykes cropping out in the respective areas. Note the correlation between alteration and tectonic architecture of the two islands. Hurd Peninsula (Livingston Island, not shown in this Fig.) has an average AI of 3.4 and an average LOI of 4.81.
(B) NW-SE oriented cross section showing the tectonic architecture of King George Island (taken from Birkenmajer 2003, p. 16).

the faults of the first generation to a distance of up to 15 km, though they are shorter and less deep-cutting than the ones produced during the first phase. They are by far more numerous, but on the other hand not reflected that clearly by the island's morphology like the strike-slip faults of the first phase. Probably they have formed after cessation of strike-slip movement along the Collins and Ezcurra Faults and other subparallel linear fractures. Their age is probably early Pliocene [Birkenmajer 1982a]. This fault generation possibly marks the change from a compressional (transpressional) to a tensional (transtensional) tectonic regime in the South Shetland Islands volcanic arc.

(3) During a third deformation phase, gravity block-faulting caused differently oriented, often radial structures expressed only along the coast of Bransfield Strait (Fig. 2-21), involving predominantly the youngest units of the late Cenozoic succession on King George Island, the Kraków Block (see below). The character of these faults is transversal or radial, partly strike-slip, but predominantly dip-slip. Maybe they are related to subsidence of the Bransfield Basin and therefore to the opening of Bransfield Strait. This would explain the exclusive occurrence along the shores of Bransfield Strait and maybe also their radial pattern. Given the probable Pliocene age of the second generation faults, these radial structures should be even younger, maybe Late Pliocene or even Pleistocene.

The aforementioned two deep-cutting faults of the first generation separate Nelson and King George Island into three elongated fragments. The part lying between these two strike-slip faults is bordered by them and has often been referred to as the 'backbone' of King George Island, named *Barton Horst* (after Barton Peninsula, Maxwell Bay, Fig. 2-21). This tectonic unit has obviously been lifted considerably with respect to the NW and SE lying blocks, with a vertical displacement corresponding approx. to the scale of movement determined for the Collins and Ezcurra Faults, i.e. between 2.5 and 4 km. As a consequence, the Barton Horst today exhibits the deeply eroded lower levels of the stratiform volcanic sequence of the volcanic arc, whereas the downthrown blocks bordering it to the NW and SE represent much higher parts (Fig. 2-21B).

The downthrown block bordering the Barton Horst to the NW is called *Fildes Block* (named after Fildes Peninsula in SW King George Island, Fig. 2-18, 2-21). Like all other tectonic units it is also strongly offset by the second generation transversal faults, especially in the northernmost parts of King George Island.

To the SE, the Barton Horst is bordered by the so-called *Warszawa Block* (Fig. 2-21), like the Fildes Block a downthrown tectonic unit. It forms a broad anticline between Ezcurra Inlet and Bransfield Strait [Birkenmajer 1980b], though strong folding is restricted locally to the vicinity of Ezcurra Fault in the area of Ezcurra Inlet, probably the result of strike-slip movements along the fault.

Another tectonic unit borders the aforementioned Warszawa Block to the SE and is called *Kraków Block* (Fig. 2-21). With respect to the units lying further to the NW it is downthrown along the dip-slip Kraków Fault system [Birkenmajer 1982a]. The area covered by this unit is far smaller than the above described three main units of King George Island. The Kraków Block is exposed only along the shores of Bransfield Strait between Admiralty and King George Bay, moreover in Sherratt Bay opposite Penguin Island (Fig. 2-21). It is dissected by the faults of the third generation described above.

Regional geology and lithology

In contrast to Hurd Peninsula (Livingston Island), where a pre-arc, turbiditic sedimentary sequence represents the host rock of the investigated dykes, on King George Island non-volcanic sediments are scarce. Instead, the stratigraphy of the island comprises predominantly ?Upper Cretaceous to Lower Miocene [Birkenmajer 1989], mostly calc-alkaline effusive and intrusive suites connected mainly to the subaerial volcanic activity of the arc. Thus, the products of this volcanism are terrestrial basaltic, andesitic and dacitic lavas, pyroclastic rocks and volcanic sediments which sometimes feature terrestrial plant fossils like carbonized wood and leave imprints. The up to 3000 m thick volcanic suite [Birkenmajer 1980a, 1994] is intruded rarely by moderate-scale plutons, scarce sills, and more often by hypabyssal dykes and plugs of basaltic to andesitic chemism. Being of minor importance before Oligocene, fossiliferous marine and glaciomarine sediments become more frequent during Oligocene and Lower Miocene [Birkenmajer 1989].

A lithostratigraphy for King George Island has been introduced and defined by many authors [e.g. Hawkes 1961; Barton 1965; Smellie et al. 1984; Birkenmajer 1980a, 1989]. Though differing considerably in other aspects, nearly all authors agree that the lithological characteristics observed on King George Island are tightly bound to the island's subdivision into several tectonic units (see above at general tectonic outlines).

The most comprehensive and detailed lithostratigraphy so far has been set up by Birkenmajer [e.g. 1980a, 1989]. He introduced an older, up to 3000 m thick, mainly calc-alkaline suite of stratiform subaerial volcanics as King George Island Supergroup (KGIS), subdivided further into numerous units of group rank. According to Birkenmajer et al. [1982], this supergroup spans a time range between Campanian (77 ± 4 Ma) and Chattian (24.5 ± 0.5 Ma). For a detailed lithological description and geochronological data obtained for the different groups see Birkenmajer [1980a, 1989], Birkenmajer et al. [1981, 1982, 1991] and references therein.

A younger, approx. 600 m thick stratiform volcanic-sedimentary succession, the Kraków Icefield Supergroup (KIS, Pliocene and early Pleistocene?), has also been subdivided further into several groups [Birkenmajer 1980a]. The intrusive suites piercing King George Island have been introduced by the same author as Wegger Peak Group (WPG, plutons), Admiralty Bay Group (ABG) and Cape Syrezol Group (CSG), the latter two consisting of hypabyssal intrusions. As already mentioned before, the complete arc-related sequence of the South Shetland Islands has been dated to span the range between 130 and 14 Ma, with a renewal of magmatic activity during Pleistocene and Holocene times [e.g. Birkenmajer et al. 1991; Pankhurst & Smellie 1983; Smellie et al. 1984; Soliani et al. 1988].

Due to its upthrown nature, the *Barton Horst* exhibits the deeply eroded lower levels and oldest parts of the volcanic succession. The lithology comprises considerably altered, mainly andesitic stratiform volcanics (KGIS) intruded by numerous gabbroic to granodioritic plutons of small to moderate size (WPG) and a younger generation of hypabyssal, basaltic to andesitic plugs and dykes (ABG) [Birkenmajer 1982a].

Two main characteristics distinguish the Barton Horst from the adjacent downthrown blocks: (1) The exclusive occurrence of the gabbroic to granodioritic plutons of the Wegger Peak Group. Probably these plutons intruded also the lower levels of the other tectonic units but are exhibited only in Barton Horst due to elevation and subsequent erosion. One prominent example for such a pluton is Noel Hill on Barton Peninsula. (2) the considerably high degree of alteration, sometimes resulting in completely altered rocks composed exclusively of secondary minerals. This strong alteration may be due to a closer vicinity to the metasomatic front of the subduction zone, or also to metasomatism related to the aforementioned plutons. It affects also the dykes cropping out in the areas belonging to the Barton Horst, reflected by the considerably higher degree of alteration as compared to the adjacent tectonic blocks (Fig. 2-21). The average AI assigned to Hurd Peninsula (Livingston Island) is 3.4 (average LOI 4.81), thus correlating well with the AIs observed in the Barton Horst. Maybe this indicates, that also on Livingston Island there exists such an upthrown horst structure featuring the corresponding high degree of alteration.

The age of the rocks building up Barton Horst ranges between ?Late Cretaceous and Early Eocene, but with Paleocene ages prevailing [Birkenmajer 1989].

The adjacent *Fildes* and *Warszawa Blocks* represent corresponding levels of the volcanic stratiform succession and are both downthrown with respect to the axial elevated Barton Horst (Fig. 2-21). Thus, not only their lithology is quite similar, but also their degree of alteration and their age. The lithology comprises arc-related, stratiform volcanic rocks of predominantly basaltic to andesitic composition (KGIS), sometimes with intercalated sediments, intruded by hypabyssal plugs and dykes (ABG). Only the moderate-scale plutons are absent because they are restricted to the Barton Horst. The degree of alteration within the Fildes and Warszawa Blocks is relatively low as compared to the rocks of the Barton Horst, and the obtained ages range between Mid Paleocene (59 Ma) and Mid Eocene (42 Ma) for the Fildes Block [Fensterseifer et al. 1988; Pankhurst & Smellie 1983; Smellie et al. 1984; Soliani et al. 1988] and ?Late Cretaceous to Oligocene for the Warszawa Block [Birkenmajer 1989], but with Eocene ages prevailing.

A younger suite of mainly Eocene to Upper Oligocene terrestrial lavas, pyroclastics, agglomerates, lahars and also terrestrial and marine glaciogenic de-

posits (KIS) crops out on *Kraków Block*, the small tectonic unit bordering the Warszawa Block to the SE (Fig. 2-21).
At Cape Melville (Melville Peninsula, Fig. 2-21), Early Miocene (23.6 - approx. 20 Ma) terrestrial basaltic lavas and marine fossiliferous, partly pyroclastic, glaciomarine and non-glacial deposits occur and are assigned to the so-called *Melville Block*.

The youngest rocks cropping out on- and offshore King George Island are bound to quaternary volcanoes related to the backarc volcanism of Bransfield Strait. They comprise mildly alkaline olivine-bearing basalts occurring on Penguin Island (dormant) and at Melville Peak (extinct).

2.3.1 Fildes Peninsula & Nebles Point

Fildes Peninsula is located at the southwestern end of King George Island (Fig. 2-18) and home to scientific bases of Chile, China, Russia and Uruguay. A short gravel airstrip is operated here by Chile and represents - besides natural flat surfaces on the glacier - the only possibility in the whole South Shetland Islands archipelago for airplanes (mostly C-130 Hercules) to touch down. Fildes Peninsula extends approx. 10 km from NE to SW and approx. 3.5 km in NW-SE direction, covering about 30 km^2 and thus being by far the largest ice-free area on King George Island.

General characteristics

Field work has been carried out on Fildes Peninsula and at Nebles Point during a short stay in January 2001, investigating the area around the Uruguayan Base 'Artigas' and the coast towards Nebles Point (Fig. 2-18). The host rocks comprise the lithology described above and the dykes do often appear morphologically as monadnocks, apparently because of higher resistance against erosion.

The thickness of the dykes varies between 2 and 10 m and their composition is predominantly basaltic, sometimes andesitic. An eyecatching fact is the relative freshness of the dykes as compared to the average alteration observed in other parts of King George Island and also Nelson Island (Fig. 2-21). Indeed, the dykes investigated on Fildes Peninsula show the lowest alteration index of all investigation areas (except for Penguin Island). Qz-cc-mineralizations do occur, but are mostly restricted to joint planes and do not extend into the dykes. Xenoliths occur seldom, their magmatic character and their mineralogy pointing towards an origin from the stratiform volcanic sequence by which the dykes are hosted.
Close to the Uruguayan Base, a 4 m thick, 140° striking basaltic dyke (FP-1, UTM coordinates 21E 401228 / 3103763) is displaced several times en echelon towards SW. The displacement is dextral and occurs along NE-SW striking small faults parallel to the deep-cutting Collins Fault which runs at about 2.3 km distance (Fig. 2-21). Maybe they represent subordinate, secondary faults related to the movement along the deep-cutting strike-slip fault. The sense of the Collins Fault remains unknown up to now, but maybe the sense of these subordinate faults indicates also a dextral character for the Collins Fault.

Tectonics

Like on Nelson Island, no folding axis could be determined directly on King George Island. Strong folding related to the strike-slip translation along Ezcurra Fault has been reported from Ezcurra Inlet [Birkenmajer 1982a] but is not suitable to reconstruct deformation phases related to the regional tension pattern. Therefore, again the cautious attempt has been undertaken to interpret the observed tectonic directions (joints and dykes) within the frame of the directions identified on Hurd Peninsula (Livingston Island). Due to the very short stay on Fildes Peninsula and to bad weather, only 8 dykes were investigated and few joint measurements undertaken (Fig. 2-22). However, the results are in good agreement with the data from Hurd Peninsula and Nelson Island.
The directions determined on Fildes Peninsula differ only 5-7° from the ones observed on Hurd Peninsula. A strongly expressed direction of 109° could correspond to the a-axis, ac-joints are apparently oriented 109/78 N and taken by two dykes and some joints. The corresponding b-axis can be deduced as 19°, a dextral first order shear system as 89/81 S and a sinistral first order shear system as 140/83 SW. A second order shear system is not expressed in the data, maybe due to the low number of investigated dykes and joints.

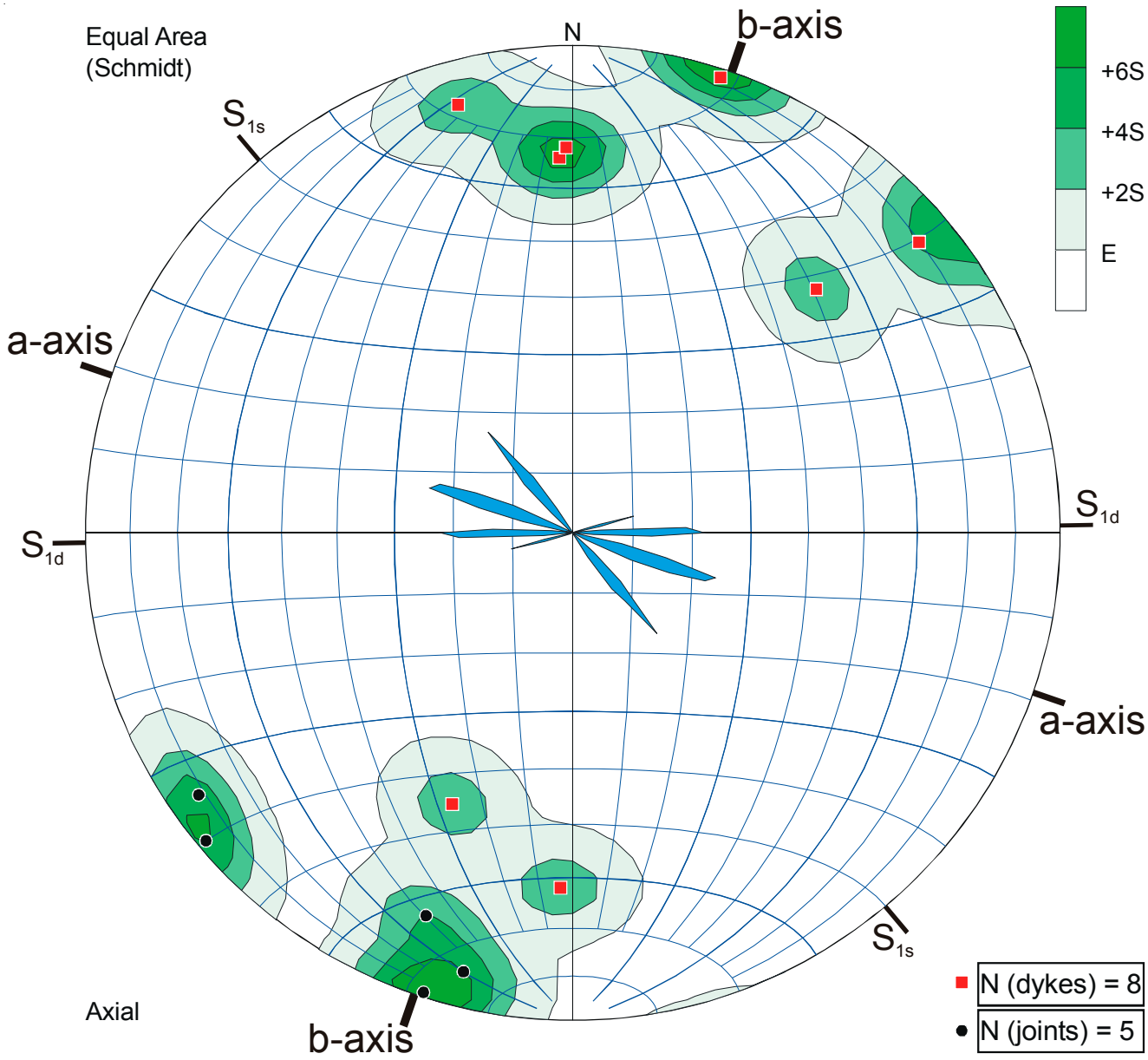

Abbr.	Explanation (with average strike)
b-axis	19°
a-axis	109°
ac	ac-joints: 109/78 N
S_{1d}	dextral first order shear direction: 89°
S_{1s}	sinistral first order shear direction: 140°

Fig. 2-22: Schmidt net showing the orientation of joints (black circles) and dykes (red squares) on Fildes Peninsula around the Uruguayan Base 'Artigas' and at Nebles Point. Cooling joints within the dykes are not plotted. Density contours calculated as explained in Fig. 2-2. Principal strike directions are shown by the rose diagram in the center. The tectonic directions shown have been determined assuming a stress field oriented similar as on Hurd Peninsula. Poles to planes.

2.3.2 Weaver Peninsula

Weaver Peninsula is located at (58° 47.5' W / 62° 12.5' S) approx. 1.5 km NNW of the South Korean Base 'King Sejong' (Barton Peninsula) just across Marian Cove (Fig. 2-18). It comprises less than 2 km^2, measures about 1 km across and is framed by Collins Harbour to the NW, Marian Cove to the SE and the huge Arctowski Icefield to the NE.

It has been visited in two short day-trips during a stay at the South Korean Base 'King Sejong' on Barton Peninsula in December 2000.

The morphology of this relatively small peninsula is characterized by smooth hills in the interior, covered in large parts by glacial detritus, and rugged cliffs at the coast leading down to rather narrow gravel beaches.

The lithology comprises a stratiform volcanic sequence characterized mainly by basaltic and basaltic-andesitic lava-flows with intercalated tuffs and volcanic agglomerates. The lavas occur as both porphyritic and aphanitic varieties, grey-green to black in color, depending on their respective degree of alteration. The agglomerates crop out along the coast of Collins Harbour (Fig. 2-18) north of the peninsula's tip and feature clast sizes between several cm and up to 50 cm.

The arc-related suite has subsequently been pierced by a moderate-scale, calc-alkaline pluton of granodioritic to dioritic to quartz-gabbroic composition. This pluton is probably a part of the Noel Hill intrusion on Barton Peninsula; the two parts have been dissected by a sinistral strike-slip fault running NE-SW along Marian Cove [Birkenmajer 1998a].

The true geological age of this pluton has been determined as 63.4-60.7 Ma (Paleocene), whereas younger obtained ages (53-42.1 Ma) have been interpreted as a resetting effect due to successive thermal events, predominantly during the Middle Eocene at approx. 44 Ma [Birkenmajer 1998a and references therein]. This period of thermal events is well documented from several locations within the Barton Horst. Quartz-pyrite veins striking NW-SE occur also N of the peninsula's tip and are probably caused by migrating hydrothermal fluids of volcanic origin like the corresponding quartz-pyrite veins well known from Barton Peninsula [Park 1991; Willan & Armstrong 2002].

The youngest group of rocks cropping out on Weaver Peninsula is a suite of hypabyssal basaltic and andesitic intrusions. The dykes considered here belong to this group.

The strong folding of the sequence observed by Birkenmajer [1998a] could not be confirmed during own field work, but a tectonic history marked by strong stress which led to cataclastic brittle failure is evident in all rocks including the dykes, far more prominent than in other parts of King George Island. At some localities, the rocks appear virtually shattered. This feature may be due to the peninsula's position between the left-lateral strike-slip fault running NE-SW along Marian Cove and the deep-cutting, probably dextral Collins Fault bordering it to the NW running also NE-SW along Collins Harbour.

One of the most striking characteristics on Weaver Peninsula is the high degree of alteration visible already in the field, affecting effusive and intrusive rocks likewise. This strong alteration is most probably due to the peninsula's position within Barton Horst; possible origins of the alteration have been discussed above. The type of alteration has been determined as propylitic and argillic [Birkenmajer 1998a]. The macroscopically visible consequences are e.g. strong granular disintegration in some parts and a generally gritty appearance. Weaver Peninsula features the highest Alteration Index (4.0) of all investigated areas (Fig. 2-21), though alteration does not affect all rocks to the same degree, as some dykes appear considerably fresher than others.

24 dykes have been examined on Weaver Peninsula. They are 0.5 to 10 m thick (averaging 3.3 m). Except for the strong alteration, the appearance of the dykes is inconspicuous with chilled margins of up to 10 cm and phenocrysts often aligned parallel to the dykes' strike, reflecting the flow direction of the magma. The majority of the phenocrysts are plagioclase grains of up to 2 cm length, but pyroxene also is common.

Assuming a similar stress field as observed on Hurd Peninsula, the tectonic directions can be assigned as follows:

Obviously, the shear systems belonging to the a- and b-axis are developed much stronger on Weaver Peninsula than directions corresponding to the axes themselves. A possible a-direction is developed very weakly at 129° (Fig. 2-23), an inferred corresponding b-axis would strike 39° but is not expressed at all, neither as joints nor dykes. Two strike directions prevail on Weaver Peninsula: a sharply defined 100° striking set of dykes could represent the dextral first order shear direction (S_{1d}) and seems to be older than a 3° striking second set, as dykes of the latter

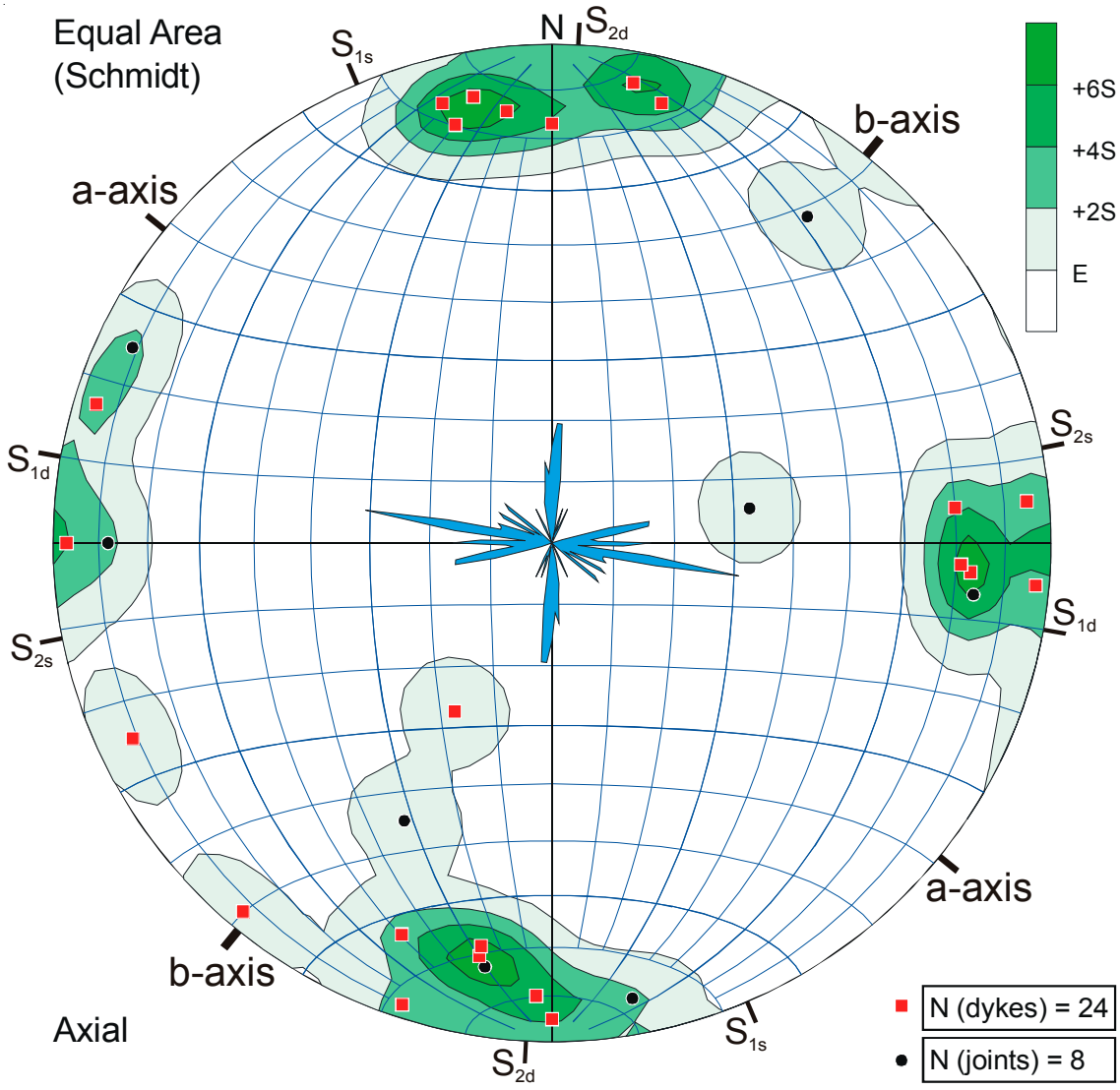

Abbr.	Explanation (with average strike)
b-axis	39°
a-axis	129°
S_{1d}	dextral first order shear direction: 100°
S_{1s}	sinistral first order shear direction: 157°
S_{2d}	dextral second order shear direction: 3°
S_{2s}	sinistral second order shear direction: 79°

Fig. 2-23: Schmidt net showing the orientation of joints (black circles) and dykes (red squares) on Weaver Peninsula. Cooling joints within the dykes are not plotted. Density contours calculated as explained in Fig. 2-2. Principal strike directions reflected by the rose diagram in the center. The tectonic directions shown have been assigned assuming a stress field oriented similar as on Hurd Peninsula (Livingston Island). Poles to planes.

sometimes cut the first set but never vice versa. This second set could correspond to a dextral second order shear direction (S_{2d}). A third set of subordinate importance strikes 79° and might be assigned to a sinistral second order shearing (S_{2s}). Only one dyke striking 157° marks a direction corresponding to a possible sinistral first order shear direction (S_{1s}). The first order shear system is oriented at angles of 36°-40° around the supposed b-axis, the second order shear system at 28°-29° around the a-axis.

Summarizing, the tectonic directions on Weaver Peninsula have to be assigned tentatively, but the observed directions indicate a stress field rotated 10-15° clockwise as compared to Hurd Peninsula. This might be due to the peninsula's position within the root of the upthrown Barton Horst and processes related to the immense vertical displacement. Another explanation might be rotations caused by the lateral movement along the strike-slip faults bordering the peninsula on both sides, in other words processes related to Late Cenozoic block faulting and tilting of single blocks relative to the adjacent ones.

2.3.3 Barton Peninsula

This peninsula is located south of Weaver Peninsula at 58° 42.3' - 58° 47.9' W and 62° 12.4' - 62° 14.6' S (Fig. 2-18). It measures 4.3 km NE-SW and 4.2 km NW-SE at its broadest parts, comprising around 10 km^2 of unglaciated area. The South Korean Base 'King Sejong' is located at the shores of Marian Cove at 58° 47' 30.5'' W / 62° 13' 22.0'' S. From here, field work on Weaver and Barton Peninsula has been carried out during a five day visit in December 2000.

The lithology on Barton Peninsula is very similar to that of Weaver Peninsula, also the degree of alteration and the locally cataclastic appearance induced by the tectonic stress. The stratiform volcanic sequence cropping out on Barton Peninsula has been subdivided into three subunits, separated from each other by angular unconformities [Tokarski 1988].

Gently dipping greenish, black and reddish lava flows and pyroclastic sequences are common and up to 80 m thick, especially the lava flows contribute as prominent steps and cliffs to the peninsula's morphology. Barton Peninsula is one of the few localities on King George Island where continental freshwater sediments have been recognized. These sediments crop out in a coastal cliff approx. 500 m east of a small basaltic plug at the peninsula's southern coast. They contain a fossil flora represented by leaf imprints attributed to *Laurelia guinazui Berry, Nectandra prolifica Berry, Nothofagus densinervosa Dusén, Ocotea menendezi Hünicken* and *Sterculia washburni Berry*. Del Valle et al. [1984] argued for an Early Eocene with a possible extension up to the Early Oligocene age of these beds, Tokarski et al. [1987] considered the flora not to be younger than Paleocene.

A pluton of gabbroic to granodioritic composition crops out in the northern part of the peninsula at Noel Hill. It has been interpreted to represent the bigger part of an intrusion dissected by a sinistral strike-slip fault running NE-SW along Marian Cove, with the other part cropping out on Weaver Peninsula [Birkenmajer 1998a]. As mentioned above, age determinations of the Noel Hill pluton range between 60.7 and 42.1 Ma, with the Paleocene age having been interpreted as the true geological age and the younger ages as a resetting effect caused by thermal reheating [Birkenmajer 1998a]. Consequently, 60.7 Ma would also be the minimum age for the stratified volcanic succession.

Most works dealing with Barton Peninsula do not state folding of the stratiform succession but instead gentle dipping to different directions at angles around 20° [Barton 1961, 1965; Davies 1982; Smellie et al. 1984; Willan & Armstrong 2002]. However, Birkenmajer [1982b] and Tokarski [1988] emphasize strongly folded, locally vertical oriented lavas, tuffs and agglomerates. Following these authors' conclusion, the general orientation of the stated folds is controlled by the shape of the intrusions piercing Barton Peninsula (especially the Noel Hill intrusion) and the fold axes run parallel to the strike of these intrusions.

However, during this work no folding could be observed directly in the field nor have the NW-SE striking folding axes stated by Tokarski [1988] been confirmed by own tectonic data.

The dykes on Barton Peninsula tend to crop out predominantly at or near the beach, piercing the coastal cliffs and offshore pyroclastic platforms formed by erosion, which are accessible only at low tide. In contrast to Weaver Peninsula, dykes are very scarce in the interior. In most cases, the dykes are morphologically not emphasized with respect to their host rocks, though some form monadnocks or platy bodies of up to 30 m height.

Normally, the dykes appear as isolated hypabyssal intrusives cutting the lava flows and pyroclastic sequences of the stratiform succession. Dyke crossings or systems are scarce. Typically, they can be traced over a length of several meters up to tens of meters and average - as on Weaver Peninsula - about 3 m in thickness. Their composition ranges from basaltic to dacitic. Macroscopically visible phenocrysts are common, especially plagioclase and pyroxene. Locally, the dykes yield pyrite-crystals of mm-size and/or cc- and qz-filled amygdales, giving evidence of the geothermal and volcanic-hydrothermal events reported by Willan & Armstrong [2002]. Columnar jointing appears well developed in some dykes but is completely absent in others.

Chilled margins up to 15 cm wide are common, mostly of darker color (dark grey) than the main body of the dyke. Sometimes the rims of the dykes are not straight but rather irregular or sinuous with indentations and inlets, indicating that the dyke did not follow a well developed joint plane but rather migrated through a heterogeneous host rock along irregular planes. In one case (location: 408535 / 3097805, UTM Zone 21E, WGS 84) a 4.5 m thick

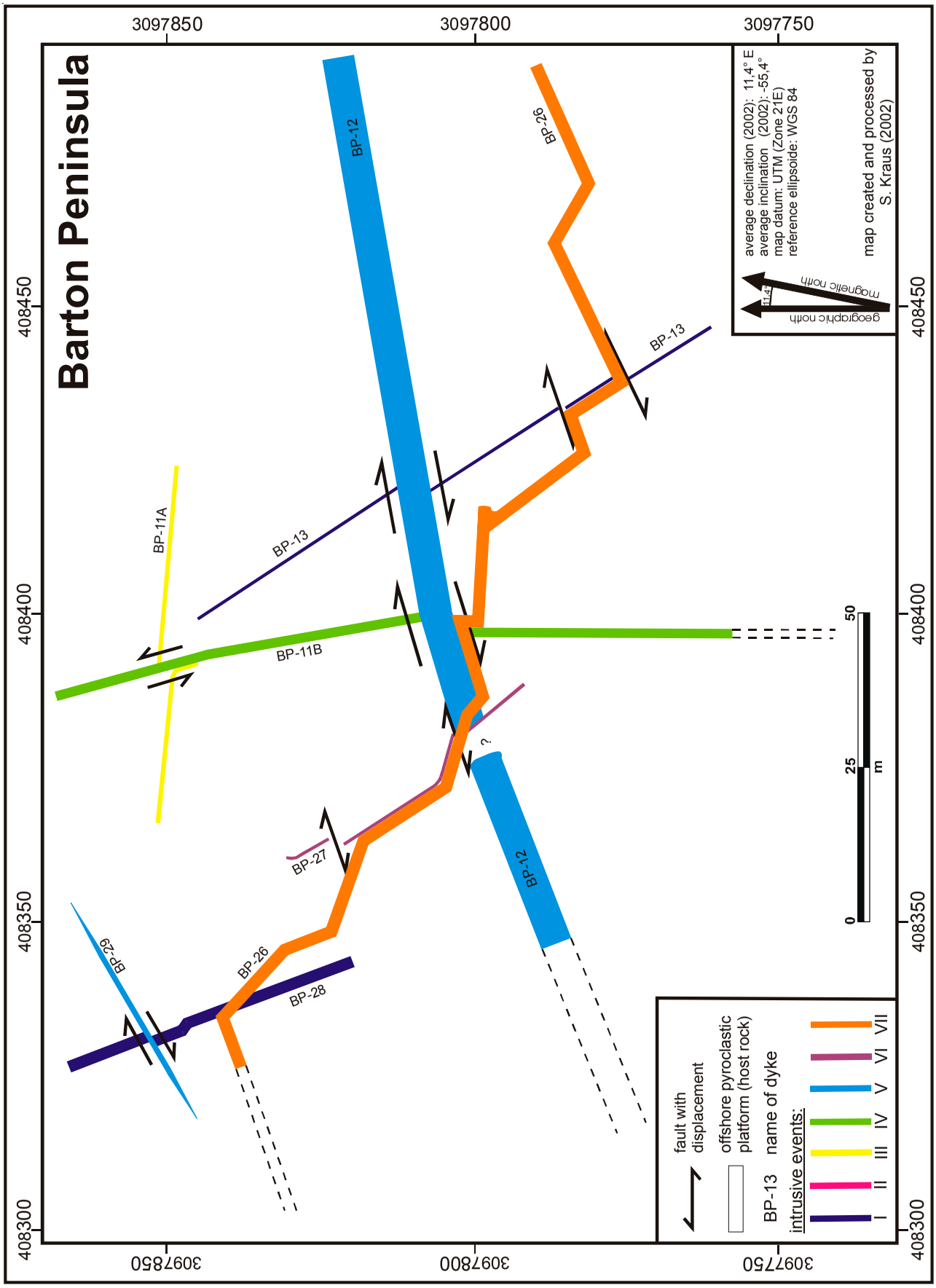

Fig. 2-24: Map of a dyke system on Barton Peninsula comprising 8 dykes. The system cuts an offshore lying, flat pyroclastic platform which is accessible only during extremely low tide. Assuming a similar tectonic stress field as on Hurd Peninsula, the relative time sequence of the dykes corresponds well to the sequence set up for the different intrusive events on Hurd Peninsula. Note the system's clockwise rotation of 10-15° as compared to Hurd Peninsula, maybe due to Late Cenozoic block faulting. Note also, that some of the faults displayed in the map are older than some dykes crossing them, leading to a short-distance jump in the course of the respective dyke.

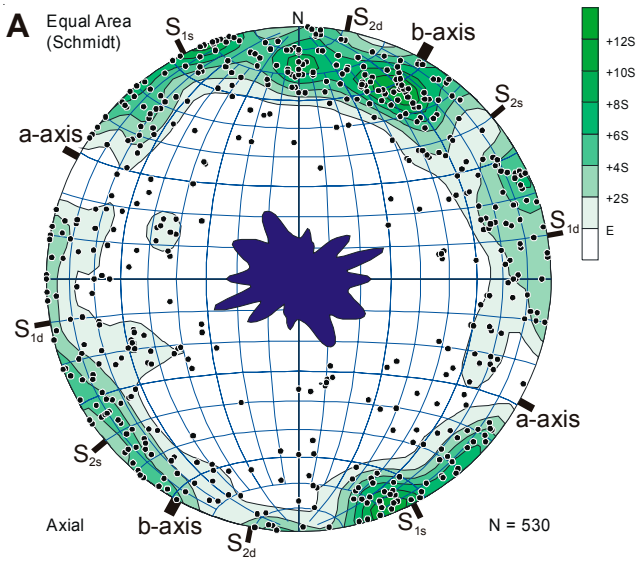

Abbr.	Explanation (with average strike)
b-axis	29°
a-axis	119°
S_{1d}	dextral first order shear direction: 70-90°
S_{1s}	sinistral first order shear direction: 153°
S_{2d}	dextral second order shear direction: 11°
S_{2s}	sinistral second order shear direction: 50°

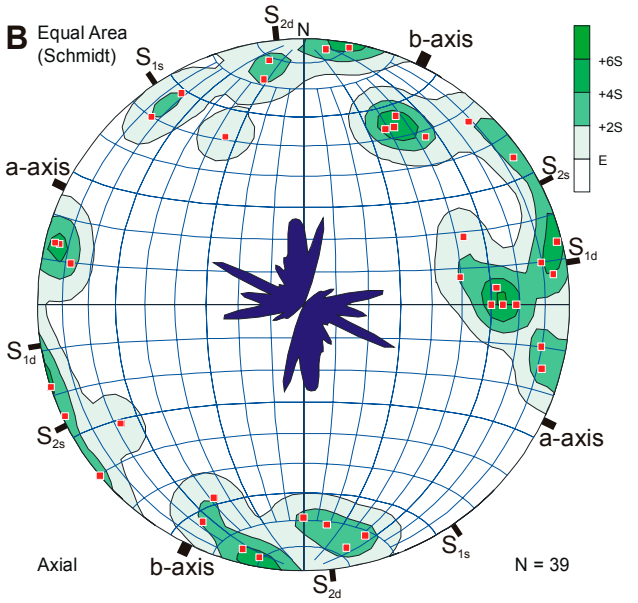

Abbr.	Explanation (with average strike)
b-axis	26°
a-axis	116°
S_{1d}	dextral first order shear direction: 81°
S_{1s}	sinistral first order shear direction: 146°
S_{2d}	dextral second order shear direction: 174°
S_{2s}	sinistral second order shear direction: 63°

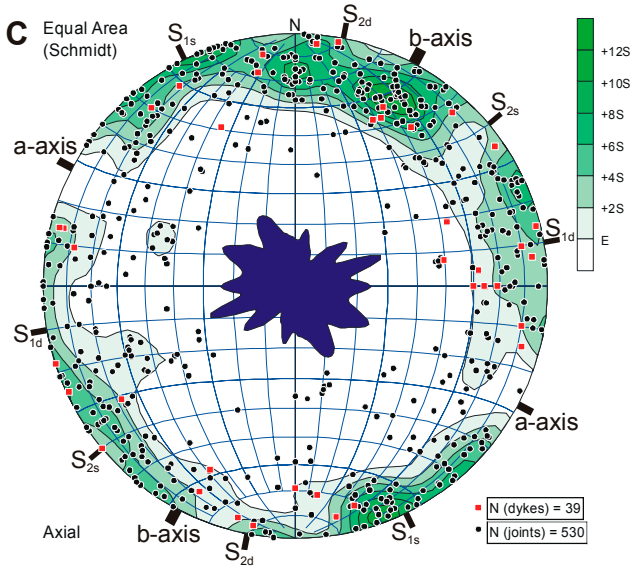

Abbr.	Explanation (with average strike)
b-axis	28°
a-axis	118°
S_{1d}	dextral first order shear direction: 70-90°
S_{1s}	sinistral first order shear direction: 154°
S_{2d}	dextral second order shear direction: 11°
S_{2s}	sinistral second order shear direction: 50°

Fig. 2-25: Schmidt Net showing all joints measured on Barton Peninsula (A), the orientation of the investigated dykes (B) and a compilation of all tectonic data (C). Cooling joints within the dykes are not plotted. Contours as explained in Fig. 2-2. Poles to planes. The tables to the right of the stereograms summarize the principal tectonic directions of the respective net.

dyke (BP-30) shows multiple splitting into several branches, then reuniting again. Moreover, it features pockets of several meters in diameter and also a heterogeneous petrology with varying size and amount of phenocrysts. Another dyke (BP-32, location 408938 / 3097711, UTM Zone 21E, WGS 84) carries numerous grey, porous and partially absorbed xenoliths of up to 5 cm diameter.

From the South Korean Base 'King Sejong' along the coast towards SE several single dykes are cropping out. At 407308 / 3098683 and at 408392 / 3097851 (WGS 84, UTM Zone 21E) crossings of N-S and E-W striking dykes can be observed. At the first locality, the E-W striking dyke cuts and offsets the N-S striking one, at the second locality the E-W striking dyke is the older one and cut and offset by the N-S striking dyke. This indicates that no time gap existed between the two directions, but that they belong to the same stress pattern, and that the dykes intruded during the same time interval, sometimes taking the N-S and sometimes the E-W direction.

About 600 m further to the SE a small basaltic plug named 'Narebski Point' crops out. It features some well preserved radial dykes which are probably related to the final stages of activity of this small volcanic center and do therefore not reflect the regional stress pattern, thus they were excluded from the tectonic dataset.

The most interesting set of dykes cropping out on Barton Peninsula is located about 700 m SE of Narebski Point, piercing an offshore pyroclastic platform. It is accessible only at very low tide and comprises 8 dykes which define 7 subsequent intrusive events, based on the relative age relationships deduced from the crossings observed in the field (Fig. 2-24). The sequence of these dykes, regarding their relative age in combination with the strike, is identical to the sequence set up on Hurd Peninsula (Livingston Island), though the strike directions are sometimes slightly different. This may be due to rotational effects related to block faulting.

Two sets of faults are existent. Both displace some of the dykes, but are themselves crossed by younger dykes, thus obviously having formed during the same time interval as the hypabyssal intrusions (Fig. 2-24). The older set of faults is sinistral and strikes approx. 165°, the younger and more intense set is dextral, striking approx. 70°. Whereas the stress field active during dyke emplacement appears to have remained stable without major changes, considerable differences can be observed between the different dykes of the system. Dyke BP-28, for example, is a relatively thin, nearly aphanitic finegrained basaltic trachyandesite, BP-12 (Fig. 2-24) is a thick dacitic dyke (6 m) featuring zoned alignment of feldspar phenocrysts parallel to well developed chilled margins, moreover dark-grey schlieren and bands in a predominantly yellowish bulk mass.

The most interesting dyke of this system is certainly BP-26 (Fig. 2-24). First of all, it defines a 7th intrusive event not observed on Hurd Peninsula, thus the youngest of all events which are confirmed by relative field relationships. Moreover, whereas the dykes normally tend to change their direction not at all or only slightly and not more than once or twice within dozens of meters, BP-26 is strongly zigzagging along its course with numerous sharp turns.

Thus, it is not only the youngest dyke of this system, but its zigzagging course does also prove a considerably different stress field at the time of intrusion as compared to preceding events. Whereas the respective stress situation usually forced earlier events to prefer one direction, BP-26 was obviously not bound to such limitations. Apparently, compressional principal stresses were decreasing in favor of extensional forces operating to all directions, letting the melt intrude all available joints and fractures along its course. This could be explained only by a very late, near-surface emplacement of the dyke after upthrow and erosion of Barton Horst.

Extensive joint measurements have been carried out in the dykes as well as in the host rock, dyke-parallel and -orthogonal cooling joints have been eliminated from the datasets (Fig. 2-25). The tectonic pattern shown by these joints and the principal directions as deduced from the orientation of the dykes are very similar (Fig. 2-25A & B). Only the second order shear system shows differing directions. Puzzlingly, whereas the dextral second order shear system (S_{2d}) expressed by dyke orientation (Fig. 2-25B) seems to be rotated by 17° *anticlockwise* compared to the corresponding joint direction (Fig. 2-25A), the dyke orientation reflecting the sinistral second order shear system (S_{2s}) is rotated by 13° *clockwise* compared to the corresponding joints. The available data do not allow an explanation of this phenomenon, further work is required.

As stated for Nelson Island and the other parts of King George Island, the following tectonic directions are assigned tentatively and under the assumption of

a stress field similar as on Hurd Peninsula. Indeed, the observed directions correlate pretty well with the directions observed on Livingston Island.

An a-axis can be stated striking approx. 118°, with possible ac-joints averaging 118/73 SW in orientation (Fig. 2-25C). From the 39 dykes investigated on Barton Peninsula, 4 seem to have intruded along ac-joints. As mentioned above, folding could not be observed directly in the field, but a b-axis striking approx. 28° can be deduced from the a-axis assuming an orthogonal relation between the axes. A dextral first order shear system (S_{1d}) is clearly expressed by the joints as well as by the dykes, though the latter cluster sharply around 81° whereas the joints cover a wider range between 70° and 90°. The prominent dextral faults belong to this system (Fig. 2-24).

The corresponding sinistral first order shearing (S_{1s}) is clearly expressed at 154° ± 8° and the aforementioned older, sinistral faults (Fig. 2-24) may belong to this shear system. Dextral second order shearing (S_{2d}) exists but is expressed rather weakly at 11° ± 15°, whereas sinistral second order shearing (S_{2s}) produces a sharp cluster of joints at 50° but is virtually not used by the dykes. The directions preferred by the dykes (Fig. 2-25B) are the ac-direction (116°), the dextral first order shear system (81°) and the dextral second order shear system (174°).

As compared to Hurd Peninsula, all directions observed on Barton Peninsula differ no more than 4° from the corresponding directions on Livingston Island, giving good support for the assumption of a similar stress field.

2.3.4 Potter Peninsula

Potter Peninsula is located at the southernmost extreme of King George Island (Fig. 2-18), stretching from 58° 35.0' to 58° 41.0' W and from 62° 13.9' to 62° 15.7' S. The unglaciated area comprises around 6 km^2, bordered by the Warszawa Icefield to the NE, Bransfield Strait to the SE, Maxwell Bay to the SW and Potter Cove to the NW.

Like on adjacent Barton Peninsula, the morphology on Potter Peninsula is predominantly characterized by a glacial landscape with abrasion platforms offshore, in parts steep cliffs along the coast, and a rather smooth, hilly countryside in the interior. The most prominent morphological feature is Three Brothers Hill (196 m), a well known andesitic plug showing conspicuous columnar jointing (Fig. 2-26). It marks the final stage of activity of a Paleogene volcano, whose eruption products (lava flows and pyroclastic rocks), together with hypabyssal intrusions related to the volcanism, make up most of the lithology observed on Potter Peninsula.

Fig. 2-26: View towards SW at Three Brothers Hill (196 m), a Lower Eocene andesitic plug showing prominent columnar jointing.

The Argentine station Teniente Jubany with the associated German/Argentine Dallmann Laboratory, located at 58°39'51.63'' W / 62°14'13.07'' S at the shore of Potter Cove, was homebase for fieldwork on Potter Peninsula during several stays in austral summers 1998/1999, 2000/2001 and 2001/2002 (Fig. 2-27).

Among the first who carried out geological work in that area were Ferguson [1921] and Tyrell [1921], who supplied short descriptions of the volcanic sequence cropping out on Potter Peninsula. Later on, Hawkes [1961], Barton [1961, 1965], Smellie et al. [1984] and Birkenmajer [1998b] published more detailed geologic and petrographic information, Smellie et al. [1984] also geochronological and geochemical data. Geological drafts and sketch maps of Potter Peninsula have been published by Fourcade [1960], González-Ferran & Katsui [1970] and Birkenmajer [1998b].

Geological frame

Potter Peninsula forms part of the downthrown Warszawa Block (Fig. 2-21). The volcanic sequence cropping out here belongs to the King George Island Supergroup [Birkenmajer 1998b] with an observed local minimum thickness of approx. 90 m.

According to Smellie et al. [1984], the sequence can be referred to as part of the Fildes Formation introduced by these authors. Some geochronological data are available from Potter Peninsula. Watts [1982] reports an Ypresian age (K-Ar, 50.6 ± 0.7 Ma) for Three Brothers Hill and Thanetian to Ypresian ages (57.9 ± 0.8 to 49.1 ± 0.9 Ma) for three andesitic lava flows. Smellie et al. [1984] obtained Ypresian to Lutetian K-Ar ages (49 ± 1 to 42 ± 1 Ma) for 6 basaltic to andesitic lava flows and hypabyssal intrusions, among them a Lutetian age (47 ± 1 Ma) for Three Brothers Hill. Given the time range spanned by the King George Island Supergroup (Campanian to Chattian), the stratigraphic position of the volcanic series cropping out on Potter Peninsula seems to be quite in the middle of the KGIS. Birkenmajer [1998b] assigned the Potter Peninsula volcanics more precisely to the Paradise Cove Group.

Three volcanic centers contributed to the volcanic sequence cropping out in the area: the former position of a stratovolcano is marked by the prominent and well known andesitic Three Brothers Hill plug, measuring about 500 m in diameter. Nearby

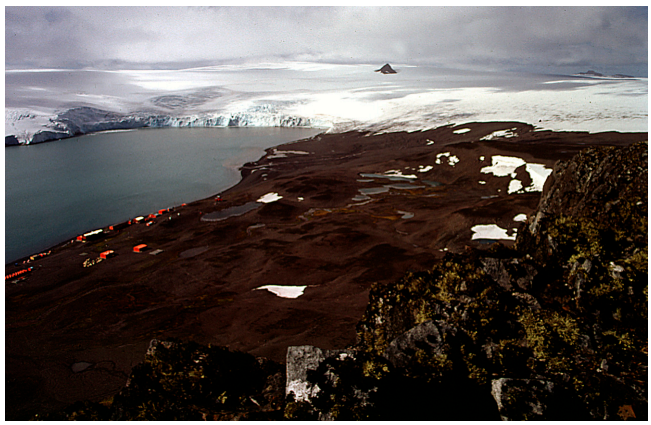

Fig. 2-27: View from top of Three Brothers Hill over Potter Peninsula towards NE. At the left side Teniente Jubany Station (Arg) located at the shore of Potter Cove, in the background Florence Nunatak piercing the Warszawa Icefield.

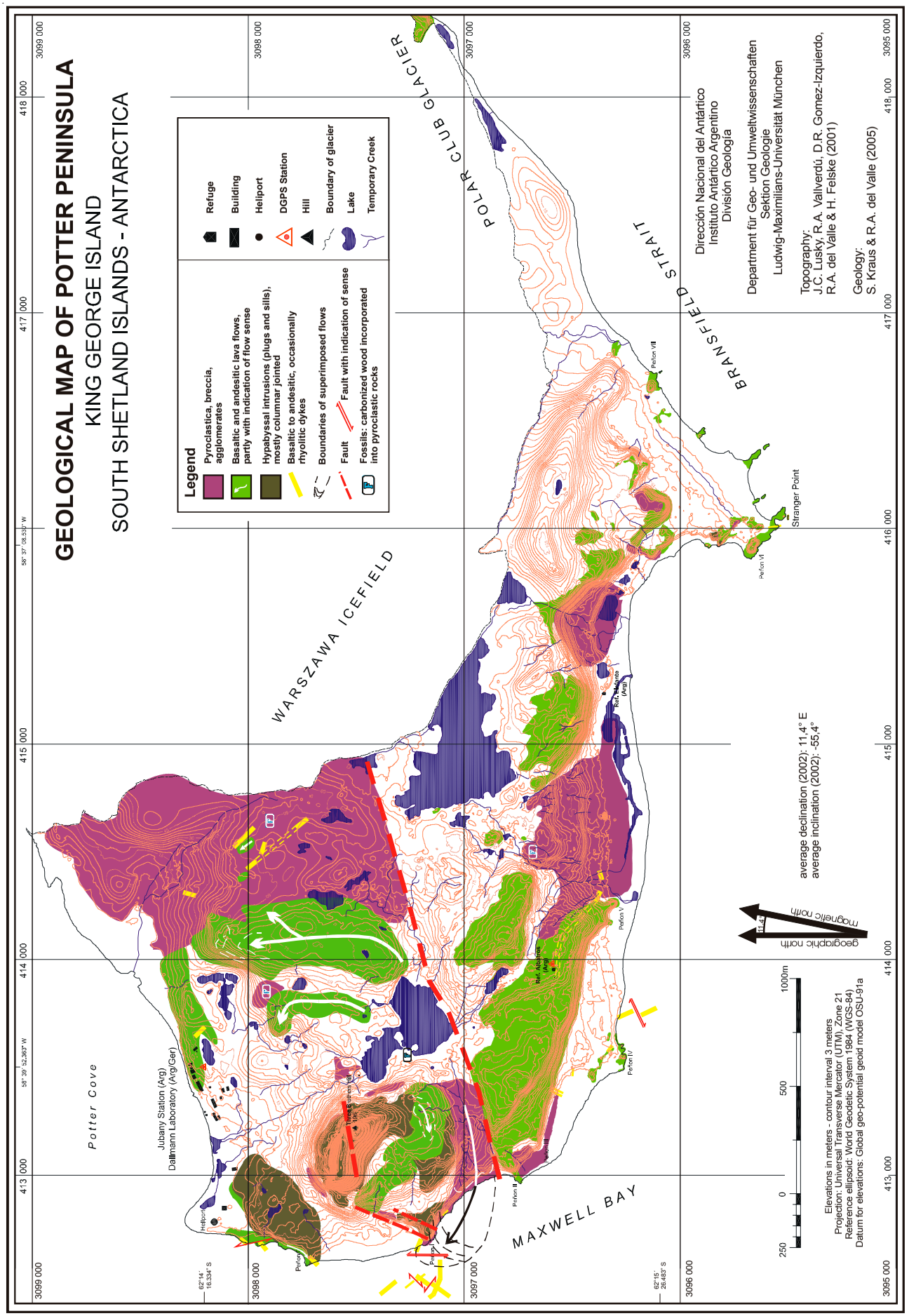

Fig. 2-28: Topographic and geological map of Potter Peninsula (King George Island, South Shetland Islands). Geology NW of the prominent, NE-SW running fault and all dykes by S. KRAUS, geology SE of the fault (except dykes) by R.A. DEL VALLE (Instituto Antártico Argentino, Buenos Aires). Dyke thickness not scale appropriate.

Florence Nunatak, piercing the Warszawa Icefield about 4.7 km to the NE of Three Brothers Hill, is also a plug and marks the location of another extinct volcanic center (Fig. 2-27). It is of basaltic andesitic composition and like Three Brothers Hill strongly columnar jointed. The remnants of a third but smaller stratovolcano are located at Stranger Point (Fig. 2-28). Today, this stratocone is completely eroded and only the reminders of the two feeding vents and the eruption products are left.

The same applies to the Three Brothers Hill volcanic complex, which is eroded down to its deepest levels. Thus, the stratigraphically deepest units from the initial phase of volcanic activity are cropping out in some parts. The lithology on Potter Peninsula comprises lava flows (~50%), pyroclastic rocks (ash-fall-out, pyroclastic flow deposits, volcanic breccia and agglomerates, ~30%) and hypabyssal intrusions (dykes, sills and small subvolcanic intrusive bodies, ~20%).

The initial phase of volcanic activity on Potter Peninsula produced primarily basalts of tholeiitic affinity, then changing to basaltic andesites and andesites featuring a calc-alkaline character, furthermore scarce dacites [Kraus et al. 2000]. Early effusive activity generated numerous tholeiitic basalt lava flows with scarce, thin intercalations of pyroclastic material, mostly ash-fallout deposits.

Later, a more explosive volcanism of andesitic composition produced more pyroclastic material and less lava flows. Volcanism terminated in a phase of intensified hypabyssal intrusive activity. Geochemical data confirm, that at least the volcanoes at Three Brothers Hill and Florence Nunatak were fed by the same magma source [Kraus et al. 2000], and in combination with field evidence it can be assumed that they were probably active during the same or at least overlapping time intervals. Possibly also the activity of the double vent at Stranger Point [Birkenmajer 1997b] falls within this time span.

The lava flows are basaltic to andesitic in composition, 1-15 m thick (seldom more) and often columnar jointed (diameter up to 70 cm), sometimes forming multiple overlying sequences. Px and pl are the most common phenocrysts, some of the flows bear ghost xenoliths of up to 15 cm diameter. Amygdales are common and either filled with secondary chlorite and/or zeolite or small, sometimes bluish qz-crystals, also agate geodes of up to 10 cm diameter occur. Flow directions, observed in the northwestern part of the peninsula, give hints on a possible origin from a vent located at the southeastern foot of the present day Three Brothers Hill. The length of these flows is generally not more than 2 km (Fig. 2-28).

Explosive phases of volcanic activity produced red to redbrown, more seldom grey-greenish tuffs, sometimes intercalated with the lava flows, and more often pyroclastic flows. The embedded clasts are of mm- to dm-size, the thickness of the flows lies between 0.5 - 1 m and several tens of meters. The flows followed predominantly morphological depressions and valleys and are therefore tightly interlocked with the lava flows. One fine example is the multiple flow sequence located S of Three Brothers Hill, following a valley down to the coast towards W, then changing its direction towards NW. The tip of these flows is located offshore Peñón I and accessible only at very low tide (Fig. 2-28).

A huge area of about 1 km^2, east of Teniente Jubany Station towards the border of the Warszawa Icefield, is covered by numerous pyroclastic flows. Their flow direction seems to be roughly NW to N, indicating a possible origin at Stranger Point volcano. At some localities, these pyroclastic rocks contain carbonized wood fragments, indicating the destruction of paleo-forests by the respective flow (Fig. 2-28).

Numerous hypabyssal intrusions pierce the effusive rocks, including sills, dykes and irregular formed subvolcanic bodies featuring diameters of up to several tens of meters (e.g. at Peñón I, Fig. 2-28). Many of these subvolcanic bodies are located in the surroundings of Three Brothers Hill and possibly related to the activity of this volcano.

Block faulting and subsequent tilting is evident everywhere on Potter Peninsula, though the individual blocks are tilted no more than 10-20° and without a prevailing direction. The prominent, NE-SW running fault separating Potter Peninsula in a northwestern and a southeastern sector was probably created during Late Cenozoic block faulting.

The dykes on Potter Peninsula

26 dykes crop out on Potter Peninsula, featuring a thickness between 30 cm and 10 m (average 3.68 m). They are far more abundant in the northwestern sector of Potter Peninsula than in the SE towards Stranger Point (Fig. 2-28). Most of them are single, isolated dykes cutting the stratiform volcanic suite, and can be traced from several meters to up to 200 m (with interruptions). Like on adjacent Barton Pen-

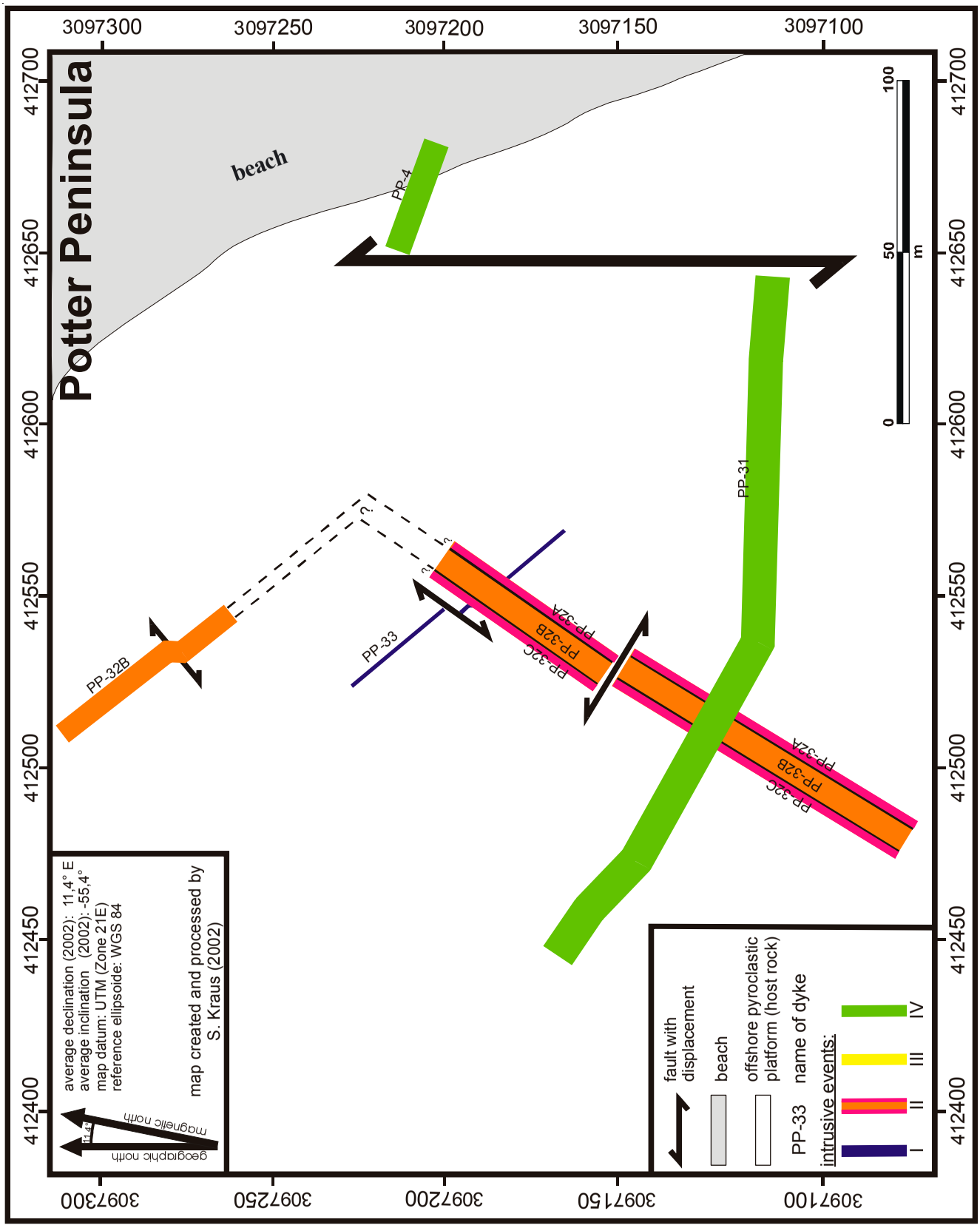

Fig. 2-29: Dyke system mapped at the western side of Potter Peninsula (see Fig. 2-28). The system is located offshore, cutting an abrasion platform consisting of pyroclastic rocks. Accessibility is restricted to days with extremely low tide. The system comprises 5 dykes taking directions corresponding to intrusive events I, II and IV as determined on Hurd Peninsula (Livingston Island). Event III is not represented here. Note the multiple intrusion comprising dyke PP-32B (rhyolite, 7.6 m thick) flanked by two thin basaltic andesitic dykes (PP-32A and PP-32C, 1.0 - 1.2 m thick). Ar-Ar age determinations yielded same ages (Lutetian, approx. 46 Ma) for all dykes of the system, suggesting that only one intrusive event occurred, using different tectonic directions.

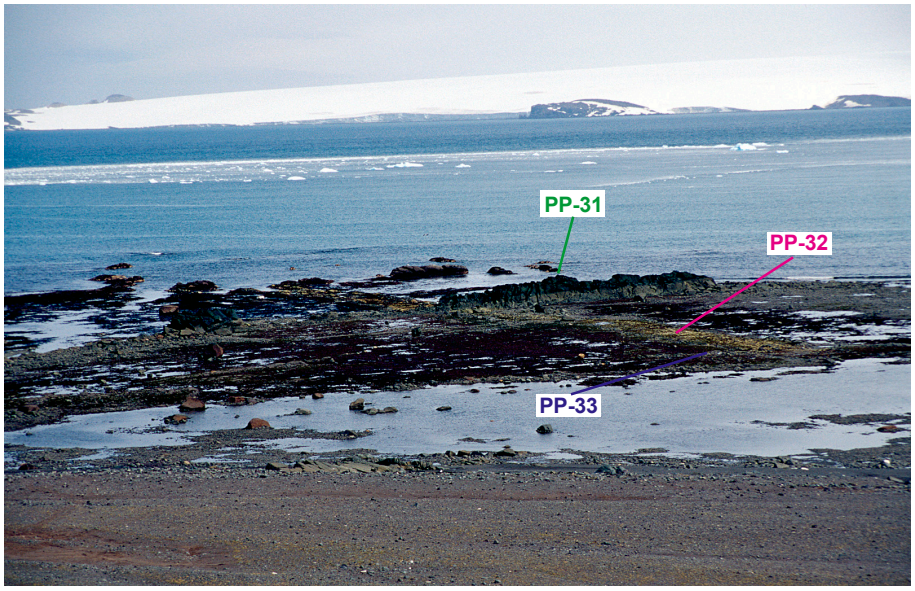

Fig. 2-30: View towards SW onto the dyke system offshore Potter Peninsula, cutting a pyroclastic platform. The colors of the dyke-names correspond to the colors given in Fig. 2-29. Barton Peninsula in the background.

insula, the only existing outcrop of a dyke system allowing the observation of relative age relationships is an offshore pyroclastic abrasion platform near Peñón I (Fig. 2-28, 2-29, 2-30). It is pierced by 5 dykes, some of them zigzagging, and a multiple intrusion (Fig. 2-29). The dykes are offset by three sets of faults. The oldest one is dextral and strikes approx. 35-45°, the second sinistral striking approx. 120° and the third set is also sinistral, running exactly N-S (0° strike).

Most of the dykes are inconspicuous concerning their main characteristics and general appearance, they resemble well the dykes found in other parts of the South Shetland Islands. However, two outcrops deserve special attention, due to their unique appearance and features.

An especially spectacular example is PP-9, an andesitic dyke cropping out in the northern part of Potter Peninsula near the border of Warszawa Icefield at 414533 / 3098052 (UTM, WGS 84, Zone 21E). It is oriented 136/64 NE, about 4 m thick and can be traced over a length of approx. 60 m along a ditch approx. 1.8 m deep (Fig. 2-31). Here, the extensive pyroclastic rock sequence borders a small basaltic lava flow (Fig. 2-28), and the dyke has intruded exactly along this border between the two units. At approx. 150 m distance from the icefield, the dyke is located within an area from which the glacier retired only during the last 40 years. Thus, the ditch most probably represents the bed of a melt water creek which has fallen dry meanwhile. The water ran along the border between the dyke and the pyroclastic host rock, removing only the latter because of its lower resistance against erosion, thus laying open the outer wall of the dyke over a length of approx. 60 m.

Its appearance is characterized by torose, more seldom globular structures and redbrown to greenish schlieren (Fig. 2-32). The bulges reflect clearly the magma's movement while intruding the fissure, mostly in a vertical but sometimes also subhorizontal direction. The color of the redbrown areas is due to fragments of the northeasterly lying pyroclastic host rock being baked onto the surface of the dyke, the greenish schlieren mark the chilled margin of the dyke itself, to a great extent

Fig. 2-31: About 60 m long ditch representing the bed of a meltwater creek now fallen dry. The left wall of the ditch is the outer surface of dyke PP-9. View towards NW.

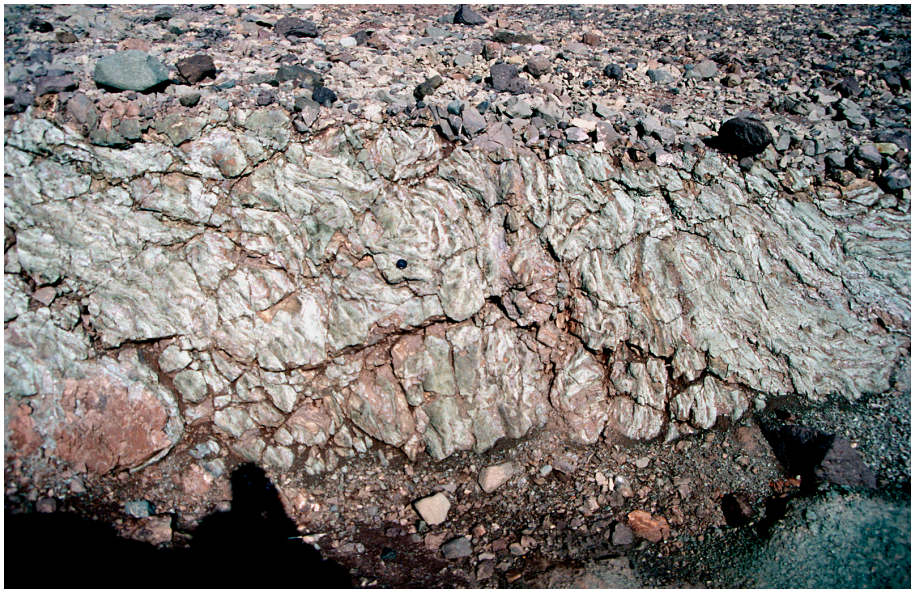

Fig. 2-32: Torose structures on the outer surface of dyke PP-9, reflecting clearly the movement of the magma during intrusion. The greenish parts are the dyke's chilled margin, the brownish areas are fragments of the pyroclastic host rock baked onto the surface of the dyke. The ditch is approx. 1.5 m deep.

consisting of secondary minerals like chlorite. Fragments of the pyroclastics are sometimes lined up in a string, also demonstrating the movement of the magma (Fig. 2-32). The dyke's about 4-5 cm thick chilled margin consists of a schlieren-like melange of greenish dyke- and redbrown pyroclastic material. Sometimes flame-structured amygdales of up to cm-size occur within this zone, often filled with a microcrystalline mineral of deep orange color, possibly zeolite. Within small geodes, this mineral sometimes forms dodecahedrons of up to 1 mm diameter.

Further towards the dyke's interior, the color of the dyke rock changes to brownish-grey, then to grey. Small pores (< 1 mm) are aligned parallel to the dyke's outer wall and filled with calcite. They are aligned according to the orientation of the aforementioned bulges and thus reflect the magma's movements also in the dyke's interior. At about 15 cm distance from the dyke's surface, another zone of up to 1 cm big amygdales is visible, also partly filled with calcite. The bulk rock of the dyke consists of a light-grey, dense matrix hosting phenocrysts like px (up to 1.5 mm, euhedral, greenish), pl (up to 2 mm, euhedral, whitish) and opaque minerals. Scarce amygdales of up to 2 cm diameter and irregular form are filled with chl and/or cc.

A second outcrop (PP-5) is well worth mentioning, comprising a multiple intrusion consisting of three dykes. The outcrop is located at the shore SW of the Heliport at 412683 / 3097998 (UTM, WGS 84, Zone 21E). A yellowish, rhyolitic dyke is sandwiched between two dykes of basaltic andesitic composition (Fig. 2-33), the orientation is 30/84 SE. The rhyolitic dyke is 4 m thick, features tight cleaving and a smooth surface with small pores (mm-range) and single feldspar grains (< 0.5 mm). The rhyolite reacts with HCl, indicating presence of calcite, and bears accessory, mostly cubic pyrite (< 0.5 mm). An alteration rim is yellowish, 3-4 cm thick, and changes its color towards the fresher interior to grey-whitish. The contact with the two enclosing basaltic andesitic dykes is not sharp, but a rather blurry, approx. 2-3 cm (max. 5 cm) wide transition zone featuring a schlieren-like intermingling of the two materials (Fig. 2-34). Pyrite cubes (< 0.5 mm) appear more frequently in the vicinity of the contact but are restricted to the rhyolitic dyke. Pores become more frequent towards the contact, indicating a stronger degassing towards the rim.

Each of the two flanking dykes is 1.6 m thick. Their contacts to the rhyolitic dyke feature sometimes a finegrained darker banding about 1 cm thick but without glass. Mostly this margin is rather vague and in some parts missing, instead the aforementioned intermingling of the two magmas is prevailing. Plagioclase crystals are aligned parallel to the contact and sometimes arranged in a tile-like pattern. Like the rhyolitic dyke between them, these two flanking dykes are lacking a chilled margin at the contact with their acidic counterpart (Fig. 2-34), being a strong hint on contemporaneous intrusion.

About 60 m to the S (412679 / 3097935, UTM, WGS 84, Zone 21E), a very similar situation occurs. Here, the orientation of the dykes is 50/80 NW, the rhyolitic dyke is only 3 m thick and the basaltic andesitic dykes each 1.6 m. A small, NW-SE running fault has cut and brecciated the dyke system. At both outcrops, the rhyolitic dyke morphologically steps backward as compared to the flanking ones and is also stronger jointed. This latter effect may be due to the considerable differences in acidity, resulting in a lower resistance against brittle failure of the rhyolite as compared to the basaltic andesite.

Fig. 2-33: A multiple intrusion at outcrop PP-5 reflecting bimodal volcanism and maybe also bimodal flow. A rhyolitic dyke (left side) is sandwiched symmetrically between two basaltic andesitic dykes (one of them at the right side) of 1.6 m thickness.

Two more outcrops on Potter Peninsula show the same situation of a rhyolitic dyke sandwiched symmetrically between two basaltic andesitic dykes: PP-32 (412529 / 3097149, UTM, WGS 84, Zone 21E, see Fig. 2-29 and 2-30) and PP-1 (413381 / 3096562, UTM, WGS 84, Zone 21E). The unique character of these outcrops has to be emphasized, as this type of multiple dyke intrusion has been observed nowhere else on the South Shetland Islands.

Concerning the development of this remarkable intrusion, one explanation might be that the rhyolitic dyke intruded first, followed by tearing of the contacts to the wall rock during cooling. Subsequent intrusion of the basaltic andesitic magma might have occurred along these new planes, accompanied by intermingling with the still not completely crystallized rhyolite. However, to my mind this theory is not satisfying concerning the missing chilled margins of the rhyolitic dyke and the schlieren-like intermingling of the two magmas (Fig. 2-34), as especially the contacts of the rhyolite to the host rock should have cooled rapidly. Moreover, the outer surfaces of a dyke do often carry fragments of the host rock baked onto them (Fig. 2-32). According to the above theory, such fragments should be found along the contact between the rhyolite and the flanking basaltic andesitic dykes. However, this has not been observed at any of the aforementioned outcrops.

A more comprehensive and maybe promising but unproven theory is bimodal flow [McClarren 2003], requiring the contemporaneous intrusion of the crack by two types of magma, one of high viscosity and the other of low. The rhyolitic magma may have derived from the mush-zone of a differentiated magma chamber, whereas the basaltic andesitic material might have come from the chamber interior, both being pulled out through a crack in the chamber wall. In such a scenario, the magma flow is probably rather chaotic when entering the dyke, but the higher viscous magma (rhyolite) then should become surrounded/sandwiched by the lower viscous (higher fluid) basaltic andesitic material. Because of the much higher viscosity of the rhyolitic magma, mixing is highly unlikely. This phenomenon has been utilized for years by the petroleum industry, injecting water into oil pipelines in order to speed up the oil flow. In case of the dyke, the consequence would be that only the lower viscous (and hotter) magma is touching the host rock, whereas the rhyolitic magma remains insulated and does therefore suffer neither friction (which would lead to a slowdown) nor cooling. In other words, the basaltic andesitic magma in this scenario acts like a lubricant for the rhyolite. This process might allow a highly viscous rhyolitic magma to travel much longer distances than without participation of the more basic lubricant [McClarren 2003].

This second explanation appears plausible in this case, because the aforementioned schlieren-like intermingling and the missing chilled margins (Fig. 2-34) along the contacts between the basaltic andesitic and the rhyolitic dyke argue against a temporal gap between the intrusion of the two melts but instead for a contemporaneous one. Moreover, the position of the rhyolite sandwiched *between* the two basaltic andesitic dykes corresponds well to the above mentioned theory of the lower viscous magma acting like a lubricant, with the rhyolite placed in between.

Fig. 2-34: Schlieren-like intermingling along the contact between the rhyolitic dyke (upper half) and the bordering basaltic andesite (lower half), indicating contemporaneous intrusion of the two magma types. The camera cap measures 6 cm in diameter.

However, this theory is not without weaknesses. In contrast to the mechanism observed in petroleum pipelines, it requires the contemporaneous injection of two liquids not only highly diverse in chemical composition but also in temperature. The difference should be several hundreds of degrees Celsius, and the question is what effect this might have concerning the interaction of the two magma types during flow. Another question is, if the conditions within a magma chamber really allow the contemporaneous injection of two such different magma types into a crack.

However, at least the occurrence of bimodal volcanism is indicated by the observed situation at the four outcrops, and probably related to the magma chamber which has fed Three Brothers Hill volcano. This assumption is supported by the relatively low distance (not more than 1 km) of all four outcrops to Three Brothers Hill (Fig. 2-28), furthermore by parallel trends displayed in certain geochemical diagrams (Fig. 4-14B).

Tectonics

Concerning the tectonic situation on Potter Peninsula, the situation is quite similar as observed on the adjacent Barton Peninsula: due to the lack of folding visible in the field, a b-axis striking 30° and an a-axis striking 116° has to be inferred from the overall tectonic pattern (Fig. 2-35). As stated for Nelson Island and the other parts of King George Island, the following tectonic directions are assigned tentatively and under the assumption of a stress field similar as on Hurd Peninsula.

Indeed, the observed directions correlate pretty well with the directions observed on Livingston Island. 423 joints measured on Potter Peninsula predominantly within the pyroclastic rocks and the dykes (cooling joints eliminated) reflect ac-planes oriented 116/87 NE, a dextral first order shear plane at 87/90 N (S_{1d}), a sinistral first order shear plane at 158/79 NE (S_{1s}), a dextral second order shear plane at 3/78 E (S_{2d}) and a sinistral second order shear plane at 63/80 SE (S_{2s}).

As on Barton Peninsula, these directions correspond unexpectedly well with the directions observed on Hurd Peninsula (Livingston Island). Concerning the ac-, S_{1d}- and S_{2d}-directions, difference in strike is no more than 5°, whereas the sinistral first and second order shear directions deviate 13-14° from the corresponding values on Hurd Peninsula.

However, like on Barton Peninsula, the average orientation of the dykes on Potter Peninsula deviates much stronger from the directions shown by the joints as well as from the directions observed on Hurd Peninsula. The Potter Peninsula dykes suggest a b-axis striking 37° and an a-axis oriented at 138° (Fig. 2-35), the latter deviating 22° clockwise from the corresponding direction inferred from the joints. The same applies to S_{1d} (23° difference clockwise), and only S_{1s} is close to the direction shown by the joints (difference of 4° clockwise). At present, no convincing explanation can be presented for the differing behavior of the dykes.

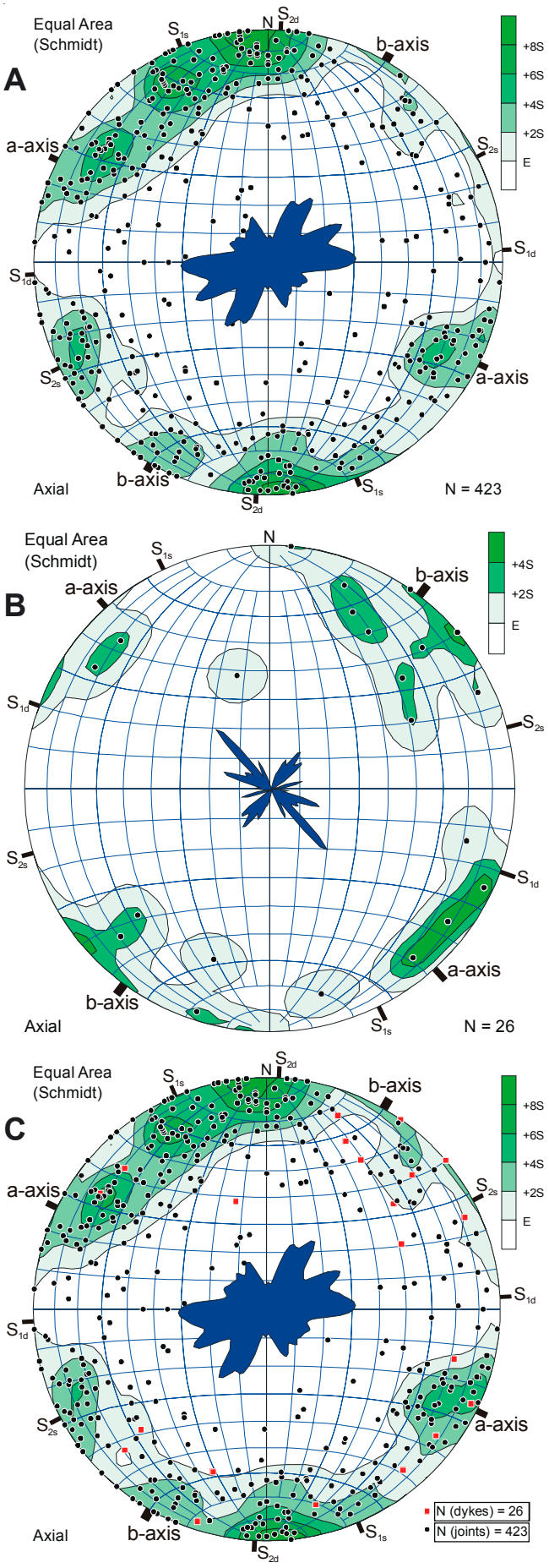

Abbr.	Explanation (with average strike)
b-axis	30°
a-axis	116°
S_{1d}	dextral first order shear direction: 87°
S_{1s}	sinistral first order shear direction: 158°
S_{2d}	dextral second order shear direction: 3°
S_{2s}	sinistral second order shear direction: 63°

Abbr.	Explanation (with average strike)
b-axis	37°
a-axis	138°
S_{1d}	dextral first order shear direction: 110°
S_{1s}	sinistral first order shear direction: 154°
S_{2s}	sinistral second order shear direction: 75°

Abbr.	Explanation (with average strike)
b-axis	30°
a-axis	116°
S_{1d}	dextral first order shear direction: 87°
S_{1s}	sinistral first order shear direction: 157°
S_{2d}	dextral second order shear direction: 3°
S_{2s}	sinistral second order shear direction: 62°

Fig. 2-35: Schmidt Net showing all joints measured on Potter Peninsula (A), the orientation of the investigated dykes (B) and a compilation of all tectonic data (C). Cooling joints within the dykes have not been plotted. Contours as explained in Fig. 2-2. Poles to planes. The tables to the right of the stereograms summarize the principal tectonic directions of the respective net.

2.3.5 Admiralty Bay

This locality is situated NE of Maxwell Bay (Fig. 2-18, at approx. 62° 8' S, 58° 25' W) and forms the largest fjord system of King George Island. Towards the south it opens to Bransfield Strait (Fig. 2-36), to the north it branches into three embayments (Ezcurra Inlet, Mackellar Inlet and Martel Inlet). Already during the last century, the protected coves and ice-free areas around Admiralty Bay have frequently been used by whalers, and hundreds of whale-skulls and -ribs today still scattered along the shores give testimony of this time. Admiralty Bay is home to several scientific bases and summer stations: "Comandante Ferráz" (Brazil), "Machu Picchu" (Peru), "Copacabana" (USA) and "H. Arctowski" (Poland). The latter was used as homebase during few days of field work in January 2002.

Most of the rocks cropping out around Admiralty Bay belong to the King George Island Supergroup (KGIS), a stratiform volcanic sequence of 2500-3500 m thickness which has been assigned Late Cretaceous through Late Oligocene ages [Birkenmajer 2001]. This succession consists predominantly (approx. 90%) of lavas and pyroclastic rocks and subordinately of intercalated freshwater deposits of pyroclastic origin [e.g. Birkenmajer 2003].

At inner Admiralty Bay, stratiform piles of metavolcanics and metasediments have been distinguished into Cardozo Cove Group, Martel Inlet Group and Dufayel Island Group. These successions have been assigned to the Upper Cretaceous through Eocene [e.g. Birkenmajer 2003].

Plutonic intrusions of the Wegger Peak Group and hypabyssal dykes and sills of the Admiralty Bay Group pierce the King George Island Supergroup. Most of the dykes investigated at this locality belong to the Admiralty Bay Group, subdivided by Birkenmajer [2003] into five informal units of formation rank: (1) Sphinx Hill dykes, (2) Panorama

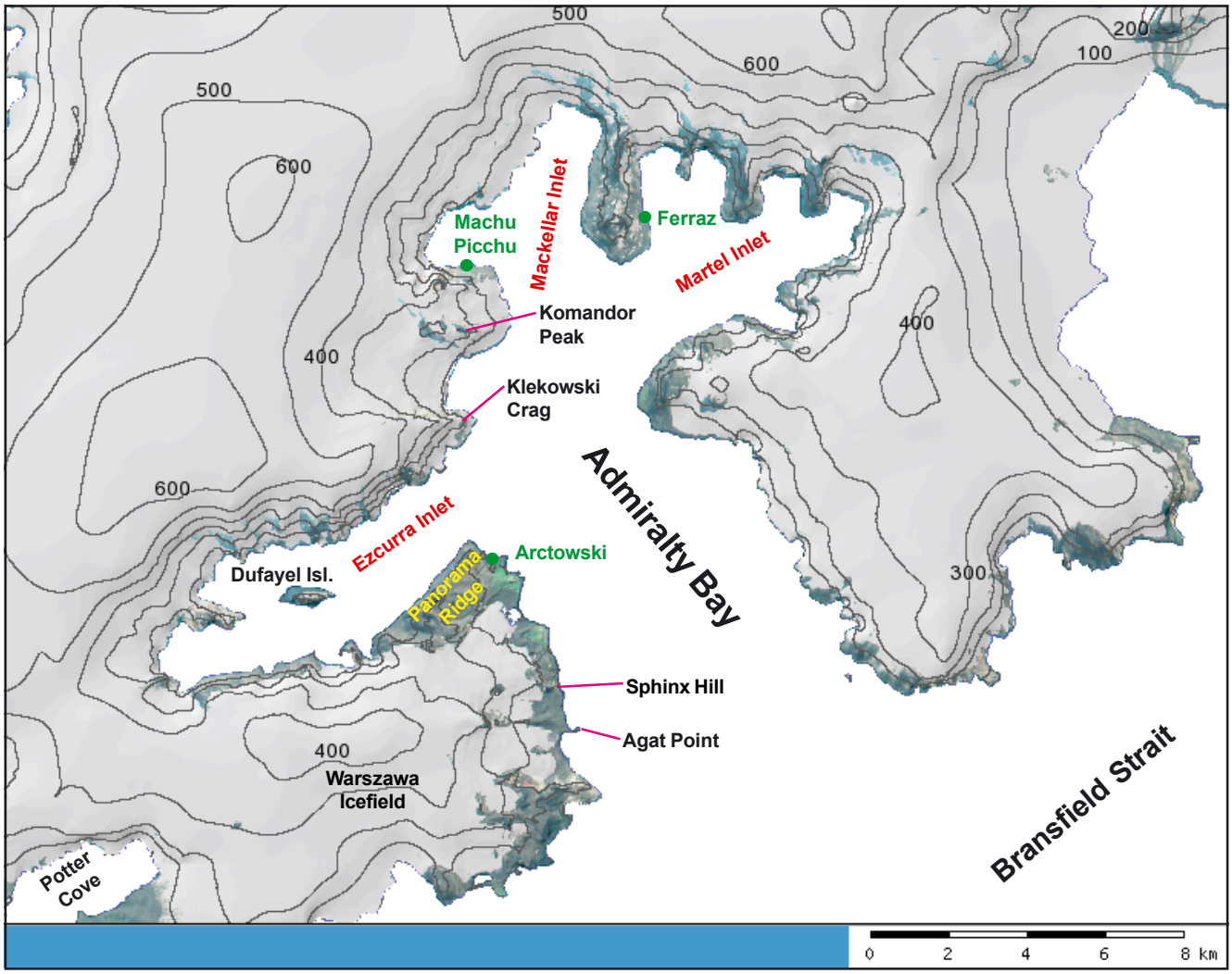

Fig. 2-36: Geography of Admiralty Bay, the largest fjord system on King George Island. Map created by S. Kraus (2004), topographic subset courtesy of IPG Freiburg.

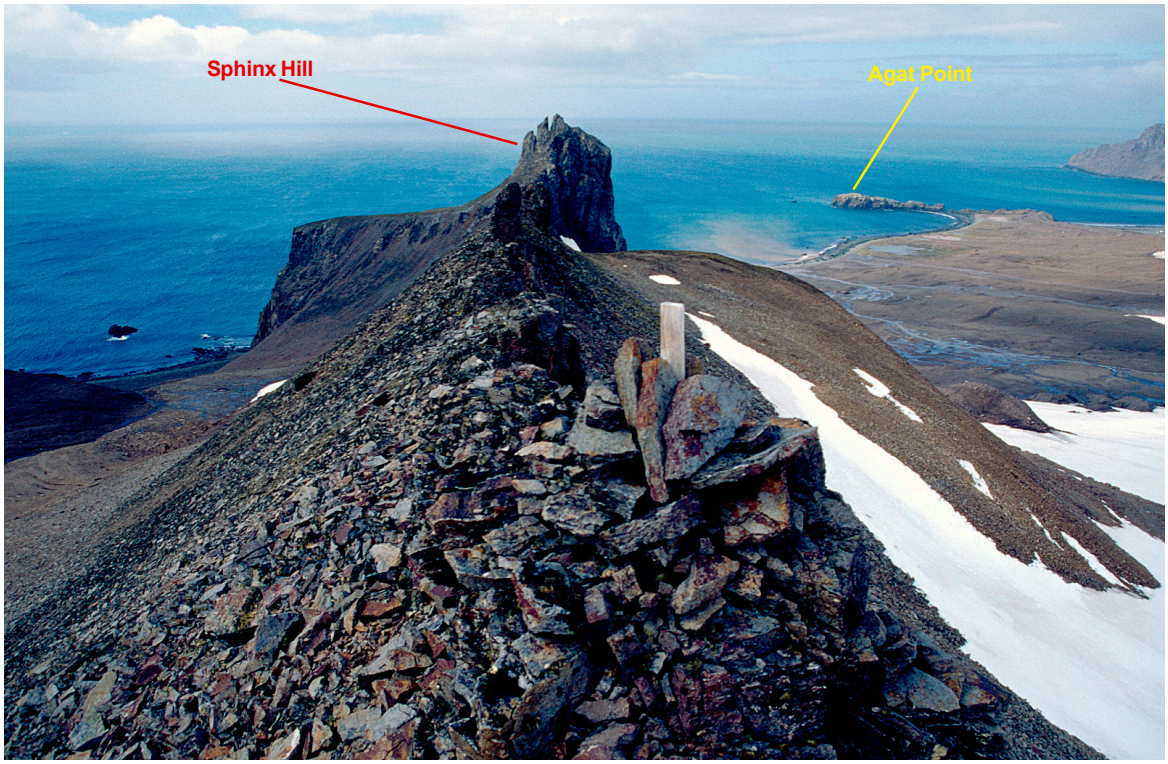

Fig. 2-37: Sphinx Hill, the longest and thickest dyke known on the South Shetland Islands so far. View towards SE along the ridge of the dyke. Agat Point (Fig. 2-39) is visible on the right side.

Fig. 2-38: Crisscrossing dykes cutting Panorama Ridge (south side of Ezcurra Inlet). View towards southwest.

Fig. 2-39: Agat Point, a huge dyke forming a promontory at the entrance of Admiralty Bay. View towards east.

Ridge dykes, (3) Jardine Peak plugs, (4) Jersak Hills plugs and dykes, (5) Hervé Cove dykes (in this stratigraphic order).

The field work has been carried out by foot and Zodiac boat along the western coast of Admiralty Bay between Bransfield Strait and Ezcurra Inlet, along the southern shore of Ezcurra Inlet (including Dufayel Island), and on two mountainous ridges directly north of the entrance of Ezcurra Inlet, Klekowski Crag and Komandor Peak (Fig. 2-36). It has been pointed out before, that one of the major strike-slip faults which transects King George Island, the Ezcurra Fault, is running in NE-SW direction along Ezcurra Inlet.

The dykes closest to the Ezcurra Fault appear to be also the most alterated ones. This might be due to hydrothermal activity affecting the wall rocks of the fault and therefore also the dykes cropping out in close vicinity. The following description of the different dyke groups follows the order of the aforementioned subdivision by Birkenmajer [2003].

(1) The type locality of the *Sphinx Hill dykes* is Sphinx Hill (Fig. 2-36, 2-37), a huge dyke forming a prominent ridge located at the coast half way between Bransfield Strait and Ezcurra Inlet. It stretches about 1 km in NW-SE direction (strike approx. 110°) and is about 200 m wide. The rock consists of porphyritic rhyodacite/rhyolite, locally showing dark banding (cm-scale, flow banding?) oriented vertically or steeply dipping towards SE. Platy disintegration of the rock is oriented parallel to this banding. The dyke limits can not be determined precisely due to voluminous debris coverage. The weathering surface is winered-grey and bears brown lines along the mentioned dark banding (effect of Fe^{3+}?), moreover numerous whitish feldspar-phenocrysts (mm-scale). Scarce angular andesitic xenoliths are whitish-grey and measure up to 10 cm in diameter. Sphinx Hill is by far the biggest dyke investigated within this project and is of Lutetian age (47.09 Ma, see chapter 5).

(2) A conspicuous swarm of relatively thin (average 1.1 m), porphyritic basaltic to andesitic dykes represents the *Panorama Ridge Dykes* which cut the likewise named ridge stretching along the southern shore of Ezcurra Inlet close to Arctowski Base (Fig. 2-36, 2-38). Panorama Ridge consists mostly of lenticular lavas alternating with pyroclastic rocks and shows locally strong alteration, probably due to the close vicinity of Ezcurra Fault. This holds also for many of the dykes belonging to this group. Their strike directions vary between 14° and 74° with a peak around 40°. A brownish weathering surface with whitish plagioclase (up to 1 cm) and less frequently dark-green pyroxene phenocrysts (up to 3 mm) is typical, as well as blocky disintegration and the absence of columnar jointing. Tectonic joints are often sealed by calcite. Some of the dykes show slightly varying course (zigzagging) and thickness, in other cases flow banding has been observed. Folding stated along the southern shore of Ezcurra Inlet within the rocks of Panorama Ridge is restricted to the host rocks and most probably related to the movement along the major Ezcurra strike-slip fault, resulting in drag folds. This assumption is supported by the restriction of folding to outcrops along this coast but its absence further away from Ezcurra Inlet. Because of this supposedly local character, these folds have not been included into the tectonic dataset. However, the lack of folding within the dykes leads to the conclusion that movement along the Ezcurra Fault occurred *before* intrusion of the dykes. No age determinations have been attempted at samples of this dyke group due to the overall high degree of alteration.

(3) No dykes have been attributed to the *Jardine Peak* group. It consists only of plugs.

(4) According to Birkenmajer [2003], two of the investigated dykes belong to the *Jersak Hills* dyke and plug group: A prominent dyke at Agat Point (Fig. 2-36, 2-37, 2-39) and another one at Shag Point (at close vicinity to Arctowski Base). Both dykes strike approx. 75° and are considerably thicker and fresher than the Panorama Ridge Dykes. The Agat Point dyke is about 70 m thick and forms a promontory at the coast close to the entrance of Admiralty Bay. It consists of fresh basaltic andesite showing a brownish weathering surface and blocky cleavage. Columnar jointing is absent. The fresh surface is grey and aphanitic and the dyke is displaced along a small, NW-SE trending fault belonging to a system which is believed to postdate the Ezcurra strike-slip fault [Birkenmajer 2001]. The name-giving agate occurs as multicolored geodes of up to football-size widely distributed within the dyke and indicates a considerable gas content at the time of intrusion. Agat Point yielded an Ar-Ar age of 54.0 Ma

(Ypresian, see chapter 5) and is thus older than Sphinx Hill. This stands in conflict with the stratigraphical order put up by BIRKENMAJER [2003], according to which the Agat Point dyke should be younger than Sphinx Hill and the Panorama Ridge Dykes. The dyke at Shag Point is a basalt of similar freshness as Agat Point, about 10 m thick and can be interpreted as an apophysis of a small adjacent plug. The vertical dyke is accessible only at very low tide. Plagioclase phe-

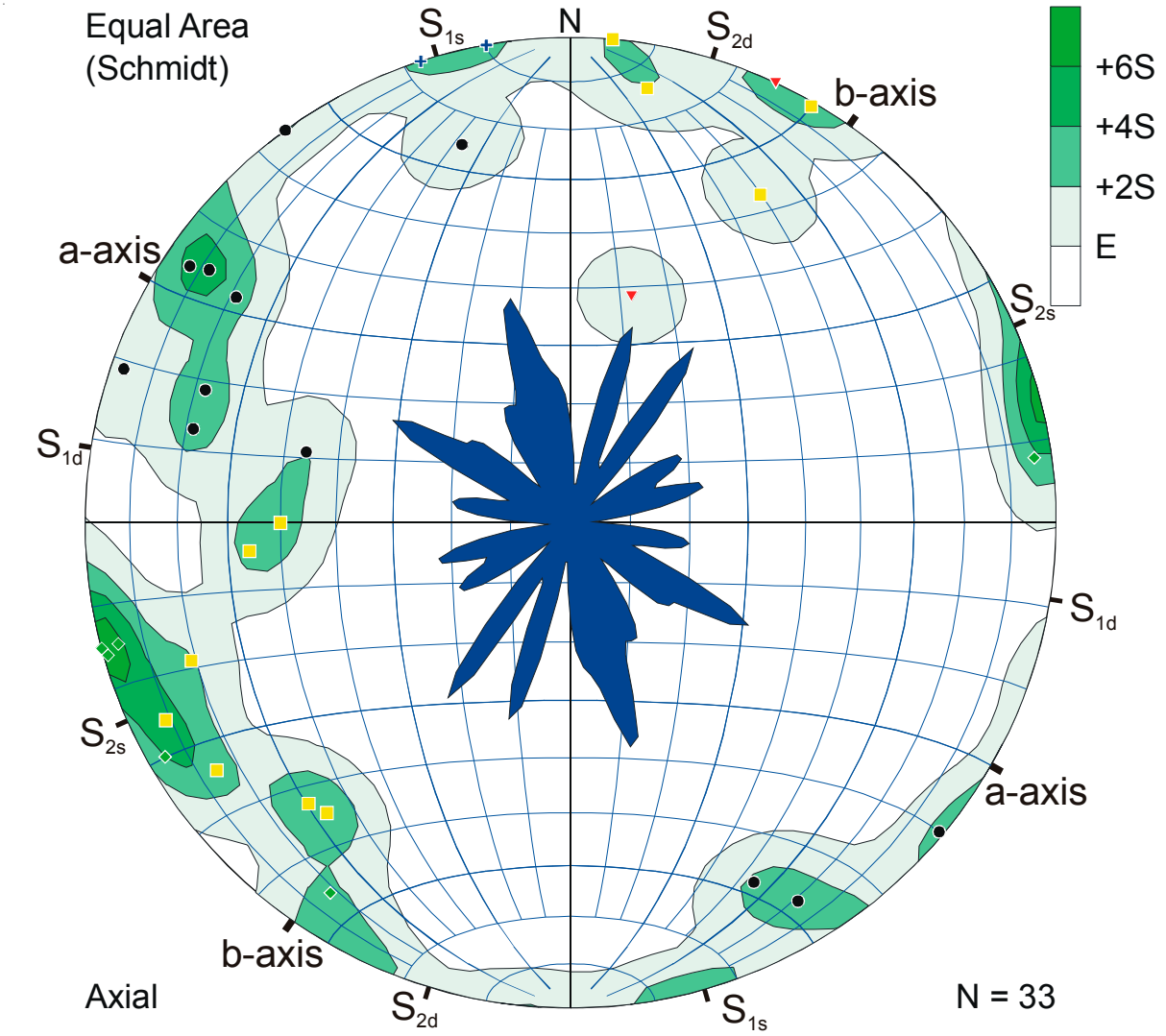

V	◆	Klekowski Crag & Komandor Peak Dykes (45 Ma, average orientation: 158/88 NE)
IV	■	Hervé Cove Dykes (average orientation: 136/77 NE)
III	▼	Sphinx Hill Dyke (47 Ma, average orientation: 111/65S)
II	+	Jersak Hills Dykes (54 Ma, average orientation: 76/90 S)
I	●	Panorama Ridge Dykes (average orientation: 38/80 SE)

Abbr.	Explanation (with average strike)
b-axis	35° (bc-planes: 35/82 SE)
a-axis	120° (ac-planes: 120/84 NE)
S_{1d}	dextral first order shear direction: 99°
S_{1s}	sinistral first order shear direction: 164°
S_{2d}	dextral second order shear direction: 17°
S_{2s}	sinistral second order shear direction: 66°

Fig. 2-40: Schmidt Net showing the orientation of all dykes studied in Admiralty Bay. Contours as explained in Fig. 2-2. Poles to planes. The stratigraphical order (lower left) is only tentative and by no means definite (see text). The table (lower right) summarizes the principal tectonic directions.

nocrysts visible on the grey weathering surface are aligned and of mm-size.

(5) The type locality of the *Hervé Cove Dykes* is a likewise named small cove located at the southern shore of Ezcurra Inlet opposite Dufayel Island (Fig. 2-36). This group comprises basaltic to andesitic dykes which followed NW-SE trending faults (average strike 137°), interpreted as transversal to and thus postdating the Ezcurra strike-slip fault [Birkenmajer 2001, 2003]. Due to rather strong alteration, no age determinations have been carried out on these dykes within this work, but Birkenmajer [2001] supposes an Early Miocene age for this group. The thickness of the Hervé Cove dykes averages 4 m, but scatters considerably between 0.5 and 20 m. They show a brownish to brownish-green, sometimes porous weathering surface and often calcite/quartz/zeolite-sealed joints. Phenocrysts comprise up to 1 cm long dark green, euhedral pyroxenes and numerous plagioclase crystals, but some dykes are also aphanitic. Amygdales occur and are elongated along-strike of the respective dyke. Some dykes feature small quartz-geodes, predominantly towards the rim. Columnar jointing is scarce, blocky cleavage common, also flow banding has been observed.

(6) Additional dykes not included in the groups mentioned by Birkenmajer [2001, 2003] have been investigated on two mountain ridges immediately north of Ezcurra Inlet. On the northern slopes of Klekowski Crag and Komandor Peak (Fig. 2-36), NW-SE trending dykes cut strongly altered stratiform volcanics (lava alternating with tuffs and agglomerates) attributed to the Cardozo Cove Group [Birkenmajer 2003]. This group belongs to the tectonic unit called Barton Horst (Fig. 2-21) and is located north of the dextral Ezcurra strike-slip fault. Barton Horst is well known for its comparatively high degree of alteration (see pp. 35-39). The average strike of the dykes is 157° and their inclination is generally subvertical. Their composition is basaltic to andesitic, and the often brownish-yellowish weathering surface shows plagioclase- and pyroxene-phenocrysts of up to cm-size, the fresh surface is grey. The dykes at Komandor Peak tend to form morphologically conspicuous, up to 30 m high and 100 m long ridges protruding from the slope of the mountain. Most of the dykes are approx. 5 m thick, others only 30 cm. In contrast to the Panorama Ridge Dykes, orthopyroxene occurs as phenocrysts, and columnar jointing is frequent in this group. From all dyke groups studied in Admiralty Bay, this one shows the highest degree of alteration, probably due to its position within the Barton Horst. However, one of the dykes from Komandor Peak (KP-1, 422579 / 3113331, UTM, WGS 84) gave an Ar-Ar age of 45.41 Ma (Lutetian), the youngest dyke-age determined in Admiralty Bay within this project.

No joint measurements have been carried out in Admiralty Bay due to the very short stay and because extensive joint data are available from literature [e.g. Tokarski 1984, 1987]. These data will be considered in combination with own data on the orientation of the dykes.

A b-axis as inferred from the overall tectonic regional schedule observed in Admiralty Bay strikes 35° (Fig. 2-40), differing no more than 5° from the axis determined on Potter Peninsula (Fig. 2-35), and about 10° clockwise from the folding axis observed on Hurd Peninsula (Fig. 2-7). A sharply expressed orientation at 35/82 SE may represent bc-planes. The a-axis strikes 120° and well developed ac-planes are oriented 120/84 NE. The dextral first order shearing (S_{1d}) is weakly developed at 99/72 S. The corresponding sinistral first order shearing (S_{1s}) lies at 164/85 E, is the strongest developed shearing direction (Fig. 2-40) and varies between 150° and 175°. The dextral second order shearing (S_{2d}) is sharply expressed at 17/62 E. A corresponding sinistral second order shearing (S_{2s}) oscillates between 59° and 74° and has an average orientation of 66/88 NW.

Tokarski [1981, 1987] distinguishes three sets of predominantly extensional joints: (1) Set I (90-120°), (2) Set II (160°), (3) Set III (40-70°) and states a temporally separated development for these joints due to a clockwise rotation of σ_1, rejecting a contemporaneous one.

However, in many of the stereonets published by him (e.g. Tokarski 1987, p. 143, Fig. 12) he assigns two or more maxima to the same set of joints. These maxima can also be attributed separately to the different shear directions described above. For example, in most of his stereonets his set I (90-120°) is composed of two maxima which can be split up into the dextral first order shear direction (99°, S_{1d}) and the ac-direction stated here as 120°. Another maximum interpreted by him as part of his set II (160°), does

well correspond to the sinistral first order shear system (164°, S_{1s}) distinguished here. The same applies to his set III (40-70°), which shows maxima corresponding well with the sinistral second order shearing (66°, S_{2s}), maybe also including some ac-joints.

Summarizing, it can be stated that the tectonic data published by TOKARSKI [1981, 1984, 1987] confirms fully the shear directions deduced here from the orientation of the dykes, but his interpretation differs considerably from the one presented here.

Having a look at the different dyke groups studied in Admiralty Bay, the Panorama Ridge Dykes used different directions evenly distributed: a third of them seem to have intruded along bc-planes, another third along S_{2d} and the remaining third along S_{2s} (Fig. 2-40). The Jersak Hills Dykes (Agat Point and Shag Point) seem to have intruded along S_{2s} (Fig. 2-40). The main part of the long Sphinx Hill dyke intruded along an ac-plane, an apophysis used the S_{1d}-direction. The Hervé Cove Dykes intruded mainly along S_{1s}- and ac-planes, few of them along S_{1d}. The dykes cropping out north of Ezcurra Fault at Klekowski Crag and Komandor Peak used predominantly sinistral first order shear planes (S_{1s}), subordinately ac-planes.

Due to the lack of outcrops of dyke crossings in Admiralty Bay, it has not been possible to establish a relative time sequence based on field relationships as in case of Hurd Peninsula. The low number of Ar-Ar age determinations is a consequence of the high alteration grade especially in the vicinity of the Ezcurra Fault, thus, a chronological order of the studied dyke groups remains speculative at present. Comparing the sequence of the different directions taken by the dykes on Hurd Peninsula with the preferred directions in Admiralty Bay, it seems as if the Panorama Ridge Dykes are the oldest group, corresponding to the second intrusive event on Hurd Peninsula.

The Jersak Hills Dykes could be correlated with the third event on Hurd Peninsula, and their Ypresian age (54 Ma) would thus constrain an earliest Eocene or even Paleocene age for the Panorama Ridge Dykes. The very high degree of alteration shown by the latter might therefore also be due to their possibly lowest stratigraphical position, not only to the vicinity to the Ezcurra Fault. The Sphinx Hill Dyke might correspond to the dykes of the fourth event that used ac-planes also on Hurd Peninsula, and the remaining two groups (Hervé Cove Dykes and Klekowski Crag / Komandor Peak Dykes) are doubtlessly younger, as indicated by their lower degree of alteration and an 45.4 Ma Ar-Ar age obtained for the Klekowski Crag and Komandor Peak dykes.

Summarizing, hard evidence for a chronological order of the Admiralty Bay dyke groups is sparse, but three arguments support the supposed sequence:

(1) The three Ar-Ar ages obtained in Admiralty Bay are in good agreement with the inferred relative time sequence.

(2) The conspicuous high degree of alteration of the Panorama Ridge Dykes as compared to the other groups supports their low stratigraphical position. The Hervé Cove Dykes, though in the same vicinity to Ezcurra Fault, are less altered.

(3) The sequence of the directions preferred by the different events on Hurd Peninsula (Table 2-3, p. 29) corresponds largely with the sequence of directions inferred for Admiralty Bay. For example, the supposedly older Panorama Ridge Dykes use the bc- and S_{2s}-directions like the second intrusive event on Hurd Peninsula. The younger groups - Hervé Cove Dykes and Klekowski Crag / Komandor Peak Dykes - prefer the S_{1s}- and ac-directions.

2.4 Penguin Island

This island volcano is situated at 62° 6' 7" S, 57° 55' 42" W at the northeastern entrance of King George Bay (Fig. 2-18), thus being located at the northern margin of the Bransfield Strait rift which is separating the South Shetland Islands from the Antarctic Peninsula crustal block. Penguin Island measures between 1.4 and 1.8 km in diameter and covers an area of 1.84 km^2.

Penguin Island has been assigned a Pleistocene/Holocene age [Barton 1965; Birkenmajer 1980c, 2001; González-Ferrán & Katsui 1970] and thus has been related to the recent opening of Bransfield Strait. The development of the volcano certainly postdates the activity of the South Shetland Islands magmatic arc and therefore no relation should be expected to the dykes cropping out elsewhere on the archipelago.

However, during a three hours stop, the opportunity has been taken to sample radial dykes cutting the stratocone in order to compare their mineralogy, geochemistry and isotopy with the much older dykes studied within this project. It was expected to get some hints on common features (e.g. a crust derived component reflected by the isotopy) and an insight into changes of magmatism since cessation of activity of the magmatic arc.

Geological frame

Penguin Island consists of a 171 m high, recent basaltic stratocone featuring a central plug and radial dykes (Fig. 2-41, 2-42). This stratocone is built upon a basaltic platform [Birkenmajer 1982c]. The volcano is the type locality of the Penguin Island Group, subdivided further into (1) Marr Point Formation (oldest), (2) Deacon Peak Formation and (3) Petrel Crater Formation [Birkenmajer 1980c;

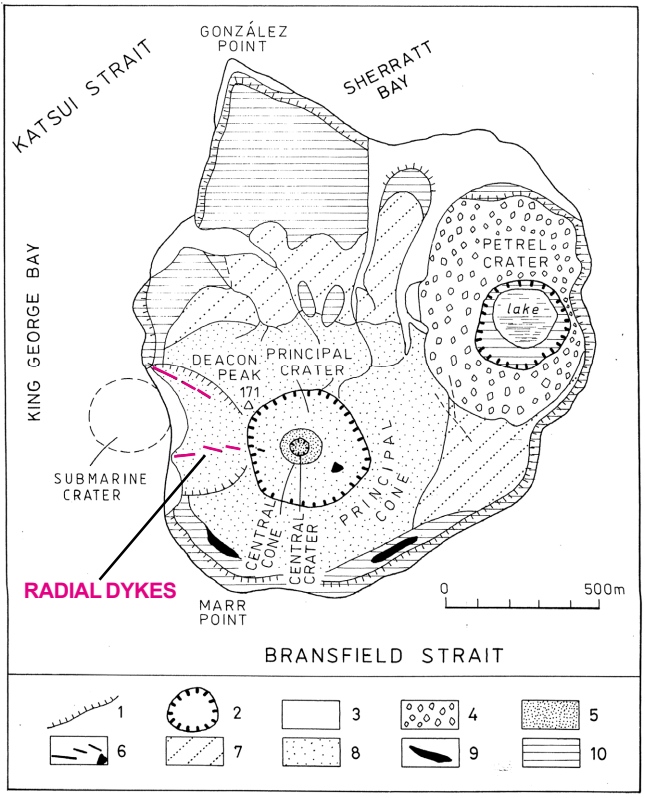

Fig. 2-41: Geological map of Penguin Island volcano (slightly mod. after Birkenmajer 2001, p. 71). (1) escarpment; (2) crater rim; (3) alluvia, beach; (4) Petrel Crater Fm.; (5-8) Deacon Peak Fm. [(5) central cone; (6) radial dykes and plug; (7) thin ash cover; (8) principal cone]; (9) raised beach gravel; (10) Marr Point Fm. (plateau basalt alternating with beach deposits).

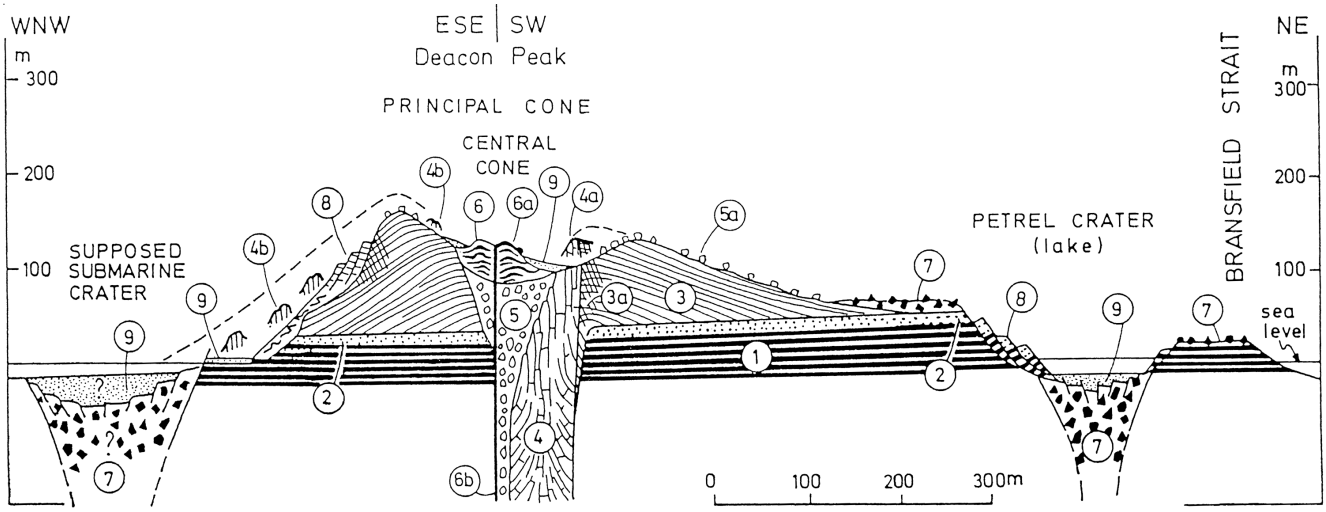

Fig. 2-42: Geological cross section of Penguin Island volcano [taken from Birkenmajer 2001, p. 72]. *Marr Point Fm.* (1) plateau basalt with beach-gravel intercalations; (2) sand with basalt blocks; *Deacon Peak Fm.* (3) stratocone; (3a) welded agglomerate and tuff; (4a) plug; (4b) radial dykes; (5) supposed explosion breccia from fragmented plug; (5a) loose fragments of basalt from fragmented plug; (6a, b) central cone [(6a) last basalt flow; (6b) supposed basalt feeder vein]; *Petrel Crater Fm.* (7) vent rim breccia; (8) collapse structures; (9) crater fill and beach.

1982c]. The Marr Point Formation (stratigraphically lowest) comprises the mentioned platform, built up by olivine-augite lavas alternating with beach deposits, and features an exposed thickness of max. 50 m (Fig. 2-42). It has been suggested to be of Late Pleistocene age [Birkenmajer 1982c].

The Deacon Peak Formation builds up the stratocone resting upon the aforementioned platform and consists of redbrown basaltic material comprising lava flows, pyroclastics, a central plug and the sampled radial dykes. Its age has been determined by lichenometric dating as 18th to mid-19th century [Birkenmajer 1980c].

The stratigraphically uppermost unit is the Petrel Crater Formation, comprising a water-filled explosive maar (Petrel Crater) at the northeastern side of the island and a submarine crater on its western side (Fig. 2-41). The explosive activity of the latter removed large parts of the western slopes of Deacon Peak, leaving the radial dykes of the Deacon Formation protruding from an amphitheater-like caved slope. The Petrel Crater Formation and thus these craters are believed to have formed in 1905, as determined by lichenometric dating [Birkenmajer 1980c]. Penguin Island is supposed to be a dormant volcano [Barton 1965; Birkenmajer 1980c, 2001; González-Ferrán & Katsui 1970].

The olivine basalts of Penguin Island have been reported to feature the most primitive chemistry (low SiO_2, high MgO) of all Bransfield Strait lavas and are thus thought to represent the least modified mantle melts [Weaver et al. 1979]. This is fully confirmed by the geochemical and isotopic data obtained from the radial dykes sampled within this project (chapter 4).

The radial dykes

The studied radial dykes crop out at the western slope of Deacon Peak between the beach and 120 m above sea level (Fig. 2-41, 2-42). Their strike varies between 95° and 120°, and they cross the slope diagonally. The dykes show prominent segmentation, with the individual segments forming up to 50 m long and 20 m high fragments arranged en echelon (Fig. 2-41). In general, they consist of massive basalt with varying degrees of vesicularity. Olivine is present as sub- to euhedral phenocrysts. Subordinately, also plagioclase occurs.

Like for large parts of the island, a redbrown to rusty color of the weathering surface is characteristic and might be a hint on reaction of the fresh and still hot material with rain water subsequently to magmatic activity.

Due to the very short stay on Penguin Island, no joint measurements have been possible. However, interpretation and comparison of tectonic data of Penguin Island with the datasets of the rest of the South Shetland Islands would not make sense anyway because of the much younger age of Penguin Island. This view is confirmed by Tokarski [1984], who stated that the volcanics on Penguin Island apparently are devoid of tectonic joints and that only thermal joints seem to be present.

Surprisingly, a plagioclase separate from the freshest dyke sample yielded a Tortonian (8.8 ± 2.4 Ma) Ar-Ar age (see chapter 5), not only far older than the Holocene age expected for the Deacon Peak Formation (to which the dykes belong), but also far older than the maximum age (Pleistocene) postulated for any unit on Penguin Island so far. The most probable explanation, the presence of older basement xenoliths in the dated sample, is highly unlikely.

Not the slightest sign of xenoliths has been noted, neither in the field nor during microscopy studies of the samples. The lack of xenoliths of pre-Quaternary rocks has also been emphasized as a characteristic feature of Penguin Island by other authors [e.g. Birkenmajer 1982c].

Hence, Penguin Island might be far older than believed so far, and all the features supporting a Pleistocene/Holocene age (unconsolidated tephra, young lichenometric ages, lack of alteration) may be due to recent activity of the volcano covering and destroying older features.

The dated radial dyke might represent part of an older unit not known so far which was buried until the explosive activity of the submarine crater on the western side of the island blew away its pyroclastic coverage.

To my knowledge, only lichenometric datings have been attempted on rocks of Penguin Island so far, thus the Tortonian age obtained within this project raises questions concerning the history of Penguin Island as well as the history of Bransfield Strait (see chapter 1).

3. Petrology

Deductions on petrologic characteristics are based on microscopic analyses and on microprobe data (see also Appendix II). The thin sections have been studied and digitally photographed using a Leica microscope. Microprobe analyses have been carried out on a Cameca SX50 on feldspar of the same 19 dykes as selected for Ar-Ar geochronology in order to determine the K_2O-content and the an-, ab- and or-components. Macroscopic characteristics of the studied dykes like thickness, weathering surface (incl. visible phenocrysts and their possible alignment), fresh rock appearance, columnar jointing, alignment of amygdales etc. has been discussed in chapter 2. For explanation of abbreviations see Appendix I.

3.1 General characteristics

3.1.1 Typical mineralogy and fabric

The dykes of the South Shetland Islands are predominantly of basaltic, basaltic andesitic and andesitic composition. Dacites and rhyolites occur subordinately. The dominant mineral is feldspar. On Hurd Peninsula, alkali feldspar- and plagioclase-bearing dykes occur, but on Nelson, King George and Penguin Island plagioclase is the only feldspar mineral present in the dykes. Typically, it occurs in two generations, as phenocryst and as groundmass constituent, but three or more generations or also serial fabrics occur in some cases. Albite-twinning is typical, Karlsbader twins are scarce.

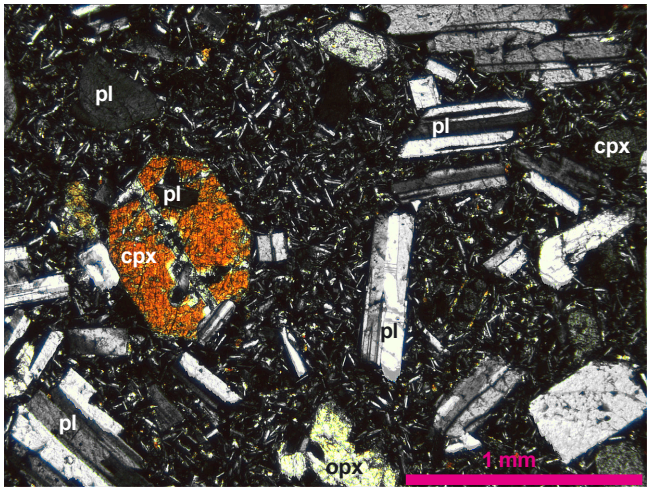

Fig. 3-1: Typical porphyric fabric of a very fresh basaltic andesite (sample EI-16) from Ezcurra Inlet, Admiralty Bay (King George Island). A euhedral, twinned cpx- and subhedral to euhedral pl-phenocrysts showing albite-twinning are embedded into a matrix consisting of pl, px (opx+cpx), ap, opq and devitrified glass. Note the ophitic fabric of pl enclosed by the cpx. At the central lower margin of the photo, an opx-phenocryst shows signs of corrosion. (X Nichols).

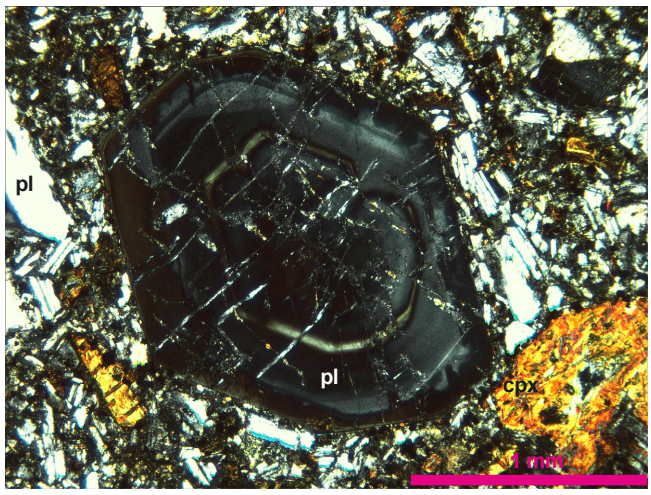

Fig. 3-2: A complexly zoned, euhedral plagioclase phenocryst showing abnormal interferences and pressure release cracks. The matrix consists of lath-shaped pl, subhedral cpx-crystals and opaque minerals. The phenocryst in the lower right corner is a cpx showing advanced alteration. Sample PP-2 is an andesite from Potter Peninsula (X Nichols).

Typically, the dykes show a (glomero-) porphyritic fabric (Fig. 3-1), with clinopyroxene- (augite) and feldspar-phenocrysts of 1-5 mm length (max. 8 mm). The percentage of the phenocrysts in the bulk rock is normally around 20% but may become as large as 35% in single cases. Ophitic enclosure of small plagioclase laths into pyroxene phenocrysts as well as the reverse case is common (Fig. 3-1).

In many cases, large plagioclase phenocrysts show conspicuous, complex zoning (Fig. 3-2) and sometimes concentrically aligned melt inclusions, evidence that they have not always been in equilibrium with the melt in which they grew. Magma mixing is the most probable explanation for this phenomenon, but disability of the phenocrysts to re-equilibrate with the melt during ascent through the lithosphere might also be a contributing factor. Another characteristic feature of many large plagioclase phenocrysts are pressure release cracks (Fig. 3-2).

These phenocrysts are of intratelluric origin and suffered fracturing caused by pressure release during ascent of the melt. This feature might be an indicator for a very rapid ascent of the respective melt, as slower rising should have allowed the phenocrysts to adjust their crystal structure to lower pressures without fracturing.

The phenocrysts are embedded into a matrix consisting predominantly of feldspar and clinopyroxene

(augite), subordinately of opaque minerals (magnetite, ilmenite), accessory apatite and variable amounts of alteration minerals (see below). Apatite is present in nearly all dykes as groundmass-mineral sharing around 5% and forms up to 100 µm long, thin needles, sometimes tightly intergrown with plagioclase.

In some cases orthopyroxene (bronzite) occurs as additional phenocryst phase (Fig. 3-1, 3-4), nearly always altered more strongly than the accompanying clinopyroxene and in single cases surrounded by a clinopyroxene rim, indicating earlier growth. Olivine is absent in all areas except for Penguin Island (see below). Hornblende has been observed in none of the studied dykes.

Summarizing, the typical and representative magmatic paragenesis of the South Shetland Islands dykes is akf+cpx±opq±ap for Hurd Peninsula and pl+cpx±opx±opq±ap for the other areas.

3.1.2 Alteration

Alteration is common in any of the dykes of the South Shetland Islands with only very few exceptions. The most common alteration minerals are calcite, chlorite and sericite, less frequently also epidote, albite, quartz and zeolite.

According to microscopic observations, an alteration index (AI, Table 2-2) has been assigned to each studied dyke. Based on this AI, samples were chosen for geochemical, isotopic and geochronological work. The average AI calculated for each investigation area

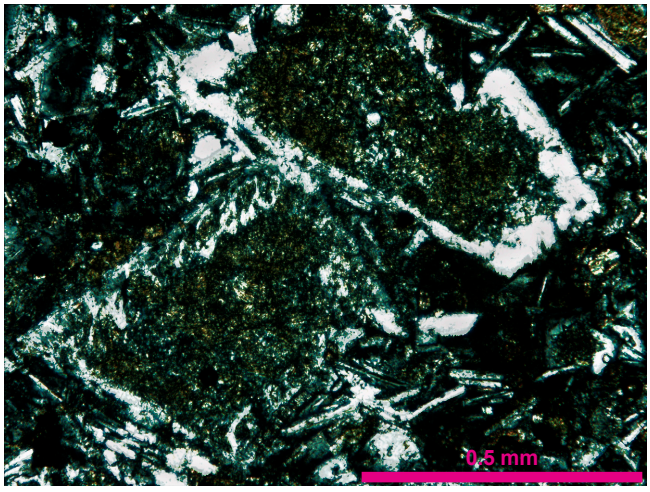

Fig. 3-3: "Filled plagioclase". The anorthite-rich cores of two plagioclase phenocrysts are completely altered to a microcrystalline mixture of sericite and chlorite. The albite-rich rims remained stable under the given conditions. This type of alteration displays a normal crystallization history of the plagioclase: an anorthite-rich core forming during early phases and an albite-rich rim during later phases (X Nichols).

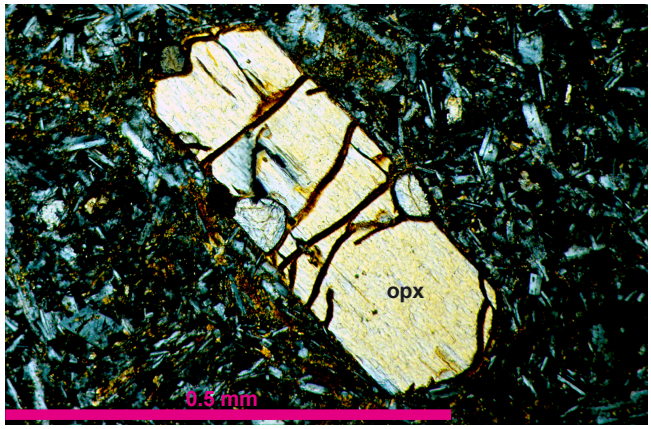

Fig. 3-4: A bronzite phenocryst showing beginning opacitization along fractures and corrosion embayments caused by disequilibrium with the melt (X Nichols).

confirmed well the stratigraphical distinct (lower) position of all areas belonging to the upthrown Barton Horst (high AI), as compared to adjacent, downthrown tectonic blocks (low AI, Fig. 2-21). Hurd Peninsula (Livingston Island) possibly also represents

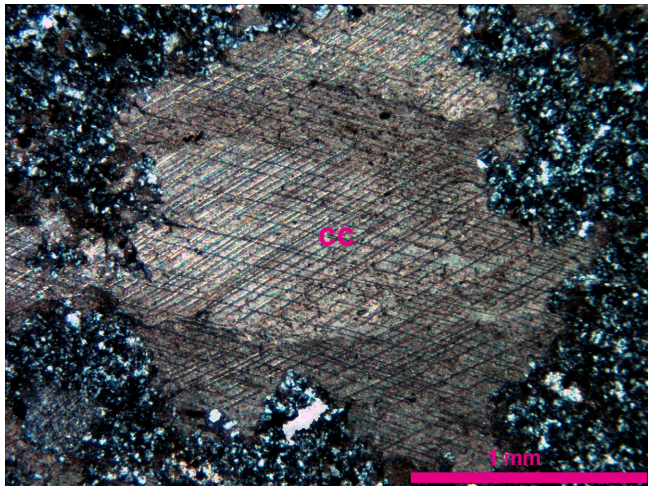

Fig. 3-5: Anhedral calcite in dyke HP-10B on Hurd Peninsula which has suffered pressure twinning as a consequence of tectonic deformation (X Nichols).

part of an upthrown structure and might therefore be correlated with Barton Horst.

Concerning plagioclase, partial or complete alteration of anorthite-rich cores to sericite and chlorite (Fig. 3-3), leading to so-called "filled plagioclase", has been observed in many cases. This phenomenon is due to the albite-rich rims having a higher resistance against hydrothermal alteration than the anorthite-richer interior of the crystal, causing an earlier breakdown of the latter.

Orthopyroxene shows a type of alteration called opacitization, a process starting along fractures within

the crystal (Fig. 3-4), leading finally to complete disintegration under formation of opaque Fe-minerals. Pyrite occurs as accessory opaque alteration mineral especially in the acidic dykes, zeolite often represents the filling of amygdales with a rim of quartz around it.

The typically occurring secondary minerals (cc, chl, ser) indicate a hydrothermal type of alteration, maybe of autometasomatic character without change of chemistry. Calcite tends to form nests and fillings of amygdales or represents the major alteration product from disintegrating phenocrysts (plagioclase as well as pyroxene). In some cases, pressure twinning of calcite has been observed (Fig. 3-5), reflecting the tectonic deformation history. Chlorite and sericite derive predominantly from alteration of plagioclase, forming the filling of phenocrysts that have an albite-rich rim, but are also evenly distributed in the matrix.

However, especially in the areas belonging to the Barton Horst and correlated tectonic units (Weaver Peninsula, Barton Peninsula, part of Nelson Island and Hurd Peninsula), the additional occurrence of epidote/clinozoisite together with albite and quartz indicates lower greenschist facies conditions. This might be explained with the stratigraphically much lower position of these units as part of the "root" of the magmatic arc, coming along with higher temperatures and pressures. Whereas the albite commonly forms anhedral blasts usually of sub-mm size and is evenly distributed throughout the rock, epidote/clinozoisite and quartz occur most often in paragenesis with calcite and chlorite, especially as fillings of amygdales, alteration products of pyroxene or along fractures within plagioclase phenocrysts.

Some of these dykes have suffered complete alteration, consisting exclusively of secondary minerals, only pseudomorphs giving hints on the original magmatic phases.

3.2 The dyke groups on Hurd Peninsula

Two major mineralogical differences distinguish the dykes on Hurd Peninsula from the dykes elsewhere on the South Shetland Islands. First of all, only the two youngest dykes (HP-1A and HP-23, Fig. 2-8 & 2-9) bear plagioclase, whereas all other dykes contain alkali-feldspar or albite, the latter probably being an alteration product in most cases. The comparatively high potassium content reflected by the presence of alkali-feldspar in combination with

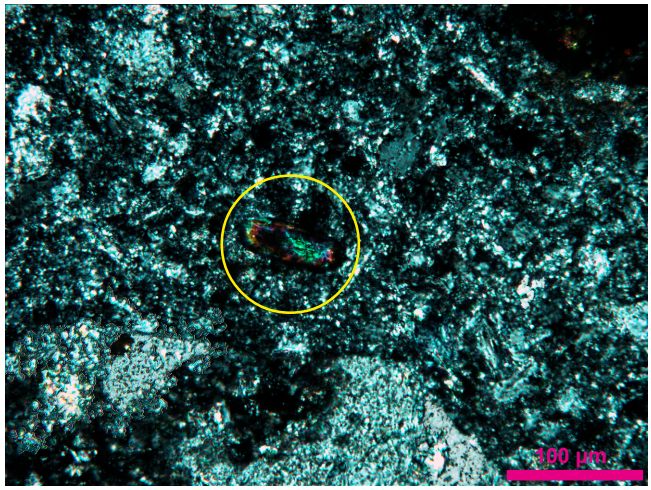

Fig. 3-6: A euhedral zircon (80 µm long, encircled) embedded in a matrix of cryptocrystalline feldspar and alteration minerals (predominantly chl) in the rhyolitic dyke HP-12 (X Nichols).

the low εNd-values (see chapter 4) indicates that these melts ascended through a still relatively unstretched continental crust during an initial phase of subduction zone volcanism in that area. Moreover, this corroborates the assumption that the dykes on Hurd Peninsula are older than all other investigated dykes, and that dyke intrusion started earlier in the SW than in the NE.

The second difference to the dykes studied elsewhere is the complete absence of opx in any of the dykes, indicating temperature conditions and Fe-Mg-Ca compositions allowing only the formation of cpx, if any. Some dykes on Hurd Peninsula do not even contain cpx. Having a look at the dyke groups defining the different intrusive events on Hurd Peninsula, no striking mineralogical differences can be stated between these groups (except for the mentioned presence of plagioclase in the two youngest events). Obviously, identification of events having a different age, history or even magma source is hardly possible only by means of petrologic constraints, at least in case of the first four intrusive events. Likewise, rock types are the same and the fabric is very similar to dykes in other parts of the South Shetland Islands. However, some differences between the groups are to be mentioned. In the following, a brief description of the group-specific features will be given in the order of the distinguished intrusive events (I-VI, Fig. 2-8), concentrating on the "abnormal" characteristics:

(I) This event consists of one single, porphyric dyke (HP-7D) of trachyandesitic composition. Feldspar is represented predominantly by orthoclase

(Or_{91-97}) and secondary albite. It contains no pyroxene but is furthermore inconspicuous.

(II) This group consists of 8 dykes of predominantly andesitic/dacitic composition. Feldspar is present as anorthoclase and albite. 50% of the dykes contain clinopyroxene, indicating a change in the magma source and the crystallization conditions as compared to event I.

(III) Event III is represented by 16 dykes of basaltic to rhyolitic composition with an emphasis on andesites. Albite is the major feldspar phase present in the dykes of this group. $^2/_3$ of the dykes contain cpx, continuing the trend towards a stronger presence of that mineral group. Some exotic dykes belong to this group, e.g. a rhyolitic dyke (HP-12) containing scarce euhedral zircons of up to 80 µm length (Fig. 3-6). The same dyke features approx. 70 cm thick rims on both sides which are not part of the chilled margin but nevertheless characterized by a markedly darker color and a lower frequency of phenocrysts, gradually passing into the lighter and phenocryst-richer interior. Though these rims are undoubtedly *not* separate dykes sandwiching a third one between them, as in the case of the multiple intrusion described from Potter Peninsula, the pattern is similar. The gradual concentration of the phenocrysts towards the dyke centre could possibly be explained by gravitational separation of early formed crystals in a magma chamber followed by injection of the crystal-stratified magma into the dyke. Subsequent flow differentiation might have resulted in the effect described for the multiple intrusion on Potter Peninsula, with the phenocryst-poor (and therefore lower viscous) magma enclosing the phenocryst-richer (and thus higher viscous) batch, facilitating propagation for the whole dyke. The same effect has been observed in two other dykes of this group (HP-10B and HP-26).

(IV) Group IV comprises 17 dykes of basaltic to andesitic composition, but the general tendency is more mafic (basaltic) as compared to the preceding events. At least in some dykes of this group, alkali-feldspar is the dominant feldspar phase, ranging from albite to orthoclase in composition. Some bear plagioclase. All except for two dykes contain clinopyroxene, and most show a porphyritic fabric. Four dykes of this group draw special attention because of the noticeable predominance of cpx-phenocrysts over plagioclase. One of them (HP-18) is a basalt completely lacking plagioclase phenocrysts, but bearing plenty of euhedral, sometimes twinned cpx-phenocrysts of up to 2.5 mm length. Surprisingly, in some of the dykes the clinopyroxene is preserved much better than the plagioclase, sometimes not showing the slightest sign of alteration. This stands in contrast with the majority of the studied dykes, in which the alteration grade of the px is mostly the same or higher than that of pl.

(V) This event produced only two dykes in the study area on Hurd Peninsula, both of basaltic andesitic composition. Plagioclase (An_{10-37}) and secondary albite are the prevailing feldspar phases. Both dykes bear pyroxene and are aphyric but furthermore inconspicuous.

(VI) The last intrusive event on Hurd Peninsula produced an andesitic dyke showing a porphyric fabric and bearing also euhedral pyroxene of up to 1.5 mm length. Its feldspar content comprises albite and plagioclase (An_{20-36}).

Summarizing, the dominant and most prominent features distinguishing the dykes cropping out on Hurd Peninsula from the dykes elsewhere on the South Shetland Islands are:

- the lack of plagioclase in dykes of the first four events
- the complete lack of orthopyroxene
- the gradual introduction of clinopyroxene from event to event, tightly correlated with a decrease in potassium content and orthoclase-component in the feldspars, finally leading to the introduction of plagioclase during the last two events.
- the occurrence of zircon in single dykes
- dyke banding as a probable consequence of flow differentiation

3.3 The dykes on Nelson Island

Petrologic characteristics of the dykes on Nelson Island are tightly bound to their strike, probably defining different intrusive events. Three of the dykes studied at O'Cain Point (Fig. 2-18) are running parallel at approx. 110° and share the following characteristic features:

- all three are porphyritic dacites
- complete lack of pyroxene
- relatively few, strongly altered pl-phenocrysts
- thin, dyke-parallel joints sealed with cc and qz
- cc alteration prevails

The mentioned joints are probably cooling joints, running dyke-parallel and bound by diffuse brown banding on either side (Fig- 3-7), maybe induced by

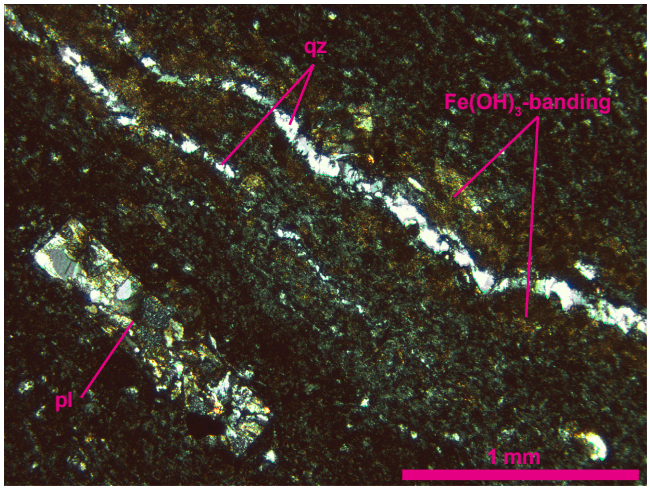

Fig. 3-7: Dyke NI-2 at O'Cain Point (Nelson Island), a porphyric dacite bearing few plagioclase phenocrysts. The qz-sealed joint crossing the photo diagonally is oriented dyke parallel, probably a cooling joint later infiltrated by Fe- and SiO_2-rich fluids that led to qz-mineralization and the marked brown banding (possibly $Fe(OH)_3$) on either side (X Nichols).

Fe-infiltration derived from fluids running along the cracks that also caused the noticeable qz-mineralization. The same phenomena have been observed in the Sphinx Hill Dyke in Admiralty Bay.

The fourth dyke at O'Cain Point and one dyke studied at New World Point (Fig. 2-18) strike 68° and 95°, respectively, and are of basaltic and basaltic andesitic composition. They contain clinopyroxene, are furthermore of inconspicuous character and do certainly represent another intrusive event in that area. The age relationship between these two (or three) events is not clear, due to missing outcrops of dyke crossings in the field.

3.4 The dykes on King George Island

3.4.1 Fildes Peninsula

Most of the dykes studied in the northeastern part of Fildes Peninsula around the Uruguayan Base Artigas and at Nebles Point are porphyric basaltic andesites and andesites. Besides the common features described above, most of these dykes show relatively unaltered, euhedral, strongly zoned plagioclase phenocrysts (An_{22-52}) incorporating also melt pockets. The pyroxene (opx+cpx) phenocrysts are twinned, often fractured and have rounded rims, thus not displaying their euhedral habit. The melt pockets present in the plagioclase grains and the rounded rims of the pyroxene phenocrysts indicate an intratelluric history of these phases. Later on, the equilibrium between the crystals and the melt has apparently been disturbed (due to magma mixing?), leading to the melt inclusions present in the plagioclase and the rounded rims of the pyroxene.

The plagioclase continued growing after re-equilibrating with the melt, thus forming the concentric zoning, but the pyroxene seems to have stopped growing, thus preserving its rounded rims and corroded habit. Further unusual mineralogical features of these dykes include fibrous zeolite filling amygdales and in single cases (FP-8) extraordinary huge percentages (up to 25%) of apatite as groundmass mineral.

3.4.2 Weaver Peninsula

The lithology of the dykes on Weaver Peninsula comprises predominantly basalts and basaltic andesites with scarce dacites. The most conspicuous feature of these dykes is their high grade of alteration. Sometimes unusually large (up to 8 mm long) plagioclase and pyroxene phenocrysts are common, in some of the dykes only remaining as "ghost-phenocrysts", due to complete alteration to chl+cc+ser. WP-15 bears a special type of clinopyroxene; the sandglass-shaped internal structure indicates titanaugite.

Amygdales are common and always completely filled by secondary minerals. These sometimes form concentric, ringlike structures (WP-16), e.g. a core of quartz surrounded by a ring of calcite containing itself a ring of epidote, and an outermost ring formed by chlorite.

3.4.3 Barton Peninsula

On Barton Peninsula, lithology ranges from basalts to dacites, but with basaltic andesites prevailing. The plagioclase composition corresponds to pure anorthite (An_{93}) in some dykes. Characteristic for the dykes of this peninsula is their unusually high degree of alteration (Fig. 2-21) and the occurrence of sphene as secondary mineral. It forms clusters and so-called sphene-eggs and occurs frequently in dykes on Barton Peninsula but very seldom in dykes of the other areas.

A possible explanation for the origin of the strong alteration are fluids or hydrothermal activity related to the Noel Hill pluton, an intrusion influencing strongly all stratigraphical units on Barton Peninsula.

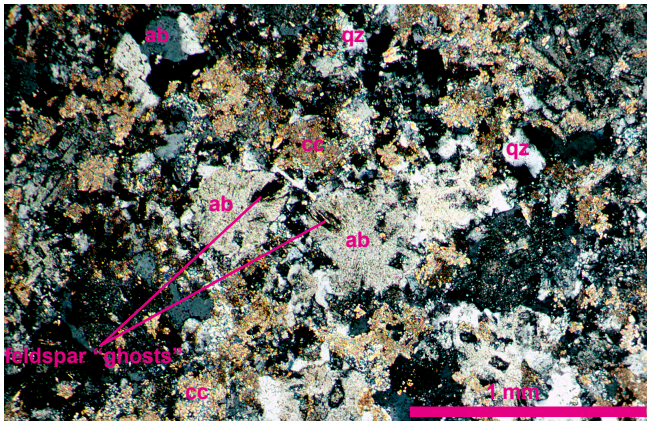

Fig. 3-8: Dyke PP-5B, the rhyolitic part of a multiple intrusion on Potter Peninsula. The photo demonstrates the high degree of alteration, shadowy feldspar grains are the only magmatic remnants in this thin section (X Nichols).

3.4.4 Potter Peninsula

The vast majority of the dykes on Potter Peninsula corresponds to porphyritic basaltic andesites, moreover a group of rhyolites. Basalts are virtually absent. The very sharp distinction of the occurring dykes into only two rock types suggests (1) a relatively short intrusion event and (2) differentiation within a magma chamber, leading to highly acidic residual melts. This conclusion is strongly supported by the plagioclase composition: exclusively labradorite (An_{52-61}) in the basaltic andesitic group and albite/anorthoclase in the rhyolites. The overall characteristic features of the basaltic andesites correspond to the introductory general description given above, moreover following observations are worth to be mentioned:

- opx occurs in nearly all dykes except the rhyolites and shows the longest magmatic history (corrosion, alteration grade, scarce cpx-rims)
- most phenocrysts show signs of dissolution suggesting magma mixing during growth
- the percentage of phenocrysts (up to 40% in some dykes) is unusually high

These features indicate a magma chamber history of the dyke melts involving differentiation and phenocryst growth (opx, cpx, pl), subsequent injection of fresh magma batches and finally the injection of phenocryst-rich melts (including the early-stage orthopyroxene) forming the dykes.

A unique feature of Potter Peninsula are the rhyolitic dykes forming part of the multiple intrusions described in chapter 2. Naturally, these rocks display a very distinct mineralogy as compared to the other dykes, whereas their accompanying dykes are inconspicuous and seem to have been fed by the same magma as the majority of the dykes on Potter Peninsula. The mineralogy of the rhyolites is highly diverse and consists of fsp (albite, anorthoclase) +qz+opq+cc+ab+ser±chl ±ap±ep.

The opaque minerals consist mostly of euhedral pyrite which is thought to be of secondary origin. The dense ground mass (Fig. 3-8) comprises equigranular anhedral quartz, calcite and albite, subordinately strongly altered, lath-shaped feldspar (probably alkali-feldspar), chlorite and/or sericite and scarce aggregates of epidote. Calcite forms evenly distributed nests of up to 3 mm diameter. No flow structure is visible.

Phenocrysts are evenly distributed, mostly euhedral and do only very seldom show glomerophyric fabric. They are strongly, often completely altered (mostly to cc) and only some of them still show albite twinning. Only ghost- or shadow-like remnants have been left from most of these phenocrysts, sometimes fragments. Same applies to the lath-shaped feldspar grains present in the ground mass (Fig. 3-8). Accessory apatite occurs as thin needles, sometimes ophitically intergrown with quartz. The latter appears in three generations, the first apparently comagmatic and evenly distributed, the second in nests, showing mosaic texture. These two generations form anhedral grains, whereas a third generation consists of bigger and euhedral crystals, evenly distributed in the ground mass. The second and third generation are believed to be of secondary origin.

In some of these rhyolitic dykes a marked, uniform sericitization of the ground mass is evident, probably deriving from disintegration of feldspar.

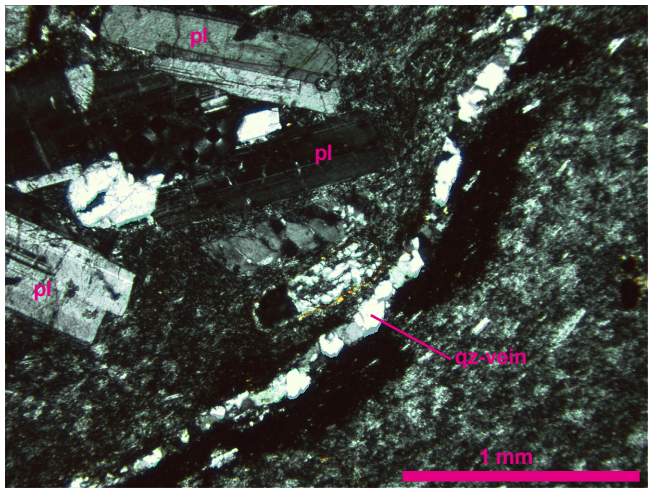

Fig. 3-9: Glomerophyric plagioclase phenocrysts in a micro/cryptocrystalline ground mass showing flow banding (sample SH-2 from Sphinx Hill). A dyke-parallel joint sealed with mosaic textured quartz crosses diagonally (X Nichols).

3.4.5 Admiralty Bay

Generally, the dykes studied in Admiralty Bay are rather inconspicuous and show much of the general characteristics. A short description of the differences between the individual groups will be given.

(1) Panorama Ridge Dykes

This group is relatively strongly altered (average AI = 3) and comprises predominantly basalts and a few basaltic andesites. The dykes are absolutely opx-free, the other phenocrysts (pl and cpx) are strongly fractured and show signs of dissolution, indicating disequilibrium with the melt. The strong fracturing of the phenocrysts may be due to pressure release cracking, but the vicinity to Ezcurra Fault and strike-slip movements along that fault might also have played a role, though not leading to an overall deformation of the dykes.

(2) Jersak Hills Dykes

These dykes are slightly more acid, comprising basaltic andesites and andesites with an average alteration index of AI = 2.5. They are also opx-free but furthermore inconspicuous. Some contain three generations of plagioclase (An_{60-70}): two phenocryst generations of different size and one ground mass generation.

(3) Sphinx Hill Dyke

This enormous dyke is a porphyric rhyolite of surprisingly low alteration (average AI = 2.5). As it would be expected, it contains no pyroxene at all. The only phenocryst phases are (partly glomerophyric) feldspar and opaque minerals. The most conspicuous feature are dyke-parallel joints sealed with mosaic textured quartz (Fig. 3-9) and accompanied by brown (Fe-infiltration?) bands on both sides. These bands are very similar to the ones described from Nelson Island (Fig. 3-7) and the explanation proposed for these will probably also apply for Sphinx Hill.

(4) Hervé Cove Dykes

Besides scarce basalts and andesites, the majority of the dykes of this group represent basaltic andesites. Though cropping out along the southern coast of Ezcurra Inlet, this group shows relatively low alteration (average AI = 2.6), in contrast to the Panorama Ridge Dykes. Most of the Hervé Cove Dykes are opx-free, but a few dykes bear considerable quantities of opx and are furthermore extremely fresh. This suggests that despite sharing the same strike with the rest of the group, these opx-bearing dykes represent an own (possibly younger) intrusive event and a distinct magmatic history.

(5) Klekowski Crag and Komandor Peak Dykes

Also of basaltic andesitic composition, these dykes are located north of the Ezcurra Fault, thus belonging to the Barton Horst. Consequently, they show the highest average alteration of all dykes investigated in Admiralty Bay (average AI = 3.3). In contrast to the majority of the other dykes, most of them bear orthopyroxene, and a relation with the opx-bearing dykes of the Hervé Cove group cannot be excluded. However, as long as the exact age for the strike-slip movement along Ezcurra Fault is unknown, and therefore also no conclusion can be drawn whether the dykes are younger or older than this movement, such correlations must remain speculative.

3.5 Radial dykes on Penguin Island

The radial dykes cropping out on the western slope of Deacon Peak are all porphyric basalts and extremely fresh (average AI = 1.9). These are the only dykes studied within this project bearing olivine. This phase shares approx. 15 % of the rock and appears as phenocrysts of up to 2 mm size and is an- or subhedral, sometimes also euhedral. Rounded rims and resorption embayments point towards an early growth and subsequent disequilibrium with the melt (Fig. 3-10). In some cases, the crystals show an advanced state of disintegration, forming opaque Fe-minerals (Fig. 3-11). Typically, the olivines are clustered in a glomerophyric way. The same applies to the plagioclase phenocrysts (An_{45-60}), which show

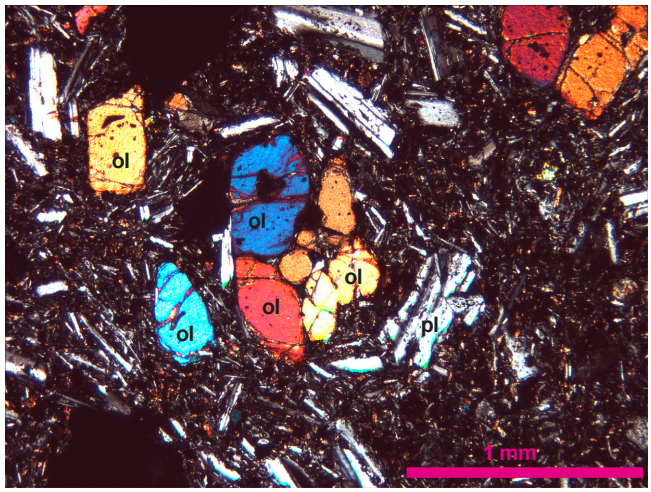

Fig. 3-10: Glomerophyric fabric of olivine and plagioclase phenocrysts in a dyke (PI-4) on Penguin Island. Note the flow structure displayed by the ground mass crystals around the cluster of phenocrysts (X Nichols).

very similar characteristics (size, resorption, clustering) and are often associated with olivine, indicating a shared history. Cpx is present as a third phenocryst phase and the internal hour glass structure points towards Ti-augite. The ground mass consists of sub- to euhedral plagioclase laths and fragmentary, mostly anhedral cpx grains, furthermore of considerable amounts (up to 40%) of opaque material, much of it certainly being glass.

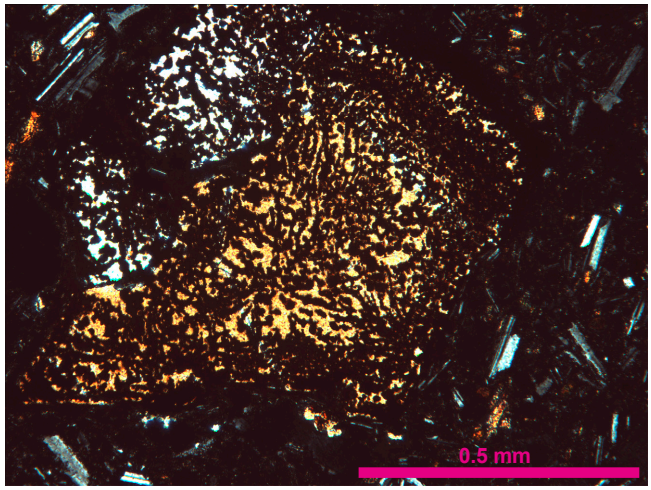

Fig. 3-11: An olivine phenocryst in dyke PI-2, disintegrating into microcrystalline, opaque Fe-minerals (X Nichols).

4. Geochemistry and Sr-Nd-Pb isotopic data

4.1 Sample selection, preparation and analytical methods

Principally based on the degree of alteration determined under the microscope (Alteration Index AI, Table 2-2), the freshest samples of each group of dykes have been selected for geochemical analyses. Dykes, which are part of a system and thus display clear relative age relationships in the field, have been analyzed preferentially. Major element concentrations are given in wt%, trace element and REE concentrations in µg/g. For abbreviations see Appendix I. The resulting datasets have been processed using the programs PbDAT [Ludwig 1993], Isoplot/Ex ver. 2.49x [Ludwig 2000] and PostAnalysis ver. 5.54 (© 2002 BEGUMA, Berlin).

Major, minor and trace elements

The geochemical dataset comprises 131 dykes from the South Shetland Islands, including 11 dykes from Potter Peninsula analyzed previously [Kraus et al. 2000] and 120 new analyses.

For all 131 dykes, sample preparation has been carried out in Munich and the whole rock (WR) powder then has been sent to ACTLABS (Activation Laboratories, Ancaster, Ontario, Canada) for analysis. The identical pre-analysis treatment and the analysis of all samples in one and the same laboratory guarantees comparable precision, accuracy and thus a homogeneous dataset. The complete dataset is listed in Appendix III.

During a first step of preparation, weathering crusts, xenoliths (if present) and veins (calcite and quartz) have been removed from approx. 2 kg sample using a diamond-staffed saw blade. After careful washing, the samples were dried over night at 100° C, then crunched using a steel press. Next, the samples were milled (max. 60 sec. to avoid contamination with mill-derived attrition) using a WIDIA-mill and a tungsten-carbide pot. The latter was cleaned between different samples by milling crushed glass and subsequent thorough washing. Furthermore, the first passage of each sample was discarded in order to cause a self-contamination of the mill before producing the rock powder intended for further analytical work.

At Activation Laboratories (ACTLABS), major elements were analyzed by lithium metaborate/tetraborate fusion ICP technique, trace elements and REE by ICP-MS. Detection limits were ≤ 0.01 wt% for major elements, ≤ 5 µg/g (mostly ≤ 1 µg/g) for trace elements, and ≤ 0.1 µg/g for REE (for details see http://www.actlabs.com). For a detailed description of the analytical technique (ICP-MS) see Potts [1987], Heinrichs & Herrmann [1990] and Rollinson [1993].

Sr-Nd-Pb isotopy

Tectonic and geochemical data served as a basis for selecting samples for Sr, Nd and Pb isotopic analyses. Pb and Nd isotopes have been determined for 30 dykes from Livingston, Nelson, King George and Penguin Island. Sr isotopes have been determined for 12 dykes from King George Island (11) and Penguin Island (1). The dykes from Nelson and Livingston Island could not be analyzed for their Sr isotopic composition due to laboratory problems.

For isotope analyses, WR-powder from the same fractions as sent to ACTLABS has been used. The chemical separation of the elements of interest has been carried out at the "Zentrallabor für Isotopengeochemie" at the Department of Earth and Environmental Sciences, Ludwig-Maximilians-Universität München. Details of the separation scheme can be found in Hegner et al. [1995a and b].

(1) Pb isotope analyses

50 mg of samples with Pb > 5 µg/g and 100 mg of samples with Pb < 5 µg/g (ICP-MS detection limit), respectively, were weighted into teflon beakers (PFA type). 3-5 g of HF+HNO_3 (5:1) solution were added and the samples then baked 24 h at 130° C. Next, the capsules were left open on the hotplate at 80° C until the solution appeared nearly dry (subsequent dissolution in HCl works more efficiently if added into the hot beakers *before* the solution is completely dry). Then approx. 3 ml 6N HCl were added and the samples baked for another 24 h at 130° C (closed capsules). After drying the solution once more at 80° C, the samples were dissolved in 0.5 ml 1N HBr and dried again in order to transfer chlorides into bromides. After drying, 1 ml 1N HBr was added and the samples dissolved in an ultrasonic bath. In a last step, the solution was centrifuged for 15 min. at 6500 rpm to separate the dissolved sample from undissolved residues (e.g. organic matter).

Lead separation and cleaning was carried out in 400 µl- and 100 µl-columns, respectively, using DOWEX AG1-x8 resin. The applied elution scheme which is based on HBr-HCl-chemistry is shown in Appendix IV (Table 4).

Mass spectrometric analyses have been performed on a Finnigan MAT 261 mass spectrometer, using a single-filament (Re) technique. NBS 981 standard has been loaded with each sample batch. Samples have been measured at least 6 blocks (15 scans per block), the NBS 981 standard 7 blocks (10 scans per block). During measurements of the NBS standard, the temperature with the lowest linear mass fractionation (F = 1.08‰) was about 1300-1320° C. At lower temperatures (1180-1200° C), a linear mass fractionation of F = 1.50‰ has been observed. However, using an imprecise optical thermometer, this temperature can not be regarded as an exact temperature. The mass fractionation has been calculated (Appendix IV, Table 3) considering the recommended values for NBS 981 by Todt et al. [1996] and all measurements were corrected accordingly. Average 2σm (%) errors were 0.0084 ($^{206}Pb/^{204}Pb$), 0.0094 ($^{207}Pb/^{204}Pb$) and 0.0102 ($^{208}Pb/^{204}Pb$). Individual results are listed in Appendix IV (Table 1 & 2). Blanks have been determined measuring 3 blocks (10 scans per block) and ranged between 250 and 400 pg, an acceptable value for Pb analyses.

(2) Sr and Nd isotope analyses

35-40 mg of WR powder were weighted into teflon beakers (PFA type). The powder was then homogenized with 5 drops $HClO_4$. After adding 2 ml HF, the samples were dissolved in closed beakers on a hotplate at 80° C for about two days, then evaporated until dry (mainly removal of SiF_4). The temperature then was risen to 130° C and the samples were baked overnight until turning black/red (evaporation of $HClO_4$). In a next step, the samples were dissolved in 3 ml 6N HCl in closed beakers at 80° C. After evaporating the sample solutions at 80° C, the temperature was risen to 130-140° C. As a last step, the samples were dissolved in 1 ml 2.5 N HCl and then centrifuged for 15 min. at 13000 rpm to separate insoluble components from the solution (organic matter, fluorides).

Sr, Sm and Nd separation was carried out according to Hegner et al. [1995a and b].

Measurements were performed using a Finnigan MAT 261 mass spectrometer, applying a single filament (W) technique for Sr, and a double filament (Re) technique for Nd measurements. The NBS 987 standard has been loaded with the Sr sample batches, the AMES standard with the Nd sample batches. Measurements of the NBS 987 standard yielded $^{87}Sr/^{86}Sr = 0.7102101 \pm 0.00002$ (2σm = 0.0016%; n = 3). Measurements of the AMES standard yielded $^{143}Nd/^{144}Nd = 0.512145 \pm 0.000015$ (2σm = 0.0026%; n = 7).

Mass fractionation has been corrected internally by normalizing Sr isotope ratios to $^{86}Sr/^{88}Sr = 0.1194$, Nd isotope ratios to $^{146}Nd/^{144}Nd = 0.7219$, and Sm isotope ratios to $^{147}Sm/^{152}Sm = 0.56081$. Total procedural blanks were < 95 pg for Nd and < 0.9 ng for Sr. Average in-run errors (2σm) were 0.0033 % for $^{87}Sr/^{86}Sr$ and 0.0026 % for $^{143}Nd/^{144}Nd$. Individual results are listed in Appendix IV (Table 1 & 2).

4.2 Alteration

The question, whether the studied samples have undergone mass exchange or not, is of crucial importance in order to accurately interpret the geochemical data. Alteration processes may result in transformation of the primary magmatic minerals into hydrated secondary minerals or in hydration of glass, thus rising the volatile content of the respective rock. The LOI-value (loss on ignition) represents the volatile content (in weight percent) released by the sample during heating, thus being a useful indicator for the degree of alteration. The higher the LOI, the stronger the alteration of the sample. Conventionally, LOI values < 3 indicate relatively fresh rocks, whereas samples with an LOI > 4 are interpreted as altered. However, it has been emphasized, that primary subduction zone magmas contain in general higher and more variable volatile contents (0-4 wt%) than magmas from other tectonic settings [Tatsumi & Eggins 1995]. In contrast, typical N-MORB normally contains between 0.1 and 0.2 wt% volatiles. I conclude, that the relatively high LOI values observed in the dykes of the South Shetland Islands must not necessarily be the result of alteration processes, but that at least part of this volatile content might be of primary magmatic origin.

The average LOI-values have been calculated for each of the investigated areas (Fig. 2-21), paying heed to the observed correlation between the tectonic architecture of the islands and the degree of alteration of the rocks. The Neogene radial dykes from Penguin Island feature by far the lowest average LOI (0.15), and the dykes belonging to Barton

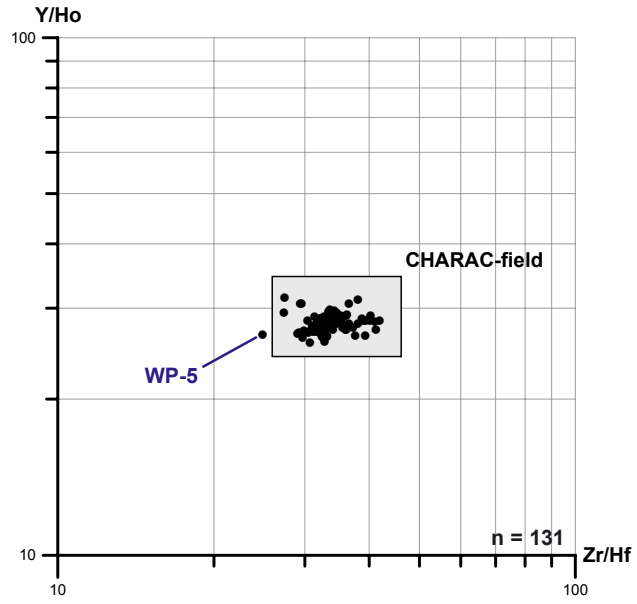

Fig. 4-1: CHArge- and RAdius-Controlled (CHARAC) trace element behavior. Field defines area of ± 30% of chondritic ratios [Bau 1996]. Except for WP-5, all dykes plot inside the CHARAC-field, indicating chondritic Zr/Hf and Y/Ho ratios and therefore low alteration of immobile elements.

Horst the highest (Barton Peninsula: 4.26, Weaver Peninsula: 5.57, Nelson Island: 4.05). As expected, the dykes on Warszawa Block lie in between (Admiralty Bay: 2.99, Potter Peninsula: 3.37). The dykes on Fildes Peninsula show an unexpectedly high average LOI (4.28), contrasting with the tectonic position of Fildes Block which is believed to correspond to that of Warszawa Block [Birkenmajer 2001]. Hurd Peninsula (Livingston Island) shows an average LOI of 4.81, correlating well with the strongly altered dykes of Barton Horst, as already observed in case of the alteration index (AI, Fig. 2-21). A tectonically upthrown position of Hurd Peninsula in form of a horst-like structure similar to Barton Horst seems possible.

Macro- and microscopically discernible alteration features have already been described in previous chapters and point to an autometasomatic origin of the observed secondary minerals, thus not necessarily indicating major mass exchange of the dykes with the host rock.

The impact of hydrous fluids on basic to intermediate rocks might be estimated using Zr/Hf- and Y/Ho-ratios [Bau 1996]. CHArge- and RAdius-Controlled (CHARAC) behavior of these elements is typical in silicate melts, whereas in hydrous fluids also the electron configuration plays a major role. Under such conditions, the formation of chemical complexes is possible, resulting in contrasting interelemental partition coefficients as compared to the silicate melt-rock system. In general, both Zr/Hf and Y/Ho ratios are uniform and close to chondritic in most magmatic and metamorphic rocks.

However, if basic to intermediate rocks display Zr/Hf- and Y/Ho-ratios significantly different from chondritic ratios, they have been subjected to significant alteration [Bau 1996]. The CHARAC-field (Fig. 4-1) reflects the chondritic Zr/Hf- and Y/Ho-intervals, considering also the Zr/Hf variation demonstrated by David et al. [2000] for oceanic and continental rocks.

Concerning the dykes investigated on the South Shetland Islands, all but one sample plot well inside the CHARAC-field (Fig. 4-1), indicating CHARAC-behavior and therefore a supposedly low degree of alteration with respect to immobile trace elements. The one rock plotting outside the CHARAC-field is sample WP-5 from Weaver Peninsula, one of the most basic of all analyzed dykes ($Zr/TiO_2 = 0.0035$ and $SiO_2 = 46.14$ wt%). This dyke also features a very high LOI (6.86 wt%) reflecting a strong alteration which may have also affected immobile trace elements. WP-5 plots well apart from the other dykes in many diagrams, displaying a depleted REE pattern (Fig. 4-5) and a generally low content in incompatible elements (Fig. 4-7).

4.3 General geochemical features

Concerning the complex geochemical signatures of subduction zone derived magmas, there is general agreement about a contribution of the downgoing slab as well as of the overlying mantle wedge. The slab contributes two distinct components to the arc lavas [Elliott 2003]: (1) melt of the subducted sediment controlling the budgets of most incompatible trace elements and (2) an aqueous fluid derived from the altered mafic oceanic crust, dominating a smaller set of elements, predominantly Ba, Pb and Sr. Both components have considerably elevated concentrations in incompatible elements relative to typical mantle rocks and thus can be expected to impart a strong chemical signature during arc magma generation. As confirmed by melting experiments, dehydration of the underlying oceanic crust and partial sediment melting can occur at the same temperature of approx. 650-700° C and pressures between 10 and 40 kb [Nichols et al. 1994].

The mantle wedge serves as a third component participating in melt generation. The wedge is believed

to be of similar composition as the usual MORB source, depleted upper mantle.
Summarizing, three main components are thought to contribute to the compositional diversity of subduction zone magmas [Elliott 2003]:

- depleted mantle wedge
- melt of subducted sediment
- aqueous fluid derived from altered oceanic crust

At active continental margins, crustal contamination might also play a major role.
When discussing subduction zone magmatism, it has become common practice to classify incompatible elements either as "fluid mobile" (corresponding to large ion lithophile elements, LILE) or as "fluid immobile" (high field strength elements, HFSE). The following discussion will focus mainly on the information given by these immobile elements.

4.3.1 Rock type and magma series

The standard methods commonly applied to discriminate between different magma series and rock types (e.g. TAS-diagram, Le Maitre 2002) mostly use element oxides bearing the risk of mobility during alteration and metamorphism (e.g. K_2O and Na_2O). Paying heed to the comparatively high degree of alteration of the investigated dykes (AI and LOI, Fig. 2-21 and Appendix III, Table 1 & 2), mobile elements have been avoided in the discussion.

In contrast, immobile elements are known to allow the identification even of altered and metamorphosed rocks [Floyd & Winchester 1978]. For all but the most siliceous rocks, a constant Nb/Y ratio of 0.67 has been recognized as a valuable indicator of alkalinity to distinguish between subalkali- and alkali-series [Winchester & Floyd 1977]. The Zr/TiO_2 ratio has been established by the same authors as providing a reliable differentiation index. Because these four elements are highly immobile during alteration processes, they are considered to reflect rock type and magma series of the South Shetland Islands dykes more reliably than the classic diagrams based on major elements. This assumption is confirmed by the very homogeneous and compact distribution pattern shown in Fig. 4-2A.
To check for possible alteration processes, the classic differentiation index SiO_2 has been applied in Fig. 4-2B. The original diagram of Winchester & Floyd [1977] has been modified, replacing the horizontal boundaries delimiting the fields within the subalkali-series with the nowadays widely accepted, also straight-running SiO_2-boundaries used in the total alkali-silica diagram (TAS-diagram, Le Maitre 2002). Doing so, the advantage of the reliable distinction between the magmatic series provided by the ratio of the immobile elements Nb and Y can be combined with the well known and widely applied distinction of rock types based on SiO_2-content as differentiation index.

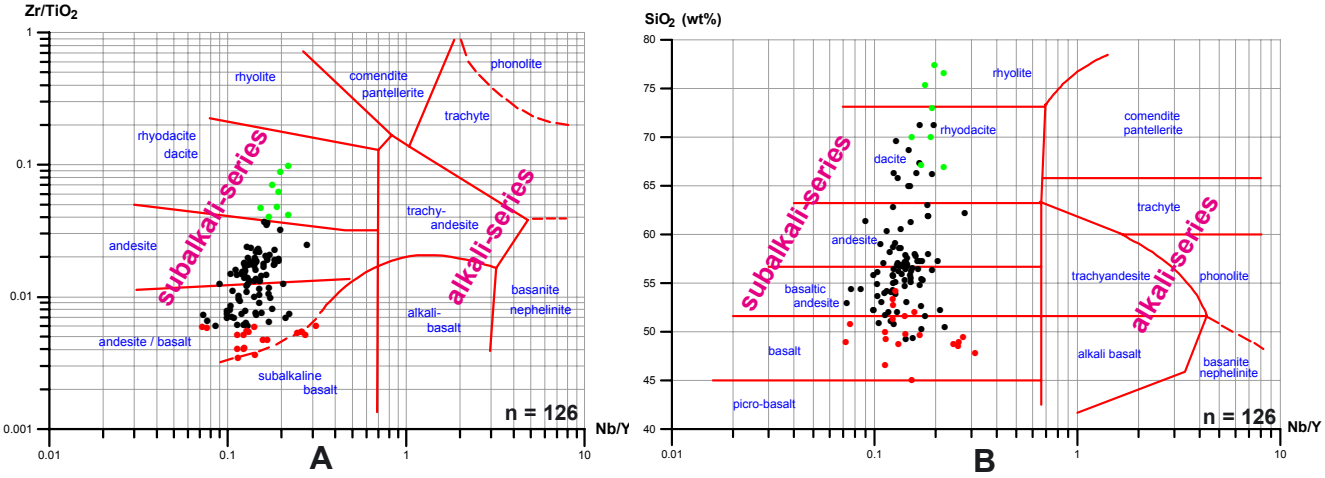

Fig. 4-2: Determination of magma series and rock type classification of the South Shetland Islands dykes using SiO_2 and immobile elements. All dykes belong to the subalkali-series and their composition ranges from basaltic to rhyolitic. The most basic (red dots) and the most evolved (green dots) dykes have been denoted according to their position in (A) in order to control the position of the same samples using SiO_2 as differentiation index (B). A fairly good correlation between the two diagrams can be stated.
(A): Nb/Y vs. Zr/TiO_2 using Nb/Y as indicator of alkalinity and Zr/TiO_2 as differentiation index [Winchester & Floyd 1977].
(B): Nb/Y vs. SiO_2 diagram modified after Winchester & Floyd [1977]. Except for the dacite/rhyolite-boundary, all original, horizontal (SiO_2-content defined) boundaries delimiting the fields of the subalkali-series have been replaced with the now widely accepted SiO_2-boundaries used in the total alkali-silica-diagram (TAS, Le Maitre 2002). The (sub-)vertical boundaries and the boundaries delimiting the fields of the alkali-series correspond to the original diagram published by Winchester & Floyd [1977].

To cross-check the comparability of the two diagrams and to determine if SiO_2 has been affected by alteration or not, the most basic samples in Fig. 4-2 were plotted as red dots and the most acid ones as green dots. Assuming an undisturbed SiO_2-system, the relative position of the marked samples should remain fairly the same. This is true for most dykes.

Three conclusions can be drawn from Fig. 4-2:

(1) As expected for a subduction zone environment, all dykes of the South Shetland Islands belong clearly to the subalkaline series. This is also true for the five dykes from Penguin Island, believed to be related to the opening of the Bransfield Strait backarc basin and therefore expected to show a higher degree of alkalinity.

(2) The rock composition of the South Shetland Islands dykes ranges from basalts to rhyodacites with Zr/TiO_2 applied as differentiation index (Fig. 4-2A), and from basalts to rhyolites with SiO_2 used as differentiation index (Fig. 4-2B).

(3) Generally, the distribution of the samples in the two diagrams is very similar, clustering in both cases around the basic boundary of the andesite field. Moreover, the most basic and the most acid dykes in diagram 4-2A are also among the most basic and most acid ones in diagram 4-2B, respectively. The same applies to intermediate examples. This indicates a good correlation between SiO_2 and Zr/TiO_2 differentiation indices, though the red and green marked samples in Fig. 4-2B show scatter and overlap with unmarked samples.

The generally less homogeneous and compact distribution pattern in Fig. 4-2B might indicate an alteration component affecting SiO_2 which may be partly responsible for the rhyolitic compositions not displayed in Fig. 4-2A.

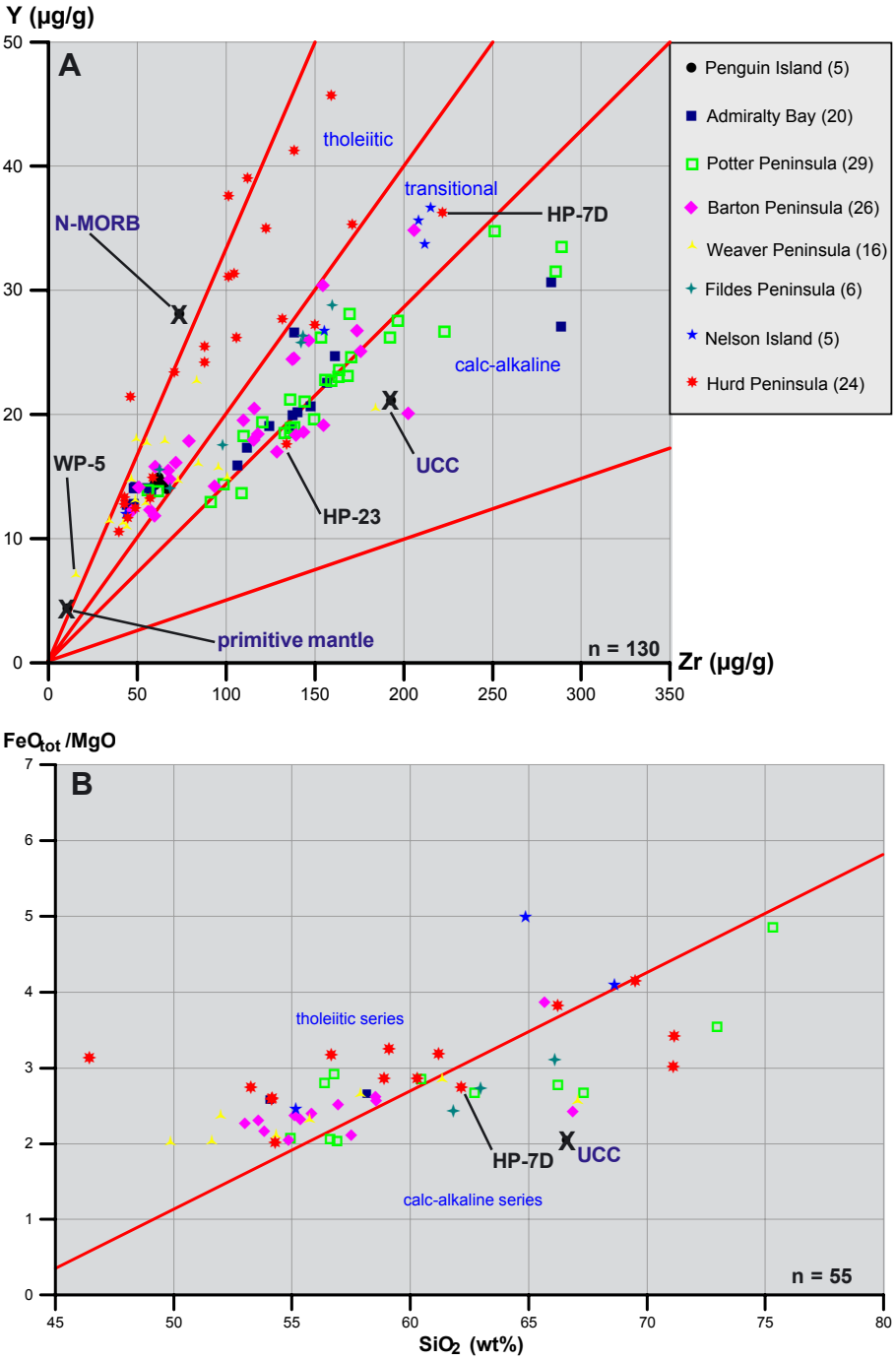

Fig. 4-3: Magmatic affinity of the South Shetland Islands dykes. Note the correlation between geographical area and magmatic trend, especially in (A). Digits in brackets refer to the number of plotted dykes from the respective area. Primitive mantle values from McDonough & Sun [1995], N-MORB values from Sun & McDonough [1989], upper continental crust (UCC) values from Rudnick & Gao [2003].
(A) Zr vs. Y plot after MacLean & Barrett [1993].
(B) SiO_2 vs. FeO_{tot}/MgO after Miyashiro [1974].

4.3.2 Magmatic affinity

Subdivision of the subalkaline series

The subalkaline series to which all dykes belong is further subdivided into a calc-alkaline and a tholei-

itic series (Fig. 4-3). As in the case of rock classification, the risk of mobility of some major element oxides (especially Na_2O and K_2O) does not recommend the use of classic diagrams like the AFM-diagram of Irvine & Baragar [1971] for determination of magmatic affinity.

A plot that is based on the immobile elements Zr and Y (Fig. 4-3A) has therefore been applied. It exhibits a strong tholeiitic trend for the dykes on Hurd Peninsula (see also Fig. 4-22), the majority of the dykes on Weaver Peninsula and part of the dykes on Barton Peninsula and in Admiralty Bay. The dykes from Penguin Island also plot entirely within the lower part of the tholeiitic field, this affinity also being confirmed by their low Al_2O_3-content of less than 16 wt% (Fig. 4-4 and Appendix III, Table 3). The other areas show transitional to calc-alkaline trends.

A very similar distribution pattern of the magmatic affinity is revealed using SiO_2 and the FeO_{tot}/MgO ratio [Miyashiro 1974], though the resolution is much lower here (Fig. 4-3B). According to the originally intended application of this diagram by Miyashiro, only dykes showing intermediate degrees of differentiation (i.e. $2.0 < FeO_{tot}/MgO < 5.0$) are plotted.

In accordance to Fig. 4-3A, this diagram classifies most of the dykes from Hurd and Weaver Peninsula as tholeiitic, along with the majority of the dykes from Barton Peninsula and Nelson Island. In contrast, the dykes from Potter Peninsula and Fildes Peninsula are predominantly calc-alkaline. This pattern corresponds to the tectonic architecture of the South Shetland Islands, with Weaver and Barton Peninsula and the sampled part of Nelson Island belonging to the upthrown horst structure (like supposed also for Hurd Peninsula), and Potter Peninsula like Fildes Peninsula representing part of the downthrown blocks.

However, the more homogeneous, tighter clustering and less scattered distribution pattern in Fig. 4-2A and Fig. 4-3A indicates, that highly immobile elements obviously reflect the original rock composition more reliably than less immobile or even mobile elements.

High-Alumina Basalts

Basaltic members of the calc-alkaline series are referred to as high-alumina basalts [Wilson 1989] and characterized by Al_2O_3-contents of 16-20 wt%. On Hurd Peninsula, 12 out of 17 basalts and basaltic andesites match the criteria of high-alumina basalts, thus suggesting a calc-alkaline character (Fig. 4-4). This is in contrast to the immobile trace element systematics that argue strongly for the tholeiitic affinity of these dykes (Fig. 4-3A & 4-22). Accumulation of plagioclase crystals might be an explanation for the unexpectedly high alumina values. Moreover, the alumina values of *all* Hurd Peninsula dykes are well below the values of dykes from the other areas (Fig. 4-4). The alumina values of the Penguin Island dykes confirm their tholeiitic character. Only one of them shows high-alumina characteristics (PI-5). For the rest of the investigation areas, alumina values correspond to high-alumina basalts and thus to calc-alkaline affinity (Fig. 4-4).

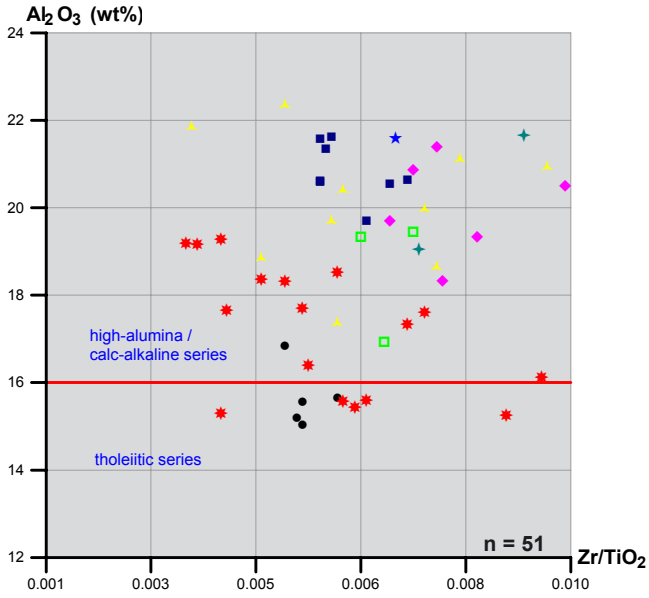

Fig. 4-4: High-alumina and tholeiitic characteristics of the basaltic and basaltic andesitic dykes of the South Shetland Islands. Zr/TiO_2 ratio used as differentiation index. Symbols as in Fig. 4-3.

4.3.3 Rare Earth Elements (REE)

The REE belong to the least soluble trace elements and are relatively immobile during low-grade metamorphism, weathering and hydrothermal alteration. In igneous rocks, REE patterns are controlled by the REE composition of their magma sources, the degree of partial melting and by crystal fractionation during their evolution. In general, the REE show very similar chemical and physical behavior, but some petrological processes exploit small differences in their ionic size, leading to fractionation of the REE series.

In a primitive mantle normalized REE plot (Fig. 4-5, the most basic dykes of the South Shetland Islands show all relatively low REE-enrichment and only part of them displays higher fractionation between LREE and HREE, leading in general to a

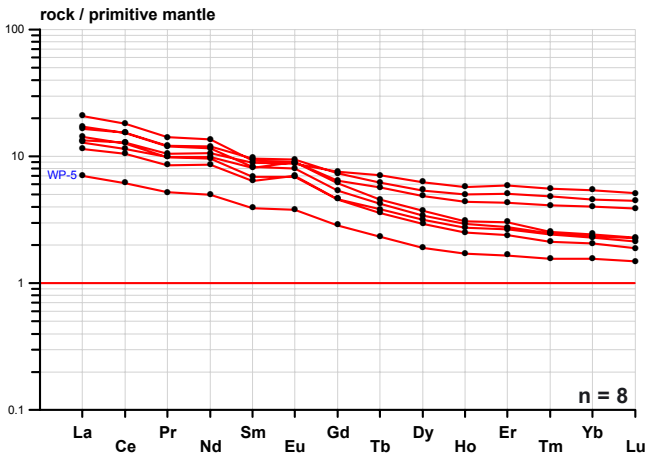

Fig. 4-5: REE distribution pattern of the most basic dykes (basalts) of the South Shetland Islands. Normalization using primitive mantle values from McDonough & Sun [1995].

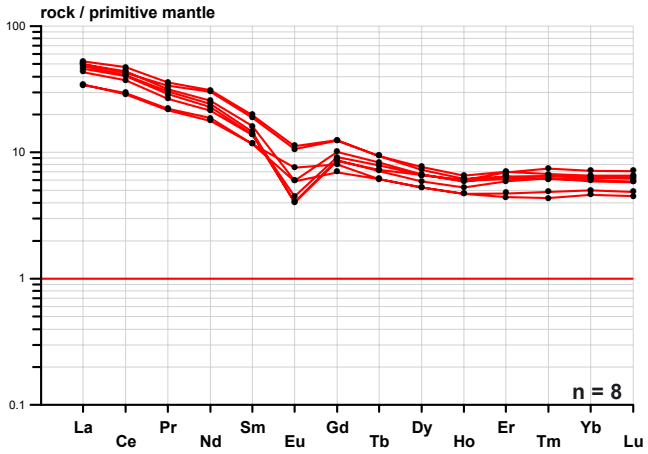

Fig. 4-6: REE distribution pattern of the most acid dykes of the South Shetland Islands. Note the evident Eu-anomaly indicating feldspar fractionation. Normalization using primitive mantle values from McDonough & Sun [1995].

rather smooth curve with a shallow slope and without major anomalies. About 80% of the basic dykes from the South Shetland Islands display a fractionation factor between LREE and HREE (La/Lu) of 2.5 - 6 times, an LREE-enrichment of up to 20 times as compared to primitive mantle and HREE-enrichment not exceeding 5 times.

The REE patterns of these dykes are remarkably consistent, moreover some of them display a high Mg-number. This could indicate relatively small degrees of partial melting in the source region, leading to preferential enrichment of the LREE in the melt and thus to the observed slope. Enrichment of LREE relative to HREE is also typical for sediment input. Also fractionation of orthopyroxene has been considered as responsible for negative REE slopes like observed in Fig. 4-5, because the partition coefficients of the HREE are higher with respect to this mineral than those of the LREE [Philpotts 1990; Rollinson 1993].

Accumulated plagioclase might be responsible for the slight positive Eu-anomaly observed in some basic dykes (Fig. 4-5). This assumption is supported by the very high quantity (up to 50%) of plagioclase phenocrysts in some dykes as observed under the microscope. Alternatively, fractionation of Hornblende also causes a slight positive Eu-anomaly. However, this effect is only weakly pronounced. The complete absence of negative Eu-anomalies at least argues against separation of plagioclase from the melts prior to dyke emplacement.

20% of the basaltic dykes show different behavior, displaying a steeper slope which indicates higher fractionation between LREE and HREE (factor 6x - 9x) and low HREE-enrichment factors of 2x - 3x. Most of them belong to the Hurd Peninsula dykes, though to different intrusive events. Other dykes from the same intrusive events do not show such behavior. Thus, a possible explanation might be variable degrees of orthopyroxene fractionation and not necessarily different magma sources or degrees of partial melting, because such conditions would obviously affect *all* dykes from the respective intrusive events and not only selected ones.

The fact that the REE patterns are fanning out towards the HREE side of the diagram (Fig. 4-5) is a strong indication for the absence of residual garnet in the mantle source. The capability of garnet to buffer HREE abundances would not allow such patterns.

The REE-fractionation factor of the most silica-rich dykes from the South Shetland Islands ranges from 6x to 9.5x. During crystal fractionation, the general incompatibility of the REE also leads to higher enrichment levels of up to 50x for the LREE and up to 7x for the HREE as compared to primitive mantle. All of these silica-rich dykes display a marked negative Eu-anomaly (Fig. 4-6), especially the highly acidic dykes from Potter Peninsula. Feldspar fractionation during magma differentiation is the most probable explanation for the negative Eu-anomaly.

4.3.4 Multi-element spider diagrams

Arc signature and sediment influence

In order to decipher the geotectonic setting and facilitate the identification of the magma sources without masking these primary signatures by any differentiation process, only the most basic dykes were plotted into a primitive mantle normalized multi-element spider diagram (Fig. 4-7). The elements are

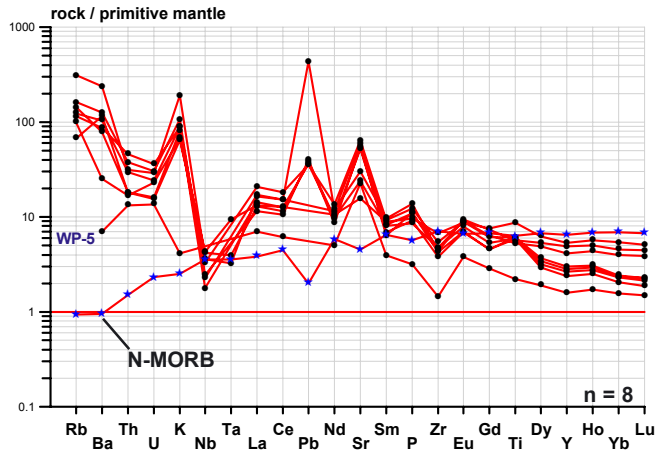

Fig. 4-7: Primitive mantle normalized spidergram of the most basic dykes of the South Shetland Islands, displaying a clear subduction zone pattern. Primitive mantle values from McDonough & Sun [1995], N-MORB values from Sun & McDonough [1989].

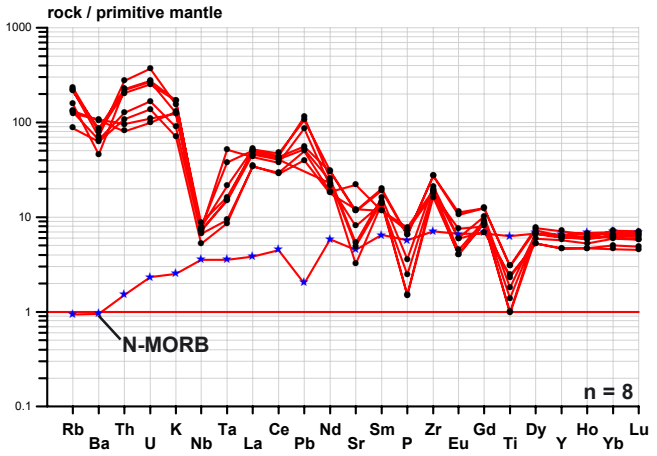

Fig. 4-8: Primitive mantle normalized spidergram of the most acid dykes of the South Shetland Islands, displaying subduction zone characteristics as well as fractionation during petrogenesis. Normalizing values from McDonough & Sun [1995], N-MORB values from Sun & McDonough [1989].

ordered according to their relative incompatibility during mantle melting [Hofmann 1988]. This method produces a smooth pattern for MORB. Any concentration peak or trough observed in the "spidergram" indicates processes or source effects not related to normal upper mantle melting.

In case of the South Shetland Islands dykes, a strong arc signature is evident and most possibly due to contributions from slab derived components.

In general, the highly incompatible elements at the left side of the diagram reflect predominantly the effects of slab derived components, whereas the moderately incompatible element abundances to the right of the "spidergram" can mainly be attributed to melting and fractionation processes [Elliott 2003]. Accordingly, the patterns of the most basic dykes from the South Shetland Islands (Fig. 4-7) reflect a strong influence of slab derived components, along with melting processes not very different from depleted upper mantle melting, as indicated by the N-MORB pattern.

The prominent enrichment in incompatible alkali metals and alkaline earths (K, Rb, Cs, Sr, and Ba) is typical for subduction zones. Significantly, these are the most enriched elements in sediments, and also the most soluble ones. Whereas K, Rb, and Cs enrichment can be attributed to both subducted sediments as well as to slab derived fluids, the positive Sr-peak is characteristic only for the latter. In contrast, major influence of subducted and partially melted sediment would lead to a negative Sr-anomaly [Elliott 2003; Sun & McDonough 1989; Turner et al. 2000]. In any case, the observed pattern can be attributed to enrichment of the mantle source by components induced by the subducted slab. The strong positive Pb-anomaly is also typical for slab derived fluid signatures but might also express sediment addition [Sun & McDonough 1989]. However, Chauvel et al. [1995] attribute the origin of Pb in subduction zone magmas predominantly to leaching of the subducting slab and not to sediment input. According to their model, migration of Pb from the interior of the oceanic crust to the surface during hydrothermal alteration is more efficient than that of Ce, and this may explain the effective fractionation of the two elements, which have a similar incompatibility during melting. At the surface of the oceanic crust, Pb concentrates in sulfides and oxides which break down during subduction, releasing Pb dissolved in the fluid phase which then migrates into the overlying mantle wedge [Chauvel et al. 1995; Miller et al. 1994].

The marked Nb-Ta trough is also typical for subduction zone signatures. It is diagnostic for both island arcs and active continental margins. The debate concerning the reason for the Nb-Ta depletion still continues. Nb and Ta belong to those elements that are least enriched in sediments and are also highly insoluble in aqueous solutions (derived from the oceanic crust). Their specific geochemical behavior is partly due to their high ionic potential (ratio of ionic charge to radius, Z/r). The same holds for Ti, Hf and Zr, and indeed the latter also displays a slight negative anomaly (Fig. 4-7).

Since Y may behave slightly mobile during alteration [MacLean & Barrett 1993], it is plotted between Dy and Ho (according to its ionic radius of 1.019 Å) to check for any alteration induced depletion/en-

richment effect. Such processes should lead to either a positive or a negative Y-anomaly. The absence of an obvious Y anomaly (Fig. 4-7) indicates that it largely retained its immobile behavior during alteration. Therefore, Y is a reliable element that can be used for determining the petrogenetic history of the South Shetland Islands dykes.

Fractional crystallization processes

Whereas the basic dykes are the most reliable source of information about magma source characteristics and processes, a comparison of their spidergrams with those of the most silica-rich or evolved dykes provides information about petrogenetic and differentiation related processes. This comparison is justified, because except for the negative Eu-anomaly and the higher concentration, the REE-patterns of the silica-rich dykes (Fig. 4-6) are very similar to the REE-patterns of the basic dykes (Fig. 4-5). This observation rejects the possibility that these dykes represent material generated by melting of the continental crust underlying the South Shetland Islands. Such melts would certainly display completely different REE-patterns. I therefore conclude, that these acidic melts were generated by simple differentiation from basic parent magmas. This assumption is strongly supported by the nearly identical $^{87}Sr/^{86}Sr$ ratios (Fig. 4-17A).

The concentrations of Th and U are 5x to 8x higher in the acidic dykes, a consequence of the incompatible behavior of these elements during differentiation. Far more interesting is the behavior of Nb and Ta. Whereas Nb shows the well known negative anomaly typical for subduction zones, the negative Ta anomaly scatters considerably and is virtually nonexistent in some of the dykes (Fig. 4-8). Maybe Nb and Ta do not behave as "geochemical twins" anymore in these acidic dykes, suggesting a process causing fractionation of these two elements in highly evolved systems (see also Fig. 4-14B and discussion there). At present, the responsible process remains unknown, but such behavior has been recognized in highly evolved aqueous systems also for other "geochemical twins" like Zr and Hf [Bau 1996]. The Nb-Ta systematics will be discussed more in detail in chapter 4.4.3 (The mantle wedge).

The most prominent features of Fig. 4-8 are the strong negative anomalies of Sr, P and Ti. They are related almost certainly to crystal fractionation of plagioclase (causing Eu- and Sr-depletion of the melt), apatite (extracting P) and ilmenite/sphene (leading to Ti-depletion of the melt). This conclusion is supported by the observed mineralogy (see chapter 3), stating plagioclase as major rock forming mineral for almost all basic to intermediate dykes, and apatite as frequent constituent of the ground mass. Both minerals play only a minor role or are absent in the silica-rich dykes.

4.4 Components of magma genesis

Besides the mantle wedge and eventual crustal contamination, some older models of arc magmatism state only one single component derived from the subducting slab contributing to arc magma genesis. Meanwhile, it is widely accepted that in most cases at least two discrete slab-related components are contributing: (1) subducted sediments and (2) fluids derived from the altered mafic oceanic crust [Class et al. 2000; Elliott 2003; Elliott et al. 1997; Hawkesworth et al. 1997; Turner et al. 1996, 1997, 2000].

Trace element and isotopic constraints were used to identify the different contributors to arc magma genesis beneath the South Shetland Islands. Apart from geochemical data, the following isotopic data have been used:

- Sr (WR) isotopic data of 12 dykes (this work)
- Nd and Pb isotopic data (WR) of 30 dykes (this work)
- Sr, Nd and Pb isotopic data (WR) of 14 samples of MORB dredged from the Drake Passage [Pearce et al. 2001]
- Sr (8) and Nd (9) isotopic data of WR sediment samples dredged from the Drake Passage [Walter et al. 2000]
- Pb isotopic data of 5 WR sediment samples dredged from the Drake Passage [kind p.c. E. Hegner, Univ. Munich]
- Sr (WR) of 32, Nd (WR) of 24 and Pb (leached feldspars) isotopic data of 8 samples from the basement of the northern Antarctic Peninsula (Graham Land). These data are from Millar et al. [2001] and have been obtained courtesy of I. Millar. Only pre-Jurassic basement samples from Graham Land have been included in this work and their isotopy recalculated to 50 Ma (the average around which the age of the SSI dykes is clustering). Pre-Jurassic samples are considered as being representative for the original, Gondwana-related basement of the Peninsula and the recalculation was done in order to get values as

close as possible to the material which might have contributed to crustal contamination during the magma genesis of the dykes.

4.4.1 Subducted sediments

Trace element systematics

Key sediment signatures include enrichment of the LREE relative to HREE, generally high Th abundances also expressed as high Th/Ce and low U/Th, moreover low Ta/Nd and Nb/Nd, high Pb isotopic ratios, low εNd values and negative Ce anomalies [Elliott 2003; Hawkesworth et al. 1997; Turner & Hawkesworth 1997; Turner et al. 2000]. Whereas Th is unlikely to be transported in fluids from the subducting plate, it is strongly enriched in partial melts derived from subducted sediments. Thus, LREE enrichment combined with elevated Th abundances is typical, though not diagnostic of sediment contribution to the arc magma source [Elliott 2003].

Fig. 4-9A shows a plot of Nb/Ta vs. primitive mantle normalized La/Sm (reflecting LREE fractionation). The $(La/Sm)_N$ ratio reflects the enrichment of the LREE relative to HREE (Fig. 4-5, 4-6). The higher the $(La/Sm)_N$ value, the steeper the slope of the REE pattern. A clear distinction is visible in Fig. 4-9A between the dykes from Hurd Peninsula exhibiting relatively low LREE fractionation and the dykes from King George Island (Admiralty Bay, Potter, Barton, Weaver and Fildes Peninsula). The dykes from Hurd Peninsula plotting at low $(La/Sm)_N$ belong to the early intrusive events. The apparent correlation of rising LREE fractionation with time suggests increasing sediment input into the subduction zone.

Nb/Ta ratios lower than N-MORB and primitive mantle have been considered as robust measure of source depletion prior to arc magma genesis [Elliott 2003] and will be discussed in detail below (see chapter 4.4.3: The mantle wedge). The pattern shown in Fig. 4-9A indicates a mantle source beneath the South Shetland Islands more depleted than the ambient upper mantle. This is reflected by most dykes, giving strong evidence for melt depletion *prior* to arc magma genesis. In contrast, the LREE enrichment displayed by the elevated La/Sm ratios reflects a process occurring *during* arc magma genesis and is probably related to subducted sediments.

The tight clustering observed for part of the dykes from Hurd Peninsula and the dykes from Nelson Island and Penguin Island in Fig. 4-9A indicates stable source conditions during the respective intrusive

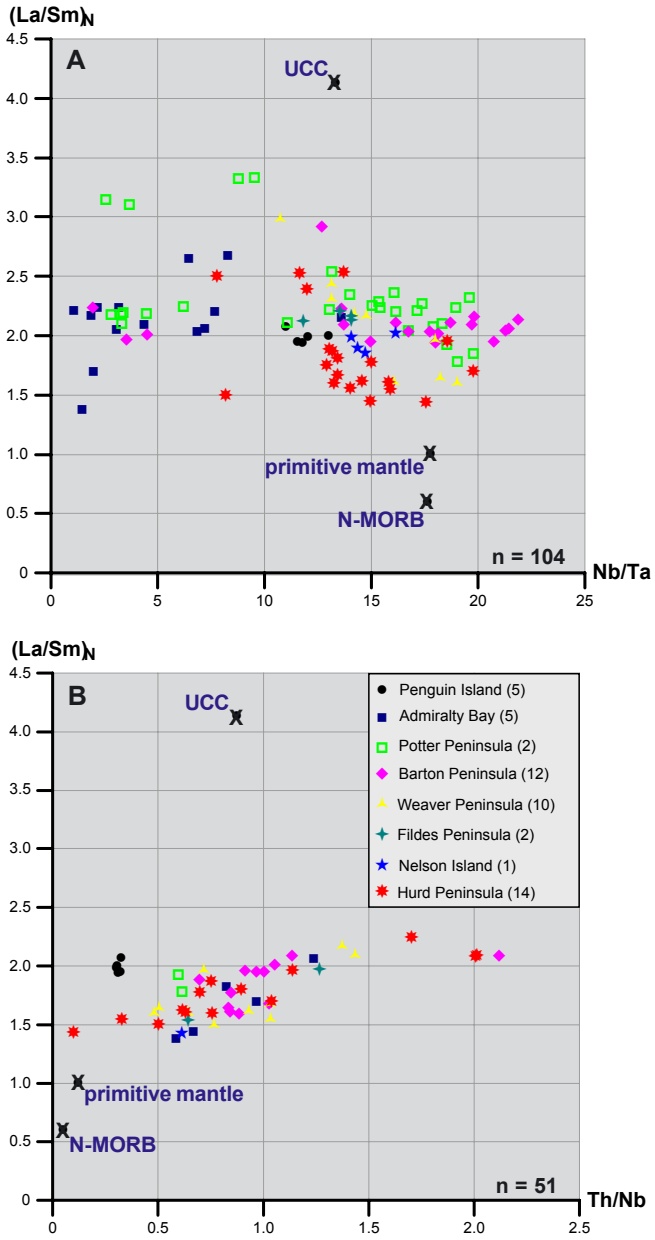

Fig. 4-9: Sediment influx into the South Shetland Islands subduction zone as indicated by LREE and HFSE behavior. LREE ratios normalized to primitive mantle values from McDonough & Sun [1995], N-MORB values from Sun & McDonough [1989], upper continental crust (UCC) values from Rudnick & Gao [2003].
(A) Nb/Ta ratio plotted versus LREE fractionation, indicating least sediment input during early stages beneath Hurd Peninsula and a highly depleted mantle source for the Admiralty Bay dykes. Symbols as in (B).
(B) Positively correlated Th/Nb and $(La/Sm)_N$ ratios. Note the separate position of the Penguin Island dykes, plotting on a line defined by N-MORB, primitive mantle and UCC. Only basalts and basaltic andesites were plotted in this diagram in order to avoid differentiation and fractionation effects.

phases. In contrast, the dykes from Weaver Peninsula exhibit a linear trend.

A strong hint on sediment input given by trace elements is also the positive correlation of Th/Nb and LREE enrichment (Fig. 4-9B). Elevated Th/Nb ratios of arc magmas as compared to N-MORB and primitive mantle are typical for sediment input and a

consequence of several combined effects. The well known Nb-Ta trough (and thus high Th/Nb ratio) expressed in arc magma "spidergrams" is also typical for many subducting sediments [Plank & Langmuir 1998]. Strong fractionation of Nb and Ta from elements like Th and La during transfer of sedimentary material to the sub-arc mantle further intensifies this effect. This is caused by residual rutile holding back Nb and Ta during partial melting of the sediment [Elliott & Plank 1997; Turner et al. 2000]. Significant Th mobilization from subducted sediments has been shown experimentally to require temperatures in excess of the sediment solidus (650-700° C) [Plank & Johnson 1997]. Based on the enhanced Th concentration in most subduction zone volcanics, it was concluded, that the sediment component of the subducting slab is transferred into the overlying mantle wedge as partial melt rather than as fluid [e.g. Elliott 2003; Turner et al. 2000].

The linear positive trend observed in Fig. 4-9B supports this interpretation. Accordingly, Th/Nb and $(La/Sm)_N$ can both be considered as sensitive tracers for sediment added to the mantle wedge beneath the South Shetland Islands.

The variation of sediment influx as deduced from Fig. 4-9A is confirmed by Fig. 4-9B. Though the variation along the trend is biggest for the dykes from Hurd Peninsula, the majority, in accordance to Fig. 4-9A, tend towards lower values, thus suggesting lower sediment influx to the source region of that area during early phases. The linear trend as displayed in Fig. 4-9B does not suggest upper continental crust to play a major role for the budget of these elements, as UCC does not plot in an end-member position for that trend.

Note that the radial dykes from Penguin Island plot well above the general trend defined by the other SSI dykes. The low Th/Nb and relatively high $(La/Sm)_N$ ratios in these rocks question the role of major sediment participation. The geographical position of Penguin Island further east and the young age (Tortonian) of these dykes suggest a relationship to the opening of the Bransfield Strait as a backarc basin rather than to subduction processes. The relatively high $(La/Sm)_N$ of the Penguin Island rocks may therefore indicate an enrichment process by fluids (Th is considered immobile under aqueous conditions) rather than sediment melts. Crustal contamination as suggested by the position of these dykes on the line with UCC as end-member is contradicted by the isotopic data.

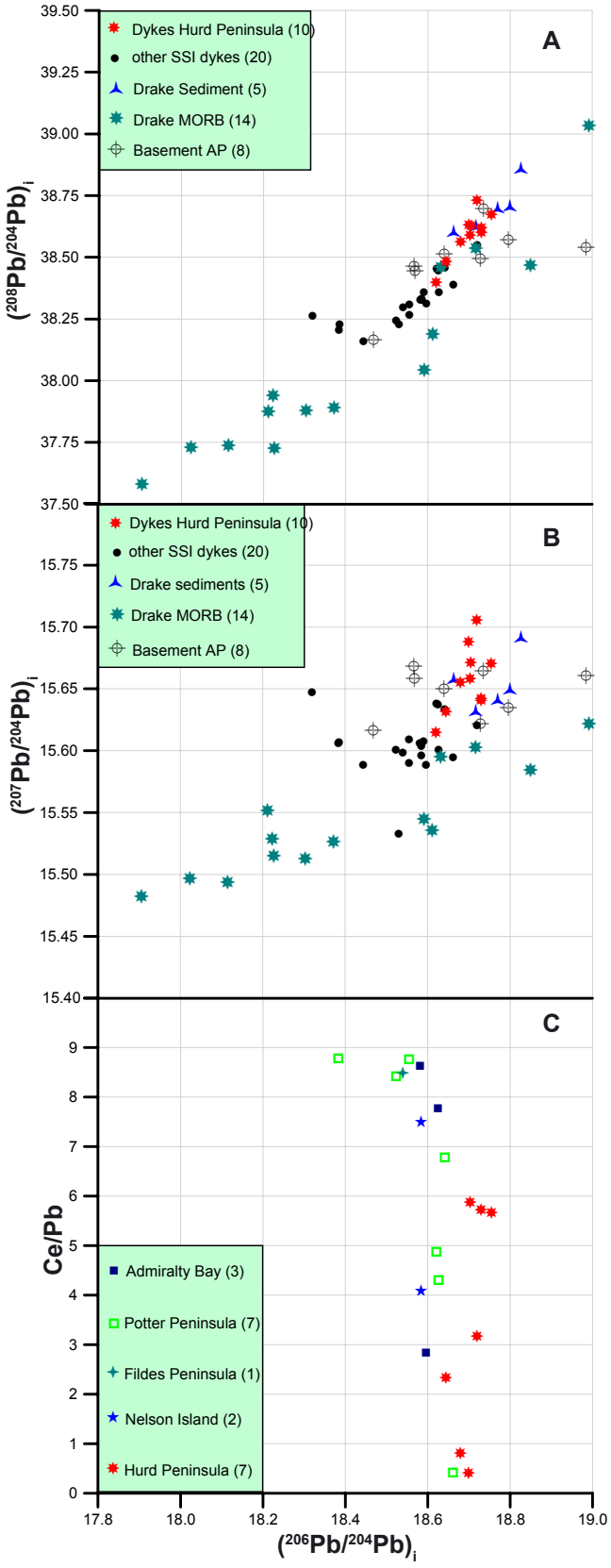

Fig. 4-10: Ce/Pb ratio and lead isotopy of the South Shetland Islands dykes. Basement isotopy from Millar et al. [2001], Drake MORB isotopy from Pearce et al. [2001], Drake sediment isotopy courtesy E. Hegner (Univ. Munich, p.c.). 2σm uncertainties for the SSI dykes average 0.0084% ($^{206}Pb/^{204}Pb$), 0.0094% ($^{207}Pb/^{204}Pb$) and 0.0102% ($^{208}Pb/^{204}Pb$).

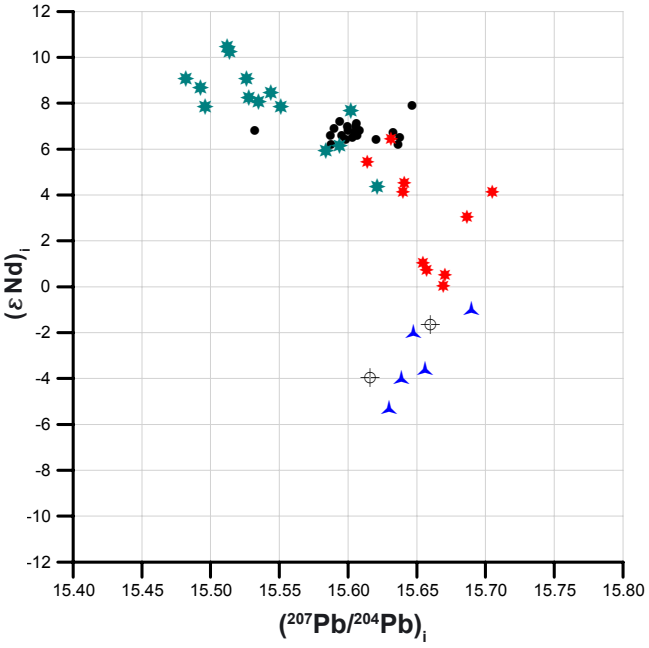

Fig. 4-11: Pb and Nd isotopy of the SSI dykes, confirming considerable crust or sediment influence on Hurd Peninsula and a rather uncontaminated mantle source for the other areas. Symbols as in Fig. 4-10A. Drake MORB isotopy from PEARCE et al. [2001], Drake sediment isotopy from WALTER et al. [2000], AP basement isotopy from MILLAR et al. [2001].

Cerium, thorium, and lead (isotope) constraints

The Ce/Pb ratio closely reflects the composition of the magma source and is largely unaffected by partial melting and differentiation processes at shallow levels of convergent margins [HOFMANN et al. 1986; MILLER et al. 1994]. The generally low Ce/Pb ratios of arc magmas (< 10 as compared to approx. 20-40 for MORB and OIB) are due to the preferential transfer of Pb in relation to Ce from the subducting plate into the mantle wedge [MILLER et al. 1994]. Fig. 4-10C exhibits a steep negative correlation between Ce/Pb and initial $^{206}Pb/^{204}Pb$ ratios, with the Hurd Peninsula dykes tending towards higher $^{206}Pb/^{204}Pb$ and lower Ce/Pb. As constrained by the superimposed correlation trends in a $^{208}Pb/^{204}Pb$ - $^{206}Pb/^{204}Pb$ diagram (Fig. 4-10A), this trend could either reflect higher sediment influx or crustal contamination with MORB and sediment/basement as end-members. From both the Pb and Nd isotopes it becomes clear, that the Hurd Peninsula dykes experienced the highest degree of contamination. These rocks lie entirely within the field covered by the basement of the Antarctic Peninsula and sediments dredged from the Drake Passage (Fig. 4-10A & 4-10B). In a Pb versus Nd isotope diagram (Fig. 4-11), the dykes and the sediments/basement form two contrasting trends converging around $\varepsilon Nd = 0$ and $(^{207}Pb/^{204}Pb)_i = 15.67$. However, neither Nd nor Pb isotopy allow to decide which of these two possible sources caused the observed pattern.

The dykes from the other areas plot closer to the Drake MORB field, indicating less contamination and a stronger mantle component.

At a first glance, the trace element and isotopic systematics of the Hurd Peninsula dykes appear contradictory. On the one hand, sediment influx seems to have been lowest beneath Hurd Peninsula (Fig. 4-9), on the other hand these dykes display the lowermost Ce/Pb ratios of all samples and the most radiogenic lead (Fig. 4-10). A plausible explanation is that the Hurd Peninsula dykes suffered higher crustal contamination but that their mantle source received less sediment input. In contrast, the dykes from the other areas were apparently not contaminated by assimilation of continental crust (see also Fig. 4-18), while their trace element systematics suggest higher sediment influx.

This assumption is supported by the linear relationship between Ce/Th ratio and the age of the dykes (Fig. 4-12). As mentioned before, high sediment input may cause a negative Ce anomaly but also increasing Th abundances. Thus, a low Ce/Th ratio might reflect a strong sedimentary component. The linear trend towards lower Ce/Th ratios with time suggests that the early intrusive events on Hurd Peninsula contain the lowest sedimentary component. With time, crustal contamination (see also chapter 4.4.4: Continental crust) ceased and sediment influx

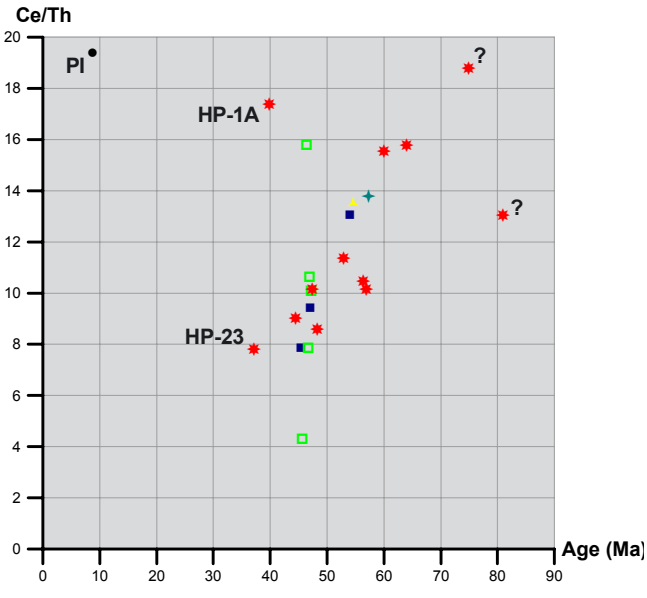

Fig. 4-12: Linear relationship between age and Ce/Th ratio, suggesting increasing sediment input with time. The question marks indicate uncertain ages. Note that the high Ce/Th ratio displayed by Penguin Island (Pl) indicates low sediment contribution to its magma source. Symbols as in Fig. 4-9.

to the mantle source got stronger, leading to lower Ce/Th ratios.
This does not apply for Penguin Island, featuring the highest Ce/Th ratio of all dykes. A low input of sediment to its magma source seems plausible, considering its geotectonic position related to a back-arc-basin.

4.4.2 Slab derived fluids

A useful method to discriminate the different components transferred from the subducting plate to the mantle wedge is plotting the primitive mantle normalized La/Sm ratio versus Ba/Th (Fig. 4-13). Sediment addition to the mantle wedge should result in LREE enrichment and therefore increased La/Sm ratios, whereas high relative Ba (e.g. Ba/Th) abundances can be attributed to fluids derived from altered oceanic crust [Elliott 2003; Hawkesworth et al. 1997; Tatsumi & Eggins 1995; Turner & Hawkesworth 1997; Turner et al. 2000]. This relationship reflects the high mobility of LIL elements such like Ba in hydrous fluids derived from the subducting slab, whereas HFS elements like Th behave essentially immobile during such processes. However, it has been stated that during arc magma genesis U behaves similar to LILE, and that U and Th are highly fractionated during processes related to dehydration of the subducting oceanic crust [Hawkesworth et al. 1997]. Such a fractionation is not expected for normal mantle melting, as all of the mentioned elements are highly incompatible and should therefore enter the melt equally or only insignificantly fractionated.
Concerning sediments, Ba has been shown to be retained in residual biotite. Strong sediment involvement may therefore be capable to cause relative Ba depletion of the melt [Nichols et al. 1994], at least it is unlikely to be responsible for Ba enrichment. Thus, elevated Ba/Th ratios give essential hints on enrichment induced by fluids derived from the subducting oceanic crust, especially if accompanied by low La/Sm and $^{87}Sr/^{86}Sr$ ratios.
In a $(La/Sm)_N$ versus Ba/Th diagram (Fig. 4-13), rocks containing the greatest sedimentary component are supposed to plot to the right, while a component predominantly derived from the oceanic crust is expected to plot at elevated Ba/Th ratios. Only basaltic and basaltic andesitic dykes (as determined by their Zr/TiO_2 and SiO_2 contents), but no evolved rocks have been plotted in order to avoid any blurring induced by differentiation processes.
Fig. 4-13 shows a clear fluid induced component, especially for dykes from Hurd and Barton Peninsula, with Ba/Th ratios elevated by a factor of up to 15 as compared to melts generated from the depleted mantle (N-MORB).
The question is if the high Ba abundances might also be the result of contamination by continental crust. As has been shown by Wilson [1989], assimilation of continental crust indeed raises Ba abundances, but the same would apply to Th. Thus, depending on the Ba/Th ratio of the assimilated crustal material, contamination would not unequivocally fractionate Ba and Th in a way to explain the elevated Ba/Th. However, crustal contamination has been identified for Hurd Peninsula, as reflected by the correlation of Nd isotope data with the Mg-number (Fig. 4-18).
Considering the comparatively high degree of alteration of Hurd and Barton Peninsula, an alternative explanation involves the addition of Ba by postmagmatic hydrothermal alteration. Th is highly insoluble at least in oxidizing aqueous fluids [Turner & Hawkesworth 1997] and consequently would not be mobilized under such conditions. Thus, alteration caused by aqueous fluids may be capable to explain the raised Ba/Th ratios observed in Fig. 4-13.

However, because Ba/Th ratios in dykes from Weaver Peninsula (i.e. the locality with the highest

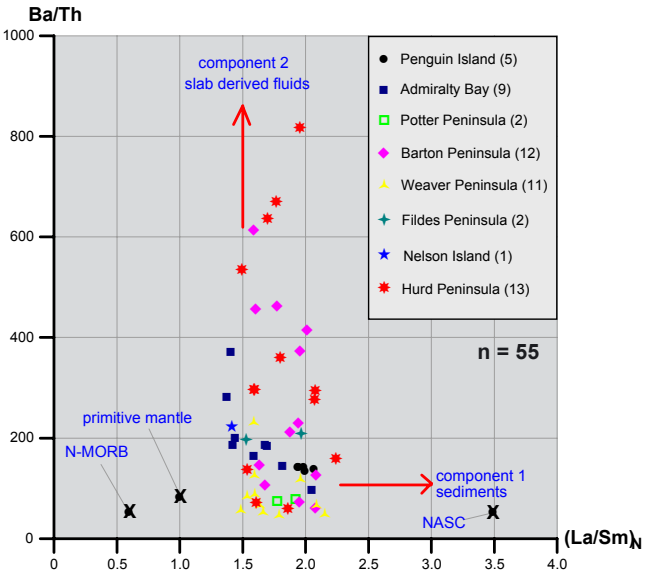

Fig. 4-13: Determination of slab derived components using primitive mantle normalized [McDonough & Sun 1995] La/Sm vs. weight ratio Ba/Th. $(La/Sm)_N$ serves as an index for enrichment caused by sediment addition, Ba/Th reflects the relative Ba abundances induced by fluids from the altered mafic oceanic crust [after Elliott 2003]. N-MORB values from Sun & McDonough [1989], North American Shale Composite (NASC) values from Gromet et al. [1984].

alteration of all areas) cluster tightly at low values and without large scatter, I favor an origin from slab derived fluids.

4.4.3 The mantle wedge

Trace element systematics

Due to masking caused by subduction contributions (additions from altered oceanic crust and sediment), it is difficult to determine the original composition of the mantle wedge (i.e. prior to enrichment). One way to address this problem is to study the abundances and ratios of the HFSE, because these elements are less abundant in sediments as compared to other elements of similar incompatibility and thus cause the least enrichment in the mantle wedge by sediment addition [Woodhead et al. 1993]. HFSE are also little affected by aqueous fluids from the oceanic crust, because they are not readily mobilized and transported by fluids [Tatsumi et al. 1986, Wilson 1989]. However, the influence of subducted sediment on HFSE abundances in arc magmas is not completely negligible, thus these elements do only provide a minimum constraint on the original composition of the mantle wedge. Most significance can probably be attributed to the highest incompatible HFSE like Nb and Ta because of two reasons [Elliott 2003]:

(1) Abundances of the highest incompatible elements should be most affected by prior mantle depletion under normal mantle melting conditions.
(2) In contrast to ratios of the less incompatible HFSE, the highly incompatible element ratios are little influenced by variations in melting and fractional crystallization.

Due to the development of the ICP-MS technique, nowadays high quality data are available, assessing even small variations in the Nb/Ta ratio. This pair of elements has been used successfully to trace prior melt depletion in the arc magma source [Eggins et al. 1997; Elliott et al. 1997; Plank & White 1995].

Still, the quality of Nb and Ta measurements can be affected by different factors: (1) especially the abundances of Ta frequently approach the detection limit in ICP-MS measurements, (2) sample preparation during this work has been carried out in a tungsten-carbide mill, which is known to bear the risk not only of W but also of Nb and Ta contamination.

Though milling times were kept as short as possible (max. 60 sec.), it is therefore absolutely necessary to check for Nb- and Ta-contamination caused by attrition from pot material.

Except for the dykes from Admiralty Bay and partly from Potter Peninsula, Ta plotted versus Nb displays a marked linear trend for the dykes from the South Shetland Islands (Fig. 4-14A). The difficulty in fractionating Nb and Ta has long been recognized, and this linear trend confirms the expected correlated behavior of the two elements.

Following observations argue against contamination of Nb and Ta by mill derived attrition:

(1) primitive mantle and upper continental crust plot in end-member positions for the South Shetland Islands dykes (Fig. 4-14A). Also average N-MORB lies on this trend. The dykes from Hurd Peninsula plotting nearest to upper continental crust in Fig. 4-14A are the same for which Nd and Pb isotope data indicate the highest degree of crustal contamination (Fig. 4-18, 4-20). This is especially true for dyke HP-7D, which according to field relationships is the oldest of the investigated dykes on Hurd Peninsula. Thus, contamination with upper continental crust seems to be at least partly responsible for the linear trend observed in Fig. 4-14A.
(2) The fact that nearly all dykes from Admiralty Bay and part of the dykes from Potter and Barton Peninsula plot to the right of the general trend in Fig. 4-14A is primarily due to variations in Ta abundances (and not to Nb), as proved by the good correlation displayed in a plot of Nb/Ta versus Ta (not shown) and the very weak correlation between Nb/Ta and Nb. This unusual behavior of Ta has already been observed causing the missing negative Ta anomalies in the "spidergram" of the silica-rich dykes (Fig. 4-8).

The dykes from Potter Peninsula plotting towards elevated Ta abundances (Fig. 4-14A) are those forming the multiple intrusions described in chapter 2.3.4 (Potter Peninsula). The highly acidic, rhyolitic dykes sandwiched between two basic dykes flanking them plot along a horizontal trend at rather high, but fairly uniform Nb abundances and variable Ta contents (Fig. 4-14B). Strikingly, the flanking basic dykes display a subparallel trend at lower Nb abundances but also towards considerably elevated Ta contents. Explaining these trends as a consequence of Ta contamination is rejected by two observations.

Firstly, a comparatively high degree of mill derived attrition could be explained in case of the rhyolites as being related to considerable quartz contents because of the relatively high hardness

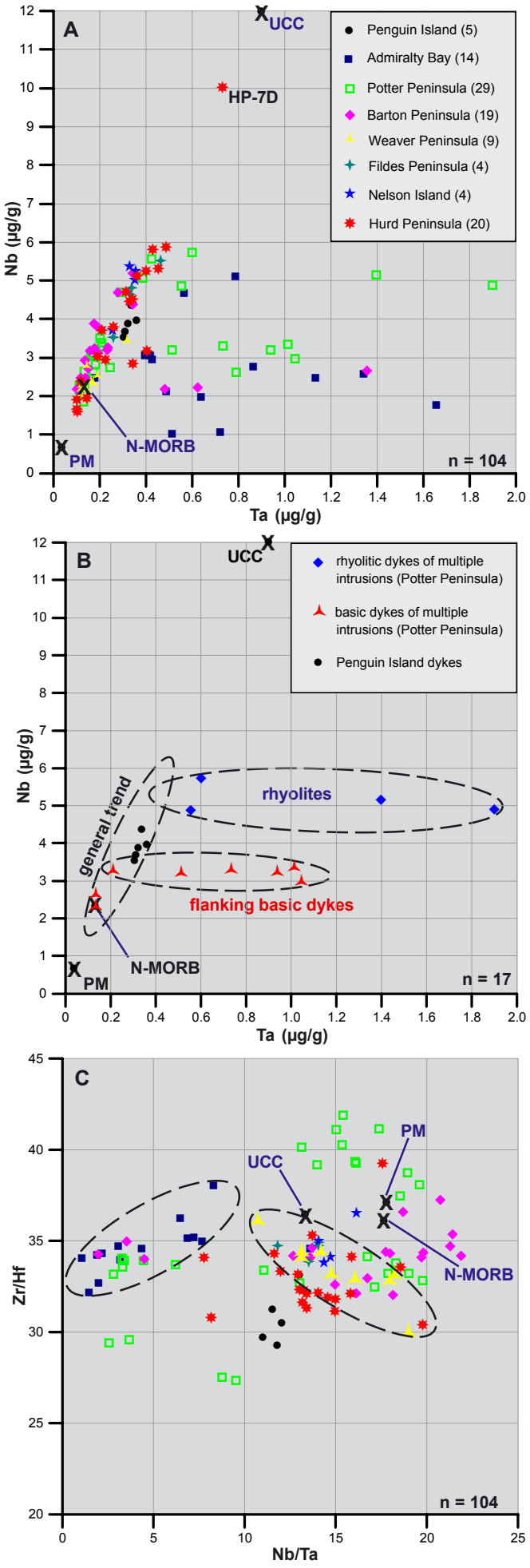

of this mineral. However, as confirmed by microscopy, quartz is absent in the flanking basic dykes nor do they yield any other minerals uncommon in the South Shetland Islands dykes, but they nevertheless display a subparallel trend.

Secondly, it is assumed that the strongest contaminated samples are those displaying the highest tungsten abundances. These are the dykes from Penguin Island (see also Appendix III, Table 5). However, they do *not* display the Ta anomaly causing the horizontal trends in Fig. 4-14B, but instead plot along the general trend as observed in Fig. 4-14A. Furthermore, none of the three groups (rhyolites, flanking basic dykes, Penguin Island dykes) displays a correlation when plotting Ta vs. W (not shown).

I therefore conclude, that the horizontal, subparallel trends displayed in Fig. 4-14B by the dykes forming the multiple intrusions are *not* related to contamination caused by the tungsten-carbide mill. Instead, I assume that they reflect a hitherto unknown, magma chamber bound process fractionating Nb and Ta, maybe related to highly evolved systems. The identical age of the rhyolitic and their flanking basic dykes indicated by both field observations and geochronological data (chapter 5) supports this assumption by proving a contemporaneous evolution of the two melts.

Similar processes might account for the elevated Ta abundances observed for almost all dykes from Admiralty Bay and three dykes from Barton Peninsula (Fig. 4-14A).

(3) The dykes from Admiralty Bay and Weaver Peninsula display linear trends when plotting Nb/Ta vs. Zr/Hf (Fig. 4-14C), and dykes from other areas (e.g. Penguin Island) show tight clustering.

Fig. 4-14: Highly immobile trace element systematics. UCC: upper continental crust (values from Rudnick & Gao [2003]), PM: primitive mantle (values from McDonough & Sun [1995]), N-MORB values from Sun & McDonough [1989].
(A) The strict linear trend between primitive mantle and upper continental crust displayed by the majority of the dykes from the South Shetland Islands indicates strongly correlated behavior of Nb and Ta and suggests mixing between the displayed end-members.
(B) Behavior of the rhyolitic and basic dykes forming the multiple intrusions on Potter Peninsula, differing strongly from the general trend.
(C) The marked linear trends (encircled) displayed by the dykes from Weaver Peninsula and Admiralty Bay, respectively, argue against contamination or analytical problems as reason for the scattered distribution of the latter group in (A), because Zr and Hf should not be affected by such effects. Symbols as in (A). Generally, Nb/Ta of most dykes is below primitive mantle and N-MORB values, suggesting a mantle source even more depleted than an average N-MORB source.

This argues against low data quality due to sample preparation or analytical problems, because contamination derived by the tungsten-carbide mill is not expected to affect Zr and Hf abundances. Correlations between Nb/Ta and Zr/Hf therefore argue against contamination. Such behavior occurs also when plotting Nb/Ta vs. $(La/Sm)_N$ (Fig. 4-9A) and versus Y/Ho (not shown), in this last case the dykes from Potter and Weaver Peninsula define the linear trends.

For the reasons outlined above, I conclude that the observed trends and correlations are natural. Nb and Ta contamination caused by the tungsten-carbide mill was, if at all, insignificant with respect to overprinting natural trends.

In order to avoid effects of differentiation and crustal contamination, only basaltic and basaltic andesitic dykes are studied to determine the composition of the original mantle wedge. This subgroup of samples is characterized by $Zr/TiO_2 < 0.0125$ and $SiO_2 < 57$ wt% (Fig. 4-2). Only dykes matching both criteria have been selected and comprise a group of 56 dykes, 29 of which are plotted in Fig. 4-15. For the rest, Nb and more frequently Ta values are below ICP-MS detection limits.

A striking first order observation are the very low Nb abundances (< 2 µg/g) displayed by part of the dykes from Hurd Peninsula and Admiralty Bay (Fig. 4-15). These low contents contrast with the higher abundances of other elements of comparable incompatibility (e.g. Th). One possibility is, that the mantle wedge component of these dykes was strongly depleted in Nb. However, besides the composition of the mantle source, the degree of melting also plays a major role for elemental abundances in melts, though this should affect all elements of comparable incompatibility likewise.

An even more robust tracer for depletion of the mantle source is the Nb/Ta ratio [Elliott 2003]. The two elements are both highly incompatible, have the same valency and an apparently identical ionic radius [Shannon 1976] and should therefore be very difficult to fractionate during melting. However, experimentally determined distribution coefficients suggest that Nb is slightly more incompatible in common mantle minerals than Ta [Green et al. 1989]. Consequently, melt extraction should reduce the Nb concentration and Nb/Ta ratio in the residue [Elliott 2003]. Great parts of the South Shetland Islands dykes display Nb/Ta ratios lower than primitive mantle and, to a lesser degree, also lower than MORB (Fig. 4-9A, 4-14C, 4-15). These observations indicate a heterogeneous mantle wedge beneath the South Shetland Islands volcanic arc, partly even more depleted than normal MORB source.

In Fig. 4-15, almost all dykes displaying Nb/Ta ratios lower than MORB plot outside the field delimited by the compilation of island arc rocks from Elliott [2003]. This compilation is restricted to island arcs, whereas the South Shetland Islands volcanic arc represents an active continental margin. No data exist so far comparing the Nb/Ta systematics of these two geotectonic settings. However, these dykes plot subparallel to the island arcs field in Fig. 4-15 and might indicate a shift towards higher Ta contents for active continental margins under special conditions.

High LILE/HFSE ratios like Ba/Th in combination with low $^{87}Sr/^{86}Sr$ and low Th abundances have been considered as generally typical for arc rocks derived from a depleted mantle source [Hawkesworth et al. 1997]. These conditions are matched by many dykes from the South Shetland Islands (Fig. 4-16 & 4-17), thus supporting the conclusion drawn from Fig. 4-15.

Th abundances and the U/Th ratio reflect melting processes in the mantle wedge. Basalts and basaltic andesites have been plotted, and a sedimentary or continental crust derived component seems likely for

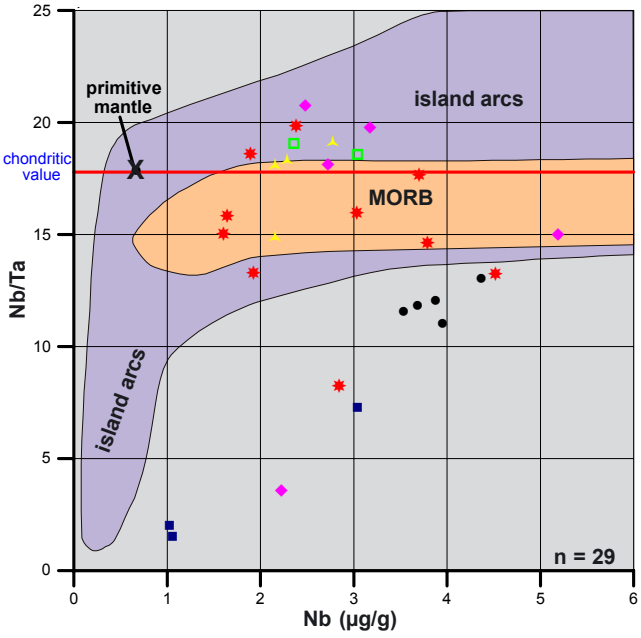

Fig. 4-15: Nb vs. Nb/Ta plot of the most basic dykes, suggesting heterogeneity of the mantle wedge. Primitive mantle values from McDonough & Sun [1995]. Fields for MORB and island arc rocks after Elliott [2003]. Symbols as in Fig. 4-14.

the dykes from Hurd and Barton Peninsula (Fig. 4-16A).

The U/Th ratios plot mostly at sub-MORB level, contradicting a significant fluid induced fractionation of U and Th, which would lead to relative U enrichment as postulated by Hawkesworth et al. [1997] and Turner et al. [2000]. Either contribution of subducted sediments (which have relatively low U/Th ratios as displayed in Fig. 4-16A), or a mantle source depleted in U might be responsible for the observed pattern. Interestingly, U/Th correlates with the geographic position. Whereas most of the Hurd Peninsula dykes and especially the radial dykes from Penguin Island display ratios lower than primitive mantle, the dykes from King George Island (Barton, Weaver and Potter Peninsula, Admiralty Bay) tend towards higher U/Th ratios. The dykes from Admiralty Bay do even show ratios higher than N-MORB (Fig. 4-16A) and are thus the most probable candidates to be affected by the U enrichment process stated by Hawkesworth et al [1997].

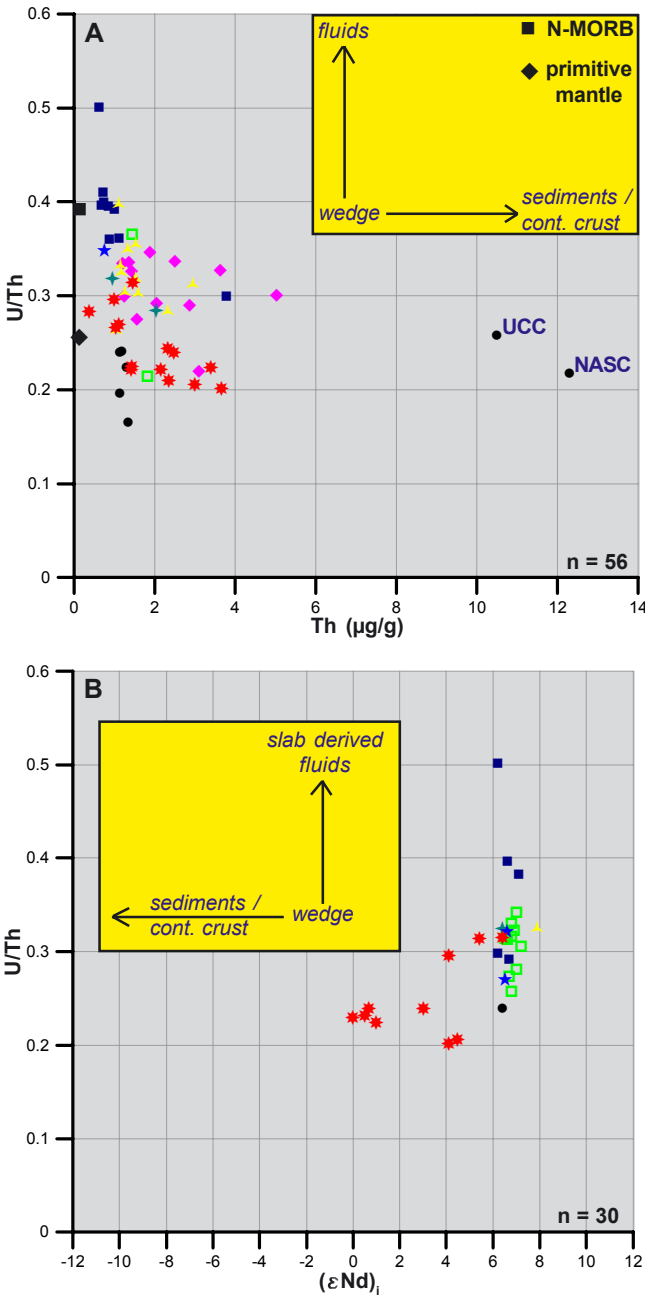

Fig. 4-16: Nd isotope, Th and U/Th systematics. Primitive mantle values from McDonough & Sun [1995], N-MORB values from Sun & McDonough [1989], upper continental crust (UCC) values from Rudnick & Gao [2003], North American Shale Composite (NASC) values from Gromet et al. [1984]. Symbols as in Fig. 4-14.
(A) Th abundances and U/Th ratios do not indicate significant contribution of slab derived fluids, but a sedimentary or crust derived component for the dykes from Hurd and Barton Peninsula. Only basic dykes plotted.
(B) Nd isotope data vs. U/Th ratio suggesting a sedimentary or crust derived component for the dykes from Hurd Peninsula. No isotope data available for Barton Peninsula.

Unlike U, Th has been attributed a much higher fluid mobility than Th [Hawkesworth et al. 1997; Turner et al. 2000]. However, despite of its mobility, a depletion of U caused by postmagmatic hydrothermal alteration is unlikely because of the homogeneous and tight clustering of the different geographical areas not showing large scatter (Fig. 4-16A). Especially in the case of the Penguin Island dykes, which represent the freshest of all samples, such a process is highly unlikely. Therefore, I conclude that the differing U/Th ratios reflect true differences in the mantle wedge for all areas but Hurd Peninsula.

For Hurd Peninsula, crustal contamination is evident (Fig. 4-18). Because crustal materials have low U/Th ratios, such contamination would result in reduction of the U/Th ratio [Turner et al. 2000]. This applies to the Hurd dykes, as shown in Fig. 4-16.

Isotopic constraints

Except for the dykes from Hurd Peninsula, a relatively uncontaminated, mantle derived origin is clearly visible from lead and neodymium isotope data (Fig. 4-11). All dykes on Nelson, King George and Penguin Island plot close to the MORB field, suggesting a depleted mantle source.

Concerning Sr isotopes, the initials calculated for the South Shetland Islands dykes range from 0.703270 to 0.703790 and are thus relatively unradiogenic (Fig. 4-17). Since the average $^{87}Sr/^{86}Sr$ ratio of altered oceanic crust sampled in ophiolites is approx. 0.7055 [Bickle & Teagle 1992] and of ocean floor approx. 0.7046 [Staudigel et al. 1996], the subducted oceanic crust can possibly be ruled out as main contributor of Sr to the arc magmas. The same applies to subducted sediment, as the calculated Global Subducting Sediment Composition (GLOSS) has an

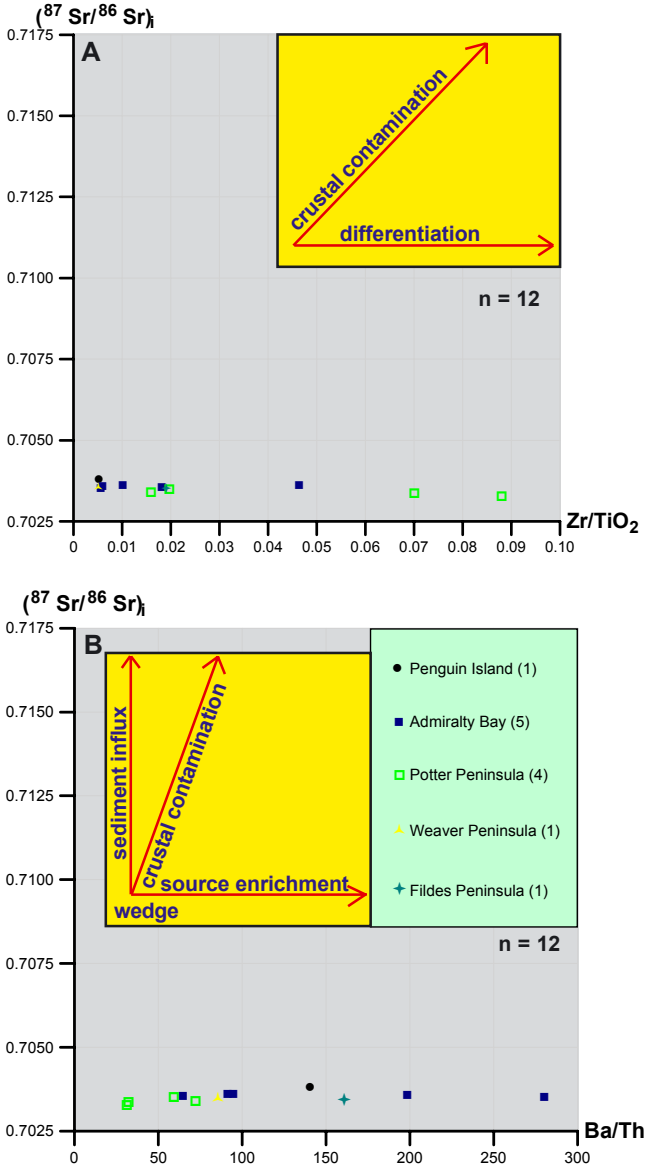

Fig. 4-17: Differentiation index Zr/TiO_2 (A) and Ba/Th (B) plotted versus $(^{87}Sr/^{86}Sr)_i$ of 11 dykes from King George and one dyke from Penguin Island to determine crustal contamination and source enrichment. No crustal component can be identified in these dykes, but a considerable source enrichment, probably caused by fluids from the subducted slab. Digits in brackets refer to the number of plotted dykes from the respective area.

even higher $^{87}Sr/^{86}Sr$ ratio of 0.7174 [PLANK & LANGMUIR 1998], and sediments dredged from the Drake Passage [WALTER et al. 2000] an average value of 0.7087. A major Sr contribution from these sources or assimilation of continental crust would have led to much higher $^{87}Sr/^{86}Sr$ ratios than observed, thus indicating that the measured Sr isotopic composition reflects largely that of the mantle wedge. No Sr isotopic data are available for the dykes from Hurd Peninsula. According to their trace element behavior and Nd and Pb isotopy (Fig. 4-11, 4-16), I assume that these rocks would probably plot towards higher $^{87}Sr/^{86}Sr$ ratios.

4.4.4 Continental crust

From Sr, Nd and Pb isotope data alone, it is difficult or impossible to distinguish between sediment influx and crustal contamination in active continental margin settings (Fig. 4-10, 4-11). However, crustal contamination usually occurs during shallow level differentiation. Consequently, if such a process takes place, the most differentiated rocks should also be the most contaminated. Thus, plotting isotopic data (e.g. εNd) versus some differentiation factor (e.g. Mg-number) may display a correlation in case that contamination occurred. This is obviously the case for the Hurd Peninsula dykes, but not for the dykes from the areas further to the NE (Fig. 4-18). Moreover, the Hurd dykes plot roughly according to their relative ages as deduced from field relationships and Ar-Ar data, i.e. the oldest dykes have the lowest εNd and Mg-numbers (see also chapter 4.6.1: Hurd Peninsula).As shown by the geochronological data, dyke intrusion on Hurd Peninsula started at least 10 Ma earlier than on Nelson and King George Island.

Therefore, I assume that these dykes reflect intrusive events that took place during initial stages of magmatic arc activity in that area. Such a scenario would also be consistent with a still relatively unstretched continental crust and therefore higher degrees of crustal contamination, leading to lower εNd values and higher incompatible element abundances. Moreover, the tholeiitic character of these rocks (Fig. 4-3, 4-22) is typical for initial stages of a young immature arc [TATSUMI & EGGINS 1995; WILSON 1989]. Consequently, the two youngest events (HP-1A and HP-23, Fig. 2-8 & 2-9), that even postdate the dykes from the other areas, plot within the "uncontaminated" field occupied by the areas further to the NE.

As outlined above, low U/Th ratios may also reflect crustal contamination (Fig. 4-16A). Whereas the Hurd Peninsula dykes generally tend towards low U/Th ratios as compared to the other areas, the two youngest events indeed have the highest U/Th ratios from all Hurd Peninsula dykes, providing further evidence for a gradual decrease of the crustal contamination.

These observations give strong evidence, that crustal contamination was high during initial phases of intrusive activity, then decreased gradually and had virtually expired at the time the dykes on Nelson and King George Island intruded. Apparently the situation did not change anymore until recent times, as proved by the uncontaminated character of the Penguin Island dyke.

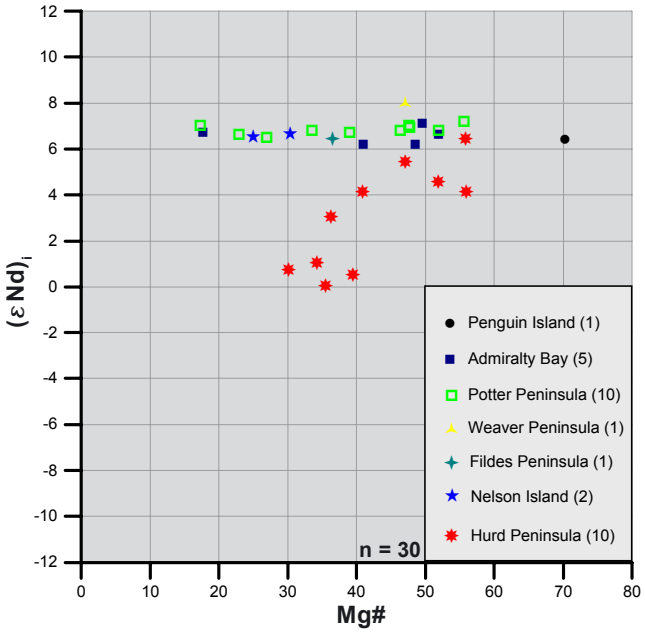

Fig. 4-18: Mg-number plotted versus Nd isotopy to determine crustal contamination. The correlation in case of Hurd Peninsula proves assimilation of crustal material during shallow level differentiation. Such processes did obviously not occur on Nelson, King George and Penguin Island. Average $2\sigma m$ for Nd isotope data is 0.0026 %.

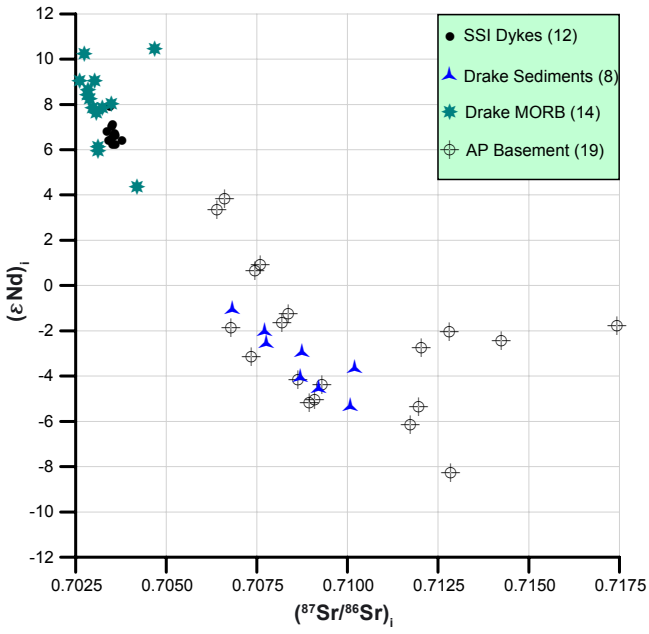

Fig. 4-19: Influence of crustal contamination and/or sediment input on the dykes of the South Shetland Islands. Sr vs. Nd isotopic data of 11 dykes from King George Island and one from Penguin Island. A mantle derived origin is clear for these dykes. Note that no dykes from Hurd Peninsula plot in this diagram.
Isotope data of Antarctic Peninsula Basement from MILLAR et al. [2001], initials recalculated at 50 Ma. Drake Passage MORB data from PEARCE et al. [2001] and sediment data from WALTER et al. [2000].

These observations are fully confirmed for the dykes from King George and Penguin Island by a plot of differentiation index (Zr/TiO_2) and source enrichment index (Ba/Th) versus Sr isotopic data (Fig. 4-17). According to the above given arguments, also a positive correlation between $^{87}Sr/^{86}Sr$ and differentiation index (SiO_2, Mg# or Zr/TiO_2) can be attributed to crustal contamination at shallow levels [DAVIDSON 1987, DAVIDSON & HARMON 1989, HAWKESWORTH et al. 1997], particularly if accompanied by increases in oxygen isotopes. Obviously, the 12 dykes display distinct degrees of differentiation (Fig. 4-17A) and also source enrichment caused by fluids derived from the subducting slab (Fig. 4-17B), but no crustal component. This also means, that the highly acidic (rhyolitic) dykes from Potter Peninsula (plotting to the right of Fig. 4-17A) are *not* the result of crustal assimilation, but simply of high degrees of differentiation from the same parent magma as their more basic counterparts.

The magma source of some areas on King George Island (e.g. Potter Peninsula) seems to be even less enriched in Ba than the source of the Penguin Island dykes (Fig. 4-17B), though the latter are assumed to be related to backarc spreading in Bransfield Strait and not to subduction.

Further evidence is demonstrated convincingly by a plot of Nd versus Sr isotopes (Fig. 4-19). The 12 samples from King George and Penguin Island plot close to MORB dredged from the Drake Passage, but are slightly displaced towards Drake Passage sediments and granitoids from the basement of the Antarctic Peninsula (isotopic data of the Drake sediments from WALTER et al. [2000], of the basement from MILLAR et al. [2001]). Crustal contamination can be ruled out according to the above arguments. Thus, I conclude, that during dyke emplacement on King George Island and still much later on Penguin Island, the melt was of mantle derived origin but with a sedimentary component.

4.5 Magmatic phases

The geochronological data (chapter 5) suggest that the time interval, during which dyke intrusion occurred in the investigated areas, was restricted to the Paleocene and Eocene. However, this does certainly not exclude possible earlier intrusive activity in other parts of the archipelago, especially as arc related magmatic activity has repeatedly been reported to have started already during Cretaceous times [e.g. BIRKENMAJER 1994; SMELLIE et al. 1984].

A rough correlation between the degree of crustal contamination and the sequence of the different in-

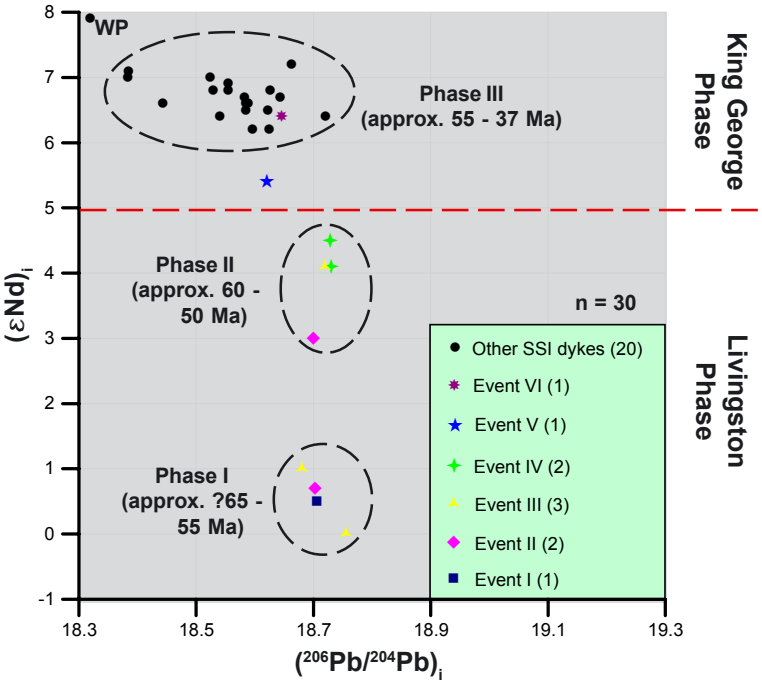

Fig. 4-20: Pb and Nd isotope data demonstrating different phases of intrusive activity as characterized by decreasing degrees of crustal contamination and by their age. Event I to event VI are the different intrusive events observed on Hurd Peninsula (Livingston Island). WP: Weaver Peninsula.
The first two phases (event I to event IV) are entirely restricted to Hurd Peninsula and reflect decreasing degrees of crustal contamination. The third phase expressed mainly on Nelson and King George Island displays very uniform isotopy and no crustal component.

trusive phases is evident from Fig. 4-20. The most contaminated melts comprise dykes from Hurd Peninsula, attributed to events I, II and III, termed here "Phase I". Geochronological data (Ar-Ar and K-Ar) yielded uncertain Campanian ages for the oldest dykes from this phase, and Selandian to Thanetian ages for the youngest. The second phase, also restricted to Hurd Peninsula, includes single dykes from event II and III and the dykes from event IV ("Phase II"). Geochronological data indicate Thanetian to Ypresian ages for this phase. These first two phases are entirely restricted to Hurd Peninsula and therefore termed "Livingston Phase" (Fig. 4-20). Only during a third cycle intrusive activity on Nelson and King George Island commenced. Single dykes belonging to phase III yielded Thanetian and Ypresian ages, but the vast majority intruded during the Lutetian around 46 Ma. The two last intrusive events on Hurd Peninsula (event V and VI) can also be assigned to phase III. The position of event V in Fig. 4-20 suggests an already much decreased but still visible influence of continental crust, whereas event VI plots entirely within the field occupied by the dykes from King George Island.

Given the temporal overlap between the different phases, the following development seems plausible:

(1) Intrusive activity started earlier on Hurd Peninsula (Livingston Island) and lasted longer than on King George Island, accompanied during initial stages by considerable crustal contamination, probably during shallow level differentiation. The degree of crustal contamination decreased with time (Fig. 4-21), maybe due to an increasingly stretched crust letting the melts rise more directly and with shorter storage times at shallow levels. The last event on Hurd Peninsula seems to be free of contamination and is younger than the last event on King George Island. This interpretation is supported by petrologic observations in the dykes from Hurd Peninsula, stating a decrease in potassium content and orthoclase-component in the feldspars, tightly correlated with the gradual introduction of clinopyroxene from event to event (see chapter 3).

(2) Intrusive activity further to the NE on Nelson and King George Island started later than on Livingston Island and was charac-

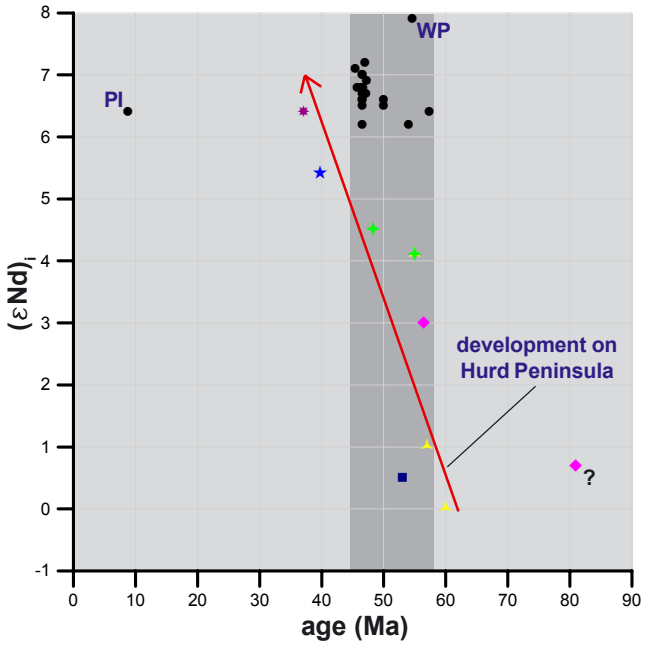

Fig. 4-21: Development of εNd with time and dependent on the area. PI: Penguin Island, WP: Weaver Peninsula. The question mark (lower right) indicates the uncertainty of this age, the dark grey area denotes the time of intrusive activity on King George Island. Note that some older dykes from Hurd Peninsula do not plot in this diagram due to missing Nd isotopic data. Symbols as in Fig. 4-20.

terized by the absence of crustal contamination from the beginning on. The vast majority of the dykes on King George Island intruded around 46 Ma, indicating an intense, ephemeral event.

(3) Crustal contamination is also absent in the Tortonian dyke from Penguin Island (Fig. 4-21).

Further geochronological constraints are discussed in chapter 5.

4.6 Characteristics of individual areas

As well as profound differences are obvious comparing the different investigation areas, also different intrusive events within one and the same area may be distinguished according to their geochemical characteristics.

4.6.1 Hurd Peninsula

Discussion of tholeiitic affinity

As the different bivariate plots commonly applied for determination of magmatic affinity give contradictory results, another plot besides Fig. 4-3A is recommended to control whether the tholeiitic trend shown by the Hurd Peninsula dykes is confirmed or not. In a plot of Zr vs. TiO_2, these dykes plot well along the idealized fractionation curve of a tholeiitic suite (Fig. 4-22). Due to the suppression of Fe- and Ti-enrichment by the early crystallization of Fe-Ti-oxides, a calc-alkaline suite would define a linear trend straight across the diagram. The strong Ti-enrichment observed for the dykes from Hurd Peninsula in Fig. 4-22 accompanies the Fe-enrichment typical for tholeiitic suites and supports the interpretation of these dykes as of tholeiitic affinity. Consequently, the dykes from Potter Peninsula, plotting as calc-alkaline in Fig. 4-3A, do not show such a Ti-enrichment trend (Fig. 4-22).

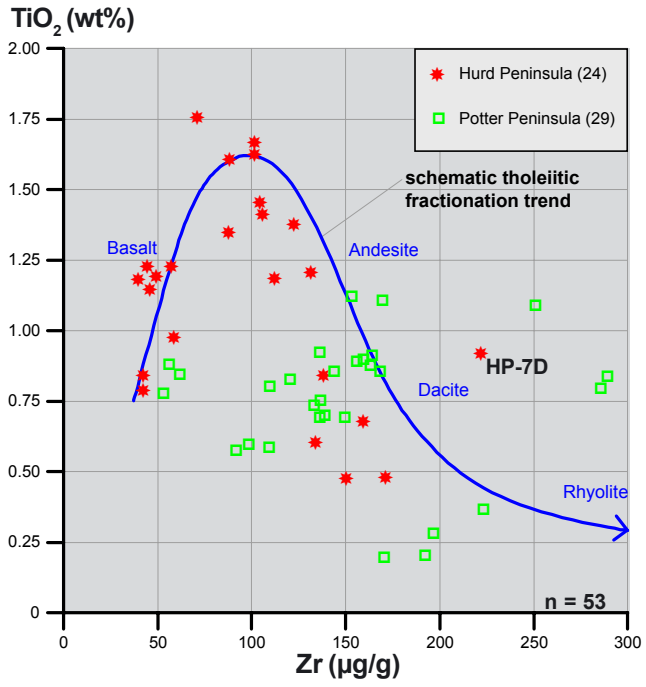

Fig. 4-22: The dykes from Hurd Peninsula, plotting along the idealized fractionation curve for immobile elements in a tholeiitic volcanic suite [MacLean & Barrett 1993]. Strong Ti-enrichment is characteristic for the initial phases (basalts), followed by marked Ti-depletion from andesite to rhyolite.

The degree of differentiation of the Hurd Peninsula dykes, as indicated by Zr/TiO_2 and SiO_2 (Fig. 4-2), corresponds well with their respective position along the fractionation curve. The same behavior is observed in plots of Zr vs. Al_2O_3 and TiO_2 vs. Al_2O_3, all referred to as immobile. This is interpreted as a further argument for the tholeiitic character of the Hurd Peninsula dykes. Tholeiitic magmas are typical for young immature arcs and do also occur closest to the trench in more mature arcs [Tatsumi & Eggins 1995; Wilson 1989], or at continental margins with subduction rates exceeding 7 cm per year [Philpotts 1990]. In contrast, the calc-alkaline series is strictly bound to more mature arcs and active continental margins. In case of Hurd Peninsula, the tholeiitic trend correlates with the following observations:

(1) The focus of activity of the South Shetland Islands magmatic arc is thought to have migrated from SW to NE [Birkenmajer 1994; Birkenmajer et al. 1986b; Pankhurst & Smellie 1983], thus the dykes on Hurd Peninsula should be older than the dykes on King George Island. This is confirmed by own age determinations at least for the dykes cropping out in the investigated areas (see chapter 5). Assuming, that a tholeiitic melt is generated during initial stages of arc activity and that these melts in case of an active continental margin setting have to travel through a still relatively unstretched continental crust, they should show stronger contamination than melts generated during later stages. Indeed, crustal contamination of the Hurd Peninsula dykes is convincingly demonstrated plotting Mg-number versus εNd (Fig. 4-18).

(2) Two-pyroxene (cpx + opx) andesites are typical for the calc-alkaline series but not for the tholeiitic series. The dykes on Hurd Peninsula do not contain any opx (see chapter 3), thus indirectly supporting their tholeiitic character. Two-pyroxene rocks are characteristic for the dykes on Potter Peninsula, and indeed these plot predominantly

within the transitional and calc-alkaline fields (Fig. 4-3A).

As mentioned in chapter 1, a first magmatic arc was built during Mesozoic times resting upon the Antarctic Peninsula. During the Cretaceous, the subduction trench shifted oceanward (NW), only then initiating magmatic arc activity also in the area of the South Shetland Islands. Own Ar-Ar age determinations yielded earliest Paleogene (Paleocene) and some uncertain Late Cretaceous ages for the dykes from Hurd Peninsula (see chapter 5), thus supporting their generation during initial arc activity in that area. A further argument is given by the fact that 40% of the dykes from Hurd Peninsula display Ti/Zr ratios higher than average N-MORB, interpreted as indicative for primitive arc magmas [TATSUMI & EGGINS 1995].

Non-tholeiitic intrusive events

Only two intrusive events on Hurd Peninsula do not show tholeiitic characteristics: event I represented by dyke HP-7D and event VI represented by dyke HP-23.

Dyke HP-7D (event I in Fig. 2-8) shows markedly different geochemical characteristics as compared to the other dykes from Hurd Peninsula (e.g. Fig. 4-3, 4-14A, 4-22, 4-24). As this dyke, based on field relationships, is interpreted as representing the first intrusive event in the investigated area, for the reasons outlined above it should be amongst the dykes showing highest crustal contamination. This assumption is supported by its εNd value, being the second lowest of all dykes, and by its unusually high Nb and Ta abundances, getting close to upper continental crust values (Fig. 4-14A). However, its non-tholeiitic character is puzzling, as especially the oldest events should not be of calc-alkaline affinity. Maybe its tholeiitic origin is masked by the high degree of crustal contamination. The very distinct geochemical behavior, causing HP-7D to plot separately from the other Hurd Peninsula dykes in most diagrams, in combination with field evidence at least justifies its classification as a separate intrusive event.

The youngest dyke on Hurd Peninsula, as deduced from field relationships (intrusive event VI represented by dyke HP-23, Fig. 2-8), also gave the youngest Ar-Ar age (Priabonian, 37.16 Ma), thus indicating its generation during final stages of intrusive activity on Hurd Peninsula. This should correspond to the mature phase of the arc, and consequently, it plots as calc-alkaline in Fig. 4-3A.

Characteristics of the individual intrusive events

Generally, the dykes on Hurd Peninsula display the highest Fe_2O_3 and TiO_2 contents of all areas, corresponding to their tholeiitic character.

Profound geochemical differences can be stated between the dyke suites from the different parts of the South Shetland Islands (e.g. Fig. 4-9A, 4-14C), and likewise the different intrusive events on Hurd Peninsula also have characteristics allowing to distinguish them from each other (Fig. 4-23 & 4-24).

The Mg-number is insensitive to the degree of partial melting but is a powerful tool serving as an index of subsequent fractional crystallization, especially of olivine. The Yb enrichment relative to primitive mantle displays the degree of partial melting in the source if applied only to the basaltic members of a rock suite, and serves as differentiation index if applied also to the higher differentiated members. In Fig. 4-23, all geochemically analyzed dykes from Hurd Peninsula have been plotted and following deductions can be made:

(1) Intrusive events I-III and to a lesser degree also V have undergone considerable fractional crystallization as indicated by their low Mg-numbers. Event II and especially event III display a notable negative linear trend, suggesting that these dykes intruded subsequently over a longer time period during which crystal fractionation and differentiation took place in the magma chamber, such

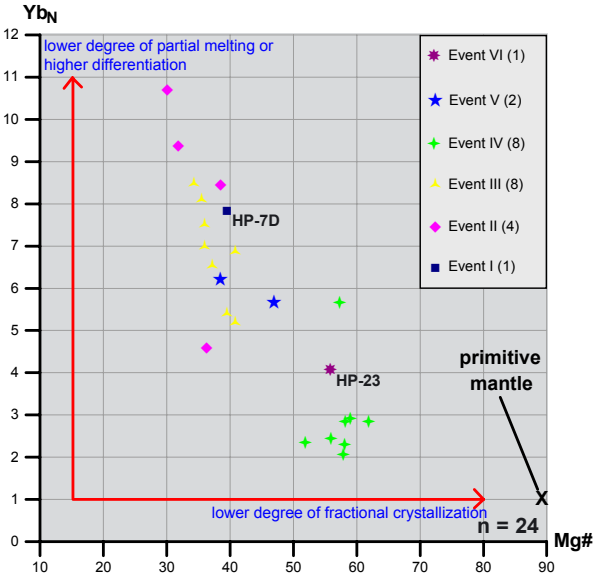

Fig. 4-23: Mg-number vs. Yb_N to distinguish different intrusive events on Hurd Peninsula according to degree of crystal fractionation and HREE enrichment. Yb normalized to primitive mantle values from MCDONOUGH & SUN [1995]. Symbol colors corresponding to those assigned to the different events in Fig. 2-8 and 2-9. Digits in brackets indicate the number of analyzed dykes from the respective intrusive event.

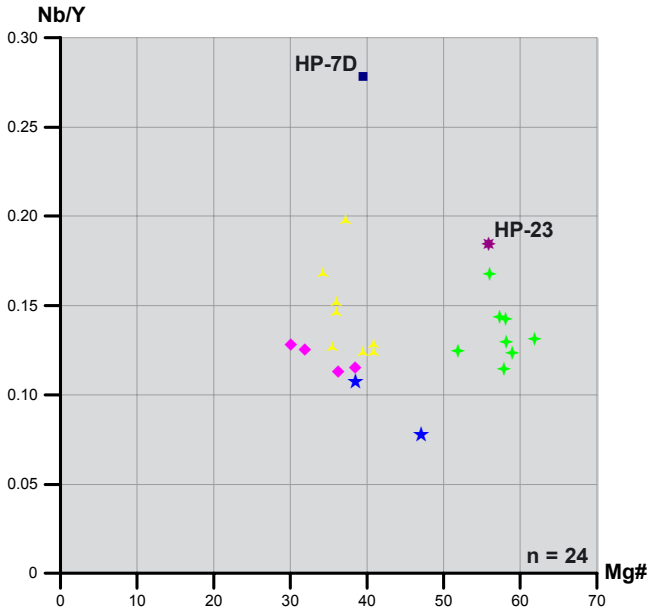

Fig. 4-24: Mg-number versus Nb/Y ratio to demonstrate distinct geochemical behavior of the individual intrusive events on Hurd Peninsula (Livingston Island). Note the extraordinary high Nb/Y ratio of the first intrusive event, probably caused by strong crustal contamination. Colors as in Fig. 2-8 and 2-9, symbols as in Fig. 4-23.

that each dyke represents magma which was a little more fractionated and differentiated than the preceding one. This is perfectly true for event II, whose members become progressively more differentiated (according to their Zr/TiO_2 content) with rising Yb_N values. In case of event III, the correlation between rising Zr/TiO_2 and Yb_N is not perfect, but also in this group the more basic members tend to low and the more acidic ones to high Yb_N values.

(2) Event IV displays a considerably different history. The higher Mg-numbers indicate that these dykes have not been affected too strongly by crystal fractionation processes and thus represent a less evolved magma. A lower degree of differentiation is also indicated by the low Yb enrichment relative to primitive mantle and is confirmed by very low Zr/TiO_2 values (not plotted), belonging to the lowest of all investigated dykes. Moreover, this group shows by far the highest Ni (up to 100 µg/g) and Cr (up to 170 µg/g) abundances. These observations suggest that this was a comparatively short-lived event without long storage times in a shallow level magma chamber. This assumption is supported by the cluster-like plotting of event IV, as any magma chamber bound processes combined with non-contemporaneous intrusion of the dykes would have produced a linear trend as in case of events II and III. Further characteristics of event IV include very high Ba/La and Ba/Th ratios, indicating higher influx of slab derived fluids to the mantle source during that time.

(3) The last event, represented by dyke HP-23, also represents a magma less evolved than those of events I-III. Obviously, it was affected by a shorter history of fractional crystallization, as displayed by its Mg-number.

A clearer demonstration of the distinct geochemistry of each individual intrusive event is given by Fig. 4-24. As reflected by its high Nb/Y ratio, the first intrusive event (HP-7D) displays the highest degree of alkalinity, also reflected by its extremely high K_2O content (5.2 wt%). The same applies to a dyke from event II (HP-19, not shown). This might be due to stronger crustal contamination and corresponds well with their role as early intrusive events. The other events plot within well defined areas, event III, IV and VI showing intermediate, event II and V low degrees of alkalinity.

The variations in the Nb/Y ratio observed within some suites (e.g. the trend displayed by event III in Fig. 4-24) might reflect different residence times in shallow level magma chambers and therefore different degrees of crustal contamination of the respective melts.

The differences displayed by the Mg-number have been discussed before.

4.6.2 Weaver Peninsula

The dykes from Weaver Peninsula are characterized by low to moderate Ba/Th ratios, indicating a lower influence of slab derived fluid. On the other hand, a tendency towards high Cs/Th ratios can be observed. However, Cs might also be mobilized from subducted sediment.

At least some of the dykes on Weaver Peninsula seem to represent direct mantle fractionates without major contribution of other sources, as indicated e.g. by a very high εNd value (7.9) of dyke WP-20B (Fig. 4-20, 4-21) and the generally very high Co abundances in this group. I assume, that the dykes on Weaver Peninsula represent an event fed by depleted mantle melts that ascended and emplaced unusually fast, without contamination or long storage times at shallow levels. The generally low Nb abundances and Nb/Ta ratios, mostly lower than primitive mantle and N-MORB (Fig. 4-14), support this assumption.

Though also average upper continental crust has been attributed relatively low Nb/Ta values between 12.5

[Barth et al. 2000] and 13.3 [Rudnick & Gao 2003], the high Mg-numbers and εNd values shown by some of the dykes from Weaver Peninsula argue against crustal contamination as reason for the observed Nb and Ta characteristics.

WP-5, one of the geochemically most conspicuous dykes, is cropping out here. According to its SiO_2 content (46.14 wt%), it is the most basic dyke of all, also having a high Mg-number (63.49) and the second highest Ti/Zr ratio (173.4). Very high Al_2O_3 (21,83 wt%) and very low TiO_2 (0.442 wt%) and P_2O_5 (0.065 wt%) abundances are also noteworthy. Except for Penguin Island, WP-5 shows the highest Co content (41.35 µg/g) of all samples. Its REE pattern is similar to the other dykes but with notably lower abundances (Fig. 4-5). The same applies to the multielement "spidergram" (Fig. 4-7). Nb and Ta abundances are even below ICP-MS detection limit. Part of this behavior might be due to an unusual high degree of alteration, as reflected by the high LOI (6.86 wt%). This is supported also by the fact that WP-5 plots outside the CHARAC-field (Fig. 4-1) and has by far the highest CaO content (13.69 wt%). A massive, hydrothermal introduction of CaO may have caused a kind of dilution process in the bulk rock. Such an interpretation is, however, contradicted by the fact that WP-5 also shows by far the lowest Zr/Hf ratio. This ratio should remain unaffected during usual alteration processes. It has been stated [Bau 1996], that non-chondritic Zr/Hf ratios occur only occasionally in basalts, but that Zr-Hf fractionation is usually restricted to highly evolved felsic magmatic systems. Even in case that the observed unusual chemical characteristics are not primary but were induced by hydrothermal alteration, it can be stated that this process must have been exceptionally intense.

4.6.3 Potter Peninsula

The dykes from this area show generally low LILE/HFSE ratios (e.g. Ba/Th) and part of them also unusually high Ce/Pb ratios (Fig. 4-25). Ba is an element preferably transferred from the subducting slab, and the same holds for 40 - 60% of the lead added to arc magma sources [Miller et al. 1994; Turner et al. 2000]. The observed low Ba/Th and high Ce/Pb ratios thus are both consistent with unusually low influx of slab derived fluids to the mantle source of the Potter dykes.

Further characteristics include low Ce/Th and high Ce/Yb ratios.

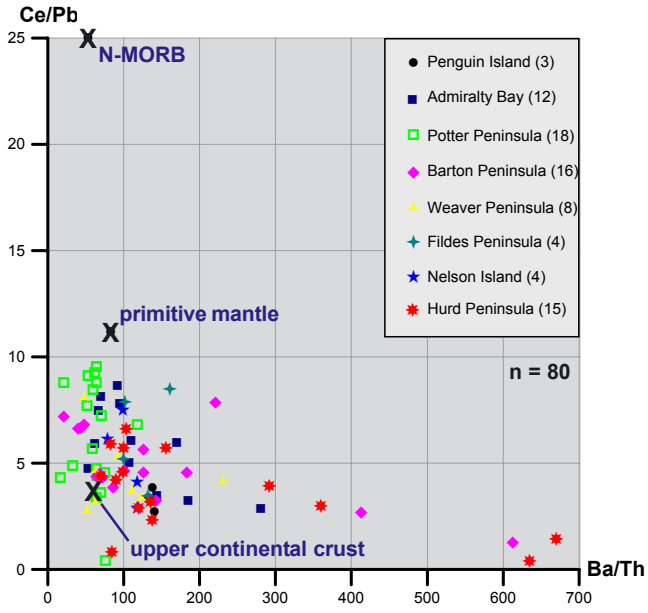

Fig. 4-25: Ba/Th vs. Ce/Pb ratio indicating unusually low fluid influx from the subducted slab to the magma source of Potter Peninsula. N-MORB values from Sun & McDonough [1989], primitive mantle values from McDonough & Sun [1995], upper continental crust values from Rudnick & Gao [2003].

A large spread in the Nb/Ta, Y/Ho and Zr/Hf ratios is evident (e.g. Fig. 4-14C). Whereas the vast majority of the South Shetland Islands dykes have Zr/Hf ratios lower than average N-MORB (36.1 according to Sun & McDonough [1989]), a subgroup of 10 dykes from Potter Peninsula shows higher ratios of 38 - 42 (Fig. 4-14C). However, this effect is not due to differentiation processes, as the Zr/Hf variation shown by the most acid dykes of the South Shetland Islands (27.3 - 37.9) is entirely bracketed by the variation of the most basic dykes (24.9 - 39.2). An influence of differentiation processes on the Zr/Hf ratio is therefore not evident from South Shetland Islands data. This holds also for Nb/Ta, and with limitations for Y/Ho (not shown).

Due to their similar chemical properties, the element pairs Nb/Ta, Zr/Hf and Y/Ho are each considered to be very difficult to fractionate during melting and differentiation processes even in highly evolved magmatic systems ("geochemical twins"). Therefore, Nb/Ta and Zr/Hf ratios observed in igneous rocks are assumed to reflect closely the respective mantle source [Bau 1996; Elliott 2003].

Judging from the unusual wide scatter shown by the dykes from Potter Peninsula as compared to the other areas (Fig. 4-14C), the magma source of these dykes might have been comparatively heterogeneous. It is unlikely, that this scatter has been induced by hydrothermal alteration, as all Potter dykes plot within

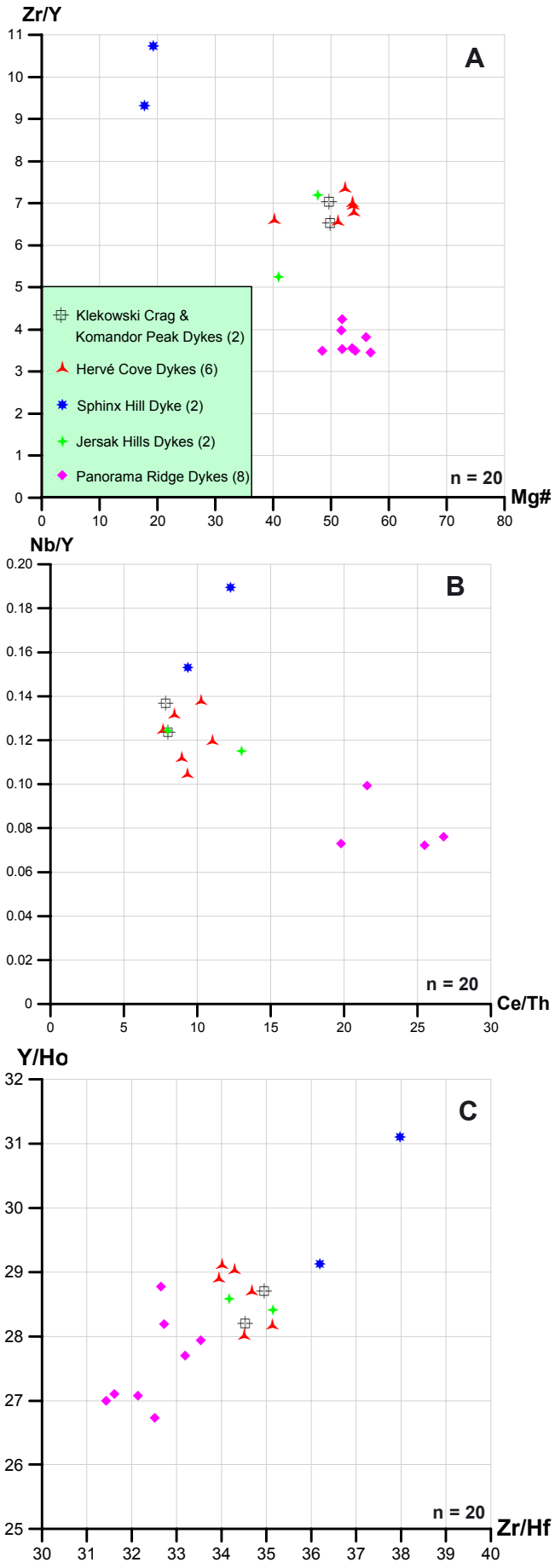

Fig. 4-26: Mg# and trace element ratio variation of the different dyke groups from Admiralty Bay (King George Island). Legend of (A) applies for all three diagrams.

the CHARAC field (Fig. 4-1), thus confirming charge and radius rather than aqueous fluid controlled behavior for these elements.

4.6.4 Admiralty Bay

Based on field work, Ar-Ar data and the stratigraphy set up by Birkenmajer [2003], the dykes sampled in Admiralty Bay could be subdivided into several groups. According to the obtained ages and the structural data, a tentative stratigraphic order was established (Fig. 2-40).

As prominently evident from Fig. 4-26, the geochemical characteristics of the Admiralty Bay dykes correspond closely to these groups. Following observations can be made:

(1) The relatively high Mg-numbers displayed by the Panorama Ridge dykes, the Hervé Cove dykes and the dykes at Klekowski Crag and Komandor Peak indicate comparatively short storage times in low level magma chambers (Fig. 4-26A). This holds especially for the Panorama Ridge dykes, comprising mostly basalts and few basaltic andesites. In contrast, the other groups consist predominantly of basaltic andesites and andesites, Sphinx Hill is rhyolitic in composition. Whereas the Panorama Ridge dykes are all tholeiites (not shown), all other groups are of calc-alkaline character.

(2) The Ce/Th ratios of the Panorama Ridge dykes (Fig. 4-26B) are the highest observed in the South Shetland Islands and might be an indication for low or no sediment input to their source. This assumption is supported by the considerably lower LREE fractionation of these dykes as compared to the other subgroups (not plotted, see also Fig. 4-9 and explanations there).

(3) The Sphinx Hill dyke displays the highest degree of alkalinity, as reflected by its high Nb/Y ratio (Fig. 4-26B) and also extremely high alkali content ($Na_2O + K_2O$ = 8.9 wt%).

(4) The correlated Zr/Hf and Y/Ho ratios give hints on a continuing development of the mantle source (Fig. 4-26C).

The Admiralty Bay dykes show extraordinary low Nb/Ta ratios (Fig. 4-14C), most extremely expressed in the Panorama Ridge dykes (approx. 6 times lower than primitive mantle, Fig. 4-15), at Nb abundances approx. 40% of N-MORB. Moreover, the Panorama Ridge dykes have the highest U/Th and Ba/Th ratios. This implicates an extremely depleted mantle source enriched in selected elements (e.g. Ba, U) by fluids derived from the subducted slab.

Following model is proposed here as indicated by the geochemical data:

(1) Intrusive activity started in Admiralty Bay fed by an extremely depleted mantle source only selectively enriched by slab derived fluids. Sediment input seems to have been negligible during that phase. The tholeiitic Panorama Ridge dykes, strongly enriched in Ba and U but extremely depleted in Nb, intruded during that phase. Apparently, storage times in shallow crustal magma chambers have been short.

(2) The mantle source then became gradually enriched, leading to lower Ce/Th, higher Nb/Ta and Th/Yb ratios, higher Nb abundances, rising LREE and REE fractionation at simultaneously rising REE abundances. Taken together, these changes indicate increasing input of sediments to the source region. In contrast to Hurd Peninsula (Fig. 4-18), obviously no crustal contamination took place, thus not masking deep level processes.

This change in mantle source composition is closely reflected by positively correlated Zr/Hf and Y/Ho ratios (Fig. 4-26C), displaying a well defined linear trend. For the reasons outlined above, it is unlikely that this trend is just a consequence of differentiation processes.

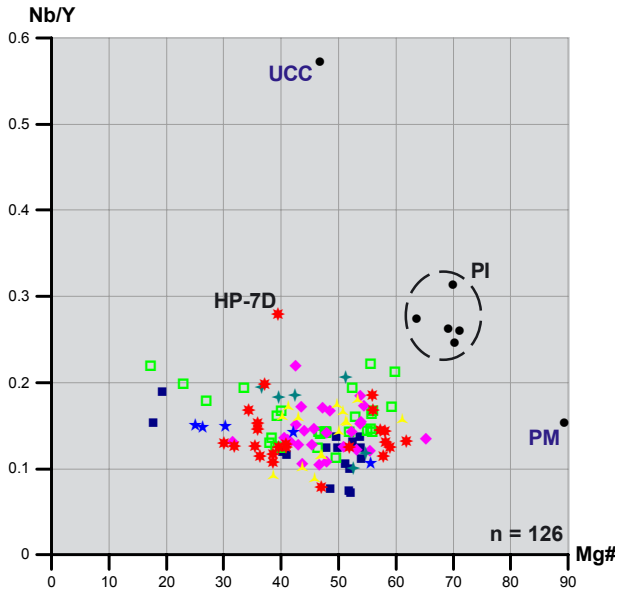

Fig. 4-27: Mg-number versus Nb/Y ratio to demonstrate key geochemical features of the Penguin Island (PI) dykes. Primitive mantle (PM) values from McDonough & Sun [1995], upper continental crust (UCC) values from Rudnick & Gao [2003]. Symbols as in Fig. 4-25.

4.6.5 Penguin Island

The most characteristic features of the radial dykes from Penguin Island are their high Mg-numbers (64 - 71, Fig. 4-27), along with high Cr (approx. 500 µg/g), Ni (approx. 200 µg/g) and TiO_2 (> 1.1 wt%) contents.

They are also characterized by Al_2O_3 contents lower than 16 wt% (Fig. 4-4), very low Th/Nb ratios (Fig. 4-9B) and U/Th ratios even lower than primitive mantle (Fig. 4-16A).

These dykes are clearly undifferentiated, primitive tholeiites. The rather high εNd (6.4) argues against crustal contamination and shallow level storage prior to emplacement.

However, together with HP-7D (Hurd Peninsula), these rocks show the highest Nb/Y ratios observed in the South Shetland Islands (Fig. 4-27), indicating a considerably higher degree of alkalinity than typical for the South Shetland Islands dykes. This may be explained by the geotectonic setting of Penguin Island related to the recent opening of the Bransfield Rift as a backarc-basin.

4.7 Conclusions from geochemical and isotopic data

(1) Alteration processes mainly affected the major element oxides, but not the immobile trace elements.

(2) The dykes from the South Shetland Islands comprise basaltic to rhyolitic rock types and belong to a subalkaline magmatic series. Tholeiites occur on Hurd Peninsula, Weaver Peninsula, Barton Peninsula and in Admiralty Bay, but the majority of the investigated dykes is of calc-alkaline affinity.

(3) Negative slopes in the REE distribution patterns indicate LREE enrichment caused by sediment addition to the mantle wedge, maybe also subsequent orthopyroxene fractionation. Residual garnet in the mantle source region is not indicated by the observed patterns.

(4) Trace element systematics (LREE enrichment, Th/Nb and Ce/Th ratios) indicate increasing sediment input into the subduction zone with time. The early intrusive events on Hurd Peninsula display the lowest sedimentary influence, whereas later phases here and further to the NE (King George Island) reflect an increased sedimentary component.

(5) Elevated Ba/Th ratios especially on Hurd and Barton Peninsula suggest addition of slab derived fluids to the magma source region.

(6) Nb/Ta, Zr/Hf and U/Th systematics indicate a heterogeneous, depleted mantle wedge beneath the South Shetland Islands volcanic arc, partly even more depleted than a normal MORB source.

(7) Continental crust contributed to arc magma genesis only on Hurd Peninsula.

(8) This crustal contamination, in combination with the ages obtained for the dykes, indicates that part of the dykes from Hurd Peninsula represent early phases of activity of a young immature arc. The melts ascended through a still relatively unstretched crust and were contaminated, probably during storage times in shallow level magma chambers. This assumption is supported by the tholeiitic affinity of these dykes, which is typical for young immature arcs but not for later, more mature stages. The degree of crustal contamination decreased with time. In contrast, the dykes from Nelson and King George Island correspond to a later phase of arc activity and do not show signs of crustal contamination. This is also true for the youngest dykes from Hurd Peninsula, confirming a parallel development in different parts of the South Shetland Islands.

(9) Low REE and Nb abundances, relatively low Nb/Ta ratios and very high εNd values give hints on exceptionally low degrees of sediment input and crustal contamination for the dykes from Weaver Peninsula. These rocks seem to represent mantle fractionates without marked contribution from other sources.

(10) The radial dykes on Penguin Island represent the most primitive rocks studied within this work. They are undifferentiated, primitive tholeiites characterized by high Mg-numbers and εNd values. Moreover they show the highest degree of alkalinity from all investigated areas, as reflected by their high Nb/Y ratios. This is probably due to their backarc-basin related geotectonic setting.

5. Geochronology

In order to assign a time frame to the pattern obtained by structural and geochemical data, Ar-Ar and K-Ar age determinations were carried out.
$^{40}Ar/^{39}Ar$ datings were performed on plagioclase separates of 19 dykes. Sample preparation was carried out by myself partly in Munich, partly at Stanford University (California, USA). The samples were then sent to Oregon State University for irradiation. Subsequently they were stored a couple of weeks at the reactor site, then shipped back to Stanford for the measurements. These were executed by Prof. Michael McWilliams in September 2004, applying the stepwise heating technique. The full datasets including all age spectra are stored as Excel files on the attached CD-ROM.
Additionally, K-Ar datings were performed on 7 whole rock samples. Only dykes from Hurd Peninsula were selected, because the complete relative time sequence known from this area allows full control over the quality of the K-Ar age data. Moreover, the oldest ages from Hurd Peninsula are especially interesting, because they yield constraints on the age of the host rocks (Miers Bluff Formation) and the deformation phases. Two samples (HP-1A and HP-23) scheduled for Ar-Ar dating were additionally K-Ar dated in order to double check the reliability of the K-Ar ages and possible alteration induced shifts of the obtained ages. Sample preparation was carried out in Munich and the samples then sent to the Institute of Nuclear Research of the Hungarian Academy of Sciences (ATOMKI) in Debrecen, Hungary. The age determinations were executed there by Dr. Zoltan Pecskay in May 2004.
The results are summarized in Table 5-1.

5.1 Sample selection and preparation

As in case of isotopic analyses, sample selection was based principally on the degree of alteration and whether the respective dyke forms part of a dyke system, i.e. if field relationships reveal relative ages or not. Preference was given to dykes with known relative ages in order to gain control on the quality of the obtained age data. In case of the mapped dyke systems on Hurd Peninsula, at least one dyke from each intrusive event was dated even though especially the first intrusive events are characterized by high degrees of alteration. The attempt was justified considering the comprehensive control on relative age relationships not provided in any of the other investigation areas. Despite single, barely interpretable measurements, the overall data yielded results in good agreement with field data.

5.1.1 Ar-Ar age determinations

Sample preparation technique

19 dykes were selected for Ar-Ar dating, comprising basalts to rhyolites (Table 5-1). Feldspar phenocrysts are ubiquitous in the SSI dykes, consisting of plagioclase in basic to intermediate rocks and plagioclase plus K-feldspar in acidic rocks (see Appendix II - Microprobe data).
Dykes containing plagioclase full of inclusions and adhering phases were avoided. Pyroxene or olivine fragments can contain significant amounts of trapped Ar that is not of atmospheric composition and can produce artificially old ages [McDougall & Harrison 1999]. This is also true for glass and fluid inclusions.
Feldspar contents in the analyzed dykes range from 10 to 50% at grainsizes between 0.5 and 8 mm and variable degrees of alteration. Major effort has been put into removal of alteration minerals and production of highly pure plagioclase separates.
First steps of preparation (sawing and crushing) are identical to the procedures described for geochemistry sample preparation (see the respective section). The use of the WIDIA-mill has been restricted to max. 10 sec. in order to (1) avoid punctual heating above the closure temperature of plagioclase (approx. 250° C) and (2) to avoid decreasing the grain size below a minimum of 5 µm. Very small grains suffer from the ^{39}Ar recoil effect, but this happens only with grains smaller than about 2-3 µm [McDougall & Harrison 1999].
In a next step, the samples were wet sieved in order to separate a 63-125 µm fraction. The fraction smaller than 63 µm was discarded, the fraction >125 µm dried overnight at 100° C, then run once more through the WIDIA-mill and subsequently sieved. For each sample, this procedure was repeated until a minimum of 150 g was achieved for the 63-125 µm whole rock fraction.
The samples then were spread upon clean paper and magnetic minerals removed in a first run using a handheld magnet. Subsequently, the mafic mineral

Sample/locality	latitude[1]	longitude[1]	strike	dip	thickness	lithology (microscopy / TAS-geochemistry)	AI	LOI (wt%)	Ar-Ar age (Ma)	MSWD (Ar-Ar)	K-Ar age (Ma)	K-Ar age (second run)
Penguin Island												
PI-4	451033	3113943	115	82NE	2.0 m	basalt / basalt	1	0.00	**8.8** ± 2.4	0.7		
Admiralty Bay												
KP-1	422579	3113331	164	89NE	5.5 m	basalt / bas. andesite	2-3	1.15	**45.41** ± 0.61	4.3		
SH-1	424421	3104230	115	90NE	min. 100 m	andesite / rhyolite	2-3	1.41	**47.09** ± 0.56	2.3		
AP-1	425284	3102865	72	90SE	70 m	basalt / bas. andesite	1-2	1.95	**54.0** ± 1.5	9.9		
Potter Peninsula												
PP-32B	412529	3097149	35	76SE	7.6 m	rhyolite / rhyolite	4	4.08	**45.7** ± 1.2	184		
PP-33	412546	3097200	140	60SW	70 cm	andesite / trachyandesite	4-5	5.76	**46.43** ± 0.56	1.6		
PP-11	414308	3098266	15	72W	4 m	andesite / andesite	2-3	3.05	**46.61** ± 0.37	5.8		
PP-31B	412514	3097131	110	71N	6.2 m	andesite / bas. Andesite	2-3	2.76	**46.98** ± 0.62	10.6		
PP-32C	412529	3097149	35	76SE	1.0 m	basalt / andesite	2	2.35	**47.19** ± 0.50	0.61		
Weaver Peninsula												
WP-20B	407062	3101977	3	71W	~50 cm	andesite / basalt	3-4	6.75	**54.6** ± 3.8	4.4		
Fildes Peninsula												
FP-8	401204	3103845	88	66S	~8 m	andesite / dacite	1-2	3.48	**57.4** ± 2.1	1.5		
Hurd Peninsula												
HP-23	635368	3051794	135	79SW	~6 m	andesite / andesite	2-3	3.35	**37.16** ± 0.92	10.5	**39.99** ± 1.74	
HP-1A	635142	3051777	54	78SE	5.5 m	bas. andesite / bas. andesite	2-3	2.96	**39.8** ± 7.3	8.6	**56.38** ± 3.27	
HP-10B	635315	3051673	64	90S	8 m	dacite / ---	1-2	---			**43.32** ± 1.73	
HP-17	635287	3051758	141	74SW	90 cm	bas. andesite / trachybasalt	2-3	4.51			**44.52** ± 1.81	
HP-7G	635503	3052309	85	73S	3 m	andesite / trachyandesite	2-3	4.41			**47.43** ± 2.13	
HP-10A	635315	3051673	149	90NE	90 cm	bas. andesite / bas. trachyandesite	2-3	2.82	**48.3** ± 1.5	1.7		
HP-7D	635539	3052276	138	74SW	55 cm	dacite / trachyandesite	3-4	5.43	**53** ± 16	5.3		
HP-26	635246	3051788	60	59SE	min. 3 m	dacite / rhyolite	2-3	2.97	**55-60**	n.d.		
HP-7J	635517	3052303	83	63S	~2.5 m	andesite / andesite	3	3.32	**55-65**	n.d.		
HP-19	635293	3051812	26	55E	~1 m	andesite / tephrite	4	7.79			**56.45** ± 2.28	
HP-7A	635548	3052291	63	70NW	30 cm	dacite / andesite	2-3	6.96	**64** ± 13	18		
HP-33	635363	3051694	44	49NW	2.0 m	dacite / dacite	3-4	4.48	**60-90**	n.d.		
HP-15	635337	3051807	21	78SE	1.6 m	dacite / dacite	3	4.03			**80.12** ± 3.12	**82.73** ± 3.28

[1]UTM, WGS 84

Caution: ages in red denote samples which did not yield formal plateaus and are estimated ages as deduced from age spectra

AI = Alteration Index (microscope)
1 absolutely fresh, no secondary minerals
2 slight signs of alteration; scarce secondary minerals in groundmass or along fractures/rims of phenocrysts
3 medium alteration; groundmass enriched in secondary minerals; many phenocrysts show partial alteration
4 heavy alteration; most phenocrysts at least partly altered
5 basically no primary minerals left; rock completely altered

K-Ar age determinations:
Sample preparation: Stefan Kraus, Univ. Munich, Germany
Data produced by: Zoltan Pecskay, Univ. Debrecen, Hungary
Technique: K-Ar whole rock analysis

Ar-Ar age determinations:
Sample preparation: Stefan Kraus, Univ. Munich, Germany
Data produced by: Michael McWilliams, Stanford University, California, USA
Technique: Ar-Ar stepwise heating of plagioclase mineral separates

Table 5-1: Summary of the dykes selected for Ar-Ar and K-Ar age determinations and relevant information on the samples and the used technique. The full Ar-Ar datasets are stored as Excel files on the attached CD-ROM.

fraction was removed using a Frantz magnetic separator. At least two runs per sample were necessary to achieve the wanted pureness (< 3% mafic minerals), in some cases three or even four runs were required. The fractions were controlled for quality using a binocular.

Subsequent laboratory work aimed on removing alteration minerals. Especially calcite *must* be removed because it produces CO_2 that can flood the mass spectrometer and can cause error at best and damage at worst. However, HCl *must not* be used to do so, because (1) a HCl residue will remain in

the sample and the mass of $H^{35}Cl$ is almost the same as ^{36}Ar, which would cause interference; and (2) ^{35}Cl would combine with H in the mass spectrometer producing $H^{35}Cl$, causing the same problem [McDougall & Harrison 1999].

Instead, dilute nitric acid (2.5 N) in ultrasound has been used to remove secondary minerals. The strongest altered samples (e.g. HP-7D) contained also pyrite, the feldspar fractions of such samples were treated with 6N nitric acid. It could be observed that 6N nitric acid reliably removes the pyrite but does not damage the feldspar crystals. As a final step of laboratory work, the samples were rinsed repeatedly using distilled water in ultrasound to remove all traces of chemicals. Heavy liquids, usually applied to remove further unwanted mineral phases, were not necessary to achieve the required pureness.

In a last step of preparation, each separate was controlled under the binocular and remaining unwanted grains (mafic components, discolored plagioclase) removed by handpicking. The final separates consisted of better than 99% pure plagioclase at a minimum quantity of 1 g.

The $^{40}Ar/^{39}Ar$ stepwise heating technique

What follows is a short summary of the method; a detailed description of Ar-Ar dating techniques is presented in McDougall & Harrison [1999].

The sample to be dated is irradiated in the core of a nuclear reactor to transform a fraction of the ^{39}K to ^{39}Ar by an (n,p) reaction with fast neutrons. A mineral standard of known K/Ar age is irradiated together with the sample as a neutron fluence monitor.

Following irradiation, the sample is stepwise heated in ultrahigh vacuum (UHV), starting at temperatures well below fusion. The argon isotopes extracted in each heating step are analyzed using a sector mass spectrometer. The abundances of ^{40}Ar, ^{39}Ar, ^{37}Ar, ^{36}Ar, and sometimes also ^{38}Ar are measured and the $^{40}Ar^*/^{39}Ar_K$ ratio is determined. $^{40}Ar^*$ is the radiogenic argon and $^{39}Ar_K$ is the ^{39}Ar produced from ^{39}K during irradiation in the reactor. The $^{40}Ar^*/^{39}Ar_K$ ratio is then corrected for interfering isotopes produced from Ca and K using the measured ^{37}Ar and ^{36}Ar, the latter to correct for the presence of nonradiogenic ^{40}Ar.

The determined $^{40}Ar^*/^{39}Ar_K$ ratio is proportional to the $^{40}Ar^*/^{40}K$ in the sample, because the $^{39}Ar_K$ depends on the amount of ^{39}K in the sample. As $^{39}K/^{40}K$ is basically constant in nature, the $^{40}Ar^*/^{39}Ar_K$ ratio therefore is proportional to the age of the sample, which is calculated by comparison with the $^{40}Ar^*/^{39}Ar_K$ ratio of the fluence monitor standard.

In the stepwise heating technique [Merrihue & Turner 1966], argon isotopes extracted at progressively higher temperature steps yield a series of apparent ages. In the ideal case where the sample has remained a closed system, each gas heating step would yield indistinguishable $^{40}Ar^*/^{39}Ar_K$ ratios and hence indistinguishable apparent ages. In this case, a plot of the apparent age of each step versus the cumulative fraction of ^{39}Ar released will yield a flat array termed a plateau.

In contrast, a sample that experienced alteration or was subjected to metamorphism may lose part or all of its radiogenic argon after initial crystallization. In other cases, K-poor minerals incorporate radiogenic argon derived e.g. from neighboring minerals into the outer parts of the crystal, producing an excess of ^{40}Ar.

However, Ar loss as well as excess Ar will not be evenly distributed in such samples, and therefore the $^{40}Ar^*/^{39}Ar_K$ ratios measured on the successively released gas fractions will vary. This can result in an age spectrum that is not flat (Fig. 5-3, 5-5, 5-6).

The measurements must finally be corrected for any contaminating atmospheric argon contained in the sample. After excluding other known interfering sources, it is assumed that all of the ^{36}Ar is of atmospheric origin and an atmospheric $^{40}Ar/^{36}Ar$ ratio of 295.5 [Nier 1950] is used for correction.

Plotting the results on an isochron diagram offers an independent control of assumptions concerning the isotopic composition of the trapped argon component. Usually a model assumption is made that the trapped argon is of atmospheric composition. The initial $^{40}Ar/^{36}Ar$ values quoted in all isochron diagrams of this chapter are a measure for the difference from the normally expected atmospheric value.

Plotting $^{39}Ar/^{40}Ar$ vs. $^{36}Ar/^{40}Ar$ (thus using ^{40}Ar as reference isotope) precludes problems such as highly correlated errors and misleading linear correlations that occur if using ^{36}Ar as denominator. This approach has been used in the diagrams presented here and results in a closed array of data with a negative slope. The age is given by the intercept of the isochron with the x-axis, and the trapped argon composition by the y intercept. The digits quoted next to the error ellipses indicate the temperature at which the respective data was measured.

5.1.2 K-Ar age determinations

A detailed description of the K-Ar dating method is given e.g. by DICKIN [1995] and FAURE [1986].

Sample preparation was carried out in Munich, producing 50-100 g whole rock fraction (125-355 µm) of each sample. Concerning sawing, crushing, milling and wet sieving, the same procedures were applied as described above for Ar-Ar sample preparation.

Subsequently, each sample was rinsed using distilled water in ultrasound until the suspension remained clear. The samples were then sent to Hungary. Further chemical treatment to remove secondary minerals and subsequent age determinations were carried out there by Dr. Zoltan Pecskay. The analytical methods as applied in Debrecen are supplemented in Appendix IV (p. A-18) as provided by Dr. Pecskay. Only the final age data were submitted via eMail, therefore no (isochron) diagrams are available for the K-Ar ages.

5.2 Results

The coordination of the isotope derived ages to the geological time scale follows the International Stratigraphic Chart published by the IUGS International Commission on Stratigraphy (ICS, website: www.stratigraphy.org).

The obtained age data in general confirm the relative time sequence as deduced from field relationships. However, on Hurd Peninsula some datings did not yield unequivocal results, most probably due to the advanced state of alteration of these dykes and/or excess argon. The results obtained by K-Ar dating generally correlate well with the ages obtained by the Ar-Ar method (Table 5-1).

An earliest Danian age is most probable for incipient dyke intrusion on Hurd Peninsula (Livingston Island). Dykes from this first phase cluster around 65-60 Ma. Two subsequent intrusive phases are expressed throughout the South Shetland Islands. The first of them took place during Thanetian and Ypresian (approx. 57-53 Ma) and is expressed on Hurd Peninsula, Fildes Peninsula, Weaver Peninsula and in Admiralty Bay. A second phase marks the main phase of dyke intrusion in the South Shetland Islands, is restricted to 48-43 Ma (Lutetian) and concentrates strongly at 47-45 Ma (Fig. 5-1). A last and final phase is expressed only on Hurd Peninsula and comprises Bartonian and earliest Priabonian dykes (40-37 Ma). A summary of the deduced main phases is given in Table 5-2.

5.2.1 Hurd Peninsula (Livingston Island)

Results obtained during this work

Intrusive activity on Hurd Peninsula started earlier and lasted longer than on Nelson and King George Island.

A maximum age for the dykes on Hurd Peninsula is set by the Campanian nannofossils determined in the metasedimentary host rocks [PIMPIREV et al. 2005; STOYKOVA et al. 2002]. For this reason, the earliest Campanian K-Ar age obtained for dyke HP-15 (approx. 81 Ma, Table 5-1 & 5-3) is most probably artificially old and might be the consequence of excess argon.

The sequence of intrusive events on Hurd Peninsula, as deduced from field relationships, is confirmed within error by the age determinations (Table 5-3). Most conflicting results have been obtained for the first three intrusive events. These are also the ones most affected by alteration.

The true age of event I (HP-7D) is probably older than 53 Ma (Fig. 5-2), intrusion around the Cretaceous/Paleogene boundary seems geologically more plausible and lies within the error. This assumption is supported by the higher age given by the age spectrum of HP-7D (58.2 ± 2.2 Ma, see supplemented CD-ROM). Alteration or later reheating (perhaps due

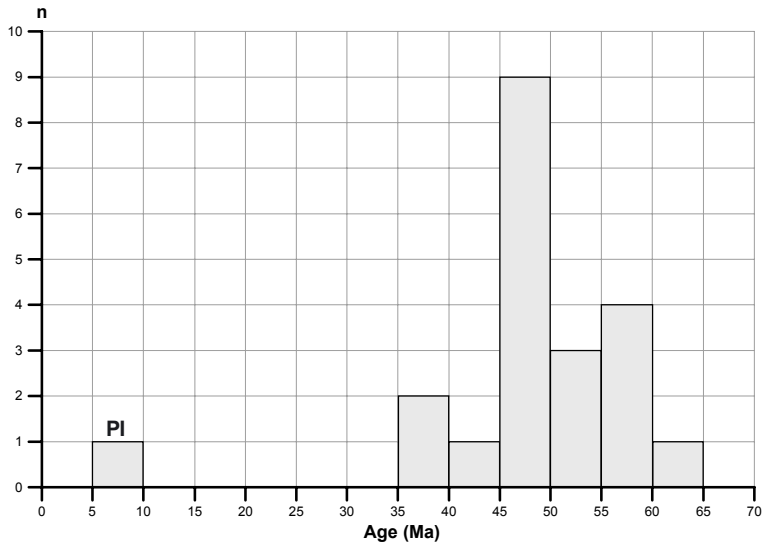

Fig. 5-1: Histogram displaying the relationship between frequency and obtained ages. Pl: Penguin Island (1 dyke). All other ages correspond to dykes from King George and Livingston Island (18 Ar-Ar and 4 K-Ar ages). The two highly uncertain Cretaceous K-Ar ages have been excluded from this histogram (see text).

to subsequent nearby intrusive events) might have led to argon loss in this case.

Ages for event II spread from approx. 65 to 56 Ma (Fig. 5-3 & 5-4), not considering the highly uncertain Campanian age of HP-15 (see above). The age spectrum of HP-33 (Fig. 5-3) is basically uninterpretable, a probable intrusion time between 90 and 60 Ma might be assumed. It is unlikely that this spectrum is the result of excess argon. In that case it would be characterized by high initial ages, decreasing to a minimum and subsequently rising to high ages again during the last stages of gas release, forming a so-called "saddle-shaped" spectrum [McDougall & Harrison 1999]. This is clearly not the case (Fig. 5-3), instead it is more likely that the feldspar was not completely free of inclusions (e.g. pyroxene or fluid) which contained significant amounts of trapped argon of non-atmospheric composition. Such inclusions can produce artificially old ages [McDougall & Harrison 1999].

Considerable overlap exists with event III, which yielded two estimated Ar-Ar plateau ages around 60 Ma (Fig. 5-5 & 5-6) and an unexpectedly young Lutetian K-Ar age (43.32 Ma). The data at least seem to confirm that event III started later than event II.

Age data are better for event IV and indicate intrusion of the respective dykes during the Lutetian (Fig. 5-7; Table 5-3).

A large spread in possible ages can be observed for event V (Table 5-3). As outlined in chapter 2 (Geology and tectonics), HP-1A represents a dyke cutting dozens of other dykes over a length of more than one km. There is no doubt concerning its relative age. Moreover, event V is represented by only two dykes (HP-1A and HP-7G) in the whole area and therefore interpreted as a single, short-lived magma pulse rather than a long lasting event. Within error, the ages obtained for the two dykes are identical. Assuming a more or less contemporaneous intrusion, the data suggest emplacement between 47 and 45 Ma. However, a younger (Bartonian) age of HP-1A seems more plausible in the light of geochemical and isotopic data (e.g. Fig. 4-20), though excluding contemporaneous intrusion with dyke HP-7G.

There is less debate about the age of event VI (HP-23). The Ar-Ar and K-Ar method yielded well correlating ages of 37.16 and 39.99 Ma, respectively (Fig. 5-9; Table 5-1). Within error, these two ages are almost identical and prove HP-23 not only to reflect the last intrusive activity within the investigation area on Hurd Peninsula, but also to be the youngest of all investigated dykes (with exception of Penguin Island, see below).

Main phase	Time interval (Ma)	Geographic area
IV	40-37	Hurd Peninsula (Livingston Island)
III	48-43	throughout the South Shetland Islands, culminating at 47-45 Ma
II	57-53	Hurd, Fildes, Weaver Peninsula, Admiralty Bay
I	65-60	Hurd Peninsula (Livingston Island)

Table 5-2: Summary of the main phases of dyke intrusion in the working areas on the South Shetland Islands.

Comparison with results from former works

Two important works have been carried out on Hurd Peninsula dealing with the dyke systems cropping out there [Willan & Kelley 1999; Zheng et al. 2003]. Both works included Ar-Ar and K-Ar age determinations. However, the interpretation of these data was in both cases based on the then widely believed Triassic age of the host rocks (the sedimentary Miers Bluff Formation, MBF). In the meanwhile, the MBF proved to be not older than Campanian [Pimpirev et al. 2005; Stoykova et al. 2002].

Magmatic phase (as of Table 5-2)	Intrusive event (Hurd P.)	obtained ages (Ma)	dated dyke (incl. method)
IV	VI	37.16 ± 0.92 39.99 ± 1.74	HP-23 (Ar-Ar) HP-23 (K-Ar)
IV	V	39.8 ± 7.3 56.38 ± 3.27 47.43 ± 2.13	HP-1A (Ar-Ar) HP-1A (K-Ar) HP-7G (K-Ar)
III	IV	44.52 ± 1.81 48.3 ± 1.5	HP-17 (K-Ar) HP-10A (Ar-Ar)
II, III	III	43.32 ± 1.73 60-55 (est.) 65-55 (est.)	HP-10B (K-Ar) HP-26 (Ar-Ar) HP-7J (Ar-Ar)
I, II	II	56.45 ± 2.28 64 ± 13 80.12 ± 3.12 90-60 (est.)	HP-19 (K-Ar) HP-7A (Ar-Ar) HP-15 (K-Ar) HP-33 (Ar-Ar)
I	I	53 ± 16	HP-7D (Ar-Ar)

Table 5-3: Summary of age determinations from dykes on Hurd Peninsula (Livingston Island). The ages labeled "est." did not yield formal plateaus and are estimated probable ages as deduced from the respective age spectrum. Subdivision of intrusive events according to field relationships (Fig. 2-8, 2-9).

This new age for the host rocks also sheds new light on the evaluation of the dyke ages published by Willan & Kelley [1999] and Zheng et al. [2003].

Willan & Kelley [1999] distinguished eight groups of mafic dykes and related high-level stocks ranging in age between mid Cretaceous and Oligocene (~108 - 29 Ma). Though all of these datings (Ar-Ar as well as K-Ar) were carried out on plagioclase separates and not on whole rock powder, it is conspicuous that only two dykes and one stock yielded Cretaceous ages (108.0 ± 5.0, 66.8 ± 2.0 and 73.8 ± 13.0 Ma, respectively). Of these, the 108 Ma age has been considered problematic by the authors themselves, stating an Ar-Ar age of 62 ± 1.34 Ma for muscovite from the same rock. The 66.8 Ma age obtained for the second dyke and the very imprecise 73.8 Ma age yielded by the stock do both within errors not exclude Danian ages for these rocks. All other age determinations gave Cenozoic ages which are in good agreement with the data obtained during this work. This includes a peak in intrusive activity between 51 and 45 Ma, which has been confirmed and specified within this work as 47-45 Ma.

Zheng et al. [2003] published fifteen K-Ar and three Ar-Ar ages in the range of 79-31 Ma for dykes from Hurd Peninsula. Their results are especially interesting because these authors concentrated on the same investigation area located in the NW of Hurd Peninsula around the Bulgarian Antarctic Base, as this work. However, their K-Ar as well as their Ar-Ar ages were determined from whole rock powder and not from mineral separates, challenging the reliability of these data in the light of the strong alteration evident throughout Hurd Peninsula. These authors determined four intrusive events between 79 and 31 Ma. However, as in case of the datings performed by Willan & Kelley [1999], Cretaceous ages are the exception. Only one dyke yielded a Cretaceous K-Ar age (78.8 ± 1.8 Ma). Two peaks of intrusive activity stated by these authors (56-52 and 45-42 Ma, respectively) correspond well with the third and fourth intrusive event determined in the present work. The youngest ages obtained by Zheng et al. [2003] (38-31 Ma) reflect possibly the same event marking the final phase of intrusive activity as the 37.16 Ma age obtained for event VI (HP-23) during this work.

However, the cited authors emphasize the problematic degree of alteration of the dykes from Hurd Peninsula. Judged especially under the light of the new, Campanian nannofossil ages evident for the host rocks (MBF), I conclude that these Cretaceous ages might be due to excess argon and that dyke intrusion on Hurd Peninsula did not start before Danian.

5.2.2 King George Island

In contrast to Hurd Peninsula (Livingston Island), the host rocks on King George Island consist predominantly of volcanic rocks related to the magmatic arc. Numerous Cretaceous and above all Cenozoic age determinations exist for lava flows, plugs and other magmatic rocks, mainly carried out using the Rb-Sr and the whole rock K-Ar technique [e.g. Shiling et al. 1996; Smellie et al. 1984; Watts 1982]. However, the majority of the ages obtained from King George Island are in the range 60-40 Ma and many works failed to confirm the existence of pre-Cenozoic ages [e.g. Smellie et al. 1984]. This is in good agreement to the dyke ages presented here, which are also restricted to the Cenozoic (Paleocene and Eocene). Summarizing, pre-Cenozoic intrusive activity on King George Island cannot be excluded but is also not confirmed at least for the areas investigated within this project.

Dykes belonging to magmatic phase II (Table 5-2) intruded on Fildes Peninsula (Thanetian, Fig. 5-10), Weaver Peninsula (Ypresian, Fig. 5-11) and in Admiralty Bay (Ypresian, Fig. 5-17). This phase seems to be rather weakly expressed, comprising only three of the dykes studied on King George Island. The prominent, huge Agat Point dyke (AP-1, Fig. 2-37, 2-39, 5-17) in Admiralty Bay is among them. The most intense intrusive activity on King George Island can be attributed to phase III (Table 5-2), which is entirely restricted to the Lutetian (Fig. 5-12, 5-13, 5-14, 5-15, 5-16, 5-18, 5-19). The majority of these dykes intruded between 47 and 45 Ma (Table 5-1, Fig. 5-1), indicating a single, intense event during that time. No dyke intrusions younger than 45 Ma can be stated for the areas investigated on King George Island.

5.2.3 Penguin Island

As already mentioned in chapter 2.4, the unexpected Tortonian age (Fig. 5-20) obtained for one of the radial dykes on Penguin Island sheds some new light on the development of this small island. Hitherto believed to be the product of volcanism related to backarc-spreading in the Bransfield Strait, Penguin Island traditionally has been assigned a Pleistocene / Holocene age, mainly based on lichenometric dating and stratigraphical constraints [Birkenmajer

2001; González-Ferrán & Katsui 1970; Weaver et al. 1979].
However, the newly obtained Tortonian age is not without uncertainties. Only about 40% of the ^{39}Ar define this age and during measurement, the radiogenic argon values never got larger than about 20-25% over the range of interest, which explains the relatively poor precision. The possibility cannot be completely excluded that there was anything else in the separate besides feldspar that might have contributed nonradiogenic ^{40}Ar.
Formation of the Bransfield Rift is widely believed to have started around 4 Ma or later [Barker et al. 1991; Barker & Austin 1994; Barker & Austin 1998], conflicting clearly with a Tortonian age for Penguin Island. However, there is still debate about the age of initial rifting in Bransfield Strait, and other works postulate incipient rifting for as early as Oligocene (Chattian), continuing at a slow rate and with gaps in geological evidence through to recent times [Birkenmajer 1992a, 1993].
A Tortonian age for activity on Penguin Island as indicated by the here presented data certainly claims more debate about timescales for the development of the Bransfield Rift and the associated volcanoes. Incipient rifting and related subsequent volcanism at 4 Ma is at least contradictory to a Tortonian age of the Penguin Island dyke.

5.2.4 Constraints on the deformation history

As outlined above, the new findings of Campanian nannofossils in the sedimentary host rocks [Pimpirev et al. 2005; Stoykova et al. 2002] set a maximum age for the investigated dykes.
The new Ar-Ar and K-Ar age data presented here for the dykes cutting the metasedimentary sequence include unquestionable Paleocene and Eocene ages and some uncertain ages. From these, two (HP-7J and HP-26) are most probably also of Paleocene age (Fig. 5-5 & 5-6). Only two dykes yielded highly questionable older ages. One of them shows a basically uninterpretable age spectrum (HP-33, Fig. 5-3), which however does not exclude a Lowest Paleocene (Danian) age for this dyke. The other dyke (HP-15) was K-Ar whole rock dated and excess argon is a possible explanation for the apparent Campanian age.
From this point of view, I assume that dyke intrusion on Hurd Peninsula most probably was restricted to the Cenozoic (Paleocene and Eocene), starting shortly after the Cretaceous/Paleogene boundary.

Given the Campanian nannofossil age, only a short time gap of certainly not more than 5-10 Ma (predominantly Maastrichtian) is left for the deformation of the host rocks. At first sight this seems unlikely short, but heed has to be payed to the fact that the metasedimentary sequences comprising the host rocks represent a fossil accretionary wedge belonging to a subduction zone environment. In such a geotectonic setting, very fast burying and short deformation times seem more probable. Thus, the obtained dyke ages are not considered contradictory to the nannofossil evidence.

5.2.5 Ar-Ar as compared to K-Ar data

The alteration patterns observed under the microscope indicate an autometasomatic origin of the secondary minerals for most of the investigated dykes. If this is true, alteration should have occurred immediately after emplacement of the dykes, therefore being of the same age. Thus, alteration should not affect the results of K-Ar WR dating.
The K-Ar datings presented here have been executed in order to test this hypothesis and to obtain additional age data.
Part of the K-Ar data are in good agreement with the more reliable Ar-Ar data. The intense intrusive phase during the Lutetian is well reflected also by the K-Ar ages (Table 5-1).
A good constraint on the reliability of the age data is given by the relative age relationships observed in the field. Whereas the Ar-Ar ages correlate well with the relative time sequence (within error), this holds only with limitations for the K-Ar data. The ages obtained by this method must be regarded as questionable in three cases:
(1) The above discussed unlikely Campanian age (80.12 ± 3.12 Ma) obtained for dyke HP-15.
(2) The Thanetian age (56.38 ± 3.27 Ma) obtained for HP-1A (Table 5-1). This dyke was also Ar-Ar dated, and the Bartonian age (39.8 ± 7.3 Ma) obtained by this method is geologically much more plausible, as outlined above.
(3) For dyke HP-10B, a Lutetian K-Ar age (43.32 ± 1.73 Ma) was obtained (Table 5-1). This age is contradicted by two facts: (1) As evident from field relationships, HP-10B belongs to the third intrusive event on Hurd Peninsula (Fig. 2-8). Two other dykes from this group have been Ar-Ar dated at 55-60 Ma (HP-26 & HP-7J), indicating an older Thanetian age for this event. (2) Dyke

HP-10B is crossed by dyke HP-10A (Fig. 2-8 & 2-9), and for the latter a reliable Ar-Ar age of 48.3 ± 1.5 Ma has been obtained. Thus, the K-Ar age yielded by dyke HP-10B is probably too young and may be the result of Ar loss during alteration processes.

I conclude, that the K-Ar ages correlate well with the Ar-Ar data only in part (e.g. HP-23, Table 5-1), but that they generally should be interpreted with caution and only as giving a rough time frame. The true errors of the K-Ar ages are probably much larger than indicated by the data.

Reasons like Ar loss in some cases and excess Ar in others are probably responsible for the high uncertainties.

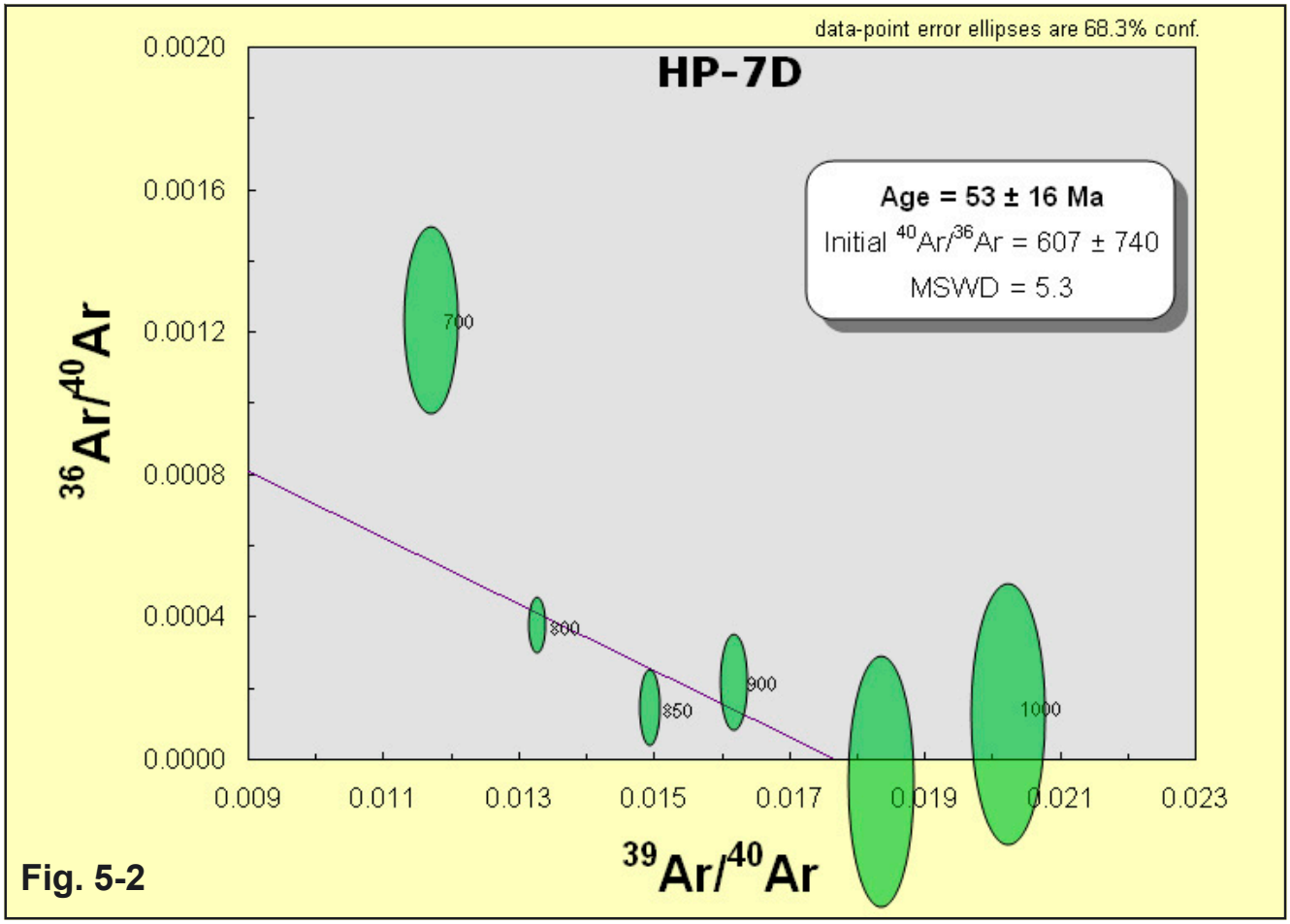

Fig. 5-2

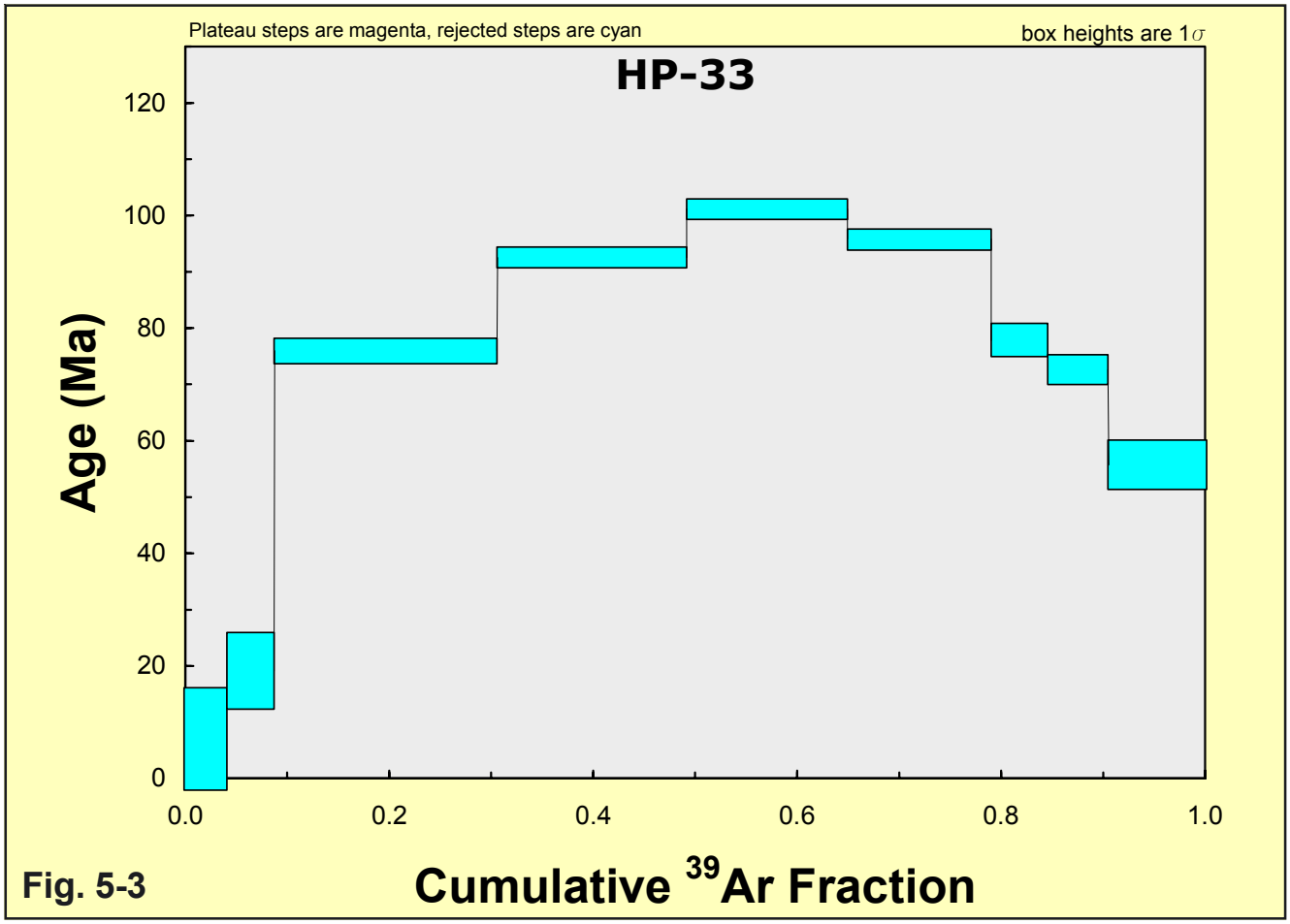
Plateau steps are magenta, rejected steps are cyan
box heights are 1σ
HP-33
Age (Ma)
120
100
80
60
40
20
0
0.0
0.2
0.4
0.6
0.8
1.0
Cumulative 39Ar Fraction

Fig. 5-3

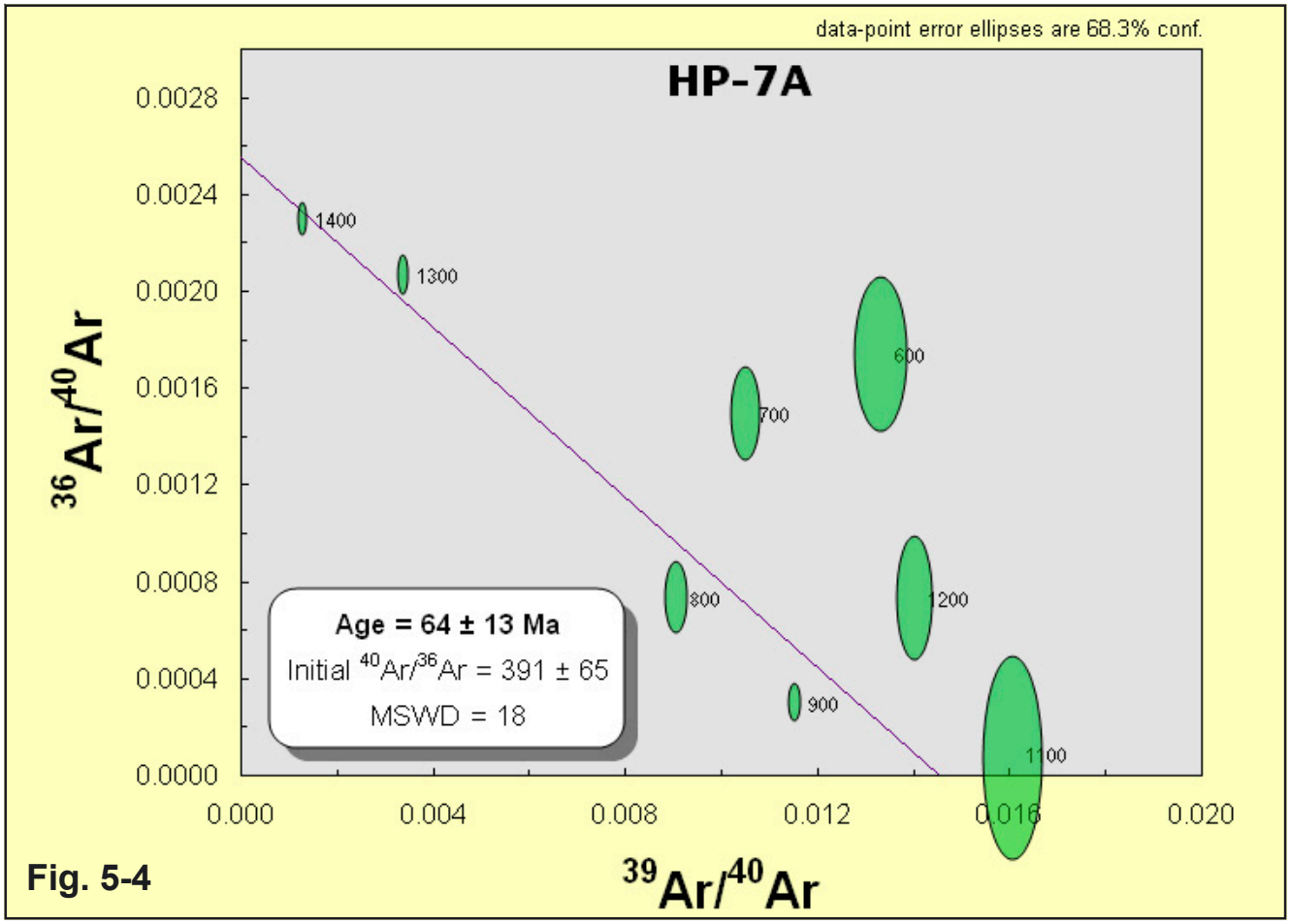
data-point error ellipses are 68.3% conf.
HP-7A
36Ar/40Ar
0.0028
0.0024
0.0020
0.0016
0.0012
0.0008
0.0004
0.0000
0.000
0.004
0.008
0.012
0.016
0.020
1400
1300
700
600
800
1200
900
1100
Age = 64 ± 13 Ma
Initial 40Ar/36Ar = 391 ± 65
MSWD = 18
39Ar/40Ar

Fig. 5-4

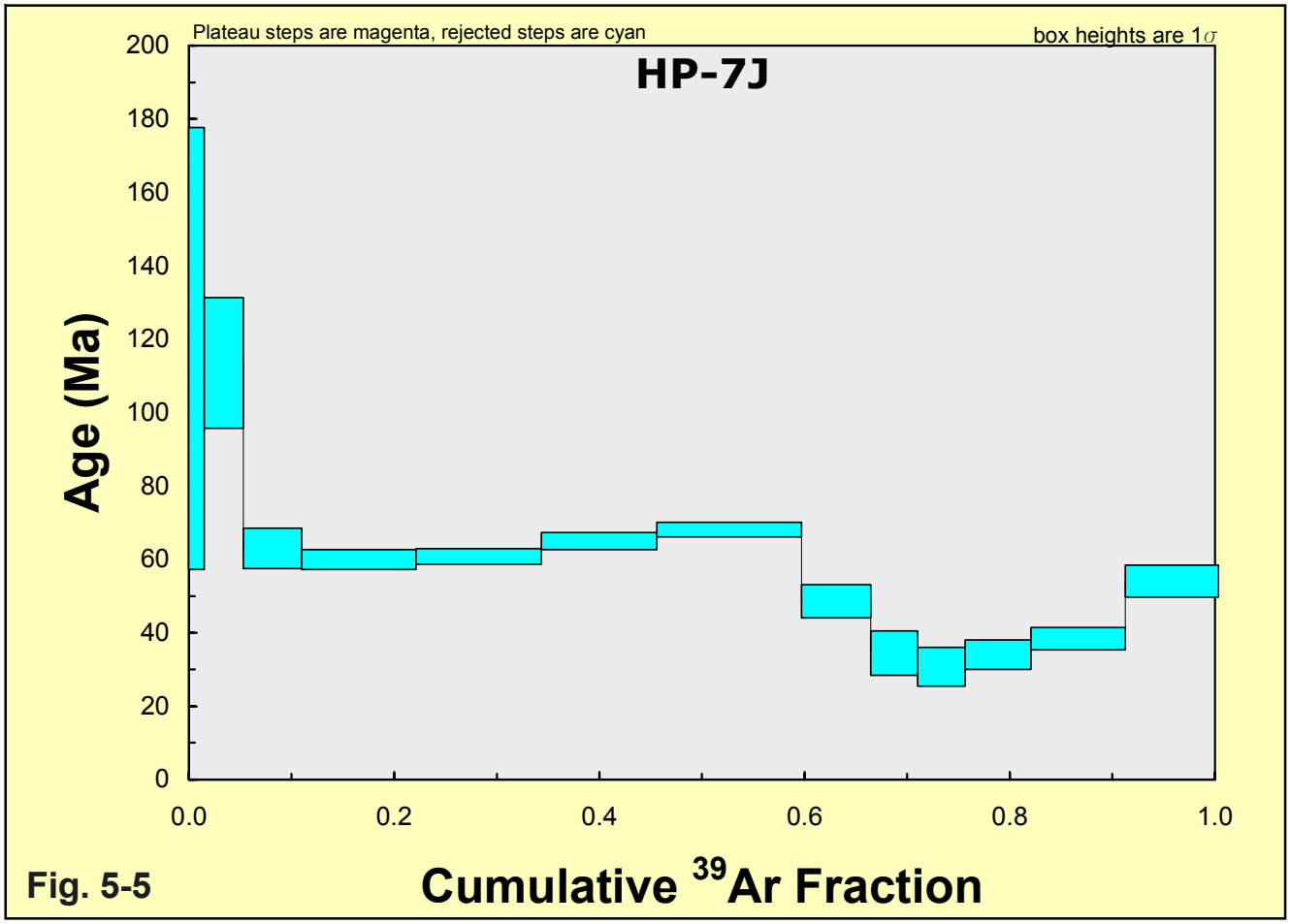
Plateau steps are magenta, rejected steps are cyan
box heights are 1σ
HP-7J
Age (Ma)
200
180
160
140
120
100
80
60
40
20
0
0.0
0.2
0.4
0.6
0.8
1.0
Cumulative 39Ar Fraction

Fig. 5-5

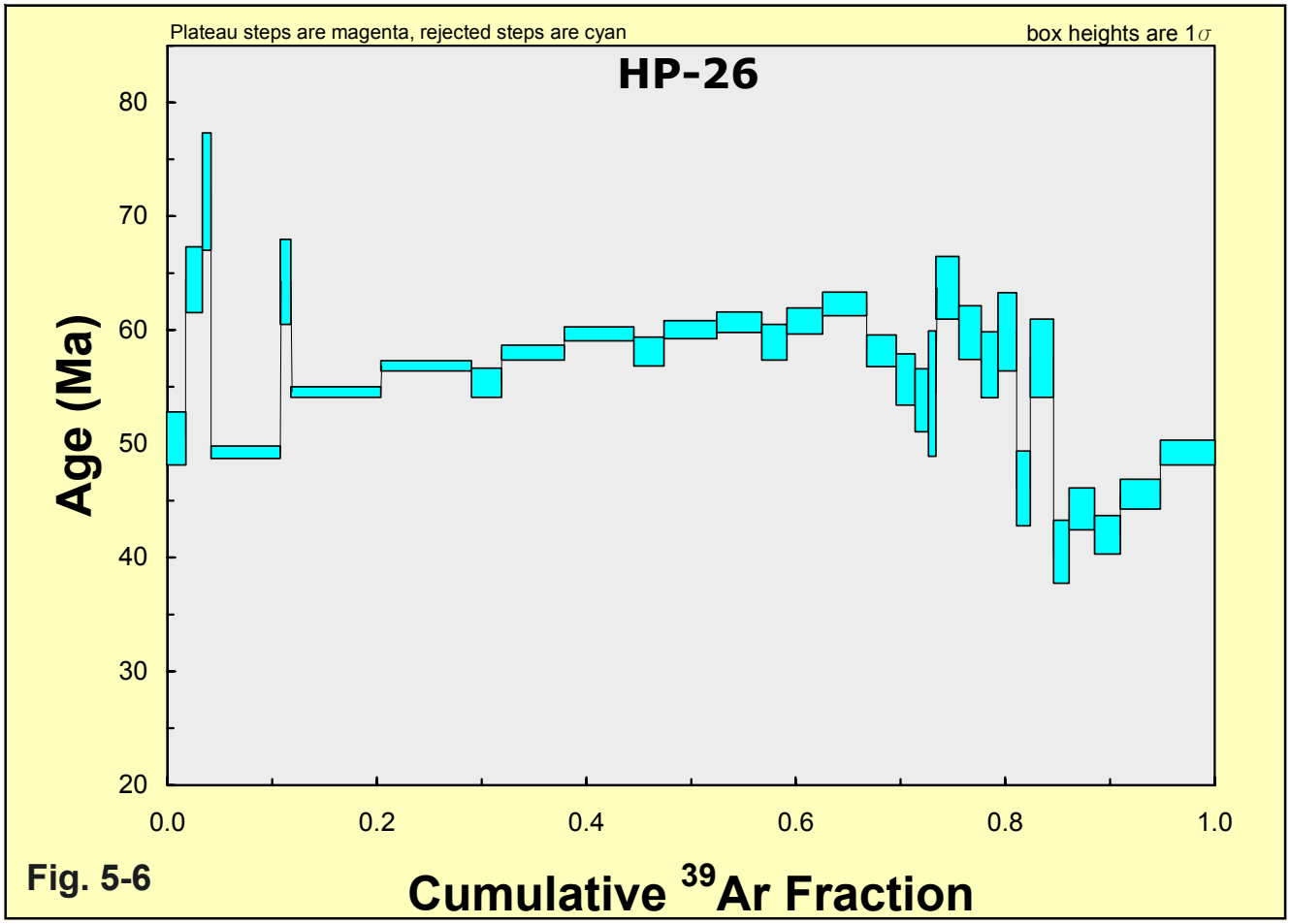
Plateau steps are magenta, rejected steps are cyan
box heights are 1σ
HP-26
Age (Ma)
80
70
60
50
40
30
20
0.0
0.2
0.4
0.6
0.8
1.0
Cumulative 39Ar Fraction

Fig. 5-6

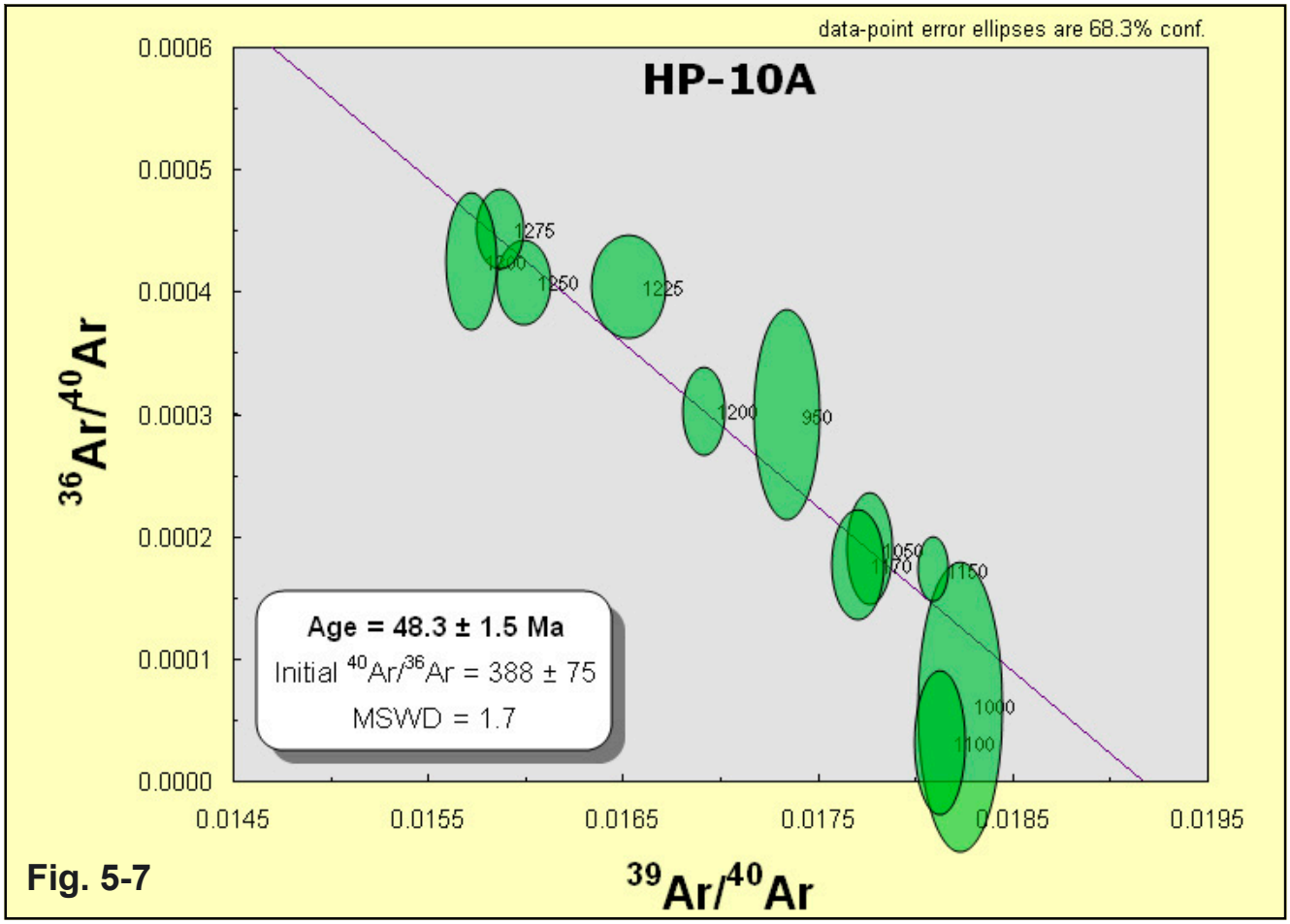
data-point error ellipses are 68.3% conf.
HP-10A
0.0006
0.0005
0.0004
0.0003
0.0002
0.0001
0.0000
$^{36}Ar/^{40}Ar$
1275
1250
1225
1200
950
1050
1150
1000
1100
Age = 48.3 ± 1.5 Ma
Initial $^{40}Ar/^{36}Ar$ = 388 ± 75
MSWD = 1.7
0.0145
0.0155
0.0165
0.0175
0.0185
0.0195
$^{39}Ar/^{40}Ar$

Fig. 5-7

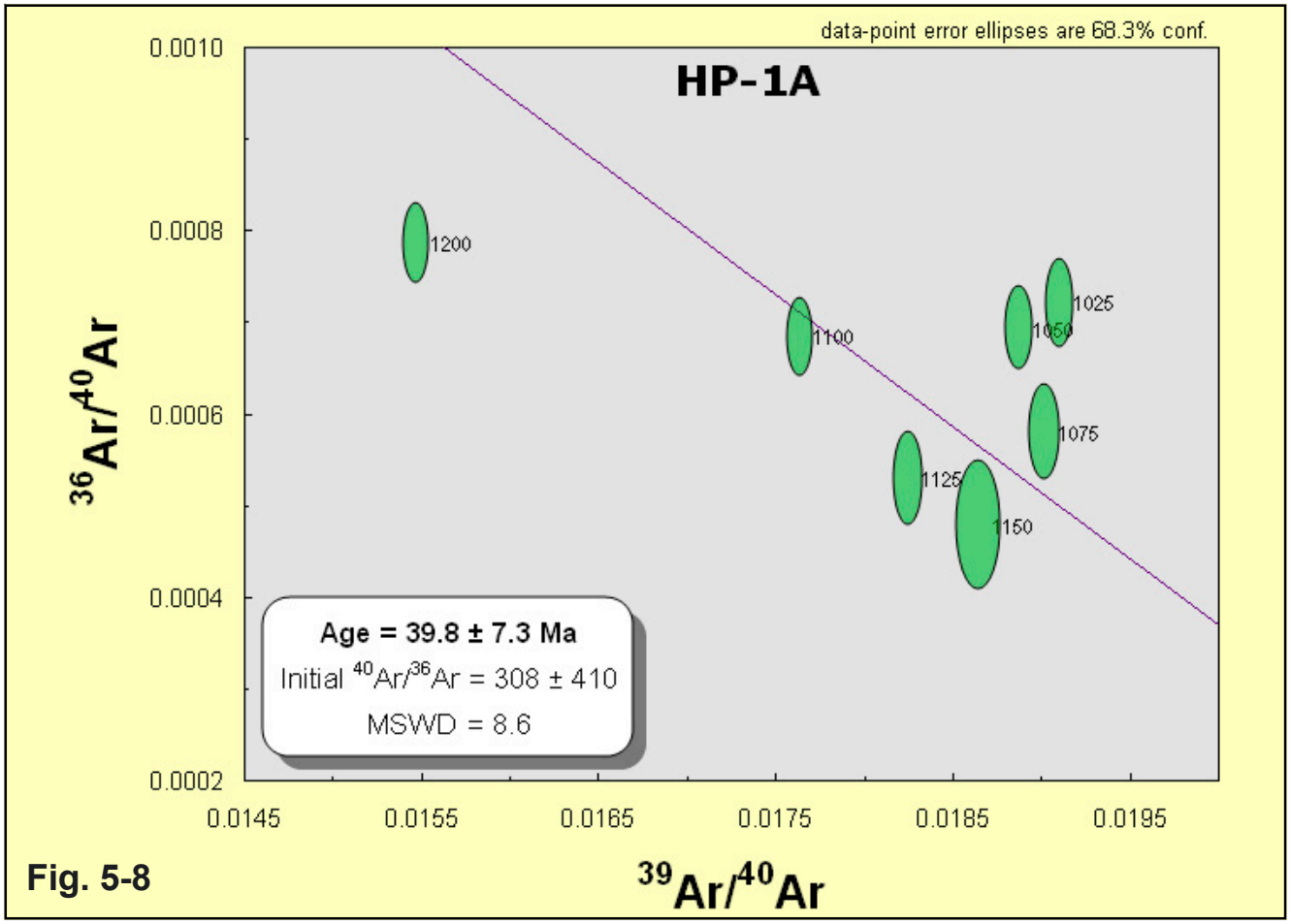
data-point error ellipses are 68.3% conf.
HP-1A
0.0010
0.0008
0.0006
0.0004
0.0002
$^{36}Ar/^{40}Ar$
1200
1100
1025
1050
1075
1125
1150
Age = 39.8 ± 7.3 Ma
Initial $^{40}Ar/^{36}Ar$ = 308 ± 410
MSWD = 8.6
0.0145
0.0155
0.0165
0.0175
0.0185
0.0195
$^{39}Ar/^{40}Ar$

Fig. 5-8

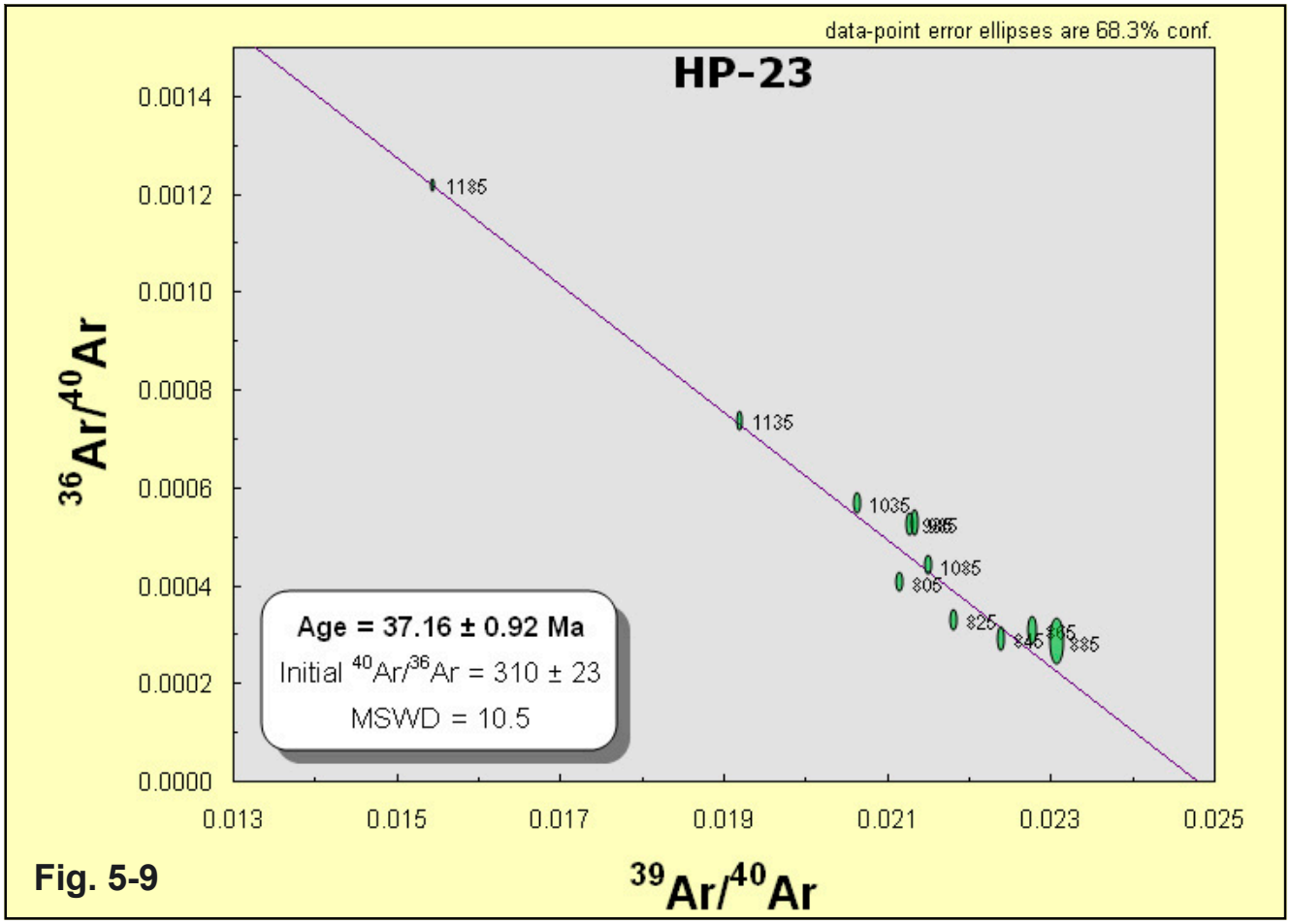

Fig. 5-9

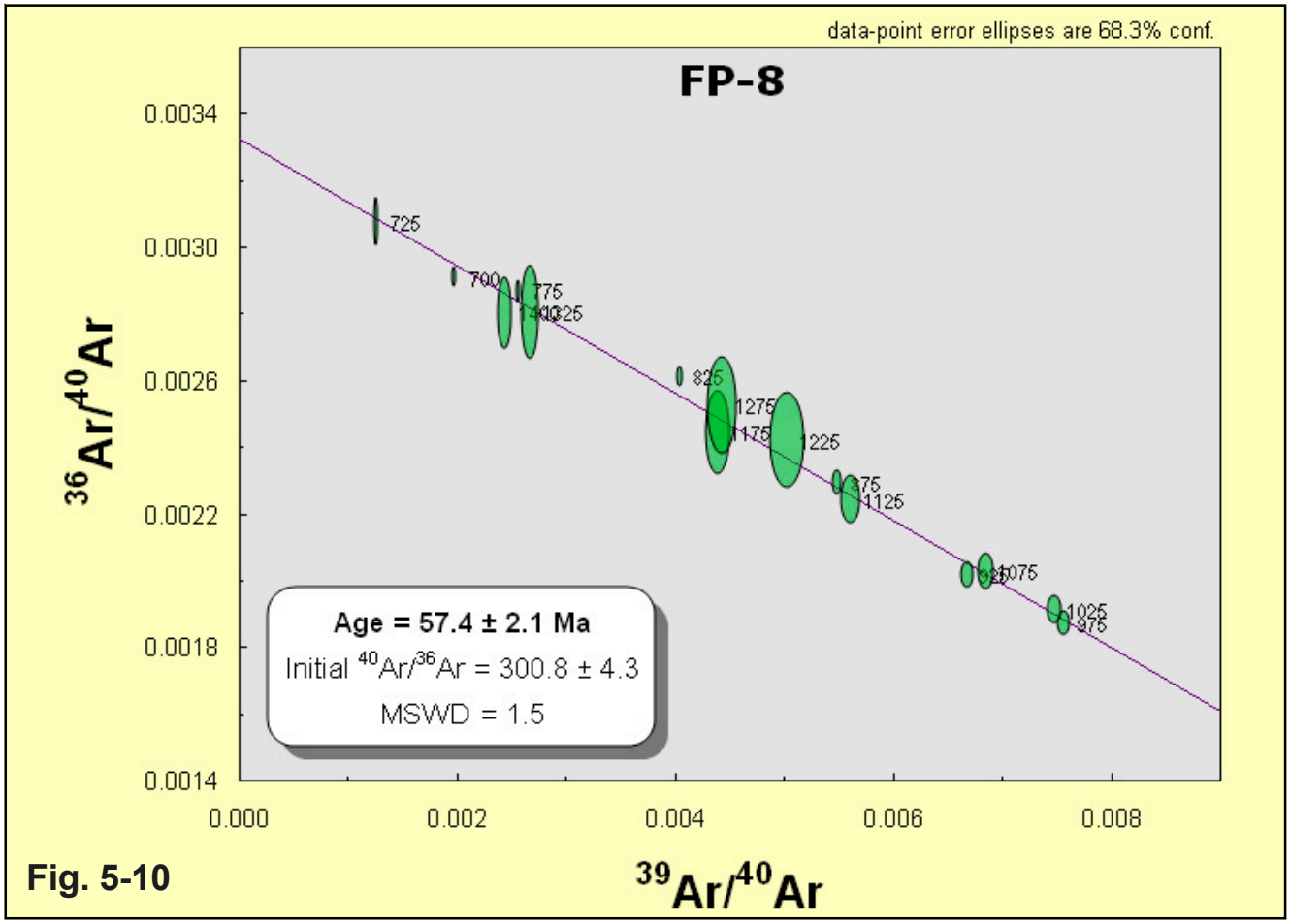

Fig. 5-10

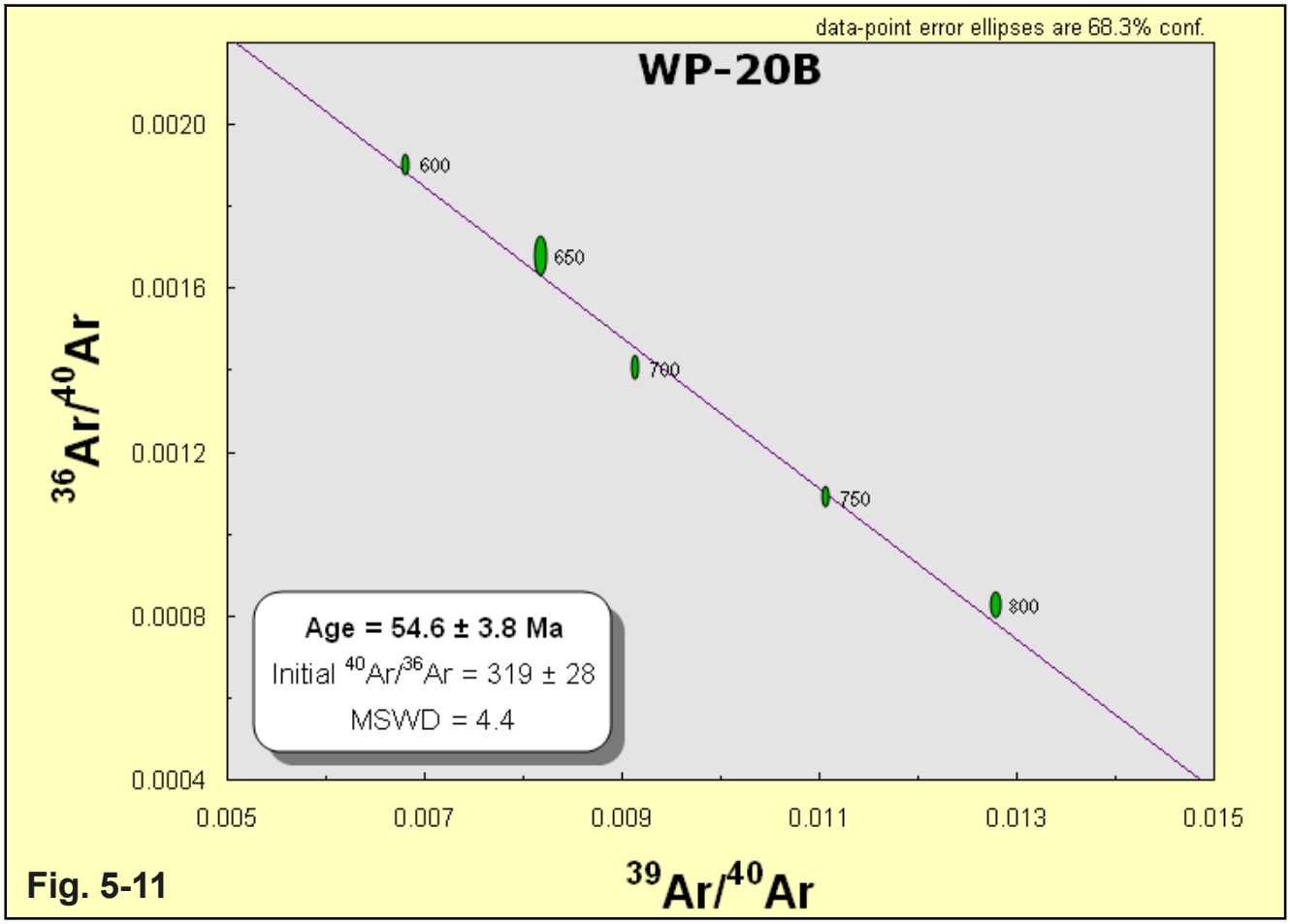

Fig. 5-11

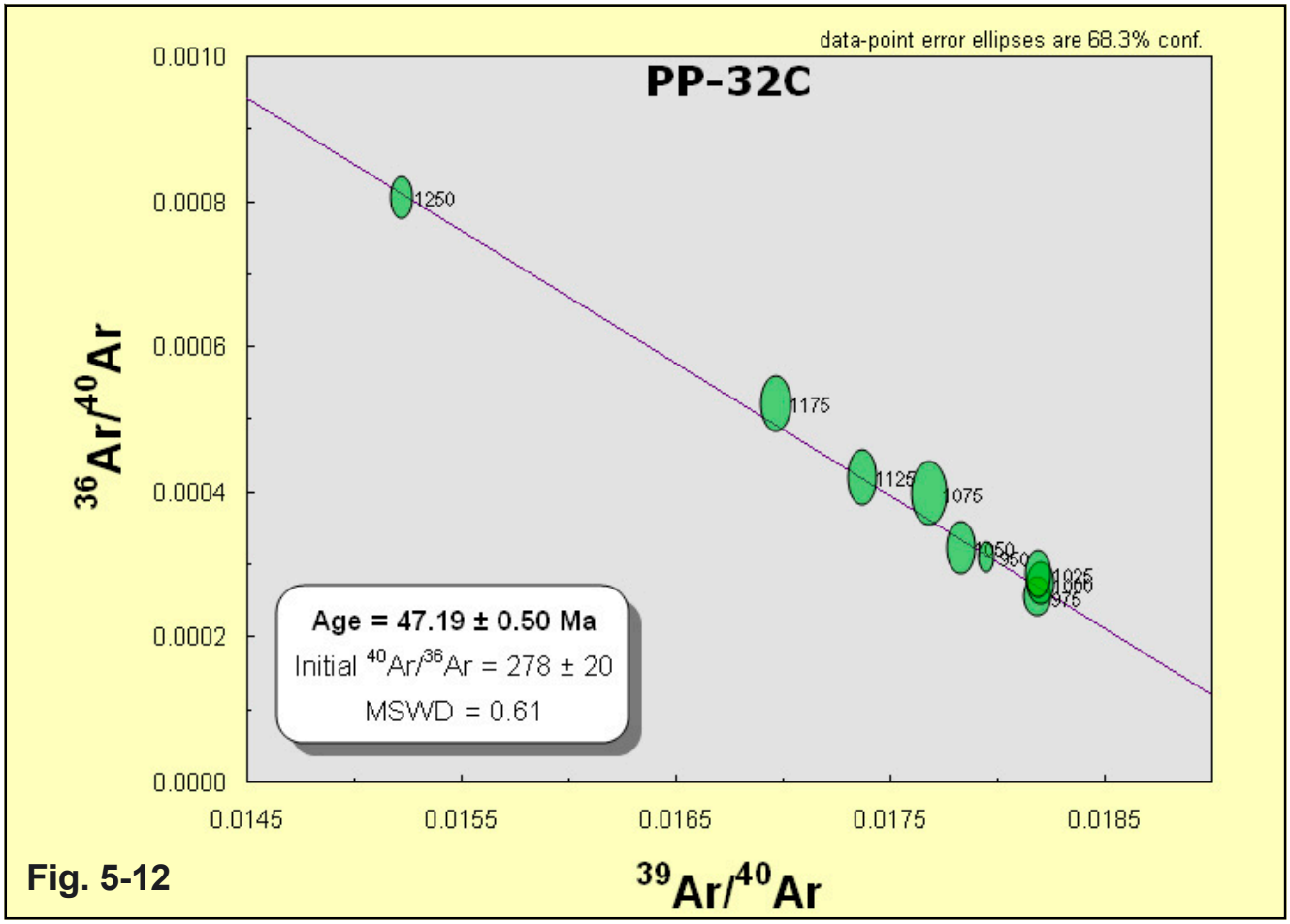

Fig. 5-12

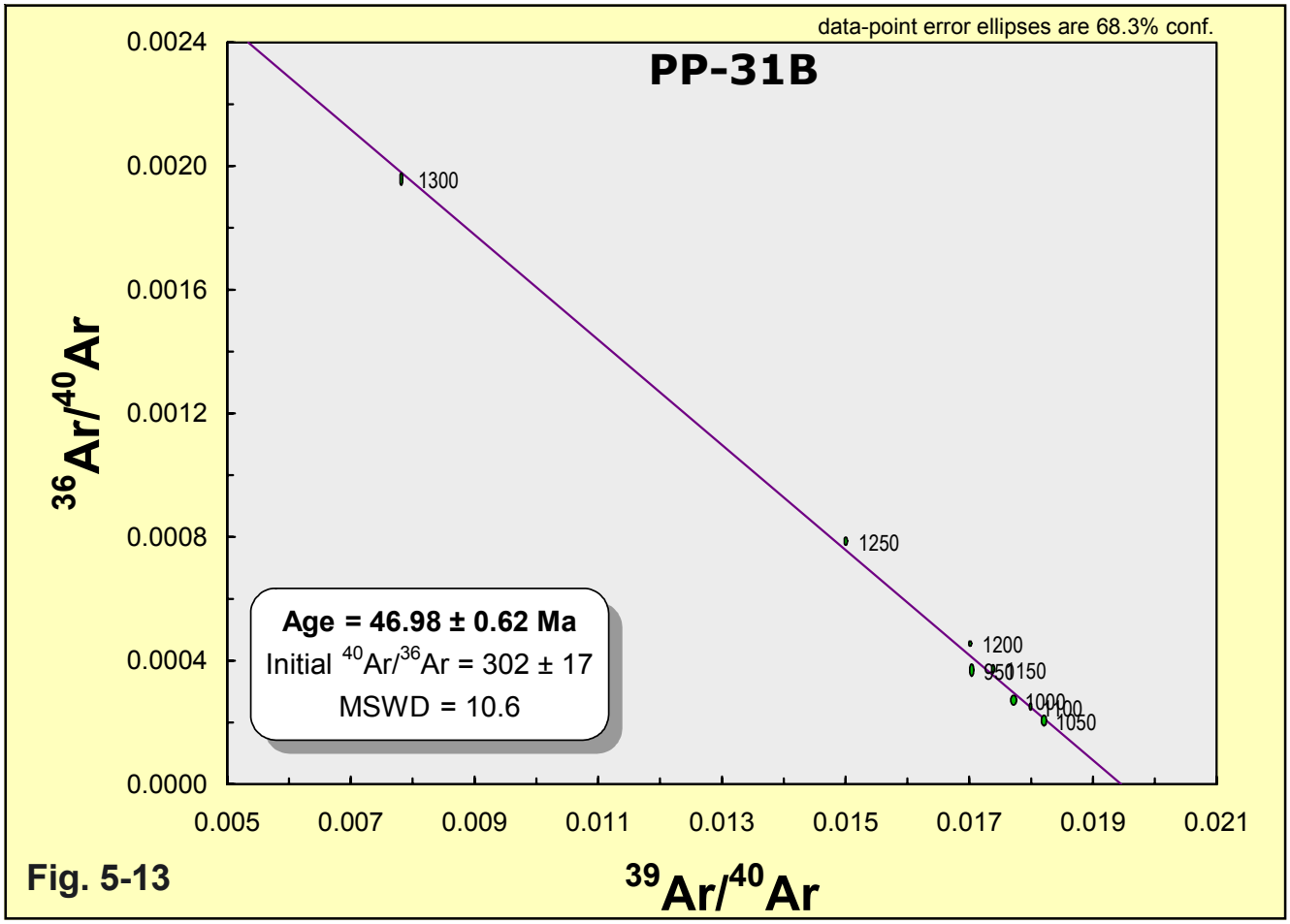

Fig. 5-13

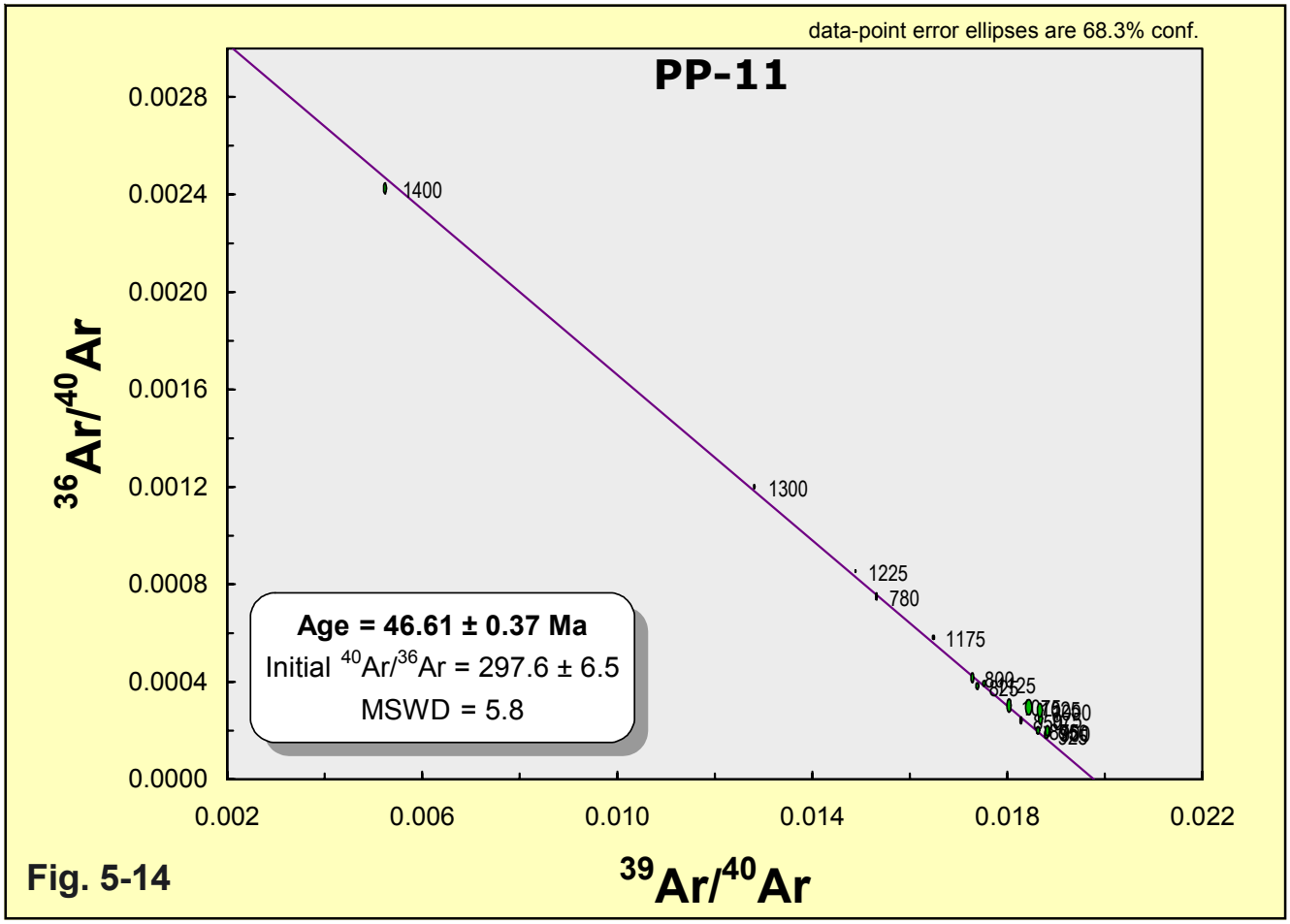

Fig. 5-14

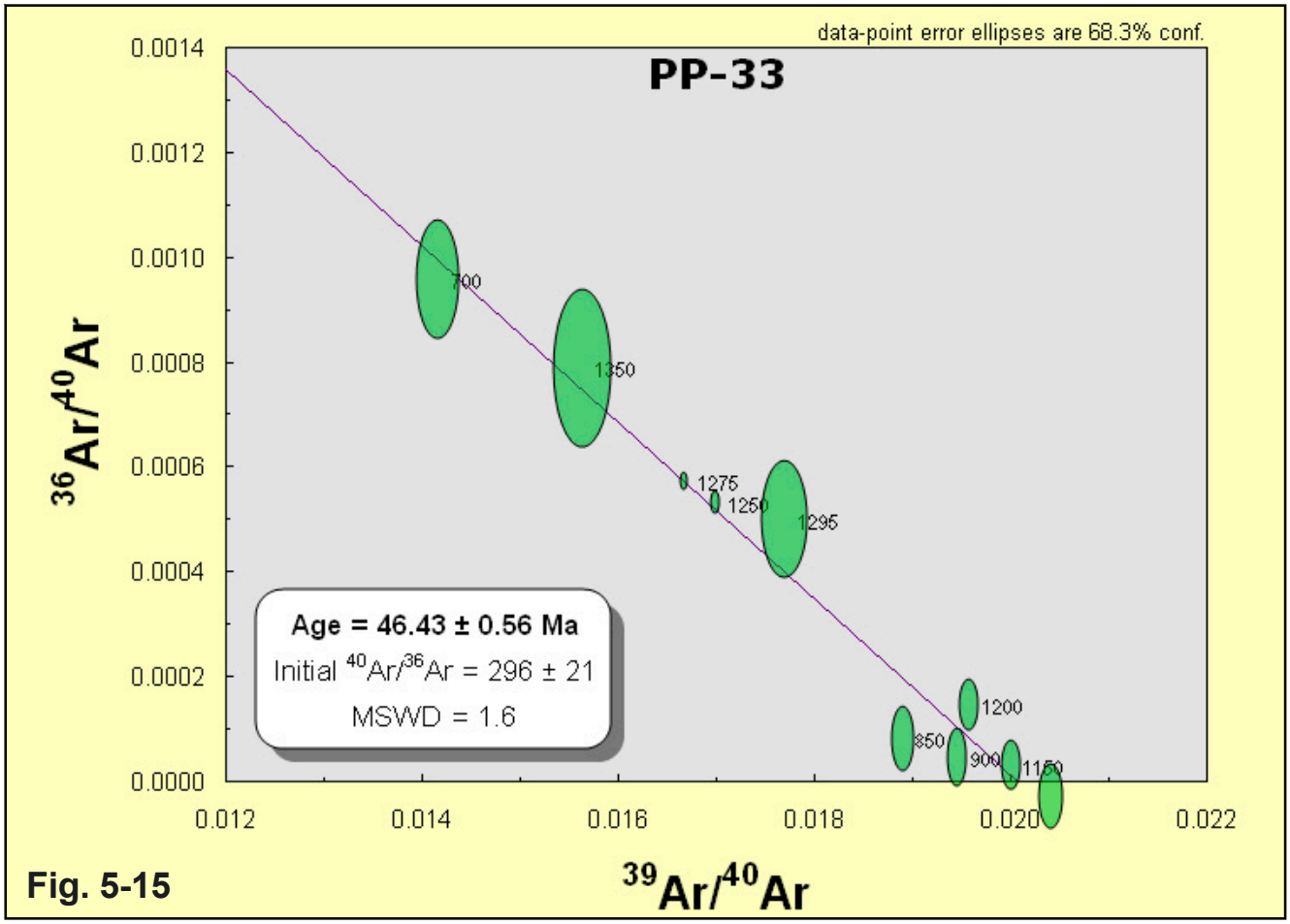

Fig. 5-15

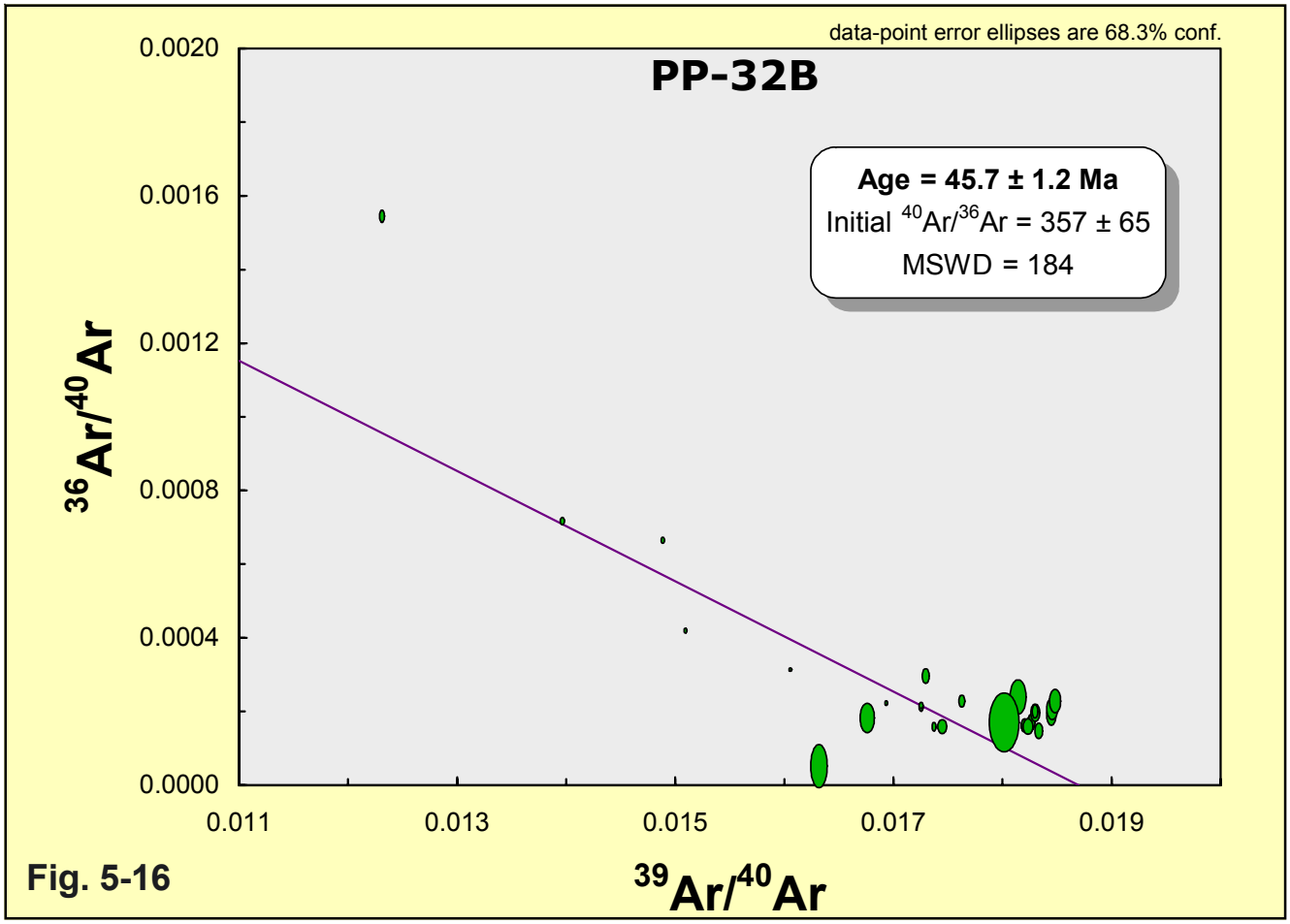

Fig. 5-16

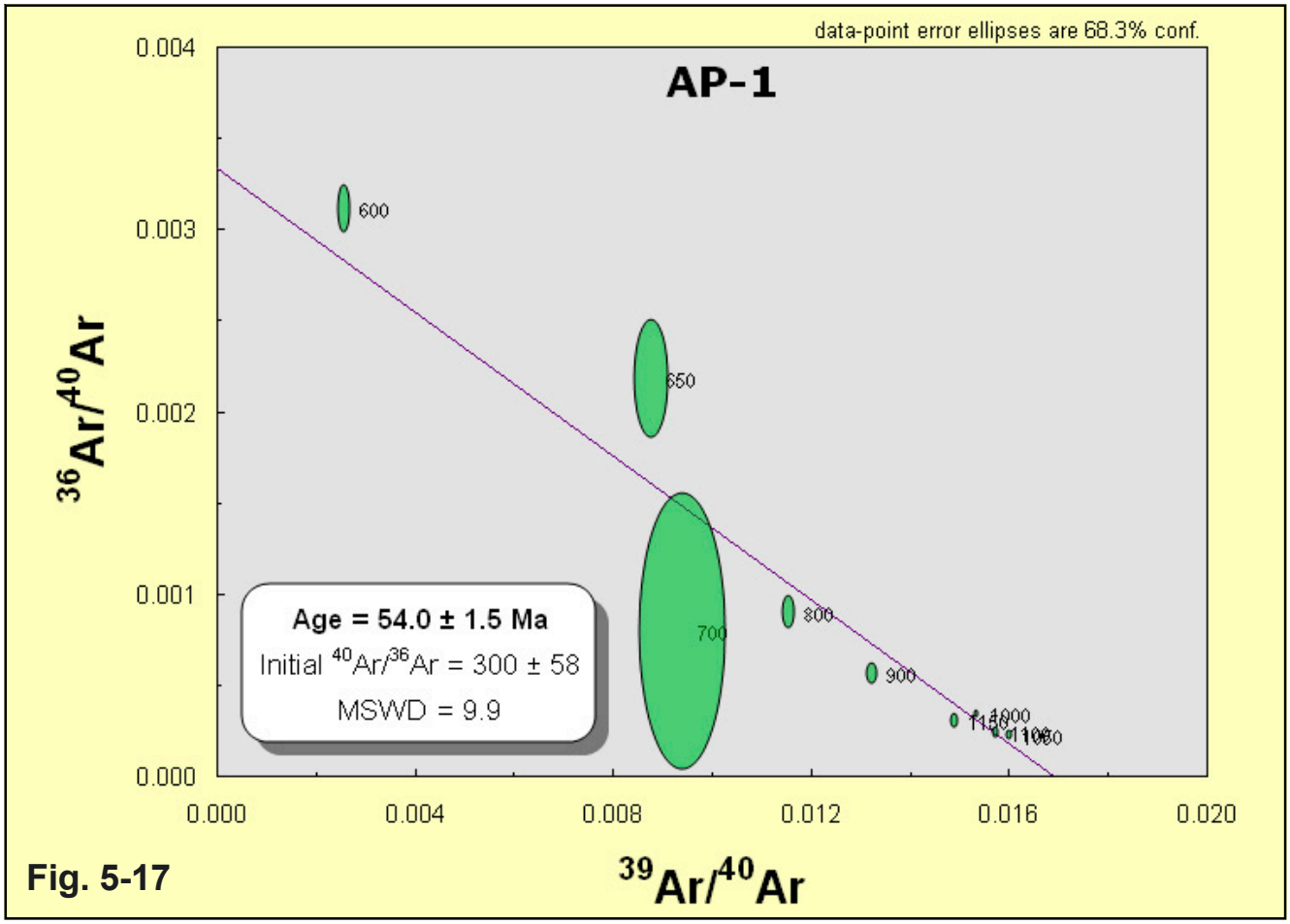

Fig. 5-17

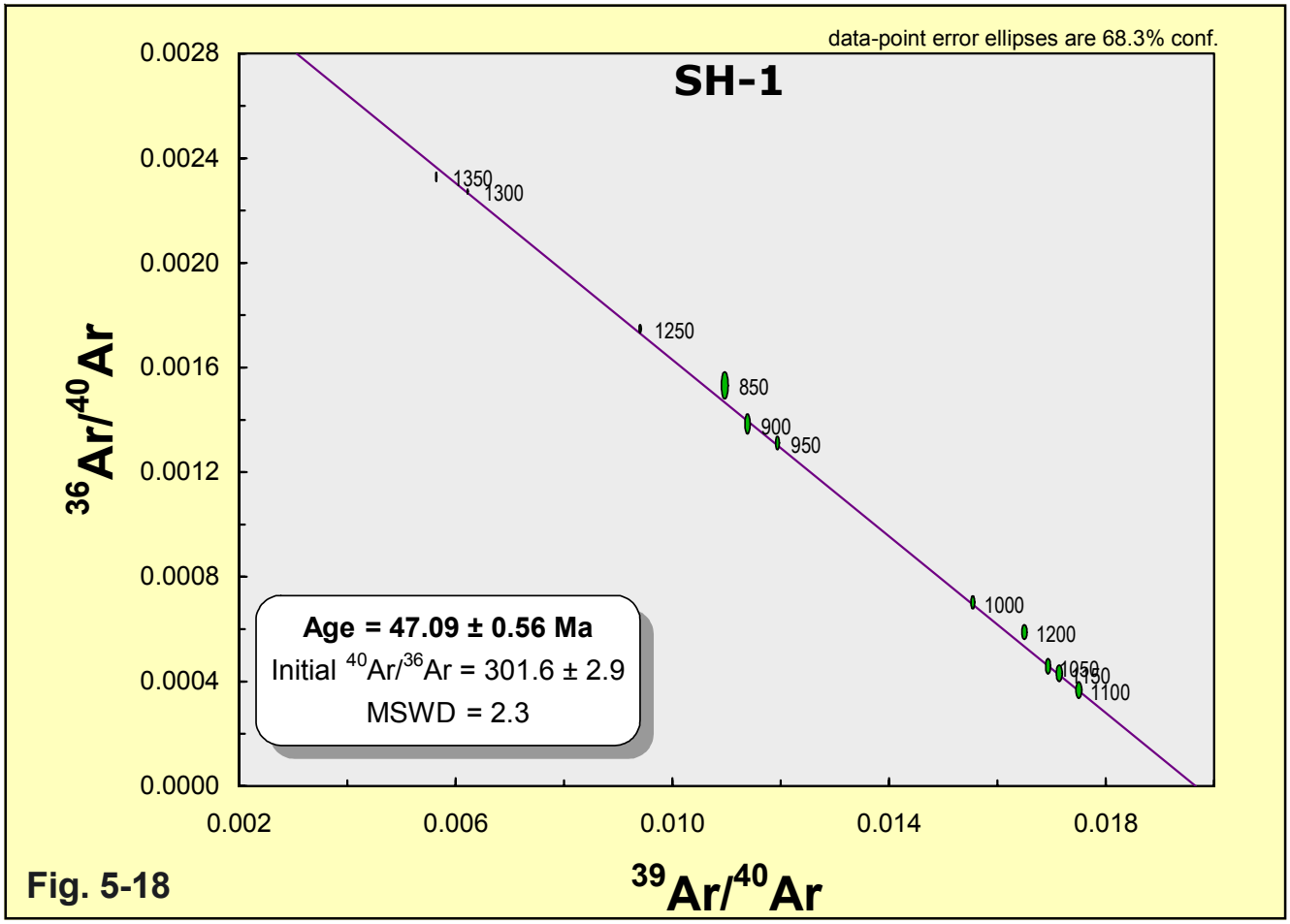

Fig. 5-18

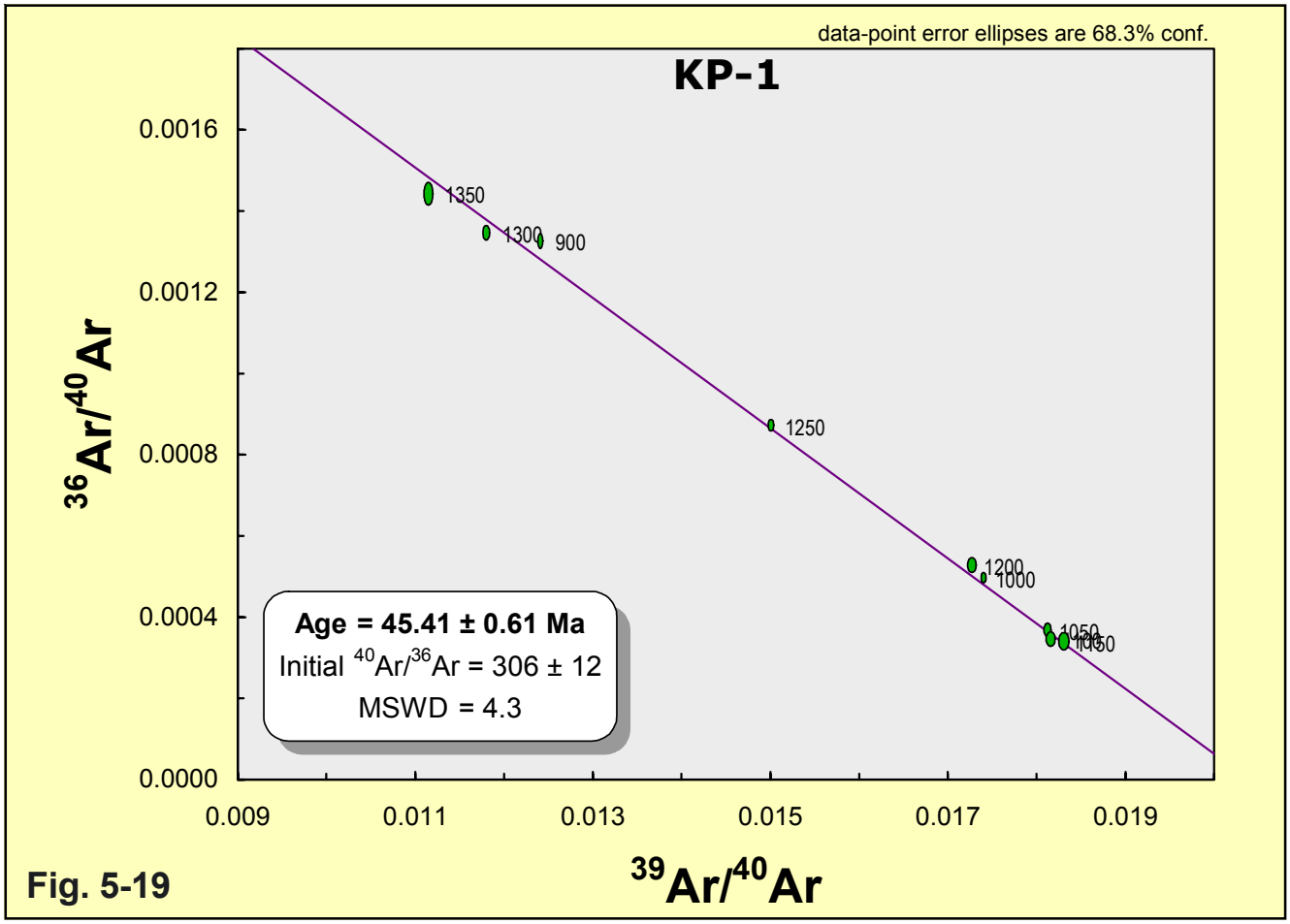

Fig. 5-19

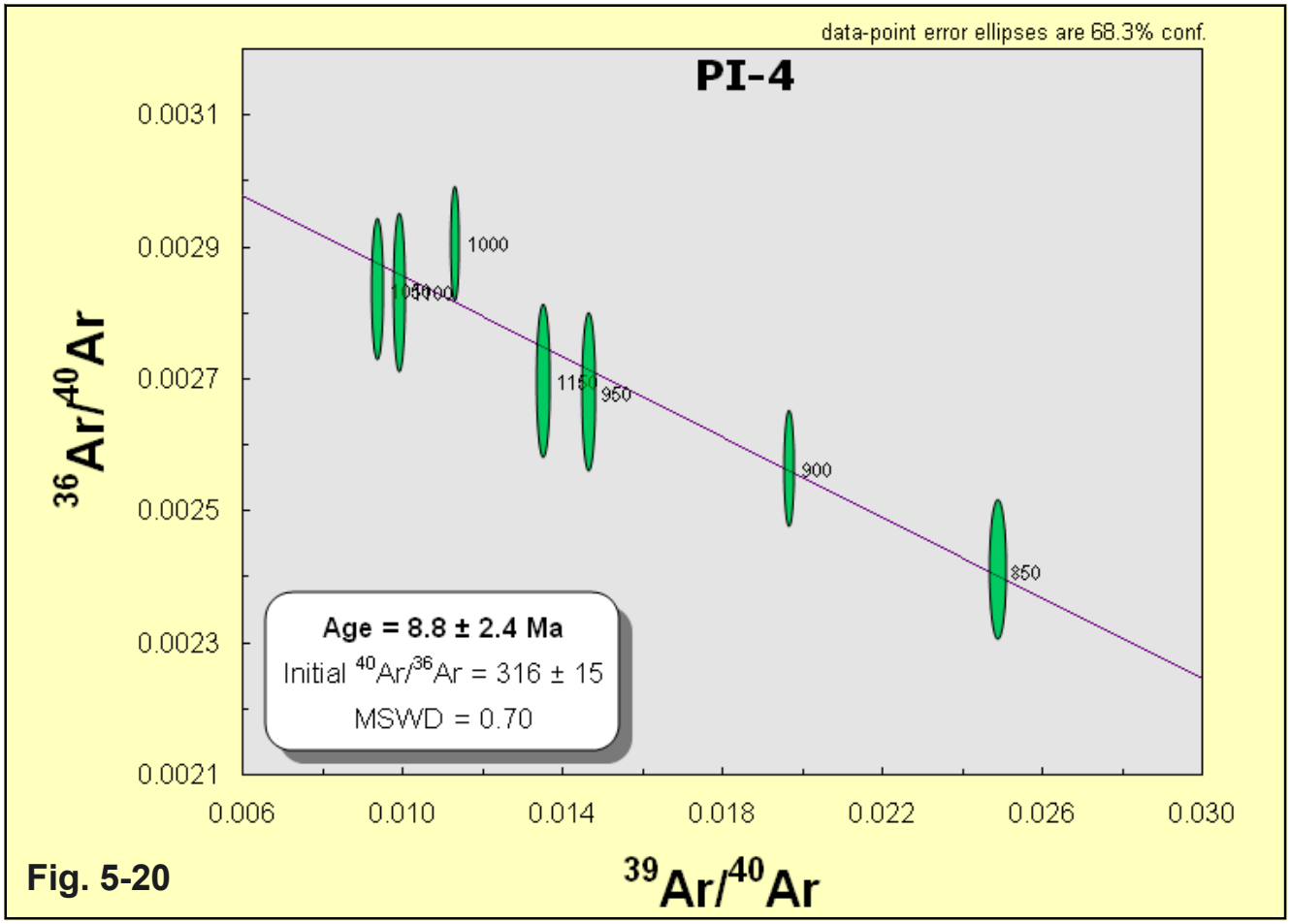

Fig. 5-20

6. Inferences for the Cenozoic geodynamic history

6.1 Summary of the results

A threefold approach combining structural, (isotope-) geochemical and geochronological data has been applied to reconstruct the geodynamic development of the South Shetland Islands as reflected by dyke systems.

The three datasets are in good agreement and record a relatively short, but intense phase of intrusive activity during the Paleocene and Eocene.

According to the structural data, the overall tectonic stress pattern remained fairly stable during that time.

Geochemical and isotopic data prove an incipiently relatively strong, but subsequently decreasing crustal component and a heterogeneous, depleted mantle wedge beneath the South Shetland Islands volcanic arc. In contrast, sediment input apparently increased with time.

Age determinations suggest incipient intrusive activity during the earliest Paleocene (Danian), lasting until the Late Eocene (approx. 65-37 Ma).

The main deformation of the host rocks was at least on Livingston Island obviously restricted to the uppermost Cretaceous. The tectonic regime thereafter remained stable throughout the time of dyke intrusion.

One of the goals of this work was to check if the dyke systems of the South Shetland Islands give any hints on ridge crest-trench collision events in that area (see chapter 1.7). No such indications are given by the datasets presented here. Nor are there any hints on adakitic melts contributing to arc magma genesis, which are usually generated related to slab window formation. Obviously, such processes did not occur during the time of dyke intrusion.

6.1.1 Structural data

An overview of the structural data is given in Table 6-1. The results include following important observations:

(1) The overall stress pattern was apparently very similar throughout the South Shetland Islands, i.e. the tectonic directions observed at the individual locations correlate well within normal variance. Differences are probably at least in part due to late block faulting and subsequent tilting of the individual blocks.

(2) The joint directions used by the dykes indicate a stable tectonic stress field during the complete time of intrusive activity, because all used directions can be interpreted as belonging to the same tectonic regime. This argument is supported by the movement directions of the subducting Phoenix plate relative to the Antarctic Peninsula as deduced from calculations of plate rotations [McCarron & Larter 1998]. According to them, the direction of the subducting plate changed considerably in the uppermost Cretaceous, but then remained stable during the Early Cenozoic (Fig. 1-3), the time during which the dykes intruded.

(3) On Hurd Peninsula, a folding axis striking 24° was determined in the host rocks. The dykes intruded the different joint directions (first and second order dextral and sinistral shear systems) correlated with this folding axis but are not folded themselves. Six different intrusive events could be distinguished on Hurd Peninsula, as deduced from crosscutting field relationships and the different strike directions. Dykes of the same relative age also share the same strike direction, indi-

Location	b-axis	a-axis	ac-plane	S_{1d}	S_{1s}	S_{2d}	S_{2s}
Admiralty Bay (KGI)	35°	120°	120/84 NE	99°	164°	17°	66°
Potter Peninsula (KGI)	30°	116°	-	87°	157°	3°	62°
Barton Peninsula (KGI)	28°	118°	-	70-90°	154°	11°	50°
Weaver Peninsula KGI)	39°	129°	-	100°	157°	3°	79°
Fildes Peninusula (KGI)	19°	109°	109/78 N	89°	140°	-	-
Nelson Island	20°	110°	110/80 S	72°	155°	1°	45°
Hurd Peninsula (LI)	24°	117°	117/87 SW	82°	145°	179°	49°

Table 6-1: Summary of the tectonic directions observed in the individual areas of investigation. Apparently, the overall stress pattern was similar throughout the South Shetland Islands. The only true folding axis was observed on Hurd Peninsula. No ac-planes were observed on Potter, Barton and Weaver Peninsula. No secondary shear system is expressed on Fildes Peninsula. KGI: King George Island; LI: Livingston Island. For further abbreviations see Appendix I.

	Hurd Peninsula (LI)	Nelson Island	Fildes Peninsula (KGI)	Weaver Peninsula (KGI)	Barton Peninsula (KGI)	Potter Peninsula (KGI)	Admiralty Bay (KGI)	Penguin Island
time of intrusion	?Danian - Priabonian	?Thanetian - ?Ypresian	Thanetian - Ypresian	Thanetian - Ypresian	?Thanetian - ?Ypresian	Lutetian	Ypresian - Lutetian	Tortonian
magmatic phase	all phases	main phase	main phase	main phase	main phase	main phase	main phase	not arc-related
# of intrusive events	6	3 (?)	4 (?)	4 (?)	7	4	5	1
magma series	subalkaline	subalkaline	subalkaline	subalkaline	subalkaline	subalkaline	subalkaline	subalkaline
magmatic affinity	tholeiitic/calc-alkaline	calc-alkaline	calc-alkaline	tholeiitic/calc-alkaline	tholeiitic/calc-alkaline	calc-alkaline	tholeiitic/calc-alkaline	tholeiitic
prevailing rock type	basalt - andesite	dacite	andesite	basalt - basaltic andesite	basaltic andesite	basaltic andesite - rhyolite	basaltic andesite	basalt
sedimentary component	initially weak, then increasing	notable	notable	notable	notable	notable	notable	weak
slab derived fluids	notable	weak	weak	weak	notable	weak	weak	weak
crustal contamination	initially strong, then decreasing	weak or absent	weak or absent	weak or absent	weak or absent	weak or absent	weak or absent	weak or absent
special features	highest Ti- and Fe-contents lowest REE-fractionation high Ba/Th			low Ba/Th highest εNd values	high REE-fractionation highest Nb/Ta high Ba/Th	high REE-fractionation largest spread in Zr/Hf low Ba/Th high Ce/Pb	high alumina-contents lowest Nb/Ta highest U/Th	highest Mg-numbers highest Nb/Y highest Ce/Th lowest alumina-contents lowest U/Th

Table 6-2: Summary of the geochemical main characteristics of the South Shetland Islands dykes. LI: Livingston Island, KGI: King George Island. The question marks in the first row indicate uncertain or estimated ages, in the third row estimated number of events according to different strike.

cating that slight changes of the overall tectonic parameters led to different preferred directions, but within the same stress field.

(4) On King George Island, up to 7 intrusive events could be distinguished in different areas, like on Hurd Peninsula each of them characterized by sharing the same relative age and the same strike.

(5) The correlation between tectonic directions as deduced from joint systems (in the host rocks and within the dykes) and directions as deduced from the strike of the dykes is generally good. However, in single cases (e.g. the dextral first order shear direction on Potter Peninsula) differences of up to 20° have been observed between corresponding directions. Currently, no convincing explanation can be given for the differing directions taken by the dykes. As the directions deduced from the measured joints are also based on joints observed *within* the dykes, a change of the stress field and thus a temporal factor can be excluded.

6.1.2 Geochemical and isotopic data

A summary of the main characteristics of the South Shetland Islands dykes as indicated by geochemical and isotopic data is given in Table 6-2.

Alteration effects are evident at least for part of the major element oxides (e.g. Na_2O, K_2O), possibly induced by hydrothermal fluids and/or seawater interaction. Thus, the evaluation of the geochemical dataset was based primarily on the discussion of minor and (immobile) trace elements, for which no alteration could be detected.

The dykes from the South Shetland Islands comprise a subalkaline series of predominantly calc-alkaline affinity. However, apparently bound to the initial stages of intrusive activity in the respective areas, also tholeiites occur. This is true for Hurd, Weaver and Barton Peninsula, as well as for Admiralty Bay.

Generally negative slopes displayed by the REE distribution patterns might be influenced by different factors like sediment

influx to the magma source region, partial melting processes or orthopyroxene fractionation during crystal fractionation processes. The presence of residual garnet in the mantle source region is contradicted by the REE patterns as well as by missing negative Y anomalies.
Trace element systematics (LREE fractionation, Th/Nb and Ce/Th ratios) suggest that sediment input has been lowest to the magma source of the dykes on Hurd Peninsula during initial stages. Later dykes from here as well as all dykes from the areas further to the NE (Nelson and King George Island) reflect a notably stronger sedimentary component.
In contrast, enrichment of the mantle source by fluids derived from the subducted slab was apparently strongest on Hurd Peninsula (Livingston Island), and on Barton Peninsula, as reflected by the considerably elevated Ba/Th ratios.
A heterogeneous and in large parts depleted mantle wedge is indicated by Nb/Ta and U/Th systematics. This is reflected especially by the dykes from Admiralty Bay, but holds also for the magma source of the much younger Penguin Island.
A signature caused by contamination with continental crust is obvious for most intrusive events on Hurd Peninsula. Especially the early events display a strong crustal component. This component decreases with time on Hurd Peninsula (Livingston Island) and is weak or nonexistent in the areas further to the NE (Nelson and King George Island).
The dykes on Weaver Peninsula (King George Island) apparently represent direct mantle fractionates without major contribution of other sources (sediment, slab derived fluids, continental crust). This is indicated by unusually low REE and Nb abundances, low Nb/Ta ratios and very high εNd values.
High Mg-numbers, εNd values and Nb/Y ratios characterize the radial dykes from Penguin Island as primitive, undifferentiated and moderately alkaline rocks. They are of tholeiitic affinity.

6.1.3 Geochronological data

Ar-Ar age determinations carried out on plagioclase separates of 19 samples and K-Ar whole rock datings performed on 7 samples suggest that the time interval during which intrusive activity occurred was restricted to the Paleocene and Eocene.
Dyke intrusion started earlier and lasted longer on Hurd Peninsula (Livingston Island) than on King George and probably also Nelson Island.
The supposedly oldest dykes from Hurd Peninsula did not yield formal Ar-Ar plateaus, but best estimates as deduced from the measured data point towards an intrusion age around the Cretaceous/Paleogene boundary, probably Danian. One K-Ar dated sample yielded an early Campanian age conflicting with the relative age of this dyke as deduced from field relationships, as well as with nannofossils from the host rocks also dated Campanian [Pimpirev et al. 2005]. Therefore, an artificially high age due to excess argon is considered probable for this dyke.
The Campanian nannofossil age of the host rocks and the inferred Early Danian age for the oldest dykes leaves a time gap of approx. 5-10 Ma for the main deformation phase (including folding) of the metasedimentary host rocks.
The main phase of dyke intrusion in the South Shetland Islands took place from Thanetian to Lutetian, culminating between 47 and 45 Ma. This phase is expressed throughout the investigated areas.
However, dyke intrusion then ceased and terminated during the Priabonian, those latest dykes once again being restricted to Hurd Peninsula.
The dyke dated from Penguin Island yielded an unexpectedly high age (Tortonian). Penguin Island represents a volcano considered as being related to the backarc-spreading that opened the Bransfield Strait between the Antarctic Peninsula and the South Shetland Islands. This backarc-spreading is widely believed to have started during the Pliocene (approx. 4 Ma ago). The Tortonian age obtained for the dyke on Penguin Island therefore rises the question if backarc-spreading in Bransfield Strait might have commenced considerably earlier than believed so far.

6.2 Discussion

In general, the structural, (isotope-) geochemical and geochronological datasets produced during this work allow a well constrained reconstruction of the geodynamic history of the South Shetland Islands during the time of dyke intrusion (Paleocene - Eocene).
However, some of the results are not unequivocal.

6.2.1 Discussion of the tectonic dataset

The good agreement of the individual tectonic directions determined in the different areas of investigation has been mentioned before and is summarized in Table 6-1. However, only on Hurd Peninsula (Livingston Island) a real folding axis could be

determined. Therefore, the directions of the corresponding dextral and sinistral shear systems can be attributed unambiguously for this area. This does not hold for the other areas. Due to missing folding axes, the tectonic directions as deduced from joint measurements and the orientations of the dykes can be assigned only tentatively and under the assumption of a stress field similar as on Hurd Peninsula. However, the correlation of the inferred directions with those of Hurd Peninsula is surprisingly good (Table 6-1), encouraging the conclusion that the stress field indeed was very similar throughout the South Shetland Islands. Nevertheless, a final evidence (which would be given by folding axes) is missing.

Another weak point are the partly very small datasets. In case of Nelson Island, for example, only five dykes and 19 joints have been measured. As compared to hundreds of joints measured e.g. on Hurd Peninsula and also on Potter Peninsula, the significance of such small datasets is limited. They are without exception due to logistic difficulties reaching remote areas, the absence of scientific bases and/or shortness of time. The work on Nelson Island e.g. was done during shorttime visits and required comparatively long journeys in Zodiac boat. More work is required to extend these datasets. On the other hand, the directions as determined for Nelson Island are in especially good agreement with the "reference" dataset from Hurd Peninsula (Table 6-1).

At first sight, another discrepancy is that from all investigated areas Fildes and Weaver Peninsula, though lying next to each other, are the areas showing the most differing tectonic directions (Table 6-1). However, they are separated by one of the deepest cutting strike-slip faults so far recognized in the South Shetland Islands (Collins Fault, Fig. 2-21A), and movement including a rotational factor along the plane of this fault may explain the differing tectonic directions. Late block faulting is evident anywhere in the South Shetland Islands and may easily account for further differences between individual areas.

6.2.2 Discussion of the geochemical dataset

A problem touching basic geochemical constraints concerns the magmatic affinity attributed to the different dyke suites. As shown in Fig. 4-3A and B and convincingly confirmed in Fig. 4-22, almost all dykes from Hurd Peninsula are of tholeiitic affinity. Nevertheless, the alumina content of more than 16 wt% shown by most of these dykes is more typical for calc-alkaline rocks. A possible explanation is given by cumulus plagioclase, but this is an unusual feature as compared to typical tholeiites.

The same applies to the Panorama Ridge Dykes in Admiralty Bay, great part of the dykes from Weaver Peninsula and a group of dykes from Barton Peninsula. However, tholeiites are anyway unusual in an active continental margin setting and commonly attributed to incipient stages of young, immature arcs [Tatsumi & Eggins 1995; Wilson 1989]. This, on the other hand, supports the interpretation of the dykes on Hurd Peninsula as marking the incipient stages of arc activity in that area. Moreover, the Panorama Ridge Dykes are also considered the oldest group of their respective area (Admiralty Bay, see chapter 2.3.5 and Fig. 2-40), and similar relationships can not be excluded for Weaver and Barton Peninsula. The possibility exists, that incipient intrusive activity in the South Shetland Islands generally was accompanied by melts of tholeiitic affinity. Another constraint is given by the velocity of the subducting slab. Philpotts [1990] states, that at active continental margins tholeiites may occur when subduction rates exceed 7 cm per year. As shown by McCarron & Larter [1998], the subduction velocity increased considerably in the area of the South Shetland Islands when the subduction direction changed during the uppermost Cretaceous (Fig. 1-3). According to them, the velocity remained high from Danian at least until Ypresian, just the time during which incipient phases of dyke intrusion took place.

Another question is why the influence of slab derived fluids was especially strong in case of the magma sources of Hurd and Barton Peninsula as compared to the other areas (Fig. 4-13 and 4-25). In case of Hurd Peninsula, the geographical distance from the other areas (more than 100 km) might justify the assumption of higher fluid influx from the down-going slab to the mantle wedge in that area. In case of Barton Peninsula, the root cause must be different. It can not be related to the tectonic architecture of King George Island, because the adjacent Weaver Peninsula belongs to the same upthrown horst structure as Barton Peninsula (Fig. 2-21A), but does not show the signature of elevated fluid influx. Maybe small scale mantle heterogeneities are responsible for the observed differences.

This argument is supported by the behavior of Zr/Hf and Nb/Ta ratios observed in the South Shetland Islands (Fig. 4-14C). As debated in chapter 4,

alteration processes or even analytical problems are considered unlikely as reason. Instead, the highly immobile element ratios of the dykes are supposed to reflect those of their mantle source. Thus, the scatter observed in Fig. 4-14C also points towards a mantle source showing small scale heterogeneities. On the other hand, mixing processes might also have influenced the Nb/Ta and Zr/Hf ratio, as supported by the linear trend shown by the dykes from Weaver Peninsula and Admiralty Bay (Fig. 4-14C).

An unsolved problem remains at present the positive Ta anomaly shown by most dykes from Admiralty Bay and part of the dykes from Potter Peninsula (Fig. 4-14A, 4-14B). As outlined in chapter 4, normal differentiation processes in the highest evolved systems (e.g. on Potter Peninsula) may, if at all, only in part be responsible for the fractionation of Nb and Ta, as also more basic dykes are amongst those showing the elevated Ta abundances.

However, on Potter Peninsula this behavior is restricted to the dykes forming the multiple intrusions described in chapter 2.3.4. The prominent, subparallel trends shown by the rhyolites and their basic counterparts in a plot of Ta versus Nb, point towards a magma chamber bound process involving highly diverse melts. At present, no such process is known.

6.2.3 Discussion of the geochronological dataset

Though a plausible estimate can be given for the time of incipient intrusive activity, the precise onset of dyke intrusion remains unknown, due to the low quality of the age data obtained for the oldest dykes. The inferred earliest Danian ages for the oldest dykes and the Campanian nannofossil ages reported by Pimpirev et al. [2005] for the host rocks restrict the time interval for deformation (folding) to a rather short period prior to dyke emplacement. This is not contradictory, especially considering the geotectonic setting of the host rocks within an accretion wedge, but at least remarkable.

An unsatisfying fact is the partly bad correlation of relative age relationships as observed in the field with the measured age data.

On Potter Peninsula, the ages determined for the dyke system mapped offshore (Fig. 2-29) do within errors coincide with the sequence given by relative relationships.

On Hurd Peninsula, this holds only if focussing on the Ar-Ar ages obtained from feldspar separates. Though partly of very low quality (possibly due to alteration of the dykes), these data correlate within errors with the relative ages observed in the field. In contrast, some of the K-Ar whole rock ages contradict clearly the relative ages. It has been discussed in chapter 5, that some of the K-Ar ages might be the result of excess Ar. This is probably true for the Campanian age obtained for dyke HP-15. Other dykes might have suffered Ar loss, the respective K-Ar data indicate too low ages as compared to the relative time sequence and the constraints given by the Ar-Ar ages. The time interval given by the K-Ar ages is roughly correct, but the true errors are probably much larger than indicated by the individual data.

6.3 Conclusions

According to the geochronological data, dyke intrusion started earlier (Danian) and lasted longer (Priabonian) on Hurd Peninsula (Livingston Island) than on Nelson and King George Island (Thanetian - Lutetian). A maximum age for incipient dyke intrusion on Hurd Peninsula is set by Campanian nannofossil ages determined for the metasedimentary host rocks (Miers Bluff Formation, MBF).

The main deformation of the MBF, including folding and the creation of primary and secondary shear systems, occurred during a time gap of approx. 5-10 Ma between the uppermost Campanian and the lowest Danian. Given the geotectonic position of these rocks forming part of an accretionary wedge, such a relatively short deformation time seems possible. Related to subduction processes, the sedimentary sequences might have been buried relatively fast to lower levels of the accretionary wedge, where they were subjected to deformation.

A folding axis striking 24° was determined, accompanied by dextral and sinistral first and second order shear systems. These directions were also used by the dykes and are further expressed as joints within the dykes, indicating that the stress field that caused the deformation of the Miers Bluff Formation remained stable also during the complete time of dyke intrusion. However, the deformation of the dykes is restricted to jointing, but in contrast to their host rocks they are not folded. Though no true folding axis could be determined for the areas investigated on Nelson and King George Island, the a- and b-axes and the shear directions as deduced from the strike of the dykes and from jointing within the dykes and their host rocks are nearly identical to the directions ob-

served on Hurd Peninsula. This suggests a uniform stress field throughout the South Shetland Islands at least from Maastrichtian to Priabonian.

Six different intrusive events can be distinguished on Hurd Peninsula, each of them represented by a dyke system of uniform strike and characteristic geochemical features. Crosscutting relationships observed in the field prove slight changes of the tectonic parameters, causing each dyke system to prefer another, but still to the overall stress field related direction for intrusion.

On King George Island, up to seven different intrusive events can be distinguished, as defined by their crosscutting relationships and different strike directions.

Age determinations yielded uncertain ages for the oldest dykes, but suggest incipient dyke intrusion on Hurd Peninsula (Livingston Island) most probably around the Cretaceous/Paleogene boundary or during the lowermost Danian. This first magmatic phase is expressed only here, but is absent on Nelson and King George Island. It comprises dykes from the first three intrusive events on Hurd Peninsula.

According to the geochemical data (e.g. Ce and Th systematics), sediment influx to the magma source was apparently low during these initial stages. On the other hand, the chemical and isotopic composition of the dykes generated during this first phase suggests considerable contamination by continental crust. This is reflected by low εNd values (0-1) and a correlation of Nd isotopic data with the degree of differentiation. A relatively unstretched continental crust during the initial stages of intrusive activity and storage of the melts in shallow level magma chambers prior to intrusion is assumed to be responsible.

A rough correlation between decreasing degree of crustal contamination and the sequence of the following intrusive events on Hurd Peninsula indicates an increasingly stretched crust that let the melts rise more directly and with shorter storage times at shallow levels. At the same time, sediment contribution to arc magma genesis apparently got stronger.

On King George Island, ages published for magmatic rocks suggest onset of arc activity already during Cretaceous times. However, most published ages range between 65 and 40 Ma. In accordance, the new ages presented here indicate dyke intrusion in the areas studied on Nelson and King George Island from the Paleocene/Eocene boundary on, then ceasing again during the Lutetian. However, these results do not exclude predating dyke intrusion in other parts.

A culmination of intrusive activity is indicated for all investigated areas during the Lutetian at 47-45 Ma. This main phase is characterized by the absence of crustal contamination (also on Hurd Peninsula), and by notable contribution of subducted sediment to arc magma genesis.

The characteristics of the magma source then remained stable, until dyke intrusion terminated during the Priabonian, producing last dykes on Hurd Peninsula (Livingston Island).

A depleted and partly heterogeneous mantle wedge beneath the South Shetland Islands volcanic arc is indicated by HFSE and LILE systematics. REE patterns in combination with missing negative Y anomalies indicate that this mantle source is free of residual garnet.

The unexpectedly high Tortonian age obtained from one of the radial dykes cropping out on Penguin Island questions the widely believed Pliocene (4 Ma) onset of backarc-spreading in Bransfield Strait. Instead, the activity of the Bransfield Rift might have started earlier.

Summarizing, the results of this work prove dykes to be a promising and suitable means to decipher the geodynamic parameters prevailing during the time of their emplacement.

A tight correlation between orientation and chemical composition of the dykes can be observed throughout the South Shetland Islands. This allows the correlation of tectonic and magmatic events and the identification of changes in the magma source.

However, thorough mapping of the dyke systems and the determination of relative age relationships proved to be an essential prerequisite for the successful reconstruction of the geodynamic history. This holds especially, as the rather high degree of alteration of some dykes made reliable age determinations difficult in these cases.

References

Acosta J. & Uchupi E. (1996): Transitional tectonics along the south Scotia Ridge, Antarctica. *Tectonophysics*, **267**, 31-56.

Anon (1821): Notizen über das neue südliche Land. *Neue allg. geogr. Ephemeriden,* **9**, Pt. 4, 514-515, Weimar.

Arche A., Lopez-Martinez J. & Martinez de Pison E. (1992): Sedimentology of the Miers Bluff Formation, Livingston Island, South Shetland Islands. *In:* Yoshida Y., Kaminuma K. & Shiraishi K. (eds.): *Recent progress in Antarctic Earth Science.* Terra Scientific Publishing Company, 357-362, Tokyo.

Ashcroft W.A. (1972): Crustal structure of the South Shetland Islands and the Bransfield Strait. *Brit. Ant. Surv. Scient. Rep.,* **66**, 43 pp.

Barker D.H.N. & Austin J.A. (1994): Crustal diapirism in Bransfield Strait, West Antarctica: Evidence for distributed extension in marginal basin formation. *Geology,* **22,** 657-660.

Barker D.H.N. & Austin J.A. (1998): Rift propagation, detachment faulting, and associated magmatism in Bransfield Strait, Antarctic Peninsula. *J. Geophys. Res.,* **103**, 24017-24043.

Barker P.F. (1976): The tectonic framework of Cenozoic volcanism in the Scotia Sea region – A review. *In:* González-Ferrán O. (ed.): *Proceedings of the Symposium on Andean and Antarctic Volcanology Problems.* International Association of Volcanology and Chemistry of the Earth's Interior, 330-346, Rome.

Barker P.F. (1982): The Cenozoic subduction history of the Pacific margin of the Antarctic Peninsula: ridge-crest-trench interactions. *J. Geol. Soc. Lon.,* **139**, 787-801.

Barker P.F. & Dalziel I.W.D. (1983): Progress in geodynamics in the Scotia Arc region. *In:* Cabre R. (ed.): *Geodynamics of the Eastern Pacific region. Caribbean and Scotia Arcs.* AGU, Geodynamics Series, **9**, 137-170.

Barker P.F., Dalziel I.W.D. & Storey B.C. (1991): Tectonic development of the Scotia arc region**.** *In:* Tingey R.J. (ed.): *The geology of Antarctica.* Oxford Science Publ., Monogr. on Geol. and Geophys., **17**, Clarendon Press, 215-248.

Barth M.G., McDonough W.F. & Rudnick R.L. (2000): Tracking the budget of Nb and Ta in the continental crust. *Chem. Geol.,* **165**, 197-213.

Barton C.M. (1961): The geology of King George Island, South Shetland Islands. *Prel. Rpts. Falkl. Isl. Dep. Surv.,* **12**, 18 pp., London.

Barton C.M. (1965): The geology of the South Shetland Islands: III. The stratigraphy of King George Island. *Brit. Ant. Surv. Scient. Rep.,* **44**, 33 pp.

Bau M. (1996): Controls on the fractionation of isovalent trace elements in magmatic and aqueous systems: evidence from Y/Ho, Zr/Hf, and lanthanide tetrade effect. *Contrib. Mineral. Petrol.,* **123**, 323-333.

Bennat H., Heidrich H., Grimm J., Sievers J., Walter H. & Wiedemann A. (1998): Das "Geowissenschaftliche Informationssystem Antarktis" (GIA) am Institut für Angewandte Geodäsie (IfAG). *In*: Goß mann H. (ed.): Patagonien und Antarktis - Geofernerkundung mit ERS-1-Radarbildern. *Petermanns Geographische Mitteilungen*, **Ergänzungsheft 287**, 13 - 34.

Bickle M.J. & Teagle D.A.H. (1992): Strontium alteration in the Troodos ophiolite: implications for fluid fluxes and geochemical transport in mid-ocean ridge hydrothermal systems. *Earth Planet. Sci. Lett.,* **113**, 219-237.

Birkenmajer K. (1980a): A revised lithostratigraphic standard for the Tertiary of King George Island, South Shetland Islands, (West Antarctica). *Bull. Acad. Pol. Sci. Ser. Sci. Terre,* **27**, 49-57.

Birkenmajer K. (1980b): Geology of Admiralty Bay, King George Island (South Shetland Islands) - An outline. *Polish Polar Res.*, **1**, 29-54.

Birkenmajer, K. (1980c): Age of the Penguin Island volcano, South Shetland Islands (West Antarctica), by the Lichenometric method. *Bull. Acad. Pol. Sci. Ser. Sci. Terre,* **27**, 69-76.

Birkenmajer K. (1982a): Late Cenozoic phases of block-faulting on King George Island (South Shetland Islands, West Antarctica). *Bull. Acad. Pol. Sci. Ser. Sci. Terre,* **30**, 21-32.

Birkenmajer K. (1982b): Report on geological investigations of King George Island and Nelson Island (South Shetland Islands, West Antarctica) in 1980-81. *Stud. Geol. Pol.,* **74**, 175-197.

Birkenmajer K. (1982c): The Penguin Island volcano, South Shetland Islands (Antarctica): its structure and succession. *Stud. Geol. Pol.,* **74**, 155-173.

Birkenmajer K. (1989): A guide to Tertiary geochronology of King George Island, West Antarctica. *Polish Polar Res.,* **10**, 555-579.

Birkenmajer K. (1992a): Evolution of the Bransfield Basin and Rift, West Antarctica. *In:* Yoshida Y., Kaminuma K. & Shiraishi K. (eds.): *Recent progress in Antarctic Earth Science.* Terra Scientific Publishing Company, 405-410, Tokyo.

Birkenmajer K. (1992b): Trinity Peninsula Group (Permo-Triassic?) at Hope Bay, Antarctic Peninsula. *Polish Polar Res.,* **13**, 35-60.

Birkenmajer K. (1993): Contemporaneous volcanoes of Bransfield Rift, West Antarctica. *Proc. XX Polar Symposium,* Lublin, 299-303.

Birkenmajer K. (1994): Evolution of the Pacific margin of the northern Antarctic Peninsula: an overview. *Geologische Rundschau,* **83**, 309-321.

Birkenmajer K. (1997a): Geology of the northern coast of King George Island, South Shetland Islands (West Antarctica). *Stud. Geol. Pol.,* **110**, 7-26.

Birkenmajer K. (1997b): Thermal jointing in Tertiary plugs on King George Island, South Shetland Islands (West Antarctica) - a comparison with Tertiary volcanoes of Lower Silesia, Poland. *Stud. Geol. Pol.,* **110**, 27-45.

Birkenmajer K. (1998a): Geological structure of Barton Peninsula and Weaver Peninsula, Maxwell Bay, King George Island (South Shetland Islands, West Antarctica). *Bull. Pol. Acad. Sci., Earth Sci.,* **46 (3-4)**, 191-209.

Birkenmajer K. (1998b): Geology of volcanic rocks (?Upper Cretaceous - Lower Tertiary) at Potter Peninsula, King George Island (South Shetland Islands, West Antarctica). *Bull. Pol. Acad. Sci., Earth Sci.,* **46 (2)**, 147-155.

Birkenmajer K. (2001): Mesozoic and Cenozoic stratigraphic units in parts of the South Shetland Islands and northern Antarctic Peninsula (as used by the Polish Antarctic Programmes). *Stud. Geol. Pol.,* **118**, 188 pp.

Birkenmajer K. (2003): Admiralty Bay, King George Island (South Shetland Islands, West Antarctica): A geological monograph. *Stud. Geol. Pol.,* **120**, 75 pp.

Birkenmajer K., Francalanci L. & Peccerillo A. (1991): Petrological and geochemical constraints on the genesis of Mesozoic–Cenozoic magmatism of King George Island, South Shetland Islands, Antarctica. *Antarct. Sci.,* **3**, 293-308.

Birkenmajer K., Narebski W., Nicoletti M. & Petrucciani C. (1982): Late Cretaceous through Late Oligocene K-Ar ages of the King George Island Supergroup volcanics, South Shetland Islands (West Antarctica). *Bull. Acad. Pol. Sci. Ser. Sci. Terre,* **30**, 133-143.

Birkenmajer K., Narebski W., Skupinski A. & Bakun-Czubarow N. (1981): Geochemistry and origin of the Tertiary island-arc calc-alkaline volcanic suite at Admiralty Bay, King George Island (South Shetland Islands, Antarctica), *Stud. Geol. Pol.,* **72**, 7-57.

Birkenmajer K., Delitala M.C., Narebski W., Nicoletti M. & Petrucciani C. (1986a): Geochronology of Tertiary island-arc volcanics and glacigenic deposits, King George Island, South Shetland Islands (West Antarctica). *Bull. Acad. Pol. Sci. Ser. Sci. Terre,* **34**, 257-273.

Birkenmajer K., Delitala M.C., Narebski W., Nicoletti M. & Petrucciani C. (1986b): Geochronology and migration of Cretaceous through Tertiary plutonic centres, South Shetland Islands (West Antarctica): Subduction and hot spot magmatism. *Bull. Pol. Acad. Sci., Earth Sci.,* **34**, 243-255.

Birkenmajer K., Guterch A., Grad M., Janik T. & Perchuc E. (1990): Lithospheric Transect Antarctic Peninsula - South Shetland Islands, Antarctica. *Polish Polar Res.,* **11**, 241-258.

Bradshaw J.D. (1989): Cretaceous geotectonic patterns in the New Zealand region. *Tectonics,* **8**, 803-820.

Cande S.C., Herron E.M. & Hall B.R. (1982): The early Cenozoic tectonic history of the southeast Pacific. *Earth Planet. Sci. Lett.,* **57**, 63-74.

Cande S.C., Raymond C.A., Stock J. & Haxby W.F. (1995): Geophysics of the Pitman Fracture Zone and Pacific-Antarctic plate motions during the Cenozoic. *Science,* **270**, 947-953.

Chauvel C., Goldstein S.L. & Hofmann A.W. (1995): Hydration and dehydration of oceanic crust controls Pb evolution in the mantle. *Chem. Geol*., **126**, 65-75.

Class C., Miller D.M., Goldstein S.L. & Langmuir C.H. (2000): Distinguishing melt and fluid subduction components in Umnak Volcanics, Aleutian Arc. *Geochem. Geophys. Geosyst.,* **1**, 1999GC000010.

Craddock C. (1975): Tectonic evolution of the Pacific margin of Gondwanaland. *In:* Campbell K.S.W. (ed.): *Gondwana Geology*. A.N.U. Press, 609-618, Canberra.

Dalziel I.W.D. (1969): Structural studies in the Scotia Arc: Livingston Island. *Ant. J. of the US,* **4**, p. 137.

Dalziel I.W.D. (1972): Large-scale folding in the Scotia Arc. *In:* Adie R.J. (ed.): *Antarctic geology and geophysics*. Universitetsforlaget, 47-55, Oslo.

Dalziel I.W.D. (1982): The early (Pre-Middle Jurassic) history of the Scotia Arc region: A review and progress report. *In:*Craddock C. (ed.): *Antarctic Geoscience,* Univ. of Wisconsin Press, 111-126, Madison.

Davey F.J. (1972): Marine gravity measurements in Bransfield Strait and adjacent areas. *In:* Adie R.J. (ed.): *Antarctic geology and geophysics.* Universitetsforlaget, 39-46, Oslo.

Davey F.J. (1990): Structure and tectonics. *In:* Glasby G.P. (ed.): *Antarctic Sector of the Pacific*. Elsevier Oceanogr. Ser., **51**, 125–154.

David K., Schiano P. & Allégre C.J. (2000): Assessment of the Zr/Hf fractionation in oceanic basalts and continental materials during petrogenetic processes. *Earth Planet. Sci. Lett.,* **178**, 285-301.

Davidson J.P. (1987): Crustal contamination versus subduction zone enrichment: examples from the Lesser Antilles and implications for the mantle source composition of island arc volcanic rocks. *Geochim. Cosmochim. Acta,* **51**, 2185-2198.

Davidson J.P. & Harmon R.S. (1989): Oxygen isotope constraints on the petrogenesis of volcanic arc magmas from Martinique, Lesser Antilles. *Earth Planet. Sci. Lett.,* **95**, 255-270.

Davies R.E.S. (1982): The geology of the Marian Cove area, King George Island, and a Tertiary age for its supposed Jurassic volcanic rocks. *Brit. Ant. Surv. Bull.,* **51**, 151-165, Cambridge.

Del Valle R.A. & Rinaldi C.A. (1992): Regional scheme of the main structural features of the northeastern extreme of the Antarctic Peninsula and the James Ross Island area. *In: Geología de la Isla James Ross*. Instituto Antártico Argentino, Dirección National del Antártico, 349-357, Buenos Aires.

Del Valle R.A., Diaz M.T. & Romero E.J. (1984): Preliminary report on the sedimentites of Barton Peninsula, 25 de Mayo Island (King George Island), South Shetland Islands, Argentine Antarctica. *Contr. Inst. Ant. Argent.,* **308**, 1-18.

Dickin A.P. (1995): Radiogenic isotope geology. *Cambr. Univ. Press*, Cambridge, 452 pp.

Dietrich R., Dach R., Engelhardt G., Ihde J., Korth W., Kutterer H., Lindner K., Mayer M., Menge F., Miller H., Müller C., Niemeier W., Perlt J., Pohl M., Salbach H., Schenke H.-W., Schöne T., Seeber G., Veit A. & Völksen C. (2000): Ergebnisse der SCAR GPS Kampagnen – ITRF-Koordinaten und Geschwindigkeiten. *In:* Dietrich R. (Hrsg.): *Deutsche Beiträge zu GPS-Kampagnen des Scientific Committee on Antarctic Research (SCAR), 1995-1998, Reihe B, Angewandte Geodäsie,* **310**, 11-20.

Dilek Y., Thy P. & Moores E.M. (1991): Episodic dike intrusions in the northwestern Sierra Nevada, California: Implications for multistage evolution of a Jurassic arc terrane. *Geology,* **19**, 180-184.

DiVenere V.J., Kent D.V. & Dalziel I.W.D. (1994): Mid-Cretaceous paleomagnetic results from Marie-Byrd-Land, West Antarctica: A test of post-100 Ma relative motion between East and West Antarctica. *J. Geophys. Res.,* **99**, 15115-15139.

Doktor M., Swierczewska A. & Tokarski A.K. (1994): Lithostratigraphy and tectonics of the Miers Bluff Formation at Hurd Peninsula, Livingston Island (West Antarctica). *Stud. Geol. Pol.,* **104**, 41-104.

Domack E.W., Burnett A. & Leventer A. (2003): Environmental setting of the Antarctic Peninsula. *In:* Domack E., Leventer A., Burnett A., Bindschadler R., Convey P. & Kirby M. (eds.): *Antarctic Peninsula climate variability*. Ant. Res. Ser., AGU, **79**, 1-13, Washington D.C.

Drewry D.J. & Morris E.M. (1992): The response of large ice sheets to climate change. *Phil. Trans. R. Soc. London, Ser. B*, **338**, 235-242.

Eggins S.M., Woodhead J.D., Kinsley L.P.J., Mortimer G.E., Sylvester P., McCulloch M.T., Hergt J.M. & Handler M.R. (1997): A simple method for the precise determination of ≥ 40 trace elements in geological samples by ICP-MS using enriched isotope internal standardisation. *Chem. Geol*., **134**, 311-326.

Eights J. (1833): Description of a new crustaceous animal found on the shores of the South Shetland Islands, with remarks on their natural history. *Transactions of the Albany Inst.,* **2**, No. 1, 53-69.

Elliot D.H. (1988): Tectonic setting and evolution of the James Ross Basin, northern Antarctic Peninsula. *Geological Society of America*, Memoir **169**, 541-555, Boulder.

Elliot D.H. (1997): The planar crest of Graham Land, northern Antarctic Peninsula: possible origins and timing of uplift. *In:* Barker P.F. & Cooper A.K. (eds.): *Geology and seismic stratigraphy of the Antarctic margin, part 2.* Ant. Res. Ser., AGU, **71**, 51-74, Washington D.C.

Elliott T. (2003): Tracers of the slab. *In:* Eiler J. (ed.): *Inside the subduction factory.* AGU Geophys. Mon., **138**, 23-45.

Elliott T. & Plank T. (1997): Subduction zone processing of oceanic crust. *7th Annual V.M. Goldschmidt Conference,* LPI Contribution No. 921, pdf # 2414.

Elliott T., Plank T., Zindler A., White W. & Bourdon B. (1997): Element transport from slab to volcanic front at the Mariana arc. *J. Geophys. Res.,* **102**, 14991-15019.

Faure G. (1986): Principles of isotope geology. *J. Wiley & Sons*, New York, 589 pp.

Fensterseifer H.C., Soliani E. Jr., Hansen M.A.F. & Troian F. (1988): Geología e estratigrafia da associacáo de rochas do setor centro-norte da Peninsula Fildes, Ilha Rei George, Shetland do Sul, Antartica. *Ser. Cient. INACH,* **38**, 29-43, Santiago de Chile.

Ferguson D. (1921): Geological observations in the South Shetlands, the Palmer Archipelago, and Graham Land, Antarctica. *Trans. Roy. Soc. Edinb.*, **53**, 29-55.

Floyd P.A. & Winchester J.A. (1978): Identification and discrimination of altered and metamorphosed volcanic rocks using immobile elements. *Chem. Geol.,***21**, 291-306.

Fontoura M.A., Fensterseifer H.C. & Troian F.L. (1988): Geology and petrography of intrusive bodies of Stansbury Peninsula, Nelson Island, South Shetland Islands, Antarctica. *Ser. Cient. INACH,* **38**, 45-58, Santiago de Chile.

Forsyth D.W. (1975): Fault plane solutions and tectonics of the South Atlantic and Scotia Sea. *J. Geophys. Res.,* **80**, 1429-1443.

Fourcade N.H. (1960): Estudio geológico-petrografico de Caleta Potter, Isla 25 de Mayo, Islas Shetland del Sur. *Publ. del Inst. Ant. Argent.,* **8**, 121 pp., Buenos Aires.

Galindo-Zaldívar J., Jabaloy A., Maldonado A. & Sanz de Galdeano C. (1996): Continental fragmentation along the South Scotia Ridge transcurrent plate boudary (NE Antarctic Peninsula). *Tectonophysics*, **258**, 275-301.

Ghidella M.E., Yáñez G. & LaBrecque J.L. (2002): Revised tectonic implications for the magnetic anomalies of the western Weddell Sea. *Tectonophysics,* **347**, 65-86.

González-Ferrán O. (1985): Volcanic and tectonic evolution of the northern Antarctic Peninsula – Late Cenozoic to recent. *Tectonophysics*, **114**, 389-409.

González-Ferrán O. & Katsui Y. (1970): Estudio integral del volcanismo cenozoico superior de las Islas Shetland del Sur, Antártida. *Ser. Cient. Inst. Ant. Chileno,* **1**, No. 2, 123-174, Santiago de Chile.

González-Ferrán O., Katsui Y. & Tavera J. (1970): Contribución al conocimiento geológico de la Peninsula Byers de la Isla Livingston, Islas Shetland del Sur, Antártica. *Ser. Cient. Inst. Ant. Chileno,* **1**, No. 1, 41-54, Santiago de Chile.

Green T.H., Sie S.H., Ryan C.G. & Cousens D.R. (1989): Proton microprobe-determined partitioning of Nb, Ta, Zr, Sr and Y between garnet, clinopyroxene and basaltic magma at high pressure and temperature. *Chem. Geol.,* **74**, 201-216.

Griffiths D.H., Riddihough R.P., Cameron H.A.D. & Kennett P. (1964): Geological investigation of the Scotia Arc. *Brit. Ant. Surv. Scient. Rep.,* **46**, 43 pp.

Gromet L.P., Dymek R.F., Haskin L.A. & Korotev R.L. (1984): The "North American Shale Composite": its compilation, major and trace element characteristics. *Geochim. Cosmochim. Acta*, **48**, 2469-2482.

Grunow A.M., Dalziel I.W.D., Harrison T.M. & Heizler M.T. (1992): Structural geology and geochronology of subduction complexes along the margin of Gondwanaland: New data from the Antarctic Peninsula and southernmost Andes. *Geological Society of America Bulletin,* **104**, 1479-1514.

Gurney A. (1997): Below the convergence: Voyages toward Antarctica, 1699-1839. W.W. Norton & Company, Inc., 315 pp., New York.

Guterch A., Grad M., Janik T. & Perchuc E. (1991): Tectonophysical models of the crust between the Antarctic Peninsula and the South Shetland trench. *In:* Thomson M.R.A., Crame J.A. & Thomson J.W. (eds.): *Geological Evolution of Antarctica.* Cambridge Univ. Press, 499-504.

Harrison C.G.A., Barron E.J. & Hay W.W. (1979): Mesozoic evolution of the Antarctic Peninsula and the southern Andes. *Geology*, **7**, 374-378.

Hawkes D.D. (1961): The geology of the South Shetland Islands: I. The petrology of King George Island. *Falkland Islands Dependencies Survey Scient. Rep.,* **26**, 28 pp.

Hawkesworth C., Turner S., Peate D., McDermott F. & van Calsteren P. (1997): Elemental U and Th variations in island arc rocks: implications for U-series isotopes. *Chem. Geol.,* **139**, 207-221.

Hegner E., Walter H.J. & Satir M. (1995a): Pb-Sr-Nd isotopic compositions and trace element geochemistry of megacrysts and melilitites from the Tertiary Urach volcanic field: source composition of small volume melts under SW Germany. *Contr. Min. Petr*., **122**, 322-335.

Hegner E., Roddick J.C., Fortier S.M. & Hulbert L. (1995b): Nd, Sr, Ph, Ar, and O isotopic systematics of Sturgeon Lake kimberlite, Saskatchewan, Canada - constraints on emplacement age, alteration, and source composition. *Contr. Min. Petr*., **120**, 212-222.

Heinrichs H. & Herrmann A.G. (1990): Praktikum der Analytischen Geochemie. *Springer,* Heidelberg, 669 pp.

Henriet J.P., Meissner R., Miller H. & GRAPE Team (1992): Active margin processes along the Antarctic Peninsula. *Tectonophysics*, **201**, 229-253.

Henry C.D., Price J.G. & James E.W. (1991): Mid-Cenozoic stress evolution and magmatism in the Southern Cordillera: Texas and Mexico: Transition from continental arc to intraplate extension. *J. Geophys. Res.,* **96**, 13545-13560.

Hernández P.J. & Azcárate V. (1971): Estudio paleobotánico preliminar sobre restos de una tafoflora de la Península Byers (Cerro Negro), Isla Livingston, Islas Shetland del Sur, Antártida. *Ser. Cient. Inst. Ant. Chileno,* **2**, No. 1, 15-50, Santiago de Chile.

Herron E.M. & Tucholke B.E. (1976): Seafloor magnetic patterns and basement structure in the southeastern Pacific. *In:* Hollister C.D., Craddock C. *et al.* (eds.): *Initial Reports of the Deep Sea Drilling Project.* US Government Printing Office, **35**, 263-278, Washington DC.

Hervé F., Miller H. & Pimpirev C. (2005): Patagonia - Antarctica connections before Gondwana break-up. *In:* Fütterer D. et al. (eds): *Antarctic Contributions to Global Earth Science*, accepted.

Hobbs G.J. (1968): The geology of the South Shetland Islands: IV. The geology of Livingston Island. *Brit. Ant. Surv. Scient. Rep.*, **47**, 34 pp.

Hofmann A.W. (1988): Chemical differentiation of the Earth: the relationship between mantle, continental crust and oceanic crust. *Earth Planet. Sci. Lett.*, **90**, 297-314.

Hofmann A.W., Jochum K.P., Seufert M. & White W.M. (1986): Nb and Pb in oceanic basalts: new constraints on mantle evolution. *Earth Planet. Sci. Let*., **79**, 33-45.

Irvine T.N. & Baragar W.R.A. (1971): A guide to the chemical classification of the common volcanic rocks. *Can. J. Earth Sci.,* **8**, 523-548.

Jarrard R.D. (1986): Relations among subduction parameters. *Reviews of Geophysics*, **24**, 217-284.

Jokat W., Boebel T., König M. & Meyer U. (2003): Timing and geometry of early Gondwana breakup. *J. Geophys. Res.,* **108(B9**), 2428, doi: 10.1029/2002/LB001802, 1-15.

Jwa Y.-J., Park B.-K. & Kim Y. (1992): Geochronology and geochemistry of the igneous rocks from Barton and Fildes Peninsulas, King George Island: A review. *In:* Yoshida Y., Kaminuma K. & Shiraishi K. (eds.): *Recent progress in Antarctic Earth Science.* Terra Scientific Publishing Company, 439-442, Tokyo.

Kamenov B.K. (1997): Geochemistry and petrology of the Hespérides Point Intrusion, Hurd Peninsula, Livingston Island. *In:* Ricci C.A. (ed.): The Antarctic Region: Geological evolution and processes. *Terra Antartica,* 341-352, Siena.

Klepeis K.A. & Lawver L.A. (1996): Tectonics of the Antarctic-Scotia plate boundary near Elephant and Clarence Island, West Antarctica. *J. Geophys. Res.*, **101**, No. B9, 20211-20231.

Kraus S., Miller H. & del Valle R.A. (2000): Geochemically corroborated stratigraphy of a Tertiary volcanic series at Potter Peninsula (King George Island, South Shetland Islands, West Antarctica). *Actas IX Congr. Geol. Chil. Puerto Varas, resúmenes expandidos*, **2**, 379-383.

LaBrecque J., Cande S., Bell R., Raymond C., Brozena J., Keller M., Parra J.C. & Yanez G. (1986): Aerophysical survey yields new data in the Weddell Sea. *Antarct. J. U.S.*, Review, **21, No. 5**, 69-71.

Larson R.L. & Chase C.G. (1972): Late Mesozoic evolution of the western Pacific Ocean. *Geological Society of America Bulletin,* **83**, 3627-3644.

Larter R.D. & Barker P.F. (1991): Effects of ridge-crest-trench interaction on Antarctic-Phoenix Spreading: Forces on a young subducting plate. *J. Geophys. Res.,* **96**, 19583-19607.

Larter R.D., Rebesco M., Vanneste L.E., Gambóa L.A.P. & Barker P.F. (1997): Cenozoic tectonic, sedimentary and glacial history of the continental shelf west of Graham Land, Antarctic Peninsula. *In:* Barker P.F. & Cooper A.K. (eds.): *Geology and Seismic Stratigraphy of the Antarctic Margin, Part 2*. Ant. Res. Ser., AGU, **71**, 1-28.

Le Maitre R.W. (2002): Igneous rocks: a classification and glossary of terms. Recommendations of the International Union of Geological Sciences subcommission on the systematics of igneous rocks. *Cambr. Univ. Press,* 252 pp.

Livermore R., McAdoo D. & Marks K. (1994): Scotia Sea tectonics from high-resolution satellite gravity. *Earth Planet. Sci. Lett.*, **123**, 255-268.

Lopez-Martínez J., Martínez de Pison E. & Arche A. (1992): Geomorphology of Hurd Peninsula, Livingston Island, South Shetland Islands. *In:* Yoshida Y., Kaminuma K. & Shiraishi K. (eds.): *Recent progress in Antarctic Earth Science.* Terra Scientific Publishing Company, 751-756, Tokyo.

Loske W., Miller H. & Kramm U. (1988): U-Pb systematics of detrital zircons from low-grade metamorphic sandstones of the Trinity Peninsula Group (Antarctica). *J. of South Am. Earth Sci.,* **1**, 301-307.

Ludwig K.R. (1993): A computer program for processing Pb-U-Th isotope data, version 1.24. *USGS Open File Rep.,* **93-0513**.

Ludwig K.R. (2000): User's manual for Isoplot/Ex version 2.2 - a geochronological toolkit for Microsoft Excel. *Berkeley Geochr. Cent.,* Spec. Pub. **1a**, 56 pp.

Lugmair G. & Marti K. (1977): Sm-Nd-Pu time pieces in the Angra dos Reis meteorite. *Earth Planet. Sci. Lett.,* **35**, 273-284.

Luyendyk B., Cisowski S., Smith C., Richard S. & Kimborough D. (1996): Palaeomagnetic study of the northern Ford Ranges, western Marie-Byrd-Land, West Antarctica: Motion between East and West Antarctica. *Tectonics,* **15**, 122-141.

MacLean W.H. & Barrett T.J. (1993): Lithogeochemical techniques using immobile elements. *J. Geochem. Expl.,* **48**, 109-133.

Maldonado A., Larter R.D. & Aldaya F. (1994): Forearc tectonic evolution of the South Shetland margin, Antarctic Peninsula. *Tectonics,* **13**, 1345-1370.

Mayes C.L., Lawver L.A. & Sandwell D.T. (1990): Tectonic history and new isochron chart of the south Pacific. *J. Geophys. Res.,* **95**, 8543-8567.

McCarron J.J. & Larter R.D. (1998): Late Cretaceous to early Tertiary subduction history of the Antarctic Peninsula. *J. Geol. Soc. Lon.*, **155**, 255-268.

McClarren C. (2003): Sills and dikes. *http://mivosys.tripod.com/dikes.html*

McDonough W.F. & Sun S.-s. (1995): The composition of the Earth. *Chem. Geol.,* **120**, 223-253.

McDougall I. & Harrison T.M. (1999): Geochronology and thermochronology by the $^{40}Ar/^{39}Ar$ method (second edition). *Oxford Univ. Press,* 269 pp.

Merrihue C. & Turner G. (1966): Potassium-argon dating by activation with fast neutrons. *J. Geophys. Res.*, **71**, 2852-2857.

Miers J. (1820): Account of the discovery of New South Shetland, with observations on its importance in a geographical, commercial and political point of view. *Edinburgh Philosophical Journal*, **9**, Pt. 4, No. 6, 367-380.

Millar I.L., Willan R.C.R., Wareham C.D. & Boyce A.J. (2001): The role of crustal and mantle sources in the genesis of granitoids of the Antarctic Peninsula and adjacent crustal blocks. *J. Geol. Soc. Lon.*, **158**, 885-867.

Miller D.M., Goldstein S.L. & Langmuir C.H. (1994): Cerium/lead and lead isotope ratios in arc magmas and the enrichment of lead in the continents. *Nature,* **368**, 514-520.

Miller H. (1981): Pre-Andean orogenies of southern South America in the context of Gondwana. *In:* Cresswell M.M. & Vella P. (eds.): *Gondwana Five*, A.A. Balkema, 237-242, Rotterdam.

Miller H. (1983): The position of Antarctica within Gondwana in the light of Palaeozoic orogenic development. *In*: Oliver R.L., James P.R. & Jago J.B. (eds.): *Antarctic Earth Science - proceedings of the fourth international symposium on Antarctic Earth Sciences, Adelaide, South Australia.* Australian Acad. of Sci., Canberra/Cambridge Univ. Press, 579-581.

Miller H., Loske W. & Kramm U. (1987): Zircon provenance and Gondwana reconstruction: U-Pb data of detrital zircons from Triassic Trinity Peninsula Formation metasandstones. *Polarforschung,* **57**, 59-69.

Miyashiro A. (1974): Volcanic rock series in island arcs and active continental margins. *Am. J. Sci.,* **274**, 321-355.

Moyes A.B. & Hamer R.D. (1983): Contrasting origins and implications of garnet in rocks of the Antarctic Peninsula. *In:* Oliver R.L., James P.R. & Jago J.B. (eds.): *Antarctic Earth Science - proceedings of the fourth international symposium on Antarctic Earth Sciences, Adelaide, South Australia.* Australian Acad. of Sci., Canberra/Cambridge Univ. Press, 358-362.

Nichols G.T., Wyllie P.J. & Stern C.R. (1994): Subduction zone melting of pelagic sediments constrained by melting experiments. *Nature,* **371**, 785-788.

Nier A.O. (1950): A redetermination of the relative abundances of the isotopes of carbon, nitrogen, oxygen, argon, and potassium. *Phys. Rev.*, **77**, 789-793.

Norton I.O. & Sclater J.G. (1979): A model for the evolution of the Indian Ocean and the break-up of Gondwanaland. *J. Geophys. Res.,* **84**, 6803-6830.

Orlando H.A. (1963): La flora fósil en las inmediaciónes de la Peninsula Ardley, Isla 25 de Mayo, Islas Shetland del Sur. *Contr. del Inst. Ant. Argent.,* **79**, 1-14, Buenos Aires.

Orlando H.A. (1964): The fossil flora of the surroundings of Ardley Peninsula (Ardley Island), 25 de Mayo Island (King George Island), South Shetland Islands. *In:* Adie R.J. (ed.): *Antarctic Geology.* North-Holland Publ. Co., 629-636, Amsterdam.

Pankhurst R.J. (1983): Rb-Sr constraints on the ages of basement rocks of the Antarctic Peninsula. *In*: Oliver R.L., James P.R. & Jago J.B. (eds.): *Antarctic Earth Science - proceedings of the fourth international symposium on Antarctic Earth Sciences, Adelaide, South Australia.* Australian Acad. of Sci., Canberra/Cambridge Univ. Press, 367-371.

Pankhurst R.J. & Smellie J.L. (1983): K-Ar geochronology of the South Shetland Islands, lesser Antarctica: Apparent lateral migration of Jurassic to Quaternary island arc volcanism. *Earth Planet. Sci. Lett.,* **66**, 214-222.

Park M.E. (1991): Epithermal alteration and mineralization zoning within the stratovolcano, Barton Peninsula, King George Island. *Korean J. of Pol. Res.,* **2**, 141-154.

Pearce J.A., Leat P.T., Barker P.F. & Millar I.L. (2001): Geochemical tracing of Pacific-to-Atlantic upper-mantle flow through the Drake Passage. *Nature,* **410**, 457-461.

Pelayo A.M. & Wiens D.A. (1989): Seismotectonic and relative plate motions in the Scotia Sea region. *J. Geophys. Res.*, **94, No. B6**, 7293-7320.

Peucat J.J., Vidal P., Bernard-Griffiths J. & Condie K.C. (1988): Sr, Nd and Pb isotopic systematics in the Archean low- to high-grade transition zone of southern India: syn-accretion vs. post-accretion granulites. *J. Geol.,* **97**, 537-550.

Philpotts A.R. (1990): Principles of igneous and metamorphic petrology. *Prentice Hall,* 498 pp., New Jersey.

Pimpirev C., Dimov D. & Miller H. (2000): Field studies of sedimentary sequences in eastern Hurd Peninsula, central Livingston Island, South Shetland Islands. *Polarforschung,* **66 (3)**, 1-5.

Pimpirev Ch., Dimov D., Ivanov M. & Stoykova K. (2005): New paleontological evidences for a Late Cretaceous age of the Miers Bluff Formation (Livingston Island, South Shetland Islands). *In*: Fütterer D. et al. (eds.): *Antarctic Contributions to Global Earth Science*, accepted.

Pimpirev C., Ivanov M., Dimov D. & Nikolov T. (2002): First find of the Upper Tithonian ammonite genus *Blanfordiceras* from the Miers Bluff Formation, Livingston Island, South Shetland Islands. *N. Jb. Geol. Paläont. Mh.*, **2002 (6),** 377-384, Stuttgart.

Pirrie D. (1991): Controls on the petrographic evolution of an active margin sedimentary sequence: the Larsen Basin, Antarctica. *In:* Morton A.C., Todd S.P. & Haughton P.D.W. (eds.): *Developments in Sedimentary Provenance Studies*. Geol. Soc. Spec. Publ., **57**, 231–249, London.

Plank T. & Johnson M. (1997): Experimental study of trace element partitioning in fluids and melts generated during sediment subduction. *7th Annual V.M. Goldschmidt Conference,* LPI Contribution No. 921, pdf # 2310.

Plank T. & Langmuir C.H. (1998): The chemical composition of subducting sediment and its consequences for the crust and mantle. *Chem. Geol.*, **145**, 325-394.

Plank T. & White W. (1995): Nb and Ta in arc and mid-ocean ridge basalts. *EOS, Trans. AGU*, **76**, p. 655.

Platt J.P. (1993): Mechanisms of oblique convergence. *J. Geophys. Res.,* **88**, 16239-16256.

Potts P.J. (1987): A handbook of silicate rock analysis. *Blackie,* London, 622 pp.

Robertson S.D., Wiens D.A., Shore P.J. Smith G.P. & Vera E. (2002): Seismicity and tectonics of the South Shetland Islands and Bransfield Strait from the SEPA broadband seismograph deployment. *Roy. Soc. New Zealand Bull.*, **35**, 549-554.

Rogers G., Saunders A.D., Terrell D.J., Verma S.P. & Marriner G.F. (1985): Geochemistry of Holocene volcanic rocks associated with ridge subduction in Baja California, Mexico. *Nature,* **315**, 389-392.

Rollinson H. (1993): Using geochemical data: evaluation, presentation, interpretation. *Longman Group UK Limited*, Essex, 352 pp.

Rudnick R.L. & Gao S. (2003): Composition of the continental crust. *In:* Rudnick R.L. (ed.): Treatise on geochemistry, **Vol. 3. The Crust**, Elsevier Ltd., 1-64.

Scarrow J.H., Vaughan A.P.M. & Leat P.T. (1997a): Ridge-trench collision-induced switching of arc tectonics and magma sources: clues from Antarctic Peninsula mafic dykes. *Terra Nova,* **9**, 255-259.

Scarrow J.H., Leat P.T., Wareham C.D. & Millar I.L. (1997b): Mantle sources for Cretaceous-Tertiary mafic magmatism in the Antarctic Peninsula. *In:* Ricci C.A. (ed.): The Antarctic Region: Geological evolution and processes. *Terra Antartica,* 327-332, Siena.

Scarrow J.H., Leat P.T., Wareham C.D. & Miillar I.L. (1998): Geochemistry of mafic dykes in the Antarctic Peninsula continental-margin batholith: a record of arc evolution. *Contr. Min. Petr.,* **131**, 289-305.

Schmidt W. (1932): Tektonik und Verformungslehre. *Borntraeger,* 208 pp., Berlin.

Shannon R.D. (1976): Revised effective ionic radii and systematic studies of interatomic distances in halides and chalcogenides. *Acta Crystallogr.,* **32**, 751-767.

Shiling H., Xiangshen Z., Molan E. & Birkenmajer K. (1996): $^{40}Ar/^{39}Ar$ and K-Ar datings on the volcanic rocks in northern Coast of King George Island, West Antarctica. *Kor. J. Pol. Res*., **7 (1/2)**, 11-21.

Sloan B.J., Lawver L.A. & Anderson J.B. (1995): Seismic stratigraphy of the Larsen Basin, eastern Antarctic Peninsula. *Geology and Seismic Stratigraphy of the Antarctic margin,* AGU, Ant. Res. Ser., **68**, 59-74.

Smellie J.L. (1990): Graham Land and South Shetland Islands. *In:* LeMasurier W.E. & Thomson J.W. (eds.): *Volcanoes of the Antarctic Plate and Southern Oceans.* Ant. Res. Ser., AGU, **48**, 303–312, Washington D.C.

Smellie J.L. (1991): Stratigraphy, provenance and tectonic setting of (?) Late Palaeozoic-Triassic sedimentary sequences in northern Graham Land and South Scotia Ridge. *In:* Thomson M.R.A., Crame J.A. & Thomson J.W. (eds.): *Geological evolution of Antarctica.* Cambr. Univ. Press, 411-417, New York.

Smellie J.L., Pankhurst R.J., Thomson M.R.A. & Davies R.E.S. (1984): The geology of the South Shetland Islands: VI. Stratigraphy, geochemistry and evolution. *Brit. Ant. Surv. Sci. Rep.*, **87**, 85 pp.

Smellie J.L., Liesa M., Muñoz J.A., Sábat F., Pallás R. & Willan R.C.R. (1995): Lithostratigraphy of volcanic and sedimentary sequences in central Livingston Island, South Shetland Islands. *Antarctic Science,***7 (1)**, 99-113.

Smith A. & Hallam A. (1970): The fit of the southern continents. *Nature*, **255**, 139-144.

Soliani E., Kawashita K., Fensterseifer H., Hansen M.A. & Troian F. (1988): K-Ar ages of the Winkel Point Formation (Fildes Peninsula Group) and associated intrusions, King George Island, Antarctica. *Ser. Cient. INACH*, **38**, 133-139, Santiago de Chile.

Staudigel H., Plank T., White W. & Schmincke H.-U. (1996): Geochemical fluxes during seafloor alteration of the basaltic upper oceanic crust: DSDP sites 417 and 418. *In:* Bebout G.E., Scholl D.W., Kirby S.H. & Platt J.P. (eds.): *Subduction: Top to bottom.* AGU Geophys. Monogr., **96**, 19-38.

Steiger R.H. & Jäger E. (1977): Subcomission on geochronology: convention on the use of decay constants in Geo- and Cosmochronology. *Earth Planet. Sci. Lett.,* **36**, 359-362.

Stoykova K., Pimpirev C. & Dimov D. (2002): Calcareous nannofossils from the Miers Bluff Formation (Livingston Island, South Shetland Islands, Antarctica): First evidence for a Late Cretaceous age. *J. of Nannoplankton Res.,* **24, 2**, 166-167.

Suárez M. (1976): Plate-tectonic model for southern Antarctic Peninsula and its relation to southern Andes. *Geology,* **4**, 211-214.

Sun S.-s. & McDonough W.F. (1989): Chemical and isotopic systematics of oceanic basalts: implications for mantle composition and processes. *In:* Saunders A.D. & Norry M.J. (eds.): *Magmatism in the Ocean Basins,* Geol. Soc. Spec. Pub., **42**, 313-345.

Tarney J., Weaver S.D., Saunders A.D., Pankhurst R.J. & Barker P.F. (1982): Volcanic evolution of the northern Antarctic Peninsula and the Scotia Arc. *In:* Thorpe R.S. (ed.): *Andesites*, 371-400.

Tatsumi Y. & Eggins S. (1995): Subduction zone magmatism. *Blackwell Science*, 211 pp., Massachusets.

Tatsumi Y., Hamilton D.L. & Nesbitt R.W. (1986): Chemical characteristics of fluid phase released from a subducted lithosphere and origin of arc magmas: evidence from high pressure experiments and natural rocks. *J. Volcan. Geotherm. Res.,* **29**, 293-309.

Thomson M.R.A. (1992): Stratigraphy and age of the pre-Cenozoic stratified rocks of the South Shetland Islands: review. *In:* López-Martínez J. (ed.): *Geología de la Antártida Occidental.* III. Congr. Geol. Esp. & VIII. Congr. Latinoamericano Geol. (Salamanca), **Simposium T3**, 75-92.

Thomson M.R.A., Pankhurst R.J. & Clarkson P.D. (1983): The Antarctic Peninsula - a late Mesozoic–Cenozoic arc (review). *In:* Oliver R.L., James P.R., & Jago J.B. (eds.): *Antarctic Earth Science.* Cambridge University Press, 289–294.

Tikoff B. & Teyssier C. (1994): Strain modelling of displacement-field partitioning in transpressional orogens. *J. Struct. Geol.,* **16**, 1575-1588.

Todt W., Cliff R.A., Hanser A. & Hofmann A.W. (1996): Evaluation of a ^{202}Pb-^{205}Pb double spike for high-precision lead isotope analysis. *In:* AGU: *Earth processes: Reading the isotopic code.* Geophys. Mon., **95**, 429-437.

Tokarski A.K. (1981): Structural events in the South Shetland Islands (Antarctica): I. The Polonez Cove Formation (Pliocene). *Stud. Geol. Pol.,* **72**, 89-95.

Tokarski A.K. (1984): Structural events in the South Shetland Islands (Antarctica): II. Tertiary volcanics and sediments south of Ezcurra Fault, King George Island. *Stud. Geol. Pol.,* **79**, 131-166.

Tokarski A.K. (1987): Structural events in the South Shetland Islands (Antarctica): III. Barton Horst, King George Island. *Stud. Geol. Pol.,* **90**, 7-38.

Tokarski A.K. (1988): Structural analysis of Barton Peninsula (King George Island, West Antarctica): An example of volcanic arc tectonics. *Stud. Geol. Pol.,* **95 (pt. 8)**, 53-63.

Tokarski A.K., Danowski W. & Zastawniak E. (1987): On the age of fossil flora from Barton Peninsula (King George Island, West Antarctica). *Pol. Polar Res.*, **8**, 293-302.

Tokarski A.K., Swierczewska A. & Doktor M. (1997): Miers Bluff Formation, Livingston Island (South Shetland Islands): diagenesis/metamorphism and early stage of structural development. *In:* Ricci C.A. (ed.): The Antarctic Region: Geological evolution and processes. *Terra Antartica,* 409-416, Siena.

Traill T.S. (1822): Mineralogische Notiz von und aus Neu-Süd-Shetland. *Neue allg. geogr. Ephemeriden*, **10**, Pt. 1, 99-102, Weimar.

Trouw R.A.J., Pankhurst R.J. & Kawashita K. (1990): New radiometric age data from Elephant Island, South Shetland Islands. *Zbl. Geol. Paläont.*, Pt. 1, **1990 (1/2)**, 105-118, Stuttgart.

Turner S.P. & Hawkesworth C.J. (1997): Constraints on flux rates and mantle dynamics beneath island arcs from Tonga-Kermadec lava geochemistry. *Nature*, **389**, 568-573.

Turner S.P., George R.M.M., Evans P.J., Hawkesworth C.J. & Zellmer G.F. (2000): Time-scales of magma formation, ascent and storage beneath subduction-zone volcanoes. *Phil. Trans. R. Soc. Lond. A,* **358**, 1443-1464.

Turner S.P., Hawkesworth C.J., van Calsteren P., Heath E., Macdonald R. & Black S. (1996): U-series isotopes and destructive plate margin magma genesis in the Lesser Antilles. *Earth Planet. Sci. Lett.,* **142**, **191-207.**

Turner S.P., Hawkesworth C.J., Rogers N.W., Bartlett J., Worthington T., Hergt J., Pearce J. & Smith I. (1997): ^{238}U-^{230}Th disequilibria, magma petrogenesis, and flux rates beneath the depleted Tonga-Kermadec island arc. *Geochim. et Cosmochim. Acta,* **61**, 4855-4884.

Tyrell G.W. (1921): A contribution to the petrography of the South Shetland Islands, the Palmer Archipelago, and the Danco Coast, Graham Land, Antarctica. *Trans. Roy. Soc. Edinb.,* **53**, Pt. 1, No. 4, 57-79.

Tyrell G.W. (1945): Report on rocks from West Antarctica and the Scotia Arc. *Discovery Reports,* **23**, 37-102.

Veit A. (2002): Volcanology and geochemistry of Pliocene to recent volcanics on both sides of the Bransfield Strait / West Antarctica. *AWI, Rep. on Polar and Marine Res.,* **420**, 177 pp., Bremerhaven.

Walter H.J., Hegner E., Diekmann B., Kuhn G. & Rutgers van der Loeff M.M. (2000): Provenance and transport of terrigeneous sediment in the South Atlantic Ocean and their relations to glacial and interglacial cycles: Nd and Sr isotopic evidence. *Geochim. et Cosmochim. Acta,* **64 (22)**, 3813-3827.

Watts D.R. (1982): Potassium-argon ages and palaeomagnetic results from King George Island, South Shetland Islands. *In:* Craddock C. (ed.): *Antarctic Geoscience.* Univ. Wisc. Press, 255-261, Madison, Wisconsin.

Weaver S.D., Saunders A.D., Pankhurst R.J. & Tarney J. (1979): A geochemical study of magmatism associated with the initial stages of back-arc spreading – The Quaternary volcanics of Bransfield Strait, from South Shetland Islands. *Contrib. Mineral. Petrol.,* **68**, 151-169.

Wharton M.R., Hathway B. & Colley H. (1995): Volcanism associated with extension in an Oligocene-Miocene arc, southwestern Viti Levu, Fiji. *In*: Smellie J.L. (ed.): Volcanism associated with extension at consuming plate margins. *Geol. Soc. Lon.*, 95-114.

Willan R.C.R. (1994): Structural setting and timing of hydrothermal veins and breccias on Hurd Peninsula, South Shetland Islands: a possible volcanic-related epithermal system in deformed turbidites. *Geol. Mag.,* **131**, 465-483.

Willan R.C.R. (1996): The Moores Peak Formation, a Cretaceous debris-avalanche deposit in the Antarctic Peninsula Volcanic Group, Livingston Island, South Shetland Islands. *J. South Am. Earth Sci.,* **9 (3/4)**, 251-264.

Willan R.C.R. & Armstrong D.C. (2002): Successive geothermal, volcanic-hydrothermal and contact-metasomatic events in Cenozoic volcanic-arc basalts, South Shetland Islands, Antarctica. *Geol. Mag.,* **139**, 209-231.

Willan R.C.R. & Kelley S.P. (1999): Mafic dike swarms in the South Shetland Islands volcanic arc: Unravelling multiepisodic magmatism related to subduction and continental rifting. *J. Geophys. Res.,* **104**, 23051-23068.

Wilson M. (1989): Igneous petrogenesis: a global tectonic approach. *Kluwer Acad. Pub.,* 466 pp., Dordrecht.

Winchester J.A. & Floyd P.A. (1977): Geochemical discrimination of different magma series and their differentiation products using immobile elements. *Chem. Geol.,* **20**, 325-343.

Woodhead J., Eggins S. & Gamble J. (1993): High field strength and transition element systematics in island arc and back-arc basin basalts: evidence for multiphase melt extraction and a depleted mantle wedge. *Earth Planet. Sci. Lett.,* **114**, 491-504.

Xiguang D., Xiangshen Z., Xiaohan L., Shu O. & Yanbin S. (2002): Terrestrial palynomorphs from the Miers Bluff Formation of Livingston Island, West Antarctica. *Roy. Soc. New Zeal. Bull.,* **35**, 269-273.

Zheng X., Kamenov B., Sang H. & Monchev P. (2003): New radiometric dating of the dykes from the Hurd Peninsula, Livingston Island, South Shetland Islands. *J. South Am. Earth Sci.,* **15 (2003)**, 925-934.

ab	albite
ABG	Admiralty Bay Group
AI	Alteration Index
akf	alkali-feldspar
an	anorthite
ap	apatite
AP	Antarctic Peninsula
AWI	Alfred-Wegener-Institute
cc	calcite
chl	chlorite
cpx	clinopyroxene
CSG	Cape Syrezol Group
E	east
ep	epidote
fsp	feldspar
HFSE	High Field Strength Elements
KGIS	King George Island Supergroup
KIS	Kraków Icefield Supergroup
LILE	Large Ion Lithophile Elements
Ma	million years
MBF	Miers Bluff Formation
ms	muscovite
N	north
n.d.	not determined
NE	northeast
NNW	northnorthwest
NW	northwest
opq	opaque minerals
opx	orthopyroxene
or	orthoclase
pl	plagioclase
PM	primitive mantle
px	pyroxene
qz	quartz
RT-C	ridgecrest-trench collision
S	south
S_{1d}	dextral first order shear system
S_{1s}	sinistral first order shear system
S_{2d}	dextral second order shear system
S_{2s}	sinistral second order shear system
SE	southeast
ser	sericite
SSI	South Shetland Islands
SSSI	Site of Special Scientific Interest
SW	southwest
TPG	Trinity Peninsula Group
UCC	upper continental crust
W	west or tungsten
WPG	Wegger Peak Group
WR	whole rock
zeo	zeolite
zir	zircon

Table 1

Feldspar Point	Label	SiO_2	TiO_2	Al_2O_3	Fe_2O_3	MgO	CaO	SrO	BaO	Na_2O	K_2O	Rb_2O	Sum Ox%	Si	Ti	Al/Al IV	Al VI	Fe^{3+}	Mg	Ca	Sr	Ba	Na	K	Rb	Sum Cat#	Ab	An	Or	Celsian	Rb-Feld	Sr-Feld
#1	Orthoklas_1	64,83	-	16,69	1,23	0,02	0	-	0,06	0,38	16	-	99,2	3,03	-	0,919	0	0,043	0,001	0	-	0,001	0,034	0,954	-	4,983	3,458	0,001	96,431	0,11	0	0
#2	Orthoklas_2	65,97	-	16,93	1,22	0,01	0	-	0,02	0,4	15,97	-	100,52	3,036	-	0,918	0	0,042	0,001	0	-	0	0,035	0,938	-	4,97	3,639	0,001	96,322	0,038	0	0
#3	Orthoklas_3	65,13	-	16,7	1,37	0	0,01	-	0	0,41	15,79	-	99,41	3,033	-	0,917	0	0,048	0	0	-	0	0,037	0,938	-	4,973	3,834	0,036	96,121	0,009	0	0
average		**65,31**	**-**	**16,77**	**1,2733**	**0,01**	**0,00333**	**-**	**0,02667**	**0,3967**	**15,92**	**-**	**99,71**	**3,033**	**-**	**0,918**	**0**	**0,0443**	**0,0006667**	**0**	**-**	**0,0003**	**0,0353**	**0,9433**	**-**	**4,9753333**	**3,6437**	**0,0127**	**96,291**	**0,05233**	**0**	**0**
#4	Albit_1	70,44	-	19,36	0	0	0,34	-	0	11,01	0,15	-	101,31	3,026	-	0,98	0	0	0	0,016	-	0	0,917	0,008	-	4,947	97,441	1,666	0,892	0	0	0
#5	Albit_2	70,19	-	19,2	0	0	0,25	-	0,07	10,91	0,16	-	100,78	3,03	-	0,977	0	0	0	0,012	-	0,001	0,913	0,009	-	4,942	97,648	1,259	0,958	0,135	0	0
#6	Albit_3	68,49	-	18,99	0,01	0	0,23	-	0,03	10,97	0,14	-	98,87	3,018	-	0,986	0	0	0	0,011	-	0,001	0,937	0,008	-	4,961	97,962	1,139	0,845	0,053	0	0
average		**69,707**	**-**	**19,18**	**0,0033**	**0**	**0,27333**	**-**	**0,03333**	**10,963**	**0,15**	**-**	**100,32**	**3,0247**	**-**	**0,981**	**0**	**0**	**0**	**0,013**	**-**	**0,0007**	**0,9223**	**0,0083**	**-**	**4,95**	**97,684**	**1,3547**	**0,8983**	**0,06267**	**0**	**0**
#7	HP-1A/2_I_1	65,8	-	21,05	0,18	0	2,76	-	0	10,07	0,04	-	99,89	2,896	-	1,092	0	0,006	0	0,13	-	0	0,859	0,002	-	4,985	86,665	13,121	0,206	0,008	0	0
#8	HP-1A/2_I_2	43,55	-	22,05	2,05	0,01	27,05	-	0,01	0	0	-	94,72	2,214	-	1,321	0	0,078	0,001	1,473	-	0	0	0	-	5,087	0,002	99,975	0,011	0,012	0	0
#9	HP-1A/2_I_3	54,84	-	21,02	0,96	0,16	15	-	0	5,83	0,06	-	97,86	2,582	-	1,166	0	0,034	0,011	0,757	-	0	0,532	0,004	-	5,086	41,19	58,535	0,275	0	0	0
#10	HP-1A/2_I_4	67,22	-	20,19	0,21	0	1,52	-	0,06	10,65	0,11	-	99,95	2,948	-	1,043	0	0,007	0	0,071	-	0,001	0,905	0,006	-	4,982	92,03	7,263	0,603	0,103	0	0
#11	HP-1A/2_I_5	67,82	-	20,06	0,15	0,01	1,43	-	0	10,55	0,06	-	100,08	2,963	-	1,033	0	0,005	0,001	0,067	-	0	0,894	0,004	-	4,966	92,678	6,959	0,363	0	0	0
average		**59,846**	**-**	**20,87**	**0,71**	**0,036**	**9,552**	**-**	**0,014**	**7,42**	**0,054**	**-**	**98,5**	**2,7206**	**-**	**1,131**	**0**	**0,026**	**0,0026**	**0,4996**	**-**	**0,0002**	**0,638**	**0,0032**	**-**	**5,0212**	**62,513**	**37,171**	**0,2916**	**0,0246**	**0**	**0**
#12	HP-1A/2_II_1	66,78	-	20,47	0,27	0	2,26	-	0,03	9,75	0,04	-	99,6	2,936	-	1,061	0	0,009	0	0,106	-	0	0,831	0,003	-	4,946	88,368	11,314	0,268	0,05	0	0
#13	HP-1A/2_II_2	66,74	-	20,33	0,21	0	2,04	-	0	9,84	0,07	-	99,23	2,943	-	1,056	0	0,007	0	0,096	-	0	0,841	0,004	-	4,948	89,34	10,249	0,411	0	0	0
#14	HP-1A/2_II_3	67,23	-	19,86	0,17	0	1,46	-	0	10,23	0,05	-	99	2,967	-	1,033	0	0,006	0	0,069	-	0	0,875	0,003	-	4,953	92,426	7,301	0,273	0	0	0
#15	HP-1A/2_II_4	67,77	-	20,29	0,21	0	1,76	-	0,04	10,35	0,05	-	100,47	2,953	-	1,042	0	0,007	0	0,082	-	0,001	0,874	0,003	-	4,961	91,075	8,567	0,285	0,073	0	0
#16	HP-1A/2_II_5	66,27	-	19,88	0,14	0	1,94	-	0	9,81	0,07	-	98,12	2,954	-	1,044	0	0,005	0	0,093	-	0	0,848	0,004	-	4,948	89,756	9,794	0,45	0	0	0
average		**66,958**	**-**	**20,17**	**0,2**	**0**	**1,892**	**-**	**0,014**	**9,996**	**0,056**	**-**	**99,284**	**2,9506**	**-**	**1,0472**	**0**	**0,0068**	**0**	**0,0892**	**-**	**0,0002**	**0,8538**	**0,0034**	**-**	**4,9512**	**90,193**	**9,445**	**0,3374**	**0,0246**	**0**	**0**
#17	HP-1A/2_III_1	42,16	-	21,65	1,89	0	27,08	-	0	0,08	0,01	-	92,88	2,193	-	1,327	0	0,074	0	1,509	-	0	0,008	0,001	-	5,111	0,54	99,425	0,035	0	0	0
#18	HP-1A/2_III_2	69,7	-	19,5	0,12	0	1,38	-	0	12,3	0,06	-	103,06	2,975	-	0,981	0	0,004	0	0,063	-	0	1,018	0,003	-	5,044	93,895	5,814	0,29	0	0	0
#19	HP-1A/2_III_3	65,53	-	20,4	0,19	0	1,47	-	0	10,34	0,04	-	97,96	2,929	-	1,075	0	0,006	0	0,071	-	0	0,896	0,002	-	4,979	92,5	7,28	0,22	0	0	0
#20	HP-1A/2_III_4	66,71	-	20,15	0,23	0	1,81	-	0	10,11	0,03	-	99,05	2,947	-	1,049	0	0,008	0	0,086	-	0	0,866	0,002	-	4,958	90,826	8,968	0,206	0	0	0
#21	HP-1A/2_III_5	68	-	19,72	0,27	0	1,24	-	0,04	10,45	0,08	-	99,81	2,978	-	1,018	0	0,009	0	0,058	-	0,001	0,887	0,004	-	4,955	93,336	6,14	0,45	0,074	0	0
average		**62,42**	**-**	**20,28**	**0,54**	**0**	**6,596**	**-**	**0,008**	**8,656**	**0,044**	**-**	**98,552**	**2,8044**	**-**	**1,09**	**0**	**0,0202**	**0**	**0,3574**	**-**	**0,0002**	**0,735**	**0,0024**	**-**	**5,0094**	**74,219**	**25,525**	**0,2402**	**0,0148**	**0**	**0**
#10	HP-7A/I_3	70,16	-	18,28	0,08	0,01	0,69	-	0	11,92	0,13	-	101,26	3,032	-	0,931	0	0,003	0	0,032	-	0	0,998	0,007	-	5,004	96,25	3,071	0,678	0	0	0
#19	HP-7A/III_2	47	-	25,26	1,04	1,08	3,31	-	0,1	2,25	5,92	-	85,97	2,49	-	1,578	0	0,042	0,085	0,188	-	0,002	0,231	0,4	-	5,016	28,14	22,878	48,718	0,264	0	0
#38	HP-7D/I_1	67,46	-	19	0	0	0,57	-	0	10,56	0,07	-	97,66	3,008	-	0,999	0	0	0	0,027	-	0	0,913	0,004	-	4,951	96,673	2,875	0,452	0	0	0
#39	HP-7D/I_2	68,32	-	18,46	0,06	0	0,41	-	0	11,17	0,02	-	98,43	3,026	-	0,963	0	0,002	0	0,019	-	0	0,959	0,001	-	4,971	97,917	1,979	0,103	0	0	0
#41	HP-7D/I_4	68,94	-	18,51	0	0	0,4	-	0	10,67	0,11	-	98,63	3,039	-	0,962	0	0	0	0,019	-	0	0,912	0,006	-	4,939	97,348	2,001	0,65	0	0	0
#42	HP-7D/I_5	67,23	-	18,68	0	0	0,42	-	0,03	10,5	0,11	-	96,97	3,018	-	0,988	0	0	0	0,02	-	0	0,914	0,006	-	4,948	97,13	2,16	0,659	0,051	0	0
average		**67,988**	**-**	**18,66**	**0,015**	**0**	**0,45**	**-**	**0,0075**	**10,725**	**0,0775**	**-**	**97,9225**	**3,0228**	**-**	**0,978**	**0**	**0,0005**	**0**	**0,0213**	**-**	**0**	**0,9245**	**0,0043**	**-**	**4,95225**	**97,267**	**2,2538**	**0,466**	**0,01275**	**0**	**0**
#43	HP-7D/II_1	64,4	-	17,13	0	0,01	0	-	0,08	0,26	15,56	-	97,44	3,043	-	0,954	0	0	0,001	0	-	0,001	0,024	0,938	-	4,961	2,518	0,001	97,332	0,149	0	0
#45	HP-7D/II_3	64,8	-	16,88	0,06	0,02	0	-	0,14	0,24	15,41	-	97,54	3,056	-	0,938	0	0,002	0,001	0	-	0,003	0,022	0,927	-	4,948	2,278	0,001	97,442	0,279	0	0
#46	HP-7D/II_4	65,32	-	16,68	0,06	0	0	-	0,07	0,28	15,66	-	98,07	3,065	-	0,922	0	0,002	0	0	-	0,001	0,025	0,938	-	4,954	2,612	0,001	97,261	0,126	0	0
#47	HP-7D/II_5	63,81	-	17,13	0,19	0	0	-	0,09	0,28	15,3	-	96,81	3,035	-	0,96	0	0,007	0	0	-	0,002	0,026	0,928	-	4,958	2,731	0,001	97,099	0,169	0	0
average		**64,583**	**-**	**16,96**	**0,0775**	**0,0075**	**0**	**-**	**0,095**	**0,265**	**15,483**	**-**	**97,465**	**3,0498**	**-**	**0,9435**	**0**	**0,0028**	**0,0005**	**0**	**-**	**0,0018**	**0,0243**	**0,9328**	**-**	**4,95525**	**2,5348**	**0,001**	**97,284**	**0,18075**	**0**	**0**
#51	HP-7D/III_4	70,89	-	11,76	0,17	0	0,03	-	0,52	0,19	10,86	-	94,41	3,334	-	0,652	0	0,006	0	0,001	-	0,01	0,017	0,652	-	4,671	2,519	0,216	95,867	1,398	0	0
#52	HP-7D/III_5	79,54	-	8,03	0,29	0,01	0,06	-	0,32	0,08	7,16	-	95,49	3,566	-	0,424	0	0,01	0,001	0,003	-	0,006	0,007	0,41	-	4,426	1,665	0,624	96,389	1,322	0	0
average		**75,215**	**-**	**9,895**	**0,23**	**0,005**	**0,045**	**-**	**0,42**	**0,135**	**9,01**	**-**	**94,95**	**3,45**	**-**	**0,538**	**0**	**0,008**	**0,0005**	**0,002**	**-**	**0,008**	**0,012**	**0,531**	**-**	**4,5485**	**2,092**	**0,42**	**96,128**	**1,36**	**0**	**0**
#55	HP-7D/IV_3	65,77	-	15,8	0,81	0,47	0,02	-	0,15	0,14	10,19	-	93,35	3,135	-	0,888	0	0,029	0,033	0,001	-	0,003	0,013	0,62	-	4,722	2,002	0,177	97,366	0,455	0	0
#57	HP-7D/IV_5	82,07	-	11,08	1,13	0,44	0,05	-	0,1	0,1	5,17	-	100,15	3,471	-	0,552	0	0,036	0,028	0,002	-	0,002	0,008	0,279	-	4,378	2,9	0,841	95,715	0,544	0	0
average		**73,92**	**-**	**13,44**	**0,97**	**0,455**	**0,035**	**-**	**0,125**	**0,12**	**7,68**	**-**	**96,75**	**3,303**	**-**	**0,72**	**0**	**0,0325**	**0,0305**	**0,0015**	**-**	**0,0025**	**0,0105**	**0,4495**	**-**	**4,55**	**2,451**	**0,509**	**96,541**	**0,4995**	**0**	**0**
#59	HP-7D/V_2	64,2	-	17,14	0,1	0,01	0	-	0,51	0,17	15,63	-	97,77	3,036	-	0,955	0	0,004	0	0	-	0,009	0,016	0,943	-	4,964	1,62	0,001	97,401	0,978	0	0
#62	HP-7D/V_5	61,32	-	17,78	0,1	0,01	0	-	0,48	1,43	14,34	-	95,46	2,975	-	1,016	0	0,004	0,001	0	-	0,009	0,134	0,888	-	5,026	13,008	0,001	86,105	0,887	0	0
average		**62,76**	**-**	**17,46**	**0,1**	**0,01**	**0**	**-**	**0,495**	**0,8**	**14,985**	**-**	**96,615**	**3,0055**	**-**	**0,9855**	**0**	**0,004**	**0,0005**	**0**	**-**	**0,009**	**0,075**	**0,9155**	**-**	**4,995**	**7,314**	**0,001**	**91,753**	**0,9325**	**0**	**0**
#52	HP-7J/I_1	66,23	-	18,92	0,39	0	0,4	-	0,05	11,21	0,04	-	97,24	2,982	-	1,004	0	0,013	0	0,019	-	0,001	0,979	0,002	-	5	97,757	1,917	0,234	0,092	0	0
#53	HP-7J/I_2	69,25	-	18,31	0,16	0	0,18	-	0,07	10,54	0,05	-	98,55	3,052	-	0,951	0	0,005	0	0,009	-	0,001	0,9	0,003	-	4,921	98,64	0,948	0,283	0,129	0	0
#54	HP-7J/I_3	68,75	-	18,76	0,3	0	0,18	-	0	10,63	0,18	-	98,8	3,028	-	0,974	0	0,01	0	0,008	-	0	0,908	0,01	-	4,939	97,988	0,898	1,105	0,008	0	0
#55	HP-7J/I_4	66,58	-	20,01	0,67	0,11	0,16	-	0	9,27	1,81	-	98,61	2,963	-	1,049	0	0,022	0,008	0,008	-	0	0,8	0,103	-	4,952	87,844	0,842	11,314	0	0	0
#56	HP-7J/I_5	69,64	-	17,94	0,25	0,02	0,13	-	0	10,85	0,06	-	98,89	3,061	-	0,929	0	0,008	0,001	0,006	-	0	0,925	0,003	-	4,934	98,977	0,669	0,353	0	0	0
average		**68,09**	**-**	**18,79**	**0,354**	**0,026**	**0,21**	**-**	**0,024**	**10,5**	**0,428**	**-**	**98,418**	**3,0172**	**-**	**0,9814**	**0**	**0,0116**	**0,0018**	**0,01**	**-**	**0,0004**	**0,9024**	**0,0242**	**-**	**4,9492**	**96,241**	**1,0548**	**2,6578**	**0,0458**	**0**	**0**
#57	HP-7J/II_1	69,2	-	19,2	0,29	0,01	0,3	-	0	11,23	0,07	-	100,3	3,01	-	0,984	0	0,009	0,001	0,014	-	0	0,947	0,004	-	4,969	98,143	1,435	0,421	0	0	0
#58	HP-7J/II_2	69,27	-	18,7	0,22	0	0,14	-	0,03	11,34	0,05	-	99,73	3,028	-	0,963	0	0,007	0	0,006	-	0	0,961	0,003	-	4,969	99,028	0,655	0,269	0,048	0	0
#59	HP-7J/II_3	68,52	-	18,6	0,18	0	0,12	-	0,05	11,71	0,02	-	99,21	3,018	-	0,966	0	0,006	0	0,006	-	0,001	1	0,001	-	4,997	99,226	0,575	0,109	0,089	0	0
#60	HP-7J/II_4	68,07	-	18,68	0,17	0	0,13	-	0	11,17	0,03	-	98,25	3,019	-	0,977	0	0,006	0	0,006	-	0	0,961	0,002	-	4,971	99,169	0,627	0,204	0	0	0
#61	HP-7J/II_5	67,82	-	18,58	0,25	0	0,07	-	0,03	11,21	0,02	-	97,99	3,019	-	0,974	0	0,009	0	0,003	-	0,001	0,967	0,001	-	4,974	99,435	0,36	0,144	0,061	0	0
average		**68,576**	**-**	**18,75**	**0,222**	**0,002**	**0,152**	**-**	**0,022**	**11,332**	**0,038**	**-**	**99,096**	**3,0188**	**-**	**0,9728**	**0**	**0,0074**	**0,0002**	**0,007**	**-**	**0,0004**	**0,9672**	**0,0022**	**-**	**4,976**	**99**	**0,7304**	**0,2294**	**0,0396**	**0**	**0**
#62	HP-7J/III_1	67,84	-	18,86	0,18	0	0,26	-	0	11,48	0,06	-	98,69	3,004	-	0,984	0	0,006	0	0,012	-	0	0,985	0,004	-	4,995	98,409	1,23	0,36	0	0	0
#63	HP-7J/III_2	67	-	18,95	0,16	0	0,21	-	0,08	11,11	0,04	-	97,56	2,999	-	1	0	0,006	0	0,01	-	0,001	0,964	0,002	-	4,982	98,575	1,048	0,238	0,138	0	0
#64	HP-7J/III_3	67,31	-	18,69	0,13	0	0,08	-	0	10,84	0,04	-	97,1	3,018	-	0,988	0	0,004	0	0,004	-	0	0,942	0,002	-	4,958	99,327	0,426	0,247	0	0	0
#65	HP-7J/III_4	59,83	-	16,85	0,26	0,01	3,09	-	0	8,39	0,1	-	88,53	2,968	-	0,985	0	0,01	0,001	0,164	-	0	0,807	0,006	-	4,942	82,559	16,778	0,663	0	0	0
#66	HP-7J/III_5	65,91	-	18,97	0,17	0,01	0,13	-	0	11,32	0,03	-	96,55	2,984	-	1,012	0	0,006	0,001	0,006	-	0	0,994	0,002	-	5,005	99,19	0,628	0,182	0	0	0
average		**65,578**	**-**	**18,46**	**0,18**	**0,004**	**0,754**	**-**	**0,016**	**10,628**	**0,054**	**-**	**95,686**	**2,9946**	**-**	**0,9938**	**0**	**0,0064**	**0,0004**	**0,0392**	**-**	**0,0002**	**0,9384**	**0,0032**	**-**	**4,9764**	**95,612**	**4,022**	**0,338**	**0,0276**	**0**	**0**

Feldspar Point	Label	SiO_2	TiO_2	Al_2O_3	Fe_2O_3	MgO	CaO	SrO	BaO	Na_2O	K_2O	Rb_2O	Sum Ox%	Si	Ti	Al/Al IV	Al VI	Fe^{3+}	Mg	Ca	Sr	Ba	Na	K	Rb	Sum Cat#	Ab	An	Or	Celsian	Rb-Feld	Sr-Feld
#1	Orthoklas_1	57,75	-	16,95	1,3	0,02	0	-	0,07	0,39	16,14	-	92,61	2,93	-	1,013	0	0,05	0,002	0	-	0,001	0,038	1,044	-	5,079	3,542	0,005	96,323	0,129	0	0
#2	Orthoklas_2	63,91	-	17,02	1,26	0,03	0	-	0,02	0,38	12,83	-	95,45	3,045	-	0,955	0	0,045	0,002	0	-	0	0,035	0,78	-	4,863	4,346	0,001	95,601	0,052	0	0
#3	Orthoklas_3	66,79	-	17,58	1,51	0	0	-	0,03	0,28	9,34	-	95,54	3,095	-	0,96	0	0,053	0	0	-	0,001	0,026	0,552	-	4,687	4,423	0,017	95,46	0,1	0	0
average		**62,8167**	**-**	**17,18333**	**1,356667**	**0,016667**	**0**	**-**	**0,04**	**0,35**	**12,77**	**-**	**94,533333**	**3,0233**	**-**	**0,976**	**0**	**0,0493333**	**0,00133**	**0**	**-**	**0,00067**	**0,033**	**0,792**	**-**	**4,8763333**	**4,10367**	**0,00767**	**95,7947**	**0,09367**	**0**	**0**
#4	Albit_1	72,18	-	19,73	0	0	0,2	-	0	4,28	0,12	-	96,52	3,144	-	1,013	0	0	0	0,009	-	0	0,362	0,007	-	4,534	95,739	2,472	1,788	0,001	0	0
#5	Albit_2	69,21	-	19,32	0,01	0	0,11	-	0,08	11,38	0,14	-	100,24	3,012	-	0,991	0	0	0	0,005	-	0,001	0,96	0,008	-	4,977	98,556	0,522	0,787	0,135	0	0
#6	Albit_3	68,98	-	19,31	0,06	0	0,09	-	0,02	11,05	0,14	-	99,65	3,014	-	0,994	0	0,002	0	0,004	-	0	0,936	0,008	-	4,959	98,724	0,436	0,807	0,033	0	0
average		**70,1233**	**-**	**19,45333**	**0,023333**	**0**	**0,13333**	**-**	**0,03333**	**8,903333**	**0,13333**	**-**	**98,803333**	**3,0567**	**-**	**0,99933**	**0**	**0,0006667**	**0**	**0,006**	**-**	**0,00033**	**0,7527**	**0,0077**	**-**	**4,8233333**	**97,673**	**1,14333**	**1,12733**	**0,05633**	**0**	**0**
#22	HP-10A/I_1	56,39	-	20,66	8,45	3,3	1,87	-	0,06	6,15	1,88	-	98,76	2,609	-	1,126	0	0,294	0,228	0,093	-	0,001	0,552	0,111	-	5,013	72,947	12,229	14,67	0,155	0	0
#23	HP-10A/I_2	63,52	-	21,29	0,59	0,18	2,15	-	0	8,29	1,56	-	97,58	2,872	-	1,134	0	0,02	0,012	0,104	-	0	0,727	0,09	-	4,959	78,925	11,332	9,743	0	0	0
#24	HP-10A/I_3	66,5	-	19,8	0,26	0	1,34	-	0,05	8,97	2,2	-	99,12	2,958	-	1,038	0	0,009	0	0,064	-	0,001	0,774	0,125	-	4,968	80,361	6,608	12,937	0,094	0	0
#26	HP-10A/I_5	67,97	-	19,79	0,36	0,01	0,99	-	0,05	10,75	0,21	-	100,12	2,972	-	1,02	0	0,012	0	0,046	-	0,001	0,911	0,011	-	4,974	93,96	4,761	1,184	0,096	0	0
average		**63,595**	**-**	**20,385**	**2,415**	**0,8725**	**1,5875**	**-**	**0,04**	**8,54**	**1,4625**	**-**	**98,895**	**2,8528**	**-**	**1,0795**	**0**	**0,08375**	**0,06**	**0,0768**	**-**	**0,00075**	**0,741**	**0,0843**	**-**	**4,9785**	**81,5483**	**8,7325**	**9,6335**	**0,08625**	**0**	**0**
#27	HP-10A/II_1	65,13	-	18,74	0	0	0,25	-	0,49	4,38	10,11	-	99,11	2,985	-	1,012	0	0	0	0,012	-	0,009	0,39	0,591	-	4,999	38,896	1,23	58,99	0,884	0	0
#28	HP-10A/II_2	65,23	-	18,52	0,04	0,01	0,29	-	0,18	3,89	10,34	-	98,5	2,999	-	1,003	0	0,002	0	0,014	-	0,003	0,347	0,606	-	4,975	35,752	1,453	62,462	0,333	0	0
#29	HP-10A/II_3	65,74	-	17,55	0,07	0	0	-	0,4	0,28	15,94	-	99,97	3,037	-	0,955	0	0,002	0	0	-	0,007	0,025	0,939	-	4,966	2,581	0,001	96,671	0,747	0	0
#30	HP-10A/II_4	64,01	-	17,87	0	0,01	0	-	0,68	0,28	15,93	-	98,78	3,006	-	0,989	0	0	0,001	0	-	0,013	0,026	0,954	-	4,989	2,571	0,001	96,161	1,267	0	0
#31	HP-10A/II_5	64,83	-	18,44	0,26	0,02	0,25	-	0,45	2,98	12,06	-	99,29	2,988	-	1,001	0	0,009	0,001	0,013	-	0,008	0,266	0,709	-	4,995	26,752	1,262	71,174	0,812	0	0
average		**64,988**	**-**	**18,224**	**0,074**	**0,008**	**0,158**	**-**	**0,44**	**2,362**	**12,876**	**-**	**99,13**	**3,003**	**-**	**0,992**	**0**	**0,0026**	**0,0004**	**0,0078**	**-**	**0,008**	**0,2108**	**0,7598**	**-**	**4,9848**	**21,3104**	**0,7894**	**77,0916**	**0,8086**	**0**	**0**
#32	HP-10A/III_1	65,85	-	17,33	0	0	0	-	0,37	0,37	15,6	-	99,53	3,049	-	0,946	0	0	0	0	-	0,007	0,034	0,921	-	4,956	3,492	0,001	95,811	0,697	0	0
#33	HP-10A/III_2	63,23	-	17,25	0,05	0,02	0	-	0,92	0,31	15,89	-	97,67	3,014	-	0,969	0	0,002	0,002	0	-	0,017	0,029	0,966	-	4,998	2,852	0,001	95,454	1,693	0	0
#34	HP-10A/III_3	63,79	-	16,84	0,06	0	0	-	0,51	0,26	16,27	-	97,73	3,033	-	0,944	0	0,002	0	0	-	0,01	0,024	0,987	-	4,999	2,337	0,001	96,723	0,94	0	0
#35	HP-10A/III_4	62,66	-	18,05	0,02	0	0	-	0,31	0,35	15,94	-	97,34	2,986	-	1,014	0	0,001	0	0	-	0,006	0,032	0,969	-	5,007	3,205	0,001	96,224	0,571	0	0
#36	HP-10A/III_5	62,12	-	17,82	0,06	0	0	-	0,74	0,35	16,06	-	97,14	2,981	-	1,008	0	0,002	0	0	-	0,014	0,032	0,983	-	5,021	3,149	0,001	95,498	1,352	0	0
average		**63,53**	**-**	**17,458**	**0,038**	**0,004**	**0**	**-**	**0,57**	**0,328**	**15,952**	**-**	**97,882**	**3,0126**	**-**	**0,9762**	**0**	**0,0014**	**0,0004**	**0**	**-**	**0,0108**	**0,0302**	**0,9652**	**-**	**4,9962**	**3,007**	**0,001**	**95,942**	**1,0506**	**0**	**0**
#57	HP-23/2_I_1	53,1	-	27,48	0,45	0,04	11,6	-	0,03	4,73	0,19	-	97,61	2,463	-	1,502	0	0,016	0,003	0,576	-	0	0,425	0,011	-	4,997	41,954	56,889	1,109	0,049	0	0
#58	HP-23/2_I_2	64,25	-	21,33	0,09	0,02	3,13	-	0,03	9,66	0,02	-	98,53	2,87	-	1,123	0	0,003	0,002	0,15	-	0	0,836	0,001	-	4,986	84,645	15,185	0,122	0,048	0	0
#59	HP-23/2_I_3	64,9	-	21,34	0,03	0	2,47	-	0	9,59	0,02	-	98,35	2,892	-	1,121	0	0,001	0	0,118	-	0	0,829	0,001	-	4,962	87,436	12,447	0,117	0	0	0
#60	HP-23/2_I_4	64,24	-	20,12	0,01	0,02	1,77	-	0,01	9,95	0,04	-	96,15	2,926	-	1,08	0	0	0,001	0,087	-	0	0,879	0,002	-	4,975	90,822	8,941	0,224	0,013	0	0
#61	HP-23/2_I_5	64,39	-	20,78	0	0	2,22	-	0	10,08	0,05	-	97,52	2,899	-	1,103	0	0	0	0,107	-	0	0,879	0,003	-	4,991	88,912	10,809	0,275	0,004	0	0
average		**62,176**	**-**	**22,21**	**0,116**	**0,016**	**4,238**	**-**	**0,014**	**8,802**	**0,064**	**-**	**97,632**	**2,81**	**-**	**1,1858**	**0**	**0,004**	**0,0012**	**0,2076**	**-**	**0**	**0,7696**	**0,0036**	**-**	**4,9822**	**78,7538**	**20,8542**	**0,3694**	**0,0228**	**0**	**0**
#62	HP-23/2_II_1	67,02	-	19,71	0,12	0	1,01	-	0,03	11,13	0,19	-	99,2	2,962	-	1,026	0	0,004	0	0,048	-	0,001	0,954	0,011	-	5,005	94,182	4,715	1,049	0,054	0	0
#63	HP-23/2_II_2	65,55	-	20,08	0,02	0	1,5	-	0,03	10,67	0,07	-	97,91	2,936	-	1,06	0	0,001	0	0,072	-	0	0,926	0,004	-	4,999	92,412	7,168	0,372	0,048	0	0
#64	HP-23/2_II_3	62,86	-	21,07	0,02	0	2,69	-	0,02	10,17	0,03	-	96,87	2,861	-	1,13	0	0,001	0	0,131	-	0	0,897	0,002	-	5,023	87,043	12,723	0,191	0,043	0	0
#65	HP-23/2_II_4	40,06	-	23,21	4,07	2,1	20,39	-	0,03	1,12	0,03	-	91	2,111	-	1,441	0	0,162	0,165	1,151	-	0,001	0,114	0,002	-	5,146	8,996	90,816	0,136	0,052	0	0
#66	HP-23/2_II_5	50,59	-	29,41	0,7	0,04	14,03	-	0,03	3,68	0,11	-	98,58	2,343	-	1,606	0	0,024	0,003	0,696	-	0,001	0,331	0,006	-	5,01	31,993	67,344	0,612	0,052	0	0
average		**57,216**	**-**	**22,696**	**0,986**	**0,428**	**7,924**	**-**	**0,028**	**7,354**	**0,086**	**-**	**96,712**	**2,6426**	**-**	**1,2526**	**0**	**0,0384**	**0,0336**	**0,4196**	**-**	**0,0006**	**0,6444**	**0,005**	**-**	**5,0366**	**62,9252**	**36,5532**	**0,472**	**0,0498**	**0**	**0**
#67	HP-23/2_III_1	69,29	-	19,87	0,04	0,01	1,21	-	0,04	10,89	0,11	-	101,46	2,985	-	1,009	0	0,001	0	0,056	-	0,001	0,91	0,006	-	4,968	93,572	5,756	0,609	0,063	0	0
#68	HP-23/2_III_2	69,29	-	19,38	0	0,01	0,98	-	0	10,98	0,11	-	100,76	3,002	-	0,99	0	0	0	0,045	-	0	0,923	0,006	-	4,967	94,71	4,658	0,631	0	0	0
#69	HP-23/2_III_3	68,34	-	19,37	0,02	0,01	0,69	-	0,01	10,93	0,08	-	99,45	2,998	-	1,002	0	0,001	0	0,032	-	0	0,93	0,005	-	4,968	96,172	3,348	0,468	0,012	0	0
#70	HP-23/2_III_4	70,14	-	19,82	0,06	0,02	1,1	-	0,03	11,31	0,06	-	102,54	2,991	-	0,996	0	0,002	0,001	0,05	-	0	0,935	0,003	-	4,979	94,56	5,062	0,332	0,046	0	0
#71	HP-23/2_III_5	69,53	-	19,26	0,05	0	0,83	-	0	10,72	0,08	-	100,48	3,015	-	0,984	0	0,002	0	0,039	-	0	0,901	0,005	-	4,945	95,416	4,096	0,488	0	0	0
average		**69,318**	**-**	**19,54**	**0,034**	**0,01**	**0,962**	**-**	**0,016**	**10,966**	**0,088**	**-**	**100,938**	**2,9982**	**-**	**0,9962**	**0**	**0,0012**	**0,0002**	**0,0444**	**-**	**0,0002**	**0,9198**	**0,005**	**-**	**4,9654**	**94,886**	**4,584**	**0,5056**	**0,0242**	**0**	**0**

Feldspar																														
Point	Label	SiO_2	TiO_2	Al_2O_3	Fe_2O_3	MgO	CaO	SrO	BaO	Na_2O	K_2O	Rb_2O	Sum Ox%	Si	Ti	Al/Al IV	Al VI	Fe^{2+}	Mg	Ca	Sr	Ba	Na	K	Rb	Sum Cat#	Ab	An	Or	Celsian	Rb-Feld	Sr-Feld
#37	HP-26/2B_I_1	66,24	-	18,67	0,36	0,01	0,38	-	0	11,19	0,06	-	96,9	2,991	-	0,993	0	0,012	0,001	0,018	-	0	0,98	0,003	-	4,998	97,834	1,823	0,343	0	0	0
#38	HP-26/2B_I_2	66,27	-	18,66	0,03	0	0,26	-	0,02	10,34	0,02	-	95,6	3,014	-	1	0	0,001	0	0,013	-	0	0,912	0,001	-	4,942	98,465	1,377	0,128	0,031	0	0
#39	HP-26/2B_I_3	57,76	-	21,07	0,09	0,03	0,27	-	0,05	7,12	2,8	-	89,19	2,854	-	1,227	0	0,003	0,002	0,014	-	0,001	0,682	0,177	-	4,961	78,046	1,63	20,218	0,106	0	0
#40	HP-26/2B_I_4	65,82	-	19,14	0	0	0,36	-	0,02	9,88	0,3	-	95,51	2,998	-	1,027	0	0	0	0,018	-	0	0,872	0,017	-	4,933	96,111	1,94	1,918	0,031	0	0
#41	HP-26/2B_I_5	66,99	-	18,61	0,08	0,02	0,18	-	0	10,87	0,02	-	96,77	3,015	-	0,987	0	0,003	0,001	0,009	-	0	0,949	0,001	-	4,965	99,005	0,898	0,097	0	0	0
average		**64,62**	**-**	**19,23**	**0,112**	**0,012**	**0,29**	**-**	**0,018**	**9,88**	**0,64**	**-**	**94,794**	**2,974**	**-**	**1,0468**	**0**	**0,0038**	**0,0008**	**0,0144**	**-**	**0,0002**	**0,879**	**0,0398**	**-**	**4,9598**	**93,892**	**1,5336**	**4,5408**	**0,0336**	**0**	**0**
#42	HP-26/2B_II_1	65,8	-	18,53	0,05	0	0,48	-	0	10,24	0,01	-	95,1	3,011	-	0,999	0	0,002	0	0,024	-	0	0,908	0	-	4,943	97,43	2,527	0,043	0	0	0
#43	HP-26/2B_II_2	66,32	-	19,09	0	0	0,35	-	0,04	10,48	0,05	-	96,34	2,998	-	1,017	0	0	0	0,017	-	0,001	0,919	0,003	-	4,954	97,801	1,814	0,303	0,081	0	0
#44	HP-26/2B_II_3	69,7	-	17,87	0,01	0	0,36	-	0,05	12,28	0,04	-	100,3	3,041	-	0,919	0	0	0	0,017	-	0,001	1,039	0,002	-	5,019	98,118	1,576	0,233	0,073	0	0
#45	HP-26/2B_II_4	65,48	-	19,01	0,03	0,01	0,19	-	0	10,03	0,57	-	95,33	2,995	-	1,025	0	0,001	0,001	0,009	-	0	0,89	0,033	-	4,953	95,444	1,017	3,539	0	0	0
#46	HP-26/2B_II_5	67,73	-	18,86	0,07	0	0,45	-	0	10,83	0,04	-	97,98	3,012	-	0,989	0	0,002	0	0,022	-	0	0,934	0,002	-	4,961	97,521	2,257	0,222	0	0	0
average		**67,01**	**-**	**18,67**	**0,032**	**0,002**	**0,366**	**-**	**0,018**	**10,77**	**0,14**	**-**	**97,01**	**3,011**	**-**	**0,9898**	**0**	**0,001**	**0,0002**	**0,0178**	**-**	**0,0004**	**0,938**	**0,008**	**-**	**4,966**	**97,263**	**1,8382**	**0,868**	**0,0308**	**0**	**0**
#47	HP-26/2B_III_1	74,26	-	17,46	0,09	0	0,25	-	0	9,75	0,05	-	101,86	3,139	-	0,87	0	0,003	0	0,011	-	0	0,799	0,003	-	4,825	98,258	1,403	0,339	0	0	0
#48	HP-26/2B_III_2	68,14	-	19,37	0,01	0,01	0,19	-	0,02	10,86	0,04	-	98,64	3,007	-	1,007	0	0	0	0,009	-	0	0,929	0,002	-	4,955	98,763	0,931	0,26	0,046	0	0
#49	HP-26/2B_III_3	64,61	-	18,51	0	0	0,17	-	0	10,87	0,02	-	94,19	2,993	-	1,011	0	0	0	0,009	-	0	0,976	0,001	-	4,99	99	0,873	0,128	0	0	0
#50	HP-26/2B_III_4	64,73	-	18,24	0,02	0	0,12	-	0,02	10,57	0,04	-	93,74	3,008	-	0,999	0	0,001	0	0,006	-	0	0,953	0,003	-	4,97	99,079	0,615	0,268	0,039	0	0
#51	HP-26/2B_III_5	65,78	-	18,68	0,01	0	0,18	-	0	11,06	0,05	-	95,77	2,998	-	1,003	0	0	0	0,009	-	0	0,977	0,003	-	4,99	98,863	0,871	0,265	0	0	0
average		**67,5**	**-**	**18,45**	**0,026**	**0,002**	**0,182**	**-**	**0,008**	**10,62**	**0,04**	**-**	**96,84**	**3,029**	**-**	**0,978**	**0**	**0,0008**	**0**	**0,0088**	**-**	**0**	**0,9268**	**0,0024**	**-**	**4,946**	**98,793**	**0,9386**	**0,252**	**0,017**	**0**	**0**
#23	HP-33/3_I_1	57,11	-	22,84	1,4	0,48	0,09	-	0,04	5,7	5,1	-	92,77	2,756	-	1,299	0	0,051	0,035	0,005	-	0,001	0,533	0,314	-	4,993	62,543	0,555	36,807	0,095	0	0
#24	HP-33/3_I_2	67,83	-	18,72	0,14	0,01	0,42	-	0	11,02	0,07	-	98,21	3,013	-	0,98	0	0,005	0,001	0,02	-	0	0,949	0,004	-	4,971	97,545	2,032	0,422	0	0	0
#25	HP-33/3_I_3	58,4	-	21,09	1,26	0,53	0,24	-	0,09	5,87	4,34	-	91,82	2,831	-	1,205	0	0,046	0,038	0,012	-	0,002	0,552	0,268	-	4,954	66,156	1,485	32,158	0,201	0	0
#26	HP-33/3_I_4	67,75	-	19,86	0,56	0,12	0,73	-	0,03	10,79	1,12	-	100,95	2,956	-	1,021	0	0,018	0,008	0,034	-	0,001	0,912	0,062	-	5,012	90,405	3,388	6,153	0,054	0	0
#27	HP-33/3_I_5	67,03	-	18,91	0,4	0,05	0,9	-	0,01	9,97	0,35	-	97,62	2,998	-	0,997	0	0,013	0,003	0,043	-	0	0,864	0,02	-	4,939	93,158	4,644	2,172	0,026	0	0
average		**63,62**	**-**	**20,28**	**0,752**	**0,238**	**0,476**	**-**	**0,034**	**8,67**	**2,2**	**-**	**96,274**	**2,911**	**-**	**1,1004**	**0**	**0,0266**	**0,017**	**0,0228**	**-**	**0,0008**	**0,762**	**0,1336**	**-**	**4,9738**	**81,961**	**2,4208**	**15,542**	**0,0752**	**0**	**0**
#33	HP-33/3_III_1	67,37	-	18,92	0,29	0	0,53	-	0,03	10,77	0,07	-	97,98	3,001	-	0,993	0	0,01	0	0,025	-	0	0,93	0,004	-	4,965	96,882	2,625	0,443	0,05	0	0
#34	HP-33/3_III_2	56,8	-	25,47	1,87	0,48	0,15	-	0,16	4,84	6,05	-	95,81	2,669	-	1,411	0	0,066	0,034	0,007	-	0,003	0,441	0,363	-	4,994	54,207	0,897	44,537	0,358	0	0
#35	HP-33/3_III_3	66,74	-	18,65	0,2	0,01	0,33	-	0,01	10,74	0,05	-	96,72	3,008	-	0,991	0	0,007	0,001	0,016	-	0	0,938	0,003	-	4,963	98,035	1,662	0,282	0,021	0	0
#36	HP-33/3_III_4	66,7	-	19,23	0,32	0,02	0,31	-	0,03	10,3	0,59	-	97,52	2,989	-	1,016	0	0,011	0,002	0,015	-	0	0,895	0,034	-	4,962	94,771	1,582	3,596	0,051	0	0
#37	HP-33/3_III_5	68,43	-	18,81	0,34	0,01	0,33	-	0	10,76	0,07	-	98,77	3,018	-	0,978	0	0,011	0,001	0,016	-	0	0,921	0,004	-	4,949	97,908	1,664	0,428	0	0	0
average		**65,21**	**-**	**20,22**	**0,604**	**0,104**	**0,33**	**-**	**0,046**	**9,482**	**1,37**	**-**	**97,36**	**2,937**	**-**	**1,0778**	**0**	**0,021**	**0,0076**	**0,0158**	**-**	**0,0006**	**0,825**	**0,0816**	**-**	**4,9666**	**88,361**	**1,686**	**9,8572**	**0,096**	**0**	**0**
#37	FP-8/I_1	54,48	-	26,33	0,6	0,06	10,81	-	0,01	5,59	0,18	-	98,07	2,514	-	1,431	0	0,021	0,004	0,534	-	0	0,5	0,011	-	5,015	47,824	51,118	1,035	0,024	0	0
#38	FP-8/I_2	51,6	-	27,07	0,8	0,07	11,36	-	0,06	4,9	0,16	-	96,02	2,441	-	1,509	0	0,029	0,005	0,576	-	0,001	0,449	0,01	-	5,019	43,373	55,59	0,923	0,114	0	0
#39	FP-8/I_3	51,97	-	26,95	0,63	0,05	11,07	-	0,03	5,3	0,16	-	96,17	2,453	-	1,499	0	0,022	0,004	0,56	-	0,001	0,485	0,01	-	5,034	45,987	53,056	0,909	0,048	0	0
#40	FP-8/I_4	56,23	-	25,03	0,66	0,08	9,87	-	0	4,99	1,25	-	98,12	2,588	-	1,358	0	0,023	0,005	0,487	-	0	0,445	0,073	-	4,98	44,297	48,418	7,285	0	0	0
#41	FP-8/I_5	54,27	-	26,5	0,59	0,06	10,82	-	0,02	5,28	0,16	-	97,7	2,51	-	1,444	0	0,021	0,004	0,536	-	0	0,473	0,01	-	4,999	46,423	52,61	0,939	0,028	0	0
average		**53,71**	**-**	**26,38**	**0,656**	**0,064**	**10,786**	**-**	**0,024**	**5,212**	**0,38**	**-**	**97,216**	**2,501**	**-**	**1,4482**	**0**	**0,0232**	**0,0044**	**0,5386**	**-**	**0,0004**	**0,4704**	**0,0228**	**-**	**5,0094**	**45,581**	**52,158**	**2,2182**	**0,0428**	**0**	**0**
#42	FP-8/II_1	65,98	-	15,08	1,26	0,04	3,28	-	0,04	3,43	0,94	-	90,06	3,15	-	0,849	0	0,045	0,003	0,168	-	0,001	0,317	0,057	-	4,59	58,398	30,9	10,569	0,133	0	0
#43	FP-8/II_2	53,97	-	22,31	0,89	0,04	6,4	-	0	6,24	0,38	-	90,23	2,672	-	1,302	0	0,033	0,003	0,339	-	0	0,599	0,024	-	4,972	62,232	35,256	2,512	0	0	0
#45	FP-8/II_4	64,38	-	12,86	1,98	0,58	2,63	-	0	2,74	1,13	-	86,31	3,203	-	0,754	0	0,074	0,043	0,14	-	0	0,264	0,072	-	4,551	55,459	29,444	15,096	0,001	0	0
average		**61,44**	**-**	**16,75**	**1,377**	**0,22**	**4,10333**	**-**	**0,01333**	**4,137**	**0,82**	**-**	**88,866667**	**3,008**	**-**	**0,96833**	**0**	**0,0507**	**0,016333**	**0,2157**	**-**	**0,0003**	**0,3933**	**0,051**	**-**	**4,7043333**	**58,696**	**31,867**	**9,3923**	**0,0447**	**0**	**0**
#47	FP-8/III_1	60,45	-	22,61	0,97	0,05	6,27	-	0,01	6,8	0,44	-	97,59	2,753	-	1,214	0	0,033	0,003	0,306	-	0	0,6	0,026	-	4,936	64,411	32,811	2,756	0,022	0	0
#48	FP-8/III_2	73,78	-	11,33	3,19	0,16	1,46	-	0	2,41	0,8	-	93,14	3,357	-	0,607	0	0,109	0,011	0,071	-	0	0,213	0,047	-	4,415	64,343	21,532	14,125	0,001	0	0
#50	FP-8/III_4	61,63	-	22,16	1,41	0,31	6,24	-	0,07	7,05	0,48	-	99,36	2,764	-	1,171	0	0,048	0,021	0,3	-	0,001	0,613	0,028	-	4,946	65,073	31,849	2,938	0,14	0	0
#51	FP-8/III_5	61,17	-	19,94	1,29	0,06	7,59	-	0,08	6,02	0,58	-	96,73	2,82	-	1,084	0	0,045	0,004	0,375	-	0,001	0,538	0,034	-	4,901	56,743	39,529	3,576	0,152	0	0
average		**64,26**	**-**	**19,01**	**1,715**	**0,145**	**5,39**	**-**	**0,04**	**5,57**	**0,58**	**-**	**96,705**	**2,924**	**-**	**1,019**	**0**	**0,0588**	**0,00975**	**0,263**	**-**	**0,0005**	**0,491**	**0,0338**	**-**	**4,7995**	**62,643**	**31,43**	**5,8488**	**0,0788**	**0**	**0**
#52	FP-8/IV_1	71,98	-	12,91	0,69	0,07	1,01	-	0	1,78	7,12	-	95,57	3,29	-	0,695	0	0,024	0,005	0,05	-	0	0,158	0,415	-	4,637	25,383	7,968	66,649	0	0	0
#53	FP-8/IV_2	67,67	-	16,43	0,48	0,03	1,46	-	0,09	2,82	8,99	-	97,97	3,093	-	0,885	0	0,016	0,002	0,071	-	0,002	0,25	0,524	-	4,843	29,514	8,422	61,871	0,192	0	0
#55	FP-8/IV_4	60,19	-	23,36	0,91	0,04	7,02	-	0,02	6,96	0,46	-	98,97	2,715	-	1,242	0	0,031	0,003	0,339	-	0	0,608	0,027	-	4,966	62,402	34,818	2,739	0,041	0	0
#56	FP-8/IV_5	75,76	-	10,61	1,78	0,02	2,06	-	0,05	1,07	1,24	-	92,57	3,437	-	0,567	0	0,061	0,002	0,1	-	0,001	0,094	0,072	-	4,333	35,343	37,485	26,87	0,303	0	0
average		**68,9**	**-**	**15,83**	**0,965**	**0,04**	**2,8875**	**-**	**0,04**	**3,158**	**4,45**	**-**	**96,27**	**3,134**	**-**	**0,84725**	**0**	**0,033**	**0,003**	**0,14**	**-**	**0,0008**	**0,2775**	**0,2595**	**-**	**4,69475**	**38,161**	**22,173**	**39,532**	**0,134**	**0**	**0**
#32	WP-20B/III_1	40,19	-	33,69	0,73	0,05	19,39	-	0,05	0,85	0,02	-	94,98	1,979	-	1,955	0	0,027	0,003	1,023	-	0,001	0,081	0,001	-	5,071	7,304	92,467	0,134	0,096	0	0
#33	WP-20B/III_2	41,4	-	33,64	0,74	0,07	19,13	-	0,02	0,88	0,01	-	95,89	2,013	-	1,927	0	0,027	0,005	0,996	-	0	0,083	0,001	-	5,052	7,701	92,192	0,075	0,032	0	0
#34	WP-20B/III_3	41,83	-	33,6	0,7	0,06	19,05	-	0,08	0,85	0,01	-	96,18	2,026	-	1,917	0	0,025	0,004	0,989	-	0,002	0,08	0,001	-	5,044	7,472	92,294	0,085	0,15	0	0
#35	WP-20B/III_4	42,78	-	33,5	0,66	0,05	19,01	-	0	0,78	0	-	96,79	2,053	-	1,894	0	0,024	0,004	0,977	-	0	0,072	0	-	5,024	6,886	93,113	0,001	0	0	0
#36	WP-20B/III_5	42,44	-	33,78	0,66	0,05	19,51	-	0	0,7	0,02	-	97,16	2,033	-	1,907	0	0,024	0,004	1,001	-	0	0,065	0,001	-	5,035	6,061	93,822	0,117	0	0	0
average		**41,73**	**-**	**33,64**	**0,698**	**0,056**	**19,218**	**-**	**0,03**	**0,812**	**0,01**	**-**	**96,2**	**2,021**	**-**	**1,92**	**0**	**0,0254**	**0,004**	**0,9972**	**-**	**0,0006**	**0,0762**	**0,0008**	**-**	**5,0452**	**7,0848**	**92,778**	**0,0824**	**0,0556**	**0**	**0**

Feldspar Point	Label	SiO_2	TiO_2	Al_2O_3	Fe_2O_3	MgO	CaO	SrO	BaO	Na_2O	K_2O	Rb_2O	Sum Ox%	Si	Ti	Al/Al IV	Al VI	Fe^{3+}	Mg	Ca	Sr	Ba	Na	K	Rb	Sum Cat#	Ab	An	Or	Celsian	Rb-Feld	Sr-Feld
#1	Orthoklas_1	64,95	-	16,94	1,06	0,02	0	-	0,05	0,41	16,05	-	99,48	3,026	-	0,93	0	0,037	0,002	0	-	0,001	0,037	0,954	-	4,986	3,691	0,001	96,22	0,088	0	0
#2	Orthoklas_1	65,12	-	16,87	1,23	0,02	0	-	0,05	0,43	14,51	-	98,24	3,043	-	0,929	0	0,043	0,001	0	-	0,001	0,039	0,865	-	4,922	4,309	0,001	95,584	0,106	0	0
#3	Orthoklas_2	67,53	-	17,66	1,36	0,02	0	-	0	0,26	9,07	-	95,9	3,107	-	0,958	0	0,047	0,001	0	-	0	0,024	0,532	-	4,668	4,241	0,009	95,75	0,001	0	0
#4	Orthoklas_3	63,61	-	16,66	1,15	0,01	0,02	-	0	0,37	15,99	-	97,82	3,019	-	0,932	0	0,041	0,001	0,001	-	0	0,034	0,968	-	4,996	3,417	0,077	96,506	0	0	0
average		**65,3**	**-**	**17,03**	**1,2**	**0,0175**	**0,005**	**-**	**0,025**	**0,368**	**13,91**	**-**	**97,86**	**3,0488**	**-**	**0,93725**	**0**	**0,042**	**0,00125**	**0,0003**	**-**	**0,0005**	**0,0335**	**0,8298**	**-**	**4,893**	**3,9145**	**0,022**	**96,015**	**0,04875**	**0**	**0**
#5	Albit_1	68,92	-	18,96	0,06	0	0,2	-	0,05	11,18	0,12	-	99,48	3,02	-	0,979	0	0,002	0	0,009	-	0,001	0,95	0,007	-	4,968	98,278	0,952	0,689	0,081	0	0
#6	Albit_2	60,35	-	16	0,01	0,01	0,13	-	0	7,96	0,13	-	84,58	3,076	-	0,961	0	0	0,001	0,007	-	0	0,787	0,008	-	4,84	98,075	0,872	1,052	0	0	0
#7	Albit_3	68,95	-	19,04	0	0	0,16	-	0	11,07	0,12	-	99,34	3,022	-	0,984	0	0	0	0,007	-	0	0,941	0,006	-	4,96	98,557	0,765	0,678	0	0	0
average		**66,07**	**-**	**18**	**0,023**	**0,00333**	**0,16333**	**-**	**0,01667**	**10,07**	**0,123**	**-**	**94,466667**	**3,0393**	**-**	**0,97467**	**0**	**0,0007**	**0,000333**	**0,0077**	**-**	**0,0003**	**0,8927**	**0,007**	**-**	**4,9226667**	**98,303**	**0,863**	**0,8063**	**0,027**	**0**	**0**
#3	PP-11/I_1	52,04	-	27,63	1,07	0,14	12,37	-	0	4,46	0,23	-	97,93	2,419	-	1,514	0	0,037	0,01	0,616	-	0	0,402	0,014	-	5,013	38,956	59,708	1,336	0	0	0
#4	PP-11/I_2	52,52	-	26,9	1,01	0,14	11,62	-	0,11	4,61	0,34	-	97,24	2,456	-	1,482	0	0,036	0,009	0,582	-	0,002	0,418	0,02	-	5,004	40,888	56,947	1,959	0,206	0	0
#5	PP-11/I_3	53,03	-	26,93	0,88	0,07	11,39	-	0,1	4,83	0,39	-	97,61	2,467	-	1,477	0	0,031	0,005	0,568	-	0,002	0,435	0,023	-	5,008	42,358	55,232	2,225	0,184	0	0
#6	PP-11/I_4	51,28	-	27,24	0,84	0,1	12,01	-	0,05	4,74	0,36	-	96,62	2,42	-	1,515	0	0,03	0,007	0,607	-	0,001	0,434	0,022	-	5,035	40,792	57,071	2,043	0,094	0	0
#7	PP-11/I_5	52,7	-	26,73	0,8	0,1	11,67	-	0	4,8	0,3	-	97,09	2,465	-	1,473	0	0,028	0,007	0,585	-	0	0,435	0,018	-	5,011	41,914	56,337	1,749	0	0	0
average		**52,31**	**-**	**27,09**	**0,92**	**0,11**	**11,812**	**-**	**0,052**	**4,688**	**0,324**	**-**	**97,298**	**2,4454**	**-**	**1,4922**	**0**	**0,0324**	**0,0076**	**0,5916**	**-**	**0,001**	**0,4248**	**0,0194**	**-**	**5,0142**	**40,982**	**57,059**	**1,8624**	**0,0968**	**0**	**0**
#8	PP-11/II_1	53,36	-	26,72	0,82	0,11	11,33	-	0,02	4,89	0,28	-	97,54	2,48	-	1,464	0	0,029	0,008	0,564	-	0	0,441	0,017	-	5,003	43,118	55,195	1,651	0,036	0	0
#9	PP-11/II_2	52,98	-	27,63	0,86	0,08	11,58	-	0,06	4,61	0,34	-	98,13	2,45	-	1,506	0	0,03	0,006	0,574	-	0,001	0,413	0,02	-	4,999	40,969	56,912	2,017	0,101	0	0
#10	PP-11/II_3	53,58	-	26,86	0,93	0,12	11,31	-	0,02	4,73	0,39	-	97,92	2,48	-	1,465	0	0,032	0,008	0,561	-	0	0,424	0,023	-	4,995	42,057	55,628	2,286	0,028	0	0
#11	PP-11/II_4	54,32	-	26,69	0,77	0,11	11,47	-	0,1	4,74	0,43	-	98,64	2,496	-	1,446	0	0,027	0,008	0,565	-	0,002	0,423	0,025	-	4,991	41,671	55,655	2,498	0,176	0	0
#12	PP-11/II_5	53,15	-	26,7	0,79	0,09	11,58	-	0,09	4,89	0,36	-	97,65	2,473	-	1,464	0	0,028	0,006	0,577	-	0,002	0,442	0,022	-	5,013	42,371	55,411	2,068	0,15	0	0
average		**53,48**	**-**	**26,92**	**0,834**	**0,102**	**11,454**	**-**	**0,058**	**4,772**	**0,36**	**-**	**97,976**	**2,4758**	**-**	**1,469**	**0**	**0,0292**	**0,0072**	**0,5682**	**-**	**0,001**	**0,4286**	**0,0214**	**-**	**5,0002**	**42,037**	**55,76**	**2,104**	**0,0982**	**0**	**0**
#13	PP-11/III_1	52,83	-	27,35	0,99	0,1	12,26	-	0	4,37	0,27	-	98,17	2,445	-	1,492	0	0,034	0,007	0,608	-	0	0,393	0,016	-	4,995	38,628	59,816	1,556	0	0	0
#14	PP-11/III_2	53,25	-	26,92	0,87	0,04	11,57	-	0,05	4,7	0,41	-	97,81	2,472	-	1,473	0	0,03	0,003	0,575	-	0,001	0,423	0,024	-	5	41,304	56,239	2,376	0,08	0	0
#15	PP-11/III_3	53,85	-	27,36	0,9	0,06	12	-	0,02	4,23	0,39	-	98,81	2,47	-	1,479	0	0,031	0,004	0,59	-	0	0,376	0,023	-	4,974	38,034	59,641	2,292	0,033	0	0
#16	PP-11/III_4	55,08	-	28,82	0,68	0,22	11,43	-	0,01	4,88	0,39	-	101,51	2,456	-	1,514	0	0,023	0,015	0,546	-	0	0,422	0,022	-	4,998	42,613	55,147	2,229	0,012	0	0
#17	PP-11/III_5	50,71	-	27,01	0,84	0,09	11,92	-	0	4,46	0,39	-	95,41	2,421	-	1,52	0	0,03	0,006	0,61	-	0	0,412	0,024	-	5,023	39,416	58,289	2,295	0	0	0
average		**53,14**	**-**	**27,49**	**0,856**	**0,102**	**11,836**	**-**	**0,016**	**4,528**	**0,37**	**-**	**98,342**	**2,4528**	**-**	**1,4956**	**0**	**0,0296**	**0,007**	**0,5858**	**-**	**0,0002**	**0,4052**	**0,0218**	**-**	**4,998**	**39,999**	**57,826**	**2,1496**	**0,025**	**0**	**0**
#18	PP-31B/I_1	51,8	-	27,18	0,84	0,1	11,49	-	0	4,8	0,31	-	96,52	2,439	-	1,508	0	0,03	0,007	0,58	-	0	0,438	0,019	-	5,02	42,247	55,93	1,822	0	0	0
#19	PP-31B/I_2	53,08	-	27,22	0,87	0,1	11,63	-	0	4,65	0,38	-	97,93	2,46	-	1,487	0	0,03	0,007	0,578	-	0	0,418	0,022	-	5,002	41,069	56,72	2,207	0,004	0	0
#20	PP-31B/I_3	55,18	-	25,17	0,74	0,2	9,21	-	0	6,31	0,3	-	97,11	2,564	-	1,378	0	0,026	0,014	0,458	-	0	0,569	0,018	-	5,027	54,434	43,862	1,704	0	0	0
#21	PP-31B/I_4	49,7	-	25,76	0,72	0,07	10,72	-	0,05	4,85	0,43	-	92,29	2,449	-	1,496	0	0,027	0,005	0,566	-	0,001	0,463	0,027	-	5,034	43,822	53,547	2,545	0,087	0	0
#22	PP-31B/I_5	54,04	-	26,86	0,88	0,09	11,34	-	0	5,01	0,4	-	98,62	2,485	-	1,456	0	0,03	0,006	0,559	-	0	0,447	0,024	-	5,007	43,407	54,289	2,304	0	0	0
average		**52,76**	**-**	**26,44**	**0,81**	**0,112**	**10,878**	**-**	**0,01**	**5,124**	**0,364**	**-**	**96,494**	**2,4794**	**-**	**1,465**	**0**	**0,0286**	**0,0078**	**0,5482**	**-**	**0,0002**	**0,467**	**0,022**	**-**	**5,018**	**44,996**	**52,87**	**2,1164**	**0,0182**	**0**	**0**
#23	PP-31B/II_1	52,09	-	28,11	1,02	0,11	12,17	-	0,06	4,54	0,32	-	98,42	2,411	-	1,533	0	0,036	0,007	0,603	-	0,001	0,408	0,019	-	5,018	39,535	58,546	1,816	0,103	0	0
#24	PP-31B/II_2	52,95	-	28,27	1,08	0,13	12,54	-	0,03	4,42	0,31	-	99,73	2,417	-	1,521	0	0,037	0,009	0,613	-	0,001	0,391	0,018	-	5,008	38,227	59,956	1,759	0,059	0	0
#25	PP-31B/II_3	54,89	-	25,21	0,48	0,2	7,73	-	0,03	6	0,37	-	94,91	2,59	-	1,402	0	0,017	0,014	0,391	-	0,001	0,549	0,023	-	4,986	57,034	40,574	2,341	0,052	0	0
#26	PP-31B/II_4	54,45	-	26,93	0,61	0,07	10,36	-	0,01	5,13	0,49	-	98,06	2,508	-	1,462	0	0,021	0,005	0,511	-	0	0,458	0,029	-	4,994	45,898	51,185	2,892	0,024	0	0
#27	PP-31B/II_5	51,91	-	27,63	0,89	0,1	12,25	-	0,02	4,25	0,31	-	97,37	2,424	-	1,521	0	0,031	0,007	0,613	-	0	0,385	0,019	-	5,001	37,817	60,306	1,844	0,032	0	0
average		**53,26**	**-**	**27,23**	**0,816**	**0,122**	**11,01**	**-**	**0,03**	**4,868**	**0,36**	**-**	**97,698**	**2,47**	**-**	**1,4878**	**0**	**0,0284**	**0,0084**	**0,5462**	**-**	**0,0006**	**0,4382**	**0,0216**	**-**	**5,0014**	**43,702**	**54,113**	**2,1304**	**0,054**	**0**	**0**
#28	PP-31B/III_1	52,65	-	27,95	1,14	0,09	12,67	-	0,01	4,21	0,27	-	98,98	2,421	-	1,515	0	0,039	0,006	0,624	-	0	0,376	0,016	-	4,997	36,978	61,445	1,565	0,012	0	0
#29	PP-31B/III_2	54,56	-	26,79	0,88	0,07	11,19	-	0	5,16	0,42	-	99,06	2,497	-	1,445	0	0,03	0,005	0,549	-	0	0,457	0,024	-	5,007	44,396	53,234	2,369	0	0	0
average		**53,61**	**-**	**27,37**	**1,01**	**0,08**	**11,93**	**-**	**0,005**	**4,685**	**0,345**	**-**	**99,02**	**2,459**	**-**	**1,48**	**0**	**0,0345**	**0,0055**	**0,5865**	**-**	**0**	**0,4165**	**0,02**	**-**	**5,002**	**40,687**	**57,34**	**1,967**	**0,006**	**0**	**0**
#30	PP-32C/I_1	53,08	-	27,74	0,93	0,1	12,35	-	0,03	4,19	0,32	-	98,75	2,442	-	1,504	0	0,032	0,007	0,609	-	0,001	0,374	0,019	-	4,987	37,291	60,77	1,882	0,057	0	0
#31	PP-32C/I_2	53,66	-	27,15	0,79	0,09	11,99	-	0,05	4,61	0,36	-	98,7	2,468	-	1,472	0	0,027	0,006	0,591	-	0,001	0,411	0,021	-	4,998	40,129	57,714	2,069	0,087	0	0
#32	PP-32C/I_3	54,19	-	27,34	0,95	0,1	12,19	-	0	4,79	0,28	-	99,84	2,466	-	1,466	0	0,032	0,007	0,594	-	0	0,422	0,017	-	5,004	40,877	57,523	1,6	0	0	0
#33	PP-32C/I_4	52,33	-	27,22	0,96	0,09	11,87	-	0,07	4,61	0,4	-	97,55	2,442	-	1,497	0	0,034	0,006	0,593	-	0,001	0,417	0,024	-	5,014	40,275	57,304	2,294	0,127	0	0
#34	PP-32C/I_5	52,27	-	27,72	0,87	0,09	12,56	-	0,09	4,34	0,38	-	98,32	2,423	-	1,514	0	0,031	0,006	0,624	-	0,002	0,39	0,022	-	5,011	37,588	60,099	2,151	0,162	0	0
average		**53,11**	**-**	**27,43**	**0,9**	**0,094**	**12,192**	**-**	**0,048**	**4,508**	**0,348**	**-**	**98,632**	**2,4482**	**-**	**1,4906**	**0**	**0,0312**	**0,0064**	**0,6022**	**-**	**0,001**	**0,4028**	**0,0206**	**-**	**5,0028**	**39,232**	**58,682**	**1,9992**	**0,0866**	**0**	**0**
#35	PP-32C/II_1	50,67	-	27,45	1,05	0,1	11,84	-	0,01	4,67	0,38	-	96,16	2,404	-	1,535	0	0,038	0,007	0,602	-	0	0,429	0,023	-	5,036	40,729	57,095	2,165	0,012	0	0
#36	PP-32C/II_2	48,71	-	27,41	0,92	0,11	11,96	-	0	4,46	0,41	-	93,96	2,369	-	1,571	0	0,034	0,008	0,623	-	0	0,421	0,025	-	5,051	39,346	58,282	2,371	0	0	0
#37	PP-32C/II_3	50,27	-	27,2	0,9	0,13	11,74	-	0	5,02	0,39	-	95,64	2,401	-	1,531	0	0,032	0,009	0,601	-	0	0,464	0,024	-	5,062	42,65	55,164	2,186	0	0	0
#38	PP-32C/II_4	48,58	-	30,49	0,96	0,06	15,69	-	0	2,9	0,18	-	98,86	2,26	-	1,672	0	0,034	0,004	0,782	-	0	0,262	0,01	-	5,024	24,84	74,166	0,994	0	0	0
#39	PP-32C/II_5	51,15	-	27,97	0,84	0,11	12,61	-	0,01	4,17	0,36	-	97,22	2,398	-	1,546	0	0,03	0,008	0,633	-	0	0,379	0,022	-	5,015	36,624	61,262	2,093	0,02	0	0
average		**49,88**	**-**	**28,1**	**0,934**	**0,102**	**12,768**	**-**	**0,004**	**4,244**	**0,344**	**-**	**96,368**	**2,3664**	**-**	**1,571**	**0**	**0,0336**	**0,0072**	**0,6482**	**-**	**0**	**0,391**	**0,0208**	**-**	**5,0376**	**36,838**	**61,194**	**1,9618**	**0,0064**	**0**	**0**
#40	PP-32C/III_1	51,64	-	27,69	1,01	0,1	12,33	-	0,07	4,38	0,34	-	97,56	2,413	-	1,525	0	0,036	0,007	0,617	-	0,001	0,397	0,02	-	5,016	38,32	59,595	1,965	0,12	0	0
#41	PP-32C/III_2	52,36	-	27,4	0,91	0,11	11,7	-	0,07	4,63	0,41	-	97,59	2,44	-	1,505	0	0,032	0,008	0,584	-	0,001	0,418	0,024	-	5,013	40,677	56,822	2,376	0,124	0	0
#42	PP-32C/III_3	52,87	-	27,17	1,03	0,15	11,47	-	0	4,62	0,4	-	97,71	2,457	-	1,488	0	0,036	0,01	0,571	-	0	0,416	0,024	-	5,002	41,183	56,469	2,348	0	0	0
#43	PP-32C/III_4	52,43	-	27,39	0,92	0,07	12,01	-	0	4,56	0,39	-	97,78	2,439	-	1,502	0	0,032	0,005	0,599	-	0	0,411	0,023	-	5,011	39,785	57,958	2,256	0	0	0
#44	PP-32C/III_5	52,05	-	27,93	1,11	0,1	12,92	-	0,05	4,08	0,32	-	98,56	2,408	-	1,523	0	0,039	0,007	0,64	-	0,001	0,366	0,019	-	5,003	35,64	62,437	1,835	0,088	0	0
average		**52,27**	**-**	**27,52**	**0,996**	**0,106**	**12,086**	**-**	**0,038**	**4,454**	**0,372**	**-**	**97,84**	**2,4314**	**-**	**1,5086**	**0**	**0,035**	**0,0074**	**0,6022**	**-**	**0,0006**	**0,4016**	**0,022**	**-**	**5,009**	**39,121**	**58,656**	**2,156**	**0,0664**	**0**	**0**

Feldspar																														
Point	Label	SiO_2	TiO_2	Al_2O_3	Fe_2O_3	MgO	CaO	SrO	BaO	Na_2O	K_2O	Rb_2O	Sum Ox%	Si	Ti	Al/Al IV	Al VI	Fe^{3+}	Mg	Ca	Sr	Ba	Na	K	Rb	Sum Cat#	Ab	An	Or	Celsian	Rb-Feld	Sr-Feld
#50	PP-32B/II	66,62	-	19,83	0,1	0,03	0,35	-	0	10,84	0,64	-	98,41	2,965	-	1,04	0	0,003	0,002	0,017	-	0	0,935	0,036	-	4,999	94,647	1,692	3,653	0,008	0	0
#51	PP-32B/II	68,53	-	19,04	0	0,01	0,19	-	0	11,37	0,06	-	99,21	3,012	-	0,986	0	0	0,001	0,009	-	0	0,969	0,004	-	4,981	98,701	0,932	0,366	0	0	0
#52	PP-32B/II	67,23	-	18,98	0,03	0,01	0,48	-	0,03	11,24	0,07	-	98,09	2,995	-	0,997	0	0,001	0,001	0,023	-	0,001	0,971	0,004	-	4,993	97,242	2,308	0,398	0,051	0	0
#53	PP-32B/II	65,79	-	18,58	0,02	0	0,22	-	0,01	11,31	0,03	-	95,98	2,996	-	0,997	0	0,001	0	0,011	-	0	0,998	0,002	-	5,005	98,707	1,08	0,189	0,024	0	0
#54	PP-32B/II	67,09	-	18,48	0	0,01	0,28	-	0	10,89	0,04	-	96,78	3,02	-	0,98	0	0	0,001	0,013	-	0	0,95	0,002	-	4,966	98,407	1,378	0,211	0,004	0	0
average		**67,05**	**-**	**18,98**	**0,03**	**0,012**	**0,304**	**-**	**0,008**	**11,13**	**0,17**	**-**	**97,694**	**2,998**	**-**	**1**	**0**	**0,001**	**0,001**	**0,0146**	**-**	**0,0002**	**0,9646**	**0,0096**	**-**	**4,9888**	**97,541**	**1,478**	**0,963**	**0,0174**	**0**	**0**
#7	PP-33/I_1	62,44	-	18,56	0,19	0	1,21	-	0	9,2	0,1	-	91,7	2,97	-	1,04	0	0,007	0	0,062	-	0	0,848	0,006	-	4,933	92,599	6,718	0,682	0	0	0
#9	PP-33/I_3	64,66	-	19,71	0,26	0,01	1,31	-	0,09	9,14	0,3	-	95,47	2,957	-	1,062	0	0,009	0,001	0,064	-	0,002	0,81	0,017	-	4,921	90,695	7,189	1,938	0,178	0	0
#11	PP-33/I_5	61,7	-	18,6	0,07	0	1,39	-	0,01	8,96	0,07	-	90,81	2,963	-	1,053	0	0,003	0	0,071	-	0	0,835	0,004	-	4,929	91,694	7,83	0,452	0,023	0	0
average		**62,93**	**-**	**18,96**	**0,173**	**0,00333**	**1,30333**	**-**	**0,03333**	**9,1**	**0,16**	**-**	**92,66**	**2,963**	**-**	**1,05167**	**0**	**0,006**	**0,0003**	**0,0657**	**-**	**0,00067**	**0,831**	**0,009**	**-**	**4,9276667**	**91,663**	**7,2457**	**1,024**	**0,067**	**0**	**0**
#12	PP-33/II_1	59,87	-	17,48	0,45	0	0,53	-	0,22	3,06	10,8	-	92,39	2,963	-	1,02	0	0,017	0	0,028	-	0,004	0,293	0,681	-	5,006	29,164	2,77	67,64	0,43	0	0
#13	PP-33/II_2	58,21	-	18,04	0,48	0,02	2,12	-	0,17	3,21	8,37	-	90,61	2,917	-	1,065	0	0,018	0,001	0,114	-	0,003	0,312	0,535	-	4,965	32,382	11,795	55,48	0,339	0	0
#14	PP-33/II_3	50,69	-	18,32	0,99	0,28	0,74	-	0,12	4,56	3,27	-	78,96	2,843	-	1,211	0	0,042	0,023	0,045	-	0,003	0,495	0,234	-	4,895	63,803	5,757	30,09	0,347	0	0
#15	PP-33/II_4	62,75	-	19,63	0,51	0	2,05	-	0,07	8,33	0,53	-	93,88	2,928	-	1,08	0	0,018	0	0,103	-	0,001	0,754	0,032	-	4,915	84,75	11,546	3,55	0,154	0	0
average		**57,88**	**-**	**18,37**	**0,608**	**0,075**	**1,36**	**-**	**0,145**	**4,79**	**5,74**	**-**	**88,96**	**2,913**	**-**	**1,094**	**0**	**0,024**	**0,006**	**0,0725**	**-**	**0,00275**	**0,4635**	**0,3705**	**-**	**4,94525**	**52,525**	**7,967**	**39,19**	**0,3175**	**0**	**0**
#19	AP-1/I_1	51,82	-	28,1	1,13	0,1	12,72	-	0,06	4,29	0,21	-	98,43	2,401	-	1,534	0	0,039	0,007	0,631	-	0,001	0,385	0,013	-	5,012	37,401	61,267	1,224	0,108	0	0
#20	AP-1/I_2	49,41	-	30,45	0,79	0,15	15,19	-	0	2,98	0,05	-	99,02	2,285	-	1,66	0	0,027	0,01	0,753	-	0	0,267	0,003	-	5,006	26,112	73,578	0,309	0	0	0
#21	AP-1/I_3	47,98	-	30,07	0,73	0,12	14,78	-	0,04	3,21	0,08	-	97,01	2,27	-	1,676	0	0,026	0,009	0,749	-	0,001	0,294	0,005	-	5,029	28,058	71,421	0,448	0,073	0	0
#22	AP-1/I_4	49,15	-	30,02	0,76	0,17	14,91	-	0	3,12	0,06	-	98,18	2,293	-	1,65	0	0,027	0,012	0,745	-	0	0,282	0,003	-	5,012	27,368	72,298	0,334	0	0	0
#23	AP-1/I_5	49,35	-	30,24	0,77	0,14	15,01	-	0,02	3,08	0,08	-	98,69	2,291	-	1,654	0	0,027	0,01	0,746	-	0	0,277	0,004	-	5,01	26,963	72,568	0,436	0,033	0	0
average		**49,54**	**-**	**29,78**	**0,836**	**0,136**	**14,522**	**-**	**0,024**	**3,336**	**0,1**	**-**	**98,266**	**2,308**	**-**	**1,6348**	**0**	**0,029**	**0,0096**	**0,7248**	**-**	**0,0004**	**0,301**	**0,0056**	**-**	**5,0138**	**29,18**	**70,226**	**0,55**	**0,0428**	**0**	**0**
#24	AP-1/II_1	48,92	-	30,09	0,89	0,12	15,22	-	0,02	2,91	0,1	-	98,28	2,283	-	1,655	0	0,031	0,008	0,761	-	0	0,264	0,006	-	5,009	25,571	73,809	0,584	0,036	0	0
#25	AP-1/II_2	48,9	-	29,77	0,75	0,15	14,82	-	0	3,08	0,07	-	97,53	2,296	-	1,647	0	0,026	0,01	0,745	-	0	0,281	0,004	-	5,01	27,253	72,359	0,388	0	0	0
#26	AP-1/II_3	49,67	-	29,94	0,77	0,16	14,99	-	0	3,14	0,08	-	98,76	2,303	-	1,636	0	0,027	0,011	0,745	-	0	0,282	0,005	-	5,009	27,336	72,19	0,473	0	0	0
#27	AP-1/II_4	49,43	-	29,49	1,1	0,43	14,53	-	0	3,28	0,1	-	98,35	2,303	-	1,62	0	0,038	0,03	0,725	-	0	0,296	0,006	-	5,019	28,835	70,56	0,604	0	0	0
#28	AP-1/II_5	47,87	-	30,29	0,78	0,15	15,09	-	0,02	2,97	0,08	-	97,25	2,259	-	1,685	0	0,028	0,011	0,763	-	0	0,272	0,005	-	5,023	26,125	73,395	0,453	0,027	0	0
average		**48,96**	**-**	**29,92**	**0,858**	**0,202**	**14,93**	**-**	**0,008**	**3,076**	**0,09**	**-**	**98,034**	**2,289**	**-**	**1,6486**	**0**	**0,03**	**0,014**	**0,7478**	**-**	**0**	**0,279**	**0,0052**	**-**	**5,014**	**27,024**	**72,463**	**0,5**	**0,0126**	**0**	**0**
#4	PI-4/I_1	57,43	-	25,53	1,1	0,07	9,21	-	0	6,08	0,52	-	99,94	2,589	-	1,357	0	0,037	0,005	0,445	-	0	0,532	0,03	-	4,995	52,818	44,21	2,971	0	0	0
#5	PI-4/I_2	53,17	-	27,86	1,13	0,09	11,95	-	0	4,53	0,25	-	98,98	2,44	-	1,506	0	0,039	0,006	0,588	-	0	0,403	0,015	-	4,996	40,115	58,441	1,443	0	0	0
#6	PI-4/I_3	53,18	-	28,02	1,05	0,09	12,03	-	0,04	4,42	0,27	-	99,09	2,437	-	1,513	0	0,036	0,006	0,591	-	0,001	0,393	0,016	-	4,993	39,263	59,068	1,599	0,07	0	0
#7	PI-4/I_4	52,64	-	28,21	1,22	0,07	12,58	-	0,04	4,33	0,24	-	99,32	2,414	-	1,524	0	0,042	0,005	0,618	-	0,001	0,385	0,014	-	5,002	37,807	60,764	1,367	0,062	0	0
#8	PI-4/I_5	60,35	-	20,48	2,56	1,2	7,34	-	0,04	7,06	0,89	-	99,91	2,73	-	1,092	0	0,087	0,081	0,356	-	0,001	0,619	0,051	-	5,016	60,279	34,649	5,01	0,063	0	0
average		**55,35**	**-**	**26,02**	**1,412**	**0,304**	**10,622**	**-**	**0,024**	**5,284**	**0,43**	**-**	**99,448**	**2,522**	**-**	**1,3984**	**0**	**0,048**	**0,0206**	**0,5196**	**-**	**0,0006**	**0,4664**	**0,0252**	**-**	**5,0004**	**46,056**	**51,426**	**2,478**	**0,039**	**0**	**0**
#9	PI-4/II_1	56,33	-	26,65	1,3	0,03	10,18	-	0,04	5,43	0,4	-	100,35	2,536	-	1,414	0	0,044	0,002	0,491	-	0,001	0,474	0,023	-	4,984	47,923	49,669	2,339	0,069	0	0
#10	PI-4/II_2	50,93	-	28,64	1,11	0,07	12,94	-	0	4,06	0,22	-	97,97	2,372	-	1,572	0	0,039	0,005	0,646	-	0	0,367	0,013	-	5,012	35,779	62,97	1,25	0	0	0
#11	PI-4/II_3	52,08	-	27,3	0,66	0,06	11,14	-	0,04	5,2	0,3	-	96,77	2,445	-	1,51	0	0,023	0,004	0,561	-	0,001	0,473	0,018	-	5,034	44,947	53,286	1,695	0,072	0	0
#12	PI-4/II_4	49,72	-	27,88	0,75	0,05	11,56	-	0	4,68	0,25	-	94,89	2,386	-	1,576	0	0,027	0,004	0,594	-	0	0,435	0,015	-	5,038	41,646	56,913	1,44	0	0	0
#13	PI-4/II_5	51,55	-	27,12	0,8	0,06	11,14	-	0,05	5,07	0,31	-	96,1	2,439	-	1,512	0	0,029	0,004	0,565	-	0,001	0,465	0,019	-	5,033	44,298	53,833	1,788	0,081	0	0
average		**52,12**	**-**	**27,52**	**0,924**	**0,054**	**11,392**	**-**	**0,026**	**4,888**	**0,3**	**-**	**97,216**	**2,436**	**-**	**1,5168**	**0**	**0,032**	**0,0038**	**0,5714**	**-**	**0,0006**	**0,4428**	**0,0176**	**-**	**5,0202**	**42,919**	**55,334**	**1,702**	**0,0444**	**0**	**0**
#14	PI-4/III_1	53,87	-	25,86	1,25	0,05	9,67	-	0,05	5,61	0,48	-	96,84	2,519	-	1,425	0	0,044	0,004	0,484	-	0,001	0,509	0,028	-	5,015	49,763	47,361	2,779	0,097	0	0
#15	PI-4/III_2	47,22	-	25,32	5,25	1,57	10,35	-	0,03	3,86	0,4	-	94,01	2,324	-	1,469	0	0,194	0,115	0,546	-	0,001	0,368	0,025	-	5,041	39,164	58,08	2,689	0,067	0	0
#16	PI-4/III_3	50,26	-	27,97	1	0,06	12,04	-	0	4,51	0,26	-	96,09	2,385	-	1,564	0	0,036	0,004	0,612	-	0	0,415	0,016	-	5,03	39,775	58,731	1,494	0	0	0
#17	PI-4/III_4	51,02	-	26,81	2,23	0,55	11,07	-	0,02	4,29	0,31	-	96,3	2,415	-	1,496	0	0,079	0,039	0,561	-	0	0,394	0,019	-	5,003	40,404	57,64	1,911	0,045	0	0
#18	PI-4/III_5	55,59	-	25,71	1,2	0,07	9,43	-	0,01	5,93	0,47	-	98,41	2,552	-	1,391	0	0,041	0,005	0,464	-	0	0,528	0,027	-	5,009	51,817	45,493	2,675	0,015	0	0
average		**51,59**	**-**	**26,33**	**2,186**	**0,46**	**10,512**	**-**	**0,022**	**4,84**	**0,38**	**-**	**96,33**	**2,439**	**-**	**1,469**	**0**	**0,079**	**0,0334**	**0,5334**	**-**	**0,0004**	**0,4428**	**0,023**	**-**	**5,0196**	**44,185**	**53,461**	**2,31**	**0,0448**	**0**	**0**

SAMPLE	SiO_2	Al_2O_3	Fe_2O_3	MnO	MgO	CaO	Na_2O	K_2O	TiO_2	P_2O_5	LOI	TOTAL	LOI
	%	%	%	%	%	%	%	%	%	%	%	%	(average)
Penguin Island													0.15
PI-1	48.52	15.44	9.46	0.157	10.69	9.80	3.29	0.56	1.140	0.26	0.27	99.59	
PI-2	47.72	14.78	9.51	0.156	11.81	9.42	3.15	0.52	1.094	0.25	0.26	98.68	
PI-3	47.78	15.65	9.94	0.159	11.66	9.69	3.24	0.64	1.103	0.26	0.33	100.46	
PI-4	48.98	15.29	9.71	0.159	11.57	9.76	3.21	0.52	1.127	0.25	0.00	100.49	
PI-5	48.91	16.68	9.36	0.153	8.28	9.91	3.64	0.66	1.248	0.29	0.00	99.14	
Admiralty Bay													2.99
AP-1	52.60	15.49	11.03	0.195	3.87	7.33	4.01	1.06	1.327	0.39	1.95	99.24	
SH-1	68.64	15.17	2.94	0.079	0.32	1.43	5.27	3.49	0.599	0.13	1.41	99.48	
SH-3	68.32	15.00	2.90	0.084	0.35	1.51	5.10	3.64	0.592	0.13	1.56	99.19	
SP-1	57.45	16.91	7.17	0.119	3.31	6.06	3.87	2.04	0.815	0.26	2.34	100.33	
EI-1	46.56	20.17	8.26	0.177	5.50	7.76	3.46	0.72	0.796	0.16	5.42	98.98	
EI-2	49.84	19.64	7.98	0.134	4.36	9.01	3.36	0.25	0.797	0.20	3.91	99.48	
EI-3	47.67	20.21	8.52	0.203	5.09	8.81	3.07	0.23	0.803	0.18	5.25	100.03	
EI-9	48.79	19.80	8.68	0.187	4.14	9.30	3.93	0.42	0.819	0.16	2.75	98.99	
EI-10	46.57	19.50	8.76	0.174	5.13	10.52	2.89	0.16	0.736	0.16	4.39	98.98	
EI-11	48.53	18.87	8.38	0.139	5.40	10.41	3.00	0.22	0.715	0.18	4.36	100.20	
EI-13	47.34	20.95	9.00	0.318	4.93	10.15	3.08	0.21	0.810	0.15	3.07	100.01	
EI-15	53.64	16.85	7.50	0.118	4.40	7.98	3.20	1.32	0.748	0.28	2.69	98.73	
EI-16	54.33	16.98	8.01	0.181	4.75	8.03	3.38	1.01	0.783	0.23	2.10	99.77	
EI-16 /R	54.28	16.89	8.01	0.180	4.71	8.00	3.38	0.99	0.759	0.23	2.10	99.52	
EI-16 (average)	54.31	16.94	8.01	0.181	4.73	8.02	3.38	1.00	0.771	0.23	2.10	99.65	
EI-17	53.56	17.18	6.78	0.134	4.01	7.36	3.67	0.41	0.635	0.23	4.72	98.69	
EI-18	56.54	16.03	9.04	0.109	3.09	3.76	3.92	3.43	1.056	0.33	2.79	100.08	
EI-18 /R	56.52	15.99	8.95	0.109	3.03	3.72	3.89	3.54	1.060	0.33	2.79	99.93	
EI-18 (average)	56.53	16.01	9.00	0.109	3.06	3.74	3.91	3.49	1.058	0.33	2.79	100.01	
EI-20	54.54	17.23	7.83	0.149	4.36	6.54	2.67	2.78	0.768	0.22	2.22	99.31	
EI-21	54.53	17.41	7.91	0.162	4.19	6.04	2.02	4.06	0.813	0.22	3.03	100.38	
EI-22A	50.27	19.62	7.59	0.123	4.12	8.71	3.52	0.27	0.724	0.17	4.61	99.72	
KC-1	54.69	17.93	7.86	0.131	3.94	7.65	2.83	2.15	0.723	0.21	2.10	100.23	
KP-1	56.08	17.24	7.68	0.144	3.82	7.51	3.31	2.04	0.854	0.26	1.15	100.10	
Potter Peninsula													3.37
PP-1A	55.05	18.44	7.14	0.117	3.97	7.92	3.25	1.20	0.572	0.21	2.53	100.38	
PP-1B	54.90	17.22	6.67	0.128	3.80	8.06	3.06	0.48	0.564	0.20	3.71	98.81	
PP-1C	73.67	12.58	1.88	0.031	0.35	1.21	2.96	4.79	0.274	0.05	1.58	99.37	
PP-2	55.69	16.58	7.45	0.286	4.80	7.67	3.15	0.88	0.673	0.19	2.84	100.23	
PP-3	55.75	16.34	7.53	0.153	4.80	7.74	3.13	1.21	0.679	0.19	2.90	100.43	
PP-4	55.71	16.90	7.73	0.140	4.77	7.47	3.32	1.48	0.679	0.19	2.49	100.87	
PP-5A	55.38	17.34	8.28	0.140	3.81	7.39	3.06	1.70	0.838	0.27	2.51	100.72	
PP-5B	73.55	12.66	1.13	0.024	0.12	2.68	1.43	4.28	0.191	0.03	4.16	100.26	
PP-5C	54.95	16.83	8.20	0.128	3.79	7.46	2.94	1.70	0.870	0.27	2.84	99.99	
PP-6A/1	47.21	15.31	7.92	0.187	5.99	8.00	4.86	0.16	0.703	0.13	9.56	100.03	
PP-6A/2	55.58	16.47	7.95	0.124	3.68	7.66	3.08	1.72	0.830	0.27	2.34	99.69	
PP-6B	74.99	12.31	1.53	0.026	0.23	0.78	2.11	4.80	0.188	0.03	1.72	98.72	
PP-6C	55.64	16.82	8.00	0.130	3.57	7.60	3.18	1.71	0.869	0.27	2.39	100.18	
PP-7	48.09	18.51	8.55	0.142	6.28	10.63	2.40	0.18	0.841	0.16	4.63	100.44	
60C4	49.24	19.00	8.82	0.150	5.60	10.94	2.74	0.34	0.824	0.16	2.80	100.62	
PP-8	54.22	15.75	9.43	0.190	2.92	7.82	3.41	0.28	1.068	0.37	5.37	100.82	
PP-9	58.35	16.45	7.85	0.210	2.48	3.77	5.55	0.31	1.049	0.47	2.79	99.27	
PP-10	59.40	14.85	7.40	0.250	2.50	3.01	6.14	0.02	0.874	0.27	4.01	98.74	
PP-11	55.23	18.10	6.94	0.130	3.79	7.74	3.14	1.09	0.556	0.21	3.05	99.96	
PP-12	55.24	16.22	9.74	0.180	3.15	6.74	3.78	1.41	1.082	0.40	2.76	100.69	
PP-13	64.82	15.69	5.36	0.120	1.75	2.18	3.83	3.06	0.777	0.26	2.82	100.66	
PP-19	55.09	16.45	7.56	0.132	4.83	7.47	3.17	1.57	0.711	0.19	2.83	99.99	
PP-31B	55.13	16.60	7.54	0.130	4.78	7.31	3.36	1.20	0.728	0.19	2.76	99.73	
PP-32A	54.77	16.80	8.14	0.118	3.58	7.15	3.25	1.76	0.878	0.28	3.20	99.92	
PP-32B	69.01	13.17	2.63	0.058	0.67	3.12	2.07	3.45	0.344	0.07	4.08	98.68	
PP-32C	56.01	16.75	8.05	0.136	3.72	7.57	3.04	1.59	0.854	0.27	2.35	100.33	
PP-33	51.76	17.09	7.60	0.135	3.32	5.51	3.37	4.41	0.756	0.22	5.76	99.94	
127A	66.43	13.58	5.21	0.107	1.76	2.82	4.03	3.48	0.824	0.42	1.75	100.44	
128A	51.02	17.98	8.23	0.160	4.10	6.64	2.88	2.62	0.780	0.21	5.31	99.92	
Barton Peninsula													4.26
BP-2	49.70	20.30	7.94	0.151	5.01	9.51	3.51	0.48	0.633	0.12	3.04	100.39	
BP-3A	51.60	19.18	8.71	0.119	4.05	9.93	2.76	0.25	0.717	0.14	2.70	100.17	
BP-4	52.66	19.71	7.17	0.141	3.33	8.16	3.76	0.62	0.560	0.17	4.20	100.49	
BP-6	56.80	14.49	9.35	0.179	3.22	5.55	3.56	2.11	1.144	0.63	3.33	100.37	
BP-7	54.88	15.46	10.51	0.171	4.09	7.61	3.02	1.67	1.328	0.40	1.33	100.52	
BP-9	56.61	17.52	7.07	0.109	4.16	6.57	2.57	2.25	0.671	0.21	2.72	100.48	
BP-10A	52.67	17.99	8.69	0.189	5.11	6.53	1.81	1.88	0.642	0.15	4.27	99.94	
BP-10B	50.48	19.46	9.29	0.164	4.22	6.10	1.78	3.58	0.667	0.17	3.84	99.76	
BP-10B /R	50.65	19.53	9.34	0.166	4.23	6.11	1.75	3.68	0.675	0.17	3.84	100.14	
BP-10B (average)	50.57	19.50	9.32	0.165	4.23	6.11	1.77	3.63	0.671	0.17	3.84	99.95	
BP-11A	52.44	17.51	8.79	0.158	3.89	5.80	2.12	3.98	0.738	0.14	3.47	99.07	
BP-11B	47.60	20.05	8.30	0.149	4.35	7.79	2.49	2.21	0.729	0.14	5.36	99.18	
BP-12B/1	62.69	14.74	4.01	0.086	1.50	5.28	2.41	2.43	0.457	0.15	4.79	98.56	
BP-13	55.11	15.22	9.47	0.153	3.34	4.77	3.82	0.89	1.008	0.35	5.66	99.80	
BP-14	53.62	16.02	7.30	0.121	4.42	7.96	3.09	0.33	0.658	0.19	5.11	98.84	
BP-15	52.97	17.19	6.85	0.123	4.05	6.60	3.74	1.33	0.616	0.22	5.00	98.70	
BP-16	55.07	16.64	9.57	0.162	3.60	6.98	3.84	1.36	1.104	0.34	1.78	100.45	
BP-17	53.77	14.69	7.00	0.137	6.65	6.67	3.66	1.41	0.611	0.16	4.24	99.01	
BP-18	49.56	17.13	7.89	0.137	4.53	7.78	3.45	0.37	0.697	0.22	7.84	99.60	
BP-18 /R	49.70	17.21	7.89	0.137	4.53	7.82	3.46	0.34	0.693	0.23	7.84	99.84	
BP-18 (average)	49.63	17.17	7.89	0.137	4.53	7.80	3.46	0.36	0.695	0.23	7.84	99.72	
BP-19	54.54	16.23	8.43	0.163	4.67	4.24	4.73	0.13	0.899	0.35	4.20	98.60	
BP-22	53.75	18.28	8.28	0.137	3.96	7.83	3.24	1.60	0.806	0.25	2.37	100.49	
BP-24	53.32	17.26	6.47	0.108	2.76	6.04	3.55	2.31	0.692	0.20	7.36	100.06	
BP-26A	52.87	19.01	7.50	0.157	2.86	7.36	3.51	1.82	0.707	0.16	4.51	100.45	
BP-27	52.95	15.56	9.54	0.178	3.43	5.72	3.57	0.62	1.036	0.35	5.98	98.96	
BP-28	52.34	17.73	9.49	0.158	3.98	6.55	4.28	1.50	0.908	0.27	3.31	100.51	
BP-29	51.15	18.44	8.73	0.152	3.43	6.16	2.73	3.77	0.763	0.14	5.02	100.48	
BP-33	49.30	17.34	8.34	0.143	3.32	7.82	4.15	1.50	0.798	0.28	6.23	99.22	
BP-34	62.23	15.08	6.04	0.102	1.41	3.53	5.01	0.12	0.854	0.34	5.59	100.30	

SAMPLE	SiO_2	Al_2O_3	Fe_2O_3	MnO	MgO	CaO	Na_2O	K_2O	TiO_2	P_2O_5	LOI	TOTAL	LOI
	%	%	%	%	%	%	%	%	%	%	%	%	(average)
Weaver Peninsula													5,57
WP-1	52,95	17,26	6,92	0,141	3,60	7,96	3,47	0,83	0,614	0,18	4,90	98,84	
WP-2	46,94	18,98	8,13	0,129	6,47	11,65	2,09	0,11	0,558	0,09	3,44	98,59	
WP-5	42,65	20,18	8,18	0,096	7,18	12,65	0,92	0,11	0,409	0,06	6,86	99,28	
WP-6	57,31	16,69	5,82	0,139	1,85	5,20	3,92	1,70	0,622	0,17	7,09	100,50	
WP-7A	52,09	19,71	6,50	0,115	3,24	3,97	6,49	1,54	0,537	0,13	4,93	99,25	
WP-7B	54,48	16,67	6,17	0,120	2,10	8,65	2,84	2,40	0,537	0,13	5,40	99,48	
WP-10	48,49	18,52	9,32	0,123	4,73	9,95	2,08	0,13	0,673	0,10	5,49	99,59	
WP-11	48,79	19,25	8,33	0,123	3,72	10,34	2,90	0,14	0,720	0,18	5,46	99,94	
WP-13	53,93	18,80	7,35	0,132	3,95	9,04	3,11	0,21	0,622	0,15	3,14	100,43	
WP-14	53,80	18,40	6,90	0,129	3,67	8,73	3,14	0,26	0,626	0,16	4,05	99,85	
WP-17	52,23	16,67	9,88	0,176	4,24	7,31	4,42	0,14	0,886	0,18	4,32	100,45	
WP-18	48,95	19,98	7,66	0,135	4,43	9,02	3,55	0,42	0,576	0,12	5,20	100,04	
WP-19	46,86	16,97	9,16	0,191	3,49	7,63	2,94	1,76	0,954	0,16	9,63	99,74	
WP-20B	46,39	20,76	7,78	0,150	3,50	11,05	2,22	0,38	0,630	0,12	6,75	99,73	
WP-20C	52,25	17,44	8,36	0,172	3,27	8,07	2,85	0,26	0,805	0,21	6,96	100,64	
WP-21	63,25	14,99	3,87	0,094	1,37	4,14	4,05	1,92	0,439	0,14	5,43	99,68	
Fildes Peninsula													4,28
NP-1	48,80	20,34	7,45	0,149	4,55	5,71	4,10	1,99	0,699	0,17	6,04	100,01	
FP-1	55,92	17,11	7,47	0,158	3,98	6,55	4,25	1,33	0,766	0,16	2,58	100,27	
FP-2	59,62	16,18	5,38	0,134	1,78	4,80	4,15	1,48	0,783	0,34	5,59	100,25	
FP-4	58,82	16,13	5,99	0,179	2,23	4,82	4,30	1,54	0,780	0,34	4,78	99,90	
FP-8	64,10	15,50	4,60	0,145	1,34	3,80	4,88	1,46	0,808	0,29	3,48	100,40	
FP-11	50,23	18,32	8,88	0,167	4,96	7,85	4,06	0,81	0,814	0,18	3,23	99,50	
Nelson Island													4,05
NI-1	66,59	14,46	4,27	0,080	0,94	2,64	3,49	3,32	0,891	0,33	3,16	100,17	
NI-2	60,85	14,75	6,05	0,178	1,02	2,93	4,47	2,22	0,907	0,33	5,23	98,93	
NI-3	61,26	14,65	5,59	0,173	1,01	3,76	4,11	2,63	0,907	0,33	5,36	99,77	
NI-4	49,13	20,86	7,60	0,184	4,82	9,01	3,91	0,51	0,601	0,11	3,33	100,06	
NI-5	53,73	18,87	7,48	0,113	4,63	8,24	3,46	1,56	0,686	0,16	1,26	100,19	
NI-6	53,21	16,29	9,47	0,151	3,49	7,82	3,66	0,91	1,144	0,28	3,15	99,58	
Hurd Peninsula													4,81
HP-1A/2	52,81	15,15	11,08	0,192	4,97	6,92	3,48	1,14	1,309	0,22	2,96	100,23	
HP-1B	47,58	18,33	9,63	0,181	6,74	6,31	3,35	2,23	1,174	0,22	4,43	100,17	
HP-7A	56,10	14,97	6,73	0,193	2,13	5,84	3,55	2,08	1,100	0,32	6,96	99,96	
HP-7B	53,17	16,25	8,90	0,190	2,53	6,38	2,79	2,01	1,362	0,27	5,78	99,62	
HP-7D	58,70	16,04	5,37	0,144	1,77	4,29	1,99	4,92	0,863	0,31	5,43	99,82	
HP-7E	47,72	17,01	8,28	0,228	5,83	6,22	2,47	3,03	0,892	0,20	7,10	98,99	
HP-7F	47,26	17,48	9,52	0,162	6,12	7,72	3,16	2,43	1,166	0,24	4,33	99,59	
HP-7G	56,35	15,39	8,72	0,142	2,76	4,64	4,39	1,86	1,149	0,24	4,41	100,06	
HP-7H	50,84	14,57	13,24	0,247	4,37	4,38	4,14	1,79	1,674	0,19	3,95	99,39	
HP-7J	56,42	14,78	8,91	0,227	2,49	5,24	4,59	0,88	1,577	0,54	3,32	98,96	
HP-7J /R	57,18	14,83	8,93	0,230	2,47	5,24	4,63	0,94	1,534	0,54	3,32	99,86	
HP-7J (average)	56,80	14,81	8,92	0,229	2,48	5,24	4,61	0,91	1,556	0,54	3,32	99,41	
HP-8A/4	58,68	14,61	7,94	0,174	2,25	3,89	4,90	1,73	1,317	0,37	4,00	99,86	
HP-10A	51,20	17,15	9,46	0,143	5,15	5,71	3,99	3,00	1,154	0,22	2,82	99,99	
HP-12/2	68,16	13,70	3,18	0,100	0,95	2,81	3,12	3,22	0,453	0,13	4,03	99,84	
HP-15/4	66,71	14,16	4,23	0,169	0,92	3,00	3,72	2,22	0,646	0,19	4,03	99,98	
HP-16/2	47,97	17,19	8,98	0,175	6,53	6,41	3,52	2,14	0,788	0,15	6,28	100,12	
HP-16/2 /R	47,42	16,90	8,85	0,172	6,40	6,32	3,44	2,14	0,772	0,15	6,28	98,84	
HP-16/2 (average)	47,70	17,05	8,92	0,174	6,47	6,37	3,48	2,14	0,780	0,15	6,28	99,48	
HP-17/2	46,89	18,29	10,16	0,164	7,04	6,15	2,97	2,44	1,126	0,18	4,51	99,91	
HP-18/2	45,96	16,68	8,33	0,146	6,83	12,89	1,58	1,08	0,742	0,14	4,63	99,01	
HP-19/1	42,59	17,63	10,56	0,242	3,04	10,21	0,99	5,08	1,048	0,26	7,79	99,44	
HP-23/2	59,81	16,66	5,27	0,117	3,37	4,49	4,06	2,28	0,580	0,16	3,35	100,14	
HP-25/6	52,00	14,92	12,47	0,204	4,35	6,53	3,12	0,54	1,599	0,23	4,15	100,10	
HP-26/2B	68,14	13,72	3,11	0,118	0,82	2,25	4,00	3,01	0,457	0,12	2,97	98,71	
HP-27/1	45,79	16,35	10,92	0,194	7,39	5,53	2,07	3,14	1,310	0,34	7,12	100,16	
HP-28/2	50,58	15,30	11,08	0,166	3,87	5,54	4,12	0,94	1,496	0,33	6,56	99,99	
HP-33/3	63,24	14,38	5,25	0,161	1,24	4,10	4,51	1,50	0,802	0,26	4,48	99,92	

SAMPLE	SiO_2	Al_2O_3	Fe_2O_3	MnO	MgO	CaO	Na_2O	K_2O	TiO_2	P_2O_5	Total		FeO_{tot}	Mg#
	wt%	wt%	wt%	wt%	wt%	wt%	wt%	wt%	wt%	wt%	wt%		wt%	
Penguin Island														
PI-1	48,85	15,55	9,53	0,158	10,76	9,87	3,31	0,56	1,148	0,26	100,00		8,57	69,12
PI-2	48,49	15,02	9,66	0,159	12,00	9,57	3,20	0,53	1,112	0,25	100,00		8,70	71,10
PI-3	47,72	15,63	9,93	0,159	11,65	9,68	3,24	0,64	1,102	0,26	100,00		8,93	69,91
PI-4	48,70	15,20	9,65	0,158	11,50	9,70	3,19	0,52	1,121	0,25	100,00		8,69	70,24
PI-5	49,34	16,83	9,44	0,154	8,35	10,00	3,67	0,67	1,259	0,29	100,00		8,50	63,67
Admiralty Bay														
AP-1	54,06	15,92	11,34	0,200	3,98	7,53	4,12	1,09	1,364	0,40	100,00		10,20	41,01
SH-1	69,99	15,47	3,00	0,081	0,33	1,46	5,37	3,56	0,611	0,13	100,00		2,70	17,74
SH-3	69,98	15,36	2,97	0,086	0,36	1,55	5,22	3,73	0,606	0,13	100,00		2,67	19,30
SP-1	58,62	17,25	7,32	0,121	3,38	6,18	3,95	2,08	0,832	0,27	100,00		6,58	47,77
EI-1	49,76	21,56	8,83	0,189	5,88	8,29	3,70	0,77	0,851	0,17	100,00		7,94	56,88
EI-2	52,15	20,55	8,35	0,140	4,56	9,43	3,52	0,26	0,834	0,21	100,00		7,51	51,98
EI-3	50,29	21,32	8,99	0,214	5,37	9,29	3,24	0,24	0,847	0,19	100,00		8,09	54,20
EI-9	50,70	20,58	9,02	0,194	4,30	9,66	4,08	0,44	0,851	0,17	100,00		8,12	48,58
EI-10	49,23	20,61	9,26	0,184	5,42	11,12	3,05	0,17	0,778	0,17	100,00		8,33	53,71
EI-11	50,63	19,69	8,74	0,145	5,63	10,86	3,13	0,23	0,746	0,19	100,00		7,87	56,07
EI-13	48,84	21,61	9,28	0,328	5,09	10,47	3,18	0,22	0,836	0,15	100,00		8,35	52,04
EI-15	55,85	17,55	7,81	0,123	4,58	8,31	3,33	1,37	0,779	0,29	100,00		7,03	53,75
EI-16	55,67	17,36	8,21	0,185	4,85	8,22	3,46	1,03	0,790	0,24	100,00		7,39	53,91
EI-17	57,00	18,28	7,22	0,143	4,27	7,83	3,91	0,44	0,676	0,24	100,00		6,49	53,95
EI-18	58,15	16,47	9,25	0,112	3,15	3,85	4,02	3,58	1,088	0,34	100,00		8,32	40,26
EI-20	56,18	17,75	8,06	0,153	4,49	6,74	2,75	2,86	0,791	0,23	100,00		7,26	52,45
EI-21	56,01	17,88	8,12	0,166	4,30	6,20	2,07	4,17	0,835	0,23	100,00		7,31	51,21
EI-22A	52,85	20,63	7,98	0,129	4,33	9,16	3,70	0,28	0,761	0,18	100,00		7,18	51,82
KC-1	55,74	18,27	8,01	0,134	4,02	7,80	2,88	2,19	0,737	0,21	100,00		7,21	49,83
KP-1	56,68	17,43	7,76	0,146	3,86	7,59	3,35	2,06	0,863	0,26	100,00		6,98	49,63
Potter Peninsula														
PP-1A	56,25	18,84	7,30	0,120	4,06	8,09	3,32	1,23	0,584	0,21	100,00		6,56	52,42
PP-1B	57,74	18,11	7,01	0,135	4,00	8,48	3,22	0,50	0,593	0,21	100,00		6,31	53,02
PP-1C	75,33	12,86	1,92	0,032	0,36	1,24	3,03	4,90	0,280	0,05	100,00		1,73	26,94
PP-2	57,19	17,03	7,65	0,294	4,93	7,88	3,24	0,90	0,691	0,20	100,00		6,88	56,07
PP-3	57,17	16,76	7,72	0,157	4,92	7,94	3,21	1,24	0,696	0,19	100,00		6,95	55,81
PP-4	56,62	17,18	7,86	0,142	4,85	7,59	3,37	1,50	0,690	0,19	100,00		7,07	55,01
PP-5A	56,39	17,66	8,43	0,143	3,88	7,52	3,12	1,73	0,853	0,27	100,00		7,59	47,69
PP-5B	76,54	13,17	1,18	0,025	0,12	2,79	1,49	4,45	0,199	0,03	100,00		1,06	17,38
PP-5C	56,57	17,33	8,44	0,132	3,90	7,68	3,03	1,75	0,896	0,28	100,00		7,60	47,80
PP-6A/1	52,18	16,92	8,75	0,207	6,62	8,84	5,37	0,18	0,777	0,14	100,00		7,88	59,97
PP-6A/2	57,08	16,92	8,17	0,127	3,78	7,87	3,16	1,77	0,852	0,28	100,00		7,35	47,84
PP-6B	77,31	12,69	1,58	0,027	0,24	0,80	2,18	4,95	0,194	0,03	100,00		1,42	22,95
PP-6C	56,90	17,20	8,18	0,133	3,65	7,77	3,25	1,75	0,889	0,28	100,00		7,36	46,92
PP-7	50,21	19,32	8,93	0,148	6,56	11,10	2,51	0,19	0,878	0,17	100,00		8,03	59,27
60C4	50,34	19,42	9,02	0,153	5,73	11,18	2,80	0,35	0,842	0,16	100,00		8,11	55,71
PP-8	56,80	16,50	9,88	0,199	3,06	8,19	3,57	0,29	1,119	0,39	100,00		8,89	38,02
PP-9	60,47	17,05	8,14	0,218	2,57	3,91	5,75	0,32	1,087	0,49	100,00		7,32	38,49
PP-10	62,72	15,68	7,81	0,264	2,64	3,18	6,48	0,02	0,923	0,29	100,00		7,03	40,09
PP-11	56,98	18,67	7,16	0,134	3,91	7,99	3,24	1,12	0,574	0,22	100,00		6,44	51,97
PP-12	56,40	16,56	9,94	0,184	3,22	6,88	3,86	1,44	1,105	0,41	100,00		8,95	39,05
PP-13	66,25	16,04	5,48	0,123	1,79	2,23	3,91	3,13	0,794	0,27	100,00		4,93	39,28
PP-19	56,69	16,93	7,78	0,136	4,97	7,69	3,26	1,62	0,732	0,20	100,00		7,00	55,86
PP-31B	56,85	17,12	7,78	0,134	4,93	7,54	3,47	1,24	0,751	0,20	100,00		7,00	55,67
PP-32A	56,62	17,37	8,42	0,122	3,70	7,39	3,36	1,82	0,908	0,29	100,00		7,57	46,56
PP-32B	72,96	13,92	2,78	0,061	0,71	3,30	2,19	3,65	0,364	0,07	100,00		2,50	33,54
PP-32C	57,16	17,09	8,22	0,139	3,80	7,73	3,10	1,62	0,872	0,28	100,00		7,39	47,79
PP-33	54,96	18,15	8,07	0,143	3,53	5,85	3,58	4,68	0,803	0,23	100,00		7,26	46,39
127A	67,33	13,76	5,28	0,108	1,78	2,86	4,08	3,53	0,835	0,43	100,00		4,75	40,09
128A	53,92	19,00	8,70	0,169	4,33	7,02	3,04	2,77	0,824	0,22	100,00		7,83	49,67
Barton Peninsula														
BP-2	51,05	20,85	8,16	0,155	5,15	9,77	3,61	0,49	0,650	0,12	100,00		7,34	55,56
BP-3A	52,95	19,68	8,94	0,122	4,16	10,19	2,83	0,26	0,736	0,14	100,00		8,04	47,95
BP-4	54,69	20,47	7,45	0,146	3,46	8,48	3,91	0,64	0,582	0,18	100,00		6,70	47,92
BP-6	58,54	14,93	9,64	0,184	3,32	5,72	3,67	2,17	1,179	0,65	100,00		8,67	40,56
BP-7	55,36	15,59	10,60	0,172	4,13	7,68	3,05	1,68	1,340	0,40	100,00		9,54	43,53
BP-9	57,92	17,93	7,23	0,112	4,26	6,72	2,63	2,30	0,687	0,21	100,00		6,51	53,83
BP-10A	55,06	18,81	9,08	0,198	5,34	6,83	1,89	1,97	0,671	0,16	100,00		8,17	53,81
BP-10B	52,61	20,28	9,69	0,172	4,40	6,35	1,84	3,78	0,698	0,18	100,00		8,72	47,33
BP-11A	54,87	18,32	9,20	0,165	4,07	6,07	2,22	4,16	0,772	0,15	100,00		8,28	46,72
BP-11B	50,74	21,37	8,85	0,159	4,64	8,30	2,65	2,36	0,777	0,15	100,00		7,96	50,94
BP-12B/1	66,87	15,72	4,28	0,092	1,60	5,63	2,57	2,59	0,487	0,16	100,00		3,85	42,56
BP-13	58,55	16,17	10,06	0,163	3,55	5,07	4,06	0,95	1,071	0,37	100,00		9,05	41,13
BP-14	57,22	17,10	7,79	0,129	4,72	8,49	3,30	0,35	0,702	0,20	100,00		7,01	54,54
BP-15	56,54	18,35	7,31	0,131	4,32	7,04	3,99	1,42	0,657	0,23	100,00		6,58	53,94
BP-16	55,81	16,86	9,70	0,164	3,65	7,07	3,89	1,38	1,119	0,34	100,00		8,73	42,70
BP-17	56,74	15,50	7,39	0,145	7,02	7,04	3,86	1,49	0,645	0,17	100,00		6,65	65,30
BP-18	54,01	18,69	8,59	0,149	4,93	8,49	3,76	0,39	0,756	0,24	100,00		7,73	53,22
BP-19	57,79	17,20	8,93	0,173	4,95	4,49	5,01	0,14	0,953	0,37	100,00		8,04	52,32
BP-22	54,77	18,63	8,44	0,140	4,04	7,98	3,30	1,63	0,821	0,25	100,00		7,59	48,65
BP-24	57,51	18,62	6,98	0,116	2,98	6,51	3,83	2,49	0,746	0,22	100,00		6,28	45,80
BP-26A	55,10	19,81	7,82	0,164	2,98	7,67	3,66	1,90	0,737	0,17	100,00		7,03	43,03
BP-27	56,96	16,74	10,26	0,191	3,69	6,15	3,84	0,67	1,115	0,38	100,00		9,23	41,60
BP-28	53,84	18,24	9,76	0,163	4,09	6,74	4,40	1,54	0,934	0,28	100,00		8,78	45,38
BP-29	53,58	19,32	9,14	0,159	3,59	6,45	2,86	3,95	0,799	0,15	100,00		8,23	43,77
BP-33	53,02	18,65	8,97	0,154	3,57	8,41	4,46	1,61	0,858	0,30	100,00		8,07	44,09
BP-34	65,70	15,92	6,38	0,108	1,49	3,73	5,29	0,13	0,902	0,36	100,00		5,74	31,62

Recalculated to 100% on a volatile free basis

SAMPLE	SiO_2	Al_2O_3	Fe_2O_3	MnO	MgO	CaO	Na_2O	K_2O	TiO_2	P_2O_5	Total		FeO_{tot}	Mg#
	wt%	wt%	wt%	wt%	wt%	wt%	wt%	wt%	wt%	wt%	wt%		wt%	
Weaver Peninsula														
WP-1	56,37	18,38	7,37	0,150	3,83	8,47	3,69	0,88	0,654	0,19	100,00		6,63	50,75
WP-2	49,33	19,95	8,54	0,136	6,80	12,24	2,20	0,12	0,586	0,09	100,00		7,69	61,19
WP-5	46,14	21,83	8,85	0,104	7,77	13,69	1,00	0,12	0,442	0,06	100,00		7,96	63,49
WP-6	61,35	17,87	6,23	0,149	1,98	5,57	4,20	1,82	0,666	0,18	100,00		5,61	38,64
WP-7A	55,23	20,90	6,89	0,122	3,44	4,21	6,88	1,63	0,569	0,14	100,00		6,20	49,69
WP-7B	57,90	17,72	6,56	0,128	2,23	9,19	3,02	2,55	0,571	0,14	100,00		5,90	40,27
WP-10	51,52	19,68	9,90	0,131	5,03	10,57	2,21	0,14	0,715	0,11	100,00		8,91	50,14
WP-11	51,63	20,37	8,82	0,130	3,94	10,94	3,07	0,15	0,762	0,19	100,00		7,93	46,94
WP-13	55,43	19,32	7,55	0,136	4,06	9,29	3,20	0,22	0,639	0,15	100,00		6,80	51,57
WP-14	56,15	19,20	7,20	0,135	3,83	9,11	3,28	0,27	0,653	0,17	100,00		6,48	51,31
WP-17	54,33	17,34	10,28	0,183	4,41	7,60	4,60	0,15	0,922	0,19	100,00		9,25	45,95
WP-18	51,61	21,07	8,08	0,142	4,67	9,51	3,74	0,44	0,607	0,13	100,00		7,27	53,40
WP-19	52,00	18,83	10,16	0,212	3,87	8,47	3,26	1,95	1,059	0,18	100,00		9,15	43,01
WP-20B	49,89	22,33	8,37	0,161	3,76	11,88	2,39	0,41	0,678	0,13	100,00		7,53	47,12
WP-20C	55,77	18,62	8,92	0,184	3,49	8,61	3,04	0,28	0,859	0,22	100,00		8,03	43,66
WP-21	67,10	15,90	4,11	0,100	1,45	4,39	4,30	2,04	0,466	0,15	100,00		3,69	41,22
Fildes Peninsula														
NP-1	51,94	21,65	7,93	0,159	4,84	6,08	4,36	2,12	0,744	0,18	100,00		7,13	54,75
FP-1	57,24	17,51	7,65	0,162	4,07	6,70	4,35	1,36	0,784	0,16	100,00		6,88	51,35
FP-2	62,99	17,10	5,68	0,142	1,88	5,07	4,38	1,56	0,827	0,36	100,00		5,11	39,59
FP-4	61,83	16,96	6,30	0,188	2,34	5,07	4,52	1,62	0,820	0,36	100,00		5,67	42,45
FP-8	66,13	15,99	4,75	0,150	1,38	3,92	5,03	1,51	0,834	0,30	100,00		4,27	36,59
FP-11	52,18	19,03	9,22	0,173	5,15	8,15	4,22	0,84	0,846	0,19	100,00		8,30	52,53
Nelson Island														
NI-1	68,64	14,91	4,40	0,082	0,97	2,72	3,60	3,42	0,918	0,34	100,00		3,96	30,37
NI-2	64,94	15,74	6,46	0,190	1,09	3,13	4,77	2,37	0,968	0,35	100,00		5,81	25,04
NI-3	64,88	15,52	5,92	0,183	1,07	3,98	4,35	2,79	0,961	0,35	100,00		5,33	26,36
NI-4	50,79	21,56	7,86	0,190	4,98	9,31	4,04	0,53	0,621	0,11	100,00		7,07	55,68
NI-5	54,31	19,07	7,56	0,114	4,68	8,33	3,50	1,58	0,693	0,16	100,00		6,80	55,08
NI-6	55,18	16,89	9,82	0,157	3,62	8,11	3,80	0,94	1,186	0,29	100,00		8,84	42,20
Hurd Peninsula														
HP-1A/2	54,29	15,58	11,39	0,197	5,11	7,11	3,58	1,17	1,346	0,23	100,00		10,25	47,05
HP-1B	49,69	19,14	10,06	0,189	7,04	6,59	3,50	2,33	1,226	0,23	100,00		9,05	58,10
HP-7A	60,31	16,09	7,24	0,207	2,29	6,28	3,82	2,24	1,183	0,34	100,00		6,51	38,54
HP-7B	56,65	17,31	9,48	0,202	2,70	6,80	2,97	2,14	1,451	0,29	100,00		8,53	36,03
HP-7D	62,18	16,99	5,69	0,153	1,88	4,54	2,11	5,21	0,914	0,33	100,00		5,12	39,50
HP-7E	51,94	18,51	9,01	0,248	6,35	6,77	2,69	3,30	0,971	0,22	100,00		8,11	58,24
HP-7F	49,61	18,35	9,99	0,170	6,42	8,10	3,32	2,55	1,224	0,25	100,00		8,99	56,02
HP-7G	58,92	16,09	9,12	0,148	2,89	4,85	4,59	1,94	1,201	0,25	100,00		8,20	38,54
HP-7H	53,27	15,27	13,87	0,259	4,58	4,59	4,34	1,88	1,754	0,20	100,00		12,48	39,54
HP-7J	59,11	15,41	9,28	0,238	2,58	5,45	4,80	0,95	1,619	0,56	100,00		8,35	35,52
HP-8A/4	61,21	15,24	8,28	0,182	2,35	4,06	5,11	1,80	1,374	0,39	100,00		7,45	35,95
HP-10A	52,69	17,65	9,73	0,147	5,30	5,88	4,11	3,09	1,188	0,23	100,00		8,76	51,89
HP-12/2	71,13	14,30	3,32	0,104	0,99	2,93	3,26	3,36	0,473	0,14	100,00		2,99	37,18
HP-15/4	69,51	14,76	4,41	0,176	0,96	3,13	3,88	2,31	0,673	0,20	100,00		3,97	30,11
HP-16/2	51,17	18,29	9,56	0,186	6,94	6,83	3,73	2,30	0,837	0,16	100,00		8,61	58,96
HP-17/2	49,15	19,17	10,65	0,172	7,38	6,45	3,11	2,56	1,180	0,19	100,00		9,58	57,85
HP-18/2	48,70	17,67	8,83	0,155	7,24	13,66	1,67	1,14	0,786	0,15	100,00		7,94	61,90
HP-19/1	46,47	19,24	11,52	0,264	3,32	11,14	1,08	5,54	1,143	0,28	100,00		10,37	36,32
HP-23/2	61,79	17,21	5,44	0,121	3,48	4,64	4,19	2,36	0,599	0,17	100,00		4,90	55,89
HP-25/6	54,19	15,55	12,99	0,213	4,53	6,80	3,25	0,56	1,666	0,24	100,00		11,69	40,87
HP-26/2B	71,17	14,33	3,25	0,123	0,86	2,35	4,18	3,14	0,477	0,13	100,00		2,92	34,31
HP-27/1	49,22	17,57	11,74	0,209	7,94	5,94	2,22	3,38	1,408	0,37	100,00		10,56	57,28
HP-28/2	54,14	16,38	11,86	0,178	4,14	5,93	4,41	1,01	1,601	0,35	100,00		10,67	40,90
HP-33/3	66,26	15,07	5,50	0,169	1,30	4,30	4,73	1,57	0,840	0,27	100,00		4,95	31,88

Recalculated to 100% on a volatile free basis.

Trace element values are in µg/g (ppm).																																												
Sample ID:	**Be**	**Sc**	**V**	**Cr**	**Co**	**Ni**	**Cu**	**Zn**	**Ga**	**Ge**	**As**	**Rb**	**Sr**	**Y**	**Zr**	**Nb**	**Mo**	**Ag**	**In**	**Sn**	**Sb**	**Cs**	**Ba**	**La**	**Ce**	**Pr**	**Nd**	**Sm**	**Eu**	**Gd**	**Tb**	**Dy**	**Ho**	**Er**	**Tm**	**Yb**	**Lu**	**Hf**	**Ta**	**W**	**Tl**	**Pb**	**Bi**	**Th**	**U**
Penguin Island																																													
PI-1	<1	29	246	506	54	197	99	73	21	1	<5	8	567	15	62	3.87	<2	<0.5	<0.2	2	<0.5	<0.5	167	9.60	22.9	2.85	13.0	3.04	1.08	3.1	0.5	2.8	0.6	1.6	0.21	1.3	0.20	2.0	0.32	138	<0.1	<5	<0.4	1.2	0.3
PI-2	<1	28	245	563	58	238	87	76	20	1	<5	7	543	14	60	3.69	<2	<0.5	<0.2	<1	<0.5	<0.5	161	8.98	21.8	2.75	12.7	2.91	1.00	3.0	0.5	2.7	0.5	1.5	0.21	1.3	0.19	2.1	0.31	149	<0.1	8	<0.4	1.1	0.2
PI-3	<1	30	264	566	64	224	120	82	20	1	<5	7	548	14	66	4.37	<2	<0.5	<0.2	1	<0.5	<0.5	179	9.60	23.2	2.89	12.8	3.02	1.04	3.1	0.5	2.8	0.5	1.5	0.21	1.3	0.19	2.0	0.34	194	<0.1	7	<0.4	1.3	0.2
PI-4	<1	30	261	535	54	211	56	118	20	1	<5	7	545	14	60	3.53	<2	<0.5	<0.2	<1	0.7	<0.5	160	9.14	22.0	2.76	12.5	2.95	1.03	2.9	0.5	2.7	0.5	1.5	0.22	1.3	0.19	1.9	0.31	136	0.6	<5	<0.4	1.1	0.3
PI-5	<1	27	270	227	50	95	125	89	22	1	<5	9	625	14	64	3.95	<2	<0.5	<0.2	1	<0.5	<0.5	178	10.46	25.4	3.15	13.9	3.17	1.13	3.1	0.5	2.9	0.6	1.5	0.21	1.4	0.20	2.2	0.36	173	<0.1	7	<0.4	1.3	0.3
Admiralty Bay																																												
AP-1	2	32	336	40	28	135	301	90	21	1	<5	8	550	26	138	3.05	3	<0.5	<0.2	1	<0.5	<0.5	358	21.92	49.2	6.22	29.5	6.69	2.01	6.4	0.9	4.9	0.9	2.8	0.40	2.5	0.36	3.9	0.42	35	<0.1	6	<0.4	3.8	1.1
SH-1	2	11	24	<20	9	<20	<10	38	18	1	<5	75	230	31	283	4.68	3	<0.5	<0.2	2	<0.5	0.9	700	32.61	71.6	8.60	37.7	7.67	1.63	6.7	0.9	5.2	1.0	3.1	0.46	2.9	0.44	7.5	0.57	69	0.4	8	<0.4	7.6	2.2
SH-3	2	11	30	<20	11	27	18	67	20	1	14	80	233	27	289	5.10	4	<0.5	<0.2	3	<0.5	1.3	691	33.97	79.0	9.07	38.6	8.05	1.73	6.8	0.9	4.9	0.9	2.8	0.42	2.7	0.39	8.0	0.79	63	0.6	16	<0.4	6.4	2.0
SP-1	2	21	183	<20	21	<20	183	64	20	1	<5	44	587	21	148	2.56	4	<0.5	<0.2	<1	<0.5	0.5	380	19.77	45.1	5.55	25.7	5.72	1.50	5.1	0.7	3.8	0.7	2.2	0.32	2.0	0.30	4.3	1.34	26	0.2	6	<0.4	5.6	1.8
EI-1	1	28	274	<20	27	22	82	68	21	<1	<5	6	676	14	48	<1	<2	<0.5	<0.2	<1	<0.5	<0.5	274	7.08	17.3	2.35	12.2	3.16	1.23	3.4	0.5	2.7	0.5	1.5	0.22	1.4	0.20	1.5	0.10	6	<0.1	<5	<0.4	0.7	0.3
EI-2	1	25	254	<20	25	<20	189	90	20	1	<5	<2	817	14	58	1.35	<2	<0.5	<0.2	1	<0.5	<0.5	161	10.46	24.1	3.10	15.3	3.61	1.35	3.6	0.5	2.6	0.5	1.5	0.20	1.3	0.19	1.7	<0.1	15	<0.1	7	<0.4	1.1	0.4
EI-3	<1	27	288	<20	26	22	187	60	22	1	<5	<2	673	14	49	<1	<2	<0.5	<0.2	<1	<0.5	<0.5	133	7.24	17.6	2.39	12.2	3.20	1.23	3.4	0.5	2.7	0.5	1.6	0.22	1.5	0.21	1.5	0.13	9	<0.1	<5	<0.4	0.7	0.3
EI-9	<1	29	267	<20	28	<20	159	69	21	1	<5	2	752	14	49	1.06	5	<0.5	<0.2	<1	<0.5	<0.5	175	6.84	16.7	2.28	11.8	3.12	1.22	3.3	0.5	2.7	0.5	1.6	0.22	1.4	0.21	1.5	0.72	22	<0.1	6	<0.4	0.6	0.3
EI-10	1	29	276	29	32	30	141	54	20	<1	<5	<2	707	13	44	<1	<2	<0.5	<0.2	<1	<0.5	<0.5	142	7.91	18.6	2.46	12.5	3.12	1.18	3.2	0.4	2.4	0.5	1.4	0.18	1.2	0.18	1.4	0.12	9	<0.1	<5	<0.4	0.9	0.3
EI-11	<1	32	238	29	31	31	146	63	20	1	<5	<2	694	13	48	<1	4	<0.5	<0.2	<1	<0.5	<0.5	160	8.55	20.2	2.66	13.2	3.20	1.20	3.3	0.5	2.4	0.5	1.3	0.19	1.2	0.18	1.5	1.14	7	<0.1	6	<0.4	0.9	0.3
EI-13	<1	29	266	<20	28	<20	166	99	23	1	<5	<2	696	14	49	1.01	<2	<0.5	<0.2	2	<0.5	<0.5	134	7.18	17.2	2.32	12.0	3.13	1.20	3.2	0.5	2.6	0.5	1.5	0.21	1.3	0.20	1.5	<0.1	14	<0.1	<5	<0.4	0.7	0.3
EI-15	2	25	216	39	30	53	158	67	20	1	9	15	684	20	140	2.76	3	<0.5	<0.2	2	<0.5	<0.5	313	19.51	46.1	5.44	24.1	5.48	1.42	4.9	0.7	3.6	0.7	2.1	0.29	1.9	0.28	4.1	0.87	39	<0.1	6	<0.4	4.5	1.5
EI-16	2	24	189	30	29	24	160	56	19	1	53	18	615	20	138	2.47	6	<0.5	<0.2	1	<0.5	1.3	344	19.02	42.7	5.20	24.1	5.31	1.41	5.0	0.7	3.7	0.7	2.1	0.30	1.9	0.29	4.1	1.26	70	0.4	8	<0.4	5.7	1.8
EI-16 rep	2	24	184	32	29	40	163	56	19	1	53	18	609	20	137	2.46	4	<0.5	<0.2	2	0.5	1.3	335	18.56	41.4	5.11	23.6	5.23	1.40	4.8	0.7	3.6	0.7	2.0	0.30	1.9	0.28	4.0	1.01	68	0.4	6	<0.4	5.3	1.8
EI-16 (average)	2	24	187	31	29	32	162	56	19	1.1	53	18	612	20	138	2.47	5	<0.5	<0.2	1.8	0.5	1.32	339.5	18.79	42.0	5.16	23.9	5.27	1.41	4.9	0.7	3.6	0.7	2.1	0.30	1.9	0.28	4.0	1.14	69	0.42	7.1	<0.4	5.49	1.8
EI-17	2	17	159	<20	22	<20	150	68	19	<1	11	2	901	16	106	1.76	4	<0.5	<0.2	1	<0.5	0.6	214	16.14	36.1	4.41	20.6	4.58	1.35	4.1	0.5	2.9	0.5	1.6	0.23	1.5	0.22	3.1	1.66	31	<0.1	8	<0.4	4.0	1.3
EI-18	2	28	291	<20	24	<20	297	105	20	1	16	81	539	25	161	2.93	3	<0.5	<0.2	2	0.7	0.9	500	21.74	50.2	6.30	29.5	6.71	1.87	6.6	0.9	4.7	0.9	2.7	0.37	2.4	0.35	4.6	0.43	20	1.0	8	<0.4	4.6	1.5
EI-20	2	23	201	<20	28	21	171	79	19	<1	7	56	585	19	137	2.46	<2	<0.5	<0.2	1	<0.5	1.1	404	18.10	41.3	5.09	23.6	5.27	1.40	4.9	0.7	3.6	0.7	2.0	0.29	1.9	0.27	4.0	0.18	45	0.7	<5	<0.4	4.9	1.6
EI-21	1	24	197	<20	24	<20	198	86	19	<1	9	92	522	19	124	1.97	4	<0.5	<0.2	1	<0.5	1.6	667	15.84	36.5	4.51	21.3	4.86	1.32	4.7	0.6	3.5	0.7	2.0	0.28	1.8	0.27	3.6	0.64	19	1.3	6	<0.4	3.9	1.3
EI-22A	1	22	221	<20	25	<20	160	54	21	<1	<5	<2	703	14	55	1.02	<2	<0.5	<0.2	<1	<0.5	<0.5	181	8.43	19.6	2.53	12.4	3.12	1.17	3.0	0.4	2.5	0.5	1.5	0.21	1.4	0.21	1.7	0.51	12	<0.1	<5	<0.4	1.0	0.4
KC-1	1	23	207	<20	28	32	139	75	19	<1	<5	35	619	17	112	2.12	4	<0.5	<0.2	1	<0.5	1.5	328	15.37	34.9	4.32	20.0	4.62	1.33	4.5	0.6	3.2	0.6	1.8	0.26	1.7	0.25	3.2	0.49	51	0.3	<5	<0.4	4.4	1.5
KP-1	2	23	214	23	28	28	166	105	18	1	<5	43	612	22	157	3.05	3	<0.5	<0.2	1	<0.5	0.9	406	21.54	48.9	5.99	27.8	6.15	1.55	5.8	0.8	4.1	0.8	2.4	0.34	2.2	0.32	4.5	0.40	72	0.3	<5	<0.4	6.3	2.4
Potter Peninsula																																												
PP-1A	<1	18	176	<20	19	<20	86	<30	17	<1	<5	18	711	14	109	2.63	<2	<0.5	<0.2	<1	<0.5	0.6	305	14.59	32.9	4.05	18.1	3.95	1.22	3.5	0.5	2.6	0.5	1.4	0.20	1.4	0.20	2.9	0.13	59	<0.1	<5	<0.4	3.4	1.1
PP-1B	<1	16	157	<20	22	<20	102	61	20	1	<5	7	783	14	99	2.29	<2	<0.5	<0.2	<1	<0.5	0.9	243	14.43	32.6	4.03	18.4	4.10	1.22	3.4	0.5	2.8	0.5	1.5	0.22	1.4	0.21	3.0	0.13	49	<0.1	10	<0.4	3.8	1.2
PP-1C	2	5	23	<20	13	33	46	<30	15	<1	43	140	159	27	197	4.89	5	<0.5	<0.2	2	<0.5	0.6	531	28.00	62.2	6.74	26.7	5.58	0.69	5.0	0.8	4.5	0.9	3.0	0.51	3.2	0.48	6.7	1.90	148	1.0	13	<0.4	16.3	5.1
PP-2	1	24	189	46	25	<20	110	62	20	1	<5	13	587	19	136	3.09	<2	<0.5	<0.2	<1	<0.5	<0.5	267	14.68	34.1	4.30	19.6	4.40	1.19	3.9	0.6	3.4	0.7	1.9	0.30	1.8	0.27	4.0	0.17	28	<0.1	7	<0.4	4.2	1.3
PP-3	<1	24	193	44	25	<20	113	66	20	1	<5	22	577	19	139	3.10	<2	<0.5	<0.2	<1	<0.5	<0.5	298	14.89	34.7	4.40	19.6	4.50	1.19	4.0	0.6	3.5	0.7	2.0	0.30	1.9	0.28	4.2	0.17	30	0.2	10	<0.4	4.2	1.3
PP-4	<1	23	202	47	27	19	131	75	20	2	<5	25	540	20	150	2.81	<2	<0.5	<0.2	<1	<0.5	<0.5	305	15.71	34.5	4.55	20.2	4.43	1.33	4.1	0.6	3.4	0.7	2.1	0.29	1.9	0.26	3.6	0.18	38	0.1	8	<0.2	4.7	1.3
PP-5A	1	24	228	33	26	94	171	63	20	<1	<5	34	489	23	168	3.26	<2	<0.5	<0.2	<1	<0.5	<0.5	410	20.88	45.5	5.96	26.4	5.72	1.59	5.4	0.8	4.0	0.8	2.4	0.35	2.1	0.32	4.2	0.21	53	0.1	5	<0.2	6.9	1.9
PP-5B	2	3	8	<20	7	<20	<10	<30	13	<1	<5	131	98	26	193	5.72	<2	<0.5	<0.2	2	<0.5	0.7	466	31.32	68.5	7.71	30.1	5.89	0.62	4.7	0.7	4.5	0.9	2.7	0.42	2.7	0.43	7.0	0.60	104	0.6	8	<0.4	21.8	7.4
PP-5C	2	24	223	<20	27	30	179	84	21	1	<5	36	560	23	159	3.21	4	<0.5	<0.2	1	<0.5	<0.5	381	21.41	51.0	6.15	27.4	6.13	1.60	5.8	0.8	4.1	0.8	2.4	0.34	2.3	0.32	4.7	0.94	41	0.2	11	<0.4	5.1	1.6
PP-6A/1	<1	27	173	74	28	31	43	54	16	<1	<5	3	189	11	53	2.26	<2	<0.5	<0.2	<1	<0.5	<0.5	23	6.51	15.4	1.98	9.4	2.22	0.79	2.1	0.3	2.0	0.4	1.2	0.19	1.2	0.18	1.6	0.11	11	<0.1	<5	<0.4	2.4	0.4
PP-6A/2	1	23	212	<20	26	29	164	66	19	<1	<5	29	532	21	144	2.95	4	<0.5	<0.2	1	<0.5	<0.5	297	20.11	47.6	5.74	25.9	5.80	1.52	5.3	0.7	3.8	0.7	2.2	0.32	2.0	0.30	4.3	1.05	52	0.2	5	<0.4	4.8	1.6
PP-6B	2	3	10	<20	10	<20	22	<30	13	<1	6	128	64	25	171	4.86	4	<0.5	<0.2	2	<0.5	<0.5	568	29.69	67.7	7.36	28.5	5.61	0.63	4.7	0.7	4.0	0.8	2.6	0.42	2.6	0.39	6.2	0.55	117	0.9	<5	<0.4	17.9	5.6
PP-6C	2	24	228	20	27	36	177	70	21	1	<5	31	560	23	156	3.19	5	<0.5	<0.2	1	<0.5	<0.5	326	21.88	51.6	6.20	27.7	6.12	1.60	5.7	0.8	4.1	0.8	2.4	0.34	2.2	0.31	4.6	0.51	51	0.2	5	<0.4	5.1	1.6
PP-7	<1	30	256	80	29	32	71	56	20	<1	<5	3	520	14	56	2.35	<2	<0.5	<0.2	<1	<0.5	<0.5	105	8.33	19.3	2.55	12.1	2.93	1.04	2.9	0.4	2.7	0.5	1.5	0.23	1.4	0.21	1.7	0.12	17	<0.1	<5	<0.4	1.4	0.5
60C4	<1	30	273	85	30	36	146	73	19	1	<5	2	512	14	62	3.04	<2	<0.5	<0.2	<1	<0.5	<0.5	139	8.90	19.0	2.60	12.1	2.90	1.20	2.8	0.4	2.5	0.5	1.5	0.21	1.3	0.20	1.6	0.16	12	<0.1	<5	0.2	1.8	0.4
PP-8	1	30	280	<20	22	<15	171	89	20	2	<5	<2	553	26	154	3.37	<2	<0.5	<0.2	<1	<0.5	<0.5	238	23.59	50.9	6.71	30.3	6.74	2.12	6.2	0.9	4.9	1.0	2.9	0.44	2.5	0.38	3.9	0.21	19	<0.1	6	<0.2	4.5	1.3
PP-9	2	22	159	<20	14	<15	102	97	20	2	<5	3	468	35	251	4.69	<2	<0.5	<0.2	1	<0.5	<0.5	397	34.36	73.3	9.64	42.6	9.14	2.39	8.4	1.2	6.3	1.2	3.6	0.54	3.2	0.49	6.4	0.29	16	<0.1	10	<0.2	7.7	2.1
PP-10	<1	20	112	<20	20	<15	18	70	15	1	<5	<2	218	21	136	2.62	<2	<0.5	<0.2	<1	<0.5	<0.5	140	17.01	38.2	4.97	22.3	4.74	1.28	4.5	0.7	3.7	0.7	2.2	0.33	2.0	0.30	3.3	0.17	44	<0.1	<5	<0.2	4.2	1.1
PP-11	<1	17	158	<20	22	18	108	61	19	1	<5	16	620	13	92	1.85	<2	<0.5	<0.2	<1	<0.5	<0.5	264	13.14	28.4	3.76	16.7	3.52	1.25	3.2	0.4	2.4	0.5	1.4	0.20	1.2	0.18	2.3	0.13	43	<0.1	<5	<0.2	3.6	0.9
PP-12	1	30	274	<20	21	<15	161	103	20	2	<5	15	582	28	170	3.50	<2	<0.5	<0.2	1	<0.5	<0.5	588	25.47	54.8	7.21	32.4	7.05	2.15	6.6	0.9	5.2	1.0	2.9	0.42	2.7	0.40	4.1	0.20	21	0.2	8	<0.2	5.0	1.4
PP-13	2	15	59	<20	12	<15	40	52	18	<1	<5	47	369	31	286	5.07	2	<0.5	<0.2	1	<0.5	<0.5	818	32.87	71.2	9.01	38.7	8.12	2.54	7.5	1.0	5.6	1.1	3.3	0.50	3.1	0.45	7.1	0.39	56	0.2	<5	<0.2	11.7	3.3
PP-19	1	24	210	55	30	35	134	62	20	1	<5	25	632	18	133	2.61	3	<0.5	<0.2	1	<0.5	<0.5	342	15.41	36.9	4.45	20.0	4.59	1.25	4.2	0.6	3.3	0.6	1.9	0.28	1.8	0.26	4.0	0.79	39	0.3	<5	<0.4	3.4	1.1
PP-31B	1	24	213	51	28	34	129	67	20	1	7	19	619	19	136	2.74	<2	<0.5	<0.2	2	0.8	1.0	270	15.88	37.7	4.55	20.7	4.73	1.26	4.4	0.6	3.4	0.6	2.0	0.29	1.9	0.27	4.1	0.25	36	0.6	91	1.1	3.6	1.1
PP-32A	2	24	237	<20	28	41	194	77	22	1	<5	34	599	24	164	3.34	4	<0.5	<0.2	2	<0.5	1.0	383	22.12	52.6	6.33	28.1	6.39	1.65	5.9	0.8	4.3	0.8	2.4	0.36	2.2	0.34	4.8	1.01	50	0.3	7	<0.4	5.4	1.8
PP-32B	2	6	36	<20	11	<20	49	40	16	<1	<5	94	106	27	223	5.13	5	<0.5	<0.2	3	<0.5	2.1	301	32.31	73.6	8.07	32.0	6.55	0.92	5.5	0.8	4.5	0.9	2.8	0.44	2.8	0.42	7.5	1.40	96	0.8	17	<0.4	17.3	5.4
PP-32C	2	24	232	25	27	41	178	78	21	1	<5	30	606	23	163	3.28	4	<0.5	<0.2	1	<0.5	<0.5	337	22.11	52.8	6.35	28.5	6.36	1.65	5.7	0.8	4.2	0.8	2.4	0.35	2.3	0.33	4.8	0.74	36	0.2	6	<0.4	5.2	1.7
PP-33	1	24	250	<20	18	20	128	33	18	<1	<5	102	1,190	18	110	2.26	<2	<0.5	<0.2	<1	<0.5	1.9	1,250	15.86	37.1	4.57	21.0	4.89	1.46	4.5	0.6	3.3	0.6	1.8	0.26	1.7	0.24	3.2	0.13	10	0.5	<5	<0.4	2.4	0.8
127A	2	15	82	<20	15	<20	257	50	18	1	<5	102	285	33	289	5.55	<2	<0.5	<0.2	2	1.2	1.0	653	32.30	75.8	9.58	43.0	9.15	1.92	7.8	1.1	6.4	1.2	3.5	0.54	3.3	0.51	8.8	0.43	93	1.0	13	<0.4	11.1	3.5
128A	<1	25	238	32	23	<15	143	53	19	1	<5	69	391	19	121	2.15	<2	<0.5	<0.2	<1	<0.5	2.1	607	17.19	37.4	4.96	22.1	4.83	1.46	4.5	0.6	3.4	0.7	2.0	0.28	1.7	0.25	3.1	0.11	11	0.5	<5	<0.2	4.9	1.3

Trace element values are in µg/g (ppm).																																													
Sample ID:	**Be**	**Sc**	**V**	**Cr**	**Co**	**Ni**	**Cu**	**Zn**	**Ga**	**Ge**	**As**	**Rb**	**Sr**	**Y**	**Zr**	**Nb**	**Mo**	**Ag**	**In**	**Sn**	**Sb**	**Cs**	**Ba**	**La**	**Ce**	**Pr**	**Nd**	**Sm**	**Eu**	**Gd**	**Tb**	**Dy**	**Ho**	**Er**	**Tm**	**Yb**	**Lu**	**Hf**	**Ta**	**W**	**Tl**	**Pb**	**Bi**	**Th**	**U**
Barton Peninsula																																														
BP-2	<1	27	212	26	28	<20	170	73	20	<1	<5	14	751	12	47	1.46	<2	<0.5	<0.2	<1	<0.5	0.7	186	8.54	18.5	2.34	11.0	2.57	0.97	2.5	0.4	2.3	0.5	1.3	0.20	1.2	0.18	1.5	<0.1	59	<0.1	<5	<0.4	3.1	0.7
BP-3A	<1	28	238	<20	23	<20	111	69	20	1	<5	2	562	14	51	1.52	<2	<0.5	<0.2	<1	<0.5	0.6	165	7.17	16.5	2.19	10.7	2.68	1.04	2.7	0.4	2.6	0.5	1.5	0.23	1.5	0.22	1.7	<0.1	34	<0.1	<5	<0.4	1.6	0.4
BP-4	<1	17	149	<20	19	<20	79	53	20	<1	<5	11	716	12	57	1.73	<2	<0.5	<0.2	<1	<0.5	1.2	256	8.40	18.9	2.47	11.7	2.80	1.04	2.6	0.4	2.3	0.4	1.3	0.20	1.2	0.19	1.8	<0.1	23	0.1	<5	<0.4	1.2	0.4
BP-6	2	25	195	<20	21	<20	182	96	20	1	<5	40	481	35	206	4.68	<2	<0.5	<0.2	2	<0.5	1.5	510	29.73	68.4	8.82	40.8	9.17	2.24	8.2	1.2	6.8	1.3	3.6	0.54	3.3	0.50	6.3	0.28	39	0.6	18	<0.4	5.9	2.0
BP-7	1	32	304	<20	25	<20	424	86	21	1	<5	33	481	30	155	5.19	<2	<0.5	<0.2	2	<0.5	<0.5	362	19.86	45.2	5.87	27.5	6.39	1.80	6.2	0.9	5.7	1.1	3.2	0.49	3.1	0.46	4.8	0.35	51	0.2	11	<0.4	5.0	1.5
BP-9	1	19	170	<20	22	<20	109	58	21	<1	<5	31	650	17	129	3.12	<2	<0.5	<0.2	<1	<0.5	0.9	328	14.95	34.8	4.41	20.0	4.45	1.20	3.9	0.6	3.2	0.6	1.8	0.26	1.7	0.25	4.0	0.19	48	0.3	8	<0.4	4.8	1.6
BP-10A	1	18	211	<20	28	23	93	61	20	1	<5	38	654	15	68	2.22	3	<0.5	<0.2	<1	<0.5	1.8	755	9.85	23.3	2.82	13.0	3.15	1.13	3.1	0.5	2.5	0.5	1.5	0.22	1.4	0.21	2.0	0.63	14	0.4	<5	<0.4	2.0	0.6
BP-10B	<1	22	204	<20	25	<20	73	57	20	<1	<5	79	587	16	72	2.70	<2	<0.5	<0.2	<1	<0.5	2.3	1,180	10.85	24.1	3.07	14.5	3.38	1.15	3.2	0.5	3.0	0.6	1.7	0.26	1.7	0.26	2.3	0.15	22	0.8	<5	<0.4	2.9	0.8
BP-10B rep	<1	23	207	<20	25	<20	74	68	20	1	<5	82	592	16	72	2.74	<2	<0.5	<0.2	<1	0.5	2.5	1,190	10.87	24.1	3.04	14.5	3.39	1.16	3.2	0.5	3.0	0.6	1.7	0.25	1.7	0.25	2.2	0.15	21	1.0	9	<0.4	2.8	0.8
BP-10B (average)	<1	23	205	<20	25	<20	73	63	20	1	<5	81	589.9	16	72	2.72	<2	<0.5	<0.2	<1	0.5	2.42	1,185	10.86	24.1	3.05	14.5	3.39	1.15	3.2	0.5	3.0	0.6	1.7	0.26	1.7	0.25	2.2	0.15	21	0.92	9	<0.4	2.87	0.8
BP-11A	<1	27	267	<20	23	<20	142	81	23	1	<5	87	509	16	60	1.61	<2	<0.5	<0.2	<1	<0.5	1.7	876	7.54	18.0	2.36	11.3	2.97	1.07	2.9	0.5	2.8	0.6	1.6	0.23	1.6	0.23	1.8	<0.1	25	10.2	14	<0.4	1.4	0.5
BP-11B	<1	26	235	<20	24	<20	136	79	22	<1	<5	44	524	12	60	1.47	<2	<0.5	<0.2	<1	<0.5	2.5	576	7.26	17.2	2.21	10.5	2.57	0.93	2.4	0.4	2.2	0.4	1.2	0.18	1.1	0.17	1.7	<0.1	14	0.5	<5	<0.4	1.2	0.4
BP-12B/1	1	10	71	<20	13	<20	67	57	18	<1	<5	77	437	20	203	4.38	<2	<0.5	<0.2	1	<0.5	2.2	433	22.12	49.3	5.65	23.2	4.75	0.91	3.8	0.6	3.5	0.7	1.9	0.29	2.0	0.30	5.9	0.35	66	0.5	7	<0.4	10.0	3.4
BP-13	<1	29	264	<20	25	<20	162	103	25	1	<5	21	276	24	138	3.24	<2	<0.5	<0.2	<1	<0.5	2.0	185	19.56	46.1	5.94	27.1	6.31	1.65	5.5	0.8	4.6	0.9	2.5	0.37	2.3	0.33	4.0	0.18	46	0.2	7	<0.4	3.9	1.2
BP-14	<1	23	193	50	29	<20	117	65	20	1	<5	<2	598	19	144	3.20	<2	<0.5	<0.2	<1	<0.5	1.4	155	16.07	36.9	4.56	20.2	4.53	1.18	3.8	0.6	3.4	0.6	1.9	0.27	1.8	0.28	4.2	0.23	92	<0.1	<5	<0.4	4.5	1.4
BP-15	<1	17	175	<20	23	<20	115	84	21	1	<5	15	687	14	94	2.17	<2	<0.5	<0.2	<1	<0.5	1.1	410	11.67	27.2	3.46	15.7	3.56	1.11	3.0	0.5	2.6	0.5	1.4	0.20	1.3	0.21	2.7	0.10	29	0.2	6	<0.4	2.2	0.7
BP-16	1	32	303	<20	23	<20	227	94	22	2	<5	28	554	26	147	3.88	<2	<0.5	<0.2	1	<0.5	<0.5	418	22.77	51.9	6.48	29.2	6.69	1.85	6.1	0.9	5.0	0.9	2.7	0.39	2.4	0.35	4.3	0.18	28	0.3	11	<0.4	4.1	1.3
BP-17	<1	26	204	189	29	63	99	75	19	2	<5	17	500	18	118	2.47	<2	<0.5	<0.2	<1	<0.5	1.3	537	13.49	31.8	3.97	17.9	4.17	1.08	3.6	0.6	3.3	0.6	1.9	0.26	1.8	0.27	3.4	0.14	31	0.2	10	<0.4	3.8	1.2
BP-18	1	24	217	<20	27	31	117	66	20	1	<5	9	737	18	114	2.16	2	<0.5	<0.2	1	<0.5	2.3	134	16.82	40.0	4.95	23.1	5.27	1.48	4.9	0.6	3.4	0.6	1.9	0.26	1.7	0.24	3.4	0.83	8	<0.1	5	<0.4	3.3	1.1
BP-18 rep	1	24	217	<20	27	31	113	72	20	2	<5	9	745	18	117	2.18	<2	<0.5	<0.2	1	<0.5	2.5	134	16.55	40.0	4.92	22.4	5.17	1.46	4.7	0.6	3.3	0.6	1.9	0.26	1.7	0.24	3.4	0.14	8	<0.1	7	<0.4	3.3	1.1
BP-18 (average)	1	24	217	<20	27	31	115	69	20	1.5	<5	9	741.2	18	116	2.17	2	<0.5	<0.2	1.2	<0.5	2.41	133.8	16.69	40.0	4.94	22.8	5.22	1.47	4.8	0.6	3.4	0.6	1.9	0.26	1.7	0.24	3.4	0.48	8	<0.1	6.1	<0.4	3.33	1.1
BP-19	1	24	213	<20	21	<20	155	115	21	1	<5	<2	516	27	174	3.78	<2	<0.5	<0.2	1	<0.5	<0.5	98	23.52	53.9	6.65	29.7	6.83	1.69	5.7	0.9	4.9	0.9	2.7	0.38	2.4	0.37	5.1	0.19	11	0.1	8	<0.4	4.7	1.6
BP-22	1	26	231	22	24	<20	152	77	20	1	<5	31	552	19	155	3.19	<2	<0.5	<0.2	1	<0.5	<0.5	306	17.38	40.9	5.15	22.9	5.17	1.36	4.6	0.7	3.7	0.7	2.0	0.29	1.9	0.26	4.2	0.17	31	0.2	9	<0.4	4.8	1.6
BP-24	2	19	187	<20	19	21	126	74	20	<1	<5	54	715	18	139	2.65	3	<0.5	<0.2	1	<0.5	1.8	522	17.10	40.4	4.87	21.7	4.79	1.28	4.4	0.6	3.3	0.6	1.9	0.28	1.8	0.26	4.1	1.36	18	0.6	9	<0.4	4.1	1.4
BP-26A	<1	22	183	<20	16	<20	94	52	19	1	<5	49	861	18	79	2.26	<2	<0.5	<0.2	<1	<0.5	0.9	272	9.77	23.3	3.06	14.6	3.75	1.30	3.8	0.6	3.4	0.7	1.9	0.29	1.8	0.27	2.2	<0.1	39	0.3	<5	<0.4	1.9	0.6
BP-27	<1	30	302	<20	24	<20	225	107	26	2	6	13	303	24	138	3.18	<2	<0.5	<0.2	<1	97.0	1.6	456	22.01	51.7	6.41	28.8	6.62	1.86	5.5	0.8	4.7	0.9	2.5	0.36	2.3	0.34	4.1	0.16	20	0.1	9	<0.4	3.6	1.2
BP-28	<1	33	295	<20	21	<20	137	51	19	<1	<5	26	852	20	110	2.48	<2	<0.5	<0.2	<1	<0.5	0.6	569	15.59	36.4	4.63	21.4	5.02	1.53	4.7	0.7	3.7	0.7	2.0	0.29	1.9	0.27	3.0	0.12	30	0.2	<5	<0.4	2.5	0.8
BP-29	<1	28	249	<20	21	<20	139	80	21	1	<5	97	692	15	67	1.61	<2	<0.5	<0.2	<1	0.9	2.7	622	7.61	17.9	2.36	11.3	2.98	1.09	3.1	0.5	2.9	0.6	1.6	0.25	1.6	0.24	1.9	<0.1	19	0.9	<5	<0.4	1.4	0.5
BP-33	<1	27	239	<20	24	22	135	72	21	<1	<5	36	662	20	116	2.93	<2	<0.5	<0.2	<1	0.5	1.8	609	19.07	43.8	5.58	25.5	5.87	1.70	5.3	0.7	4.0	0.7	2.1	0.29	1.9	0.28	3.3	0.14	14	0.3	6	<0.4	2.8	1.0
BP-34	2	20	137	<20	18	<20	49	98	16	1	18	4	231	25	176	3.26	3	<0.5	<0.2	1	<0.5	1.5	55	22.10	53.6	6.55	29.2	6.64	1.69	6.0	0.8	4.5	0.9	2.6	0.38	2.5	0.36	5.1	0.24	43	<0.1	<5	<0.4	4.1	1.2
Weaver Peninsula																																													
WP-1	<1	21	198	<20	26	<20	98	73	20	1	<5	12	656	15	96	2.52	<2	<0.5	<0.2	<1	0.6	1.6	364	14.35	32.1	3.92	17.7	3.91	1.22	3.6	0.5	3.0	0.6	1.6	0.24	1.6	0.23	2.8	0.19	95	0.1	6	<0.4	3.9	1.2
WP-2	<1	34	228	30	36	31	82	65	19	1	<5	<2	535	11	44	1.64	<2	<0.5	<0.2	<1	<0.5	0.6	67	5.46	13.2	1.75	8.5	2.30	0.84	2.3	0.4	2.1	0.4	1.1	0.16	1.0	0.15	1.4	<0.1	42	<0.1	<5	<0.4	1.3	0.4
WP-5	<1	25	184	28	41	48	62	48	16	<1	<5	<2	451	7	15	<1	<2	<0.5	<0.2	<1	<0.5	0.9	46	4.55	10.3	1.32	6.2	1.59	0.58	1.6	0.2	1.3	0.3	0.7	0.11	0.7	0.10	0.6	<0.1	16	<0.1	<5	<0.4	1.1	0.3
WP-6	<1	17	78	<20	14	<20	50	66	19	<1	<5	50	257	22	84	2.02	<2	<0.5	<0.2	1	<0.5	1.9	295	10.60	25.3	3.33	16.1	4.14	1.39	4.4	0.7	4.0	0.8	2.3	0.34	2.3	0.35	2.5	0.13	46	0.3	<5	<0.4	2.2	0.7
WP-7A	<1	15	127	<20	17	<20	67	42	18	<1	<5	47	1,030	13	55	2.16	<2	<0.5	<0.2	<1	<0.5	1.1	179	8.03	18.4	2.31	10.7	2.57	0.95	2.6	0.4	2.3	0.5	1.4	0.21	1.3	0.20	1.7	0.12	24	0.4	<5	<0.4	1.5	0.5
WP-7B	<1	18	150	<20	20	<20	86	58	17	<1	<5	45	431	15	100	2.31	<2	<0.5	<0.2	<1	<0.5	1.8	528	12.76	28.4	3.37	14.6	3.29	0.95	3.1	0.5	2.7	0.5	1.5	0.23	1.5	0.23	2.9	0.18	41	0.5	8	<0.4	4.8	1.6
WP-10	<1	28	271	<20	31	<20	129	73	21	1	<5	<2	695	11	42	1.54	<2	<0.5	<0.2	<1	<0.5	1.9	82	6.28	14.8	1.95	9.3	2.36	0.94	2.4	0.4	2.1	0.4	1.2	0.17	1.1	0.16	1.5	<0.1	24	<0.1	5	<0.4	1.6	0.5
WP-11	<1	25	245	<20	26	23	150	62	21	<1	<5	<2	679	14	47	1.62	<2	<0.5	<0.2	<1	<0.5	0.7	146	11.81	26.4	3.30	15.1	3.54	1.16	3.3	0.5	2.8	0.5	1.5	0.23	1.5	0.21	1.6	<0.1	30	<0.1	6	<0.4	2.3	0.7
WP-13	<1	23	186	27	33	24	132	61	20	1	<5	2	655	14	73	2.16	<2	<0.5	<0.2	<1	<0.5	1.5	137	11.23	25.3	3.15	14.2	3.26	1.03	3.1	0.5	2.7	0.5	1.5	0.22	1.4	0.23	2.2	0.15	64	<0.1	<5	<0.4	3.0	0.9
WP-14	<1	23	197	24	23	22	96	60	20	1	<5	3	709	16	85	2.38	<2	<0.5	<0.2	<1	<0.5	1.3	153	12.33	27.7	3.43	15.3	3.55	1.12	3.4	0.5	2.9	0.6	1.6	0.24	1.6	0.23	2.5	0.17	55	<0.1	<5	<0.4	3.3	1.0
WP-17	<1	34	327	<20	29	21	181	108	23	1	<5	<2	658	17	56	1.50	<2	<0.5	<0.2	<1	<0.5	0.9	128	9.30	22.4	2.97	14.7	3.79	1.35	3.8	0.6	3.2	0.6	1.8	0.26	1.7	0.25	1.8	<0.1	32	<0.1	<5	<0.4	1.5	0.5
WP-18	<1	23	184	<20	29	22	84	81	20	1	<5	8	675	13	49	2.28	<2	<0.5	<0.2	<1	<0.5	3.0	73	6.81	16.3	2.13	10.3	2.60	0.97	2.6	0.4	2.4	0.5	1.3	0.20	1.2	0.18	1.5	0.12	44	0.1	5	<0.4	1.2	0.4
WP-19	<1	29	267	<20	24	26	171	90	20	1	<5	59	476	18	49	2.78	<2	<0.5	<0.2	<1	0.8	6.0	165	8.33	19.2	2.53	12.4	3.28	1.38	3.5	0.6	3.3	0.7	1.9	0.28	1.8	0.26	1.7	0.15	16	0.4	6	<0.4	1.3	0.5
WP-20B	<1	26	265	<20	25	26	136	74	22	1	<5	13	678	11	34	1.25	<2	<0.5	<0.2	<1	<0.5	5.3	100	6.68	15.8	2.09	10.0	2.61	0.91	2.6	0.4	2.1	0.4	1.2	0.17	1.1	0.16	1.1	<0.1	21	<0.1	<5	<0.4	1.2	0.4
WP-20C	<1	27	252	<20	21	21	191	95	22	1	<5	7	611	18	66	1.73	<2	<0.5	<0.2	<1	<0.5	4.6	257	9.71	23.4	3.10	15.0	3.83	1.33	3.9	0.6	3.2	0.6	1.8	0.27	1.7	0.24	2.0	<0.1	26	<0.1	6	<0.4	1.1	0.4
WP-21	1	9	73	<20	17	<20	60	56	18	<1	<5	52	241	20	184	3.43	<2	<0.5	<0.2	<1	<0.5	1.9	413	22.43	48.0	5.48	22.3	4.71	1.17	4.3	0.6	3.5	0.7	2.1	0.33	2.2	0.33	5.1	0.32	112	0.4	6	<0.4	8.6	2.8

Trace element values are in µg/g (ppm).																																										
Sample ID:	**Be**	**Sc**	**V**	**Cr**	**Co**	**Ni**	**Cu**	**Zn**	**Ga**	**Ge**	**As**	**Rb**	**Sr**	**Y**	**Zr**	**Nb**	**Mo**	**Ag**	**In**	**Sn**	**Sb**	**Cs**	**Ba**	**La**	**Ce**	**Pr**	**Nd**	**Sm**	**Eu**	**Gd**	**Tb**	**Dy**	**Ho**	**Er**	**Tm**	**Yb**	**Lu**	**Hf**	**Ta**	**W**	**Tl**	**Pb**	**Bi**	**Th**	**U**
Fildes Peninsula																																												
NP-1	1	18	223	41	25	481	128	73	21	1	<5	36	522	14	68	1.61	<2	<0.5	<0.2	<1	<0.5	0.8	420	11.05	25.9	3.17	14.7	3.52	1.19	3.3	0.5	2.5	0.5	1.5	0.20	1.3	0.19	2.1	<0.1	14	0.5	<5	<0.4	2.0	0.6
FP-1	1	25	216	23	26	30	104	64	20	1	<5	25	487	17	98	3.52	<2	<0.5	<0.2	1	<0.5	<0.5	296	12.30	27.8	3.33	14.9	3.51	1.08	3.3	0.5	3.0	0.6	1.9	0.28	1.8	0.27	2.9	0.26	32	0.1	8	<0.4	2.2	0.7
FP-2	2	16	93	<20	12	<20	43	86	20	1	<5	17	547	25	142	4.64	<2	<0.5	<0.2	1	<0.5	2.5	314	19.79	45.4	5.51	25.2	5.82	1.68	5.5	0.8	4.5	0.9	2.7	0.40	2.5	0.38	4.1	0.33	23	0.2	9	<0.4	3.1	1.0
FP-4	2	17	96	48	15	100	41	75	20	1	<5	20	540	26	144	4.80	3	<0.5	<0.2	1	<0.5	1.5	317	20.09	45.9	5.54	25.1	5.83	1.69	5.6	0.8	4.6	0.9	2.7	0.41	2.5	0.39	4.1	0.34	36	0.2	6	<0.4	3.1	1.0
FP-8	2	16	42	<20	12	<20	12	86	19	1	<5	59	551	28	160	5.50	<2	<0.5	<0.2	2	<0.5	12.5	529	19.66	45.1	5.44	24.7	5.81	1.71	5.6	0.9	4.9	1.0	3.0	0.45	2.9	0.45	4.6	0.47	83	0.5	5	<0.4	3.3	1.1
FP-11	<1	29	303	<20	29	28	161	78	21	1	20	8	652	15	63	1.50	<2	<0.5	<0.2	<1	<0.5	<0.5	188	8.77	21.8	2.83	13.9	3.60	1.29	3.5	0.5	2.8	0.5	1.6	0.22	1.4	0.21	2.0	<0.1	14	<0.1	<5	<0.4	1.0	0.3
Nelson Island																																												
NI-1	2	16	48	<20	11	<20	10	93	18	1	6	57	263	35	209	5.23	<2	<0.5	<0.2	2	0.6	1.2	566	21.66	51.3	6.43	29.5	7.33	1.99	7.2	1.1	6.2	1.2	3.8	0.58	3.7	0.54	6.1	0.36	54	0.5	13	<0.4	4.8	1.5
NI-2	3	18	54	<20	8	<20	23	87	19	1	<5	46	259	33	212	5.01	<2	<0.5	<0.2	2	<0.5	0.6	498	22.10	52.3	6.42	29.5	6.99	1.87	6.6	1.0	5.8	1.2	3.6	0.56	3.6	0.54	6.1	0.36	33	0.3	7	<0.4	5.0	1.3
NI-3	2	16	53	<20	10	22	11	110	19	1	14	56	277	36	216	5.36	<2	<0.5	<0.2	2	<0.5	0.9	541	22.74	53.4	6.61	30.2	7.08	1.86	7.0	1.1	6.0	1.2	3.7	0.57	3.5	0.52	5.9	0.33	38	0.4	18	<0.4	4.6	1.4
NI-4	1	26	186	31	25	32	106	73	19	1	<5	11	665	12	44	1.23	<2	<0.5	<0.2	<1	<0.5	1.0	165	4.95	12.2	1.59	7.9	2.19	0.88	2.4	0.4	2.1	0.4	1.3	0.18	1.2	0.18	1.4	<0.1	23	<0.1	<5	<0.4	0.8	0.3
NI-5	1	25	208	28	29	24	114	64	20	1	<5	21	780	14	104	1.91	<2	<0.5	<0.2	<1	<0.5	<0.5	235	12.33	29.1	3.37	14.9	3.42	1.05	3.2	0.5	2.6	0.5	1.5	0.21	1.4	0.20	3.1	0.13	57	0.2	5	<0.4	3.0	0.8
NI-6	1	32	298	<20	25	22	130	86	19	1	6	12	471	26	155	3.70	<2	<0.5	<0.2	1	<0.5	0.5	325	16.97	40.2	5.03	23.3	5.64	1.53	5.4	0.8	4.7	0.9	2.9	0.43	2.7	0.40	4.6	0.26	24	0.2	7	<0.4	4.1	1.3
Hurd Peninsula																																												
HP-1A/2	1	36	363	39	31	43	166	88	18	1	6	36	601	25	88	1.93	<2	<0.5	<0.2	1	<0.5	0.9	432	10.61	25.3	3.29	16.0	4.18	1.39	4.5	0.7	4.4	0.9	2.7	0.42	2.5	0.38	2.7	0.15	35	0.3	<5	<0.4	1.5	0.5
HP-1B	1	30	280	72	30	46	50	60	19	1	5	86	1,090	11	45	1.62	<2	<0.5	<0.2	<1	<0.5	2.0	521	7.44	17.6	2.16	10.7	2.59	1.08	2.5	0.4	2.1	0.4	1.2	0.17	1.0	0.14	1.4	<0.1	7	0.8	6	<0.4	1.4	0.3
HP-7A	2	23	40	<20	7	<20	<10	122	19	<1	6	75	212	39	112	4.46	<2	<0.5	<0.2	2	0.7	4.4	307	16.85	40.2	4.82	23.4	5.86	1.97	6.4	1.1	6.6	1.3	4.0	0.61	3.7	0.56	3.6	0.33	25	0.8	14	<0.4	2.6	0.6
HP-7B	2	29	151	<20	16	20	27	92	23	2	<5	73	422	31	105	4.52	<2	<0.5	<0.2	<1	0.8	2.0	198	15.20	36.6	4.29	20.1	5.12	1.63	5.3	0.9	5.5	1.1	3.4	0.51	3.1	0.45	3.3	0.34	28	0.5	<5	<0.4	3.4	0.8
HP-7D	2	15	62	<20	10	<20	12	72	18	<1	<5	182	125	36	222	10.01	<2	<0.5	<0.2	2	0.6	4.3	902	28.93	65.8	7.29	32.1	7.16	1.59	6.6	1.0	6.2	1.2	3.7	0.58	3.4	0.52	6.3	0.73	29	1.5	<5	<0.4	5.8	1.3
HP-7E	3	21	235	74	28	36	57	70	18	<1	<5	107	953	15	59	1.89	<2	<0.5	<0.2	<1	0.6	3.9	1,760	11.63	28.3	3.41	16.1	3.73	1.73	3.2	0.5	2.6	0.5	1.4	0.19	1.2	0.18	1.7	0.10	6	1.0	<5	<0.4	2.2	0.5
HP-7F	2	30	300	68	30	47	60	65	18	1	7	69	1,270	13	57	2.15	<2	<0.5	<0.2	<1	0.9	1.6	572	13.50	30.5	3.58	17.0	3.77	1.38	3.4	0.5	2.5	0.5	1.3	0.17	1.1	0.15	1.8	<0.1	13	0.7	5	<0.4	3.7	0.7
HP-7G	2	29	233	<20	20	25	150	86	18	<1	6	56	391	27	132	2.93	<2	<0.5	<0.2	2	<0.5	1.1	422	12.93	30.5	3.81	18.1	4.64	1.29	4.9	0.8	4.7	1.0	3.0	0.45	2.7	0.40	4.0	0.23	40	0.4	<5	<0.4	3.0	0.9
HP-7H	2	47	331	<20	25	<20	14	95	17	1	<5	40	313	23	71	2.84	<2	<0.5	<0.2	1	0.8	1.2	761	8.63	21.4	2.67	13.2	3.62	1.34	4.1	0.7	4.2	0.9	2.6	0.38	2.4	0.34	2.3	0.35	12	0.5	<5	<0.4	1.4	0.3
HP-7J	2	32	50	<20	9	<20	<10	103	17	2	8	18	166	37	101	4.59	<2	<0.5	<0.2	1	<0.5	<0.5	233	14.15	35.8	4.56	22.9	6.13	2.11	6.9	1.1	6.6	1.3	4.0	0.59	3.5	0.51	3.2	0.31	29	0.2	5	<0.4	2.3	0.5
HP-7J rep	2	31	51	<20	9	<20	54	115	18	2	12	19	172	38	102	4.79	<2	<0.5	<0.2	1	0.7	<0.5	236	14.51	37.2	4.75	23.7	6.38	2.19	7.3	1.2	7.0	1.4	4.2	0.61	3.7	0.55	3.3	0.31	29	0.2	7	<0.4	2.4	0.6
HP-7J (average)	2	32	50	<20	9	<20	54	109	17	1.7	10	18	169.4	37	102	4.69	<2	<0.5	<0.2	1.2	0.7	<0.5	234.7	14.33	36.5	4.66	23.3	6.25	2.15	7.1	1.2	6.8	1.4	4.1	0.60	3.6	0.53	3.3	0.31	29	0.2	6.5	<0.4	2.36	0.5
HP-8A/4	2	25	79	<20	12	<20	19	94	18	1	<5	47	366	35	122	5.24	<2	<0.5	<0.2	1	<0.5	0.8	404	16.91	41.1	4.80	22.5	5.64	1.79	5.9	1.0	6.0	1.2	3.7	0.55	3.3	0.48	3.8	0.40	27	0.5	6	<0.4	3.9	0.9
HP-10A	<1	31	292	41	27	34	62	63	15	1	7	97	1,190	12	49	1.50	<2	<0.5	<0.2	<1	<0.5	1.7	828	11.15	25.6	3.04	14.4	3.37	1.23	2.9	0.4	2.3	0.4	1.2	0.17	1.0	0.15	1.5	<0.1	13	1.0	<5	<0.4	3.0	0.6
HP-12/2	2	9	34	<20	8	<20	<10	55	15	<1	8	110	186	27	150	5.30	<2	<0.5	<0.2	1	0.9	2.4	430	16.86	38.5	4.16	18.3	4.19	1.16	4.1	0.7	4.3	0.9	2.8	0.47	2.9	0.45	4.4	0.46	71	0.9	9	<0.4	4.4	1.0
HP-15/4	2	18	9	<20	4	24	<10	89	19	1	5	83	211	45	159	5.80	<2	<0.5	<0.2	1	<0.5	2.5	274	17.34	42.9	5.15	25.0	6.57	1.98	6.9	1.2	7.7	1.6	4.9	0.77	4.7	0.71	5.0	0.43	51	0.9	7	<0.4	3.3	0.8
HP-16/2	1	33	253	127	32	51	63	74	17	1	8	61	932	13	43	1.62	<2	<0.5	<0.2	1	1.2	1.0	753	6.45	15.6	1.90	9.3	2.32	0.88	2.4	0.4	2.3	0.5	1.4	0.20	1.3	0.19	1.4	0.11	8	1.0	16	<0.4	1.1	0.3
HP-16/2 rep	1	33	249	122	31	46	117	83	17	1	10	59	910	13	42	1.58	<2	<0.5	<0.2	2	1.1	0.9	742	6.45	15.5	1.88	9.0	2.25	0.88	2.3	0.4	2.3	0.5	1.4	0.21	1.2	0.19	1.3	0.11	7	0.7	6	<0.4	1.1	0.3
HP-16/2 (average)	1	33	251	125	31	48	90	79	17	1.1	8.7	60	920.5	13	43	1.60	<2	<0.5	<0.2	1.7	1.1	0.93	747.7	6.45	15.5	1.89	9.2	2.29	0.88	2.3	0.4	2.3	0.5	1.4	0.21	1.3	0.19	1.3	0.11	7	0.82	11	<0.4	1.12	0.3
HP-17/2	<1	33	308	67	32	100	39	77	18	1	10	74	1,040	10	40	1.17	<2	<0.5	<0.2	<1	<0.5	0.7	688	9.26	21.2	2.50	12.0	2.79	1.06	2.5	0.4	2.0	0.4	1.0	0.14	0.9	0.13	1.3	<0.1	9	0.9	5	<0.4	2.4	0.5
HP-18/2	1	34	256	167	29	48	81	56	21	2	<5	30	252	12	43	1.64	<2	<0.5	<0.2	6	1.9	0.6	303	5.87	14.6	1.80	8.9	2.31	0.84	2.2	0.4	2.2	0.4	1.4	0.20	1.2	0.19	1.3	0.10	13	0.3	<5	<0.4	1.0	0.3
HP-19/1	2	24	297	<20	26	33	63	157	17	2	<5	187	599	21	46	2.38	<2	<0.5	<0.2	<1	1.9	5.5	1,570	10.63	25.7	3.07	15.0	3.93	1.45	4.0	0.6	3.6	0.7	2.2	0.33	2.0	0.30	1.5	0.12	8	1.5	65	<0.4	2.5	0.6
HP-23/2	2	14	132	<20	18	32	86	65	18	1	16	57	649	17	134	3.17	<2	<0.5	<0.2	<1	0.6	4.3	618	14.83	34.7	3.97	17.5	3.72	1.05	3.4	0.5	2.9	0.6	1.8	0.28	1.8	0.28	3.9	0.41	48	0.6	15	<0.4	4.5	1.4
HP-25/6	1	41	399	<20	30	35	60	113	20	1	13	10	295	31	102	3.79	<2	<0.5	<0.2	1	0.6	<0.5	164	11.77	29.0	3.53	17.3	4.57	1.52	4.9	0.9	5.3	1.1	3.3	0.51	3.0	0.45	3.2	0.26	22	0.1	7	<0.4	2.3	0.6
HP-26/2B	2	11	32	<20	8	<20	31	124	15	<1	<5	82	199	35	171	5.85	<2	<0.5	<0.2	1	<0.5	1.1	384	19.94	45.8	5.07	22.5	5.24	1.39	5.1	0.9	5.7	1.2	3.7	0.61	3.7	0.58	5.1	0.49	74	0.7	58	<0.4	4.5	1.0
HP-27/1	2	33	248	126	39	92	46	89	17	1	9	105	701	26	106	3.70	<2	<0.5	<0.2	<1	1.4	4.1	1,230	9.32	25.9	3.29	16.1	4.07	1.52	4.4	0.7	4.4	0.9	2.7	0.41	2.5	0.38	2.7	0.21	3	1.2	<5	<0.4	0.4	0.1
HP-28/2	1	34	313	<20	26	30	23	111	19	1	<5	31	264	24	88	3.04	<2	<0.5	<0.2	1	2.0	1.6	135	9.45	23.7	2.95	14.6	3.85	1.47	4.2	0.7	4.1	0.8	2.5	0.37	2.3	0.34	2.6	0.19	9	0.3	8	<0.4	1.0	0.3
HP-33/3	2	19	19	<20	7	<20	<10	96	18	1	<5	52	216	41	139	5.11	<2	<0.5	<0.2	1	0.6	2.4	184	15.31	38.3	4.79	23.8	6.19	2.06	6.7	1.1	7.0	1.4	4.4	0.68	4.1	0.61	4.3	0.36	56	0.4	9	<0.4	2.0	0.5

SAMPLE	age	T DM_1	Sm (µg/g)	Nd (µg/g)	$^{143}Nd/^{144}Nd$	2σm (%)	$(^{143}Nd/^{144}Nd)_i$	$^{147}Sm/^{144}Nd$	$^{143/144}CHUR_i$	εNd	$εNd_i$	Rb (µg/g)	Sr (µg/g)	$^{87}Sr/^{86}Sr$	2σm (%)	$^{87}Rb/^{86}Sr$	$(^{87}Sr/^{86}Sr)_i$
PI-4	8,8	399	2,95	12,55	0,51296200	0,0019	0,51295384	0,14180348	0,51262668	6,3	6,4	6,70	545,44	0,703795	0,0032	0,035338	0,703791
AP-1	54	431	6,69	29,48	0,51293400	0,0027	0,51288555	0,13716122	0,51256852	5,8	6,2	8,21	550,21	0,70363	0,0082	0,042955	0,703597
SH-1	47,09	322	7,67	37,74	0,51295817	0,0018	0,51292035	0,12278578	0,51257742	6,2	6,7	74,54	230,37	0,704207	0,0043	0,931490	0,703584
EI-9	46	579	3,12	11,80	0,51294533	0,0041	0,51289728	0,15970670	0,51257882	6,0	6,2	2,37	751,61	0,703517	0,0028	0,009066	0,703511
EI-13	46	502	3,13	11,99	0,51296596	0,0021	0,51291852	0,15768261	0,51257882	6,4	6,6	2,00	696,49	0,70356	0,0028	0,008267	0,703555
KP-1	45,41	322	6,15	27,80	0,51298100	0,0016	0,51294133	0,13357574	0,51257958	6,7	7,1	43,06	611,61	0,703655	0,0026	0,202698	0,703524
PP-1C	46	352	5,58	26,68	0,51294852	0,0049	0,51291049	0,12640044	0,51257882	6,1	6,5	139,51	159,39	0,705145	0,0016	2,519693	0,703499
PP-5A	46	316	5,72	26,39	0,51297900	0,0018	0,51293958	0,13102748	0,51257882	6,7	7,0	34,30	488,76	0,703626	0,0031	0,202015	0,703494
PP-5B	46	280	5,89	30,12	0,51297500	0,0018	0,51293942	0,11825296	0,51257882	6,6	7,0	131,11	98,48	n.d.	n.d.	3,832592	n.d.
PP-6B	46	314	5,61	28,49	0,51295520	0,0017	0,51291937	0,11906143	0,51257882	6,2	6,6	127,79	63,84	0,707363	0,0027	5,762404	0,703598
PP-11	46,61	326	3,52	16,70	0,51296631	0,0018	0,51292743	0,12753187	0,51257803	6,4	6,8	16,42	620,21	0,703428	0,0030	0,076206	0,703378
PP-12	46	351	7,05	32,43	0,51296100	0,0021	0,51292148	0,13136042	0,51257882	6,3	6,7	15,14	582,02	n.d.	n.d.	0,074891	n.d.
PP-31B	46,98	322	4,73	20,75	0,51299000	0,0019	0,51294768	0,13771167	0,51257756	6,9	7,2	18,78	618,55	n.d.	n.d.	0,087388	n.d.
PP-32B	45,7	310	6,55	31,98	0,51296700	0,0025	0,51293003	0,12366583	0,51257920	6,4	6,8	93,59	105,93	n.d.	n.d.	2,543430	n.d.
PP-32C	47,19	342	6,36	28,45	0,51297400	0,0021	0,51293233	0,13499544	0,51257729	6,6	6,9	29,53	605,80	n.d.	n.d.	0,140345	n.d.
PP-33	46,43	377	4,89	20,97	0,51297000	0,0019	0,51292724	0,14079430	0,51257826	6,5	6,8	102,26	1190,00	n.d.	n.d.	0,247376	n.d.
WP-20B	54,6	336	2,61	10,01	0,51302700	0,0025	0,51297066	0,15775557	0,51256775	7,6	7,9	13,33	677,87	0,703499	0,0026	0,056594	0,703455
FP-8	57,4	442	5,81	24,66	0,51294400	0,0023	0,51289051	0,14246358	0,51256415	6,0	6,4	58,57	550,93	0,703676	0,0033	0,306041	0,703426
NI-1	50	456	7,33	29,52	0,51296000	0,0021	0,51291094	0,15001359	0,51257367	6,3	6,6	57,33	263,13	n.d.	n.d.	0,627273	n.d.
NI-2	50	424	6,99	29,48	0,51295400	0,0033	0,51290718	0,14317200	0,51257367	6,2	6,5	45,62	258,50	n.d.	n.d.	0,508007	n.d.
HP-1A/2	39,8	681	4,18	15,96	0,51290300	0,0027	0,51286177	0,15837396	0,51258680	5,2	5,4	36,18	600,50	n.d.	n.d.	0,173439	n.d.
HP-7D	53	975	7,16	32,13	0,51264400	0,0016	0,51259734	0,13460635	0,51256981	0,1	0,5	182,15	125,05	n.d.	n.d.	4,193096	n.d.
HP-7F	55	619	3,77	16,96	0,51282800	0,0021	0,51277970	0,13427050	0,51256724	3,7	4,1	69,03	1270,00	n.d.	n.d.	0,156474	n.d.
HP-7J	60	1536	6,13	22,88	0,51262600	0,0020	0,51256250	0,16179603	0,51256080	-0,2	0,0	18,50	169,36	n.d.	n.d.	0,314394	n.d.
HP-10A	48,3	630	3,37	14,39	0,51285200	0,0027	0,51280731	0,14146256	0,51257586	4,2	4,5	97,27	1190,00	n.d.	n.d.	0,235302	n.d.
HP-15/4	80,12	1377	6,57	25,02	0,51265200	0,0018	0,51256885	0,15864661	0,51253491	0,3	0,7	83,35	210,97	n.d.	n.d.	1,137304	n.d.
HP-19/1	56,45	1014	3,93	15,00	0,51278000	0,0020	0,51272163	0,15808917	0,51256537	2,8	3,0	187,03	599,09	n.d.	n.d.	0,898723	n.d.
HP-23/2	37,16	357	3,72	17,54	0,51295000	0,0133	0,51291884	0,12819274	0,51259019	6,1	6,4	56,92	648,91	n.d.	n.d.	0,252501	n.d.
HP-26/2B	57	1009	5,24	22,51	0,51266700	0,0018	0,51261452	0,14076133	0,51256466	0,6	1,0	82,34	198,66	n.d.	n.d.	1,193188	n.d.
HP-28/2	55	879	3,85	14,61	0,51283500	0,0016	0,51277777	0,15908510	0,51256724	3,8	4,1	30,85	263,71	n.d.	n.d.	0,336792	n.d.
Ø 2σm (%)						0,0026									0,0033		

measured values

i = calculated initial isotopy

n.d. = not determined

Ar-Ar ages (pl-separates) measured by M. McWilliams at Stanford University, CA, USA
Caution: ages in red did not yield formal plateaus and are estimated best fits
K-Ar ages (WR) measured by Z. Pecskay at Univ. of Debrecen, Hungary
Estimated rough ages, no measurements available

Calculation of $^{147}Sm/^{144}Nd$ using following isotope percentages[1]:
^{147}Sm=14.99%; ^{144}Nd=23.8%
Calculation using decay constant from Lugmair & Marti (1978)

Calculation of T DM_1 according to Peucat et al. [1988]:
143/144 DM today = 0.51315
147/144 DM today = 0.2137

Calculation of $^{87}Rb/^{86}Sr$ using following isotope percentages[1]:
^{87}Rb=27.8%; ^{86}Sr=9.9%
Calculation using decay constant from Steiger & Jäger (1977)

[1] from: Periodical System of the Elements. *VCH Verlagsges. mbH*, 2002

SAMPLE	age	U (µg/g)	Th (µg/g)	Pb (µg/g)	$^{206}Pb/^{204}Pb$	2σm (%)	$(^{206}Pb/^{204}Pb)_i$	$^{207}Pb/^{204}Pb$	2σm (%)	$(^{207}Pb/^{204}Pb)_i$	$^{208}Pb/^{204}Pb$	2σm (%)	$(^{208}Pb/^{204}Pb)_i$	$^{207}Pb/^{206}Pb$	2σm (%)	$^{208}Pb/^{206}Pb$	2σm (%)	$^{208}Pb/^{207}Pb$	2σm (%)
PI-4	8,8	0,2713	1,1367	-5,00	18,72783494	0,0044	18,72020962	15,62089211	0,0046	15,62053971	38,56025864	0,0047	38,54973457	0,83409333	0,0010	2,05898112	n.d.	2,46847637	0,0009
AP-1	54	1,1243	3,7729	6,35	18,71655815	0,0045	18,62458648	15,64122242	0,0048	15,63689116	38,54334341	0,0051	38,44191576	0,83568926	0,0010	2,05931791	n.d.	2,46424102	0,0012
SH-1	47,09	2,2233	7,6381	8,32	18,70279159	0,0049	18,58179257	15,61089299	0,0055	15,60521121	38,46036806	0,0046	38,32371289	0,83468373	0,0013	2,05639719	n.d.	2,46369580	0,0016
EI-9	46	0,3114	0,6225	5,90	18,61918134	0,0074	18,59585956	15,58897465	0,0078	15,58788002	38,32603175	0,0081	38,31070400	0,83725350	0,0016	2,05841659	n.d.	2,45853846	0,0011
EI-13	46	0,2675	0,6759	-5,00	18,62861301	0,0058	18,58920216	15,60870758	0,0061	15,60685779	38,39035166	0,0066	38,35761129	0,83788890	0,0010	2,06082716	n.d.	2,45954708	0,0019
KP-1	45,41	2,3860	6,2511	-5,00	18,73178307	0,0067	18,38473817	15,62227964	0,0082	15,60599480	38,52358829	0,0106	38,22466200	0,83399852	0,0021	2,05658950	n.d.	2,46593866	0,0029
PP-1C	46	5,0965	16,2783	12,83	18,79753581	0,0053	18,62192446	15,64589240	0,0067	15,63764993	38,63726346	0,0083	38,45285998	0,83241631	0,0020	2,05544300	n.d.	2,46934166	0,0019
PP-5A	46	1,9261	6,8847	5,42	18,68052838	0,0054	18,52352262	15,60697168	0,0055	15,59960248	38,42507968	0,0062	38,24057453	0,83546833	0,0013	2,05695893	n.d.	2,46201778	0,0015
PP-5B	46	7,4438	21,8198	7,81	18,80439586	0,0035	18,38310390	15,62523076	0,0055	15,60545705	38,60989305	0,0056	38,20390283	0,83096237	0,0019	2,05325526	0,0023	2,47083829	0,0008
PP-6B	46	5,5917	17,8832	-5,00	19,26751789	0,0054	18,44360126	15,62597916	0,0048	15,58730790	39,02354722	0,0047	38,15725437	0,81100407	0,0014	2,02535415	n.d.	2,49735216	0,0012
PP-11	46,61	0,9315	3,6332	-5,00	18,66839181	0,0077	18,52930694	15,53870000	0,0093	15,53217026	38,40363737	0,0108	38,22530385	0,83610437	0,0018	2,05714760	n.d.	2,46085394	0,0014
PP-12	46	1,3561	4,9734	8,08	18,71661917	0,0099	18,64241570	15,63643105	0,0116	15,63294824	38,54470561	0,0128	38,45523891	0,83527604	0,0018	2,05899967	0,0015	2,46493691	0,0014
PP-31B	46,98	1,0835	3,5517	90,76	18,66742947	0,0083	18,66203953	15,59429031	0,0124	15,59403723	38,39035711	0,0157	38,38454874	0,83537424	0,0043	2,05654196	0,0076	2,46182114	0,0034
PP-32B	45,7	5,4394	17,2648	17,15	18,76549219	0,0080	18,62621548	15,60672139	0,0103	15,60018513	38,50270206	0,0136	38,35736604	0,83167014	0,0026	2,05175591	0,0061	2,46703327	0,0036
PP-32C	47,19	1,6876	5,2461	6,03	18,68134021	0,0072	18,55433414	15,59591432	0,0098	15,58995020	38,39468761	0,0111	38,26490088	0,83483180	0,0028	2,05524267	n.d.	2,46184262	0,0015
PP-33	46,43	0,7741	2,3511	-5,00	18,66957415	0,0048	18,55444307	15,61378247	0,0048	15,60837772	38,42167813	0,0055	38,30672199	0,83630804	0,0014	2,05798364	n.d.	2,46067437	0,0020
WP-20B	54,6	0,3785	1,1695	-5,00	18,38543789	0,0060	18,31920126	15,64991949	0,0085	15,64679940	38,32742327	0,0102	38,26016613	0,84405576	0,0025	2,08466198	n.d.	2,45211383	0,0018
FP-8	57,4	1,0635	3,2809	5,33	18,65091594	0,0046	18,54071256	15,60352842	0,0052	15,59833116	38,40572848	0,0049	38,29402129	0,83661788	0,0014	2,05918726	n.d.	2,46133746	0,0009
NI-1	50	1,5392	4,8052	12,63	18,64269370	0,0041	18,58411123	15,59849079	0,0044	15,59573656	38,38898629	0,0046	38,32887343	0,83671307	0,0013	2,05919739	n.d.	2,46106335	0,0009
NI-2	50	1,3450	5,0059	6,98	18,67743471	0,0098	18,58482362	15,60747042	0,0099	15,60311635	38,43587499	0,0107	38,32258249	0,83563208	0,0016	2,05787763	n.d.	2,46267096	0,0015
HP-1A/2	39,8	0,4575	1,4617	-5,00	18,67890140	0,0030	18,62060977	15,61659139	0,0041	15,61386250	38,45834083	0,0034	38,39708494	0,83605489	0,0018	2,05891878	n.d.	2,46267797	0,0009
HP-7D	53	1,3364	5,8035	-5,00	18,93194459	0,0799	18,70493851	15,68102621	0,0801	15,67034020	38,94887928	0,0802	38,62491250	0,82830825	0,0068	2,05731002	n.d.	2,48393955	0,0064
HP-7F	55	0,7339	3,6591	5,34	18,80256859	0,0055	18,72983443	15,64341668	0,0070	15,63998994	38,73681189	0,0073	38,61764642	0,83198377	0,0022	2,06018724	n.d.	2,47624692	0,0011
HP-7J	60	0,5387	2,3556	5,48	18,81161339	0,0044	18,75487671	15,67233848	0,0050	15,66965983	38,75326234	0,0049	38,67175408	0,83312152	0,0013	2,06007117	n.d.	2,47271172	0,0010
HP-10A	48,3	0,6147	3,0042	-5,00	18,82440603	0,0100	18,72928084	15,64574785	0,0101	15,64127876	38,74770931	0,0106	38,59489451	0,83114410	0,0017	2,05837620	n.d.	2,47657110	0,0017
HP-15/4	80,12	0,7864	3,3051	7,31	18,78594788	0,0032	18,70284961	15,66140437	0,0038	15,65744781	38,70084807	0,0039	38,58624115	0,83367515	0,0014	2,06009557	n.d.	2,47109009	0,0007
HP-19/1	56,45	0,5886	2,4720	65,18	18,70526310	0,0030	18,70036049	15,68699733	0,0034	15,68676621	38,63758227	0,0039	38,63081737	0,83864491	0,0017	2,06559951	n.d.	2,46302189	0,0010
HP-23/2	37,16	1,4079	4,4747	15,03	18,67860893	0,0058	18,64519269	15,63265605	0,0066	15,63109341	38,51553993	0,0084	38,48060699	0,83692829	0,0012	2,06201329	n.d.	2,46379845	0,0023
HP-26/2B	57	1,0112	4,5215	58,46	18,68946145	0,0043	18,67997817	15,65466580	0,0039	15,65421864	38,57416325	0,0044	38,56023054	0,83761307	0,0012	2,06395264	n.d.	2,46406375	0,0008
HP-28/2	55	0,2934	0,9961	7,55	18,73981484	0,0088	18,71924964	15,70603152	0,0117	15,70506263	38,74882006	0,0153	38,72587957	0,83802976	0,0041	2,06772694	n.d.	2,46677682	0,0036
Ø 2σm (%)						0,0084			0,0094			0,0102			0,0020		0,0044		0,0018

negative Pb (µg/g) values equal not detected at that lower limit (ICP-MS) i = calculated initial isotopy measured values n.d. = not determined

Ar-Ar ages (pl-separates), measured by M. McWilliams at Stanford University, CA, USA

Caution: ages in red did not yield formal plateaus and are estimated best fits

K-Ar ages (WR), measured by Z. Pecskay at Univ. of Debrecen, Hungary

Estimated rough ages, no measurements available

Calculation of initial lead isotopy using following isotope percentages[1]:

^{238}U=99.275%; ^{235}U=0.72%; ^{232}Th=100%; ^{208}Pb=52.4%; ^{207}Pb=22.1%; ^{206}Pb=24.1%; ^{204}Pb=1.4%

Calculation using decay constants from Steiger & Jäger (1977)

[1] from: Periodical System of the Elements. *VCH Verlagsgesellschaft mbH*, 2002

Correlation coefficients of 2σm (%):

206/204 vs 207/204	1,00	207/204 vs 207/206	0,83	143/144 vs 87/86	-0,13	143/144 vs 208/206	0,29
206/204 vs 208/204	0,99	207/204 vs 208/207	0,81	143/144 vs 206/204	-0,08	143/144 vs 208/207	0,03
206/204 vs 207/206	0,79	208/204 vs 207/206	0,86	143/144 vs 207/204	-0,09		
206/204 vs 208/207	0,78	208/204 vs 208/207	0,84	143/144 vs 208/204	-0,08		
207/204 vs 208/204	1,00	207/206 vs 208/207	0,86	143/144 vs 207/206	-0,17		

Calculation of linear mass fractionation F (Pb isotope data):

Std.	run	$F_{206/204}$	$F_{207/204}$	$F_{208/204}$	$F_{207/206}$	$F_{208/206}$	$F_{208/207}$
NBS 981	4288	-0.000459121	-0.000297686	-0.000116742	3.88169E-05	0.000212326	0.00037324
NBS 981	4515	0.001969382	0.001816137	0.001794064	0.001507432	0.001605328	0.00170601
NBS 981	4516	0.001504679	0.001511406	0.001524166	0.001520374	0.001530206	0.00153487
NBS 981	4660	0.001597813	0.001533539	0.001584726	0.001414442	0.001558193	0.00164012
NBS 981	4671	0.001315308	0.001442105	0.00140322	0.00165814	0.001477694	0.00129372
NBS 981	4725	0.001702144	0.001614024	0.001523694	0.00141806	0.001331831	0.00125452
NBS 981	4736	0.00150895	0.00139567	0.001388921	0.00114971	0.001255464	0.00136453
NBS 981	4764	0.000981062	0.001143241	0.001281566	0.001449531	0.001568715	0.00169418
NBS 981	4818	0.001151132	0.00116789	0.001211473	0.001194315	0.001258666	0.00132301
NBS 981	4827	0.000897656	0.001021996	0.001043629	0.001265451	0.001175298	0.00108292
	$F_{ø}$=	0.00140313	0.00140511	0.00141727	0.00139750	0.00141793	0.00143265

>> F_{ges}= 0.00150171
= 1.50 ‰
(measurement at ca 1180-1200° C)

>> F_{ges}= 0.00108230
= 1.08 ‰
(measurement at ca 1300-1320° C)

	Recommended values (Todt et al., 1996)				
	206/204	207/204	208/204	207/206	208/206
NBS 981	16.9356	15.4891	36.7006	0.914585	2.16701
$2\sigma_m$	0.0007	0.0009	0.0034	0.000040	0.00013
NBS 982	36.7492	17.1621	36.7555	0.467006	1.00016*
$2\sigma_m$	0.0004	0.0003	0.0002	0.000007	-

* ratio used for the calibration of the double spike

mass fractionation factor F calculated as: $F = (\text{isotope ratio})_{rec}/((\text{isotope ratio})_{mes})^{1/\Delta M} - 1$

"power law" correction using F: $(\text{isotope ratio})_{real} = (\text{isotope ratio})_{mes} * (1+F)^{\Delta M}$

Comparative correction of Pb-mass fractionation of PI-4 using three different F's

F	206/204	2σm (%)	207/204	2σm (%)	208/204	2σm (%)	207/206	2σm (%)	208/206	2σm (%)	208/207	2σm (%)
0.0015	18.73129219	0.0044	15.62445344	0.0046	38.57059050	0.0047	0.83413582	0.001	2.05915268	0.0044	2.46858924	0.0009
0.0010	18.71259362	0.0044	15.60106354	0.0046	38.49362252	0.0047	0.83371938	0.001	2.05709712	0.0044	2.46735679	0.0009
0.0005	18.69390439	0.0044	15.57769700	0.0046	38.41676979	0.0047	0.83330293	0.001	2.05504259	0.0044	2.46612435	0.0009

Pb elution scheme using HBr-HCl chemistry (400µl- and 100µl-columns)

scientist date

column-#	1	2	3	4	5	6	7	8	9	10
analysis-#										

Pb separation

400 µl columns (= 1RV) **Pb_{com}**

column-#		1	2	3	4	5	6	7	8	9	10	time
rinse	10 RV H_2O****											
	10 RV 6N HCl											
	1 RV H_2O****											
	2 RV H_2O****											
buffer	1 RV 1N HBr											
	1 RV 1N HBr											
	1 RV 1N HBr											
sample in 1ml 1N HBr												
Fe-cleaning	2 RV 1N HBr											
	7 RV 1N HBr											
buffer	1 RV 2N HCl											
	1 RV 2N HCl											
Pb-extraction	5 RV 6N HCl											

Pb cleaning

100 µl columns (= 1RV) **Pb_{com}**

column-#	1	2	3	4	5	6	7	8	9	10	time
10 RV H_2O****											
10 RV 6N HCl											
5 RV H_2O****											
1 RV 2N HCl											
1 RV 2N HCl											
1 RV 2N HCl											
sample in ~ 1RV 2N HCl											
1 RV 2N HCl											
2 RV 2N HCl											
5 RV 6N HCl											
end											

Analytical methods and age calculation (K-Ar whole rock)

Institute of Nuclear Research of the Hungarian Academy of Sciences (ATOMKI) in Debrecen, Hungary

Potassium determination

Powder samples were digested in acids (HF, HNO_3 and H_2SO_4) in teflon beakers and finally dissolved in 0.2 M HCl and analyzed for potassium by flame photometry using a Na buffer and a Li internal standard. Multiple runs of inter-laboratory standards (Asia 1/65, LP-6, HD-B1) indicated the accuracy and reproducibility of this method to be within 2-3%.

Argon measurements

Approximately 0.5 g of each sample was wrapped in aluminium foil and copper sieve preheated for about 24h at 150-200 C° in vacuum. Argon was extracted from the samples by RF fusion in Mo crucibles, in a previously baked stainless steel vacuum system. An ^{38}Ar spike was added from a gas pipette system and the released gas was cleaned using Ti and SAES getters and liquid nitrogen traps. The purified Ar was transported directly into the mass spectrometer and the Ar isotope ratio was measured in the static mode, using a 15 cm radius magnetic sector type mass spectrometer built in Debrecen.

Details of the instruments, the applied methods and results of calibration have been described elsewhere [Balogh 1985; Odin et al. 1982].

Age calculation

Atomic constants suggested by Steiger & Jäger [1977] were used to calculate the ages. All analytical errors represent one standard deviation (i.e. 68% analytical confidence level). Since we base our analytical errors on the long time stability of the instruments and on the deviation of our results obtained on standard samples from the inter-laboratory mean, the analytical errors are likely to be overestimated.

Based on our long term experiences, K-Ar ages of suites of volcanic and metamorphic rocks generally are in good agreement with geological expectations. However, both the Ar- and K-concentration may undergo changes during the history of the rock due to diffusion solution or ion exchange.

Consequently, K-Ar ages are considered reliable, if the data can also be supported by geological, stratigraphical and petrographical arguments.

References

Balogh K. (1985): K-Ar dating of Neogene volcanic activity in Hungary: Experimental technique, experiences and methods of chronological studies. *ATOMKI Report*, **D/1**, 277-288.

Odin G.S. et al. (1982): Interlaboratory standards for dating purposes. *In*: Odin G.S. (ed.): Numerical Dating in Stratigraphy. Wiley, Chichester New York, 123-150.

Steiger R.H. & Jäger E. (1977): Subcomission on geochronology: convention on the use of decay constants in Geo- and Cosmochronology. *Earth Planet. Sci. Lett.,* **36**, 359-362.